

UNCLASSIFIED

AD NUMBER
AD913408
NEW LIMITATION CHANGE
TO Approved for public release, distribution unlimited
FROM Distribution authorized to U.S. Gov't. agencies only; Test and Evaluation; 12 SEP 1973. Other requests shall be referred to Commander, Naval Ammunition Depot, Crane, IN 47522.
AUTHORITY
NSWC ltr, 14 May 1976

THIS PAGE IS UNCLASSIFIED

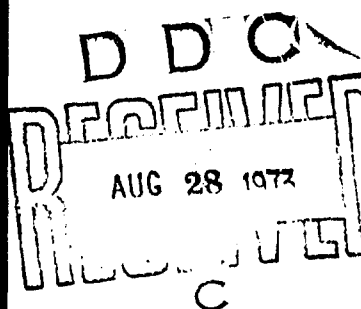
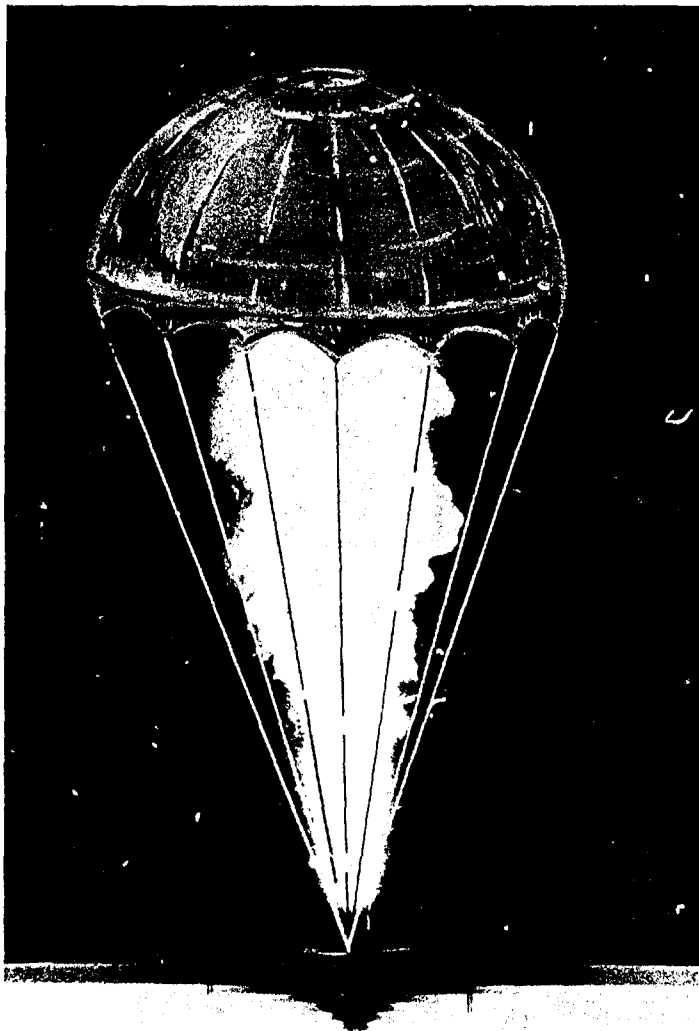
THIS REPORT HAS BEEN DELIMITED  
AND CLEARED FOR PUBLIC RELEASE  
UNDER DOD DIRECTIVE 5200.20 AND  
NO RESTRICTIONS ARE IMPOSED UPON  
ITS USE AND DISCLOSURE.

DISTRIBUTION STATEMENT A

APPROVED FOR PUBLIC RELEASE;  
DISTRIBUTION UNLIMITED.

AD-913408-1

PROCEEDINGS  
THIRD INTERNATIONAL  
PYROTECHNICS SEMINAR



Best Available Copy

ANTLERS PLAZA HOTEL  
COLORADO SPRINGS, COLORADO  
21-25 AUGUST 1972

HOSTED BY

DENVER RESEARCH INSTITUTE / UNIVERSITY OF DENVER

PROCEEDINGS OF THIRD  
INTERNATIONAL PYROTECHNICS SEMINAR  
21 AUGUST 1972

Chairman

R. M. Blunt, Denver Research Institute

Associate Chairmen

C. A. Lipscomb, Naval Ammunition Depot, Crane

R. E. Williams, Denver Research Institute

Distribution limited to U.S. Gov't. agencies only;  
Test and Evaluation; 12 SEP 1973. Other requests  
for this document must be referred to

Commander, Naval Ammunition Depot

R & D Dept. Bldg. 190

Crane, Indiana. 47522

Denver Research Institute  
University of Denver  
Denver, Colorado  
80210



## FOURTH SEMINAR PROCEEDINGS

### INTRODUCTION

Those of you who attended the Second International Pyrotechnics Seminar in 1970 will recall that I was doubtful of the success of a Third, because of the political and economic conditions then prevailing. At the time this is written, the Third Seminar shows every indication of being as successful as the Second and for once it is really a pleasure to admit how wrong I was!

My thanks to the authors of the papers; they are the backbone of these Seminars, and I hope all of you will begin to plan now for papers to be presented at the Fourth Seminar. The pyrotechnics community owes these authors a real debt for reporting their work and thus providing that exchange of information which is the justification for these Seminars.

Much of the response that justified this Third Seminar arose from the efforts of those who attended the First and Second Seminars to publicize them and attract their colleagues. To all of you, my sincere thanks. Without your help, these Seminars could not exist. Special thanks are due to Mr. Ralph Williams and Mr. Charles (Bud) Lipscomb, who sent the Seminar off to a flying start last December, and to the session chairmen for their very able assistance. The active interest and continued cooperation of the Naval Air Systems Command and of the Naval Ammunition Depot (Crane) is deeply appreciated.

With your continuing support, the presentation of a fourth seminar is very likely. Please send your comments and suggestions to me so that it may also be even better.

R. M. Blunt  
General Chairman

15 July 1972  
Denver, Colorado

## TABLE OF CONTENTS

	Page
POSSIBLE MECHANISMS FOR BURNING RATE/CANDLEPOWER ENHANCEMENT IN ILLUMINANTS - David R. Dillehay .....	1
GAS GENERATORS FOR INFLATING AUTO CRASH BAGS - George A. Lane, T. R. Torkleson, T. E. Dergazarian, and G. R. Staudacher .....	25
A COMPARISON OF GROUND AND ATOMIZED MAGNESIUM IN POUR-CAST ILLUMINANTS - George A. Lane and Keith Roberson .....	39
FORMATION OF PYROPHORIC FRAGMENTS - W. W. Hillstrom .....	49
DEVELOPMENT AND EVALUATION OF EXPLOSIVE MATERIALS FOR THE TASK OF EXPLOSIVE DISPERSION OF PROJECTILES - Allen J. Tulis, James L. Austing, and Robert F. Remaly .....	65
PYROTECHNIC FLARE SPECTROSCOPY II - Bernard E. Douda .....	97
THE CHEMICAL REACTIVITY OF FERRIC OXIDE - Charles A. Lipscomb .....	107
FEASIBILITY STUDY OF A SELF-SUSPENDING FLARE SYSTEM - D. L. Carstens .....	127
SOME FACTORS AFFECTING BURNING RATES AND VARIABILITY OF TUNGSTEN AND MANGANESE DELAY COMPOSITIONS - F. J. Valenta .....	157
THE STATE-OF-THE-ART OF NAVY PYROTECHNIC DELAYS - F. J. Valenta .....	185
ANALYTICAL AND FUNCTIONAL TESTS OF NATURALLY AGED EXPLOSIVE ORDNANCE IN THE PERSHING LEAP PROGRAM - Edward M. Storma .....	197
PROPERTIES AND APPLICATIONS OF BORON/POTASSIUM NITRATE - Paul B. Tweed .....	253
THE INFLUENCE OF TRANSITION METAL COMPOUNDS ON THE ALUMINUM-SODIUM NITRATE REACTION - P. L. Farnell, R. P. Westerdahl, and F. R. Taylor .....	271
A FLICKERING SIGNAL FLARE - Russell Reed, Jr., Richard P. Cornia, and William O. Munson .....	291
SMOKE/FLAME PYROTECHNICS - Graham C. Shaw III, and Russell Reed, Jr. ....	305

Table of Contents Cont.	Page
FLOW-CASTABLE COMPOSITIONS FOR ILLUMINATION FLARES - George A. Lane, E. M. Jankowiak, D. L. Girardin, and K. Roberson . . . . .	321
USE OF PROPELLANT GAS GENERATORS FOR THE EMPTYING OF CAPACITIES AT GREAT DIVING DEPTHS - J. Delgendre and B. Kurtzemann . . . . .	363
PYROTECHNIC SPECIAL EFFECTS IN MOTION PICTURES - Frank P. Clark . . . . .	387
IMPROVED BINDER SYSTEMS FOR FLARE COMPOSITIONS - H. E. Filter and D. L. Stevens . . . . .	403
POUR-CASTABLE COMPOSITIONS FOR COLORED SMOKE SIGNALS - Harold E. Filter, Erwin M. Jankowiak, George A. Lane, and Don L. Stevens . . . . .	419
OBSERVATIONS OF THE SURFACE DETAILS OF BURNING Mg/NaNO <sub>3</sub> /BINDER FLARES - John L. Eisel . . . . .	435
FACTORS AFFECTING THE STOICHIOMETRY OF THE MAGNESIUM-SODIUM NITRATE COMBUSTION REACTION - A. J. Beardell and D. A. Anderson . . . . .	445

# POSSIBLE MECHANISMS FOR BURNING RATE/CANDLEPOWER ENHANCEMENT IN ILLUMINANTS

by

David R. Dillehay

Thiokol Chemical Corporation  
Longhorn Division  
Marshall, Texas

## ABSTRACT

Investigations have shown that magnesium oxide does not contribute significantly to the candlepower output of illuminants. The emission of sodium atoms is the main source of visible light. This paper suggests a mechanism explaining the high efficiency of magnesium-sodium nitrate illuminants. An energy transfer between sodium and magnesium coupled with the formation of a NaMg molecule would account for the increases in light output. One resultant conclusion of this theory is that aluminum is not an effective illuminant fuel because there is no efficient energy transfer with sodium.

The burning rate response relative to flame temperature suggests that thermal input is insufficient to explain the magnitude of change observed. Photolytic reactions at the surface may be a controlling factor in surface decomposition.

## INTRODUCTION

Many theories have been propounded to account for the extraordinary amount of visible light produced by a magnesium-sodium nitrate flare. Many of the theories have dealt only with a single formulation while others assume certain characteristics which seem to be at odds with physical probabilities. Over the past three years, much has been accomplished in determining that sodium emission is the most important contributor to visible light in magnesium-sodium nitrate flare compositions. Various studies to define this mechanism have not satisfactorily explained why sodium gives this tremendous effect with increasing magnesium content even though the flame temperature is decreasing. Further, why doesn't sodium do equally well with other metal fuels, such as aluminum, where the heat of reaction exceeds that of magnesium. Burning rate variation is not adequately accounted for by thermal feedback and thermal conductivity. Very hot, sodium rich flare plumes are produced at 35 to 40% magnesium, yet light integral and burning rate are very low.

This paper will describe some alternate theories which offer a different approach to the problems and will perhaps lead to a new direction of investigation.

## EXPERIMENTAL RESULTS

To investigate the mechanism of light production, a series of mixes of varying magnesium content was made and loaded into standard 81mm candles. These formulations were tested for burning rate and candlepower and the results evaluated to elucidate some of the kinetic factors. See Table I.

A series of computer calculations were made at Thiokol Chemical Corporation, Elkton Division to determine the thermodynamic properties of these formulae. The results of these calculations are shown in Table II.

In establishing the background for using computer calculations for evaluating illuminant formulations, consideration was given to the possible role the ambient air might have on performance. A preliminary computer calculation showed that very significant quantities of high temperature gas were being generated at the illuminant surface. These gases will expand away from the surface until a pressure of one atmosphere is reached. Since the average 81mm candle generates 40

to 60 liters of gas per second, a rather high exhaust velocity would be predicted. Velocities calculated from rate of gas generation indicate approximately 1500 cm/sec for an average value. The tendency to entrain air from below would be limited to the surface of the plume. The diffusion of air into the plume is calculated to be less than 1 cm/sec. Therefore, the diffusion of air into the high velocity gaseous plume would not be significant in the central core at the mouth of the candle. Data (1,2) show that the most intense light is emitted at the mouth of the candle by the central core. Photographs of flares and direct visual observation also confirm that the light is most intense right at the mouth of the candle.

Further indication that the air would not diffuse into the center of the plume may be had by consideration of pool flames (3). It was found that varying the size of a pan containing a fuel produces a change in combustion mechanism. With small pans, sufficient air would diffuse so that combustion occurs close to the surface of the fuel. With larger pools, the rising column of hot gas prevents air from reaching the fuel until it rises so far above the fuel surface that the temperature gradient becomes negligible at the gas-fuel surface. The energy for evaporation must then be furnished by radiation, and the usual sooty flames are good radiators. This system is seen to be analogous to an illuminant surface exhausting large quantities of gas. The gases would rise undiluted by diffusion until turbulence and cooling permitted mixing with the air. As convective mixing occurred, further oxidation of sodium and magnesium would occur; however, this would be well outside the region of maximum light production.

Finally, work has been reported citing a test where nitrogen gas was allowed to flow around an illuminant and compared with still air performance (1). In this test, candlepower increased as percent magnesium increased and the reduction in candlepower (compared with air tests) showed only a 5% decrease. The fact that candlepower increased with increasing magnesium in the absence of atmospheric oxygen indicates that the mechanism for light production may be taken as independent of atmospheric oxygen.

Work being done in other laboratories (2,26) to evaluate the effect of the candle falling through air does not affect the conclusions developed for this report. It is suggested that the effect of flowing air would increase the oxidation of magnesium around the plume and provide a thermal sheath which would reduce the radiant energy loss from the plume. This, however, is outside the scope of this paper.

For these reasons, it was determined that atmospheric oxygen should be disregarded in evaluating the species and mechanisms in this study.

To study illuminant spectral output, a series of illuminant samples was tested at Thiokol Chemical Corporation, Wasatch Division. A typical spectrum is shown in Figure 1. The major features are identified on the spectrum.

## DISCUSSION

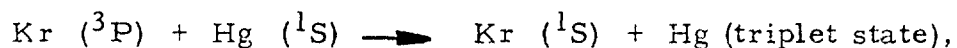
The spectroscopic data (Figure 1) shows that most of the visible light results from the sodium D-line emission, superimposed on a strong continuum. This is in good agreement with other observers (1, 2, 4, 5). From the data in Table I, it is seen that candlepower increases rapidly with increasing magnesium content, even when the flame temperature is decreasing. The calculations in Table II show that most of the major species present in the illuminant plume do not vary appreciably in concentration over a large range of magnesium contents. These data show that equilibrium thermal excitation of the sodium atoms cannot explain the increased candlepower since the candlepower increases even though the temperature decreases. The most notable change indicated from an analysis of the computer calculations is the increase in the Mg(g) content of the plume. It is seen spectroscopically that only a small fraction of the visible light results from Mg(g) radiation in the visible region. Therefore, an energy transfer involving Mg(g) and Na(g) is postulated.

Two significant complexities appear in atomic emissions at pressures of one atmosphere. The first is imprisonment of resonance radiation which increases the apparent lifetime of the resonance line. The other involves the interaction of excited and unexcited atoms which can result in a continuous rather than a line emission spectrum. The continuous emission is often characteristic of Franck-Condon transitions in molecules. (8, 23)

Hamrick et al (2) and Douda et al (4, 5) have shown that the line widths of the sodium D-lines are broadened considerably more than can be accounted for by Doppler broadening, the Stark effect, resonance broadening or collision broadening. Resonance broadening occurs due to collision (exchange of energy) between an excited atom and a ground state atom of the same species (10). Unsymmetrical broadening, usually towards longer wavelengths of

fluorescence lines, occurs when excited atoms collide with normal atoms of a different species and then in the collision state a transition takes place to a lower unstable state. This transition will also be observed as a continuous emission spectrum.

Two effects must now be considered to describe the enhancement of visible radiation. The first effect will relate to increased excitation of sodium atoms to produce more D-line radiation. Figures 2 and 3 show the Grotrian energy level diagrams for sodium and magnesium (11). General selection rules state that transitions may occur with radiation from adjacent terms to lower levels, that is, a P term can go to an S term or D term at a lower level by radiation of energy. An S term can only go to a lower level P term and a D term cannot go to a lower S term except through an intermediate P term. The difference between two levels is the excitation energy required to raise the atom from the lower state to the upper state. It also corresponds to the wavelength of light that will be emitted as the atom returns to the lower state. Other selection rules relate to the principle and inner quantum numbers and need not be discussed here. (See Reference (8) and (12) for more detailed discussions of selection rules.) Two general laws are important in examining the energy level diagrams for possible interactions between atomic species. The first one states that for a collision of the second kind (where an atom or molecule gives up excitation energy), the yield is greater, the less the energy which needs to be thereby converted to translational energy (24,25). The second general law is that, for a collision, the total spin of the two collision partners must remain unaltered before and after the collision. For example, in the following collision,



the Hg must be in a triplet state to conserve spin (12). It may be noted that this law is not as rigid as the first and frequent exceptions may be found in the literature. The phenomenon of energy transfer through collision is usually called "sensitized fluorescence".

There is a collision reaction between magnesium and sodium atoms that has a very close match in energy levels. This reaction is represented by the following:



There are three magnesium states for 3d ( ${}^3\text{D}$ ). The energy differences between the magnesium transitions and the energy required to raise the sodium to an excited state are 367, 347, and 306  $\text{cm}^{-1}$  respectively.

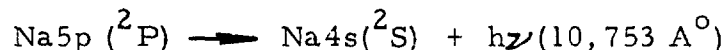


Energy differences of this magnitude may be accommodated by changes in the translational energy of the atoms. Sensitized fluorescence of sodium by mercury and other metallic vapors is widely reported in the literature. From the  $4s (^2S)$  state, the sodium will go to the  $3p (^2P)$  state and thence to the ground state by emission of the D-lines.

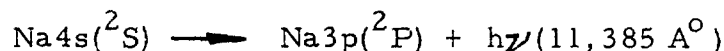
Another collision reaction that has an even closer match is represented by the following:



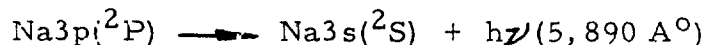
The  $\text{Na } 5p (^2P)$  is a doublet and the energy differences are 11.0 and 13.5  $\text{cm}^{-1}$  respectively. The  $\text{Na } 5p (^2P)$  can return to the ground state by radiating a 2852  $\text{\AA}$  line or it may cascade to the ground state by incremental radiation such as



then

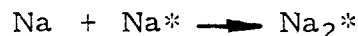


and

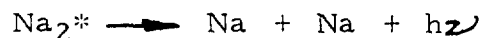


The cascade may thus produce sodium D-line radiation.

The second effect for enhancement of visible radiation is increases in the continuum by transfer of energy from one region of the spectrum to another. Continua can result from a transition from a stable electronic state of a molecule to an unstable state in which the molecules dissociate spontaneously. The formation of stable excited molecules between excited metal atoms and normal atoms give rise to continua in going to the ground state if the excited molecules decompose again with emission of spectra. An example of this type would be

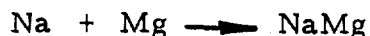


and then

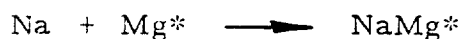


Enhancement of the continuum in these illuminants is proposed to be resultant from the formation of a temporary molecule between sodium

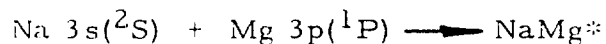
and magnesium,



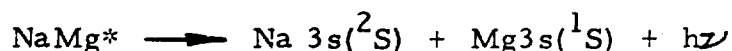
The existence of this molecule was reported by S. Barratt (20, 21, 22). The molecule was first observed in absorption as a band, degraded towards the blue with the wavelength of the band-head at  $5290.8 \text{ \AA}$ . This corresponds with Liveing and Dewar's description of a "dark line with ill-defined edges, with a wavelength about  $5300 \text{ \AA}$ " which they observed in parallel experiments in 1878. The assignment of this band spectrum to molecules of a volatile compound of magnesium and sodium is based on their persistent appearance with mixtures of these metals, and the failure of attempts to produce them in vapors not containing both constituents. The band did not appear in a series of experiments in which calcium vapor replaced the magnesium. The band appeared with undiminished intensity whether hydrogen or argon was used as a fill gas. Further experiments with intermetallic compounds revealed that these compounds form about as readily as the diatomic molecules of a single vapor. Thus, NaK forms about as readily as  $\text{Na}_2$  or  $\text{K}_2$ . Wood and Ditchburn observed the emission of the D-lines in the fluorescence accompanying absorption of light at the band frequency. This is indicative of dissociation. Assuming that the molecule of sodium magnesium breaks up on absorbing light at  $5291 \text{ \AA}$  into a normal magnesium atom and an excited sodium atom, the heat of formation is approximately 5,500 cal. Two major benefits are realized by the formation of this molecule. Consider first that if either atom is excited, then



Now, if the dissociation follows soon enough after the collision, i. e., in a period shorter than that required for one rotation, the spectrum will not possess definite lines or bands since the kinetic energies of the two atoms as they fly apart are not quantized and may assume arbitrary values (7, 8). The appearance of the spectrum is not always a definite clue as to whether or not dissociation occurs, although one may state that a definitely continuous spectrum necessarily means dissociation. The effect of this formation of an excited molecule with subsequent dissociation to emit a continuum, would be to transfer energy from the ultraviolet to the visible region of the spectrum. For example, from the energy level diagram for magnesium, it is expected that the  $2852 \text{ \AA}$  resonance line would be observed. Consider



then



where  $h\nu$  is a continuum with radiation in the visible region.

The second major benefit would be to broaden the radiation of the sodium D-line. If an excited sodium atom were to associate with a magnesium atom and then radiate the D-line energy, the effect would be a broadening of the D-line radiation. Since the D-lines show strong self-absorption or reversal, this effect would shift some of the D-line radiation to a region outside the self-absorption frequency so that the plume would then be less opaque. The increase in candlepower can then be explained in terms of increased efficiency of radiation in the visible region.

The efficacy of these transfer mechanisms would be expected to increase as the percent magnesium increases. The primary reason would be simply the increasing concentration of magnesium gas to react with the sodium. A second consideration would be the increased probability of molecular association at the lower temperatures. For example, compare the mole fractions of sodium vapor equilibrium composition in the table below (9):

Temp, °K	<u>Mole Fraction</u>		
	<u>Na<sup>+</sup></u>	<u>Na<sub>2</sub></u>	<u>Na</u>
3000	$1.3 \times 10^{-4}$	0.0253	0.97445
2000	$7 \times 10^{-7}$	0.0703	0.92974

The concentration of diatomic sodium tripled at the lower temperature. Similarly, the appearance of greater amounts of NaMg would be expected. Then, dissociation by photon absorption or through spontaneous transition to a repulsive state would enhance the background continuum producing more visible light.

Several other mechanisms can be advanced for enhanced sodium radiation. Continuous radiation from metals can result from electronic transitions in which one of the states, either the initial or final energy level of the system, is unquantized and possesses free kinetic energy (b). The emission may also arise from recombination of positive ions and free electrons, for example



Dean (6) reports that the sodium doublet at 5890 Å<sup>0</sup> is easily excited in all types of flames. However, the emissivity is affected markedly by the type of fuel and by the ratio of fuel to air or oxygen. The addition of extremely small amounts of alkaline earths to flame - gas systems containing alkali metals causes a marked increase in the concentration of free electrons in the flame gases. This increase is to values much greater than would be expected from the separate ionizations. This effect is very specific to a given pair of metals and indicates a specific interaction between them in the gas phase to form compound positive ions such as BaONa<sup>+</sup>. One can readily postulate that illuminant flames may likely give rise to MgONa<sup>+</sup>, also. The following could then result in light emission:



It seems likely that this mechanism would be favored in low magnesium compositions where the sodium to magnesium oxide ratio is high and the temperature is high.

Much experimental work has been done in trying to produce an efficient flare composition with aluminum or aluminum alloys. The reasoning being that any metal producing an energetic reaction in combustion with sodium nitrate should produce vigorous sodium emission and, indeed, the more energetic the reaction, the more sodium emission should be produced. Since aluminum is calculated to have a higher energy of reaction than magnesium, it has attracted considerable interest. However, in all instances known to this author, these attempts have resulted in poor illuminant performance, viz low candle-power, low burning rates, and low efficiencies. Table III shows the computer calculations for aluminum - sodium nitrate formulations. The values in Table IV were obtained by assuming burning rates previously reported (13). These calculations indicate that there would be very little aluminum gas present in the plume at the most efficient formulations. Kott and Lane (13) made a very complete and comprehensive study of aluminum as a flare fuel. Their results showed a peak efficiency of about 35,000 to 40,000 candle-sec/gm for aluminum fueled flares. This corresponds to a low magnesium fueled flare near the stoichiometric point (where little if any magnesium gas would be present). Their results further show that increasing the percent aluminum beyond stoichiometry causes a decrease in efficiency. Compare the flame temperatures for aluminum containing compositions in Figure 4. This would seem to indicate that the sodium radiation in aluminum containing flares is due only to thermal excitation of the sodium. Since the stoichiometric point produces the highest temperatures, this would then correspond to the maximum efficiency. They show that increasing the binder level requires a drop in percent aluminum to maintain peak efficiency and efficiency decreases as the flame temperature decreases. All of this evidence points to the fact that there is no

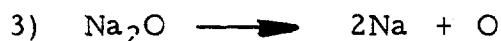
efficient energy transfer mechanism in aluminum fueled flares. The electronic structure of aluminum is shown in Figure 5. The closest energy match that could serve as a collision transfer would be  $4s (^2S)$  which is at  $25,347.69 \text{ cm}^{-1}$ . This energy level for aluminum is, however,  $391.17 \text{ cm}^{-1}$  less than that required to raise sodium from the  $3s (^2S)$  state to the  $4s (^2S)$  state. The additional energy can be supplied by thermal means; however, the probability of collision between a sodium atom and an excited atom with an energy difference requiring minimal conversion to translational energy is very low. This low probability coupled with very low concentrations of aluminum gas offers an explanation for the poor performance of aluminum rather than considering it a combustion efficiency problem.

In considering the burning rate variations of the compositions (Table I), it appears anomalous to note that the burning rate increases as the flame temperature decreases. The increase in thermal conductivity does not appear to be sufficient to offset the decrease in thermal energy radiated from the flame. The thermal conductivity increases by a factor of 2 from 35 to 60% magnesium. Thermal radiation is proportional to  $T^4$ ; therefore, from  $3000^\circ\text{K}$  to  $2000^\circ\text{K}$  the thermal radiation would decrease by a factor of 5 between 50% and 60% magnesium. If the rate were dependent solely on the thermal output from the flame, it would be expected that the rate would be lower at the higher levels of magnesium. Since the rate actually increases, it is apparent that some other factors must be contributing to the burning rate controlling reaction. Gutman (16) hypothesizes that photochemical reactions are an essential factor in propellant burning. Ullman and Meade (27) also hypothesize that ultraviolet radiation from propellant combustion increases the efficiency of aluminum containing propellants. Visible and infrared photons from equilibrium reactions at the flame temperature will supply a nominal amount of thermal energy to the surface of the illuminant. Photons from spectrally energetic atoms emitting at persistent wavelengths can provide more than enough energy to cause photochemical reactions. The reduction of sodium nitrate to sodium nitrite with liberation of atomic oxygen (17) or the rupture of polymer bonds by photolysis are examples of this type of reaction. Investigators (18, 19) have shown that with a ternary mixture of magnesium/sodium nitrate/Laminac\*, the combustion apparently begins through an intermediate reaction between sodium nitrate and some pyrolysis products from the polymer. This reaction provides sufficient thermal energy to initiate the reaction between the magnesium and sodium nitrate. Ignition of the system occurs when the sodium

---

\*Laminac is the trade name for a polyester resin manufactured by American Cyanamid Company.

nitrate has decomposed only as far as the nitrite. The following mechanism is proposed for the reaction of magnesium and sodium nitrate:



The exothermic reactions 1) and 4) produce large quantities of energy which overcome the endothermic reactions 2) and 3) and stimulate the species present to radiate energy. It is spectroscopically shown that ultraviolet light is produced by the combustion of the composition. A rate controlling energy feedback may then occur as:



It is calculated from thermodynamics that this reaction requires an energy of approximately 85 kcal/mole. This corresponds to ultraviolet light of wavelength 3360 Å°. Assuming that some of the activation energy can be supplied by exothermic reactions and radiative feedback, once the surface sodium nitrate melts, only about 78 kcal/mole is required. This corresponds to ultraviolet light of wavelength 3700 Å°. This value coincides with a strong spectroscopic peak associated with MgO - MgOH.

Krishman and Guha attribute absorption of light at 2060 Å° to the decomposition of sodium nitrate to form sodium nitrite and an excited oxygen atom. Ellis and Wells (17) report that NaNO<sub>2</sub> absorbs very strongly at 3660 Å°. Both of these reactions may contribute to the surface energetics.

The reaction of atomic oxygen produced by photochemical dissociation with magnesium atoms right at the surface may produce sufficient energy to overcome the decrease in thermal radiation from the flame. The increase in thermal conductivity and increased reaction sites produced by higher concentrations of magnesium then accounts for the increased burning rate.

## CONCLUSIONS AND RECOMMENDATIONS

From the considerations outlined, it is felt that the following conclusions can be reached:

- 1) The efficacy of magnesium/sodium nitrate illuminant compositions is due to an energy exchange between sodium and magnesium gases in the plume, especially through association to form NaMg.
- 2) Burning rates of magnesium/sodium nitrate illuminant compositions are probably influenced by photolytic decompositions of the binder and oxidizer.
- 3) Aluminum is not an efficient illuminant fuel because there is no efficient energy exchange with sodium and, as a result, only thermal excitation of the sodium is possible.

Application of these conclusions should direct studies to finding additives which would be efficient in transferring energy to the sodium present in the plume. One approach would be additives which produce radiation at an overlapping frequency to stimulate the sodium atoms directly. Another approach would be to find an additive that would stimulate the formation of excited magnesium atoms which will then transfer the energy to the sodium atoms.

If the burning rate is controlled to a large extent by the feedback of ultraviolet radiation to the surface, then burning rate modifiers may be found which will improve the tailoring of illuminants to meet burn time - candlepower requirements. The effect of ultraviolet radiation on the pyrolysis of polymers should be evaluated in the development of new formulations.

TABLE I

Burn Rate Candlepower Results

$\frac{\% \text{ MP 60}}{5\% \text{ Buader}}$	$\text{CP} \times 10^{-3}$	$r_b \text{ (in/sec)}$	$r_b \text{ (gm/sec)}$	$\frac{\text{CP sec}}{L_o \text{ gm}}$
35	410	0.060	8.4	48,600
40	480	0.065	9.1	52,600
45	575	0.070	9.8	58,800
50	740	0.075	10.5	70,700
55	940	0.083	11.8	79,900
60	1,265	0.094	13.4	94,800



Table II

Computer Calculations on Magnesium-Sodium Nitrate Composition

% Mg @ 5% Binder	Moles/Sec			Na(g)	N <sub>2</sub> (g)	CO(g)	T <sub>c</sub> , °K	WT	
	Mg(g)	MgO (s)						Fraction	MW
								Gas	Gas
35	.00931	.0960		.0521	.0281	.0161	3037	.529	27.14
40	.0238	.1066		.0547	.0287	.0250	3069	.526	26.51
45	.0484	.1176		.0563	.0290	.0270	3040	.524	25.59
50	.0819	.1262		.0552	.0282	.0314	2931	.522	24.39
55	.132	.1382		.0564	.0283	.0371	2605	.536	23.48
60	.193	.1413		.0557	.0280	.0350	1954	.574	23.42

Table III

Computer Calculations on Aluminum-Sodium Nitrate Compositions

% Al @ 5% Binder	Moles/100 gin							T <sub>c</sub> , °K	Wt Fraction Gas	MW Gas
	Al(g)	Al(l)	Al <sub>2</sub> O(g)	Al <sub>2</sub> O <sub>3</sub> (l)	AlC(g)	Na(g)	N <sub>2</sub> (g)			
30	.0041	---	.0005	.55100	.0047	.7336	.3697	3420	.438	23.35
35	.0876	---	.0283	.5640	.0245	.6963	.3482	3564	.425	23.23
40	.2069	---	.1122	.5192	.0108	.6437	.3231	3325	.471	25.58
45	.2387	---	.3080	.4030	.0001	.5860	.2942	2630	.589	30.92
50	.1665	.3734	.3098	.2458	---	.5270	.2647	2337	.549	31.57
55	.1271	.8179	.2357	.1293	---	.4684	.2353	2315	.463	30.19
60	.0818	1.2901	.1418	.2823	---	.4096	.2059	2274	.364	27.87

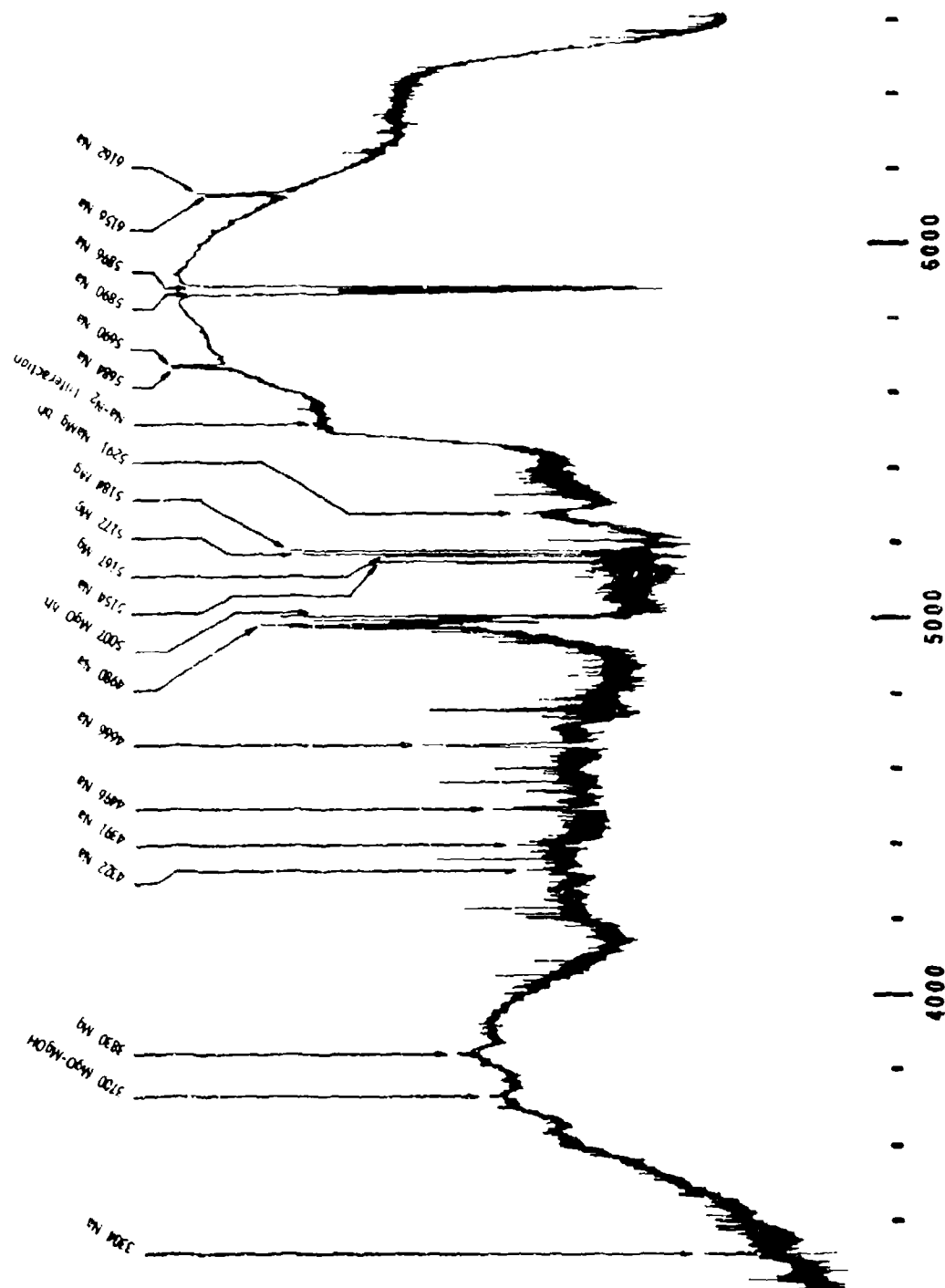
Table IV  
Calculations of Plume Species in 8mm Candle  
Aluminum-Sodium Nitrate

Moles/Sec

% Al @ 5% Binder	Al(g)	Al(l)	Al <sub>2</sub> C(g)	Al <sub>2</sub> O <sub>3</sub> (l)	AlC(g)	Na(g)	N <sub>2</sub> (g)	CC(g)	r <sub>b</sub> (in/sec)	r <sub>b</sub> (gm/sec)
35	.0043	---	.0014	.0274	.0119	.0338	.0169	.0146	.035	4.9
40	.0129	---	.0070	.0325	.0007	.0402	.0202		.045	6.3
45	.0167	---	.0216	.0282	.0001	.0419	.0206	.0216	.050	7.0
50	.0105	.0235	.0195	.0155	---	.0332	.0167	.0194	.045	6.3

Figure 1

SPECTRAL OUTPUT 3200 Å - 6600 Å



10

DIAGRAM FOR Na I



Figure 4

FLAME TEMPERATURE  
VS  
PERCENT METAL FUEL

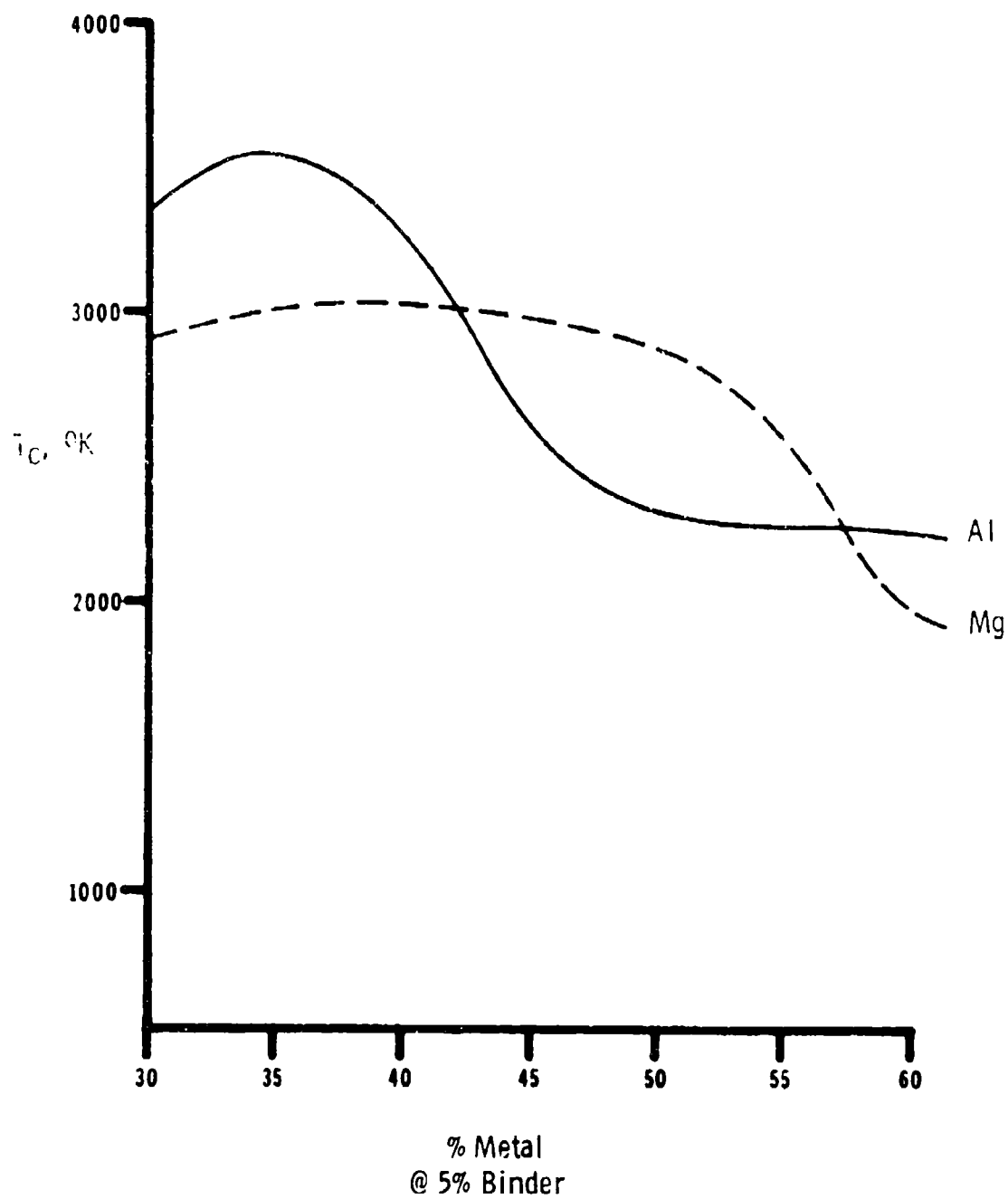
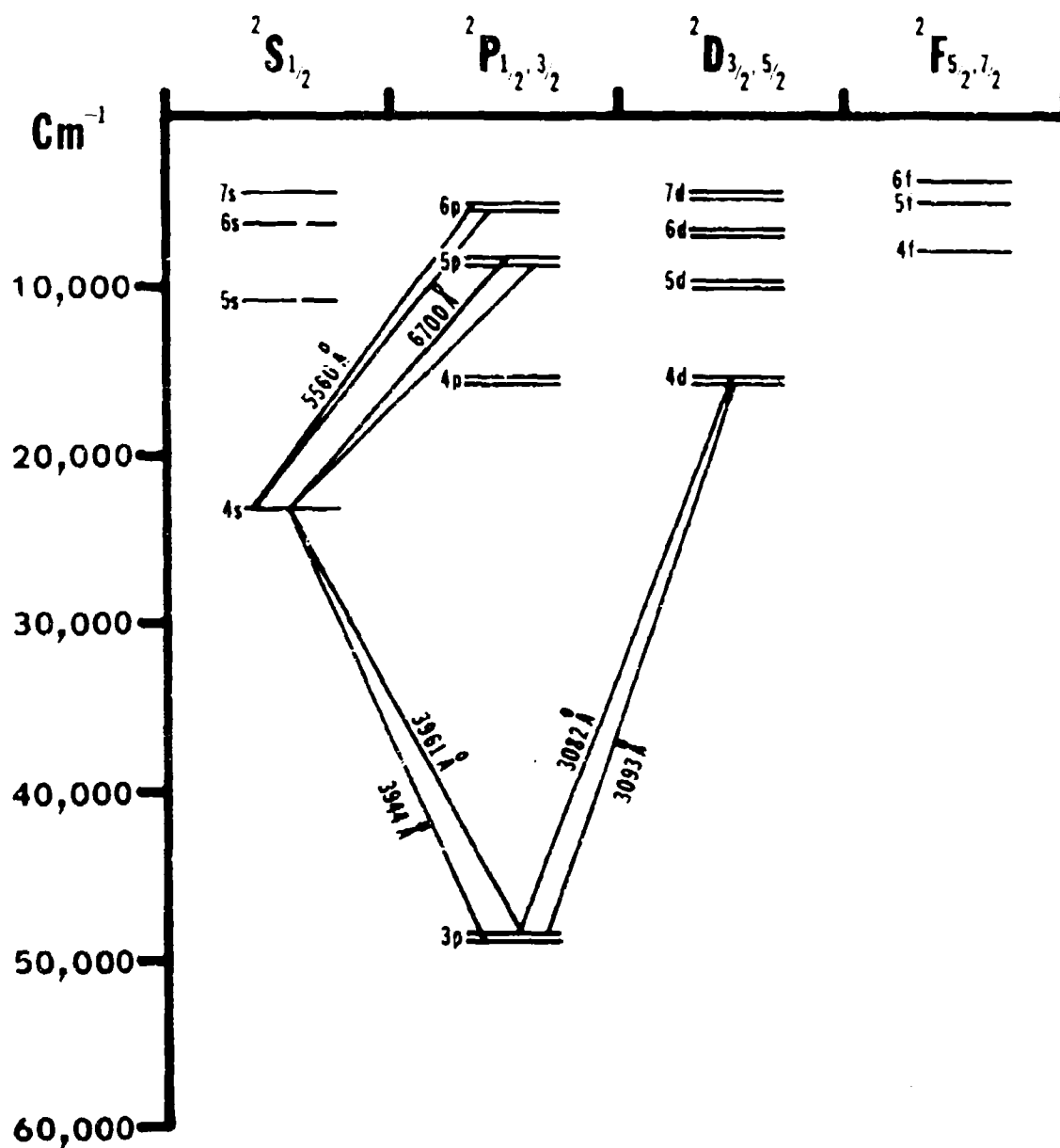


Figure 5

GROTRIAN ENERGY LEVEL

DIAGRAM FOR Al I



## REFERENCES

- 1) Hamrick, J. T.; Stanitz, J. D.; Blackshear, Jr., P. L. et al: "Exploratory Development of Illuminating Flares". Technical Report AFATL-TR-68-91, Elgin AFB, Florida, 1968
- 2) Hamrick, J. T.; Stanitz, J. D.; Blackshear, Jr., P. L. et al: "Exploratory Development of Illuminating Flares, Phase II". Technical Report AFATL-TR-69-107, Elgin AFB, Florida, 1969
- 3) Fristrom, R. M.; Westenburg, A. A.: Flame Structure. McGraw-Hill, New York, 1965
- 4) Douda, B. E.; Blunt, R. M.; Bair, E. J.: Journal of the Optical Society of America. Volume 60, Number 8, 1116 (1970)
- 5) Douda, B. E.; Bair, E. J.: Journal of the Optical Society of America. Volume 60, Number 9, 1257 (1970)
- 6) Dean, John A.: Flame Photometry. McGraw-Hill. New York, 1960
- 7) Technique of Organic Chemistry, Volume II. "Catalytic, Photochemical, and Electrolytic Reactions". A. Weissberger, Editor, Interscience Publishers, Inc., New York, 1956
- 8) Handbook of Physics. Condon, E. U. and Odishaw, H., Editors, McGraw-Hill, New York, 1967
- 9) Pomerantz, J.; Piacesi, R.: "The Equilibrium Composition and Thermodynamic Properties of Sodium Vapor from 400° to 10,000°K". NOLTR 62-170. 1965 AD-420172
- 10) Hindmarsh, W. R. Atomic Spectra. Pergamon Press. New York, 1967
- 11) Atomic Energy Levels. NBS Circular 467, Volumes I, II, III. 1949
- 12) Herzberg, G. Atomic Spectra and Atomic Structure. Dover Publications. New York. 1944



- 13) Kott, A. C. ; Lane, G. A. ; Proceedings of the Second International Pyrotechnics Seminar. "Aluminum-Fueled Flares". Denver Research Institute, 1970
- 14) Bryustowski, T. A. ; Glassman, I. "Spectroscopic Investigation of Metal Combustion". Volume I, Page 203, Bulletin of the 17th Meeting, JANAF, APPA, NASA Solid Propellant Group. May, 1961
- 15) Cassel, H. M. ; Liebman, I. "Combustion of Magnesium Particles". Combustion and Flame, Volume VI, Butterworths, London, 1962
- 16) Gutman, V. R. "Solid Propellant Burning Rate Theory". Aircraft Engineering. Volume 32, 1960
- 17) Ellis, C. ; Wells, A. A. : The Chemical Action of Ultra-violet Rays. Reinhold Publishing Corporation, New York, 1941
- 18) Bond, B. D. ; Jacobs, P. W. M. "Chemical Reaction and Ignition in Mixtures of Magnesium and Sodium Nitrate". Combustion and Flame. Volume X. Butterworths, London. 1966
- 19) Hogan, V. D. ; Gordon, S. : "Pre-ignition and Ignition Reactions of the Propagatively Reacting System Magnesium - Sodium Nitrate - Laminac". Combustion and Flame. Volume III, Butterworths, London. 1959
- 20) Barratt, S. : Proceedings of the Royal Society of London. Volume 105, Page 221 (1924)
- 21) Barratt, S. : Proceedings of the Royal Society of London. Volume 109, Page 194 (1925)
- 22) Walter, J. M. ; Barratt, S. : Proceedings of the Royal Society of London. Volume 119, Page 257 (1928)
- 23) Christophorou, L. G. : Atomic and Molecular Radiation Physics. John Wiley and Sons, Ltd., New York, 1971
- 24) Hasted, J. B. : Physics of Atomic Collisions. Butterworths, London, 1964
- 25) Ruark, A. E. ; Urey, H. C. : Atoms, Molecules and Quanta McGraw-Hill, New York, 1930

- 26) Hamrick, J. T. : Proceedings of the Second International Pyrotechnics Seminar. "Exploratory Development of Illuminating Flares". Denver Research Institute, 1970
- 27) Ullman, L. L. ; Meade, E. F. : "A Theory of the Behavior of Aluminum Metal in Solid Propellants". Thiokol Chemical Corporation, Huntsville Division, Report Number TM-96, Control Number U-C-59-1219, 1959

#### BIBLIOGRAPHY

- 1) Friend, J. N. : The Chemistry of Combustion. Gurney and Jackson, London, 1922
- 2) Gardon, A. G. : Spectroscopy and Combustion Theory. Chapman and Hall, London, 1948
- 3) Markstein, G. H. : "Magnesium-Oxygen Dilute Diffusion Flame". Ninth Symposium on Combustion. Academic Press, New York, 1963
- 4) Kroger, F. A. : Some Aspects of the Luminescence of Solids. Elsevier Publishing Company, Inc., New York, 1948
- 5) Morton, R. A. : Radiation in Chemistry. D. Van Nostrand, New York, 1928
- 6) Tsuchiya, S. ; Kuratam, K. : "Excitation and Quenching of Sodium Atoms Behind a Shock Wave". Combustion and Flame. Volume VIII. Butterworths, London, 1964
- 7) Cummings, G. A. McD. : "Chemi-Ionization and Excitation in the Reaction Zones of Hydrocarbon Flames". Combustion and Flame. Volume X, Butterworths, London, 1966
- 8) Nichols, E. L. ; Howes, H. L. ; Wilber, D. T. : Cathodo-Luminescence and the Luminescence of Incandescent Solids. Carnegie Institution of Washington, Washington, D. C. , 1928
- 9) Sutherland, G. S. : "The Mechanism of Combustion of an Ammonium Perchlorate - Polyester Resin Composite Solid Propellant". Doctorate Thesis, Princeton University, 1956

- 10) Engineering Design Handbook. Military Pyrotechnics Series, Part One. "Theory and Applications". AMC Pamphlet, AMCP 706-185, 1967
- 11) The Encyclopedia of Spectroscopy. Clark, G. L., Editor, Reinhold Publishing Corporation, New York, 1960
- 12) Yarwood, J.: Atomic Physics. University Tutorial Press, Ltd, London, 1960
- 13) Finkelburg, W.: Atomic Physics. McGraw-Hill, New York, 1950
- 14) Csgood, T. H.; Ruark, A. E.; Hutchisson, E.: Atoms, Radiation and Nuclei. John Wiley and Sons, Inc., New York, 1955
- 15) Guilbault, G. G.: Fluorescence: Theory, Instrumentation, and Practice. Marcel Dekker, Inc., New York, 1967
- 16) Gilmore, F. R.; Bauer, E.; McGowan, J. W.: Journal of Quantitative Spectroscopy and Radiative Transfer. Volume 9, Number 2. "A Review of Atomic and Molecular Excitation Mechanisms in Non-Equilibrium Gases up to 20,000°K". Pergamon Press, 1968
- 17) Peck, G. P.: Journal of Quantitative Spectroscopy and Radiative Transfer. Volume 9, Number 2, 1419 (1968)
- 18) Noyes, W. A.; Leighton, P. A.: The Photochemistry of Gases. Reinhold Publishing Corporation, New York, 1941
- 19) Flame Emission and Atomic Absorption Spectrometry. Dean, J. A.; Rains, T. C., Editors. Volume 1, Theory, and Volume 2, Components and Techniques. Marcel Dekker, Inc., New York, 1971

# GAS GENERATORS FOR INFLATING AUTO CRASH BAGS

by

George A. Lane, T. R. Torkleson, T. E. Dergazarian, and  
G. R. Staudacher

The Dow Chemical Company, Midland, Michigan

## ABSTRACT

For inflating automobile safety cushions, gas generators are required which produce a very rapid evolution of cool, non-toxic gas. We have developed several such generators for inflating steering wheel bags of different sizes. All-Solid pyrotechnic compositions are employed. Compositions have been developed which give nearly pure nitrogen gas, or which give mainly carbon dioxide. Deployment time, cushion temperature, sound level, and gas non-toxicity are satisfactory. Numerous tests have been performed with these generators in static firings, sled tests, and automobile barrier crashes with anthropomorphic dummies. These tests indicate the potential for preventing thousands of deaths and injuries in auto accidents.

## I. INTRODUCTION

Automatic inflating occupant restraint systems, often called air bags, crash bags or air cushions, have the potential for preventing thousands of automobile fatalities and injuries each year. Several gas sources have been studied or proposed for filling these bags:

1. Bottled gas.
2. Bottled gas, augmented with solid pyrotechnic.
3. Solid pyrotechnic, augmented with vaporizable liquid.
4. All solid pyrotechnic.

The potential advantages of solid pyrotechnic gas generators are smaller size and lighter weight, less leakage problems, and greater design versatility. This paper describes the problems encountered and solved in the development of a series of all-solid gas generators.

The principal obstacles in adapting conventional gas generator technology to the inflation of auto air cushions can be summarized:

1. Time - The cushion must be inflated in 20-100 milliseconds, depending on the system. Propellant combustion must be essentially complete in 5-50 msec.
2. Temperature - The bag surface must not cause thermal burns. Product gas, if inhaled must not cause thermal damage. Cool burning propellants must be used, or hot product gases must be cooled in the generator.
3. Toxicity - Gases and smoke vented from the generator and cushion must be sufficiently safe that occupants are not injured. The concentration in the bag of flammable gases, such as hydrogen or methane, should be below the explosive limit. Highly toxic gases, such as HCN or NO<sub>2</sub>, should be held to less than a few hundred ppm. Less toxic gases, such as NH<sub>3</sub> or CO, should be held to less than about one percent. Nitrogen and CO<sub>2</sub> are desirable products, as is O<sub>2</sub> up to the concentration in air. Exhaust of N<sub>2</sub> and CO<sub>2</sub> from several large bags may lead to oxygen depletion or CO<sub>2</sub> toxicity effects.

#### A. GENERATOR DESIGN

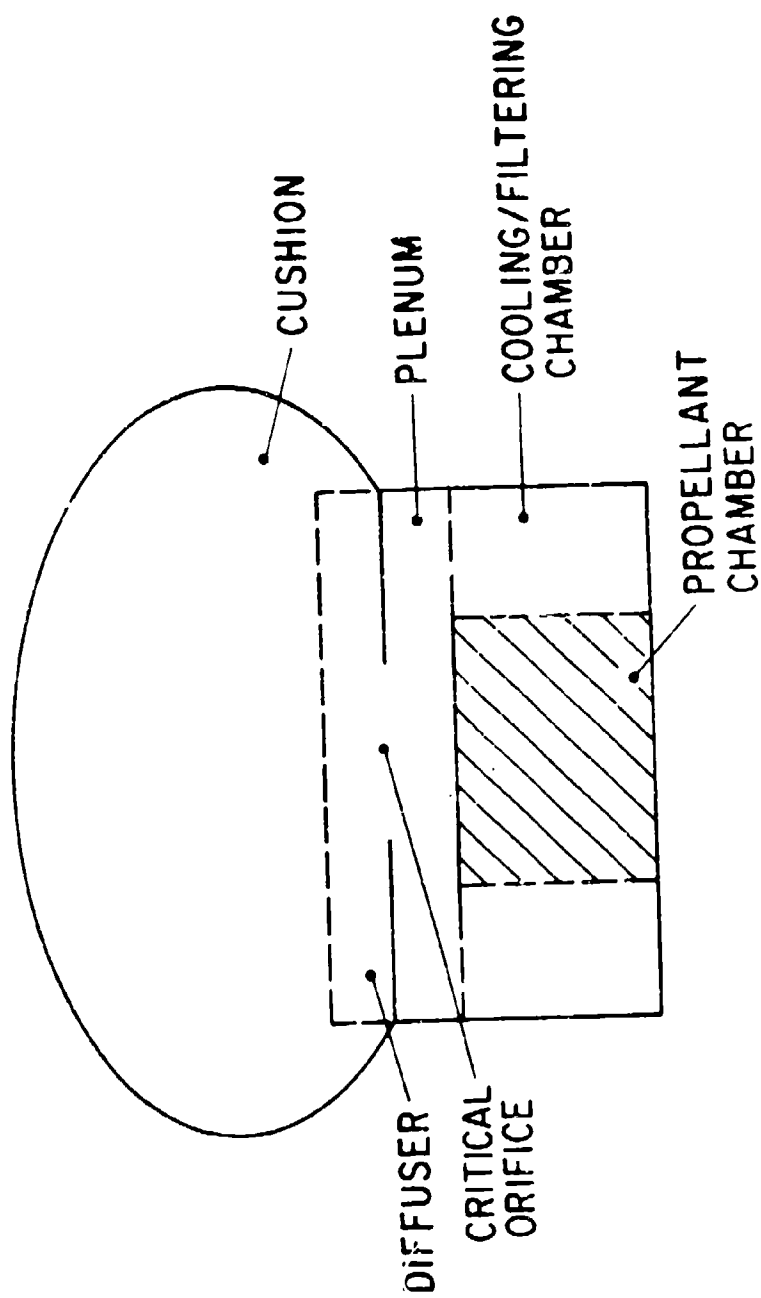
Figure 1 shows one particular generator design with a flat aspect, accomplished by situating the propellant chamber centrally and allowing the gases to flow radially outward into the cooling chamber. This might be particularly applicable to a steering wheel-generator package.

The propellant combustion takes place in a chamber, and product gases and smoke are expanded into a cooling or filtering chamber. This volume can be filled with a particulate chemical coolant. For propellants of sufficiently low flame temperature, no coolant is required, and particle traps or filters can be substituted.

From the cooling chamber the gas stream is throttled down and expanded into a plenum chamber. If needed, additional filters may be employed in this area. The exit from this chamber is the critical or controlling orifice for the generator. A frangible seal is usually employed in this orifice to seal the generator unit and contain the gas until operating pressure is reached.

The gas leaves the critical orifice and enters a diffuser, which serves to distribute the gas flow to the air cushion. In most of our work, we have employed a flat plate diffuser. Filters or screens may be used in the diffuser to trap particulates and retain metal parts, e.g., frangible fragments.

FIGURE 1  
LOW FORM GENERATOR CONFIGURATION



Several other generator designs have been tested successfully, based on these principals. In addition to the low form configuration described, a tall form generator with small diameter to length ratio, a toroidal generator (low form) for inflating a doughnut-shaped cushion, and a multi-modular generator with a plurality of sub-generators have been developed.

## B. INTERIOR BALLISTICS

Since air bag generators must produce a specified pressure in the cushion in a very short time, the rate at which gas products exhaust through the nozzle,  $\dot{m}_g$ , is critical. However, the requirements for safe, non-toxic product gases and cool or warm exhaust gas put severe restraints on the combustion temperature,  $T_c$ , the molecular weight of the gas,  $M$ , and the propellant composition. In addition, because of propellant design considerations, the mass of condensed phase produced during the burn can be anticipated to be relatively high.

Using a cushion volume of 3.5 ft.<sup>3</sup>, a cushion pressure of 2.0 psig, and an exhaust temperature computed from thermodynamic data, the weight of nitrogen needed to fill the bag was computed. Assuming that this amount of gas must enter the cushion in 25 msec., a value for  $\dot{m}_g$  of 2.5 pounds/sec. was calculated. Assuming a generator pressure ( $P_c$ ) of 2000 psi, a value for  $A_t$ , the nozzle throat area, of 0.76 in.<sup>2</sup> was derived from the relation

$$\dot{m}_g = P_c A_t C_d,$$

$C_d$  being the discharge coefficient.

The mass rate at which propellant is combusted,  $\dot{w}$ , is:

$$\dot{w} = S R_B \rho$$

where  $S$  is the burning surface area. For propellants which give both solid and gaseous products, the gas production rate, after the condensibles have been filtered out in the generator, is:

$$\dot{w}_g = (1-x) \dot{w}$$

where  $x$  is the mass fraction of condensibles. The situation is further complicated if a chemical coolant is used, since additional gas and condensed phase can be produced by its decomposition.

By using the measured density,  $\rho$ , the linear burning rate determined from strand burning experiments, a value of  $x$  derived from stoichiometric considerations, and setting

$\dot{w}_g = \dot{m}_g$ , the propellant surface area,  $S$ , was calculated to be 36.7 in.<sup>2</sup>.

Using sufficient propellant to provide the calculated amount of nitrogen gas, and with the computed burning surface area, a generator with a critical orifice area of 0.78 in.<sup>2</sup> was functioned. The bag filled to a pressure of 2.0 psig in 20 msec. The generator chamber reached a maximum pressure of 3300 psi. The result is in reasonable agreement with theory.

As illustrated later, isobaric combustion conditions are never obtained in this generator, except perhaps momentarily at the pressure peak. Experience has shown that reasonable agreement can be obtained between theoretical and experimental values, if an average pressure and the corresponding burning rate are used. By adjusting  $S$  and  $A_t$ , a value of  $P_c$  may be obtained consistent with material strength requirements, which will yield a large enough value of  $\dot{m}_g$  to fill the cushion within the necessary time.

### C. GENERATOR PERFORMANCE

Various versions of generator concepts similar to that of Figure 1 have been employed successfully in inflating neoprene-coated nylon fabric cushions ranging from 1 ft.<sup>3</sup> to 12 ft.<sup>3</sup> in volume. Considerable work has been done with the low form type of generator. Typical results are described below.

Figure 2 depicts the inflation sequence for a typical test using a 3.5 ft.<sup>3</sup> bag. Figure 3 shows the pressures measured. Generator pressure rises to a maximum within 10 msec. after squib actuation, and then drops as the vessel vents. Bag pressure shows a high initial spike as the tape holding the folded bag breaks and the bag begins to unfold. Bag pressure oscillates, sometimes even becoming negative as the inertia of the opening bag outpaces the filling process. After 30-40 msec. the cushion pressure stabilizes. Cooling of the gases eventually causes the bag to become flaccid.

Table I presents data obtained on cushion temperature, measured with a thermocouple. In most firings we press the hands, forearm, or face against the cushion immediately after functioning, to determine the sensible heat. In no case was the temperature painful to the skin. It was always possible to keep the hands in contact with the bag indefinitely. This is regarded as evidence of a safe cushion temperature.

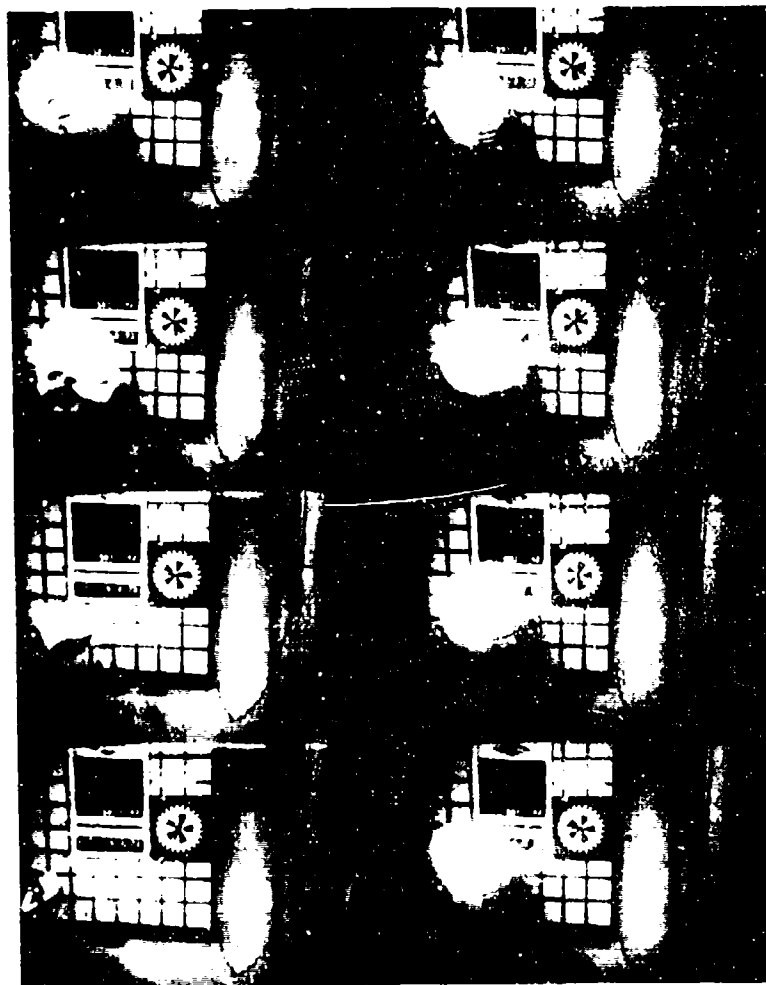


23 msec.

11 msec.

6 msec.

0 msec.



60 msec.

50 msec.

44 msec.

32 msec.

Figure 2 - Sequence Photographs of Cushion Inflation

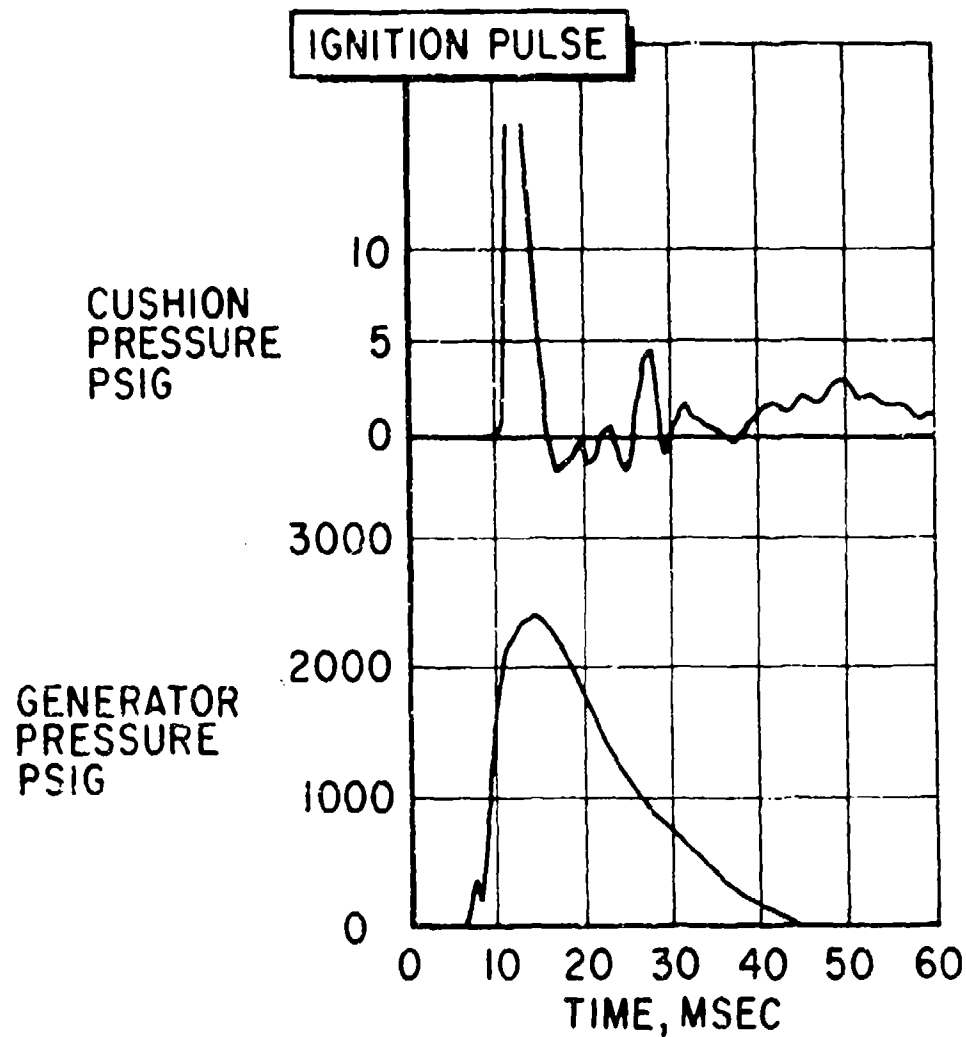


Figure 3 - Generator and Cushion Pressure During Functioning

TABLE I MEASURED BAG EXTERIOR TEMPERATURE

Test	1	2	3	4
Propellant Product	N <sub>2</sub>	N <sub>2</sub>	CO <sub>2</sub>	CO <sub>2</sub>
Bag Temperature, °C.	66	71	73	64
Bag Pressure, psig	2.1	1.8	3.7	4.6

#### D. PYROTECHNIC COMPOSITION

Ammonium perchlorate, ammonium nitrate, and potassium perchlorate are the most common oxidizers used in gas generators, giving as principal products water, carbon monoxide, hydrogen, and nitrogen (and hydrogen chloride in the case of ammonium perchlorate). For reasons of toxicity and flammability, in safety cushion generators carbon monoxide and hydrogen must be further oxidized to safe-products, carbon dioxide and water.

Because of the toxicity of hydrogen chloride, ammonium perchlorate cannot be used unless the chloride is reacted to a harmless compound in the generator. Experience has shown that formulations based on ammonium nitrate, if oxidized sufficiently to yield a minimum carbon monoxide level, produce undesirable quantities of nitrogen oxides. Potassium perchlorate is the most desirable of the three, but produces copious quantities of the non-toxic solid, potassium chloride. Several other oxidizers, such as  $\text{KClO}_3$ ,  $\text{LiNO}_3$ ,  $\text{KNO}_3$ ,  $\text{NaClO}_4$ , or  $\text{NaClO}_3$  might also be used.

For the crash bag application, two types of propellant were developed. The first gives mainly carbon dioxide, and the second yields only nitrogen. Composition of the  $\text{CO}_2$  propellant is shown in Table II. Because of the high exhaust temperature, powdered sodium bicarbonate was used as a coolant in the second chamber. This material decomposes endothermically to carbon dioxide, leaving a residue of sodium carbonate,  $2 \text{NaHCO}_3 \rightarrow \text{Na}_2\text{CO}_3 + \text{H}_2\text{O} + \text{CO}_2$ , absorbing 188.1 cal./g. of heat.

TABLE II PYROTECHNIC CARBON DIOXIDE GENERANT

Ingredient	Description	Wt. %
XFS-4008L	Epoxy Resin	6.26
Maleic Anhydride	Curing Agent	4.39
Ethylene Carbonate	Plasticizer	4.39
Oxamide	Fuel	12.64
$\text{KClO}_3$	Oxidizer	72.31
		100.00%
$\text{NaHCO}_3$	Coolant	100.00%

Theoretical exhaust products and other parameters of the pyrotechnic are given in Table III. Assuming removal of the condensibles (KCl, KOH, H<sub>2</sub>O), the theoretical exhaust composition would be 84.4% CO<sub>2</sub>, 13.60% N<sub>2</sub>, 1.62% O<sub>2</sub>, 0.35% HCl, 0.02% NO, and 0.01% CO.

TABLE III THEORETICAL EXHAUST COMPOSITION

Species	Chamber		Exhaust	
	Moles/100 g.	Mole, %	Moles/100 g.	Mole, %
H <sub>2</sub>	0.0049	0.21	0.0000	0.00
H	0.0004	0.02	0.0000	0.00
H <sub>2</sub> O	0.6325	26.95	0.6727	30.67
OH	0.0118	0.50	0.0002	0.01
CO	0.0411	1.75	0.0001	0.005
CO <sub>2</sub>	0.8504	36.23	0.8914	40.60
O	0.0006	0.03	0.0000	0.00
O <sub>2</sub>	0.0346	1.47	0.0171	0.78
N <sub>2</sub>	0.1412	6.02	0.1434	6.54
NO	0.0046	0.20	0.0002	0.01
Cl	0.0020	0.09	0.0000	0.00
HCl	0.0331	1.41	0.0039	0.17
K	0.0015	0.06	0.0000	0.00
KO	0.0002	0.01	0.0000	0.00
KOH	0.0334	1.42	0.0038	0.17
KCl	0.5549	23.65	0.4628	21.09
KCl (1)	0.0060	0.00	(0.1233)	--
Total Moles Gas	2.3472	--	2.1958	--

Table IV shows analytical data on gases generated from the crash bag pyrotechnics. The gas samples were obtained by functioning the generator into a safety cushion, piercing the bag with a hypodermic needle, and drawing off a gas sample into an evacuated flask. When Dräger gas analysis tubes were used, the gas was pumped directly from the bag through the analysis tube.

TABLE IV GAS PRODUCT COMPOSITION FROM GENERATOR

Gas	Composition of Gas Product	
	Carbon Dioxide Propellant <sup>(e)</sup>	Nitrogen Propellant <sup>(f)</sup>
Nitrogen	9.17 vol. % <sup>(a)</sup>	96.2 vol. % <sup>(a)</sup>
Nitric Oxide	0.74 vol. % <sup>(a)</sup>	1.5 ppm <sup>(b)</sup>
Nitrogen Dioxide	0(<5 ppm) <sup>(a)</sup>	0(<0.5 ppm) <sup>(b)</sup>
Hydrogen	0.7 vol. % <sup>(a)</sup>	0.35 vol. % <sup>(a)</sup>
Ammonia	0(<1 ppm) <sup>(d)</sup>	0(<5 ppm) <sup>(b)</sup>
Hydrogen Cyanide	0(<1 ppm) <sup>(d)</sup>	100 ppm <sup>(b)</sup>
Hydrocarbons	0.23 vol. % <sup>(c)</sup>	0.19 vol. % <sup>(a)</sup>
Oxygen	3.2 vol. % <sup>(a)</sup>	0.84 vol. % <sup>(a)</sup>
Carbon Monoxide	1.01 vol. % <sup>(a)</sup>	2900 ppm <sup>(b)</sup>
Carbon Dioxide	84.9 vol. % <sup>(a)</sup>	1000 ppm <sup>(b)</sup>
Chlorine	--	0(<0.2 ppm) <sup>(b)</sup>
Phosgene	0(<0.5 ppm) <sup>(c)</sup>	0(<0.05 ppm) <sup>(b)</sup>
<p>(a) Mass spectroscopy.</p> <p>(b) Dräger gas analysis tube.</p> <p>(c) Infrared spectroscopy.</p> <p>(d) Gas chromatography.</p> <p>(e) Lower levels of carbon monoxide and nitric oxide are attainable by composition modification. For the toxicity tests described later, these high levels were deemed more meaningful.</p> <p>(f) The comments of footnote (e) should be noted with regard to hydrogen cyanide and carbon monoxide.</p>		

The results are in good agreement with theory, except for the minor constituents. For the toxic species CO and NO, chemical equilibrium is not maintained upon expansion, leaving more of these gases than predicted. Water is also dissociated more than expected, and does not all recombine.

#### E. TOXICITY TESTING

The inflating gases will, by design or by accident, be vented from the bag into the passenger compartment of the automobile and will be inhaled by the occupants. Therefore, the generator effluent should not cause significant toxic effects and thereby present a hazard greater than the crash itself.

Preliminary experiments were carried out to evaluate a simple, inexpensive experimental procedure to determine the toxicity of potential propellant systems, and to see if specific fuel systems are injurious to animals.

A 144 ft.<sup>3</sup> stainless steel exposure chamber was used in these studies. The animal exposure cages were placed directly in front of the inflating devices so that the products of combustion could blow directly over the animals. The cages were situated either 8.5, 20, or 24 inches from the front of the devices. Figure 4 is a diagram of the experimental set up.

Either 5 or 10 adult male rats and 1 or 2 male dogs were used for each of the exposures. The dogs, beagle hounds obtained from the local dog warden, appeared to be normal and healthy, but heart worm disease is endemic in the area and at least two of the dogs were subsequently shown to have these parasites.

The generators used yielded sufficient gas to inflate safety cushions of 2.5 to 4.5 ft.<sup>3</sup> size. In some experiments no cushion was used on the generator; in others a cushion with numerous vents was employed. The first four experiments were done with the carbon dioxide generating propellant, and the last with the composition yielding nitrogen.

Samples of the chamber air were taken for analysis 15 seconds, 2, 10, 20, and 30 minutes after firing. The temperature and animal appearance were observed and recorded at intervals during the exposure. Thirty minutes after ignition, the last air sample was withdrawn and the chamber exhausted. The animals were observed and weighed periodically during a 14-day observation period.

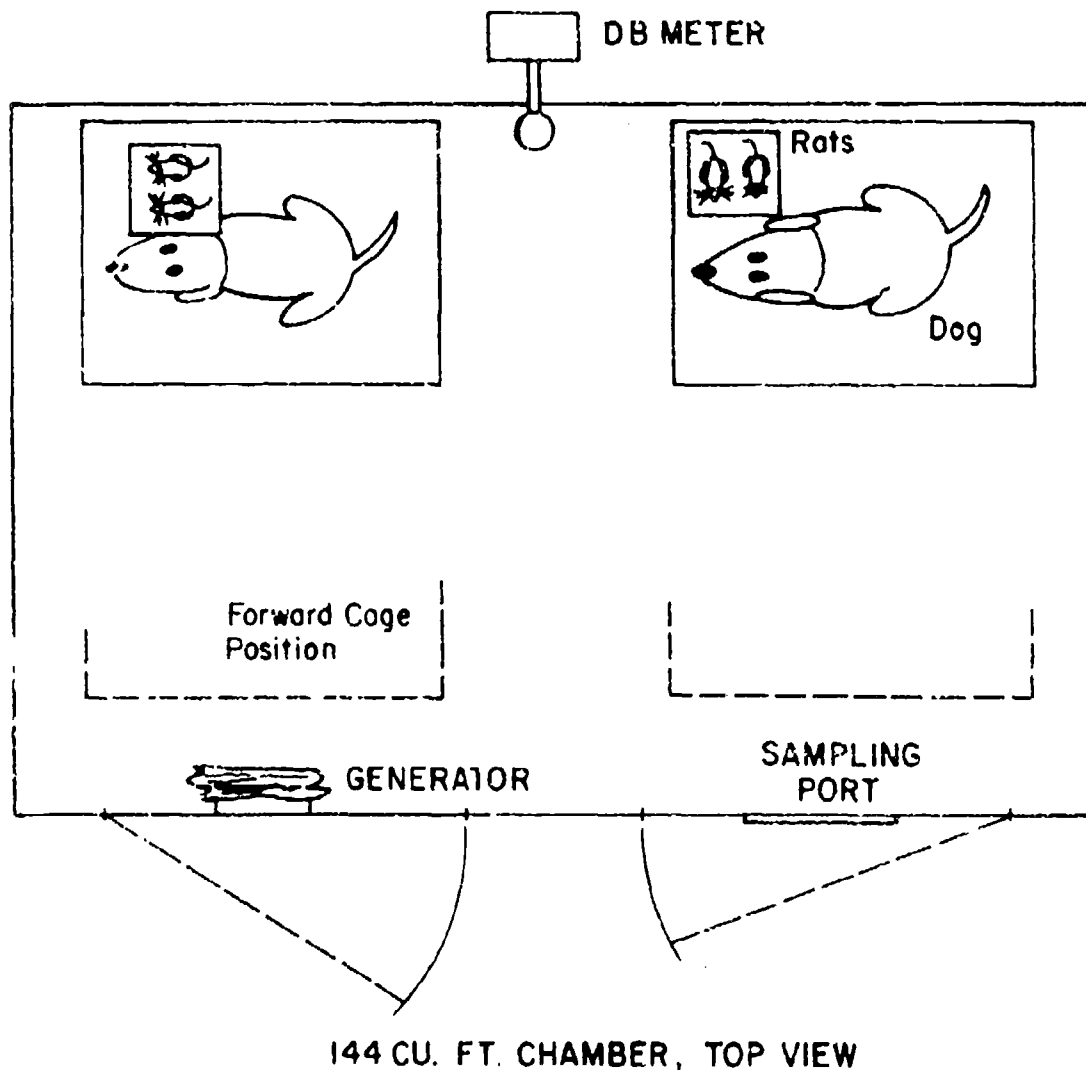


Figure 4 - Experimental Setup For Animal Toxicity Tests

The results are summarized in Table V. Analysis of the gases in the chamber showed approximately the correct ratios of  $N_2$ ,  $O_2$ , and Argon from the original air in the chamber. Firing the generators introduced measurable amounts of  $NO$ ,  $CO_2$ , and  $CO$ . About 40 ppm  $NO$  was measured in the case of the  $CO_2$  generator; however, analysis for  $NO$  may be unreliable, since this concentration is near the lower limits sensitivity of the analytical technique used. About 5 ppm  $NO_x$  was obtained from the  $N_2$  generator. Prior to firing the generator, the chamber contained about 1000 ppm

TABLE V SUMMARY OF EXPOSURES OF RATS AND DOGS TO THE COMBUSTION PRODUCTS OF  
PASSENGER RESTRAINT SYSTEM GENERATOR

Expt. No.	Variables			Observations			
	Crash Bag Attached	Number of Animals	Inches Between Device and Cage	Max. Temp., °C.	Sound Level Peak db	Response of Animals	
						During Exposure	Post Exposure
1	Yes	1	24	28.3	148	Normal	Normal
2	No	2	8.5	28.3	148	Rats somewhat quiet. Dust in chamber.	Normal
3	Yes	2	24	30.2	--	Considerable dust. Dogs were quiet.	No abnormal response. No gross pathological effects seen in rats at autopsy. Dogs normal and saved for reuse in other experiments.
4	No	2	24	32.8	--	Dust obscured observation.	No effects seen during observation period. No gross pathological effects at autopsy.
5	No	1	8.5	28.0	--	Dog somewhat dazed. Rats active.	No adverse effects. Gross necroscopy of rats revealed no abnormality.



CO<sub>2</sub>. Firing the CO<sub>2</sub> generator raised this to about 4000 ppm CO<sub>2</sub>. Respiration of the animals further increased this value to about 6000 ppm by the end of the experiment. With the N<sub>2</sub> generator, about 2000 ppm CO<sub>2</sub> was observed late in the experiment. Firing the generators also introduced 100-150 ppm CO for the CO<sub>2</sub> propellant and 50 ppm CO for the N<sub>2</sub> propellant into the chamber. About 1 ppm HCN was found in the case of the N<sub>2</sub> generator, and none from the CO<sub>2</sub> generator. No H<sub>2</sub>, CH<sub>4</sub>, N<sub>2</sub>O, NH<sub>3</sub>, HCl, Cl<sub>2</sub>, or phosgene could be detected in any case. Varying amounts of water were detected. In addition, smoke and dust were emitted from the generators in Runs 2, 3, 4, and 5. Nearly all the dust was retained in the vented crash bag in Run 1.

Expect for slight discomfort due to heat and dust there was no apparent adverse effect on rats and dogs exposed during the experiments. The most severe conditions occurred during Experiment 4. Since no bag was used on the generator, the dust was quite dense. The temperature reached 33°C. during this experiment. Despite these conditions, the animals appeared to be only slightly affected by the dust and increased temperature.

#### F. SUMMARY AND CONCLUSIONS

A gas generator design has been developed in several shapes and sizes. Ballistic relationships have been useful in designing and optimizing generator and propellant configurations.

Gas generating propellants have been developed which yield either nitrogen gas or mainly carbon dioxide. Gas generators containing these propellants inflate neoprene-coated nylon safety cushions of a size suitable for driver protection (1-3.5 ft.<sup>3</sup>) in about 30 msec. Cushions up to 12 ft.<sup>3</sup> size have been inflated with these compact generators. Sound impulse values are less than 150 db, a safe range. Bag temperatures are less than 75°C., safe for skin contact.

Preliminary toxicity tests with dogs and rats indicate that the combustion products from these generators, at the concentrations studied, do not produce observable untoward effects.

In addition to the tests described, other tests have been conducted in cooperation with automobile manufacturers and suppliers. Sled crash tests and automobile barrier crashes with anthropomorphic dummies have been successful at speeds of 30-50 mph. Instrumentation indicated compliance with federal survivability standards.

A COMPARISON OF GROUND AND ATOMIZED MAGNESIUM IN  
POUR-CAST ILLUMINANTS

by

George A. Lane and Keith Roberson  
The Dow Chemical Company, Midland, Michigan

ABSTRACT

Previous work showed that good pour-castable illuminant compositions can be obtained, using an oxygenated, energetic binder, sodium nitrate, and fine particle size atomized magnesium. A study now has been completed on the use of ground ellipsoidal magnesium powder in such compositions. Based on experience with cast illuminants, special ground magnesium particle size distributions were obtained. A nitrate ester-plasticized, anhydride-cured epoxy resin binder was used for these studies. Compositions were optimized for rheology, and good castability was obtained. Studies undertaken to optimize flare performance resulted in a castable composition with luminous efficiency of 44,700 cd. sec./g., and burning rate of 0.049 in./sec.

## I. INTRODUCTION

At the Second International Pyrotechnics Seminar, July 22, 1970, at Aspen, Colorado, we presented a paper on "Pour Castable Magnesium Illumination Flare Compositions." The work in that program was done mostly with atomized magnesium. It was believed that the more spherical shape of the atomized material would give greater mix fluidity, allowing castability at lower percentages of binder, and leading to higher efficiencies.

The promising results obtained at Dow on pour cast flares are mainly the result of three factors:

- Oxygen-rich binder
- Nitroplasticizer
- Tailored Mg particle distribution

The magnesium should have a broad particle size distribution, with a substantial fraction of material smaller than 100 mesh. The broad distribution facilitates castability, and the fine fraction improves combustion efficiency sufficiently to offset the losses caused by high binder levels. Fine particle magnesium generally is not used in pressed flares, as it promotes excessive combustion rates.

In equivalent particle sizes, ground magnesium yields higher combustion rates than atomized Mg. This phenomenon probably results from the particle structure. The ground magnesium resembles a long chip which has been rolled up into an ellipsoid, and the "web" for burning is less than for a solid sphere. If this speculation is correct, one might expect to attain good efficiency in a cast flare by using a broad distribution of ground magnesium, compensating for the more ovoid shape of the particles by using a larger average size of particle.

## II. EXPERIMENTAL TECHNIQUES AND MATERIALS

The sodium nitrate used was ground very fine and thoroughly dried. A Mikro-pulverizer was used, followed by 16 hours drying at 80°C. and screening through a 400 mesh sieve. The addition of 0.5% MgO and 0.25% Cab-o-sil before grinding aided in preventing agglomeration of the  $\text{NaNO}_3$  particles. Ground magnesium powder was used for all this work.

The binder used in this study consisted of 27.1% XFS-400BL (glycerin diglycidyl ether) epoxy resin, 18.9% maleic anhydride (MA) curing agent, 19.0% ethylene carbonate (EC)

plasticizer, and 35.0% diethylene glycol dinitrate nitro-plasticizer. The MA and EC were used as a premixed liquid solution. The plasticizers used were free of inhibitors.

For mixing, a KitchenAid Model K5-A mixer was used, with an A-B beater and pastry knife blade, using the following procedure: add curing agent, add plasticizer, add resin, mix 1-2 minutes, add  $\text{NaNO}_3$ , mix 5-10 minutes, add Mg, mix 15-20 minutes. Viscosity of the mixed formulation was determined at 25°C., using a Brookfield RVF viscometer with a T-type spindle.

After mixing, the composition was poured into a plastic funnel and allowed to flow into a mold. The candles were cured overnight at 70°C. After curing, one end of the candle was closed off by casting an epoxy-sand plug to form the flare base.

The flares were encased in paper tape after curing by bifilar spiral winding two layers of masking tape on the candle. Before the tape was applied, a coat of spray primer paint was applied for case bonding.

The flares were fired in a 18 foot 8-inch deep by 10 foot 5-inch wide by 10 foot 4-inch high concrete block hearth. The bottom of the flare was 4 foot 9 inches above the floor. Ventilation was accomplished by an inlet in the floor, below the flare, and an external 2-speed blower above the flare in the roof. The flare tunnel itself, connected to the hearth by a 4 foot by 9 foot doorway, was 60 foot long by 10 foot 5-inch wide by 14 foot high. The interior of the hearth and tunnel were painted black.

Two selenium photovoltaic cells were positioned 51.95 feet and 62.57 feet from the flare, at heights above the floor of 5.1 and 5.5 feet. The outputs of the photocells were amplified, and light output was recorded on an oscillograph. A voltage-to-frequency converter and an electronic counter were used to integrate the light output and record the integrated luminosity. The photocell was standardized with a standard lamp, which at a constant amperage yields a specific horizontal candle-power.

The 1 1/4-inch candles were burned vertically, ignited on the upper surface. Air flow was upward. Time of functioning was determined visually with a stop watch. At least four candles were fired for each data point, unless noted otherwise.

### III. MAGNESIUM SAMPLES

Three samples of experimental ground magnesium powder, especially designed for this work were obtained. Table I shows the particle size distribution, and Figures 1, 2, and 3 show photomicrographs of the material.

TABLE I GROUND MAGNESIUM PARTICLE SIZE DISTRIBUTION

Percent on Mesh No.	Sample No.		
	Spec 2 Lot 1	Spec 3 Lot 2	133850
40	0.4%	Trace	0
50	20.0	25.8%	0
60	36.2	52.0	Trace
80	35.0	21.8	8.2%
100	8.0	0.4	73.1
(-100)	(0.4)	(Trace)	--
120	--	--	18.2
160	--	--	0.4
(-160)	--	--	(Trace)

Specifications 2 and 3 were received at the beginning of the study, while sample 133850 was requested later, after the need to investigate a fine particle additive was apparent.



Figure 1 - Photomicrograph of Ground  
Magnesium Spec 2, Lot 1 (30X)



Figure 2 - Photomicrograph of Ground  
Magnesium Spec 3, Lot 2 (30X)

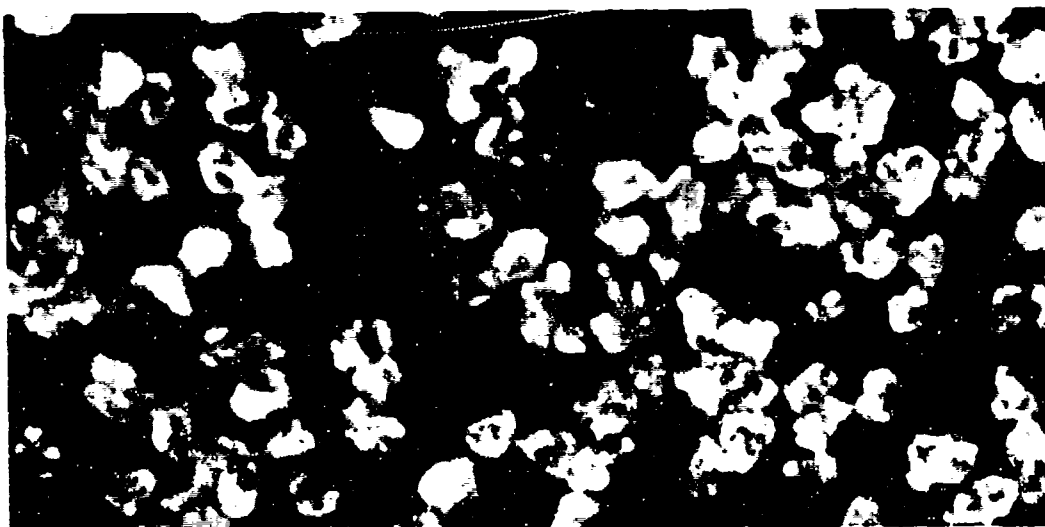


Figure 3 - Photomicrograph of Ground  
Magnesium No. 133850 (30X)

A comparative study was made of the relative effects of the SPEC 2 and somewhat coarser SPEC 3 on the castability and performance of flare compositions. As shown in Table II, formulations based on SPEC 3 Mg are much lower in viscosity, but give burning rates and luminous efficiencies equivalent to the SPEC 2 material. Therefore, the SPEC 3 material was selected for subsequent development efforts.

TABLE II CASTABILITY AND PERFORMANCE OF CANDLES

Binder Percent	Mg/ $\text{NaNO}_3$ <sup>a</sup>	Mg Type	Visc. $10^6$ cps.	Burn Rate in./sec.	Lum. Eff. Kcd.sec./g.
22	1.79	SPEC 2	>2.50	0.059	40.7
22	1.79	SPEC 3	1.88	0.051	41.9
25	1.79	SPEC 2	1.50	0.051	36.9
25	1.79	SPEC 3	0.48	0.051	34.5
24.3	1.79	SPEC 3	0.21	0.049	38.9
26.4	1.79	SPEC 2	0.30	0.050	38.2

<sup>a</sup>Mikro-pulverized and dried, not screened.

At this point a change in mixing procedure was adopted to enhance castability. The  $\text{NaNO}_3$  was screened through a 400 mesh sieve before use, and the Mg was added in increments so as to keep the mix always fluid during processing. This improved the viscosity of the second composition shown in Table II from  $1.88 \times 10^6$  cps. to  $0.39 \times 10^6$  cps.

A series of formulations was prepared to determine the optimum Mg/ $\text{NaNO}_3$  ratio. As shown in Table III and Figure 4, at 22% binder maximum efficiency was found at Mg/ $\text{NaNO}_3$  = 1.8 or more. At 25% binder the maximum appears to be lower than this.

TABLE III OPTIMIZATION OF MAGNESIUM LEVEL

Binder Percent	Mg/ $\text{NaNO}_3$	Visc. $10^6$ cps.	Burn Rate in./sec.	Lum. Eff. Kcd.sec./g.
20	1.67	2.50	0.053	40.8
22	1.44	0.28	0.053	40.5
22	1.60	0.38	0.050	40.7
22	1.79	0.39	0.049	44.7
22	2.00	0.98	0.052	44.6
25	1.50	0.07	0.045	44.2
25	2.00	0.06	0.049	42.1

An investigation was begun of adding fine Mg to these cast compositions, since previous work had shown that this improves the performance. A Mg/ $\text{NaNO}_3$  ratio of 1.79 was selected, and 24% binder was used. Table IV shows the results. The burning rate increases with addition of fine Mg, as expected. No viscosity improvement or increase in efficiency was obtained by adding fine magnesium. The effect of fine magnesium on viscosity is shown in Figure 5 and on efficiency in Figure 6.



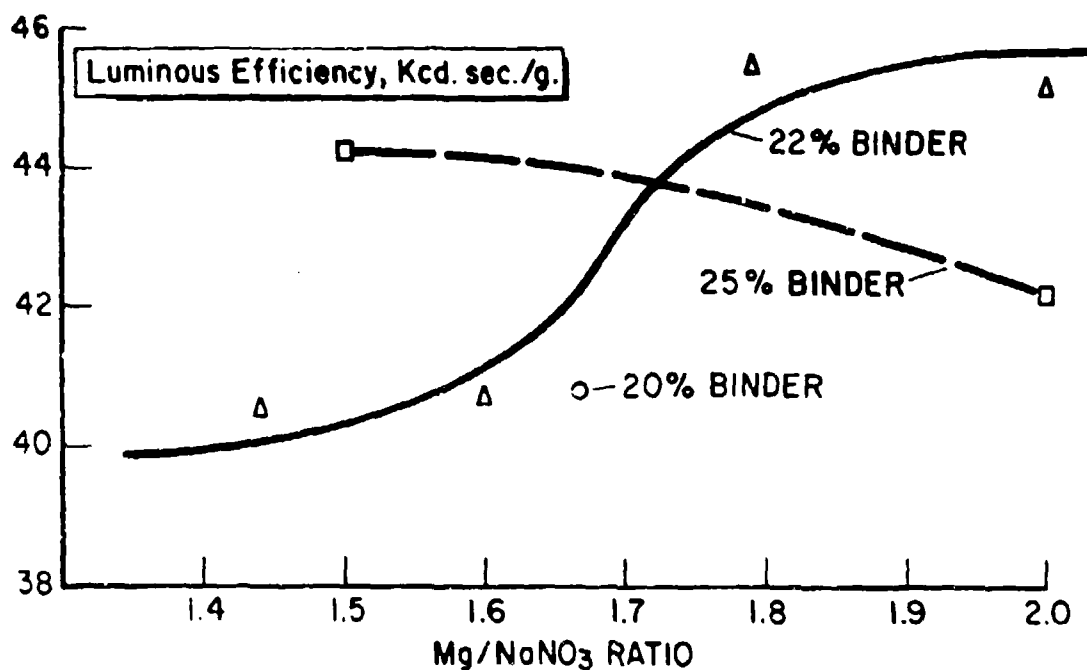


Figure 4 - Optimization of Magnesium - Sodium Nitrate Ratio

TABLE IV EFFECT OF ADDING FINE GROUND MAGNESIUM TO FORMULATION<sup>a</sup>

Mg Additive 60/120 Mesh Percent <sup>b</sup>	Viscosity 10 cps.	Burn Rate in./sec.	Lum. Eff. Kcd.sec./g.
0	0.26	0.048	42.6
5	0.33	0.051	39.4
10	0.43	0.051	38.0
15	0.82	0.052	36.3

<sup>a</sup>48.72% Mg (total), 27.28% NaNO<sub>3</sub>, 24.00% Binder.  
<sup>b</sup>% of total Mg content replaced by additive.

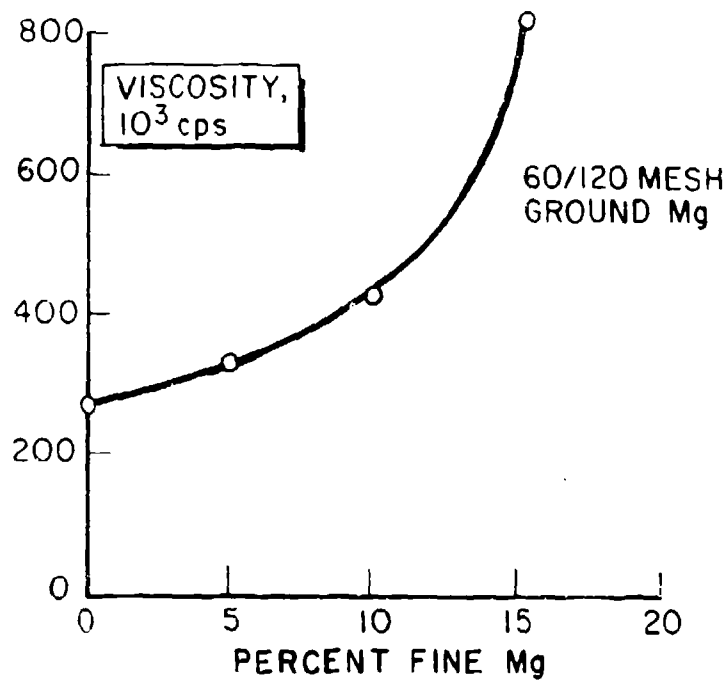


Figure 5 - Effect of Fine Mg on Mix Viscosity

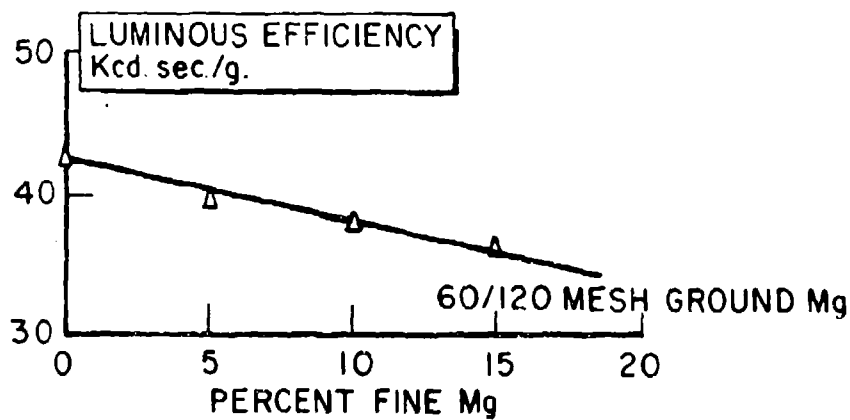


Figure 6 - Effect of Fine Mg on Luminous Efficiency

## V. SURVEILLANCE

Cast candles containing ground magnesium were stored at 70°C. for 4 weeks. The composition used contained 50% SPEC 3 Mg, 28%  $\text{NaNO}_3$ , and 22% binder. The mix viscosity was 725,000 cps.<sup>1</sup> Before surveillance this batch gave 41,600 cd. sec./g. efficiency at 0.057 in./sec. burning rate. After surveillance the efficiency was 39,100 cd. sec./g. and 0.059 in./sec. The candles experienced an average weight loss of 0.46%. The composition appears to be stable in high temperature surveillance.

## VI. CONCLUSIONS

This work has demonstrated that ground magnesium powder can be used in pour-cast flare compositions. The best formulation studied gave 45 Kcd. sec./g. luminous efficiency and 0.05 in./sec. burning rate. Mix viscosity was 390,000 cps.

In our paper at the Aspen meeting two years ago, we reported a composition of 52 Kcd. sec./g. efficiency and 0.06 in./sec. burning rate, with mix viscosity of 250,000 cps. However, this formulation contained nitroplasticizer in excess of the solubility limit, and therefore is not practical. Reduction of nitroplasticizer to a compatible level resulted in a composition yielding 41 Kcd. sec./g. efficiency and 0.05 in./sec. burning rate.

Because of the less spherical particle shape, a somewhat higher binder level will be necessary with ground Mg than with atomized material. Because of combustion characteristics, ground Mg should be employed with a larger average particle size than for atomized material.

In recent work at Dow, reported in a companion paper, an optimized flow-cast composition has yielded 53 Kcd. sec./g. efficiency at 0.066 in./sec. burning rate. A mix viscosity of 275,000 cps. was obtained with 20% binder. The atomized Mg used was a carefully selected laboratory blend of production lots and sieve fractions.

The final choice of magnesium type for use in flow-cast flares will be made by the flare manufacturer on the basis of cost, availability of specified particle distribution, and performance in production flares.

---

<sup>1</sup>This batch was larger (2000 g.) than previous mixes, and evidently was not mixed enough to achieve lowest viscosity. Marginal castability resulted in an increased burn rate and lower efficiency than expected.

## FORMATION OF PYROPHORIC FRAGMENTS

by

W. W. Hillstrom  
Ballistic Research Laboratories  
Aberdeen Proving Ground, Maryland 21005

### Abstract

Pyrophoric metals are usually studied in very small particle sizes resulting in very large surface effects. A simple test was developed to study large pyrophoric fragments and their formation in the laboratory. This paper describes the test and its results with several reactive metals. Widely different threshold conditions were found for initiation of pyrophoricity in different metals.

## FORMATION OF PYROPHORIC FRAGMENTS

W. Hillstrom

Ballistic Research Laboratories  
Aberdeen Proving Ground, Md. 21005

### I. INTRODUCTION

Pyrophoric materials are defined by Webster as those that (1) ignite spontaneously and/or (2) emit sparks when scratched or struck. Many materials ignite spontaneously in oxidizing atmospheres as a result of their extreme reactivity. Examples of such materials are metal hydrides and alkyls such as lithium hydride and trimethyl aluminum. Dusts of very small diameter metal particles may also ignite at room temperature. The ignition temperatures of these dusts usually vary with particle size and surface history.<sup>1,2,3</sup>

In this paper we are concerned primarily with the second definition where bulk metal pieces spark profusely when ground, abraded, impacted, or otherwise subjected to mechanical shock. This sparking type of pyrophoricity is a unique, little understood property of a few metals.

Cerium, zirconium, uranium and some of their alloys are commonly described as pyrophoric metals. Some of the chemical and physical properties of these metals are shown in Table I. Cerium, of course, is the major constituent of misch metal which is used in the manufacture of lighter flints. The ease of sparking of lighter flints is well known. The character of the sparks from present day lighter flints is somewhat different from the old flint and steel sparks. The former ignites hydrocarbon fuel-air mixtures while the old flint and steel sparks could only ignite extremely flammable material such as tinder or charred cloth. Sparks from pyrophoric materials also sometimes appear to multiply in a cascade effect.

Powdered zirconium and uranium have relatively low spontaneous ignition temperatures. When such temperatures are measured for powders,

Table 1

	<u>Zr</u>	<u>Ce</u>	<u>U</u>
Atomic Number	40	58	92
Electronic Structure	4d <sup>2</sup> 5s <sup>2</sup>	4f <sup>1</sup> 5d <sup>1</sup> 6s <sup>2</sup>	5f <sup>3</sup> 6d <sup>1</sup> 7s <sup>2</sup>
Density, g/cm <sup>3</sup> (4)	6.49	6.78	19.05
M.P., °C (4)	1857	815	1132
B.P., °C (4)	>2900	2417	3818
Heat of Comb., K cal/g	2.84	1.9	1.09
Heat of Comb., K cal/cm <sup>3</sup>	18.1	13	20.4
Spontaneous Ignition Temperature, °C (5)	150	150-180	20

they may vary greatly with surface history, such as annealing and the presence or lack of surface oxide coatings. Normally, high surface area to mass ratios greatly magnify metal surface effects. Thus, experiments involving ignition of powders require careful attention to experimental conditions and metal surface history for meaningful, consistent results.

The electronic structure of these pyrophoric metals disclose two common similarities. They are transition metals and all three have largely unfilled d shells. Cerium has  $5d^1$ ; uranium has  $6d^1$  and zirconium has  $4d^2$ . Thus, large numbers of orbitals are available for coordination and reaction.

Field tests are used widely to evaluate the effectiveness of pyrophoric metals in munitions against a variety of targets. However, many loosely controlled factors significantly affect these tests, often leading to inconsistent and questionable results. Some of these variable factors include fuel temperature, contamination, and evaporation and the target geometry and environment. Adequate control of all of these factors is a difficult and continuing task.

On the other hand, a laboratory test has the advantages of better controlled test conditions, lower manpower and cost requirements, and quick response. A test method for sparking pyrophoric materials could also furnish a means to study the formation of pyrophoric fragments and their ability to ignite hydrocarbon gases and liquids in the laboratory.

## 11. EMPIRICAL TREATMENT OF PROPERTIES

Since an intuitive examination of metal sparking indicated that some physical and chemical properties might correlate with the degree of pyrophoricity, the known properties of some pyrophoric metals were compared with those of non-pyrophoric metals. Two properties of interest are (1) the reactivity of the metal with oxygen or air, and (2) oxide volume compared with metal volume. The correlations might then be used to find a better based understanding of the nature of pyrophoricity and furnish a means of estimating the pyrophoricity of new and untested materials.

The standard free energy of formation per oxygen atom in the metal oxide is a parameter indicating relative metal reactivity with oxygen. It is also a good indicator of the heat available from reaction of the metal with oxygen.

The violent expansion of metal during its oxidation may account for the explosive cascading observed with pyrophoric sparks. To explore this theory the ratios of the metal oxide and metal specific volumes were calculated by means of the following formula.

$$\frac{\frac{F_o}{D_o}}{\frac{A_m}{D_m}} = \frac{F_o D_m}{A_m D_o}$$

where  $F_o$  = formula weight of oxide/atom of metal

$D_m$  = metal density

$A_m$  = atomic weight of the metal

$D_o$  = metal oxide density.

For example, the ratio of oxide to metal for titanium is

$$\frac{(79.9)(4.50)}{(47.9)(4.26)} = 1.76.$$

Comparison of this ratio with those of other metals gives a relative order of magnitude for the expansion of the reacting metal oxide. A correlation of this ratio and the free energy of formation of the oxide is shown in Figure 1.

It can be seen that these measures of reactivity and oxide expansion allow a general separation of known pyrophoric and nonpyrophoric elements. Uranium, cerium, zirconium and thorium have both relatively high reactivity and oxide volume ratio. Aluminum is an exception. Its dust ignites easily, but the metal is too soft to spark appreciably when abraded.



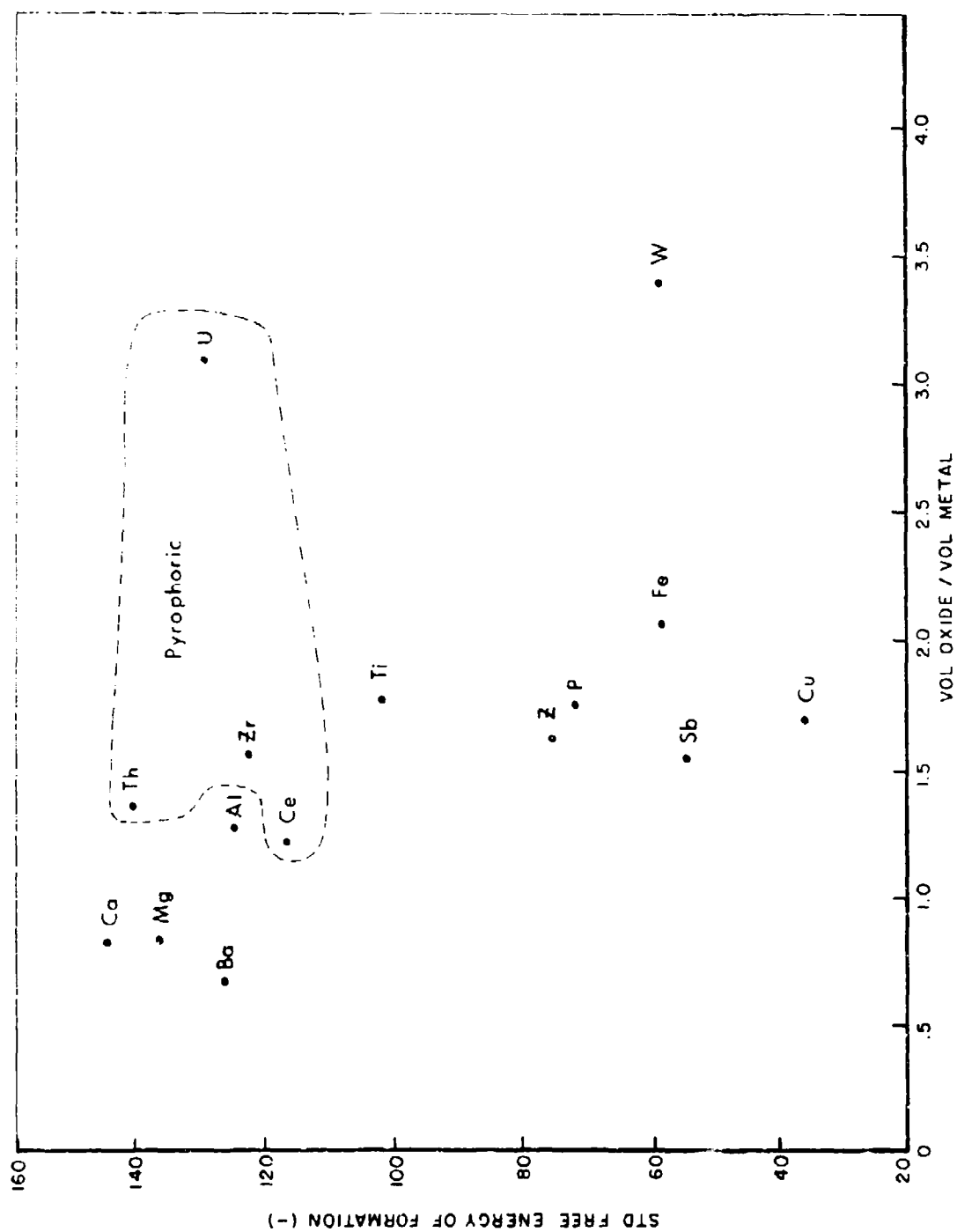


Figure 1 - Free Energy of Formation vs Oxide Expansion

Thus, some metal property such as hardness may also have to be considered for metals that are very reactive in order to call them pyrophoric.

### III. EXPERIMENTAL

Metal samples were used as obtained from the suppliers. Sponge, solid rod, and dust samples of zirconium as Commercial Grade II were supplied by Amax Specialty Metals, Inc., Akron, New York. Lengths of 3/16" diameter misch metal rod were purchased from Ronson Metals Corporation, Newark, N.J. Both 75M2 and 95M grades were used. Pure cerium (99.9%) ingots were purchased from Research Organic/Inorganic Chemical Corp., Sun Valley, Calif. and machined to the desired shapes.

### IV. METAL OXIDATION

Many values for the autoignition, spontaneous ignition, and kindling temperatures of metals are reported in the technical literature. In general, these temperatures were measured with dusts or powders rather than with bulk samples of the metals. Particle size, surface oxidation, and surface conditions such as chemical or physical surface films play an important role in the ignition or burning behavior of dusts due to the large surface area to mass ratio.<sup>6</sup>

Pyrophoric metal pieces larger than dusts were heated to temperatures much higher than the reported "auto-ignition temperatures" of their dusts without observing ignition. In this work only glowing was observed after heating misch metal at temperatures up to 1000°C in a 1" diameter tube furnace in air. No flames, sparks, or burning were seen. Even this glowing was seen at much higher temperatures (as seen in later figures) than its 150-180°C Spontaneous Ignition Temperature from Table 1. Zirconium and titanium exhibit both orange glowing and white incandescence when heated at temperatures up to 900°C. The effect of the particle size of sponge zirconium on time to orange glow in air is shown in Figure 2. As might be expected, the smaller particles begin to glow in a much shorter time than larger pieces. Particles larger than 0.7 grams only glowed orange. They did not progress to a white incandescence unless heated strongly at some sharp point or edge with a propane torch. The two temperatures used, 790° and 880°C,

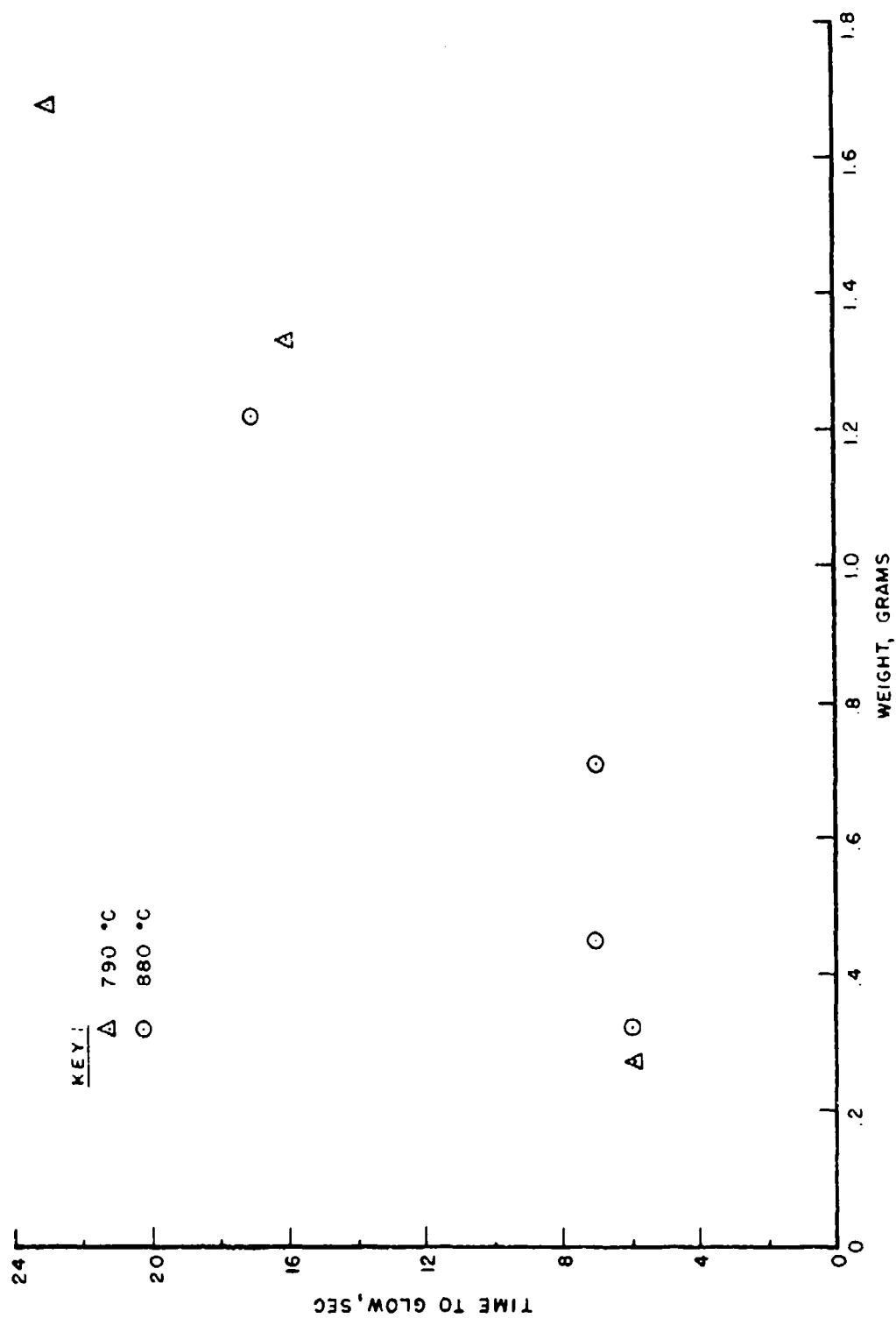


Figure 2 - Zirconium Oxidation

seemed to be equivalent, but temperatures lower than these would not initiate glowing in sponge zirconium. Pieces of solid zirconium rod in the same weight range did not progress to the white incandescent stage upon heating to 900°C.

Lower Temperature Limits for the initiation of glowing in air are also observed with samples of misch metal. Figure 3 shows the time to glow as a function of furnace temperature. Small rods, 3/16" diameter by 1/2" length, were set in a combustion boat in the hot furnace and the time measured for the onset of a bright orange glow. The Lower Glow Temperature Limit of around 400°C for 75M2 misch metal is much lower than the 790°C for zirconium sponge.

The time to glow for 95M misch metal is shown in Figure 4. Shorter times to the beginning of bright glowing were observed, but the Lower Temperature Limit is about the same within experimental error.

The bright orange glow was observed to propagate down 6" lengths of misch metal rod with a 3/16" diameter. The rods were initially at about 22°C and were held horizontal by an asbestos insulated clamp at one end. The other end of the rod was heated intensely by a propane torch. The heated end began to glow with a bright orange color and the torch was removed. The glow propagated down the 95M rod in air at an average of 2.75 cm/minute leaving a grey deformed rod behind it. The rod gained 4.5% in weight during the glowing. The glow would not propagate more than one cm. down a similar rod of 75M2 misch metal.

The glowing was an important step in the sparking of the pyrophoric metals since nonglowing large pieces would not spark on impact with a weight. Glowing misch metal pieces and incandescent zirconium pieces gave off a literally blinding multitude of sparks when impacted with weights ranging from 88 to 169 grams falling from 39.1 to 40.5 cm.

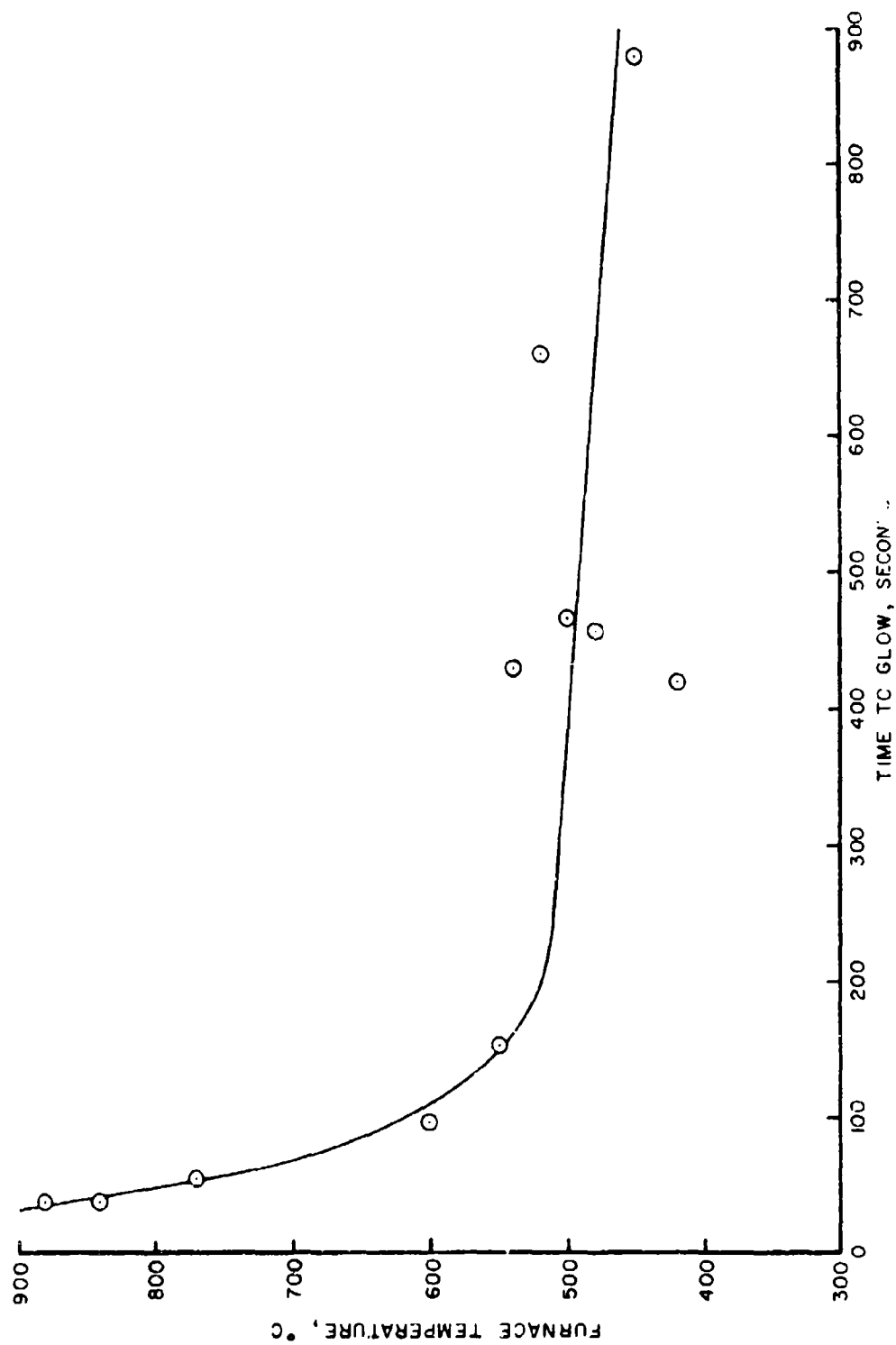


Figure 3 - 75M2 Misch metal

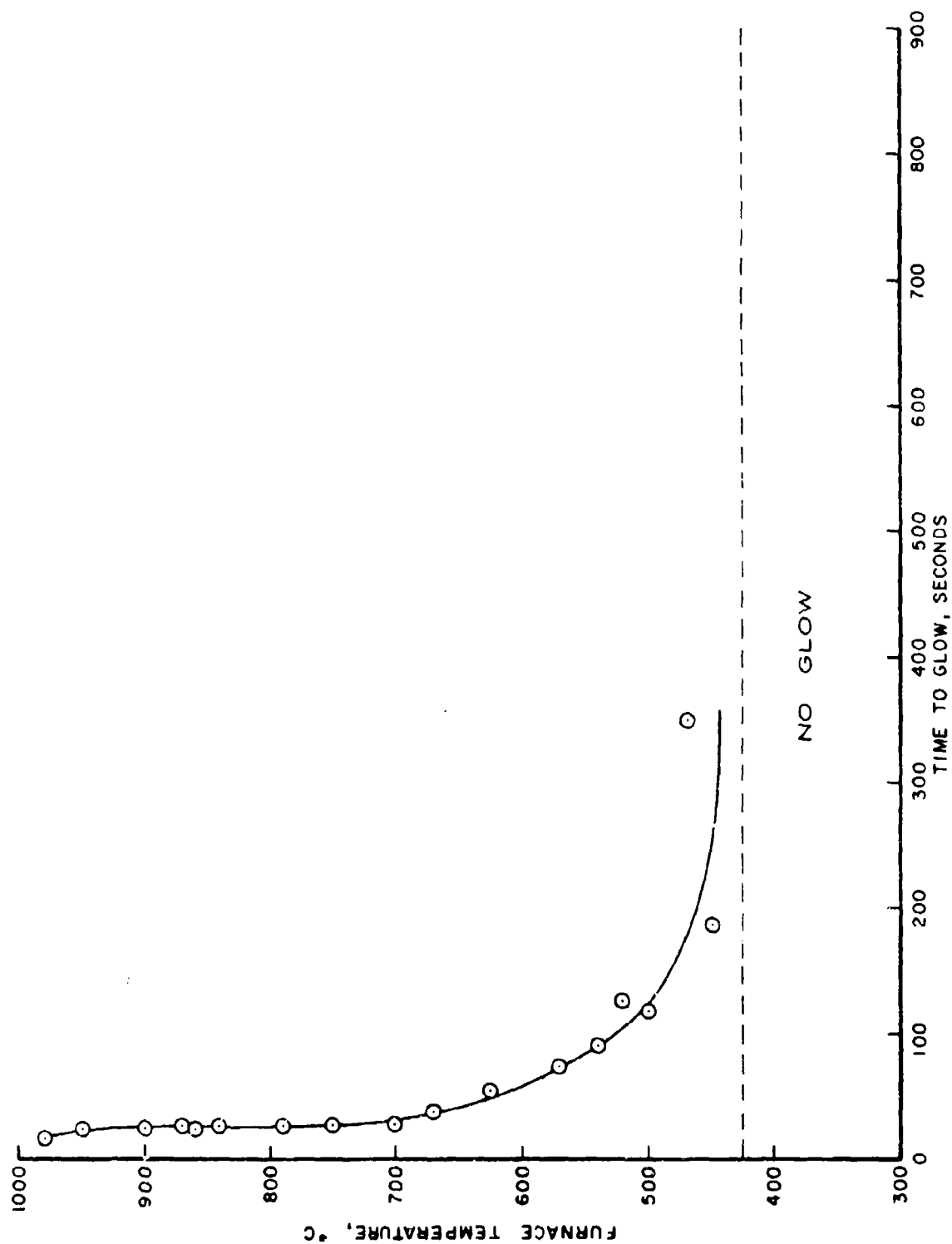


Figure 4 - 95M Misch Metal

## V. GENERATION OF PYROPHORIC FRAGMENTS

The drop weight impact apparatus that was used to generate pyrophoric sparks and fragments is shown in Figure 5. The recovered fragments varied in shape and were generally less than 0.1 gram in weight. The sparks were directed at a 45° inclined stainless steel plate which led to a long enclosed tray where terminal ballistics experiments were carried out to study fragment properties and ignition of combustible materials.

The height and weight of the drop weight were varied to give an approximate order of magnitude of kinetic energy necessary to initiate sparking. For this work, the following standardized test conditions were used: The 169 gram drop weight falls 39.1 cm in the above apparatus to give a kinetic energy impact of 65 newton-cms. Higher KE impacts do not give much greater sparking, but lower KE impacts produce fewer sparks. In some tests glowing pellets were merely dropped from small heights. In these tests some sparking occurred, but it was not as profuse as those generated in the impact apparatus.

It was found that sparking could not be initiated in the impact apparatus with the respective metals unless the misch metal pellet was glowing orange or the zirconium was incandescent white. High temperatures alone did not cause sparking in the pellets, but heat and impact in the ranges discussed here gave profuse sparks. Although either extremely high temperatures ( $>1000^{\circ}\text{C}$ ) or very high KE shocks alone may lead to sparking, the point to be emphasized is the necessity for both heat and impact in the sensitive test conditions described here.

An interesting experiment was carried out to study fragment formation in an inert atmosphere. A pellet of 75M2 misch metal was heated in air at  $700^{\circ}\text{C}$ . It was glowing brightly when it was placed on the anvil of the impact apparatus which was in a covered tray filled with argon. After impact, small glowing particles dispersed from the impact apparatus, but they were not sparking fragments. Thus, the misch metal was sufficiently softened or melted at  $700^{\circ}\text{C}$  to easily breakup upon impact. The hot fragments did not "explode" or spark in the inert argon atmosphere. Thus,

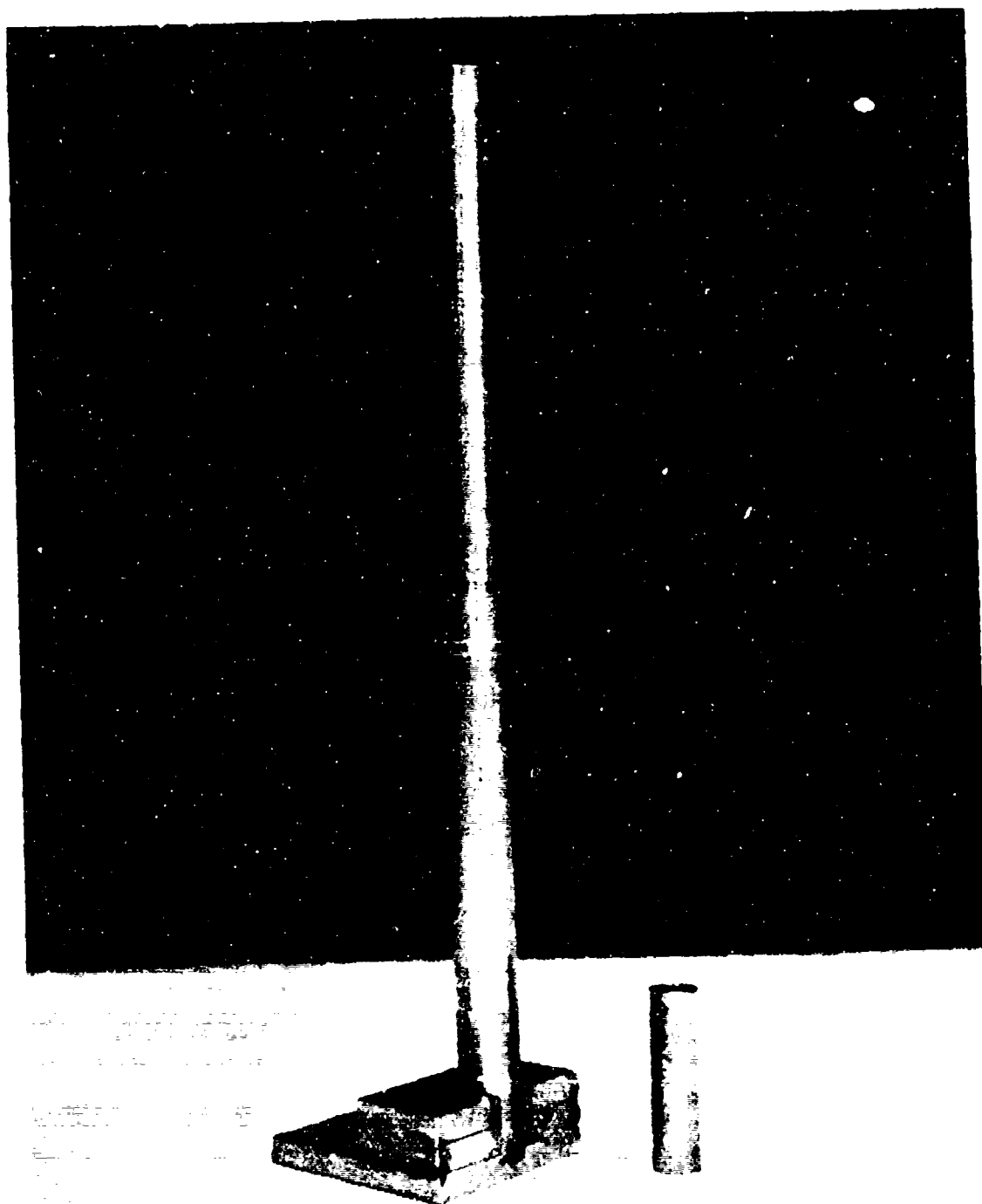


Figure 5-Drop Weight Impact Apparatus



as expected, an oxidizing atmosphere appears to be necessary to the sparking process.

High speed cinematographic studies of free flying fragments show an eroding type of breakup of the larger pieces during flight. The visible light from some fragments varied in intensity after they came to rest, and glow times as long as six seconds were recorded.

## VI. CONCLUSIONS

Pyrophoric metals possess a high degree of reactivity with air and have largely unfilled d electron shells. The ratio of the volumes of the metal and its oxide does not appear to be as important a property as the metal reactivity with oxygen.

The Lower Glow Temperature Limit that was needed to initiate sparking by standard impact on metal pieces may be an a priori indication of the degree of pyrophoricity of new materials. Thus, the laboratory test utilizing heating and impact may be used as a screening test in determining pyrophoricity. The sparking fragments generated from the drop weight impact apparatus can also be used in controlled experiments to investigate terminal ballistics effects of pyrophoric materials and munitions.

#### REFERENCES

1. I. Hartmann, J. Nagy, and Murray Jacobson, "Explosive Characteristics of Titanium, Zirconium, Thorium, Uranium and Hydrides," BMRI 4835 (1951).
2. B. Kopelman and V. B. Compton, "Metal Progress", 63(2), 77 (1955).
3. C. R. Schmitt, J. Fire and Flammability, 2, 157 (1971).
4. Handbook of Chemistry and Physics, The Chemical Rubber Co., Cleveland, Ohio (1964).
5. J. R. Gibson and J. D. Weber, Handbook of Selected Properties of Air - and Water-keactive Materials, U.S. Naval Ammunition Depot, Crane, Indiana, RDR No. 144, AD688422, (1969).
6. Hartman, Nagy and Brown, Inflamm. & Explo. of Metal Powders, BMRI 3722 (1943).

# DEVELOPMENT AND EVALUATION OF EXPLOSIVE MATERIALS FOR THE TASK OF EXPLOSIVE DISPERSION OF PROJECTILES

Allen J. Tulis  
James L. Austing  
Robert F. Remaly  
IIT Research Institute  
Chicago, Illinois

## ABSTRACT

One-dimensional-model experiments and three-dimensional field tests were conducted to evaluate the explosive projection and dispersion of spherical projectiles utilizing pyrotechnics and low-density explosives loaded into the interstitial spaces of close-packed projectiles. Although  $\text{Al-KClO}_4$  pyrotechnic at 1.1 g/cc dispersed aluminum-shell projectiles with negligible damage at velocities of about 500 ft/sec, it was necessary to reduce explosive densities to below 0.2 g/cc in order to achieve similar dispersion velocities without excessive damage. Development of polyurethane-foamed explosive systems was achieved using PETN, nitrocellulose, nitroglycerine, and HMX. The projected velocities of the spherical projectiles were determined to be directly related to (1) density and velocity of explosive-product gases, (2) ratio of projectile cross-sectional area to mass, and (3) explosive thickness acting on the projectile. Typical velocities for 2-in. diameter spheres, ranging in overall density from 1.4 to 7.8 g/cc, were 28 to 500 ft/sec depending on the type of experimental model that was utilized.

## INTRODUCTION

The objective of this work was to explore projectile dispersion techniques by utilizing low-density explosives and pyrotechnics in the interstitial spaces of close-packed projectiles. Dispersion from essentially unconfined charges precluded the use of fast-burning propellants, such as gun powder, for which projectile velocity is dependent on some degree of confinement. On the other hand, the use of standard high explosives was also out of consideration because of the attendant destruction of the projectiles.

Thus, the basis of this problem was to obtain an exploding system that (1) was sufficiently fast with adequate pressures generated to provide impulse to spheroids\* resulting in initial velocities in the neighborhood of 250 ft/sec and (2) was insufficiently "brisant" (high detonation velocity and pressure) to prevent fracturing of the spheroids. Impulse is the integral of pressure by its time duration. Thus exceedingly high shock pressures, which are in effect for very small periods of time, are generally inconsequential to the total impulse given to nominal-

\*The term spheroid will be used for the spherical-type experimental projectile that was specifically evaluated in this work.

sized projectiles in the proximity of a detonation. However, these same pressures can readily exceed critical stress levels of the projectile to cause fracture. A low detonation velocity explosive with prolonged pressure duration is desired. Explosive pyrotechnics, especially those containing aluminum, were candidates for such a requirement. In addition, low-density explosives were also considered. In particular the use of low-density foamed explosives was of prime consideration.

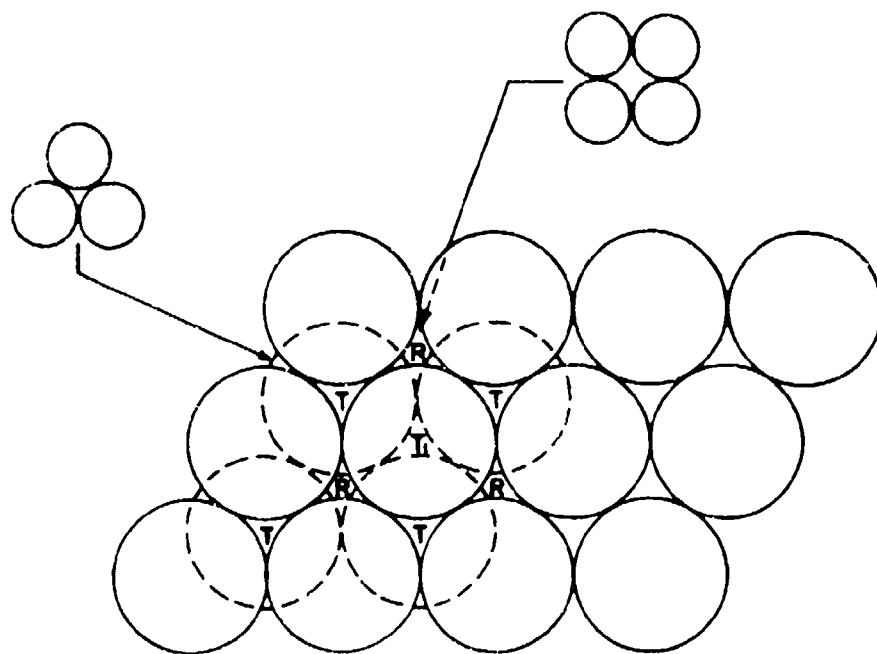
Although practical applications of explosive dispersion of projectiles involves geometrical configurations other than spherical, the use of spheres presented the least number of complicating factors for mathematical interpretation. In addition, only "close," or rhombohedral packing of these spheres was considered. Figure 1 illustrates this type of packing. As this figure shows, two types of basic cells exist in close packing: (1) tetrahedral cells and (2) rhombohedral cells; and twice as many tetrahedral cells as rhombohedral cells exist. Every sphere contacts 12 other spheres, the total porosity is 25.95%, and the narrow opening formed by contact of three spheres has an area equal to  $0.043d^2$  where  $d$  is the diameter of the sphere (Ref. 1).

The spheroid had a volume of 120 cc. In a close-pack situation this allowed 40 cc of interstitial volume per each spheroid. At 0.1 g/cc explosive, for instance, this would allow a 4-g explosive charge per spheroid. The heat of detonation of PETN is 1,385 cal/g and the kinetic energy required to accelerate a 420-g spheroid to 250 ft/sec is about 900 ft-lb, or 290 g-cal. Thus, an efficiency of 5.2% would be adequate.

#### EXPLOSIVE DISPERSION

Fadeenko (Ref. 2) considered the motion of a small sphere that was accelerated by the products of detonation of a layer of explosive material. Neglecting the effect of finite sphere size and difference of regime of flow from steady state and provided the flow remained supersonic, he showed that the velocity of the sphere was dependent on the detonation velocity, explosive loading and amount, and sphere density and size. He further indicated that the load acting on the sphere was characterized by the ratio of the accelerating forces to the cross-sectional area of the sphere. Thus, the larger the sphere the greater the damage potential.

Held (Ref. 3) evaluated the acceleration effects of steel balls embedded in an explosive as a function of various parameters, including ball size and density, embedding distance or exterior positioning of the ball, and initial positioning effects of several balls. Held also determined the effect of ball density upon the initial velocity utilizing balls of different metals. The variation was roughly proportional to the density raised to the 0.83 power; i.e., the density ratio of iron to aluminum is 2.90 so that the velocity of an aluminum ball of the



T = tetrahedral cells, top layer, solid lines

T<sub>1</sub> = tetrahedral cell, bottom layer, dotted lines

R = rhombohedral cells, top and bottom layers

Note: There are three pore types in rhombohedral packing,  
with frequency as follows:

3 rhombus : 3 square : 2 triangle

Figure 1  
RHOMBOHEDRAL (CLOSE) PACKING OF SPHERES

same size as a steel ball would be 2.40 times as great. The spheroid, at 420 g per 120 cc volume, had an average density of 3.50 g/cc. Thus, velocities of the spheroids should be about 1.85 times as great as those obtained with steel balls of similar size.

Gurney (Ref. 4) attributed the initial velocity of fragments from bombs to the energy and relative masses of the explosive and its case. Thus, in this analysis the energy imparted to the casing fragments was essentially independent of parameters usually characterizing an explosive such as detonation velocity and pressure.

Demiduk (Ref. 5) considered the working of an explosion as the work of an adiabatic expansion of the products of a detonation with the probability of uniting all the different forms of explosive work into two groups: (1) pulverizing, piercing, or fracturing the surroundings adjacent to the explosive and (2) breaking up, splitting, and throwing out of the surroundings that manifest themselves at some distance from the area of contact between the charge and its surroundings. This latter form makes up a sizable portion of the explosive work. These forms of work present themselves in connection with the significance of the whole impulse of the explosion. Thus, a substantially large shattering effect must significantly reduce the magnitude of demolition effect or dissemination of material from the area.

Explosive acceleration of projectiles can be conveniently separated into two basic processes; (1) shock-wave interaction with the projectile and (2) high pressure and high velocity gases acting on the projectile. Generally speaking, only the former process is associated with fragmentation of the projectile.

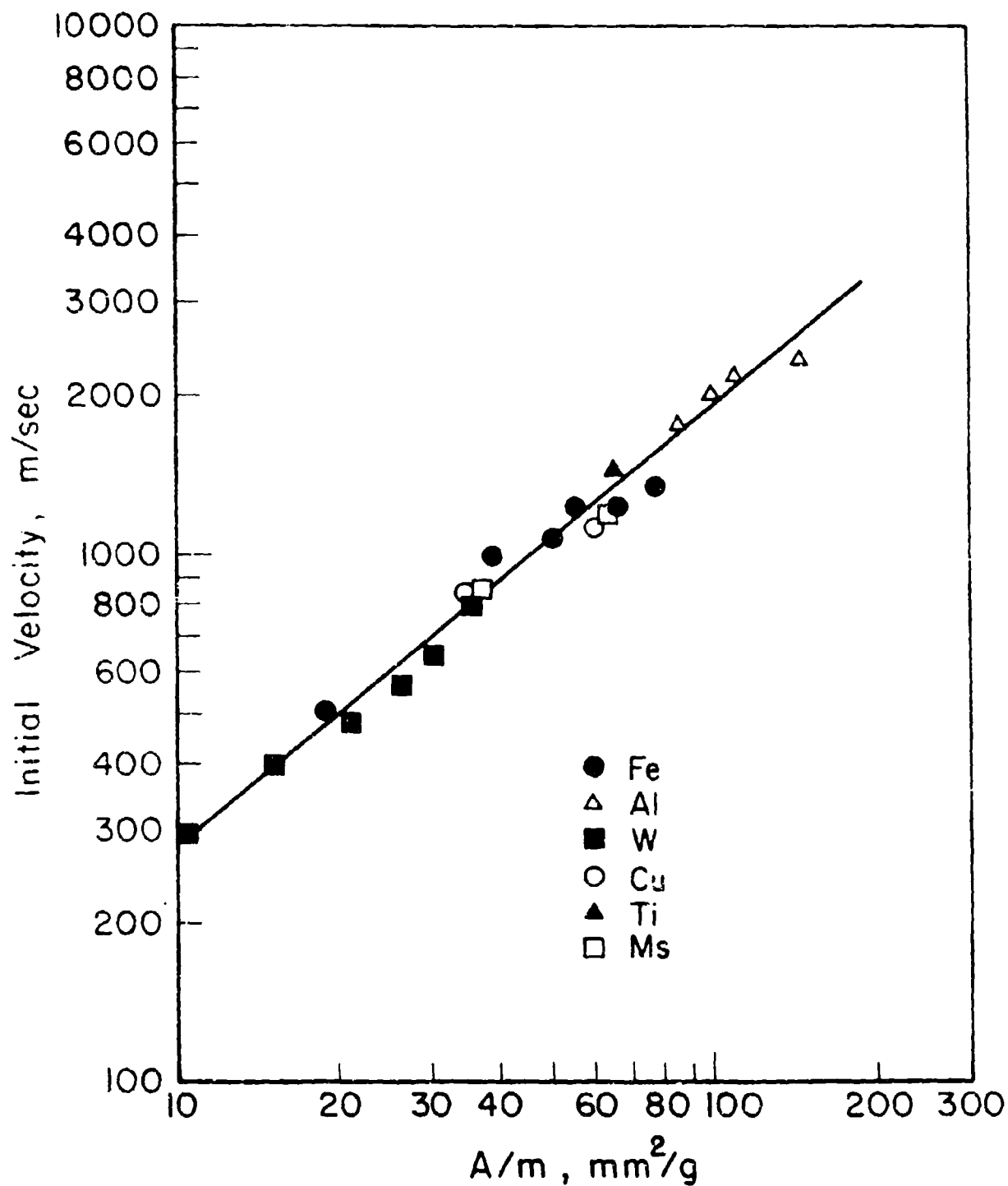
The shock-wave interaction occurs as follows (Ref. 3). As soon as the detonation wave arrives at a solid projectile, a shock wave travels through to the other surface, thereby accelerating the molecules to the particle velocity corresponding to the particular shock-wave pressure. At the opposite surface a rarefaction wave returns through the projectile to the initial surface, accelerating the molecules again to about double the initial velocity. If this rarefaction wave still encounters high pressure on this surface, another shock (compression) wave returns into the projectile, accelerating the molecules again to about triple the initial velocity. This process can continue many times. However, as the high pressure on the initial surface diminishes the highly pressurized projectile releases pressure to the initial side also, thus creating another rarefaction wave. If the action time of the shock and rarefaction waves through the projectile is longer than the duration of the high pressure, the two rarefaction waves can meet within the projectile and cause fracture. In addition, because of the complex aftermath of the first reflection of the shock wave from spherical surfaces, other stresses will preside even though the duration of high pressure is adequate.

The high velocity gases will also accelerate the projectile, based on typical fluid dynamics principles of impulse and momentum. The higher the mass, or density, of this high velocity vapor flow, the greater the force exerted upon the projectile. Thus, in theory a "foamed" explosive, or other explosive containing an inert additive, should increase the actual momentum of the explosive product particle velocity just by being carried along. This will improve the projectile dispersion independently of high pressures so that the damage potential to the projectiles can be reduced without concomitant proportional reduction of performance. The results of this work substantiated this premise.

All projectiles have a finite mass and cannot instantaneously acquire an increase in velocity. Under similar circumstances, the larger the mass the greater the time required to acquire a final velocity. Although the use of a 50-mm steel ball in place of a 3-mm steel ball implies a proportionally longer acceleration time, the acquired velocity of the 50-mm ball would be substantially less because of the disproportionate radius-to-mass relationship. Thus, as Figure 2 illustrates, a 3-mm steel ball acquired a velocity of 4,000 ft/sec, whereas the expected velocity of a 50-mm steel ball would be about 400 ft/sec.

Dynamics of the acceleration forces upon the projectile are dependent on both the explosive system and the projectile itself, as to size, shape, density, etc. In general, the acceleration period is greater the larger the explosive charge and the slower the detonation velocity. As pertains to projectile size, a larger projectile will in general be accelerated for a longer time because it takes longer for pressure pulses to overpass the larger projectile. When the pressure pulse does pass the projectile, the pressures are equalized on front and back sides (except for pressures generated by vapor-flow dynamics on the front surface and other pressure gradients), so that the projectile cannot be further accelerated even though the pressure pulse remains. In the case of a sphere the surface increase as a pressure wave is passing is linearly proportional to the distance of the pass; the acceleration force increases until the pressure wave reaches the midpoint of the sphere and then decreases as the back side of the sphere becomes progressively exposed to the pressure pulse. Figure 3 illustrates this point and shows the effect on initial velocity of the ball due to various degrees of ball-embedding in the explosive or ball-placement exterior to the explosive.

It is of interest to consider the effect on flat plates, cylinders, and other geometric shapes. In the case of a thin flat plate, flat upon the explosive, the acceleration force would be maximum nearly instantaneously although the duration would be much shorter. In addition the momentum transfer attributed to the loss of kinetic energy of high-velocity vapors impinging upon the flat surface would be maximized relative to other geometric surfaces, such as spheres.

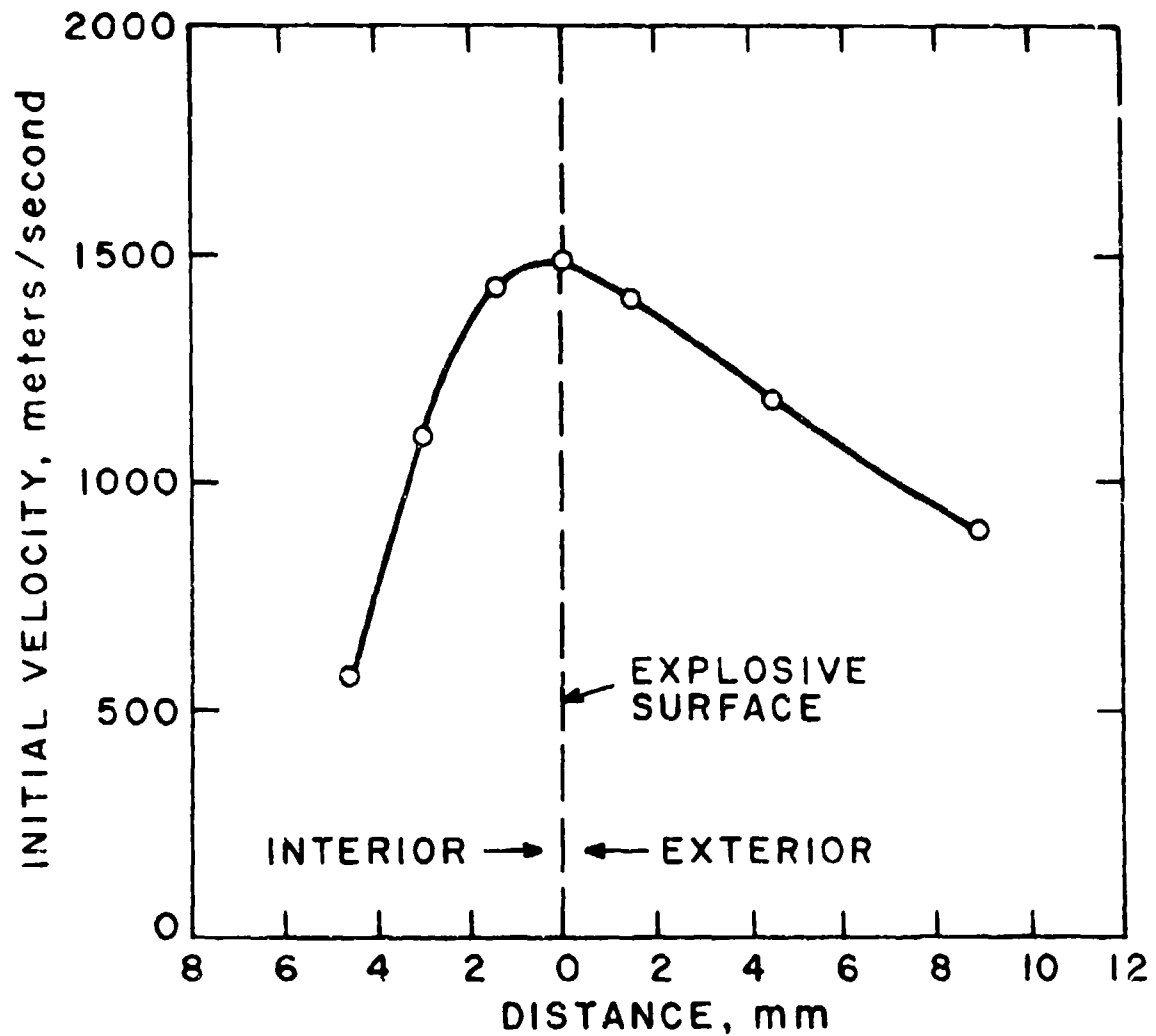


Reproduced from Reference 3

Figure 2

INITIAL VELOCITIES AS A FUNCTION OF A/m FOR SPHERES  
OF VARIOUS DENSITIES EMBEDDED IN EXPLOSIVE





Reproduced from Reference 3

Figure 3

INITIAL VELOCITY OF 3-MM SOLID STEEL BALLS AS  
A FUNCTION OF DEGREE OF EMBEDDING INTO THE  
EXPLOSIVE OR EXTERIOR PLACEMENT

Fadeenko (Ref. 2) presents a mathematical treatise on this subject, considering both large and small distances of initial separation between the explosive and the solid sphere projectile. The expression for force of gas flow upon the sphere is:

$$F = k(u) \rho r^2 u^2$$

where  $\rho$  is the density of the product gases,  $u$  their velocity relative to the sphere,  $r$  is radius of the sphere, and  $k(u)$  a constant pertaining to supersonic flow past a sphere. Solving a mathematical expression for the one-dimensional dispersion of products of detonation, the following relationship is established:

$$V/D = 1 - \sqrt{2/G} \theta^{-1}[\sqrt{G/2}]$$

where  $\theta^{-1}$  is the inverse function of  $\theta(z) = \int^z e^{t^2} dt$ ,  $D$  is the detonation velocity, and  $G = 0.304(L/r\rho)$  where  $L$  is the thickness of explosive,  $\rho$  the density of the explosive,  $\rho$  the density,  $r$  the radius of the sphere, and  $t$  the time. The sphere velocity  $V$  is shown to be dependent only upon  $D$  and  $G$  in a relationship expressed as:

$$V/D \approx \log G$$

with curvature at the higher  $G$  values.

Newton's 2nd Law states that the acceleration of a particle is proportional to the resultant force acting on it and is in the direction of this force. For the present interpretation we will consider only colinear forces, represented by direction  $x$ . Thus, the differential equation for the 2nd Law can be expressed as:

$$\frac{d^2x}{dt^2} = \frac{F(x,t)}{m}$$

where  $F(x,t)$  is the force. If  $F(x,t)$  is constant, we can write:

$$F = \frac{dV}{dt}$$

and

$$\int_1^f F dt = \int_1^f m(dV/dt) dt = m(V_f - V_i)$$

The integral  $\int_1^f F dt$ , generally denoted by  $I$ , is the impulse of the force  $F$  during the time interval  $t_f - t_i$ , or the product of the force by the time of duration of that force. The term  $m \cdot \Delta V$  is the linear momentum. Thus, the impulse  $I$  over a time interval is equal to the change in momentum of the mass under consideration during that time interval.

In an associated study of this work (Ref. 6) we have shown that the explosive projection of spherical bodies can be expressed as:

$$V = a(P/D)(g/\rho) + b(\rho uL)(A/m)$$

where a and b are constants,  $b > a$  as  $A/m$ , the cross-sectional area-to-mass ratio of the sphere, diminishes; P is pressure, g is the gravitational constant, and other notation is as used previously.

### PYROTECHNICS

The major pyrotechnic composition evaluated in this work was aluminum-potassium perchlorate ( $Al-KClO_4$ ), utilized in an oxidant-rich formulation containing 2/3 the stoichiometric amount of the fuel (Ref. 7). The aluminum was a spherical grade, type H-3\*, and the  $KClO_4$  was a commercially manufactured type identified as batch no. 2\*\*. This mixture was used without compressing or otherwise affecting the material. Its density in charge loadings was about 1.1 g/cc.

Other pyrotechnics considered were (1) boron and ammonium perchlorate ( $NH_4ClO_4$ ) and (2) aluminum and  $NH_4ClO_4$ . The boron was amorphous and about 1 micron in size\*\*\*. The aluminum was the same as that used in the  $Al-KClO_4$  pyrotechnic. The  $NH_4ClO_4$  was a finely ground NASA-spec. type. These two systems were prepared in fuel-rich formulations with 2 moles of either boron or aluminum to 1 mole of  $NH_4ClO_4$ . It should be noted that  $NH_4ClO_4$  requires a portion of the released oxygen for oxidation of the ammonium ion. These pyrotechnics were also prepared as foamed systems. The maximum loading that was practically possible was about 75% (wt) of the pyrotechnic.

### FOAMED EXPLOSIVES

Urethane foams are some of the most versatile materials in the entire spectrum of plastics. These foams are produced by the reaction between two chemicals which expand and crosslink to form a cellular structure with a density range from below 0.02 to about 1.12 g/cc; an almost limitless range of chemical and physical properties can be obtained. The foaming arises from the liberation of gas during the reaction, either  $CO_2$  when water is used as a blowing agent or a Freon gas that has been incorporated into the system. The Freon is introduced as a liquid and gasifies as a result of temperature rise of the reaction.

\*Valley Metallurgical Company, Essex, Connecticut.

\*\*Hummel Chemical Company, Newark, New Jersey.

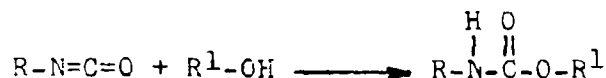
\*\*\*American Potash and Chemical Corporation, Los Angeles, California.

Both rigid and flexible foams are available, and any intermediate characteristic in between these two extremes is achievable. Rigid foams have an excellent range of compressive, shear, tensile and flexural strengths. Flexible foams have similar and other advantages, including high strength, even cell structure, high resilience and elasticity, and excellent resistance to tearing, abrasion, creep and flexural stresses.

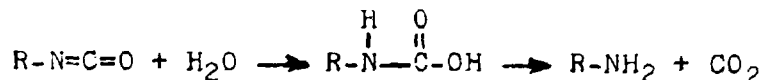
Urethanes are produced by the reaction of polyols with isocyanates. High molecular weight, low functionality polyols produce a low degree of crosslinking and consequently a flexible foam. Conversely, low molecular weight polyols of high functionality produce a high degree of crosslinking and a rigid foam. The formulation can be varied to produce any degree of flexibility or rigidity desired.

Diisocyanates are extremely reactive with compounds containing active hydrogen atoms such as amines, alcohols, carboxylic acids and water. The polyol component is a hydroxyl-terminated polyether or polyester. The polyether class polyols are generally less susceptible to the effects of humidity. Initially the polyesters had advantages of high temperature stability and strength, but the newer polyethers are presently comparable in this respect.

The chemical reaction between an isocyanate and a hydroxyl compound is:



which is a urethane. This reaction will proceed when the two components are mixed. It is an exothermic reaction, and would result in a solid polymer with a density greater than 1.0 g/cc if provision for foaming was not included. Foaming is achieved by incorporating either water or a low-boiling solvent such as Freon. The difference in these two techniques is as follows. The low-boiling solvent such as Freon does not enter into the chemical reaction but merely changes physical state from liquid to gas, due to the increased temperature of the exothermic reaction between the isocyanate and polyol. These temperatures can become quite high, generally about 100° C and sometimes as high as 165° C. Naturally the temperature depends on rate of foaming and provision for heat removal from the foam system. By not including catalysts to promote the isocyanate-polyol reaction and maintaining low initial temperatures, the reaction is moderated and much lower temperatures are encountered. The curing of the foam is not as readily completed under these circumstances. The use of water as a blowing agent involves a chemical reaction, as follows:



so that the products are an amine and CO<sub>2</sub> gas, which acts as the blowing agent. Thus it should be noted that void spaces in Freon-blown foam are filled with a Freon gas and in water-blown foam are filled with CO<sub>2</sub> gas. If the foam material enters into the chemical reaction of a detonating explosive that is incorporated, the effect of both the urethane and the gases present might be of consequence.

The amine that results in the case of water-blown foams will further react with the isocyanate to produce an urea:



The isocyanate can further react with the urea and the urethane of the primary reaction. Such further reaction is not of much consequence; however, of some concern is the possibility that the amine and possibly other intermediates would react with the explosive that is incorporated, such as nitroglycerine.

Four foam systems were utilized in the course of this investigation. They included two completely premixed systems: Nopco-foam\* and Isonate 323 (CPR)\*\*, which foamed to a pre-set density when the two portions that each system consisted of were combined; and two so-called one-shot systems: Voranol RN 490\*\*\* with Naccodate\*\*\*\* and Voranol with Papi\*\*\*\*\*, which foamed to whatever density was determined by the addition of a blowing agent (water or Freon) to the combined portions. These latter systems required the addition of a surfactant and, if desired, catalysts.

In the earlier phases of this work it was advantageous to use the one-shot systems since control of foaming density, rate, temperature, curing, and other parameters could be adjusted from experiment to experiment. However, it became convenient to fix these parameters so that the effects of type of explosive, degree of explosive loading, etc., could be determined without concomitant variations due to improper control of the previous parameters. Both the Nopcofoam and CPR systems contained Freon to achieve the desired foamed density, catalysts to promote the foaming action at the proper rate, and surfactants to control the size of the cells. In order to achieve a satisfactory foamed matrix it was necessary that the polymerization reaction and blowing action progressed simultaneously in a manner such that both were completed at the correct stage of the process; otherwise the foam broke apart with the cells growing out of control, or else the foamed matrix collapsed if the polymerization had not been completed at the correct time. Thus, the use of the catalysts was paramount and critical. The usual catalysts in these premixed systems are tertiary amines and

\*Nopco Chemical Company, Plastics Division, Los Angeles, California.

\*\*The Upjohn Company, CPR Division, Torrance, California.

\*\*\*Dow Chemical Company, Freeport, Texas.

\*\*\*\*Allied Chemical Corporation, National Aniline Division, N. Y.

\*\*\*\*\*The Upjohn Company, Polymer Chemicals Division, Kalamazoo, Mich.

organo-tin compounds such as stannous octoate and dibutyltin dilaurate. The polymerization, an isocyanate-hydroxyl reaction, was mainly controlled by the tin catalyst, and the foam action, an isocyanate-water reaction, by the amine catalyst. If Freon was used to attain foaming action, then such control was determined by the exothermicity attendant with the polymerization. It was recognized that certain amines, especially tertiary amines, are incompatible with certain explosives - especially nitroglycerine.

The preliminary polyurethane foam system selected for use in this work was a one-shot system for rigid in-place foaming based on Actol 52-460 Polyol\* (polyoxypropylene polyol with a hydroxyl number of 460) and Nacconate 4040 (modified toluene diisocyanate with an amine equivalent of 106). Water was used as the blowing agent, Silicone Fluid 113\*\* was used as surfactant, but N,N-dimethylethanolamine, a catalyst usually used with this particular system to promote the reaction, was omitted.

Preparation was as follows. The Actol, surfactant, water and explosive were mixed until a homogenous paste resulted, which was especially thick with the higher explosive density loadings. When all other preparation was made to receive the foamed explosive, the Nacconate was admixed and the system was placed into the appropriate interstitial spaces of the projectiles. Foaming was quickly attained, although with the heavily-loaded explosive foams curing required longer periods of time. All explosive charges were based on the total foamed volume and the explosive content; e.g., with 50-g PETN added and a foamed volume of 500 cc, the PETN density was reported as 0.1 g/cc. This particular foamed system without explosive attained a density of about 0.15 g/cc.

Later in this work the Actol became unavailable and was substituted by a similar amine equivalent polyol (Voranol). Also, use was made of Freon 11 as blowing agent, as a substitute for or in combination with water in order to improve the foamability of the system.

PETN of different particle size resulted in differing bulk densities. Earlier experiments had established that a fine 10-to-12-micron PETN was best suited for foamed-explosive applications. However, this type PETN had a low bulk density which precluded attainment of explosive-loading densities greater than 0.1 g/cc. The following described technique aided, to some extent, in countering this difficulty. The polyol was prepared by adding appropriate amounts of the surfactant, Freon, and isocyanate. PETN was then stirred into this combined mixture, more readily than before because the liquid portion now was about doubled. After the PETN had been completely added, the appropriate amount of water was quickly mixed in. Foaming commenced very shortly.

\*Allied Chemical Corporation, New York, N. Y.

\*\*Dow Corning Corporation, Midland, Michigan.

Two Nopcofoam systems, designated as 0.03 and 0.10 g/cc, were utilized. Initial foamed-nitroglycerine (NG) evaluation was attempted with this type foam because (1) the procedure was simple and reproducible and (2) this foam was pure white and readily indicated decomposition and/or associated reactions. It immediately became evident that decomposition would present a problem. Urethane foams are the most efficient insulators known in the industry. Thus, any exothermicity attendant with the reaction becomes adiabatic and can cause the foam to self-ignite. Several foamed-NG systems caused a high degree of NG decomposition, and in several instances these systems ignited. It is not certain whether this was due to thermal decomposition of the NG from the exothermicity of the foaming reaction or to a chemical reaction between the NG and a component of the foam system, or to a combination of both.

It was extremely difficult to mix substantial amounts of dry nitrocellulose (NC) with the foam materials. Thus, the addition of NG to the NC proved to be advantageous; namely the liquid state of NG allowed greater amounts of NC to be utilized, and an increased explosive loading was readily attained. Numerous combinations of NC and NG were investigated. Initially NG or 75% NG in triacetin was added to the combined foam materials, and then dry NC was added in maximum proportion tolerated by the system. In this manner explosive loading levels to 50% explosive were attained. Although the amount of liquid NG that could be added to the foam materials was physically unlimited, above about 33% NG the foaming action was completely inhibited. Later experiments indicated that it was more advantageous to add combined NC and NG to the unreacted foam materials. However, high loadings of NC-NG also inhibited the foaming action; thus, promoting the foaming action by the addition of water became expedient. A further development was the addition of wet NC-NG to the foam materials, in lieu of water and dry explosive. The advantages here were (1) the wet NC-NG was much more readily mixed into the unreacted foam materials and to a greater loading level and (2) the hazards associated with the handling of dry explosive were eliminated. However, the overall effects of explosive foams prepared in this manner are not completely understood.

Foamed HMX was prepared with the CPR foam system. The particular system used foamed to a predetermined density of 0.07 g/cc without any explosive being added. The HMX used was in the form of long thin needles 2-3 microns in diameter by 20-50 microns long, and as shown in Figure 4 had a rather pronounced effect on the density of the foam in the final foamed charge. The points in the figure were taken from actual foamings of this HMX, and the curve represents a design curve for proper selection of the weight of foaming agents required to achieve a final explosive density. Some HMX was recrystallized and consisted of uniform spherical crystals 50-microns in diameter along with some 60-micron crystals. Figure 5 shows the design curve for the preparation of foams utilizing recrystallized HMX. In contrast to what was observed in Figure 4, the recrystallized HMX did not have as pronounced an effect on the density of the foam. This was attributed to the coarser HMX.

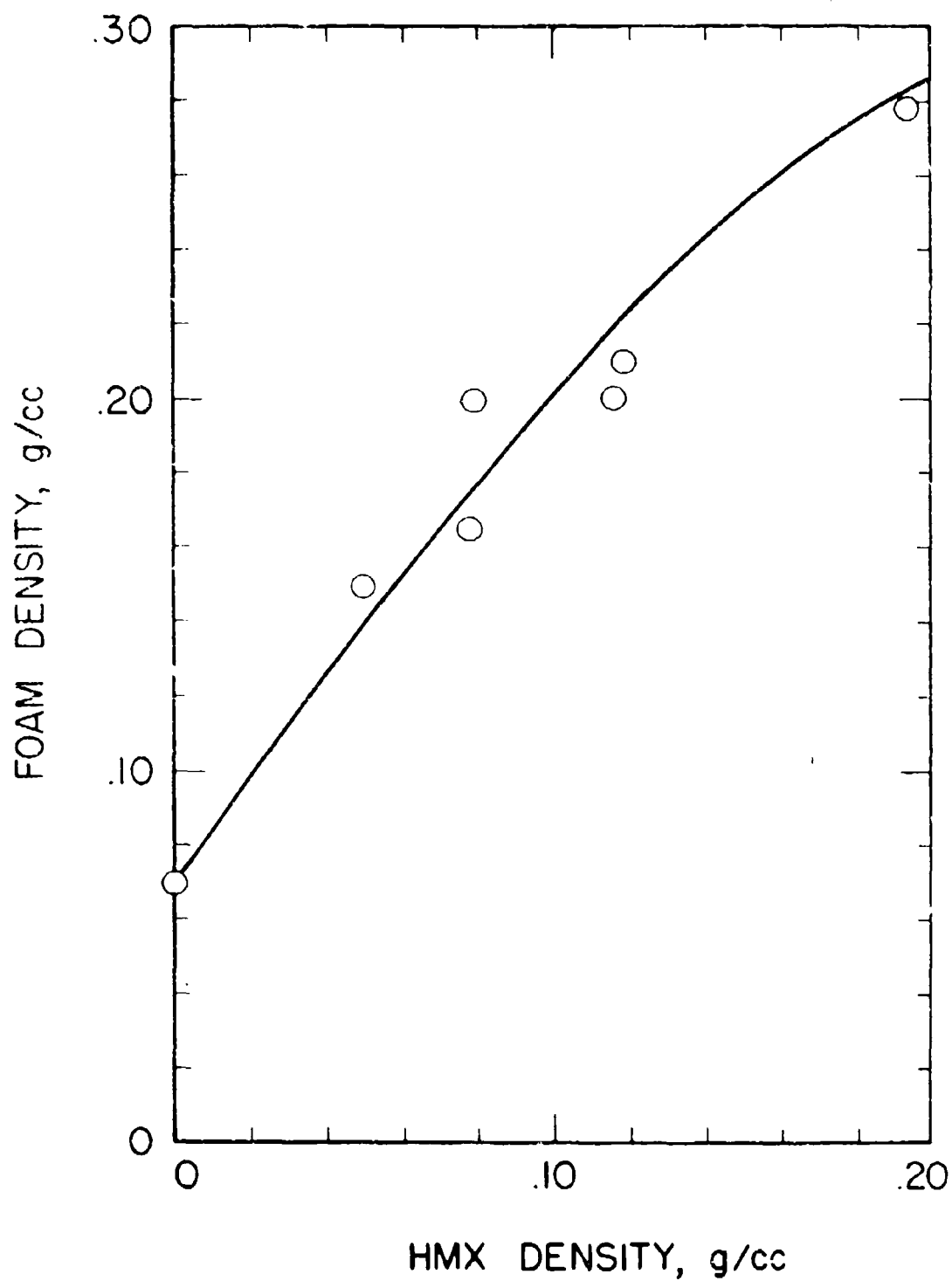


Figure 4

DESIGN CURVE FOR PREPARATION  
OF FOAMED HMX UTILIZING IITRI HMX AND ISONATE CPR 323



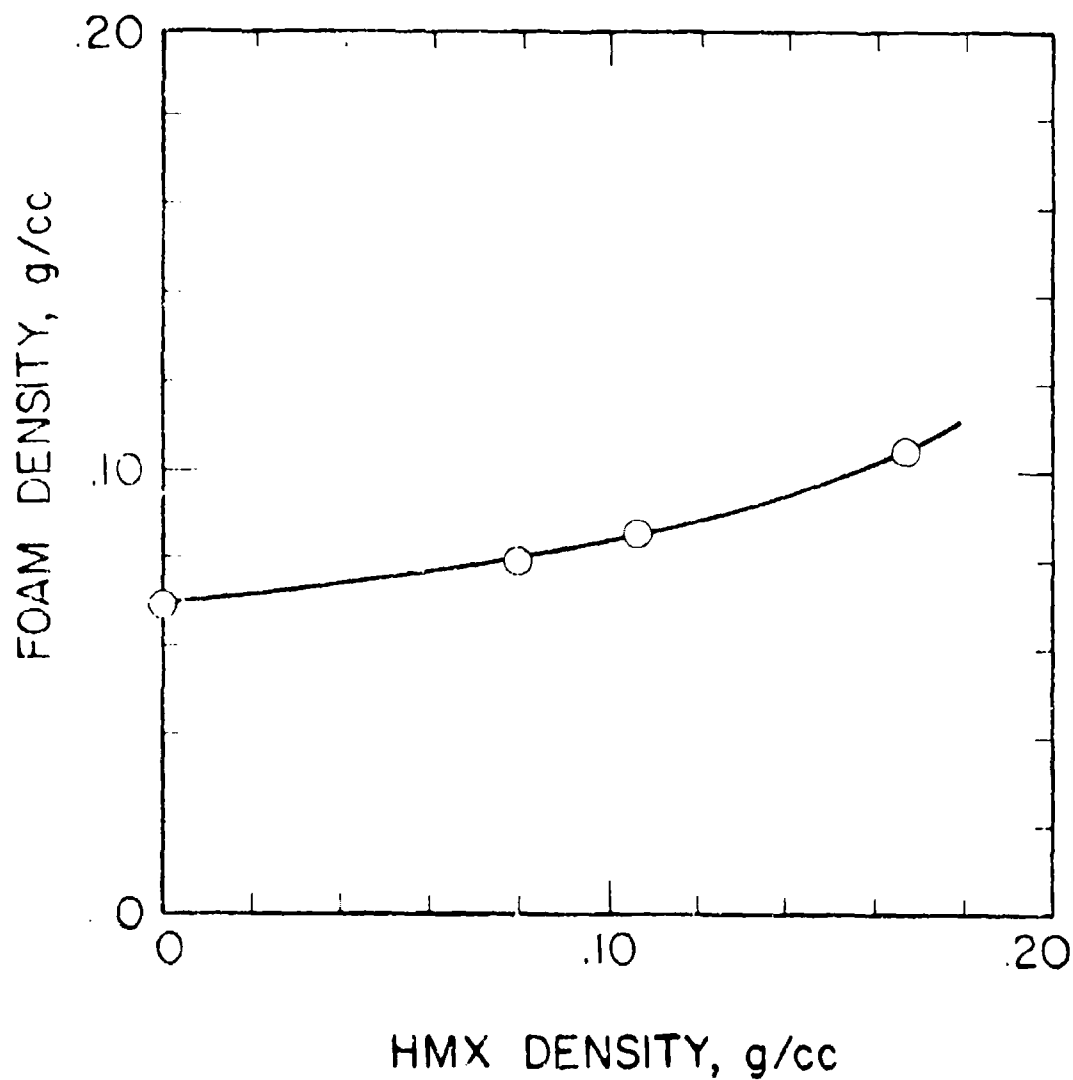


Figure 5  
DESIGN CURVE FOR PREPARATION  
OF FOAMED HMX UTILIZING RECRYSTALLIZED HMX AND ISONATE CPR 523

## EXPERIMENTAL MODELS

Figure 6 illustrates the experimental model, based on a tetrahedral cell, and the alternative model, based on a rhombohedral cell. For the experimental model, three solid-steel spheres were secured with bolts to the steel base plate, and a loose sphere was then placed on top of and into the "pocket" of these three spheres. For the alternative model, four solid-steel spheres were secured to a steel plate and the loose sphere was placed into the "pocket" of these four spheres.

Typical tests were conducted with either model as follows. The explosive or pyrotechnic was loaded into the interstitial space, and the loose ball was placed into the pocket. In the case loosely-packed explosive or pyrotechnic, the bottom openings were enclosed with heavy aluminum foil. Directly beneath the loose ball was a  $\frac{1}{2}$ -in. hole in the steel plate to accommodate the igniter. A No. 6 EBC was used in tests with explosives. In the case of pyrotechnics, an electric initiator was utilized. Figure 7 illustrates this initiator, which has a 5-amp, 5-watt no-fire and 15-amp all-fire capability (Ref. 7).

The original experimental model, termed the 3-ball-pocket model, was chosen because (1) it represented the worst condition of pressure loss due to venting and (2) it represented the least destructive technique of investigation. If the spheroids or other projectiles were destructed or heavily damaged in this model, they most likely would be damaged more so in a practical application. In practice, the spheroids would be interior to the explosive and subject to much more severe shock stresses and the mutual interaction of neighboring spheroids (Ref. 3).

The 3-ball-pocket model served well in the early phases of this work. However, initiation of detonation in this model became problematical with very-low-density foamed explosives (including foamed PETN), which required adequate boosting over a sufficiently large area. Thus for a realistic evaluation of these explosives the 3-ball-pocket model was modified as follows. Instead of a  $\frac{1}{2}$ -in. diameter hole in the plate to accommodate a No. 6 EBC, a 2-in. diameter hole was made. In addition, a 2-in. I.D. by 2-in. long section of tubing was taped to the bottom of this hole, i.e., as an extension of the hole. Foamed explosive then filled the interstitial space, the hole in the plate, and this 2-in. long extension. Detonation was then initiated at the open-ended bottom of the tube extension by utilizing a 2-in. diameter C4 sheet explosive booster. This modified 3-ball-pocket model is illustrated in Figure 8.

Figure 9 illustrates the prototype model. This model was a unit rhombohedral packing cell, composed of six 4-ball "pockets" and eight 3-ball "pockets", with a total of 14 balls. For these

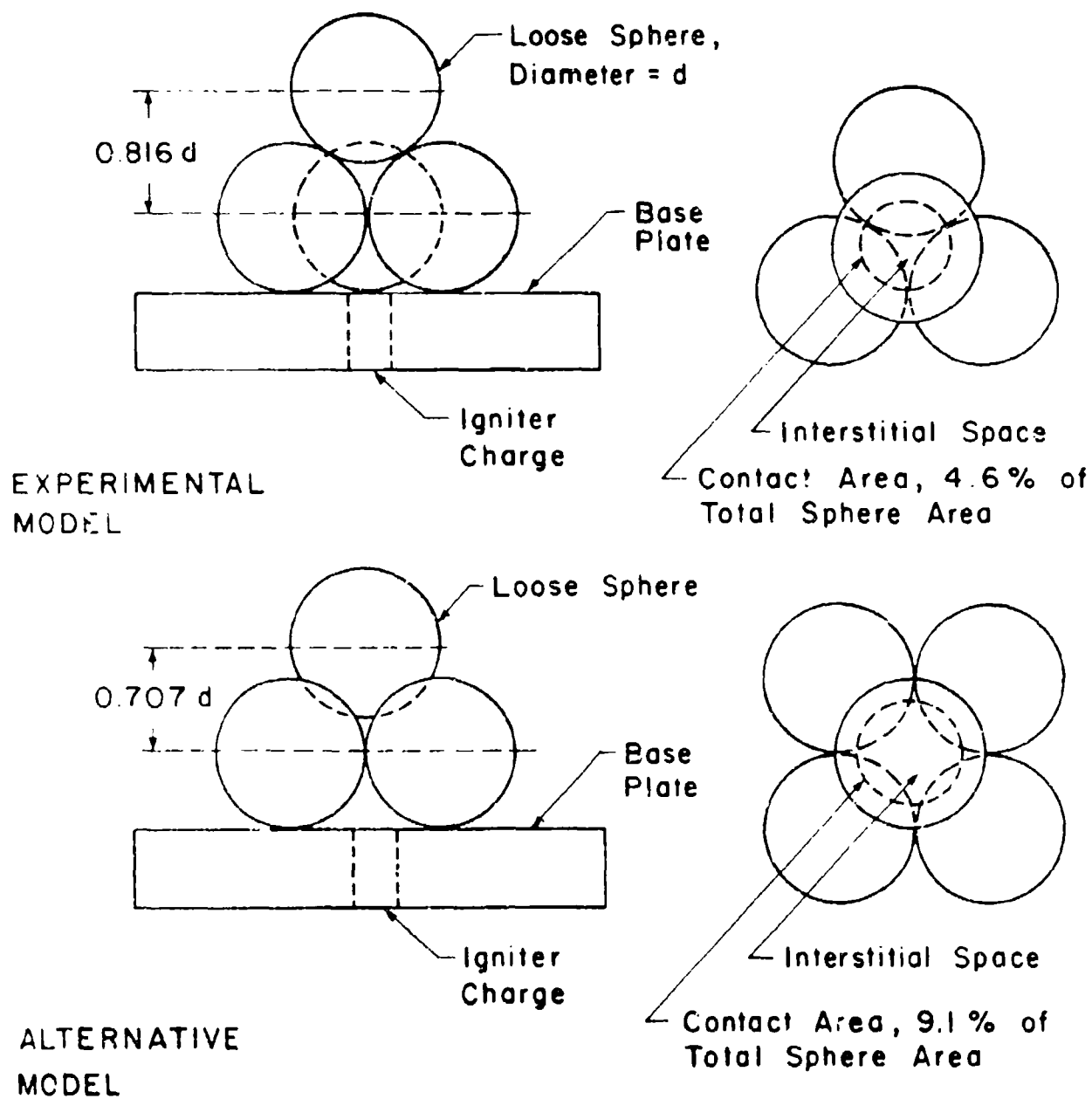


Figure 6  
EXPERIMENTAL AND ALTERNATIVE MODELS

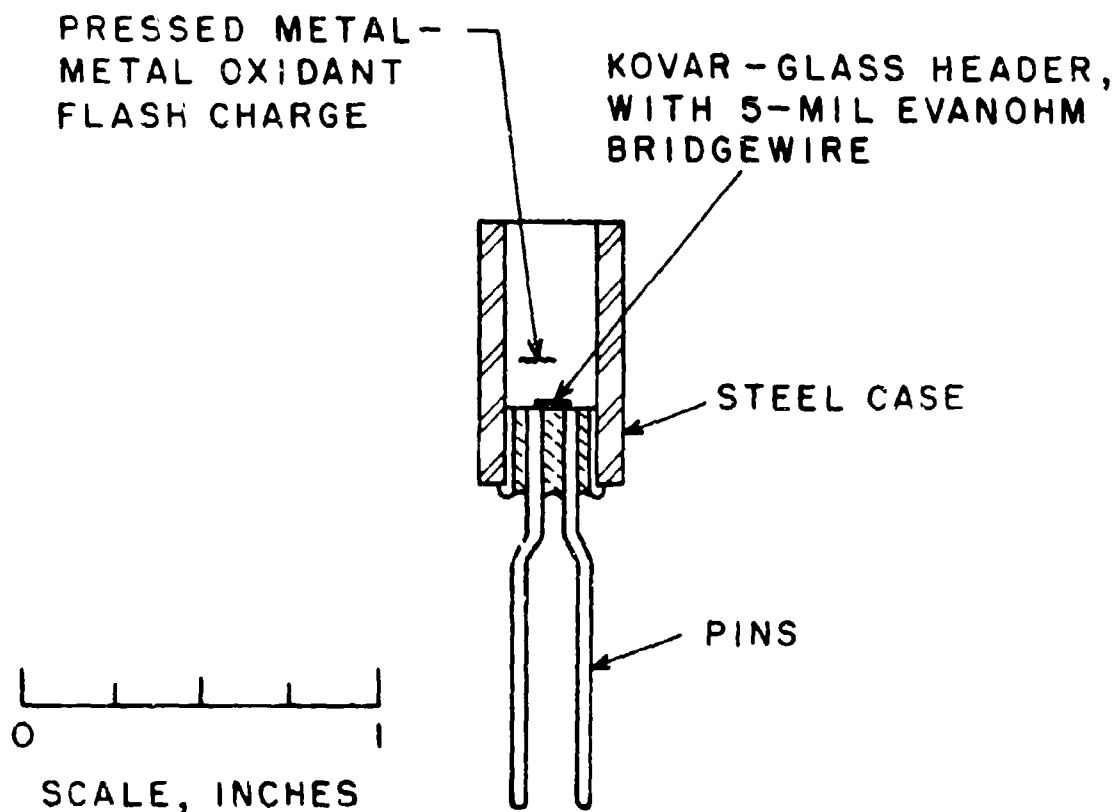


Figure 7

ELECTROEXPLOSIVE DEVICE

(Nominal bridge resistance = 0.20 ohm.  
EED has 5-amp, 5-watt no-fire capability.)

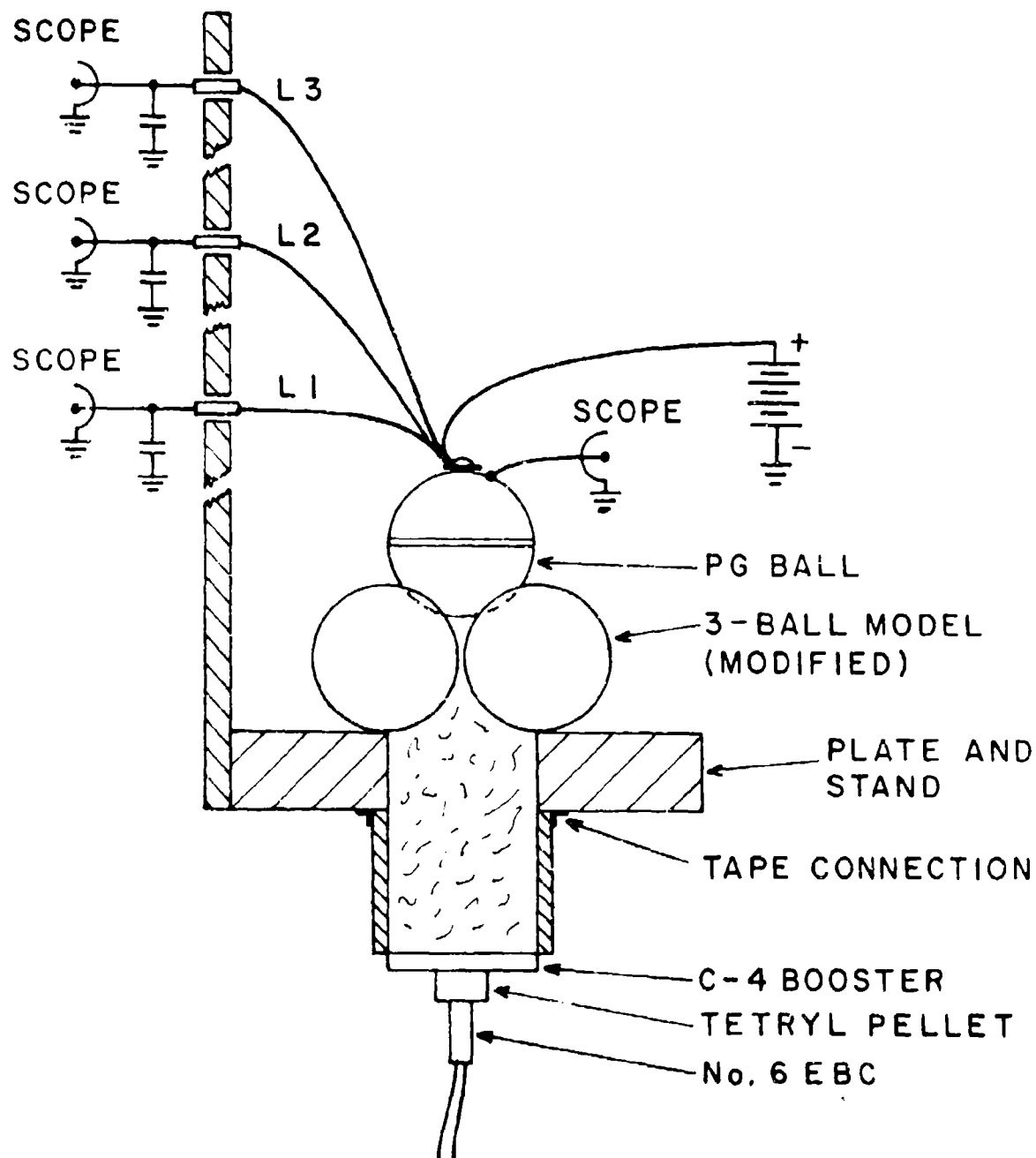
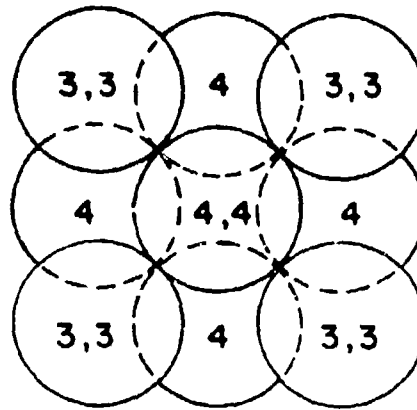


Figure 8  
MODIFIED 3-BALL-POCKET MODEL



Top, Side, and Bottom View of 14-ball Prototype Model

Eight balls sit in a 3-ball pocket

(Four of these are seen in the top layer, the other four are directly below these four balls but in the bottom layer; thus 3,3 represents two 3-ball pocket balls.)

Six balls sit in a 4-ball pocket

(Five of these are seen, one in the top layer and four in the middle layer; the sixth one is in the bottom layer, directly below the center ball of the top layer; thus 4 represents one 4-ball pocket ball and 4,4 represents two 4-ball pocket balls.)

Figure 9  
PROTOTYPE 14-BALL MODEL

tests the spheroids were used, and they were packed appropriately into a 6-in.-cubed box made from 1/8-in. Plexiglass. Two candidate materials were evaluated with this model; loosely-packed Al-KClO<sub>4</sub> pyrotechnic and foamed PETN of about 0.15 g/cc explosive loading. The tests were conducted as follows. The spheroids were painted, marked, and placed into the Plexiglass box with an open top. The explosive or pyrotechnic was loaded at the same time as the spheroids were inserted. The appropriate igniter was placed inside the one large space at the center that constituted the six 4-ball "pockets". Additionally, a booster of about 5 g loosely-packed PETN was used around the No. 6 EBC for initiation of the foamed PETN.

Figure 10 illustrates the modification to the 14-ball model that was made later in this work to evaluate other highly insensitive, low-density foamed explosives such as foamed NC-NG. This modification was similar to that required for the 3-ball-pocket model, i.e., the detonation was initiated in a 2-in. I.D. tube and brought into the interstitial space. It was determined that sufficient boosting to initiate the detonation within the interstitial space would nullify the results of the experimental model, as the size and energy of the required booster would override the effect of the foamed explosive in the interstitial space. However, it should be noted that in this modified model the detonation was directed toward the top center ball (No. 1) and away from the four lower balls (Nos. 10, 11, 12, and 13).

#### INSTRUMENTED PRESSURE-GAUGE BALL

Shock loading of projectiles by detonating explosives results in very high pressures and very short load times. There is no known way of measuring the pressure-time relation experimentally in the case of standard high explosives because of the very high detonation pressure, which exceeds the yield stress of any material. However, with the reduced detonation pressures resulting from low-density explosives and the inherent moderating effect on a spherical gauge (force is proportional to applied pressure on a time-dependent area) measurement of pressure in the several-kbar region becomes amenable.

Such a technique was developed in this work. The projectile ball was cut in half and resecured with insulated hardware to maintain electrical separation between the two halves. In between the two halves, at a contact area of 2.15 in.<sup>2</sup> (allowing for use of "O" rings) a pressure-sensitive material was located. Carbon, graphite, tellurium, and other combinations were tested, with some degree of success. However, for the sake of expediency a commercial pressure-sensitive paint was utilized. This material, called "Micro-Ducer" paint\*, is available in many types. Type R-4, the highest-pressure type available, will sense pressure to about

\*Advance Components Corporation, Clark Electronics, Santa Ana, Cal.

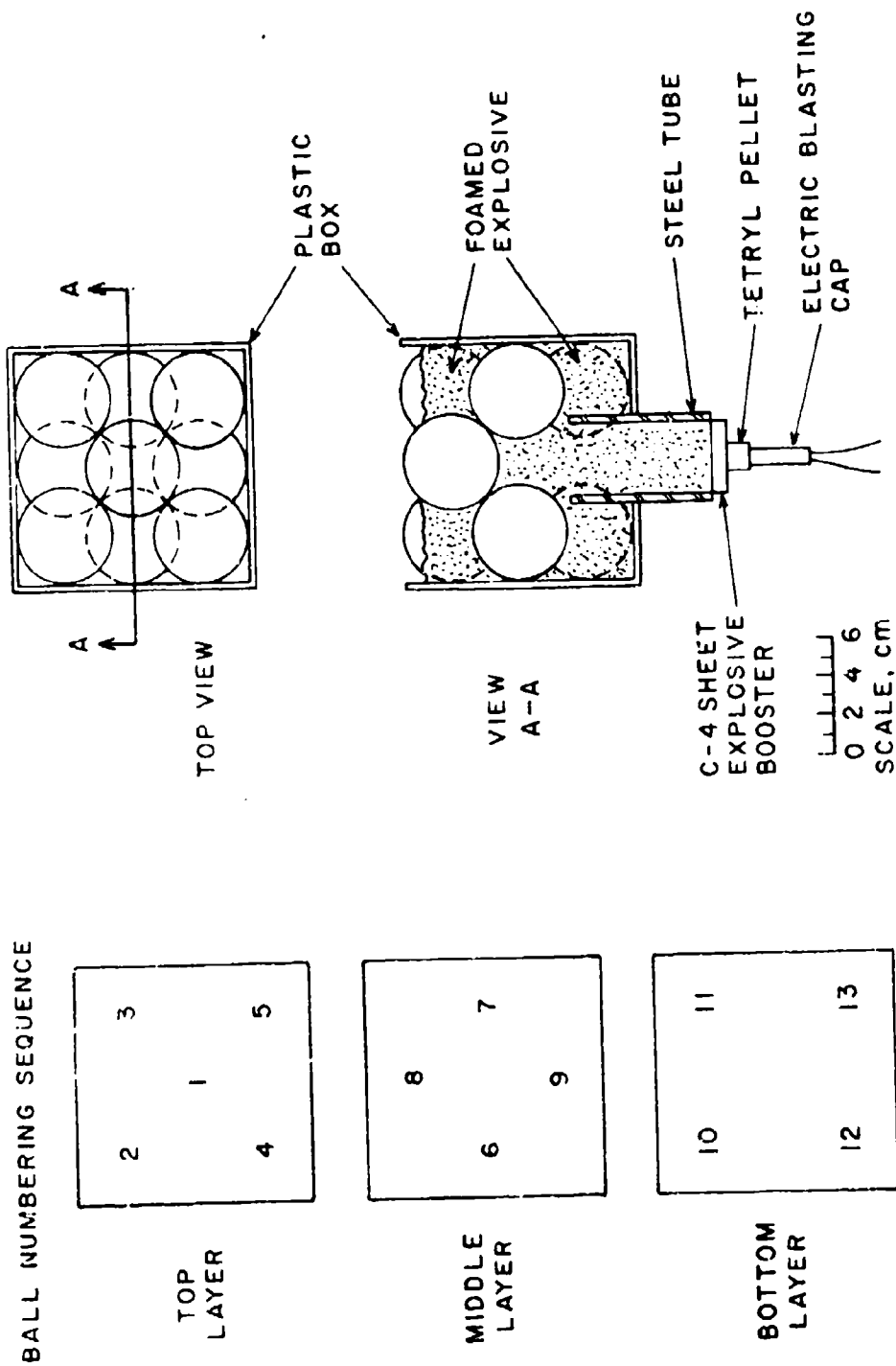


Figure 10  
MODIFIED 14-BALL PROTOTYPE MODEL



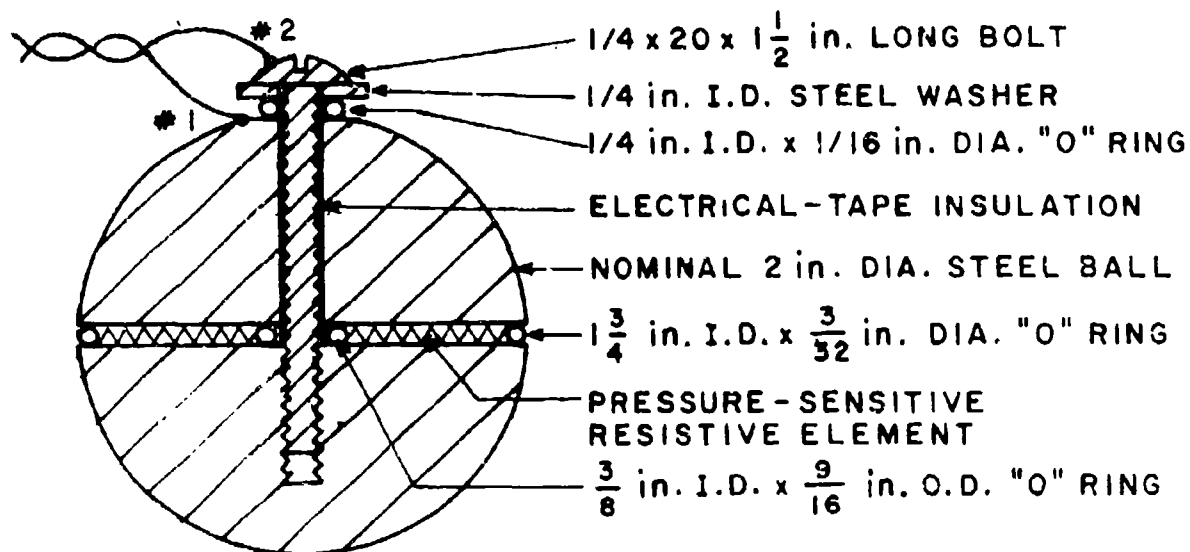
35,000 psi, or 2 to 3 kbar. Use of larger balls would allow increase of this pressure measurement, since the ball is the pressure gauge, referred to hereafter as the PG ball. The 2-in. diameter PG balls utilized in this work (Figure 11) measured pressure to about 150,000 psi. This contrasts to the 35,000 psi specified for this material.

Before being used, the PG balls were tested on a hydraulic press to static loads in excess of 40,000 psi with good results. The maximum pressure response in actual tests with explosives resulted in pressures to 144,000 psi upon the gauge surface, which is equivalent to 25,000 psi upon the whole ball surface (when the ball is totally immersed in pressure). It is not known whether the full capacity of these gauges has been exceeded, or even approached. After all the explosive evaluation tests were conducted on a specific PG ball, the PG ball was rechecked on a hydraulic press to static loads of over 400,000 lbs, or nearly 200,000 psi. The results are reported, and used as a calibration, in Figure 12. Above 250,000 lbs, at 3 volts output, permanent deformation set in and the gauge went off calibration. It is conceivable that a transient pressure beyond this "yield" point, such as is experienced in explosive shock loading, would not cause permanent deformation. The PG ball became loosened between explosive tests, especially with the more energetic explosive systems, and required retightening before reuse. The resistance was checked prior to all tests to determine tightness and effectiveness, and remained consistently at about 25 megohms.

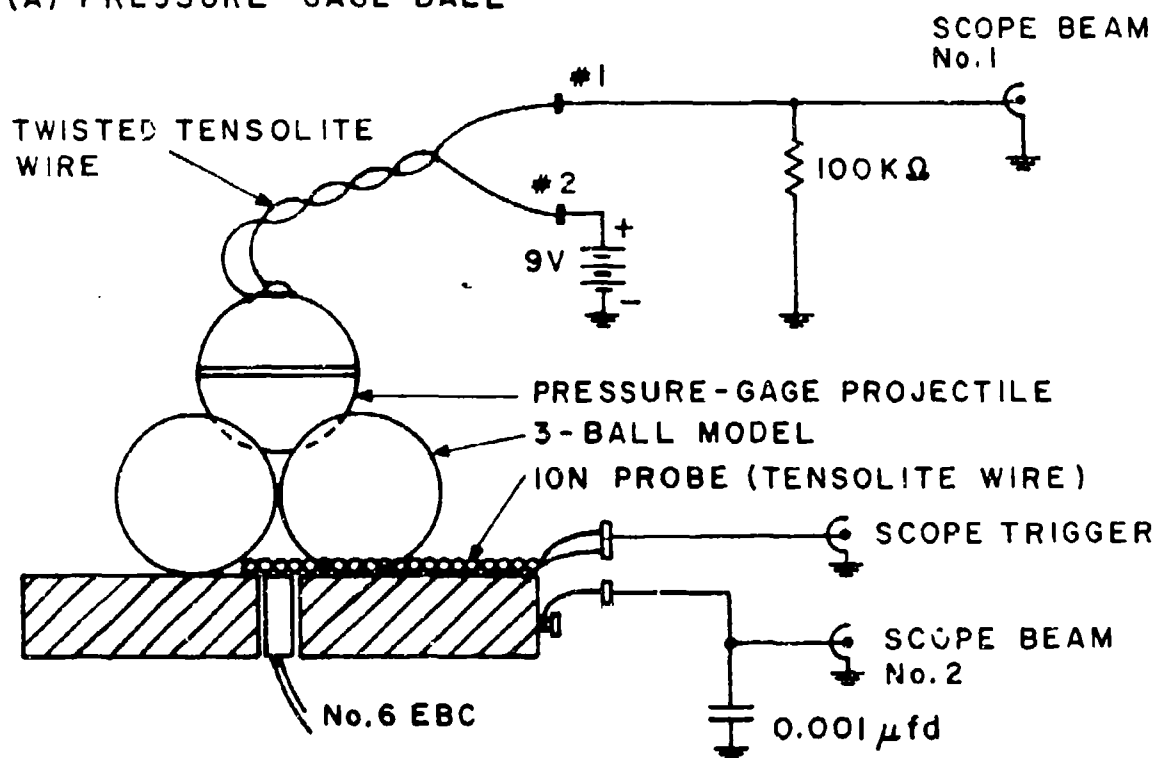
Figure 11 also illustrates the fully instrumented experimental model and PG ball. The following information was directly available (assuming correct calibration) from tests with this experimental set-up: (1) detonation velocity, (2) particle "free surface" (or air shock) velocity, dependent on test conditions, (3) force-time and acceleration-time relationships, (4) time to initial motion (including time to overcome inertia forces), (5) projectile velocity, and (6) probably yield stresses in the projectile and/or other pressure effects including factors pertaining to elastic/plastic behavior (Ref. 8). This PG gauge will be fully described in a future publication (Ref. 9). Figure 13 is similar to Figure 12, except that the basis in Figure 13 is PG-ball acceleration correlated with voltage output.

#### EXPERIMENTAL RESULTS

Results of tests conducted in the early phases of this work are reported in Table 1. The initial tests (1 through 9) in the table were conducted with loosely-packed explosives and pyrotechnics. Tests 1 through 5 were conducted with the first 3-ball-rock-ot model. In these tests loosely-packed PETN, Al-KClO<sub>4</sub>, and tetryl were evaluated. The test in which tetryl was utilized caused fragmentation of the stainless-steel test ball and extensively damaged the 1/2-in. thick stainless-steel base plate (Figure 14).



(A) PRESSURE-GAGE BALL



(B) 3-BALL MODEL TEST FACILITY

Figure 11  
INSTRUMENTED 3-BALL-POCKET MODEL TEST FACILITY

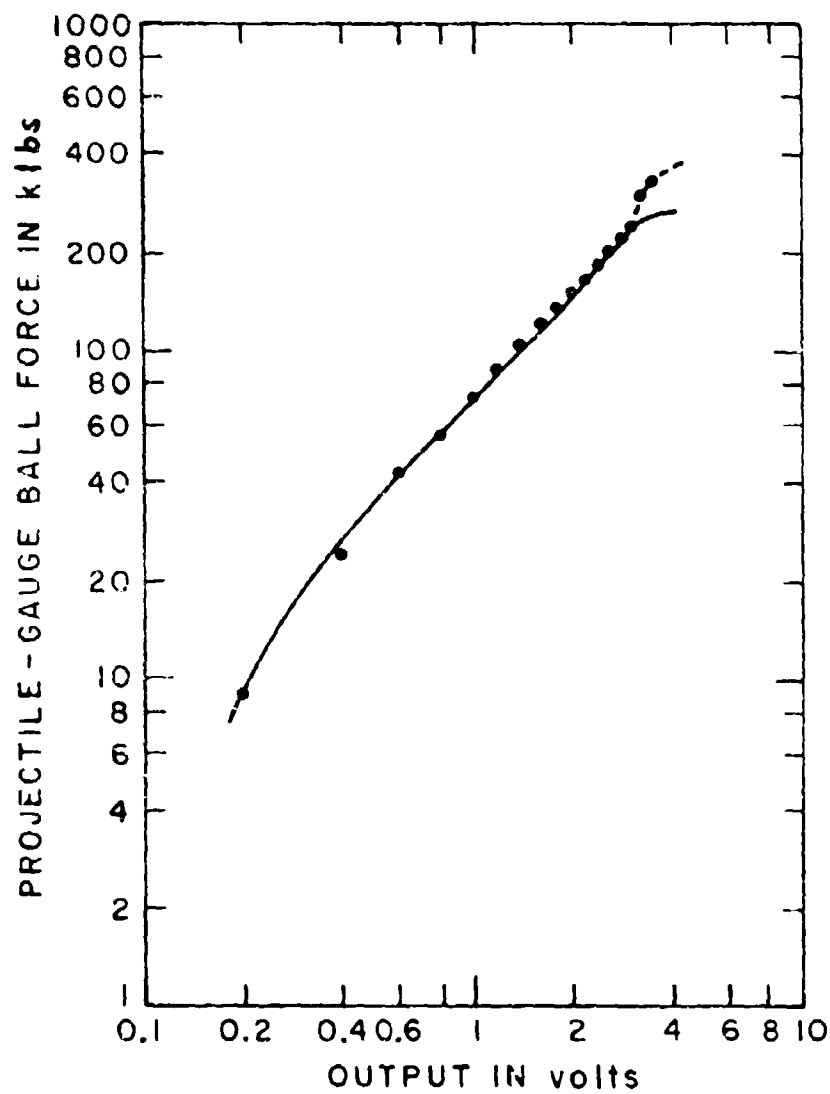


Figure 12  
PRESSURE-GAUGE BALL STATIC CALIBRATION  
WITH HYDRAULIC PRESS

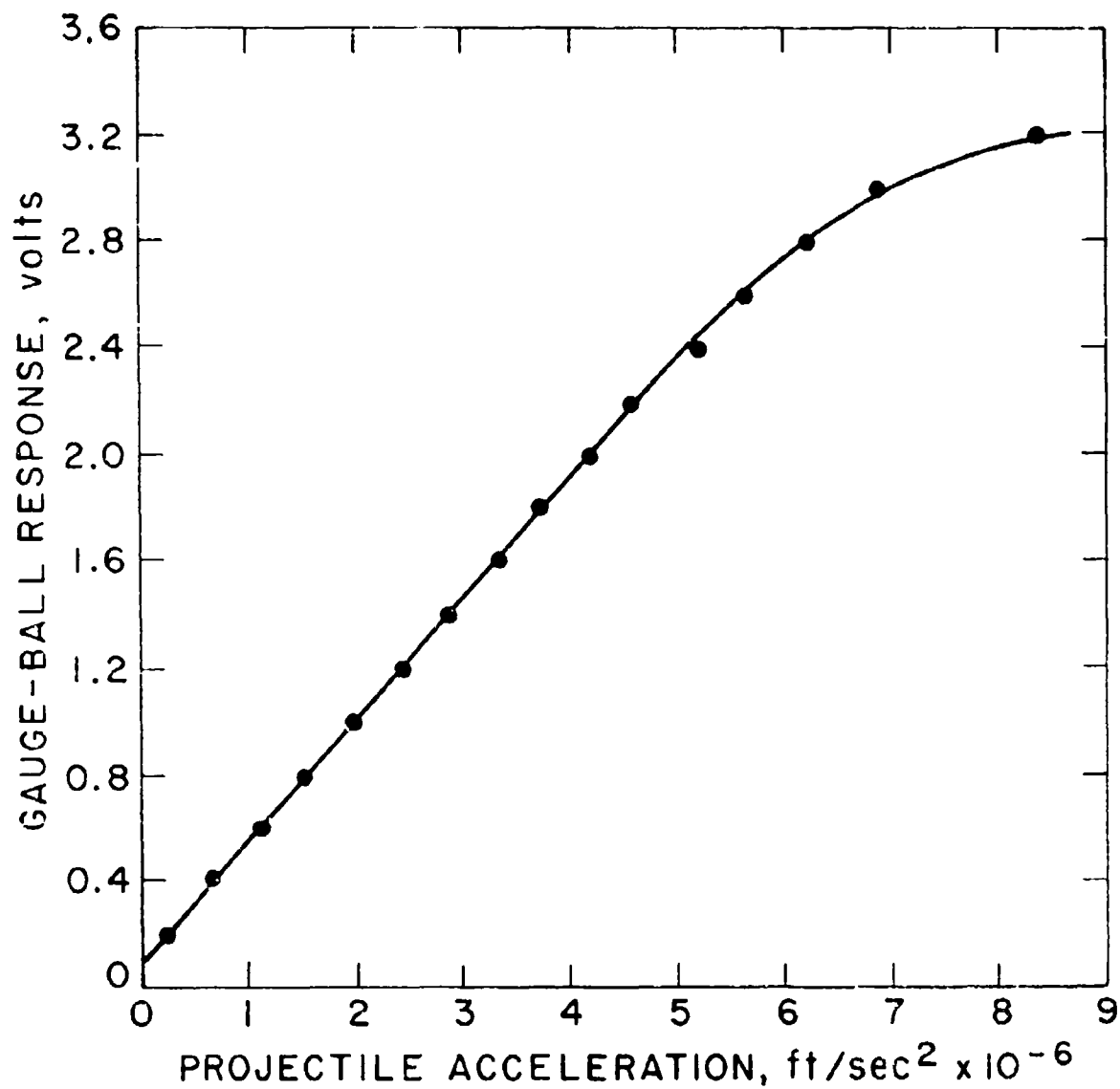


Figure 13

PRESSURE-GAUGE BALL RESPONSE-TO-ACCELERATION CORRELATION  
(Based on  $m = 0.0358 \text{ lb-sec}^2/\text{ft}$ )

Table 1

Dispersion of Various 2-in. (nominal) Spheres by Interstitially Loaded Explosive Materials

Test No.	----Explosive-----		---Projectiles---		Fastax	-----Results-----	
	Type	Density <sup>a</sup>	No	Type Model <sup>b</sup>		Velocity	Damage
	material	g/cc			use	ft/sec	
1	PETN	0.3 L	1	2 1/2" steel	yes	unknown	none
2	Al-KClO <sub>4</sub>	1.1 L	1	2 1/2" steel	yes	unknown	none
3	Al-KClO <sub>4</sub>	1.1 L	1	2 1/2" steel	yes	unknown	none
4	PETN	0.3 L	1	2 1/2" steel	yes	26	none
5	Tetryl	1.3 L	1	2 1/2" steel	yes	74	destroyed
6	Al-KClO <sub>4</sub>	1.1 L	1	2 1/2" steel	yes	76	none
7	PETN	0.3 L	1	2" steel	yes	55	none
8	PETN	0.3 L	1	2" spheroid	yes	100	destroyed
9	PETN	0.3 L	1	1.75" rubber	yes	220	destroyed
10	PETN	0.02F	1	2" steel	no	≈ 0	none
11	Blank	0.0 -	1	2" steel	no	0	none
12	PETN	0.08F	1	2" steel	yes	≈ 0	none
13	PETN	0.2 F	1	2" steel	no	≈ 35	none
14	NH <sub>4</sub> ClO <sub>4</sub>	0.1 F	1	2" steel	no	0	none
15	Al-NH <sub>4</sub> ClO <sub>4</sub>	0.1 F	1	2" steel	no	≈ 10	none
16	E-NH <sub>4</sub> ClO <sub>4</sub>	1.1 L	1	2" spheroid	no	0	heated
17	Al-NH <sub>4</sub> ClO <sub>4</sub>	1.1 L	1	2" spheroid	no	0	heated
18	Al-PETN	0.2 F	5	spheroids	yes	0	none
19	Al-KClO <sub>4</sub>	1.1 L	5	spheroids	yes	>180	distorted
20	Al-KClO <sub>4</sub>	1.1 L	1	spheroid	no	>100	distorted
21	PETN	0.2 F	5	spheroids	yes	10	none
22	PETN	0.16F	14	spheroids	yes	>500	distorted
23	Al-KClO <sub>4</sub>	1.1 L	14	spheroids	yes	200-500	distorted
24	PETN	0.12F	14	spheroids	yes	200-500	distorted

<sup>a</sup> L = loosely-packed powder load and F = foamed explosive material load<sup>b</sup> 3 = 3-ball-pocket, 4 = 4-ball-pocket, 9 = 9-ball scale-up, and 14 = 14-ball prototype models



### DAMAGED 3-BALL POCKET EXPERIMENTAL MODEL

Plate : 0.5 in. stainless steel  
Bolts : 0.5 in. diameter steel  
Balls : 2.25 in. diameter stainless steel  
Test : No. 5 using 29g loosely-packed tetryl

Note : The secured balls were blown off - one  
was recovered 500 ft. from the test site.

Figure 14  
DAMAGE TO THE EXPERIMENTAL MODEL CAUSED  
BY HIGH EXPLOSIVE DETONATION

The explosive contact area in the 3-ball-pocket model was only 25% of the total sphere cross-sectional area; in the 4-ball-pocket model, this explosive contact area was increased to about 47% (see Figure 6). It was postulated that as a result of this the velocity attained in the 4-ball-pocket model tests should be about twice as great as that in the 3-ball-pocket model tests. In addition, based on density variation, it was postulated that the spheroid should attain a velocity of almost twice (1.85) that of a similarly-sized, solid-steel ball. Comparison of test No. 4, the 3-ball-pocket model with a steel ball; No. 7, the 4-ball-pocket model with a steel ball; and No. 8, the 4-ball-pocket model with a spheroid indicates respective initial velocities of 28, 55, and 100 ft/sec, in relatively good agreement with the postulations.

In comparison of tests Nos. 4 and 9, it was noted that the density of the steel ball in No. 4 was 7.80 g/cc and that of the rubber ball in No. 9 was 1.44 g/cc. The density factor was about 4.5, as discussed earlier with reference to Held's work. However, the size of the rubber ball was smaller so that the explosive contact area for the smaller cross-sectional area rubber ball increased by a factor of 1.67, resulting in an overall factor of  $4.5 \times 1.67 = 8$ . Thus the postulated velocity of the rubber ball in test No. 9 from the results of test No. 4 was  $8 \times 28 = 225$  ft/sec. The resultant velocity of about 220 ft/sec in test No. 9 was unerringly close.

These tests sufficed to confirm the postulated effects of density, size, and model characteristics. In particular, the main variation of these models to that system used in Held's work was geometrical, with the size of the balls being a secondary but extrapolatable variation. With an explosive charge loading of 32 mm in diameter and 58 mm deep and balls between 2 and 7 mm in diameter, the surface of the explosive can be considered infinite as pertains to the balls. However, in the case of the 3-ball-pocket model used in our work, the sphere cross-sectional area that can be considered as recipient of direct force is only 25% of the total sphere cross-sectional area. In addition, the center of mass is exterior of the explosive. For a 57 mm diameter steel ball (see Figure 2) the extrapolated velocity is 330 ft/sec. Taking into account a 25% cross-sectional area, and a 10% loss due to exterior center of mass (see Figure 3), the postulated velocity should be about 75 ft/sec. This value is in excellent agreement with the 76 ft/sec obtained in test No. 5 in which tetryl was utilized, the most potent explosive evaluated with the most destructive results.

Results of the first scale-up model (not illustrated here) pertaining to foamed PETN with aluminum additive (test No. 18) and foamed PETN at 0.2 g/cc (test No. 21), indicated failure. The foamed systems using a No. 6 EBC did not detonate in either case. It is now believed that failure resulted because of (1) use of coarse PETN and (2) inadequacy of the No. 6 EBC to cause propagating detonation in the foamed explosive. Test No. 19, however,

with the  $\text{Al-KClO}_4$  pyrotechnic, proved very successful. One of the spheroids was picked up 1,000 ft from the test site, which implies a minimum initial velocity of 180 ft/sec if no friction and an optimum  $45^\circ$  trajectory is assumed.

Foamed fine-grade PETN in tests Nos. 22 and 24 at 0.16 and 0.12 g/cc, respectively, and loosely-packed  $\text{Al-KClO}_4$  in test No. 23 all performed exceptionally well with velocities in the range of 200 to 500 ft/sec, as determined by Fastax camera coverage. Because the spheroids were essentially "embedded" in the explosive or pyrotechnic in these experiments the explosive contact area was equal to the spheroid cross-sectional area. Again, an extrapolation from the data in Figure 2 would indicate initial velocities of about 500 ft/sec. Note that these velocities were attained, in particular with a foamed explosive at a loading density almost two orders of magnitude lower than the Compound B explosive utilized in Held's work!

The 14-ball model at 120 cc/ball gave a total ball volume of 1680 cc; in rhombohedral packing the interstitial volume would have been 560 cc. The actual interstitial volume used in these tests was about 150 cc for the  $\text{Al-KClO}_4$  and about 350 cc for the foamed PETN, with which excess foamed explosive oozed out of the actual interstitial spaces to exterior spaces. In the case of the foamed PETN, the total explosive weight was about 60 g, including the 5-g booster charge. This amounts to about 4 g per spheroid, which was specified in the introduction of this paper. Based on that calculation the efficiency was about 10%.

#### SUMMARY

The objective of this work was to establish feasibility of utilizing foamed explosives or pyrotechnics in the interstitial spaces of spheroids for the explosive dispersion of the latter at velocities up to 300 ft/sec without excessive damage to the projectiles. This was accomplished with both foamed PETN explosive and  $\text{Al-KClO}_4$  pyrotechnic.

It was established that high detonation velocities and pressures are not necessary for attaining high projectile velocities and, furthermore, cannot be tolerated because of the attendant damage to the projectiles.

Both Fadeenko and Held indicated that the initial velocity of solid balls, projected by the detonation of an explosive, is dependent on, among other things, ball size and density. Figure 2 illustrated the results of Held's study, indicating by extrapolation that for a nominal 2-in. diameter spheroid the initial velocity, and possibly the maximum velocity (without spalling and fracturing), should be 500 to 600 ft/sec under maximum conditions of high explosive, planar detonation, etc.



High explosives, such as PETN, can be diluted by foaming or other techniques so that shock velocities and pressures are attenuated sufficiently to preclude brisant effects, such as fragmentation, yet not degrade, and perhaps improve, impulsive characteristics. In such a manner PETN at a low density (0.1 g/cc and perhaps lower) does not excessively damage projectiles such as the spheroids, yet gives them an initial velocity in the neighborhood of 200 to 500 ft/sec. In addition, explosive pyrotechnic systems with characteristically low propagation velocities are equally proficient for such task.

As the projectile dispersing system is scaled up, the explosive charge increases accordingly. It is anticipated that cubed-root scaling factors would apply (except where the size of the projectile is small in respect to the explosive charge) and that the foamed explosives can be reduced to a minimum charge density that propagates a detonation and still would result in projectile velocities in the 200 to 300 ft/sec range.

#### REFERENCES

1. Dallovalle, J. M., "Micromeritics - The Technology of Fine Particles", Pitman Publishing Corp., New York - London, 1948.
2. Madeenko, V. I., "Projection of Spheres by Plane Layers of HE", NAVWEPS Report 9046, NOTS Tech Pub 4051, March, 1966.
3. Held, M., "Ballistics of Projectile Splinters", Explosivstoffe, 15, No. 12, 265-74, 1967. (Ger.).
4. Gurney, "The Initial Velocities of Fragments from Bombs, Shells, and Grenades", BRL Report 405, Sept. 1943.
5. Demiduk, G.P., "The Mechanism of Action of Explosion and Properties of Explosives", AD 633 490, DDC translation No. 1063.
6. Tulis, A. J., Austing, J. L., Johnson, C. D., and Blackburn, J., "On the Explosive Projection of Spherical Bodies", manuscript under preparation.
7. Austing, J. L., Kennedy, J. E., and Weber, J. P., "Ignition and Output Characteristics of Pyrotechnics for Electro-Explosive Device Applications", USNAD Report No. RTDR-131, Oct. 1, 1968.
8. Broberg, K. B., "Shock Waves in Elastic and Elastic-Plastic Media", KUNGL. FORTIFIKATION-SFURVALTNINGEN, Rap 109:12, 1956.
9. Tulis, A. J., "Novel Projectile Pressure Gauge for Continuous Pressure-Time Monitoring of Explosively Dispersed Projectiles", manuscript under preparation.

## PYROTECHNIC FLARE SPECTROSCOPY II

Bernard E. Douda\*

*Naval Ammunition Depot, Crane, Indiana 47511*

### ABSTRACT

The relative spectral radiant power distribution in the visible region is presented of flames of four different flare formulas and at environmental pressures of 760, 630, 300, 225, 150, 75, 30, and 6 torr. The spectra show the degree of sodium line broadening from these illuminating flames as the pressure and sodium atom density change.

### INTRODUCTION

The proceedings of the Second Pyrotechnic Seminar<sup>1</sup> report some of the progress made toward the interpretation of the spectral features of an illuminating flame. An experimental spectrum of a 10.8 cm dia magnesium-sodium nitrate flare, with fuel rich formula, burning in a 760 torr air atmosphere, was shown to be consistent with a theoretical model in which the flare flame is a system of thermally excited sodium atoms from which the radiant exitance is radically influenced by radiative transfer effects. Subsequently, experiments were conducted<sup>2</sup> to allow validation of the model at various ambient pressures and at differing sodium atom density in the flame. It is the general results of these experiments that will be described herein.

### EXPERIMENTAL

The relative spectral radiant power distribution in the visible region was obtained of flames from several different flare formulas at various environmental pressures. Normalized and log 10 plots will be presented, in summary form, to show the behavior of these flames as the pressure and sodium atom density change. Other parameters such as burning time, luminous intensity, and flame size were also recorded but are not included in this report.

PRECEDING PAGE-BLANK-NOT FILMED

## Experiment Design

Four different flare formulas of illuminating composition are tested at 8 levels of pressure; 760, 630, 300, 225, 150, 75, 30 and 6 torr. In most cases, four to seven spectra are obtained for each block of the formula vs pressure matrix, shown in Fig. 1.

## Test Flares

The test flares contain 50 g of a magnesium-sodium nitrate-binder mixture compressed into 3.3 cm i.d. by 5.5 cm long paper tubes, having formulas shown in Fig. 1. Formula group 24 is a typical<sup>3-6</sup> fuel rich formula. Groups 22, 25, and 26 are nearly stoichiometric mixtures, the sodium nitrate in groups 25 and 26 being about 0.1 and 0.01 of group 22 respectively. Stoichiometry is maintained in groups 25 and 26 by addition of potassium nitrate chosen because it reacts with magnesium at about the same rate as sodium nitrate and because of its reduced emission in the neighborhood of the sodium D lines, the region of interest for these studies.

## Spectral Distribution

The test flares are positioned in the approximate center of a 6 m<sup>3</sup> vacuum chamber, the flares burning cigarette fashion with the flame projecting upward. He-Ne CW and Ar CW lasers are used to maintain alignment of the spectrograph with the flare and chamber window and to provide wavelength calibration points.

A 3 m Jarrell Ash Model JA-78 spectrograph, fitted with a racking camera, using a 30 $\mu$  entrance slit, is positioned to view a 3 cm wide by 5 cm high region of the flame on the flare axis centered on a point about 3 cm above the burning surface. Kodak Linagraph Shellburst 35 mm film with typical usable range of 400 to 700 nm is exposed to the flare for a known period chosen to provide film transmission between 20% and 80% in the vicinity of the sodium D lines, the region of maximum interest. Multiple exposures of an irradiance standard are also recorded on the same film so that the upper and lower limits of film density of the flare spectrum are included in the film density range of the spectra of the irradiance standard. Densitometer traces of the standard are used to find the relationship between film transmittance and the flare relative radiant power as a function of wavelength. That relationship, representing a correction for transmittance of the spectrograph and chamber window and spectral sensitivity of the film, is applied to the flare densitometer trace to obtain the experimental relative radiant power spectrum for each flare. Although the power is not computed on an absolute basis, all the spectra form a consistent set and can be compared on a relative basis, the experimental parameters having been kept constant.

## Presentation of Data

Because of the large range (about 5 orders of magnitude) of radiant power and luminous intensity encountered during this experiment, the spectral plots were prepared in two ways. First, each spectrum is normalized so that its power maximum is unity as shown in Fig. 2. More of the spectral details are preserved on these plots. Secondly, each spectrum is plotted with the relative radiant power axis on a log 10 scale as shown in Fig. 3, ranging from -3 to +3. Visual comparison of these plots shows the large radiant power changes with pressure or sodium atom density changes.

Fig. 1 gives the wavelength scale in nanometers used to plot the data shown in Figs. 2 and 3. Groups 22 and 24 at 760 torr use a wavelength from 510 to 660 nm. Group 25 at 760 torr; groups 24, 22, and 25 at 630 torr; and groups 24 and 22 at 300 and 150 torr use a medium wavelength scale from 565 to 616 nm. The remaining spectra are plotted on an expanded scale of 585 to 593 nm.

Figs. 2 and 3 are a composite of a large number of spectra. The large size reduction required to make these figures makes the captions illegible. Full size reproductions of all of these plots, including relative luminous power distributions, are being published separately.

## DISCUSSION

A visual inspection of Fig. 2 will show how the flare spectrum and consequently the light output is affected by a change in ambient air pressure and/or sodium atom density in the flame. Before consideration of this behavior, several of the spectral features found in the spectra in Fig. 2 will be identified to prevent their confusion with the broadened sodium resonance lines.

### Spectral Features

Lines at 516.7, 517.2 and 518.3 nm which appear in the 760 torr spectra for groups 24 and 22 represent emission from elemental gaseous magnesium. The 550 nm shoulder (continuum) may be a Na/Mg interaction. The single line at 553.5 nm is the barium resonance line, barium being an impurity remaining from the boron-barium chromate ignition composition.

In all spectra, except those plotted on a wavelength scale from 585 - 593 nm, the doublet at 568.2 and 568.8 nm is due to the sodium  $3p^2P - 4d^2D$  transition. There is another sodium doublet, due to the  $3p^2P - 5s^2S$  transition, which appears at 615.4 and 616.0 nm in the 760 torr spectra of groups 24 and 22.

In the 760 and 630 torr spectra of group 25, there are two potassium doublets which appear as a quartet. These are due to the  $4p\ ^2P - 5d\ ^2D$  transition at 583.1 and 581.2 nm and the  $4p\ ^2P - 7s\ ^2S$  transition at 580.1 and 578.2 nm. In other spectra of flares containing potassium nitrate, these lines are outside the range of the plots.

The diffuse band, about 5 nm wide, with maximum near 574 nm in the 760 torr spectrum of group 25 is believed to be some form of potassium related emission.

### Sodium D Line Broadening

The sodium  $D_2$  and  $D_1$  resonance lines appear at 588.995 and 589.59 nm. It is the behavior of these lines with change of ambient pressure and/or sodium atom density that is of primary interest.

If we visually compare the spectra in Figs. 2 and 3 of group 24 (fuel rich) to group 22 (stoichiometric) at each pressure, we notice that their distributions are quite similar, except at 75 torr. Erratic burning was observed at the low pressures for all groups and particularly for group 24, the fuel rich formula. This may account for the observed inconsistency.

The spectral similarity between these two groups at each pressure level was expected, their calculated sodium atom densities, as shown in Fig. 4, being close to the same magnitude. The main reason for including the group 24 series in this experiment is because it is the formula typically used in illuminating flares.

Next we visually compare spectra of groups 22, 25 and 26 in Figs. 2 and 3 at each pressure. If we take the wavelength scale changes into consideration, it is clear that, at any constant pressure, as the sodium atom density in the flame changes by a factor of 10, there is a significant change in the spectral distribution, leading one to conclude that the distribution change is due mainly to the density change. Computed densities and adiabatic temperatures are given in Fig. 4.

Finally, by visual inspection of Fig. 2, we can deduce the influences that sodium atom density and ambient pressure have on the distribution of emitted power. First, for group 26 at 30 torr, we see two lines in emission separated 6 Å, each showing an absorption region at their respective line centers. The rather narrow lines are due to emission from the sodium  $D_2$  and  $D_1$  lines. As the pressure is increased from 30 torr to 75 to 150 to 225 torr, we observe the broadening of each of the lines with the absorption region at line center getting wider and deeper. As the pressure increases and the broadened lines overlap in an increasing amount, we see a coalescence of the two lines halfway between them, becoming completely filled near 300 and 630 torr. As the pressure increases to 760 torr, the lines and absorption region broaden even further causing the region between

the lines to become less intense in relation to the maxima on either side of the D line center frequency. This series of experiments also leads one to conclude that the observed distribution change is due mainly to the sodium atom density change caused by changing pressure.

#### FUTURE DIRECTION

It was proposed earlier<sup>10</sup> that radiative transfer theory can be used to predict the effect of parameters such as flare diameter, flare formula, and ambient pressure on the radiant output of flares.

Computations using this theory, with parameters varied as they were in these experiments, have yielded spectra consistent with those shown in Figs. 2 and 3. Although the theoretical work is not yet complete, an increasing amount of evidence is being collected which tends to lead one to conclude that the major portion of the flux radiated by flames from magnesium-sodium nitrate flares is due to emission from broadened sodium D lines, the broadening being a function of pressure, sodium atom density, and related parameters. A further conclusion is that a radiative transfer model can be used to predict the output of illuminating flares.

#### ACKNOWLEDGMENT

Thanks are due to R. M. Blunt and George Crater, Denver Research Institute, for helping with the experiments in the vacuum chamber, to Cliff Muessig, Naval Ammunition Depot, Crane, Indiana, for processing many of the spectra through the densitometer, to Mrs. Bernice Bender at NOAA, Boulder, Colorado, who processed my data through the CDC 3800 to obtain the computer plots, to the Data Processing Department, Photographic Laboratory, and the Print Shop at NAD Crane, for help in preparing the Figures, and finally to Mrs. Sondra Williams and Mrs. Pamela Bruce for typing and editing the manuscript.

## FOOTNOTES AND REFERENCES

- \* This work was supported by the Department of the Navy, Naval Air Systems Command, Research Administration Office.
1. B. E. Douda, *Formation of the Sodium Resonance Line Continuum in Proceedings - Second International Pyrotechnics Seminar*, (Snowmass-at-Aspen, Colorado, 1970), p. 191.
  2. The flares were burned in a vacuum chamber operated by the Mechanical Sciences and Environmental Engineering Division of the Denver Research Institute, University of Denver, Denver, Colorado.
  3. H. Ellern, *Military and Civilian Pyrotechnics* (Chemical, New York, 1968).
  4. B. E. Douda, U.S. Patents 3,411,963 and 3,411,964, Class 149-19 (1968).
  5. C. W. Bash and G. A. Lane, U.S. Patent 3,432,370, Class 149-19 (1969).
  6. D. Hart, J. Eppig and W. J. Powers, U.S. Patent 2,700,603, Class 52-54 (1955).
  7. B. E. Douda, *Atlas of Radiant Power Spectra of Four Flare Formulas at 8 Levels of Ambient Pressure*, RDTR No. 205 Research and Development Department, Naval Ammunition Depot, Crane, Indiana (June 1972).
  8. B. E. Douda, R. M. Blunt and E. J. Bair, *Visible Radiation from Illuminating-Flare Flames: Strong Emission Features*, J. Op. Soc. Am. 60, 1116-1119 (Aug 1970).
  9. The computer code described in NASA SP-273, entitled *Computer Program for Calculation of Complex Chemical Equilibrium Compositions, Rocket Performance, Incident and Reflected Shocks, and Chapman-Jouquet Denotations*, S. Gordon and B. J. McBride, NASA Lewis Research Center, 1971, was used to compute the adiabatic temperature and equilibrium distribution of reaction products at that temperature. The ratio of atomic sodium gas mole fraction to mole fraction of all gaseous species is used as the atomic sodium partial pressure,  $P(\text{Na})$ . The sodium atom density  $D$  is estimated by  $D = n/V = [P \cdot P(\text{Na})]/RT$  where  $n$  is the number of particles,  $V$  is volume,  $P$  is ambient pressure,  $R$  is the ideal gas constant, and  $T$  is the adiabatic temperature.
  10. B. E. Douda and E. J. Bair, *Visible Radiation from Illuminating-Flare Flames. II. Formation of the Sodium Resonance Continuum*, J. Op. Soc. Am. 60, 1257-1261 (Sep 1970).

MAGNESIUM	58.0	44.0	40.4	40.04
NANO3	37.5	51.5	5.15	0.515
KNO3	-	-	49.95	54.945
BINDER	4.5	4.5	4.5	4.5
	GROUP 24	GROUP 22	GROUP 25	GROUP 26
PRESSURE				
760	510-660	510-660	565-615	585-593
630	565-615	565-615	565-615	585-593
300	565-615	565-615	585-593	585-593
225	NO SPECTRUM	NO SPECTRUM	585-593	585-593
150	565-615	565-615	585-593	585-593
75	585-593	585-593	585-593	585-593
30	585-593	585-593	585-593	585-593
6	NO SPECTRUM	585-593	NO SPECTRUM	NO SPECTRUM

Figure 1. The column headings identify the four flare formulas used in this experiment. The ambient pressure, torr, is given in the row headings. The wavelength range in nanometers of the plots in Figs. 2 and 3 is entered in the corresponding matrix block.



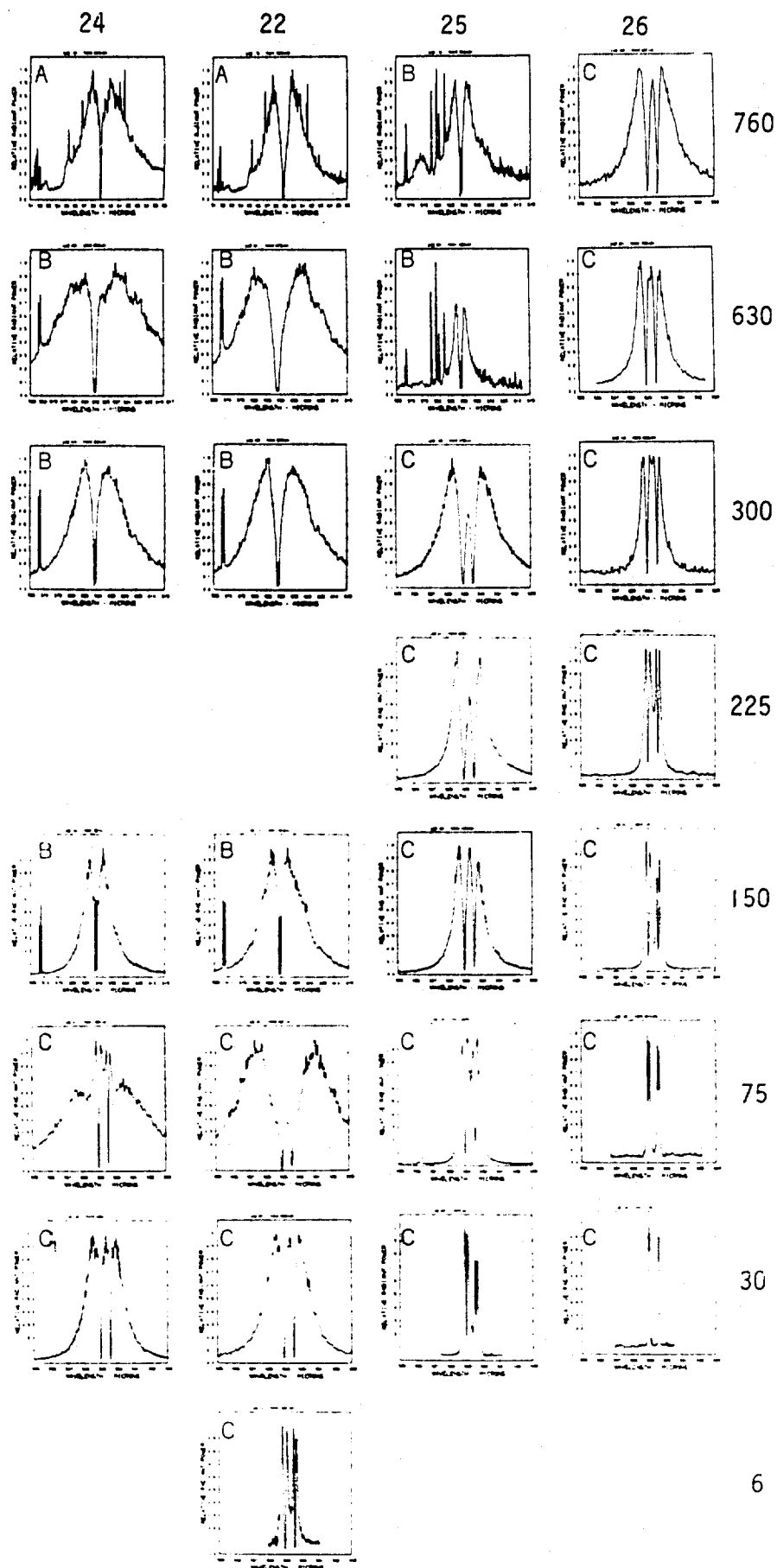


Figure 2. Relative radiant power spectra. Each spectrum is normalized so that its power maximum is unity. See Fig. 1 for wavelength scale.

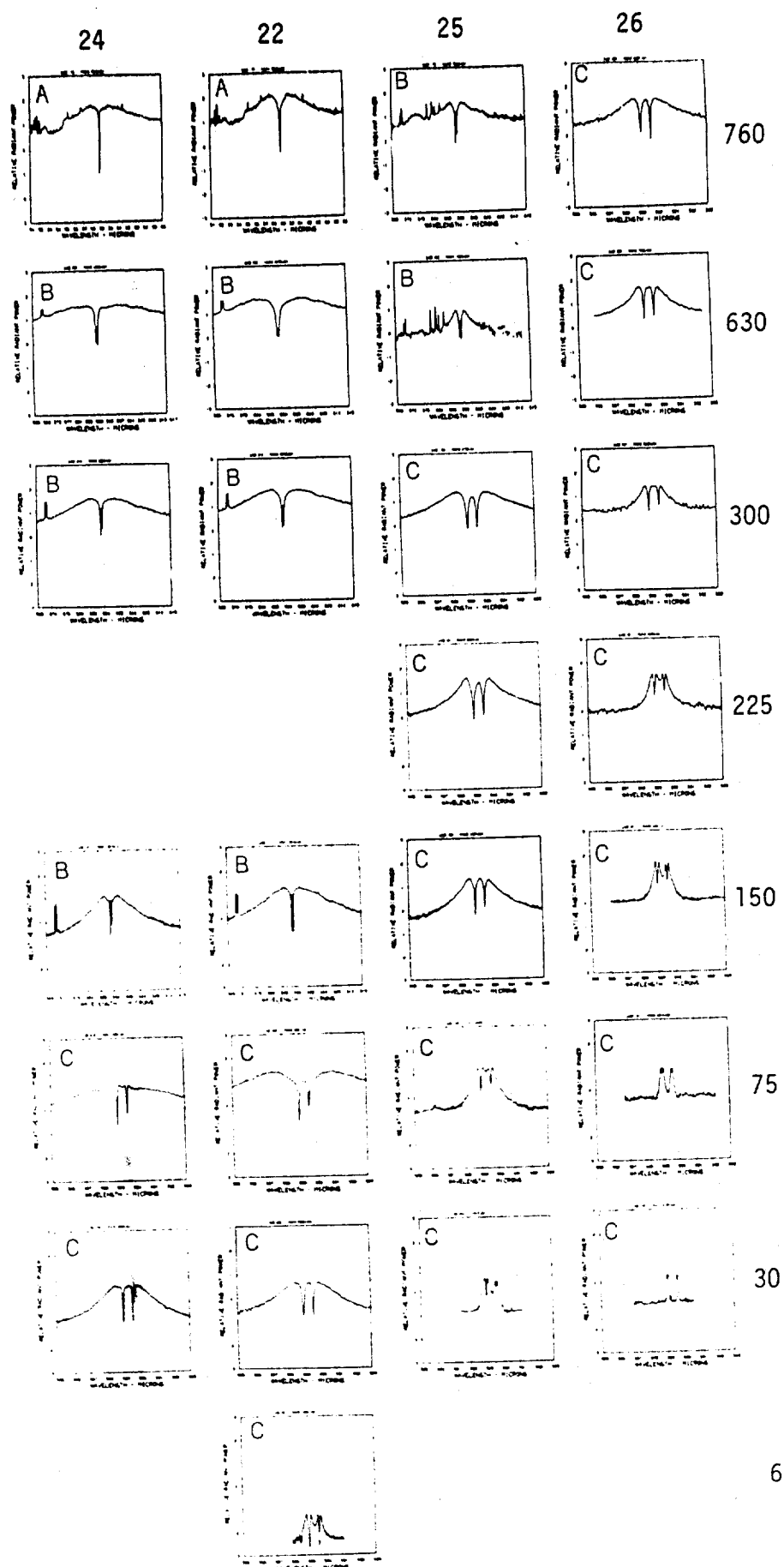


Figure 3. Relative radiant power spectra. The ordinate is plotted on a log 10 scale ranging from -3 to +3. See Fig. 1 for wavelength scale.

MAGNESIUM	58.0	44.0	40.4	40.04
NANO3	37.5	51.5	5.15	0.515
KNO3	-	-	49.95	54.945
BINDER	4.5	4.5	4.5	4.5
	GROUP	GROUP	GROUP	GROUP
	24	22	25	26
PRESSURE				
760	2631 $5.58 \times 10^{17}$	3098 $8.02 \times 10^{17}$	3098 $8.49 \times 10^{16}$	3098 $8.56 \times 10^{15}$
630	2626 $4.63 \times 10^{17}$	3098 $6.18 \times 10^{17}$	3093 $6.66 \times 10^{16}$	3092 $6.71 \times 10^{15}$
300	2601 $2.22 \times 10^{17}$	2995 $2.97 \times 10^{17}$	2988 $3.24 \times 10^{16}$	2987 $3.27 \times 10^{15}$
225			2948 $2.45 \times 10^{16}$	2948 $2.47 \times 10^{15}$
150	2572 $1.12 \times 10^{17}$	2901 $1.5 \times 10^{17}$	2898 $1.65 \times 10^{16}$	2894 $1.67 \times 10^{15}$
75	2536 $5.66 \times 10^{16}$	2812 $7.76 \times 10^{16}$	2806 $8.44 \times 10^{15}$	2805 $8.51 \times 10^{14}$
30	2483 $2.30 \times 10^{16}$	2701 $3.18 \times 10^{16}$	2696 $3.46 \times 10^{15}$	2696 $3.50 \times 10^{14}$
6		2525 $6.67 \times 10^{15}$	2521 $7.25 \times 10^{14}$	2521 $7.30 \times 10^{13}$

Figure 4. The upper value in each matrix block is the computed adiabatic temperature in degrees kelvin. The lower value is the corresponding sodium atom density. See reference 3.

# THE CHEMICAL REACTIVITY OF FERRIC OXIDE

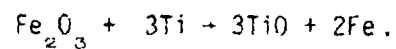
By

CHARLES A. LIPSCOME

## ABSTRACT

Ferric Oxide may experience noticeable and sometimes drastic alterations in its physical properties and in the way it reacts chemically as well.

This paper deals primarily with the effects of preparation temperature, selected impurities, and mechanical activation on such pyrotechnic properties as the heat of reaction and the pre-ignition reaction temperature for the reaction:



## BACKGROUND

In pyrotechnics, generally a field of applied Redox reactions, it is often desirable to have materials that are either more or less reactive than those that are readily available. For instance, one may wish to have a more energetic ignition mix than is readily available; faced with this situation, the pyrotechnic designer usually searches for another ignition mix that will perform in the desired manner.

Ferric oxide has been the subject of a number of investigations for several years. Pryor and Evans<sup>1</sup> in their investigations of the mechanism of direct dissolution of ferric oxide in hydrochloric acid have shown that the temperature at which the ferric oxide was prepared had a considerable effect on the rate of its dissolution in hydrochloric acid. The ferric oxide prepared at the higher temperature was less reactive than that prepared at the lower temperatures. They further point out that the density of the ferric oxide increases and the surface area decreases with preparation temperature.

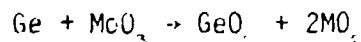
Rawlinson and Cvetanovic<sup>2</sup> show that  $\text{Fe}_2\text{O}_3$  catalyst pellets containing 1.0 Atom %  $\text{TiO}_2$  are reduced to  $\text{Fe}_3\text{O}_4$  at  $560^\circ\text{C}$  by butene at a considerably lower rate than similar  $\text{Fe}_2\text{O}_3$  pellets containing no  $\text{TiO}_2$ .

Goodman and Gregg<sup>3</sup> show that calcination temperature affects the density of the  $\text{Fe}_2\text{O}_3$  and that samples prepared from sulfates did not show appreciable signs of the onset of this effect until much higher temperatures.

Naeser and Scholz<sup>4</sup> report that  $\text{Fe}_2\text{O}_3$  when mechanically activated in a rolling mill sometimes exploded violently. They also report that  $\text{Fe}_2\text{O}_3$  was worked in a steel ball mill for several hours at room temperature to the extent that it reduced to  $\text{Fe}_3\text{O}_4$ .

#### THEORY

Altham, McLain and Schwab<sup>5</sup> give a concise theory of the reactivity effect of n-type and p-type fuels and/or oxidizers through their discussion of the solid-solid reactions



and apply it to their observed results on the B + NiO system of reactants. Briefly, their theory states that Redox reactions proceed with the transfer of electrons from the reducing agent to the oxidizing agent. Any factor which enhances this transfer of electrons will cause the reaction to occur faster and initiate at a lower temperature. If the reducing agent becomes a better donor and/or the oxidizing agent becomes a better acceptor of electrons, the reaction will be enhanced. The converse is also true.

Two steps in their derivation are deserving of further comment. First, let's refer to Fig 1. Here it is seen that the change in the activation energy for the general Redox reaction produces a corresponding change, (but of opposite sign), in the Gibbs Free Energy and Enthalpy terms. Secondly, this theory is a general one and can be applied whether the change in  $\Delta E_g$  is caused by a chemical shift in the Fermi level or is induced by some other means such as mechanical activation.

## EXPERIMENTAL

### Preparation of $Fe_2O_3$

1. Prewieghed amounts of ferric sulfate and the selected dopant, the combined weight of which is 100 grams, are dissolved in 300 ml distilled water.
2. The solution is then heated to boiling and maintained at that temperature until a persistent froth forms and the solution becomes very viscous at a volume of 70 to 100 ml.
3. The viscous solution is then stored under refrigeration at 40-45°F for 18 hours (overnight).
4. The solution is then transferred to crucibles and then placed in a furnace at 600°C for 24 hours. The remaining water is quickly driven off at this temperature, and the doped ferric sulfate decomposes to doped ferric oxide. It is necessary to periodically disturb the contents of the crucible to permit adequate venting of the sulfur dioxide

and steam decomposition products -- two or three times during the 24 hours should be sufficient.

5. The crucible and contents are then removed from the furnace and allowed to stand until cooled to ambient conditions. The  $\text{Fe}_2\text{O}_3$  will be made up largely of loosely agglomerated fine particles of about 0.5 to 1.0 microns; it will be necessary to break up these agglomerates with either a mortar and pestel or by screening.

The viscous ferric sulfate solution is a clear Terra Cotta<sup>C</sup> color while the solution was hot. After cooling, it appeared Mahogany<sup>C</sup> in color. The appearance of the material changed fairly rapidly upon being subjected to the 600°C temperatures. The outer surfaces quite rapidly began to look very dark, almost black in color, while the center changes color more slowly. The inner part turns to light yellow, then to chartreuse, and then to deeper yellow, almost Nugget Gold<sup>C</sup>. When all the mixture has decomposed, and is removed from the furnace, another color change occurs. The final color depends upon the particular dopant used. The resulting undoped  $\text{Fe}_2\text{O}_3$  becomes Terra Cotta<sup>C</sup>; the color usually referred to as Iron-Oxide-Red. The Zirconium doped  $\text{Fe}_2\text{O}_3$  is much fluffier than the other  $\text{Fe}_2\text{O}_3$  samples and is Mahogany<sup>C</sup> in color and the lithium doped  $\text{Fe}_2\text{O}_3$  becomes Burgundy<sup>C</sup> in color.



### Titanium

The titanium was used as supplied. The assay was verified as follows:

Assay Titanium - 97.8%

Granulation through #325, U.S. Standard Sieve - 97.5%

Average Particle Diameter - 8.5 micron.

This material was used for all formulation.

### Preparation of Samples

Mixes ranging in titanium/ferric oxide ratio from 2.2:1 to 10:1 were individually mixed by brushing 5 gm quantities of each mix three times through a #200 U.S. Standard Sieve; uniform mixtures resulted.

### Adiabatic Calorimetry

The results of the performed adiabatic calorimetry are seen in Figures III, IV, and V. The calorimeter used was an automatic control Parr adiabatic calorimeter. Samples weighing 0.4 gm each were burned under 30 psig argon.

### Differential Thermal Analysis

DTA results were obtained on samples of the various ferric oxide and titanium mixtures, using a DuPont 1600 instrument. The samples were

run at a rate of 75°C/min under air, starting from ambient conditions using the 1600°C high temperature cell.

## RESULTS

### Effect of Preparation Temperature

There are two noticeable and drastic effects produced by changing the preparation temperature. The temperature at which the Pre-Ignition Reaction, (PIR),<sup>6</sup> begins for the  $\text{Ti} + \text{Fe}_2\text{O}_3$  reaction is not appreciably different for  $\text{Fe}_2\text{O}_3$  prepared at temperatures ranging from 600°C to 800°C. However, when  $\text{Fe}_2\text{O}_3$  prepared at 900°C to 1000°C is used in the formulation, the PIR begins as much as 220°C lower and with such violence that the DTA quartz cups are shattered. See Fig. II.

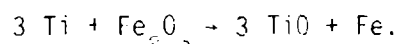
Morin,<sup>7</sup> in measuring the Seebeck effect at  $\text{Fe}_2\text{O}_3$  sintered in air at various temperatures, shows the  $\text{Fe}_2\text{O}_3$  changing from n-type to p-type at about 880°C. This result would agree with those of Altham, et al.,<sup>8</sup> that a p-type oxidizer should give a lower PIR than the n-type oxidizer in a given reaction. Further, the enthalpy and Q of the reaction continues to decrease linearly, with an increase in preparation temperatures, (See Fig. III).

Reference to Fig. I indicates that this would correspond to a linear increase in the activation energy with an increase in preparation temperature. No measurements of the activation energy have been obtained

on this system to date, but Cremer and Marshall<sup>6</sup> show a linear increase in the activation energy of the decomposition of nitrous oxide over a CuO catalyst with an increase in preparation temperature of the CuO, and Rienacker, Bremer and Unger<sup>9</sup> observed that an increase in the pre-treatment temperature of silver powder resulted in a decrease in the activation energy of the decomposition of formaldehyde.

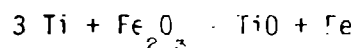
The results obtained by Altham et al.,<sup>6</sup> on the reactivity of NiO should apply to  $\text{Fe}_2\text{O}_3$ , as well. Indeed it has been reported by Hauffe<sup>10</sup> that  $\text{Fe}_2\text{O}_3$ , which has generally poor catalytical activity for some hydrogenation and dehydrogenation reactions, should become even poorer from the addition of titania, and that the catalytic activity is increased with the addition of ZnO or BeO to the  $\text{Fe}_2\text{O}_3$ . Morin<sup>7</sup> shows that with increased  $\text{Ti}^{+4}$  ionic concentration the resistivity of  $\text{Fe}_2\text{O}_3$  decreases, but that at high concentration of Ti the resistivity no longer decreases. He attributes this phenomenon to a shifting oxygen equilibrium with the higher  $\text{Ti}^{+4}$  content which introduces acceptors to compensate for some of the donors. It is clear that additions of  $\text{Ti}^{+4}$  to  $\text{Fe}_2\text{O}_3$  cause  $\text{Fe}_2\text{O}_3$  to become more n-type. We assume that  $\text{Fe}_2\text{O}_3$  becomes more n-type with the additions of cations having a valence greater than +3, and less n-type or even p-type with the addition of cations having a valence less than +3. Indeed, Hauffe<sup>11</sup>

indicates that ZnO, which is also n-type, may be made more n-type by doping with  $G_a^{+3}$  and Krylov and Roginskii,<sup>12</sup> Zhabrova, Vladimirova, and Vinogradova<sup>13</sup> indicate that  $Li^{+1}$  dopant decreases the activation of  $O_2$  i.e., becomes less n-type or even p-type. Accordingly,  $Fe_2O_3$  was doped, each with  $Li^{+1}$  and  $Zr^{+4}$ . It was observed that both dopants greatly affected the enthalpy and Q-values of the reaction.



Each dopant however, increased the enthalpy reaction with concentration (See Fig. IV). This effect was not anticipated, and the only argument that seems to apply in cases of this type is that either the reaction of the  $Zr^{+4}$  doped  $Fe_2O_3$  with Ti is different than those with  $Li^{+1}$  doped, or plain  $Fe_2O_3$  has been mechanically activated in some manner. These will be discussed individually.

By making a series of formulations containing Titanium powder and the particular  $Fe_2O_3$  sample, each formulation differing only in its Ti/ $Fe_2O_3$  ratio and obtaining the enthalpy and Q-values for the ignition reaction, a figure such as Fig. V can be obtained. The interpretation of such a figure is that inflections or maxima denote the stoichiometry of the reaction. We notice that each curve experiences a maximum at a ratio of  $Ti/Fe_2O_3 = 3$ . The reaction can be written from this relationship as:



Furthermore, X-ray diffraction examination indicates the presence of only the above materials, and no other products. A visual inspection of the products, usually a hollow sphere, plus some unreacted powder, indicated only minor amounts of titanates.

Again each of the three types of  $\text{Fe}_2\text{O}_3$  when reacted with Ti displayed the maximum at the same formulation. Thus, the tendency is to discount the argument that a reaction mechanism difference exists.

The question remaining is that of possible mechanical activation. The previous discussion of the effect of preparation temperature on the enthalpy of reaction bears further consideration.

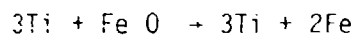
Other investigators<sup>1,2</sup> have shown that the density of  $\text{Fe}_2\text{O}_3$  increases with ignition temperature and becomes less reactive. Thus it appears that the density of  $\text{Fe}_2\text{O}_3$  is at least synergistically related to its chemical reactivity. The absolute density of both the plain and Li-doped  $\text{Fe}_2\text{O}_3$  were the same,  $4.0 \text{ gm/cm}^3$  as determined by the pycnometer method, whereas that of the  $\text{Zr}^{4+}$  doped  $\text{Fe}_2\text{O}_3$  was about  $2.5 \text{ gm/cm}^3$ .

Thus, it would appear that not only the sulfate anion<sup>3</sup> but the  $\text{Zr}^{4+}$  cation greatly affects the absolute density of the  $\text{Fe}_2\text{O}_3$ .

Since the general reactivity of  $\text{Fe}_2\text{O}_3$  seems to decrease with density, our results seem to fit this trend. This is perhaps a matter worthy of further investigation.

## CONCLUSIONS

The manner in which  $\text{Fe}_2\text{O}_3$  reacts chemically is sensitive to a variety of factors. The temperature at which the  $\text{Fe}_2\text{O}_3$  is prepared has a pronounced effect on the enthalpy of the reaction.



Here the enthalpy decreases with preparation temperature. The presence and amount of  $\text{Li}^{++}$  and  $\text{Zr}^{++}$  each have the effect of increasing the enthalpy of reaction. The increase is an anticipated one with the  $\text{Li}^{++}$  dopant. However, the increase in enthalpy with  $\text{Zr}^{++}$  dopant was not anticipated, but may possibly be explained in terms of mechanical activation deriving from strains in the  $\text{Fe}_2\text{O}_3$  crystal lattice. Additional work will center on this latter point.

## REFERENCES

1. H. J. Pryor and V. R. Evans, J. Am. Chem. Soc. 3330-3337 (1949).
2. H. C. Rawlinson and R. J. Cvetanovic, Advan. Catalysis 9, 243 (1957).
3. J. F. Goodman and S. J. Gregg, J. Am. Chem. Soc. 3612-3620 (1956).
4. G. Naeser and W. Scholz, Kolloid-Z. 156, 1-8 (1958).
5. J. A. Altham, J. H. McLain, and G. M. Schwab, Z. Physik. Chem. N. F. 74, 139-145 (1971).
6. S. Gordon and C. Campbell, Anal. Chem. 27, 1102 (1955).
7. F. J. Morin, Bell System Tech. J. 37, 1047 (1958).
8. E. Cremer and E. Marshall, Monatsh. Chem. 82, 840 (1951).

9. G. Rienacker, H. Bremer, and S. Unger, *Naturwiss* 39, 57 (1953).
10. K. Hauffe, *Advn. Catalysis* 7, 213 (1955).
11. K. Hauffe, *Angew. Chem.* 68, 776-784 (1956).
12. O. V. Krylov and S. Z. Roginskii, *Kinetika and Dataliz* 1, 15-21 (1960).
13. B. M. Zhabrova, V. I. Vladimirova, and O. M. Venogradova, *Dokl. Akad. Nauk SSSR* 133, 1375 (1960).

#### ACKNOWLEDGEMENTS

The author wishes to express thanks to his colleagues, W. T. Biggs at NAD Crane, and Dr. C. F. Parrish at Indiana State University for obtaining DTA results, Dr. J. H. McLain of Washington College for his many helpful comments regarding this work, and T. A. Sears for assistance in obtaining much of the data from which this report derives.



Potential Energy

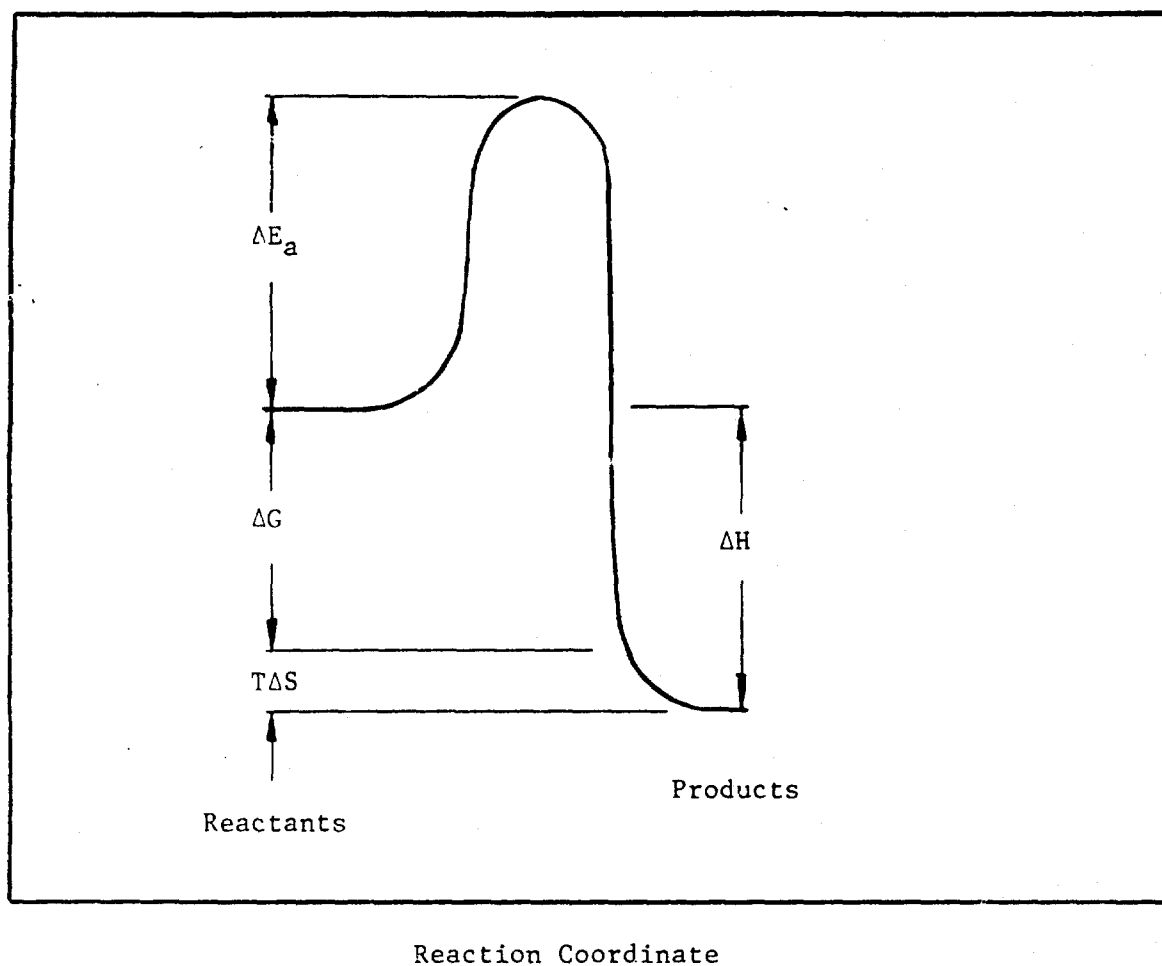


Figure I

Potential Energy Curve

$\Delta T$  in Arbitrary Units

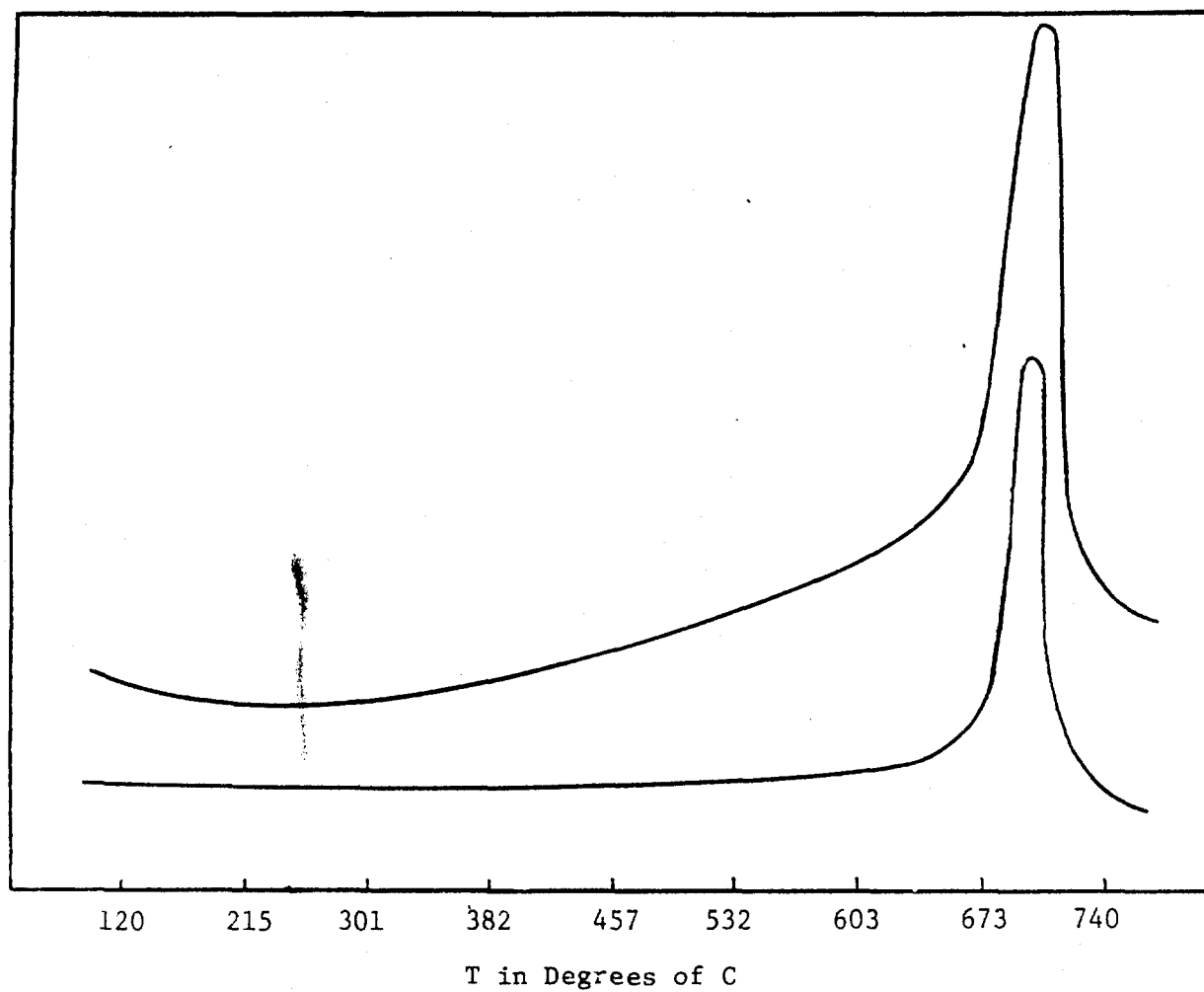


Figure II

Effect of  $\text{Fe}_2\text{O}_3$  Preparation Temperature on the  
Pre-Ignition Reaction  
 $3\text{Ti} + \text{Fe}_2\text{O}_3 \rightarrow 2\text{Fe} + 3\text{TiO}$

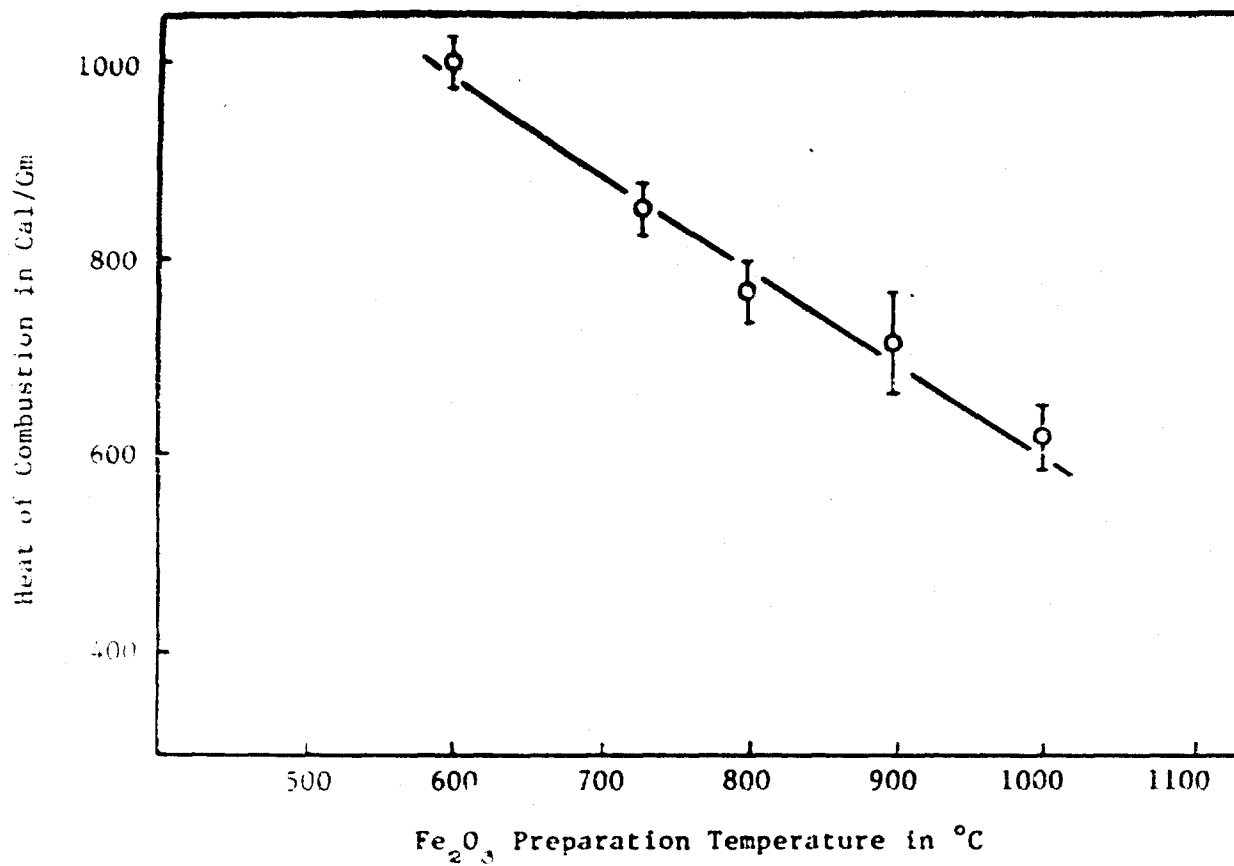


Figure III

Variation in Heat of Combustion with Fe<sub>2</sub>O<sub>3</sub> Preparation Temperature for the Reaction  $3\text{Ti} + \text{Fe}_2\text{O}_3 \rightarrow 2\text{Fe} + 3\text{TiO}$

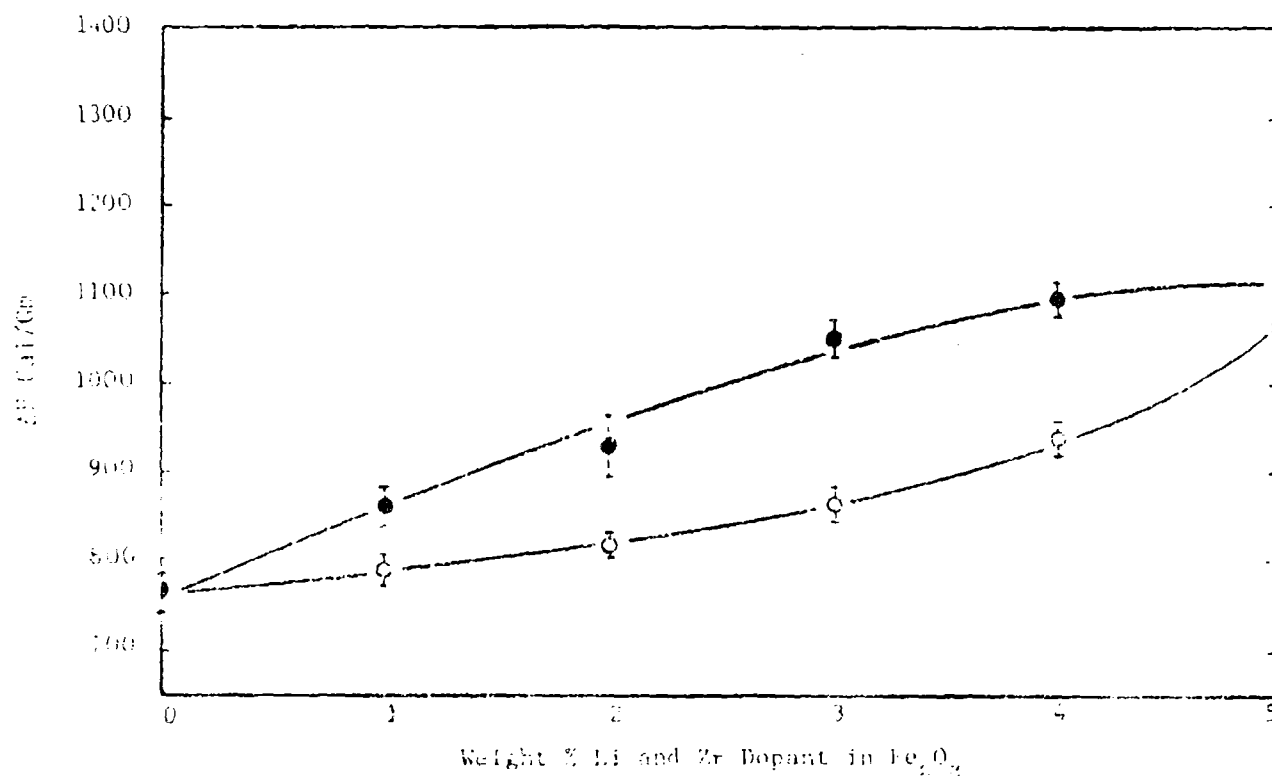


Figure IV  
EFFECT OF DOPANT CONCENTRATION ON  
HEAT OF REACTION OF  $\text{Fe}_2\text{O}_3 + \text{Ti}$  SYSTEM

● Li Doped  
○ Zr Doped

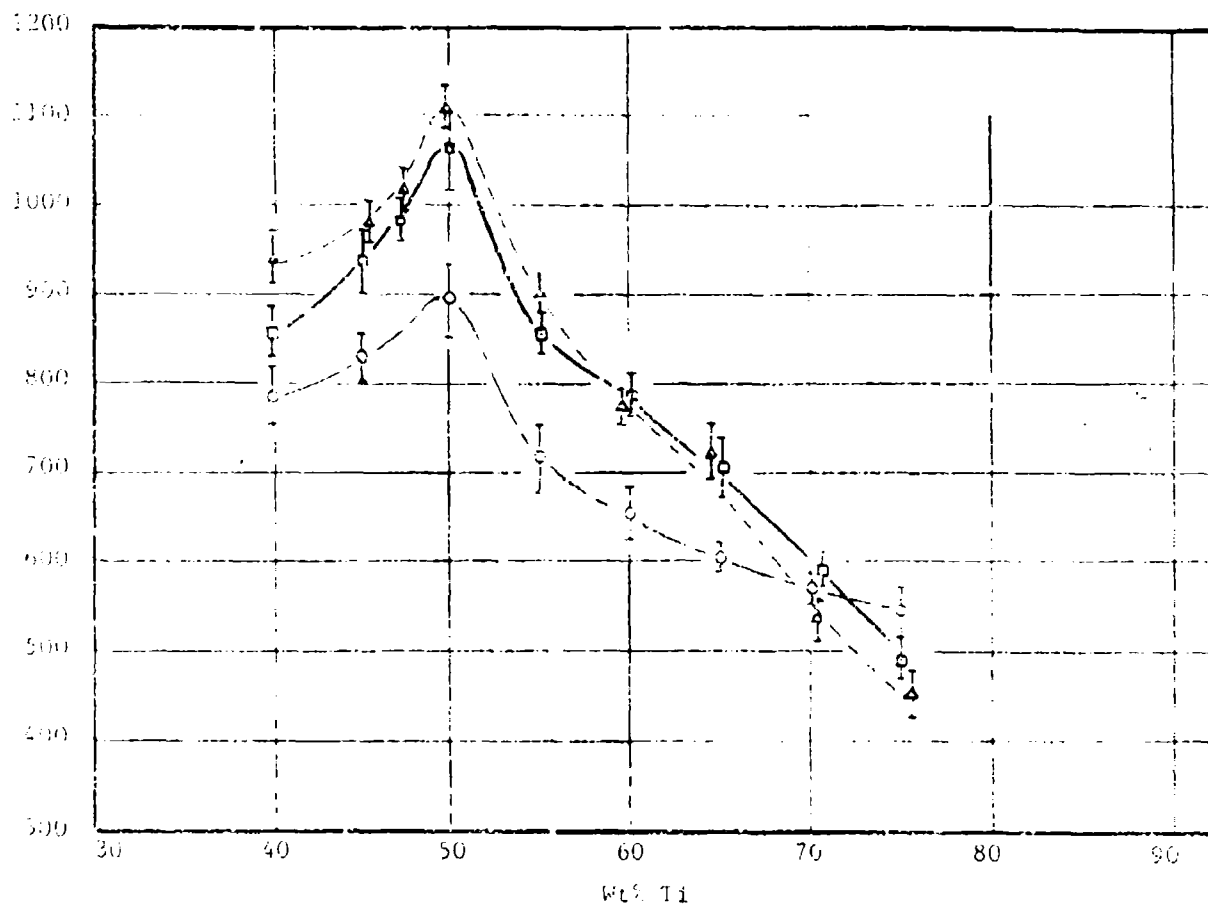


Figure V A

HEATS OF COMBUSTION  $\text{Fe}_2\text{O}_3 + \text{Ti}$  SYSTEM

- ▲  $\text{Fe}_2\text{O}_3$  - Li Doped
- ◻  $\text{Fe}_2\text{O}_3$  - Zr Doped
- $\text{Fe}_2\text{O}_3$  - Production

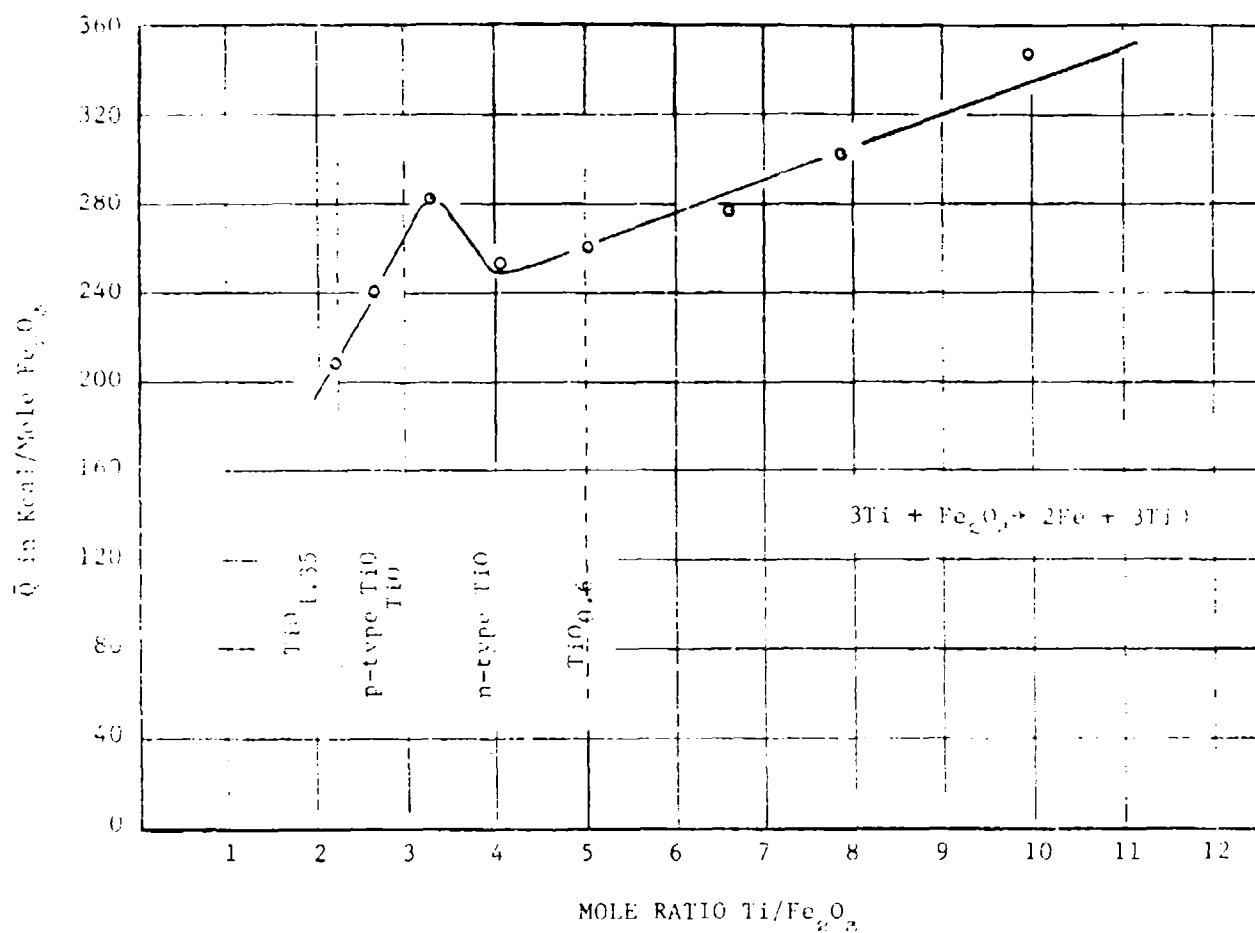


Figure V B

REACTION  $\bar{Q}$  - VALUES FOR PRODUCTION  $\text{Fe}_2\text{O}_3$  + COMMERCIAL TI

FEASIBILITY STUDY OF A  
SELF-SUSPENDING FLARE SYSTEM

D. L. Carstens  
Naval Ammunition Depot  
Crane, Indiana

ABSTRACT

The Research and Development Department of the Naval Ammunition Depot at Crane have studied a new concept in flare illumination. This concept utilizes a free-falling flare disc which is air launched and spin stabilized. This paper includes a discussion of the following: operational concepts, trajectory analysis, live and inert flare test results, proposed flare design, launcher design, fuzing techniques, and technical problems.

PRECEDING PAGE-BLANK-NOT FILMED

## INTRODUCTION

This paper is intended to present an overview of the Self-Suspending Flare (SSF) program. The SSF program is a new concept in flare illumination; namely, that of a free-falling, spin-stabilized flare disc, which is air launched. The Flare is launched from an aircraft utilizing a launcher which is attached to the aircraft. Figures 1 and 2 depict a cargo aircraft illuminating typical battlefield situations. In Figure 1 an encampment is illuminated for defense purposes. Figure 2 illustrates a target under attack utilizing SSF illumination. Figure 3 shows how an attack-type aircraft with a wing-pod type launcher can illuminate a target for interdiction.

### Sponsor

The SSF program was sponsored by the Naval Air Systems Command under Task Number A35-532/323/70F17-546-502, Work Unit No. 4, as part of the Aerial Pyrotechnic Exploratory Development Program.

### Program Objective

The objective of the SSF program as stated in the Technical Work Unit Plan\* is to investigate the feasibility of a free-falling flare for ground illumination.

## BACKGROUND

The SSF program was initiated as a feasibility study of an air-launched illuminating system in which the flares are not dependent on an external deceleration system. All of the existing aircraft-delivered illuminating flares have a parachute suspension system. Also, they have aluminum packing cannisters which are useful to the enemy. The SSF concept eliminates all of the parasitic material which litters the air from present flares.

The usual method of determining flare efficiency is to consider only the efficiency of the illuminating system in terms of total light delivered per pound of flare composition. Payload volumetric efficiency is another way of determining efficiency in terms of full-up weight. Using this method, all of the inert components used to

\*Aerial Pyrotechnics Exploratory Development, Work Unit 4, Self Suspending Flare System, NAD Crane, November 1968.





FIG. 1 PERIMETER DEFENSE

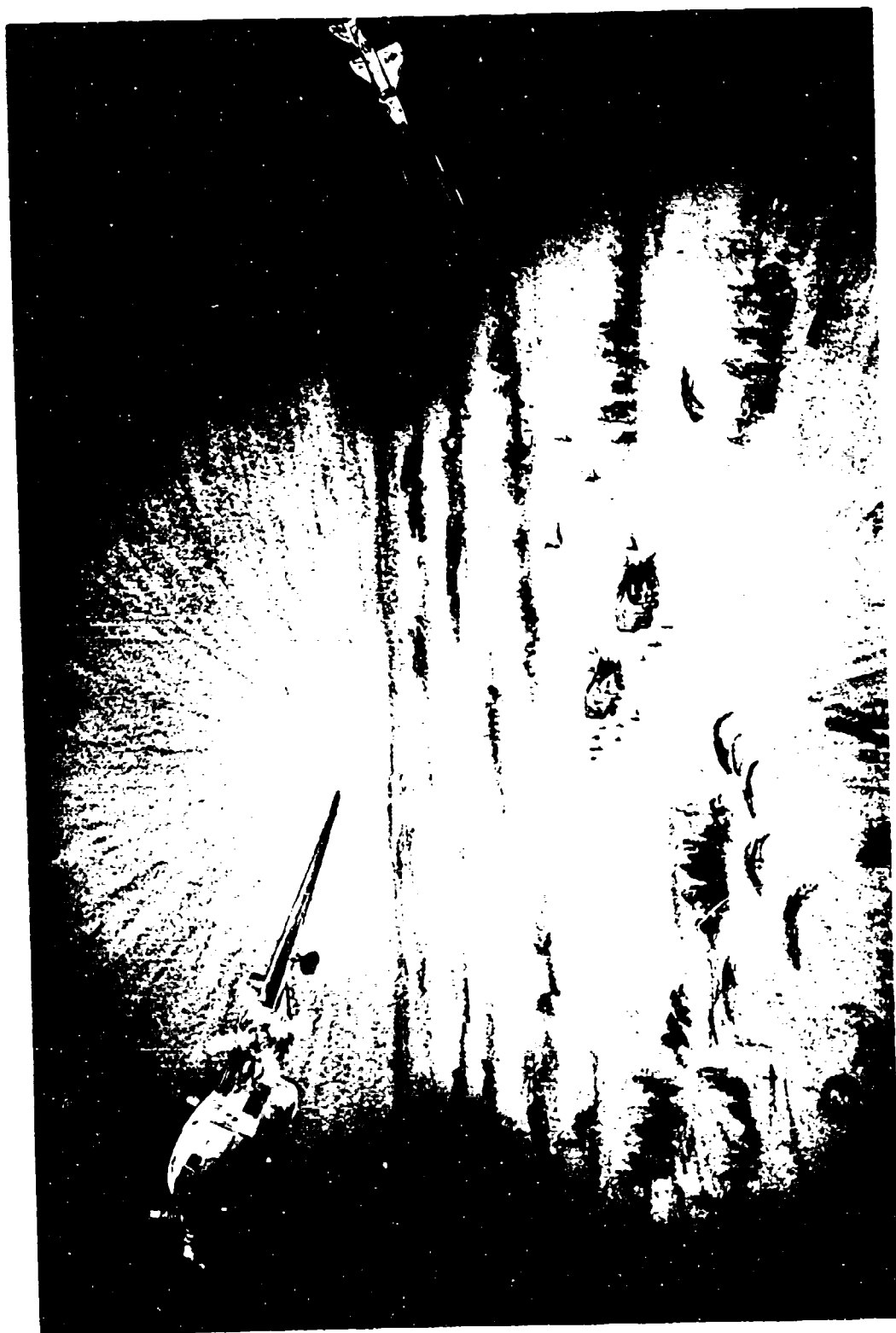


FIG. 2 NIGHT ATTACK



FIG. 3 INTERDICTION

store and deploy the suspension system, as well as the suspension system itself, drop the system efficiency by an appreciable amount. Using an illuminating composition with an efficiency of 45,000 CP-Sec/gram\* typical of the MK 45\*\* a comparison between the Mk 45 and the SSF will be made based on full-up weight. The MK 45 drops to 29,000 CP-Sec/gram of unit weight,\*\*\* while the SSF is estimated at 41,000 CP-Sec/gram of unit weight. Based on spin tests of burning flares, it appears that the efficiency of the SSF would in fact be somewhat less than 41,000 CP-Sec/gram.

Another method for comparing the cost of different illuminating systems is in terms of CP-Sec/dollar. Cost estimates for material, mixing, and pressing of illuminating composition at NAD Crane are set at \$1.00 per pound of composition.\*\*\*\* If a flare composition efficiency of 45,000 CP-Sec/gram is used then the SSF has an efficiency of  $20.4 \times 10^6$  CP-Sec/dollar, while the MK 45 has an efficiency of  $8.65 \times 10^6$  CP-Sec/dollar. The SSF is more than twice as efficient as the MK 45 based on CP-Sec/dollar.

### OPERATIONAL CONCEPTS

The primary operational concept is that of a free-falling spin-stabilized flare disc which is air launched. The SSF relies on a high drag orientation for slowing its free-fall descent. It does not have the usual suspension systems associated with flares (parachutes). The initial concept for fuzing was to utilize a fuze which would sense a spin decay and the time from flare launch until flare ignition may be varied simply by increasing the flare spin speed at the time of launch. This type of fuze would greatly increase the mission flexibility. However, films of the Hurricane Mesa\*\*\*\*\* tests indicate that the spin decay may be rather small. These tests are not conclusive, but they do discourage the spin decay method of fuzing the SSF.

The spin decay concept for fuzing the SSF would greatly increase the SSF mission flexibility. The present alternative to the spin decay type of fuze is a simple time delay type. With the fixed time delay fuze, the flare aircraft altitude would be fixed if the flare is to function within the optimum altitude range.

\* CP-Sec/gram here refers to Candlepower-Seconds per gram of flare composition.

\*\*The designation MK 45 refers to a current Navy Aircraft Parachute Flare.

\*\*\*Riester, J. J. "Interim Report on the Feasibility Study of Self Suspending Flare," NAD CRANE INTERNAL REPORT, March, 1969.

\*\*\*\*The \$1.00 per pound for flare composition is questionable, since prices have increased in the past few years; however, any increase would affect both the SSF and MK 45 numbers.

\*\*\*\*\*Hurricane Mesa is a testing area located near Hurricane, Utah. It is run by the Stanley Aviation Corp. of Denver, Colorado. A vertical drop of some 700 to 800 feet is possible at this test site with the experimental launcher.

The rate of flare launching depends on the required illumination level on target for identification and flare reliability. It is not anticipated that flare reliability will be a problem since it is a sealed unit with no manual settings.

#### Cargo Type Aircraft Flare Ship

One anticipated use of the SSF is for battlefied illumination in conjunction with a flare ship. A flare launcher will be affixed to the interior of a Cargo Type Aircraft (C130 type) which is called a flare ship. Figure 1 depicts the flare ship circling a battlefield or encampment in a banked mode ejecting flares at such a rate as to provide the necessary ground illumination.

The launcher operators do not have to set each individual flare fuze as is the case with present air-launched illuminating systems. Instead the launch velocity settings are done on the launcher. The SSF launch velocity may be changed to increase the mission flexibility to a degree. Referring to Figure 7 for a fixed time delay, it is readily seen that the horizontal range is increased with increased launch velocity while the altitude drop is reduced. The major job that the operators have is to load the SSF discs into the launcher magazine. The flare discs are then fed automatically into the power ejector part of the launcher. The flares are ejected at a preselected rate or manually by the launcher operators.

Figure 2 illustrates the flare ship accompanied by an attack-type aircraft conducting a search and destroy mission. The 12" SSF will have a burn time of 45 seconds and will produce five million candlepower, which should be adequate for this type mission.

#### Attack-Type Aircraft - Wing-Pod

Figure 3 depicts the use of the SSF for interdiction where the flare is launched from a wing-pod type launcher. The launcher and flares would be a prepackaged unit and flare ejection controlled remotely by the pilot. The wing-pod would house some 30 to 40 SSF discs and could be reloaded by ground support personnel. The wing-pod launcher is not considered an expendable item; however, in case of emergency it could be dropped and a demolition charge would destroy it. It is not anticipated that the plane carrying the wing-pod launcher be able to identify the target and destroy it. This operation would be carried out by additional high performance aircraft.

DIAMETER = 12 IN.  
 WEIGHT = 12 LB.  
 LAUNCH ALTITUDE = 10000 FT.  
 LAUNCH PATH = LEV'L  
 ALTITUDE = = =

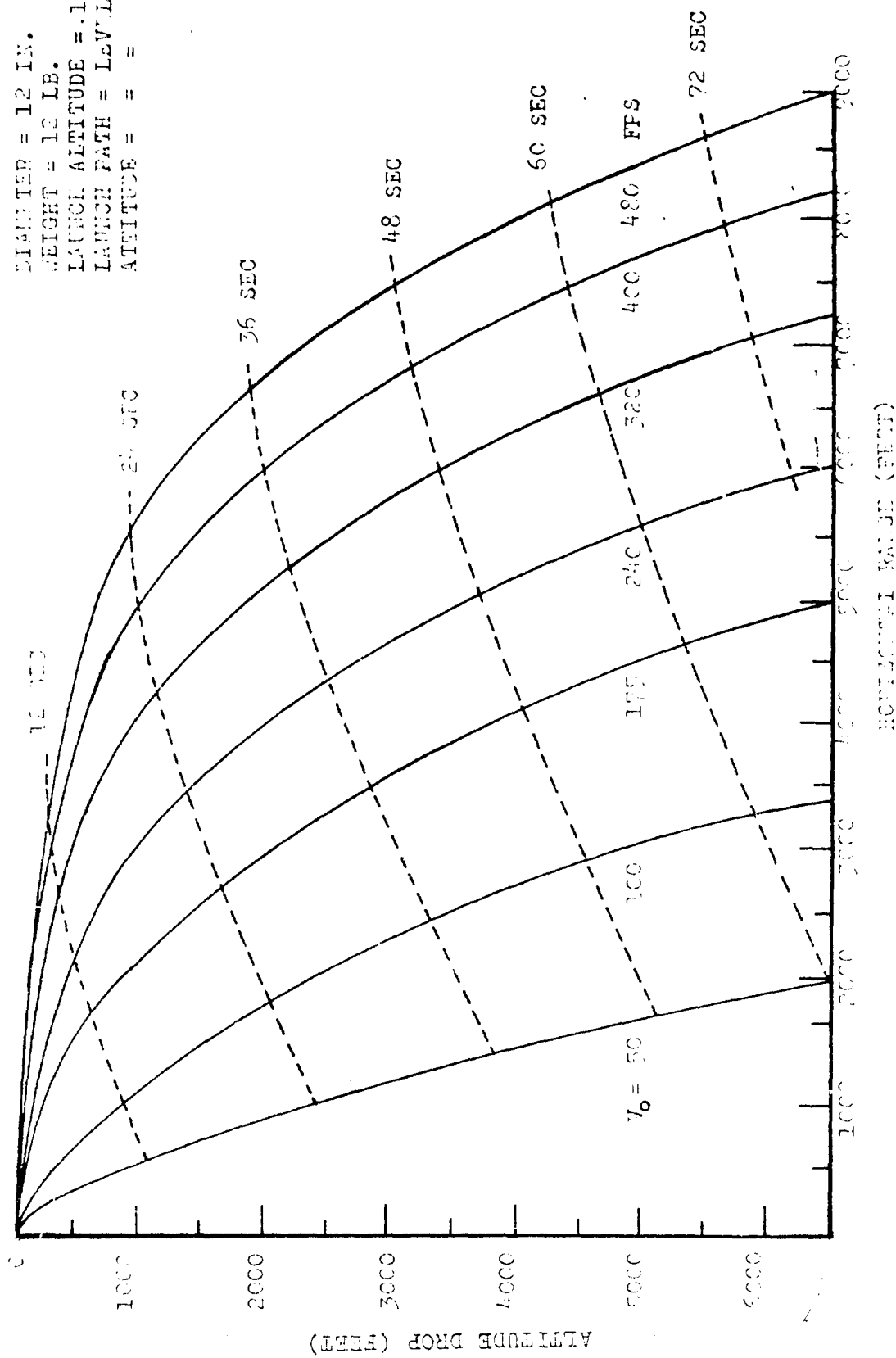


FIG. 4 TIME INTERVALS BEFORE LUNTING

### SSF Launch Altitude

The launch altitude of the SSF disc will be a function of the fuze delay time (free-fall aircraft separation) and the size of the final SSF disc. Table 1 gives the calculated light output for typical SSF disc sizes. Note that the 16" SSF shows only a slightly higher candlepower than the 12" disc. The primary reason for the 16" disc is increased burn time. The burn times and light output are both dependent on the flare composition and burning surface area. A simple change in the flare composition may reduce the burn time and increase the light output. Flare composition is sensitive to the rate of spin. Refer to the quantitative results presented in "Background." Similar to rocket propellant, an increase in the spin rate increases the burning rate. The ignition altitude will be determined by the flare light output and the required illumination level needed on the target. Figure 5 gives the flare altitude as a function of the illuminated radius on the ground for various intensity levels for a five million candlepower flare. The graph shows that a SSF may fall from 3,500 feet to 1,000 feet above the ground and maintain a minimum level of illumination of 0.2 lumens per square feet, which is considered a level of illumination equal to full moonlight, in a circular area on the ground one mile in diameter. Figure 5 reflects only the geometry involved in the problem of describing incident light. This technique involves one major fault, that is, no considerations are made for light attenuation through the atmosphere.

TABLE 1  
CALCULATED LIGHT OUTPUT

Based on flare composition efficiency of 45,000 $\frac{\text{CP-Sec}}{\text{gram}}$			
Flare Size Dia - inch	Est. Flare Composition Weight - lb.	Est. Flare Burn Time Sec.	Est. Light Output Candlepower
8	4	30	2,720,000
12	11	45	5,000,000
16	15	60	5,110,000

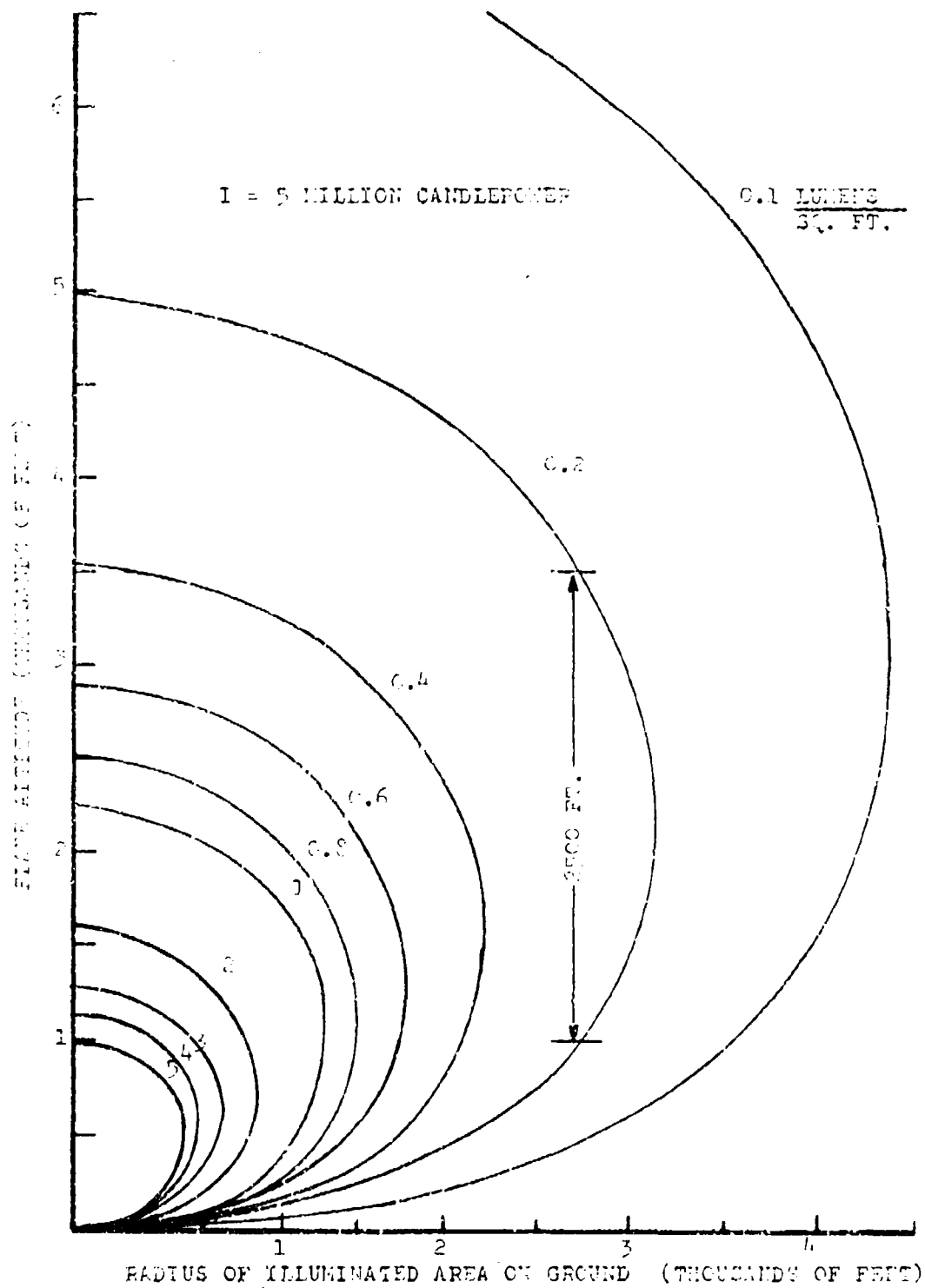


FIG. 5 CHART FOR DETERMINATION OF PLANE ALTITUDE DURING BURN



## SYSTEM CONFIGURATION

### Flare Configuration

The general SSF configuration is illustrated in Figure 6. This exploded view shows rather well that the volume available is utilized to its fullest for the packaging of illuminating composition. The star burning cavity is necessary to provide sufficient burning surface and it is partially filled with fuze and igniter.

Originally several glide shapes were considered; i.e., some lift is generated by the descending body. The major problems associated with lifting bodies are: (1) launch altitude with respect to glide altitude; (2) stability in turbulent region surrounding aircraft; and (3) inert hardware required to maintain lifting shape during burn. The complexity of the lifting body shape caused that concept to be abandoned in favor of the high drag disc shape.

### SSF Fuze

The SSF fuze was originally a spin-sensing type fuze. Several fuze requirements are necessary to keep the fuze consistent with the original concept:

1. Total cost under \$1.00 per unit.
2. All fuze intelligence in launcher.
3. Small and lightweight.
4. Consumable.

Besides these requirements there are the normal requirements of dual environmental sensing, environmental conditioning, and rough handling tests. The fuze concept under consideration will sequence through the following steps to function:

1. Sense an angular acceleration compatible with the launcher.
2. Have a fixed time delay built in either pyrotechnic delay or mechanical.

To meet the above requirements is quite simple. The fuze simply requires an overspeed to arm and then a fixed time delay to flare function. Once the fuze functions, the primer ignites a transfer composition, which in turn ignites the flare composition.

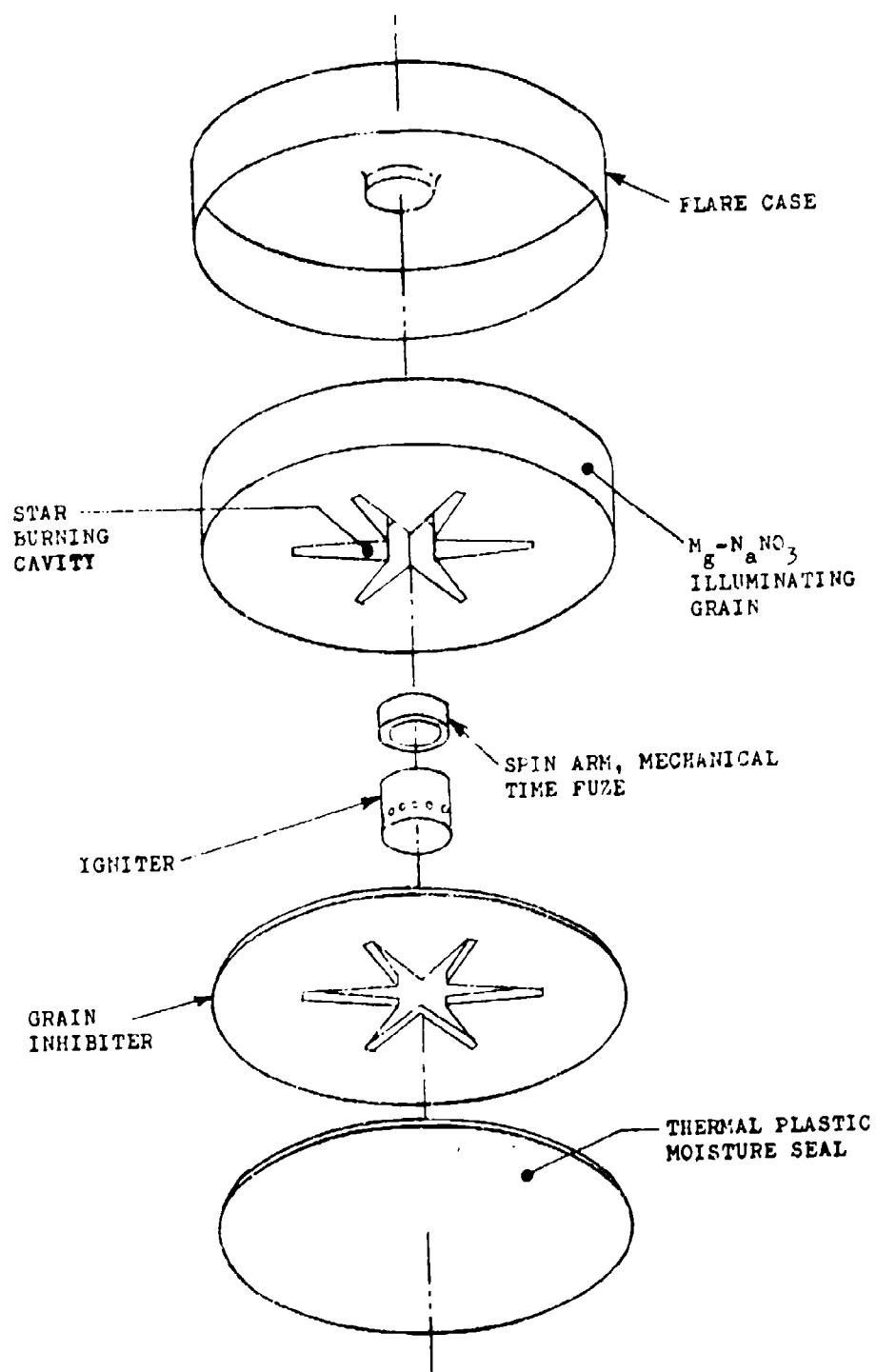


FIG. 6 SELF SUSPENDING FLARE

### *Flare Composition*

A typical flare illuminating composition consisting of 60% Magnesium (Granulation 18) and 32% Sodium Nitrate (Grade B, Class 2 dried) and 8% EPOXY binder (70% DER 321, 30% DEH 14) has been used with reasonable results. A number of formulations utilizing different oxidizers including strontium nitrate, barium-sodium nitrates, and strontium-sodium nitrates were prepared and tested to study the axial spin effects on the luminous energy output. In all cases, spinning reduced the efficiency of the flare compared to static tests.

There are two possible loading techniques for the SSF - casting and pressing. With present flare composition the binder content would be too high to allow casting of homogeneous mixtures. The variation in density would adversely affect the burning rate and flare efficiency.

The present aircraft flares (MK 45's) are pressed. In the interest of uniformity of composition density, pressing seems the only possible loading technique available with the present state-of-the-art of illuminating flares.

### *Flare Case Material*

The SSF concept of a totally consumable flare disc will be practically impossible to achieve with respect to the outer case. The outer case must act as a moisture barrier in storage and as an inhibitor during burning. Figure 6 is an exploded view of a SSF disc and it shows the portions of the flare composition which must be inhibited. The flare case will be compression molded from either asbestos phenolic or glass-filled phenolic. With the high temperature generated by the flare the case should be reduced to unusable charred remains, but not consumed.

### *Flare Grain Inhibitor*

The grain inhibitor shown in Figure 6 must perform a slightly different function than the outer case. It must inhibit the burning of the composition of the bottom side of the flare as well as erode away (burn away) at the same rate that the star burning surface recedes. This recession is necessary to prevent any orifice effect during burning.

During a series of live flare tests at Hurricane Mesa, the inhibitor did not recede at the correct rate and the resulting orifice effect provided sufficient thrust that the flare actually rose above the launch platform. More information will be given in a later section about the Mesa tests.

### *Moisture Seal*

A thermal plastic moisture barrier will be affixed to the SSF disc as a last step. The moisture seal will serve no useful purpose to the SSF. It is not presently considered feasible to use the grain inhibitor as the moisture seal due to pressure problems at flare ignition.

## LAUNCHER CONFIGURATION

### Experimental

The first launcher used in the SSF program was a modified clay pigeon trap. The major modification was to increase the spring tension for the launching arm.

Figure 7 is a photograph of the experimental launcher built by Denver Research Institute (DRI) under contract to NAD Crane. This launcher is capable of launching 4, 8, and 12" diameter 1, 2, and 2" thick discs, respectively. Minor adjustments must be made when changing disc sizes. This launcher utilizes a moving table and a fixed flat belt. The flare spin rate is dependent on the linear launch velocity with this type of launcher. The experimental launcher gives reproducible results from test to test. This launcher is powered by a gas cylinder using nitrogen, which makes it a relatively portable unit.

### SSF Launcher

There are two types of launchers envisioned for the SSF - one for a cargo-type aircraft and one mounted inside of a wing-pod. The cargo-type launcher will be larger and more versatile than the wing-pod type.

### *Cargo-Type Launcher*

The launcher consists of three basic functional elements; namely, the magazine, the feed mechanism, and the power ejector. The launcher

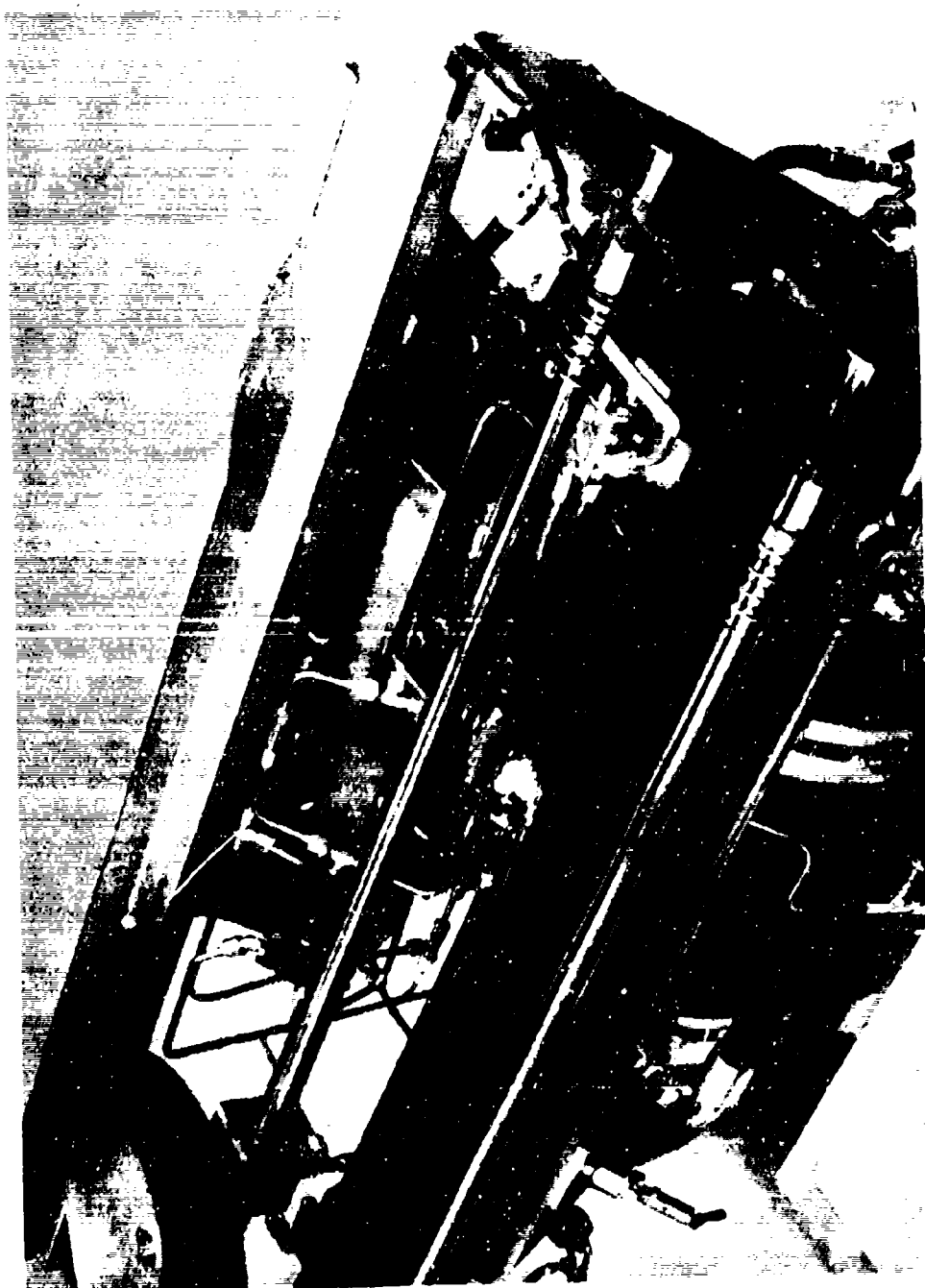


FIG. 7 PHOTOGRAPH OF THE EXPERIMENTAL LAUNCHER

design will depend on some of the aerodynamic characteristics of the flare, such as the angle of attack, initial velocity; and until these have been established, a final launcher design cannot be accomplished.

If the flare disc is found to be dependent on launch attitude, a compensating launcher platform will be incorporated in the design. The launcher will be constructed such that two men can load it into a cargo-type aircraft.

The controls may be operated either remotely by the pilot or manually by the launcher operators. There will be an overriding safety circuit which will eliminate accidental flare launching when the flare ship is on the ground. A manual override will be incorporated which requires a special key so that the launcher operation may be checked on the ground.

The principal characteristic which can be controlled by the circuit is the linear launch velocity. A minimum launch velocity is necessary for proper fuze arming and flare-aircraft separation.

The launcher will have the capability of ejecting flares at a pre-selected rate, such as every ten seconds, or randomly by the launcher operator.

It will be necessary for the launcher operators to load the flare discs into the magazine. There are no individual fuze settings on the flare discs and the operators will not handle the flares after they are placed in the magazine. The magazine will hold 20 to 25 flares. The launcher feed mechanism will locate the flare disc on the power ejector, and it will be ejected at the proper velocity.

#### *Wing-Pod Launcher*

The wing-pod type launcher will be housed in a wing-pod along with a flare feed mechanism and 25 to 50 flare discs. Launch velocity will be set by the pilot from the cockpit. He will have the same flexibility in control settings as is available in the cargo-type launcher.

Flare ejection will be accomplished either with a slinger arm or a gas cartridge pressure system. The wing-pod is reusable; however, in case of emergency it may be jettisoned. If jettisoned, a self-destruct system would destroy the launcher after aircraft separation.

There are two ejecting techniques under consideration for the wing-pod launcher - rearward and downward. Either method will be satisfactory from flare flight considerations. If flare and aircraft separation is a problem, then downward ejection may prove advantageous.

## SYSTEM PERFORMANCE

Since much of the SSF system is still in the concept stage, it is not realistic to talk system performance or try to compare it to any existing system. The operational concepts were discussed in "Operational Concepts" section. This section will discuss the actual and theoretical results of various tests of the SSF system.

### SSF Disc

The SSF disc is the most important part of the entire SSF concept. Figure 6 is an exploded view of the SSF disc. The most important part of the flare disc is the illuminating composition.

#### *Illuminating Composition*

Over the years illuminating composition has been improved and perfected to its present state. However, flares are generally cigarette burners, or end burning, and they are suspended by parachutes. Thus, they are non-spinning. Our tests on standard illuminating compositions have shown that the luminous efficiency decreases and the burn rate increases with spin.

A flare formulation study was conducted to study the effect of spinning. Compositions were prepared utilizing barium nitrate, strontium nitrate, sodium nitrate or combinations thereof with the normal fuel, magnesium, and an Epoxy binder. It was determined that the conventional system of sodium nitrate and magnesium provided the best luminous efficiency of those tested. However, all formulations tested gave the same general results mentioned in the Development Summary which is in a later section.

The above-mentioned spin tests were conducted utilizing flat (cigarette burner) four-inch diameter discs. Also, some were tests with a 1/4-inch diameter axial hole such that the burning surface increased with time. Reductions in the luminous efficiency of the compositions were observed to range up to 80 percent at 5,000 rpm as

compared to static burns. The highest average luminous efficiency obtained during spin tests was 27,400 candlepower-seconds per gram. The results of the above series of tests are somewhat erratic and it is believed that the smoke generated by the flare is obscuring the photocell.

Two sizes of flare discs (8-inch and 12-inch diameters by 1 1/3-inch thick with star-shaped center cavities) have been tested for luminous energy. These were tested statically in an instrumented tunnel for candlepower measurement. The 8-inch disc had an average burn time of 15 seconds and a candlepower of  $1.5 \times 10^6$ . Similarly, the 12-inch disc had an average burn time of 20 seconds and a candlepower of  $3.5 \times 10^6$ . The light output of these tests is somewhat below those contained in Table 1. However, the thickness of the flares listed in Table 1 are increased by over 25 percent. This increase in flare thickness will increase the burning surface area and in doing so should increase the candlepower output of each size of flare disc.

A total of four 8-inch diameter, 2-inch thick flare discs were tested (2 statically and 2 spinning) prior to a series of drops from the top of Hurricane Mesa test area. The outer case for these flares was machined from sheet asbestos phenolic to a nominal thickness of 0.100 inch. Standard magnesium-sodium nitrate with an Epoxy binder was hand tamped (packed or consolidated) into the flare case. The grain inhibitor was standard 1/16-inch thick Formica and was Epoxied into position. The two which were tested statically burned for approximately 25 to 30 seconds. No attempt was made to measure the luminous output. The next two were tested while spinning. The flare disc was spun up to 2,000 rpm and then ignited. The burn rate was increased as was expected. The average burn time for the two flares was 16 seconds. A large fan was placed near the flare in an attempt to simulate some of the wind which would exist if the flare was free falling and to help remove the smoke for candlepower measurement. The smoke cloud was so bad and the prevailing winds were in the wrong direction, which resulted in very low light output readings.

#### *Live SSF Drops Hurricane Mesa*

A total of seventeen live 8-inch diameter by 2-inch thick SSF discs were launched from the top of Hurricane Mesa Test Area. Due to technical problems with the flare ignition system, only eight ignitions occurred. In all cases the SSF disc maintained what visually appeared to be a stable attitude during the trajectory. There was no indication of pitching or rolling in any flight. Several different things happened during the flights. The first flare followed the expected trajectory\* for about

\*The expected trajectory is discussed in later section on Trajectory Analysis. Previous calculations had indicated that flare thrust would not be significant, which was not the case with this series of tests.



200 to 300 feet and then essentially exploded in midair. The second flare which ignited produced a trajectory like the one shown in Figure 8. This was unexpected and indicates that the flare produced a significant amount of thrust. The thrust is attributed to two things; namely, the increased burn rate due to spinning (which causes mass ejection at a higher rate than anticipated) and the grain inhibitor apparently did not erode away at the same rate that the flare burning surface receded, causing an orifice effect. The increased thrust may have been a combination of the two. Also, there may have been other factors which influenced the flare-like wind updrafts near the Mesa edge. However, these updrafts did not appear to influence the trajectories of the inert flares which were dropped. The third flare followed essentially the same pattern as the first flare; i.e., exploded in midair after 200 to 300 feet of free fall.

The reason for this flare breakup was attributed to the asbestos phenolic outer case. All subsequent flares were taped with a fiberglass tape (tensile strength, 400 pounds per inch) around the outer edge with at least two layers. After taping the outer case, all of the flare discs which ignited performed similar to the second flare. See Figure 8 for a typical trajectory. This does not prove conclusively that the outer case weakness was the reason two of the flares broke up, but it helps substantiate the argument.

During the Mesa test a photocell was located near the base of the Mesa (see Figure 9) for candlepower measurement. Data was obtained for three flares. The candlepower is plotted as a function of the flare burn time in Figure 10. The peak values were of short duration; however, they do have a more than adequate magnitude for an eight-inch disc. The total burn time for these flares was nine to ten seconds, but during the last three or four seconds much of the available energy was converted into kinetic energy which provided a thrust instead of illumination.

#### *Inert SCF tops*

Early in the program some four-inch diameter by one-inch thick inert discs were launched using the clay pigeon trap from an aircraft. A stability problem was noticed at this time. Further tests with the experimental launcher at Hurricane Mesa confirmed this with the four-inch disc. However, this instability did not show up in eight-inch and twelve-inch diameter two-inch thick discs. None of the larger discs have been launched from an aircraft. Both visual and movie coverage indicate the larger discs are stable throughout some 700 to 800 feet of vertical drop.



FIG. 8 PHOTO OF TYPICAL SSF AT HURRICANE MESA



FIG. 9 PHOTO OF LAUNCH AREA AT HURRICANE MESA

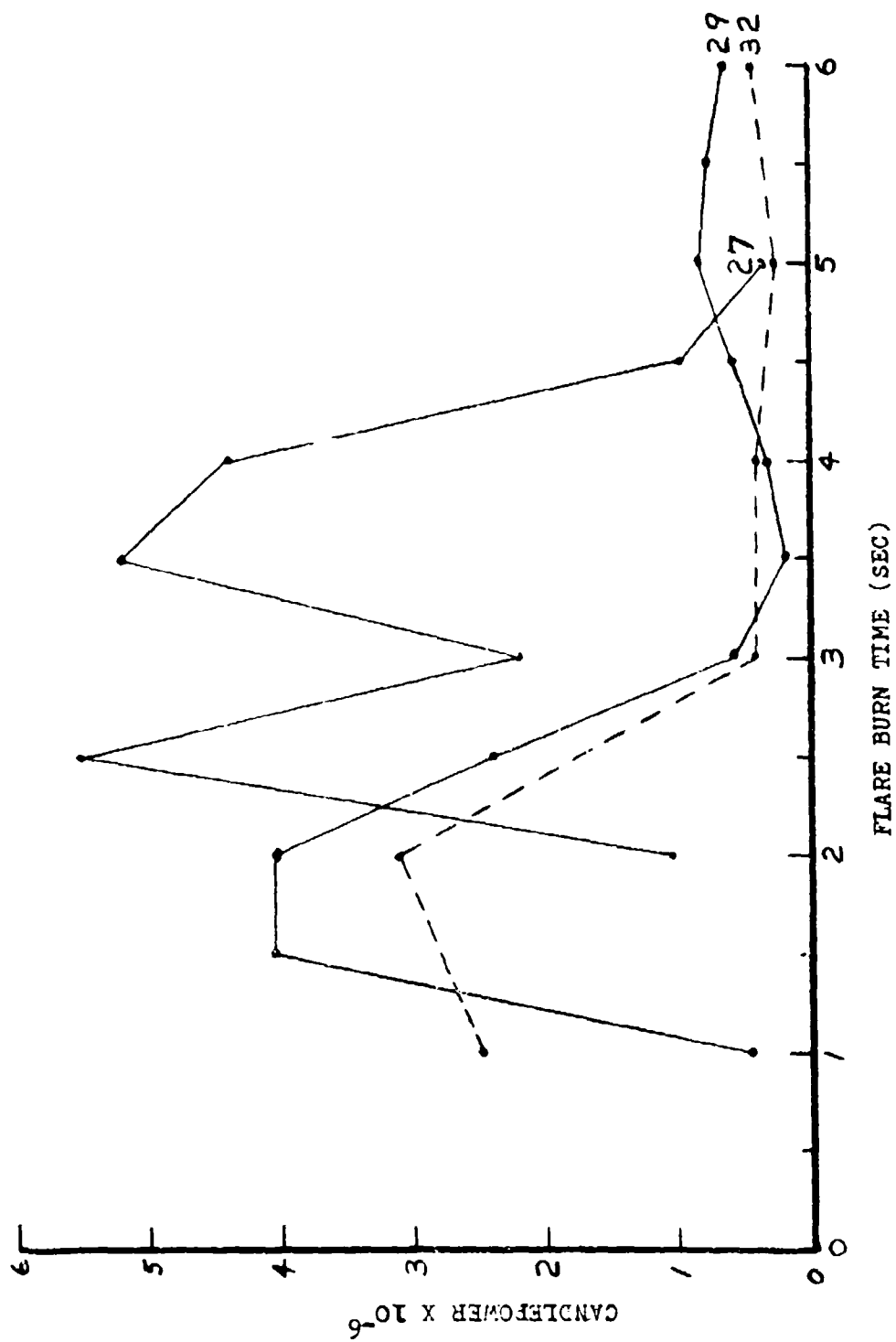


FIG. 10 HURRICANE MESA CANDLEPOWER DATA

The inert flare discs were painted with a pattern on the top such that the spin decay with time could be determined. It was intended in the original concept to use a spin decay fuze. However, these tests indicated that the spin decay was quite small. The exact data is not available, but since for reliability of fuze function a fairly large spin decay is necessary, this fuzing technique was abandoned. The impact area remained practically constant from launch to launch, indicating a high degree of reproducibility for the disc trajectory.

### Trajectory Analysis

The trajectory analysis was primarily an analytical study. Contracts were awarded to the Denver Research Institute and to Honeywell, Inc. for trajectory analysis.

#### *Summary of Honeywell's Analysis\**

Stilley's analysis was based on the separating of the high frequency dynamic motions from the slow precession and linear velocities defining the trajectory. A quasisteady math model and digital computer program were developed to simulate flare trajectories. This program allows for gyroscopic precession under the aerodynamic moments and translation under the aerodynamic forces experienced as a function of angle of attack, spin, and angular rates.

The following recommendations are taken from Stilley's report:

1. The most promising configurations appear to be the 3:1 to 2:1 diameter-to-thickness ratio right-circular cylinder and the relatively thick domed/cupped clay pigeon-like shape.
2. Because of the interaction between aerodynamics and launch conditions, the choice of configuration and/or launcher design must take into account the importance of flare orientation at launch to provide desired steady-state glide characteristics.

Stilley's trajectory simulation correlates qualitatively with available free-fall tests and analytical solutions. Inert discs or burning flares (linear burning, constant thrust) may be simulated.

Preliminary wind tunnel tests were conducted on candidate flare shapes to obtain the necessary aerodynamic coefficients.

\*Refer to "Aerodynamic Analysis of the Self-Suspended Flare Final Summary Report" by G. D. Stilley, Honeywell, Inc., Oct. 1971 (Contract Number N00164-69-C-0662).

### *Summary of DRI's Analysis*

Peterson's trajectory analysis was broken down into two phases.\* Phase I assumed a two-dimensional trajectory with the bottom face of the flare parallel to the ground. Three different sets of aerodynamic coefficients were investigated.

1. Grossly approximate coefficients for flow past a circular cylinder.
2. Coefficients obtained by extrapolating NASA data on ellipsoids of revolution.
3. Data on circular cylinders, clay pigeons, and "Frisbee"-shaped discs obtained from Honeywell, Inc.

The digital computer simulation was used to study the effects of variations of aerodynamic coefficients, launch velocity, burning rate, and base pressure. The results of these simulations conclude that:

1. The aerodynamic forces have little effect on the horizontal motion of the flare at a launching velocity of 50 fps.
2. Very significant increases in range (flight time) could be obtained by streamlining the shape of the flare.
3. Representing the effect of burning rate/mass loss by a constant rate of mass loss and constant base pressure does not allow a good match of the available experimental data.

Phase II of Peterson's analysis utilized a three-dimensional trajectory which included the gyroscopic effects produced by the spin angular momentum of the flare. The pure spinning motion is perturbed to produce a wobbling motion. It was concluded from Phase II:

1. The computed trajectories agree qualitatively with the experimental results from Hurricane Mesa.
2. The spinning disc does not behave in an inherently stable fashion; i.e., the aerodynamic pitching moment causes a precession of the disc which increases with time.
3. As a result of 2., launchings of the same discs at higher velocities will have significantly increased aerodynamic moments and angular accelerations.
4. By increasing the spin angular velocity, changing the spin angular velocity, aerodynamic shapes, base pressure, it may be possible to create a slow descent along a helical trajectory.

\*Refer to "Calculation of Self-Suspended Flare Trajectories" by Harry Peterson, Denver Research Institute, Feb. 1971 (Contract No. N00164069-C-0216)

5. The definition of the optimum configuration should be based on a combination of digital computer simulation, scale model wind tunnel tests, and similitude analysis.

Figure 4 is a typical plot of the SSF prior to ignition. This graph is for a 12-inch diameter disc and illustrates the horizontal range and vertical drop as a function of time for various launch velocities. These types of curves are valuable for determining launch parameters for fuzing purposes. Figure 11 gives the predicted trajectories of burning flares for different base pressures.\* The initial conditions of the flare and the program constants are indicated on the figure. The trajectory of an actual flare tested at Hurricane Mesa is also included on the figure. Figure 12 is a trajectory plot of a 12-inch diameter disc which has a mass decrease with time to simulate flare burning. A solid disc trajectory is shown as a reference. These trajectories assume no effect from burning other than mass decrease with time. These curves were developed before the burning flare tests were run at Hurricane Mesa. They, however, provide valuable qualitative information for proving the SSF concept feasibility. Figure 12 illustrates that for a 12-inch diameter disc launched at 175 ft/sec the vertical drop for a 30-second burn with the assumption of no thrust is in the neighborhood of 800 feet as compared to the nonburning of about 1,400 feet.

#### Development Summary

A number of different four-inch diameter inert discs were launched using a conventional clay pigeon trap to study the effects of disc shape on flight characteristics. Variations in weight and outer shape didn't appreciably affect the flight characteristics as long as there was sufficient mass to maintain a reasonable spin rate for stability.

After the four-inch inerts were tested, some live four-inch flares were launched using the clay pigeon trap. This test utilized a cigarette-type burning surface and the results were encouraging.

The ignition of these small flares occurred on the launching rail, in midair and on the ground after impact. All of the flares landed within a six-yard diameter circle approximately 35 yards from the launcher. After these tests, it was concluded that the burning process did not affect the trajectory of the flare disc. However, this conclusion proved to be somewhat in error in a later series of tests at Hurricane Mesa.

\*The pressure here refers to the average pressure acting on the underside of the flare during burning, which creates a lifting effect.

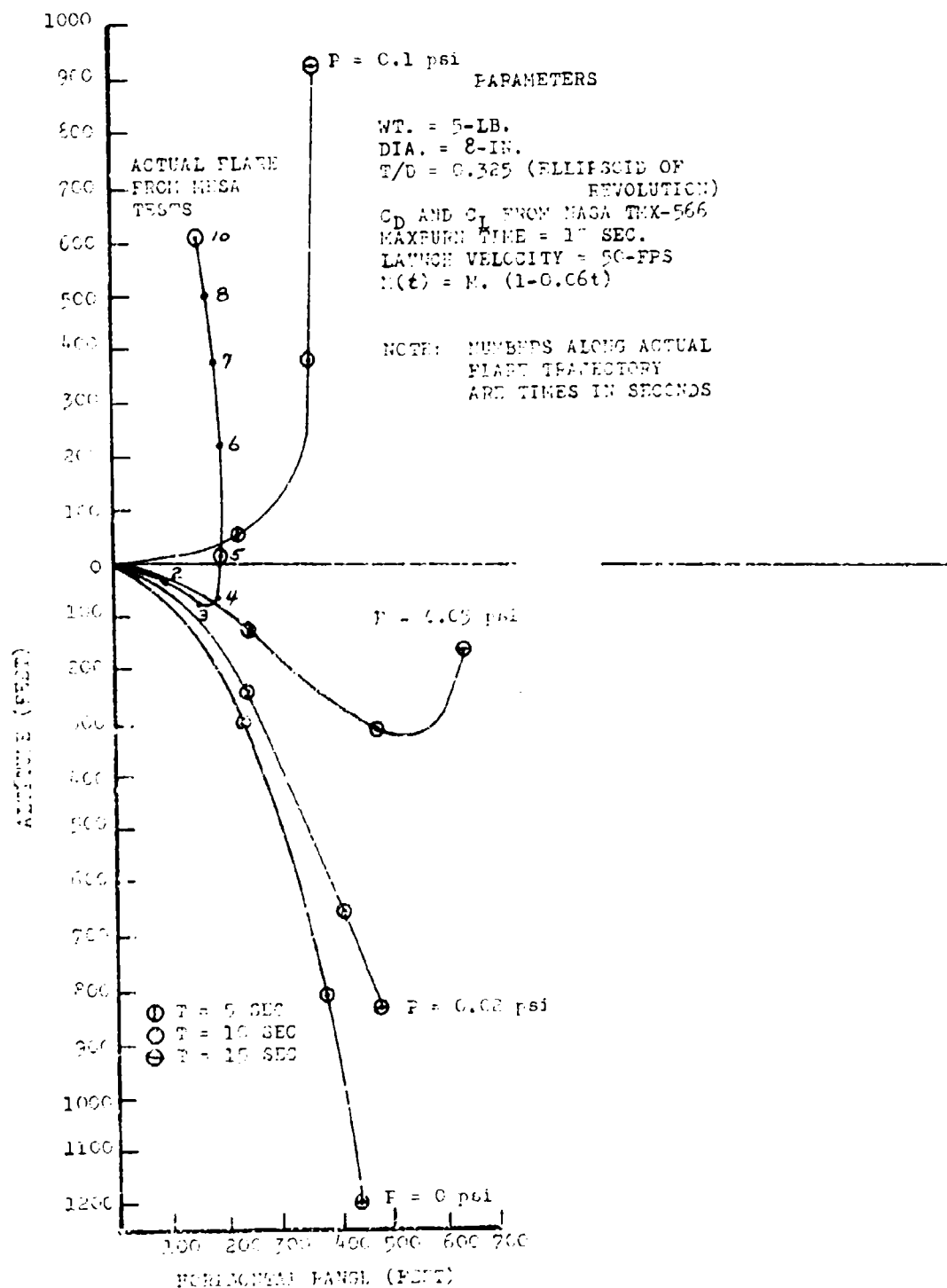


FIG. 11 PREDICTED TRAJECTORIES OF BURNING FLARE DISKS



TIME (SEC)	ALPHABET DEPTH (FEET)
0	0
10	10
20	20
30	30
40	40
50	50
60	60
70	70
80	80
90	90
100	100
110	110
120	120
130	130
140	140
150	150
160	160
170	170
180	180
190	190
200	200
210	210
220	220
230	230
240	240
250	250
260	260
270	270
280	280
290	290
300	300
310	310
320	320
330	330
340	340
350	350
360	360
370	370
380	380
390	390
400	400
410	410
420	420
430	430
440	440
450	450
460	460
470	470
480	480
490	490
500	500
510	510
520	520
530	530
540	540
550	550
560	560
570	570
580	580
590	590
600	600
610	610
620	620
630	630
640	640
650	650
660	660
670	670
680	680
690	690
700	700
710	710
720	720
730	730
740	740
750	750
760	760
770	770
780	780
790	790
800	800
810	810
820	820
830	830
840	840
850	850
860	860
870	870
880	880
890	890
900	900
910	910
920	920
930	930
940	940
950	950
960	960
970	970
980	980
990	990
1000	1000

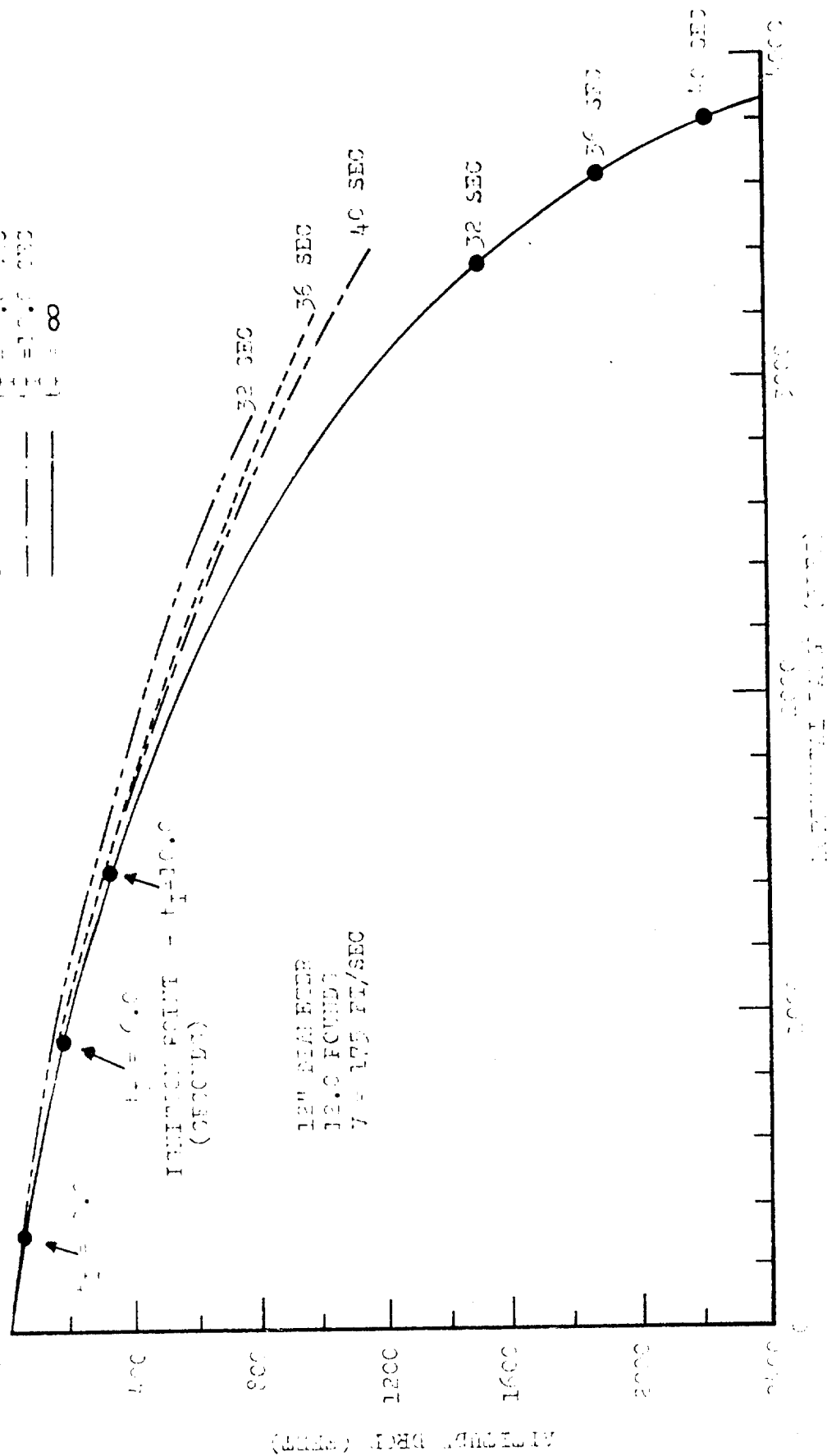


FIG. 12. ALPHABET DEPTH (FEET) vs. TIME (SECONDS) FOR 12" DIAMETER PROJECTILE

A series of tests were conducted in a static spin test fixture in which the rotational speed was controlled. The flare intensity was measured with a photo cell. These tests were conducted to determine the effects of spin on burn rate and efficiency. There was a wide variation in the results and much of it is probably due to the smoke. The following remarks are quantitative:

1. The efficiency appears to have a gradual decrease with increased spin rate.
2. The intensity seems to have a gradual increase with increased spin rate.
3. The burn rate of the flare composition increases quite markedly with increasing spin velocity.

The flare configuration used in the above tests was basically a four-inch diameter one-inch thick disc with a one-fourth inch diameter axial hole in the center. This hole provided a cylindrical burning surface which has an increasing surface area with time. This shape was chosen after testing the end burning type which exhibited considerable sparking due to centrifugal force throwing the molten burning surface off in a radial direction.

Next, contracts were awarded to Denver Research Institute for the manufacture of an experimental launcher and to Honeywell, Inc. and DRI for trajectory studies. The experimental launcher has been used for live and inert SSF launches at Hurricane Mesa. Inert eight-inch and twelve-inch diameter by two-inch thick discs which were tested maintained a relatively flat attitude with respect to the horizontal during the flight. Figure 9 is a photo of the launch area at the top of Hurricane Mesa. The launcher can be seen near the Mesa edge on the top. The inert flare impact area is in the lower left portion of the photo. The results of the trajectory analysis were discussed earlier in the paper.

A total of 17 live, eight-inch diameter, two-inch thick flares were launched from the top of Hurricane Mesa. Figure 8 is a photo illustrating a typical SSF trajectory. The flare appeared to remain stable; however, considerably more thrust was developed than anticipated. These results were discussed in detail earlier in this paper.



FIG. 18 PHOTO OF 8-INCH SSF AT HURRICANE MESA

Some Factors Affecting Burning Rates and Variability of  
Tungsten and Manganese Delay Compositions

F. J. Valenta

Naval Ordnance Station, Indian Head, Maryland

The opinions or assertions made in this paper are those of the author and are not to be construed as an official Department of the Navy position unless so designated by other authorized documents.

ABSTRACT

The reciprocal burning rates and variability of tungsten and manganese delay compositions are investigated as a function of operating pressure and fuel content. In addition, for tungsten delay, the effect of delay body material is explored. Slow burning tungsten delay compositions in a high heat loss system and fast burning manganese delay were found to be at least variable.

INTRODUCTION

Understanding the effects of physical changes, such as different burning pressures, changes in fuel content, and different delay body materials, has long been the objective of studies on pyrotechnic delay compositions. In most studies, though, pyrotechnic delay columns are burned completely inside a pressurized bomb. This situation, although of great interest from a theoretical viewpoint, does not describe the effect of pressure on a cartridge system. In a cartridge, pressure is rapidly built up in the ignition cavity which causes the hot gases to flow through the porous delay column. This pressure, in effect, acts as driving force on the combustion zone. The source of the pressure may be gas output of the ignition element, temperature change, or gassing of the "gasless" ignition composition/delay composition train. A gasless delay composition, of course, is an ideal which cannot be realized because of the imperfections of air trapped in the porous delay column and the inability to mix

perfectly homogeneous delay compositions where oxidizers and fuels are in intimate contact in the proportions necessary for perfect reaction.

In an attempt to better understand the effect of burning pressure, delay body material, and the fuel content of delay compositions, this study was undertaken to investigate the effect of these variables on delay burning rate and delay variability for both the tungsten and manganese delay systems. In specific, the objectives of this study were:

- (1) To determine the effect of operating pressure on the burning time of several tungsten and manganese delay formulations in aluminum delay bodies (since nearly all delay units in the fleet use aluminum delay bodies) under a situation which closely duplicates actual cartridge conditions.
- (2) To determine the optimum operating pressure for each formulation which would minimize delay variability and formulate functional relationships, if possible.
- (3) To determine the effect of delay body material on delay time and variability and the effective pressure coefficient for various tungsten delay formulations.

## APPROACH

### Choice of Delay Body Materials

At the outset of this study, the effect of delay body material on tungsten delay compositions was investigated in an unobturated system in accordance with OD 12051, Operating Procedures for Pyrotechnic Delay Timing Apparatus. Delay bodies of brass, stainless steel, and aluminum were chosen. Results with long burning tungsten delays indicated that stainless steel gave the longest and most consistent delay times (Table I). Note that the stainless steel gave the lowest standard deviation in five of the six tests when compared to brass and aluminum. Coupled with the longer delay time, this means that the percentage of variation is even more significant. In the temperature coefficient test, it is not known if the apparently worse temperature coefficient of the stainless steel loaded delay was due to the effect of the brass and aluminum (with their higher thermal conductivities) warming up prior to delay ignition. (Units are only conditioned to a temperature and fired at room temperature as soon as possible, approximately 30 seconds after removal from conditioning box.)

It was determined that the longer delay times of the stainless steel units was thermal in nature and its cause was exterior to the pyrotechnic materials. Dimensionally identical delays of various materials caused significant changes in the reciprocal burning rate of a given delay powder.

The choice of materials was made, not to test three specific metals, but to investigate a high heat loss system (represented by stainless steel) in comparison to two lower but different heat loss systems (represented by brass and aluminum). High/low heat loss systems can, of course, be made by physical changes in the cartridge system other than simply changing delay body material. For example, the heat capacity, mass, initial temperature, and thermal conductivity of a breech, which is in close thermal contact with the delay cartridge, could be expected to have an increasing effect as delay times increase and cartridge walls are thinner and more thermally conductive. Phenolic or ceramic delay inserts would give a low heat loss system.

#### Delay Compositions

##### Tungsten Delay Shots

Dimensionally identical delay bodies (Fig. 1) of brass, aluminum, and stainless steel were fabricated and loaded with weighed increments (400 mg) of conventional tungsten delay compositions. These compositions were E107-70, E108-70, and E109-70. With three delay body materials, three different burning rate delay compositions, and five pressures chosen, it was decided that seven repetitions of each condition would generate sufficient data to allow interpretation. The formulation of each delay composition and the loading particulars are given in Table II.

Since we were interested in thermal effects, it was decided to include one hot-burning tungsten delay composition in this study. It had been observed that exclusion of diatomaceous earth from tungsten delay compositions caused the burning temperature to increase to the point that delay melting occurred. One tungsten delay composition, E110-70, which contained no diatomaceous earth, was selected for inclusion in this study. Only aluminum delay bodies (10 for each of the five pressures) were loaded with composition E110-70, since it was of only limited interest. The formulation and loading particulars of this composition also are given in Table II.

##### Manganese Delay Shots

Fifty aluminum delay bodies each were loaded with three different burning rates of manganese delay, E1-71, E2-71, and E3-71. The delay mixes were made with the intention that nominal burning rates would be 3, 7, and 11 seconds/inch when tested in the standard unobturated test vehicle. Table III details formulation and loading particulars.

### Ignition Charge and Closure Discs

It is important at this point to remember that the ignition charge, as well as the closure disc configuration, can have an appreciable influence on both delay variability and effective pressure dependence. In this study, a three-hole closure disc was staked in over 160 mg of A1A ignition charge to insure ignition.

The A1A ignition charge was chosen because it is the most commonly used delay igniter in the fleet. The standard amount, 160 mg, used in testing delay powder in an unobtured system was pressed under 30,000-psi pressure into a 0.060-inch column with an inner diameter of 0.260 inch.

The A1A ignition charge has several qualities of interest, most of which are considered undesirable when trying to minimize delay time variability. First, it is nongassing and, when initiated, can partially (and irregularly) extrude through the three closure holes, thus rendering the delay column partially obturated from the closed bomb pressure. Second, the 160-mg A1A charge is more than adequate to ignite even the slowest delays. Ideally, the quantity of charge should have been "just enough" to ignite the delay column. Any larger amount may cause delay ignition below the A1A ignition charge/delay column interface. Also, the A1A ignition charge is considered a hard igniter. It is fairly brisant, which means that larger amounts of this charge increase the shattering effect of ignition on the delay column cracking the delay column at the delay ignition charge interface because of A1A-produced mechanical shock.

The closure configuration is also an important consideration. One-hole and three-hole closures, porous sintered stainless steel, and through bulkhead initiation would all be expected to change ignition characteristics in such a way as to change burning rate, ambient pressure dependence, and system variability.

No attempt was made to optimize ignition of each delay composition. Doubtless, better results could have been obtained for some compositions if this were done. One case in point is that composition E110 contained no diatomaceous earth and the temperature of the reaction is raised to the point where delay melting occurs. The three-hole closure discs on both ignition and output ends contained the liquid slag of the delay poorly and inconsistently, especially at or near atmospheric pressure. (The slag behind the reaction was extruded through the closure disc holes into the bomb chamber.) At higher pressures, the slag did not ooze through the ignition closure holes, but, upon ignition of the output A1A, the liquid slag was forced through the output closure by the pressure of the bomb.

## Closed Bomb Firing System

### Design Criteria

A closed bomb firing system was designed and fabricated which would permit rapid pressurization of the delay column from the ignition end. This would simulate the pressure rise caused by the percussion or electric primer in actual cartridge systems. A pressure gradient would exist through the delay column which also would simulate the real system. The pressurizing gas chosen for this study was  $N_2$ .

The system also was designed with a large free volume combustion chamber whereby the pressure in the chamber would remain effectively constant. Any delay gassing would cause a negligible pressure rise.

Heat losses were minimized in this system by thermally insulating the delay column from its surroundings. The delay column was screwed into a phenolic plug which, in turn, was screwed into the pressure bomb. In this manner, the delay body was thermally insulated from the potentially large heat sink presented by the body of the bomb, and delay time could be studied more easily.

Ignition of the delay column in the closed bomb firing system was by electric match. This would eliminate perhaps the most variable component of the delay train--the percussion primer.

### Operation

Although the closed bomb system (Fig. 2 and 3) was designed to rapidly pressurize the delay column from the ignition end from 0 to 1,500 psig, only levels of 0, 150, 300, 450, and 600 psig were used for this study. All delay bodies were conditioned to 70° F before firing.

The closed bomb system was actuated by throwing the switch closing the ac circuit to a fast acting solenoid valve which quickly pressurized the system on the bomb side of the solenoid. When pressure reached a predetermined level, the dc circuit was closed via a pressure switch causing the electric match to ignite the delay column and to trigger the electronic timer. Pressure in the bomb was continuously monitored by the pressure transducer and was displayed by both a fast sampling digital voltmeter and an oscilloscope. At the termination of delay burning, the A1A output charge was ignited causing the timer to shut off by an electrical impulse delivered by the photocell. Delay time was recorded along with pressure.



## DISCUSSION AND RESULTS

Because of the inherent variability in the  $N_2$  gas pressure regulation system coupled with the delay between test shots, pressures above 0 psig were only within  $\pm 10$  psi of the desired mean. This necessitated the normalizing of all delay times at the nominal pressure ( $\pm 10$  psi) to an adjusted delay time at the exact pressure. This was done by plotting the reciprocal burning rate versus pressure for each delay composition/delay body material combination and generating an equation which fit the data by the least-square method. Most equations were of reciprocal form but several polynomials were required for a good fit. All data were then adjusted to the standard pressures for examination of mean and variability.

### Effects of Pressure and Delay Body Material on Tungsten Delay Compositions

#### Slow Burning Tungsten

The effects of pressure and delay body material on slow burning tungsten delay are shown in Fig. 4. The stainless steel delay body consistently gave the longest delay times (slowest reciprocal burning rates) and gave the most consistent delay times (on the average) over the pressure range.

The aluminum delay body caused the delay time to be more pressure dependent (Fig. 5). The aluminum delay column represents the low heat loss system. Although the thermal conductivity of the aluminum delay body is higher than that of the stainless steel, the low mass of the aluminum body is believed to limit its ability to act as a heat sink—thus, its faster reciprocal burning rate. The strange effect noted here is that, although the pressure dependence of the delay time appears to decrease with faster delays (equals increased fuel content), similar delay compositions (same percentage of fuel) appear to be more pressure dependent in the aluminum delay body (which causes the fastest reciprocal burning rates). Figure 5 shows that all three tungsten fuel level delays, which burn fastest in the aluminum delay bodies, are most pressure dependent over the range of 0 to 600 psig. For the 30% tungsten composition, it was found that a hyperbolic equation best described the observed data.

#### Medium Burning Tungsten

The pressure dependence of the reciprocal burning rate of 45% tungsten composition assumed the same hyperbolic form exhibited by the 30% tungsten delay, but to a much lesser degree (Fig. 6).

The brass delay body data were so close to linear that a linear equation was the natural choice for adjusting data. Again, the stainless steel delay body gave the longest delay times at all pressures and the most consistent results at most pressures. Aluminum fared the worst. As shown in Fig. 5, the aluminum delay body showed the largest average pressure coefficient.

#### Fast Burning Tungsten

For the fastest burning (60% fuel) tungsten delay composition (Fig. 7), a different phenomenon was observed. As noted before, as the percentage of fuel increased, the originally hyperbolic curve flattened out to approach linearity. The curve now becomes much more complex and erratic, and results reflect this fact. The effect of delay body material on reciprocal burning rate decreases, and the choice of the optimum delay body material becomes difficult (although aluminum did give the worst coefficient of variation at three of the five pressures).

The reciprocal burning rate versus pressure curve, which was concave up on the slow burning delays and was close to linear on the 45% fuel tests, now, if anything, becomes concave down. Again the aluminum delay body gives the largest average pressure coefficient (Fig. 5).

With the fastest burning tungsten delay, every delay tested, on the average, burned slower at 150 psig than at either ambient pressure or 300 psig. This may indicate that there may be a region of low pressures over which fast burning tungsten delay may have a zero pressure coefficient. The effect of delay body material on burning time and variability appeared to be consistent with the slower burning tungsten delays tested. The high heat loss system (stainless steel) exhibited the longest burning times while the brass and aluminum gave about equal burning times up to 300 psig with the brass and aluminum assuming their expected relative positions at the two higher pressures.

A judgment on the effect of delay body material on variability is more difficult in this case. The average coefficient of variation over the pressure range is highest for the aluminum delay body. (The aluminum also gives the highest coefficient of variation for any delay body at three of the five test pressures.) The brass delay body barely gives the lowest average coefficient of variation (Fig. 7) and shows the lowest average pressure coefficient (Fig. 5).

### Effect of Pressure on Delay Composition E110

Tungsten delay (50%) composition E110 was not well-suited to this type of pressure test in the type delay column/closure combination used. Results for composition E110 were not adjusted nor was an equation computed. Generally stated, the data indicate (Fig. 8) that reciprocal burning rate decreased and that variability tended to increase at increasing pressures. The pressure coefficient was worse than any delay tested. At low pressures, composition E110 burned at about the same rate as the standard 45% tungsten delay, where at high pressures, the composition was about as fast as the 60% tungsten composition at the same pressures. The average pressure coefficient for delay composition E110 ran 86% higher than the worst of either of the faster burning (45% and 60%) tungsten delays.

### Manganese Delay Compositions

All manganese delay shots were tested in aluminum delay bodies. For this reason, the effect of pressure on delay time, the effect of fuel content on delay time, and the effect of each on variability of delay time were of prime importance. The 33.0% and 37.8% manganese delays showed no indication of nonlinearity of delay time with pressure; therefore, they were best described, and delay times corrected, with a straight line (Fig. 9). The fastest burning manganese delay (43.6%) was approximated with a polynomial because the mean delay time at 150 psig was longer than that at either 0 or 300 psig.

The fastest delay (43.6% manganese) was the most consistent (coefficient of variation of about half of either of the others, on the average) and had the lowest average pressure coefficient (less than half of those of either other manganese delays) (Fig. 5).

### General Effects of Pressure

#### Reciprocal Burning Rate

The overall effect of pressure was as expected: as pressure increased, the reciprocal burning rate decreased. With the slower burning tungsten compositions (higher reciprocal burning rate), the effect diminished as pressure increased. With the faster tungsten composition, the effect appeared to be quadratic in nature. For the manganese compositions, the effect was linear for the slower compositions and quadratic for the fastest.

### Coefficient of Variation

There was no overall effect of pressure on variability. For 30% tungsten (Fig. 4), the stainless steel units had the lowest and most consistent coefficients of variation. For 45% tungsten (Fig. 6), stainless steel again was lowest and most consistent, but only because the brass units had an extremely high coefficient of variation at 600 psig. Except at 0 psig, the aluminum delay body units were the most variable, exceptionally so at 150, 300, and 450 psig. For 60% tungsten the coefficients of variation of the stainless steel units were the most erratic, being the highest at 0 and 450 psig and the lowest at 150 and 300 psig. The brass units were the least variable. For the manganese compositions (Fig. 9), the 43.6% was the least variable with no appreciable difference overall between 33.0% and 37.8% manganese.

### General Effects of Change in Composition

#### Reciprocal Burning Rate

As already known, the reciprocal burning rate increased with increasing fuel content for both the tungsten and manganese. The effects of changes in composition at each pressure level are shown in Fig. 10 through 14. The curves on all of these graphs were not derived statistically. They were fitted by sight and are only presented to show differences between the tungsten and manganese units.

#### Coefficient of Variation

For the tungsten delay compositions, the coefficient of variation increased with increasing fuel content, while for the manganese delay compositions, the opposite effect was observed. In other words, the slow tungsten delays and the fast manganese delays were found to be the most consistent, in general, at any given pressure. Considering only the coefficient of variation as a criteria, it appears that at the low and middle fuel levels, the stainless steel/tungsten delay combination is the best. At the high composition level, the manganese units definitely are the best. The effects of changes in composition on the coefficient of variation are shown in Fig. 10 through 14.

### General Effects of Delay Body Material

Figures 4, 6, and 7 show that, of the three delay body materials, stainless steel units burned the slowest and aluminum, the fastest. However, these differences are minimal, especially at the 45.0% and 60.6% tungsten levels when they are considered in relationship to the overall range in reciprocal burning rate. This is evident in Fig. 10 through 14.

where the points representing the tungsten compositions are very closely grouped. With respect to the coefficient of variation, Fig. 4, 6, 7 and 10 through 14 indicate that, overall, the aluminum bodies are the most variable and stainless steel the least variable.

### CONCLUSIONS

The following conclusions resulted from this study:

- As measured by the average pressure coefficient, manganese units were the least affected by changes in pressure. For the tungsten units, the ones in aluminum bodies were the most sensitive to pressure.
- For the tungsten units, the coefficient of variation tended to be higher for the higher levels of fuel (faster burning). The opposite was true for the manganese units.
- For the low and intermediate tungsten fuel levels, the stainless steel units were the least variable. At the highest tungsten level, the brass units were the most consistent with the stainless steel a close second.
- Overall, of the tungsten units, the ones with stainless steel bodies were the slowest burning and least variable; the aluminum units burned fastest and were the most variable. Of the manganese units, the highest fuel content units burned fastest and were the least variable.
- Both tungsten and manganese delay compositions are pressure dependent, although, for the fastest delays, the change in delay time attributable to pressure approaches the inherent variability of the delay at that pressure.
- The effect of pressure on reciprocal burning rate is functionally more complicated for the fastest delays of either type.
- There is no indication that there is any correlation between pressure and variability for a given delay composition/delay body type.
- All tungsten delay shots of intermediate tungsten levels exhibited a lower pressure dependence than that of the slower tungsten delay over the range of 0 to 600 psig.
- Faster burning tungsten delay compositions, although their burning rates are less dependent upon pressure, are more variable at any given pressure. For this reason, using a short length of slow burning tungsten delay (potential problem: controlling length) or a longer length of fast burning manganese delay (problem: space) may be preferred.

In addition, factors suggested by this work, but not specifically treated, include:

- Delay cartridges initiated by percussion primers can be expected to be exposed to a range of pressures caused by inherent primer variability. It may be as important to minimize pressure effects by utilizing a fairly pressure-insensitive delay formulation as to strive for primer consistency.
- Although the reciprocal burning rates of faster delay compositions (both tungsten and manganese) appear to be less pressure sensitive at high pressures, generating and holding such elevated pressures over the entire delay burning period may pose an engineering challenge to the cartridge designer.
- Undesirable delay time variability caused by thermal mechanisms, such as the anticipatory effect, can be expected to be influenced by such factors as delay formulation thermal conductivity (a function of percentage of fuel) and cartridge thermal diffusivity (a function of delay body material and geometry).

#### RECOMMENDATIONS

There are many factors which affect delay time, delay variability, and the pressure coefficient of both tungsten and manganese delay compositions. These factors include (but are not limited to):

- (1) Heat loss of system
- (2) Fuel content of delay composition
- (3) Operating pressures of system
- (4) Ignition system (primer, closure disc, and ignition material).

All factors pointed out here should be considered by the cartridge designer for optimum system performance.

It is believed that very often the criticism directed at pressed pyrotechnic delays is not founded on fact. If a certain delay is chosen (often by chance) for a specific unit and the cartridge does not perform acceptably with respect to variability, there is an inclination to downgrade confidence in the consistency of pyrotechnic delays. To ask a pyrotechnic delay to perform optimally in a system which will adversely affect its variability is not reasonable. Unless there is a serious effort to achieve a match between primer output, ignition material, closure disc, delay composition, delay body material, and geometry, such criticism is unfounded.

It is recommended that the cartridge designer consider these facts and not prematurely rule out conventional pyrotechnic delays in favor of other delay systems.

It is recommended that a product improvement program be initiated on a delay cartridge which is considered unacceptably variable. It is believed that cartridge performance could be improved to the point that it could meet any realistic performance requirements if sufficient freedom in design changing and composition selection is given. It is also recommended that the full potential of the present state-of-the-art of pyrotechnic delay systems be developed before rushing into alternates to pyrotechnics.

Table I

## Aging Characteristics and Temperature Coefficient Effects of Delay Body Materials

Test no.	Delay lot	Storage at 160° F (wk)	Brass			Stainless steel			Aluminum		
			No. of shots	Reciprocal burning rate (in/sec)	Standard deviation (sec)	No. of shots	Reciprocal burning rate (in/sec)	Standard deviation (sec)	No. of shots	Reciprocal burning rate (in/sec)	Standard deviation (sec)
Aging Characteristics											
1	IHM-WD-48-69	0	6	23.24	0.635	6	24.76	0.256	6	23.55	0.425
2	IHM-WD-48-69	1	7	23.76	0.297	6	24.57	0.264	7	24.01	0.536
3	IHM-WD-48-69	3	7	23.67	0.632	7	24.28	0.365	7	23.06	0.680
4	IHM-WD-63-69	0	14	23.04	0.195	11	23.70	0.229	15	22.37	0.501
Temperature Coefficient Effects											
5	IHM-WD-2-70 <sup>a</sup>	0	7	24.60	0.228	6	25.40	0.098	7	24.52	0.228
6	IHM-WD-2-70 <sup>b</sup>	0	7	26.98	0.314	5	28.07	0.183	7	26.02	0.510

<sup>a</sup>Conditioned at 70° F.<sup>b</sup>Conditioned at -65° F.

Table II

## Tungsten Delay Compositions

(Consolidation pressure = 30 ksi; delay column diameter = 0.261 in.)

	E107-70	E108-70	E109-70	E110-70
Formulation (%)				
Tungsten (4μ)	30	45	60	50 <sup>a</sup>
Potassium perchlorate (150μ)	10	10	10	10 <sup>b</sup>
Barium chromate	55	40	25	40
Diatomaceous earth	5	5	5	0
Increments, inch	8	10	12	-
Maximum cutback for 1-in. column (in.)	0.004	0.060	0.068	-
ATA ignition charge (mg)	160	160	160	160
Reciprocal burning rate at 70° F <sup>c</sup> (10 shots) (in/sec)	22.907	9.037	4.507	8.801
Coefficient of variation (%)	0.93	2.5	2.5	1.2
Batch size (g)	2500	2500	2500	2500

<sup>a</sup>4 μg tungsten.<sup>b</sup>20μ potassium perchlorate.<sup>c</sup>Estimated.

Table III

## Manganese Delay Compositions

(Consolidation pressure = 30 ksi; delay column diameter = 0.201 in.)

	E1-71	E2-71	E3-71
Formulation (%)			
Manganese	33.6	37.8	33.0
Lead chromate	52.9	44.2	37.0
Barium chromate	3.5	18.0	30.0
Loading method	Volumetric scooping		
ATA ignition charge (in.)	0.060	0.060	0.060
Reciprocal burning rate at 70° F <sup>a</sup> (10 shots) (in/sec)	2.684	5.183	10.311
Coefficient of variation (%)	1.2	2.1	1.5
Batch size (g)	2000	2000	2000

<sup>a</sup>Estimated.



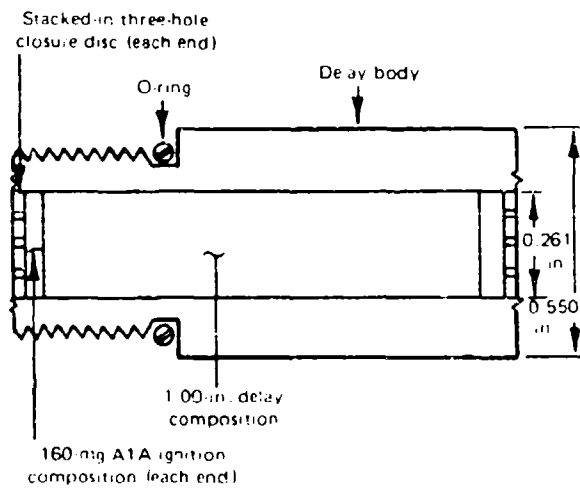


Figure 1. Delay Bodies Made of 2024 Aluminum, 304 Stainless Steel, and 360 Brass

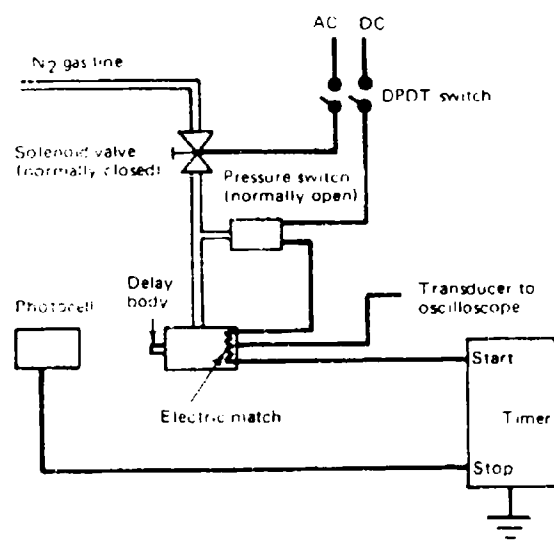


Figure 2. Closed Bomb Firing System

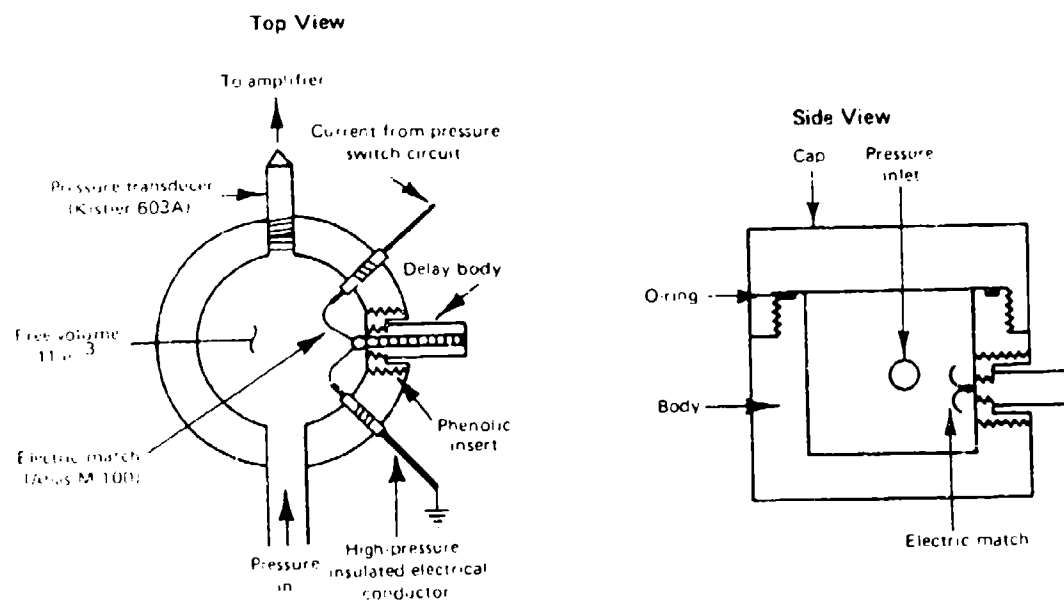


Figure 3. Detail of Closed Bomb

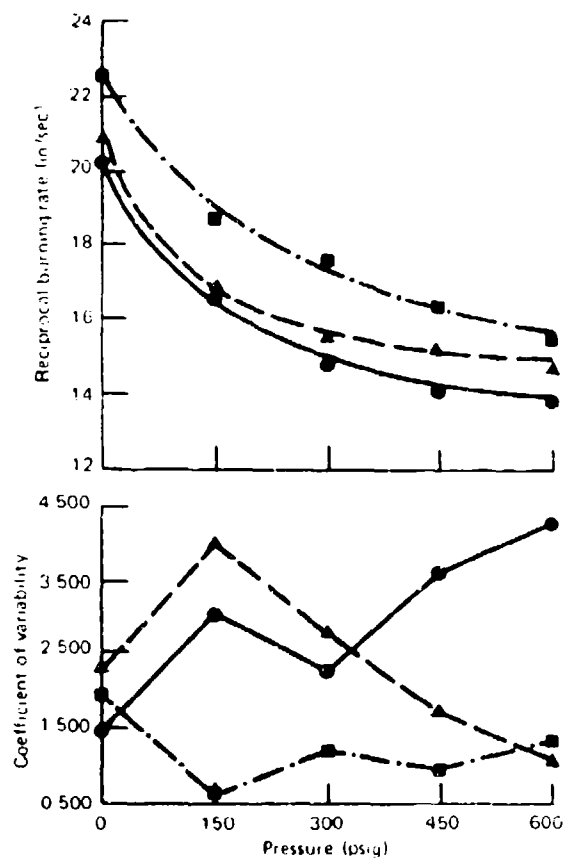


Figure 4. Effect of Pressure and Delay Body Material on Reciprocal Burning Rate and Coefficient of Variation for 30% Tungsten Composition (● Aluminum; ▲ Brass; ■ Stainless Steel)

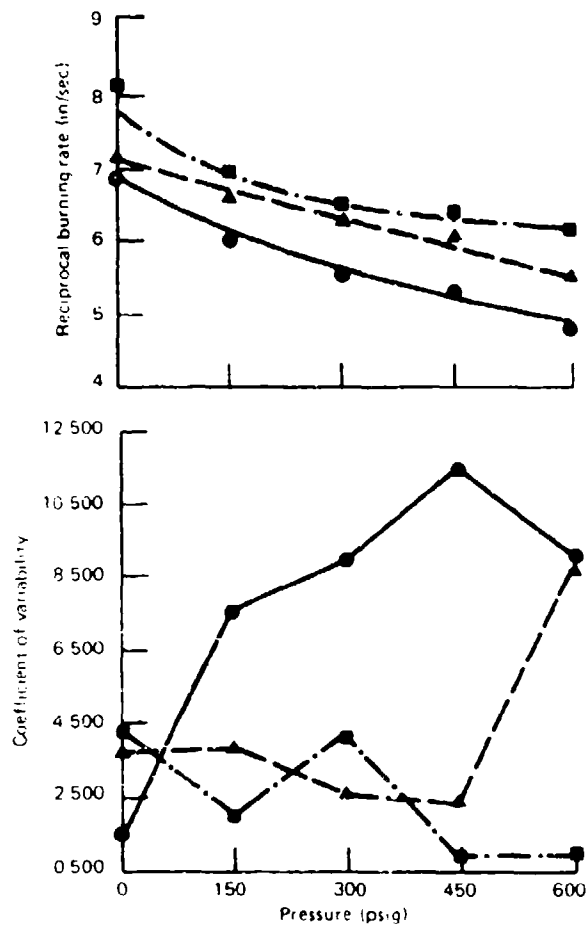


Figure 5. Relationship Between Composition and Average Pressure Coefficient Over the Range 0 to 600 psig ( • Aluminum Body, Tungsten (W); ▲ Brass Body, Tungsten; ■ Stainless Steel Body, Tungsten; ○ Aluminum Body, Manganese (Mn) )

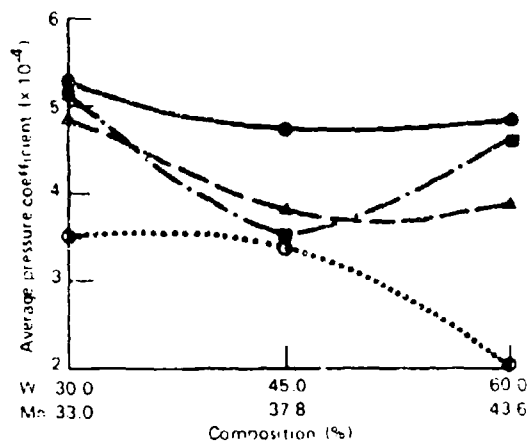


Figure 6. Effect of Pressure and Delay Body Material on Reciprocal Burning Rate and Coefficient of Variation for 45% Tungsten Composition ( • Aluminum; ▲ Brass; ■ Stainless Steel)

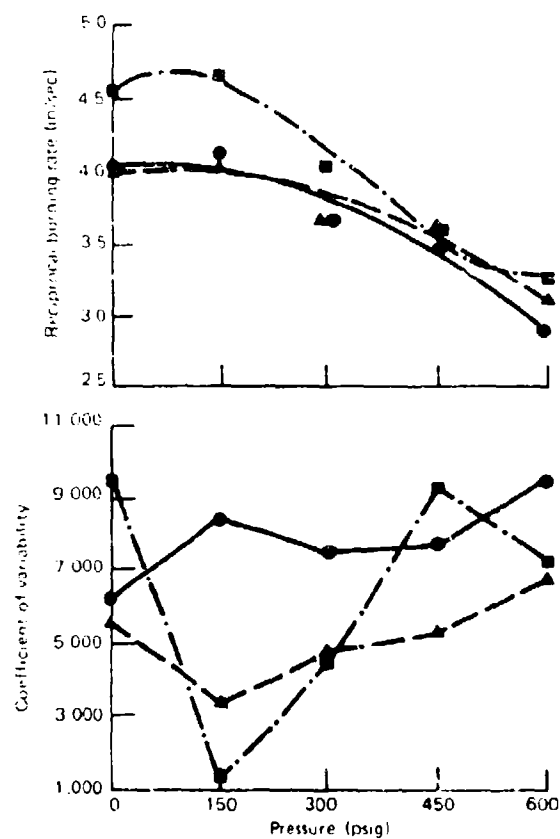


Figure 7. Effect of Pressure and Delay Body Material on Reciprocal Burning Rate and Coefficient of Variation for 60% Tungsten Composition ( ●Aluminum; ▲Brass; ■ Stainless Steel)

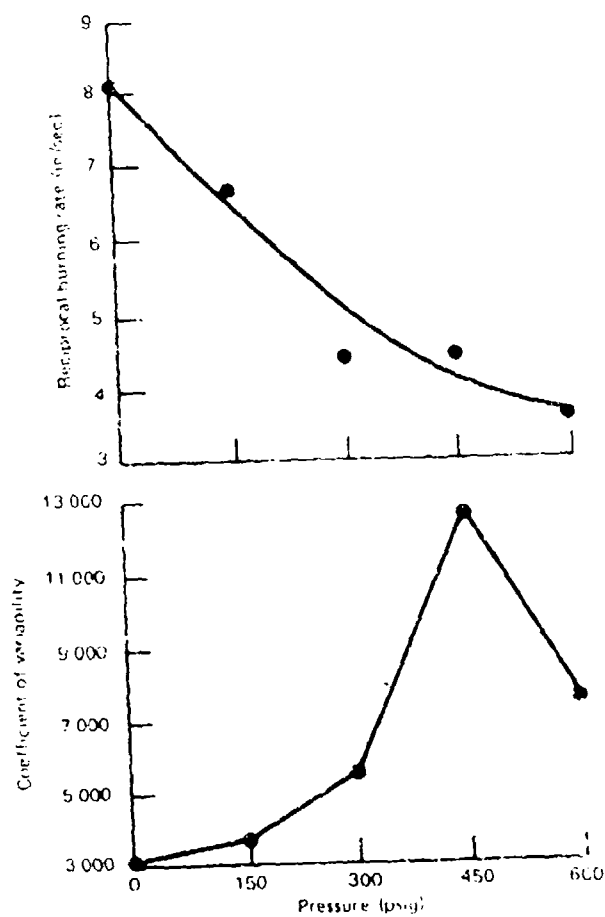


Figure 8. Effect of Pressure on Reciprocal Burning Rate and Coefficient of Variation for 50% Tungsten Composition



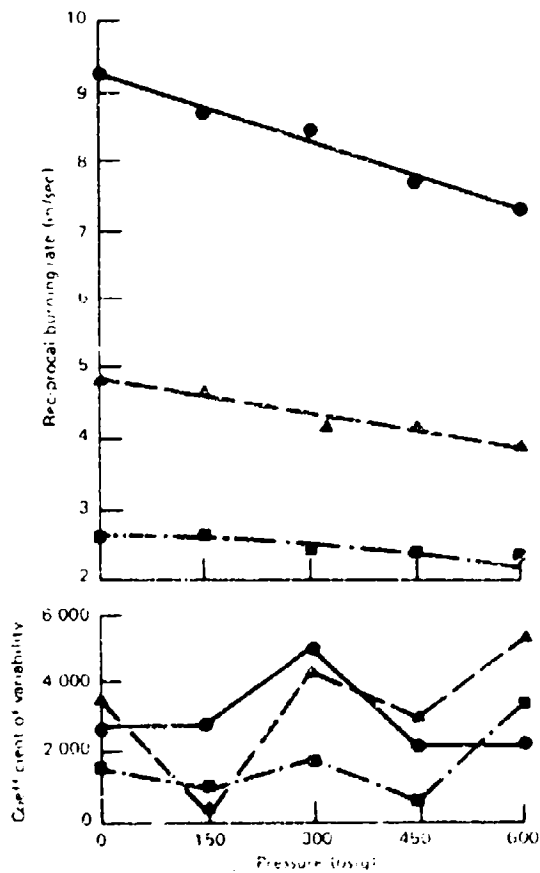


Figure 9. Effect of Pressure and Delay on Reciprocal Burning Rate and Coefficient of Variation for Manganese Compositions in Aluminum Body  
 (● 33.9% Manganese; ▲ 37.8% Manganese; ■ 43.6% Manganese)

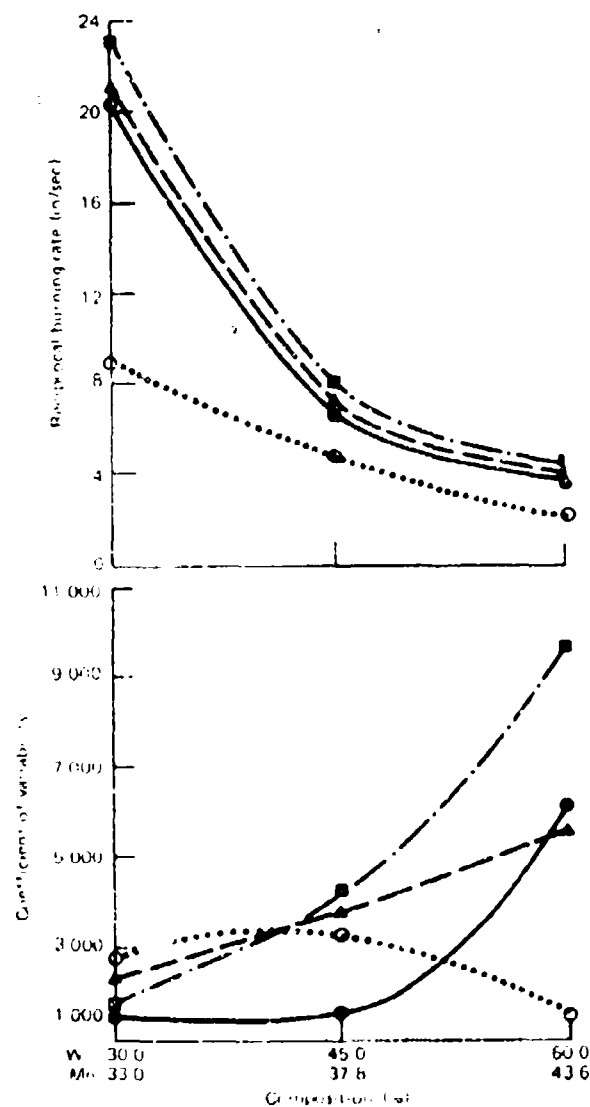


Figure 10. Effect of Changes in Composition on Reciprocal Burning Rate and Coefficient of Variation at 0 psi (● Aluminum Body, Tungsten (W); ▲ Brass Body, Tungsten; ■ Stainless Steel Body, Tungsten; ○ Aluminum Body, Manganese (Mn))

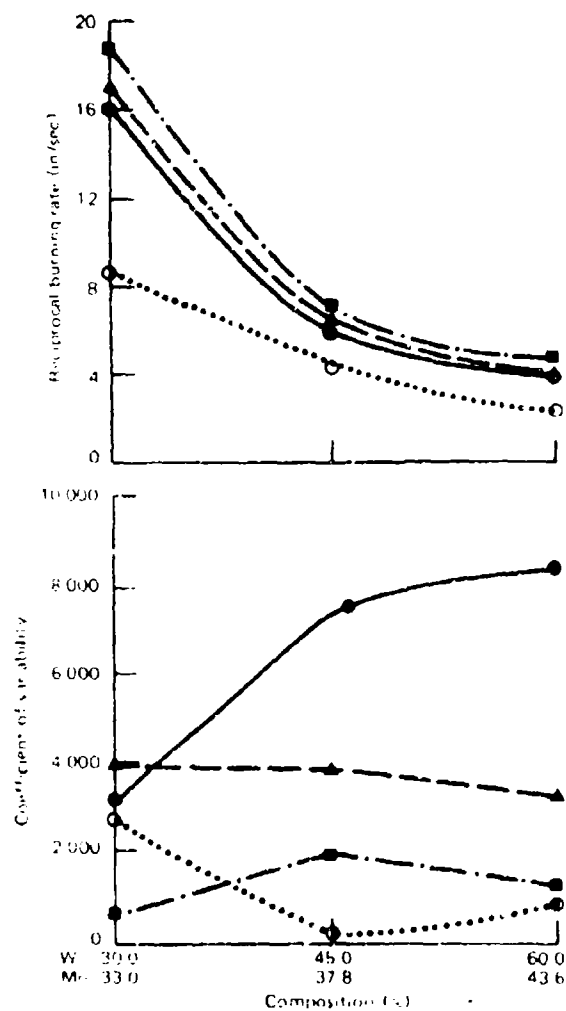


Figure 11. Effect of Changes in Composition on Reciprocal Burning Rate and Coefficient of Variation at 150 psi (• Aluminum Body, Tungsten (W); ▲ Brass Body, Tungsten; ■ Stainless Steel Body, Tungsten; □ Aluminum Body, Manganese (Mn)).

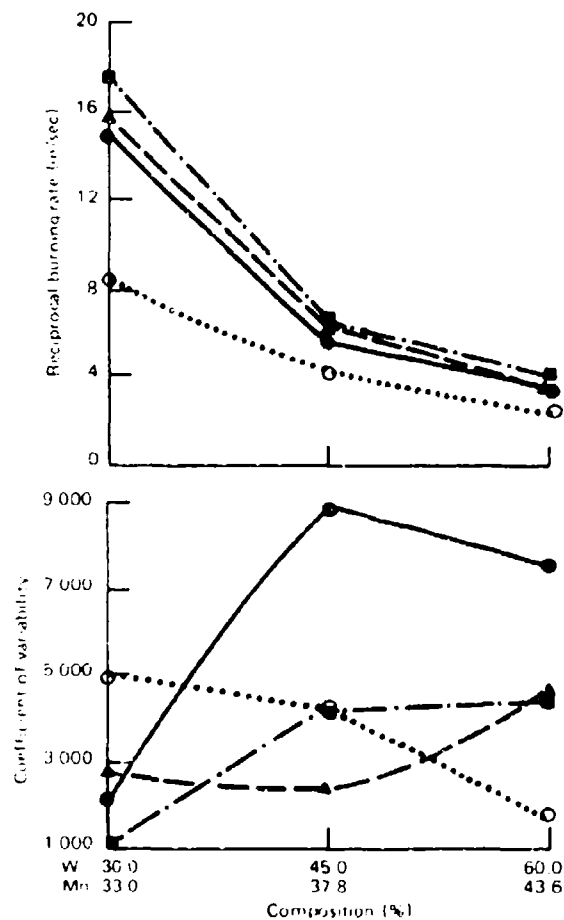


Figure 12. Effect of Changes in Composition on Reciprocal Burning Rate and Coefficient of Variation at 300 psi ( ● Aluminum Body, Tungsten (W); ▲ Brass Body, Tungsten; ■ Stainless Steel Body, Tungsten; ○ Aluminum Body, Manganese (Mn) )

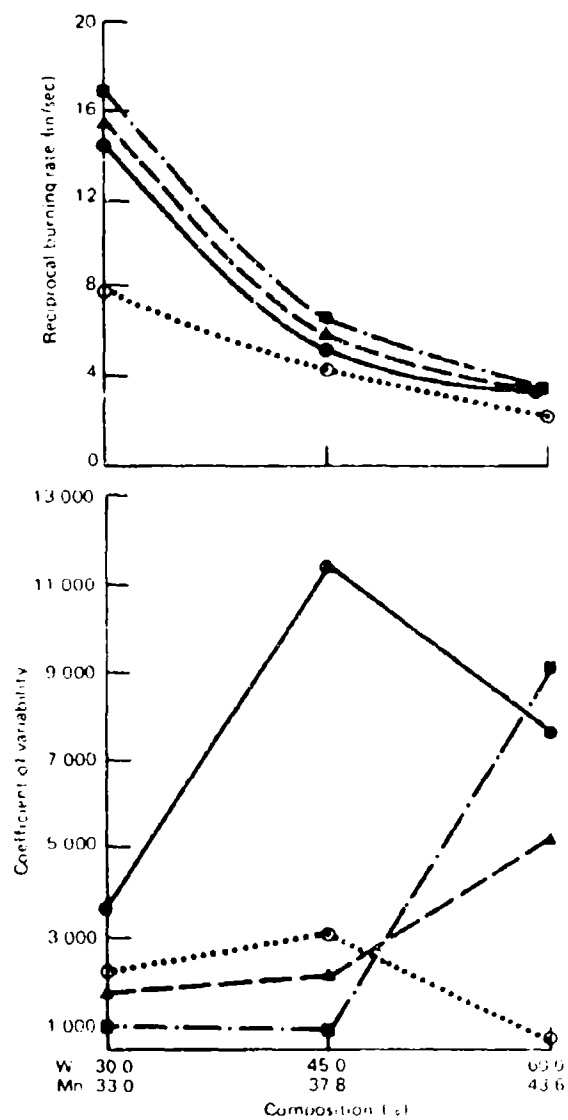


Figure 13. Effect of Changes in Composition on Reciprocal Burning Rate and Coefficient of Variation at 450 psi ( • Aluminum Body, Tungsten (W); ▲ Brass Body, Tungsten; ● Stainless Steel Body, Tungsten; - - Aluminum Body, Manganese (Mn) )

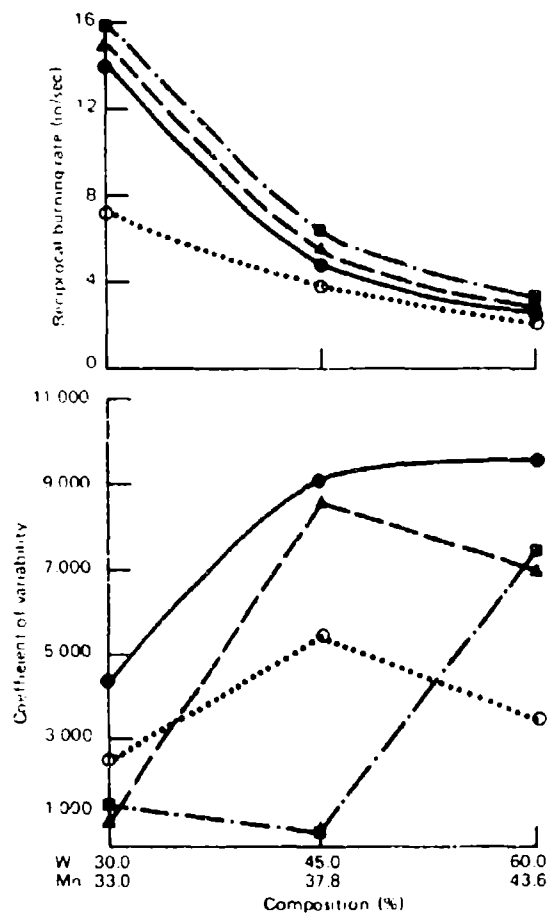


Figure 14. Effect of Changes in Composition on Reciprocal Burning Rate and Coefficient of Variation at 600 psi ( ● Aluminum Body, Tungsten (W); ▲ Brass Body, Tungsten; ■ Stainless Steel Body, Tungsten; ○ Aluminum Body, Manganese (Mn) )

## The State-of-the-Art of Navy Pyrotechnic Delays

F. J. Valenta

Naval Ordnance Station, Indian Head, Maryland

The opinions or assertions made in this paper are those of the author and are not to be construed as an official Department of the Navy position unless so designated by other authorized documents.

### ABSTRACT

The two principle pyrotechnical delay systems used by the Navy are discussed with respect to inherent variability, temperature dependence, and optimum burning rate ranges. Data are presented which show fast delays ( $\text{Mn}/\text{BaCrO}_4/\text{PbCrO}_4$ ) and slow delays ( $\text{W}/\text{BaCrO}_4/\text{KClO}_4/\text{SiO}_2$ ) to be far superior than the  $\pm 25\%$  tolerance often attributable to pyrotechnic delays.

### INTRODUCTION

Much has been written recently extolling the advantages of electronic delays and nonconventional pyrotechnic delays (swaged or bimetal alloying delays). In such discussions, reference is often made to the effect that conventional pyrotechnic delays are no more consistent than  $\pm 25\%$  over the temperature range. The purpose of this paper is to state that, as far as the Navy's experience, pyrotechnic delays are much

more consistent than their critics lead one to believe. A method of minimizing delay loading variables refined at the Naval Ordnance Station, Indian Head, Md., is also discussed.

#### STATE-OF-THE-ART

The present state-of-the-art of pyrotechnic delays can best be defined in terms of the experience, ingenuity, and insight of the delay manufacturer and loader. In short, there is, compared to fairly exact, well-defined sciences such as propellant technology and explosive technology, a nearly total lack of theory and understanding of those factors which influence the kinetics of pyrotechnic reactions.

The present experience in developing new delays and improving existing ones has been the Edisonian approach of trial and error. There are several reasons such an approach has been popular.

First, usually the improvement desired is directly tied to an end item result in a specific unit. Efforts are not directed at basic research or developing a generalized theory but at solving a specific, well-defined problem in a given unit. The accomplishments under such narrow efforts are rarely promulgated except by word of mouth and are usually not applicable to other delay units, even those with similar delay systems. Such approaches often are based on art, not science.

Second, the field of scientific delay development is so relatively new that it has been the approach of many of those in the field to concentrate on a shotgun approach—trying mixtures of various fuels and oxidizers (varying such parameters as the ratio of components, particle sizes, additives, and binders) and developing new and patentable delays. This approach is, of course, much more sensational and faster moving than formulating basic delay theories. The time is proper now to regress and take a hard scientific look at the basics of pyrotechnic delays and formulate the theories needed to understand and correct the specific problems on a general level.

Of prime interest to the Navy in the field of pyrotechnic delays are two specific formulations: tungsten delay ( $W/BaCrO_4/KClO_4/SiO_2$ ) and manganese delay ( $Mn/BaCrO_4/PbCrO_4$ ).



Table I presents the typical inherent variability and temperature dependence of the two delay systems in an unobturated test column. Better results can be obtained through optimization of the system. Both compositions are also fairly pressure dependent as shown in Fig. 1.

In end-item obturated production units, current state-of-the-art has achieved a reproducibility (at a given temperature) of 90% of the test population having a burning time less than  $\pm 4\%$  of the mean for long delay times ( $>20$  sec/in.). For short delay times ( $<4$  sec/in. delay powders), a precision of all 80 test shots falling within  $\pm 6\%$  of the mean (which was a nominal 0.75 second) has been achieved firing over the temperature range ( $-65^{\circ}$  to  $200^{\circ}$  F).

The Navy has had success in using tungsten delay in applications requiring long delay times ( $>10$  sec/in. burning rate powders) and manganese delay for shorter burning rate applications. In addition, tungsten delay composition has been shown to exhibit superior high temperature storage characteristics; 3 months storage at  $300^{\circ}$  C will change the nominal delay time only several percent.

#### MINIMIZING VARIABILITY

The Naval Ordnance Station (NOS) is a relatively recent entrant into the field of pyrotechnic delay research and development. As a result of the closing of the Naval Ordnance Plant, Macon, Ga., NOS was designated, about 7 years ago, as the cognizant field activity for Navy pyrotechnic delays.

The arts of the pyrotechnicists have been combined with science and technology in order to advance the state-of-the-art of pyrotechnic delays. The improvement in NOS delays from the period where little experience or technology existed to the present is shown in Fig. 2.

Aspects of pyrotechnic delays currently being investigated at NOS include extensive theoretical studies on the kinetics of pyrotechnic reactions, effects of additives on the burning rates, variability and pressure and temperature dependence of various delay systems, binders for gasless delays, improved pyrotechnic delay ignition concepts,

improved mixing and loading techniques, and studies on the effects of hardware and materials on delay systems.

Because of the unique position of NOS, much effort has been expended in extending the state-of-the-art in loading delays. One specific technique, which was used on long burning delays, will be discussed at length. The technique—Sublotting—was developed and refined by J. J. Trick at NOS and is recounted here for the reader.

It has been observed that certain uncontrollable factors have an influence on delay powder performance (i. e., burning rate) even if extensive efforts are made to nearly automate the entire process.

In attempts to eliminate operator variation, hand operated loading presses were replaced by pneumatically controlled air presses with standardized pressure, dwell time, and load rate. Hand scooping of delay increments was replaced by weighed increments to insure uniformity and standardization of increment size.

Data were generated which showed the time required for delay powder to come to equilibrium with the controlled humidity of the loading bay. Delay powder was allowed to achieve equilibrium each day before commencing loading.

In order to minimize variability still encountered, a sublotting technique was employed. The one day's work of each operator loading on one press out of one powder pan was taken as a sublot. The delay column was loaded slightly longer than needed for the desired delay time.

Out of each sublot (around 100 delay columns), a sample of nine delay columns was pulled, loaded into all-up units, and test-fired. Results were recorded for each sublot and, using a table based on the burning rate of the specific delay powder, the remaining delay columns of each sublot were cut back to achieve the desired mean delay time. The sublot sample also allowed a decision to be made on whether the within sublot variability was acceptable.

The variability of a typical lot before sublotting techniques were employed and the distribution of means of sublots loaded by individual operators on a given day are shown in Fig. 3. Although no individual sublot is considered too variable, unacceptable lot variation resulted from the sum of the variation of the individual groupings and the

variation between the groupings. This problem was recognized and it was determined that control of the mean of individual sublots would greatly reduce lot variability.

The effect of precisely controlling the subplot mean is shown in Fig. 4 and 5.

Although sublotting did achieve desired results of greatly reducing lot variability, it is only fair to note here that sublotting greatly increases unit price. First, nearly 10% of the units are used for in-process testing. Second, care must be exercised to insure separation and identification of individual sublots. Third, all delay columns need be cut back after the in-process sample is tested, and the amount of cutting back differs for each subplot. Because of these drawbacks, sublotting techniques should be employed only in those applications where product performance considerations far outweigh economic considerations.

### CONCLUSIONS

Variabilities in delay times of the magnitude of  $\pm 25\%$  (and even considerably lower in some units) usually stem from attempts to manufacture delay devices by personnel who have little or no experience in processing, mixing, and loading delays. This often results from the competitive bidding process. The cognizant design engineering may also be guilty of increasing the "inherent" variability of a specific unit by inadvertently suboptimizing unit design, specifying an inferior (for the specific unit) delay composition, or not giving those knowledgeable in pyrotechnics (and responsible for producing the unit) the freedom needed, within the specification, to make the unit perform as desired.

In some less sophisticated and less critical applications, a precision of less than  $\pm 25\%$  may not be needed. In such cases, the specifications on the specific unit may be, indeed, very loose, but this is not to imply that manufacturers cannot, nor do not, often greatly better the specification limits. Care must be taken not to assume that specifications reflect the state-of-the-art.

If tighter tolerances in delay time, variability, or reliability are needed, the answer is as simple as tightening up the functional requirements on the specific unit. The experienced and competent delay manufacturer, equipped with an adequate knowledge of the art and science of pyrotechnic delays should be able to meet any realistic systems requirement, given the freedom to optimize the system and the finances to afford stringent variable control techniques.

Table I  
Typical Inherent Delay Variability

Burning time (sec./in.)	Typical coefficient of variation at 22° C (%)	% Change in burning rate from 22° to -54° C
<u>Tungsten Delay</u>		
30-35	1.5-3	10-11
20-25	2-3	8-9.5
3-5	2-5	5-6
<u>Manganese Delay</u>		
2-3	1.2-2.5	5-8
3-7	1.2-2.5	5-13
9-12	1.2-2.5	10-15

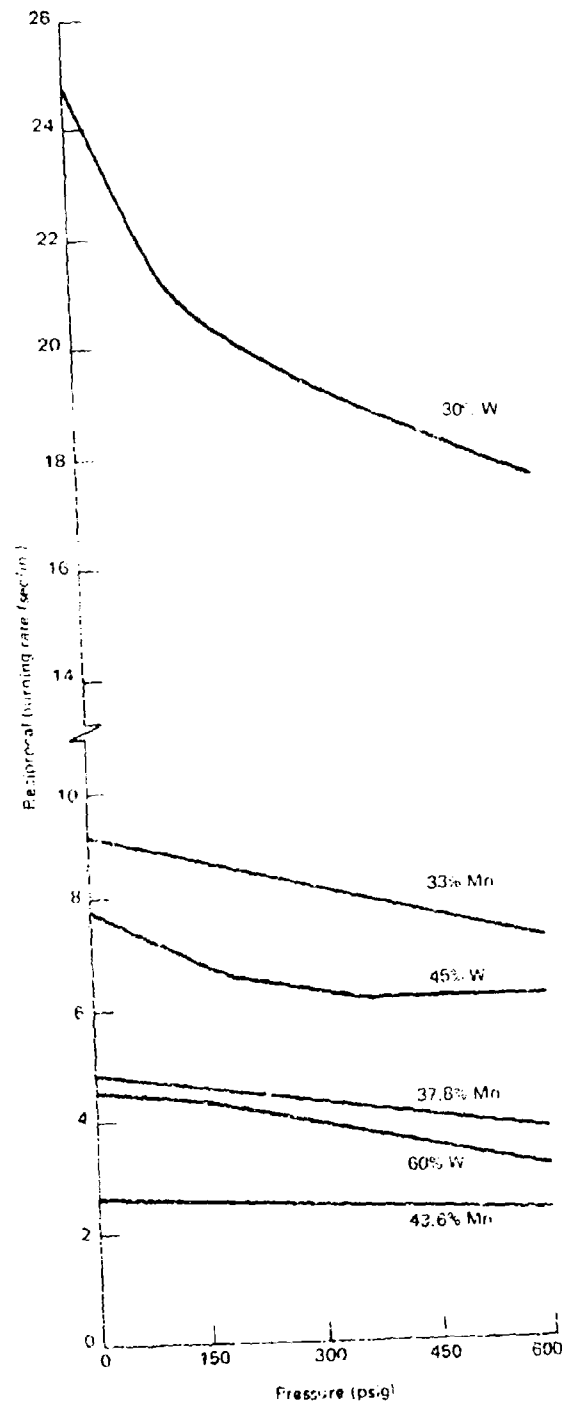


Figure 1. Effect of Pressure on Reciprocal Burning Rate

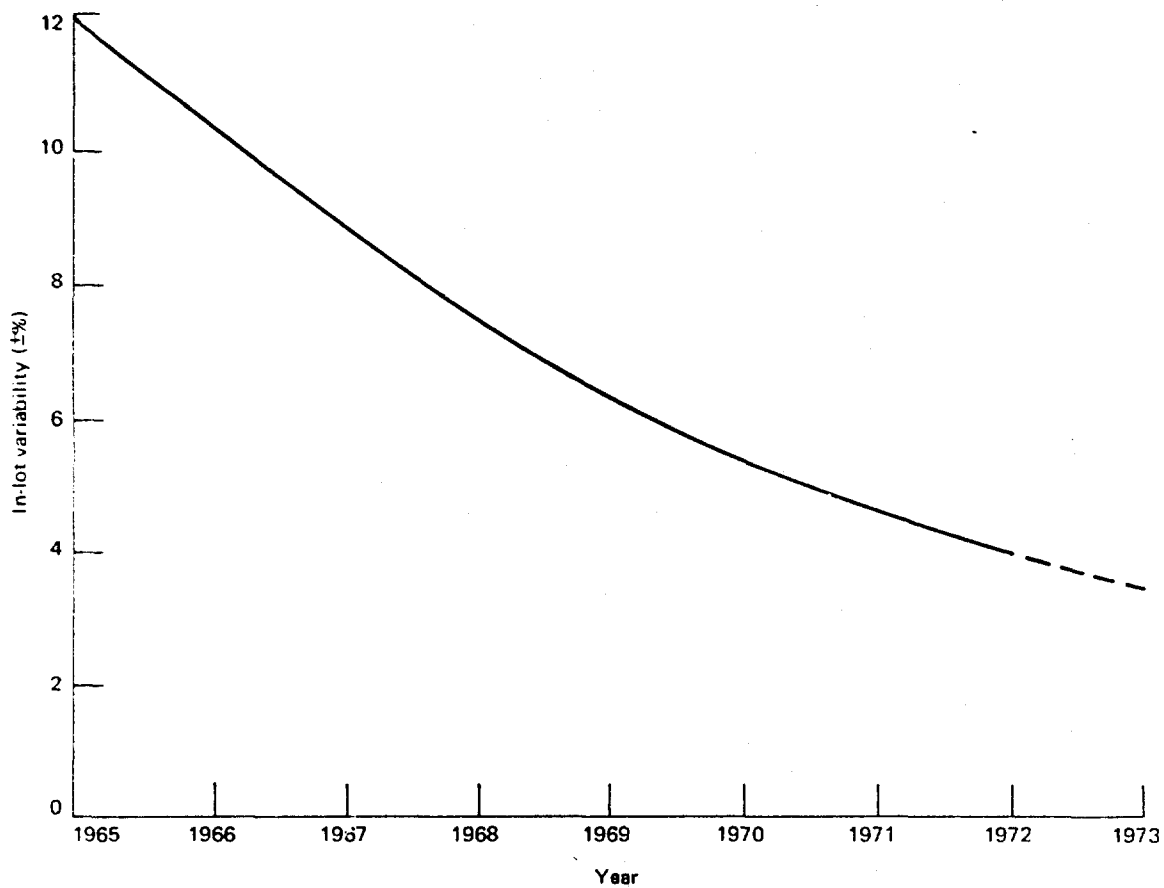


Figure 2. Improvement in NOS Delay Capability

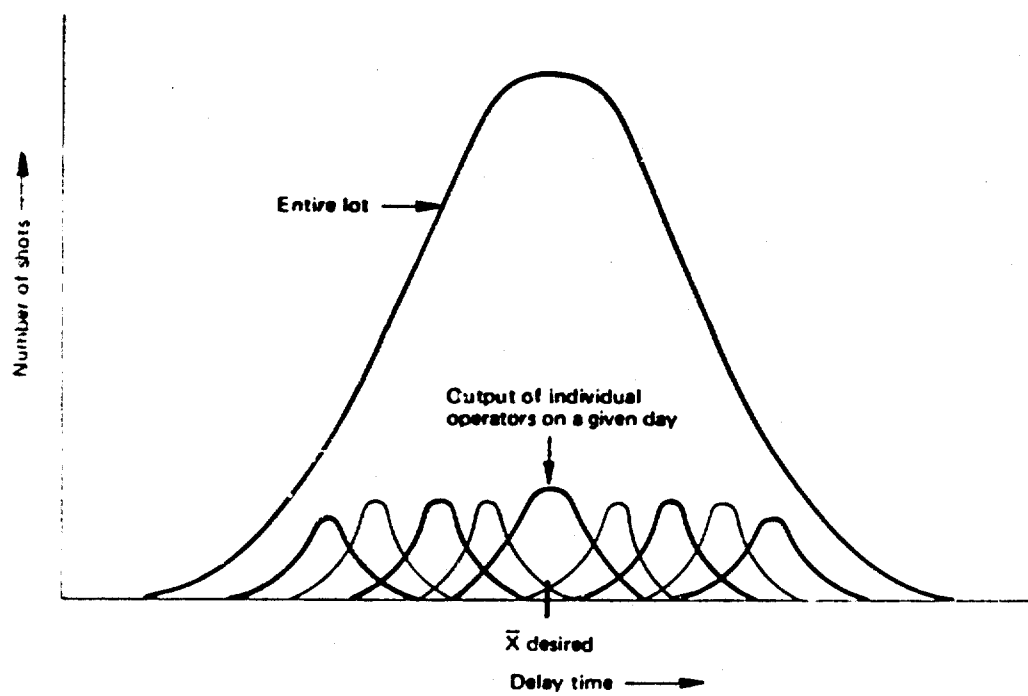


Figure 3. Lot Variability Without Sublotting

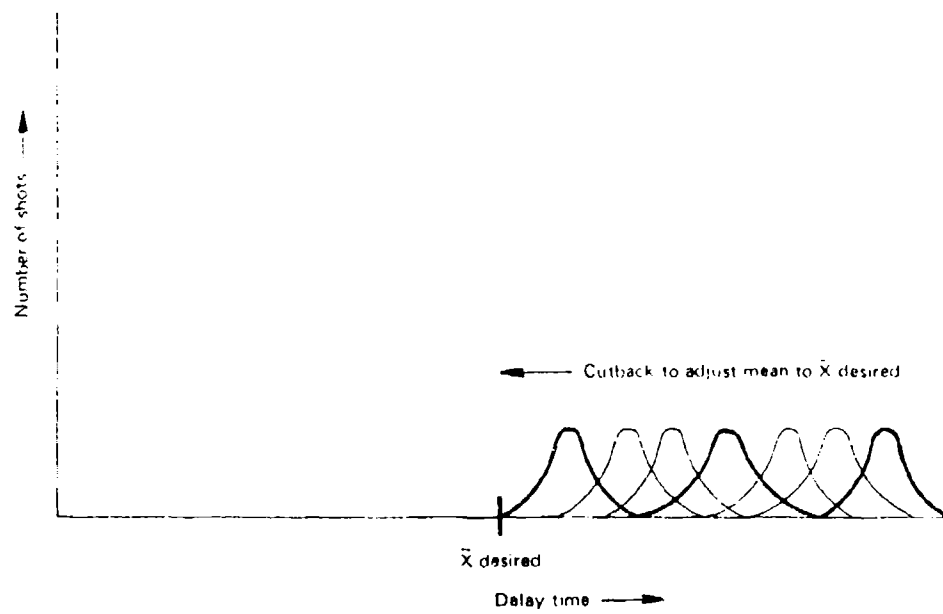


Figure 4. Sublots Before Cutback



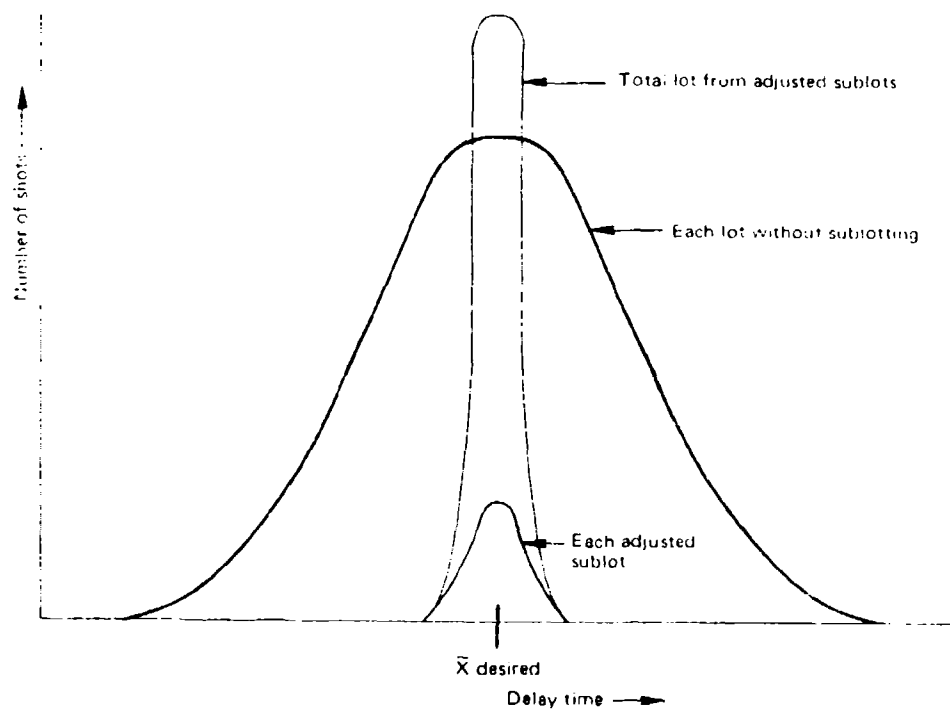


Figure 5. Comparative Results

# **ANALYTICAL AND FUNCTIONAL TESTS OF NATURALLY AGED EXPLOSIVE ORDNANCE IN THE PERSHING LEAP PROGRAM**

by

**Edward M. Storma  
Martin Marietta  
Orlando, Florida 32805**

## **ABSTRACT**

PERSHING explosive ordnance devices were tested in the Life Extension and Assessment Program (LEAP) to determine the effects of aging on the explosives and explosive assemblies. Exploding bridgewire (EBW) and hot wire electro-explosive devices, safe and arm devices (S&A), mild detonating fuse, and linear shaped charge assemblies were tested. Performance was determined from functional tests, and laboratory analyses were conducted on explosive specimens obtained from tactical assemblies. The results of these tests formed a basis for recommendations of service life, design improvements and quality control in production hardware. Pershing service life will be extended to the maximum required by the Pershing Project Manager's Office as a result of implementing the recommendations resulting from the LEAP program.

The exploding bridgewire ordnance system was developed through the joint efforts of the United States Army Ballistic Missile Agency, McCormick Selph, and the Martin Marietta Corporation.

## **I. INTRODUCTION**

The PERSHING Project Manager's Office of the Army Missile Command instituted a program in January of 1970 to extend the life of PERSHING missiles. This Life Extension and Assessment Program, referred to by its acronym LEAP, was divided into three phases:

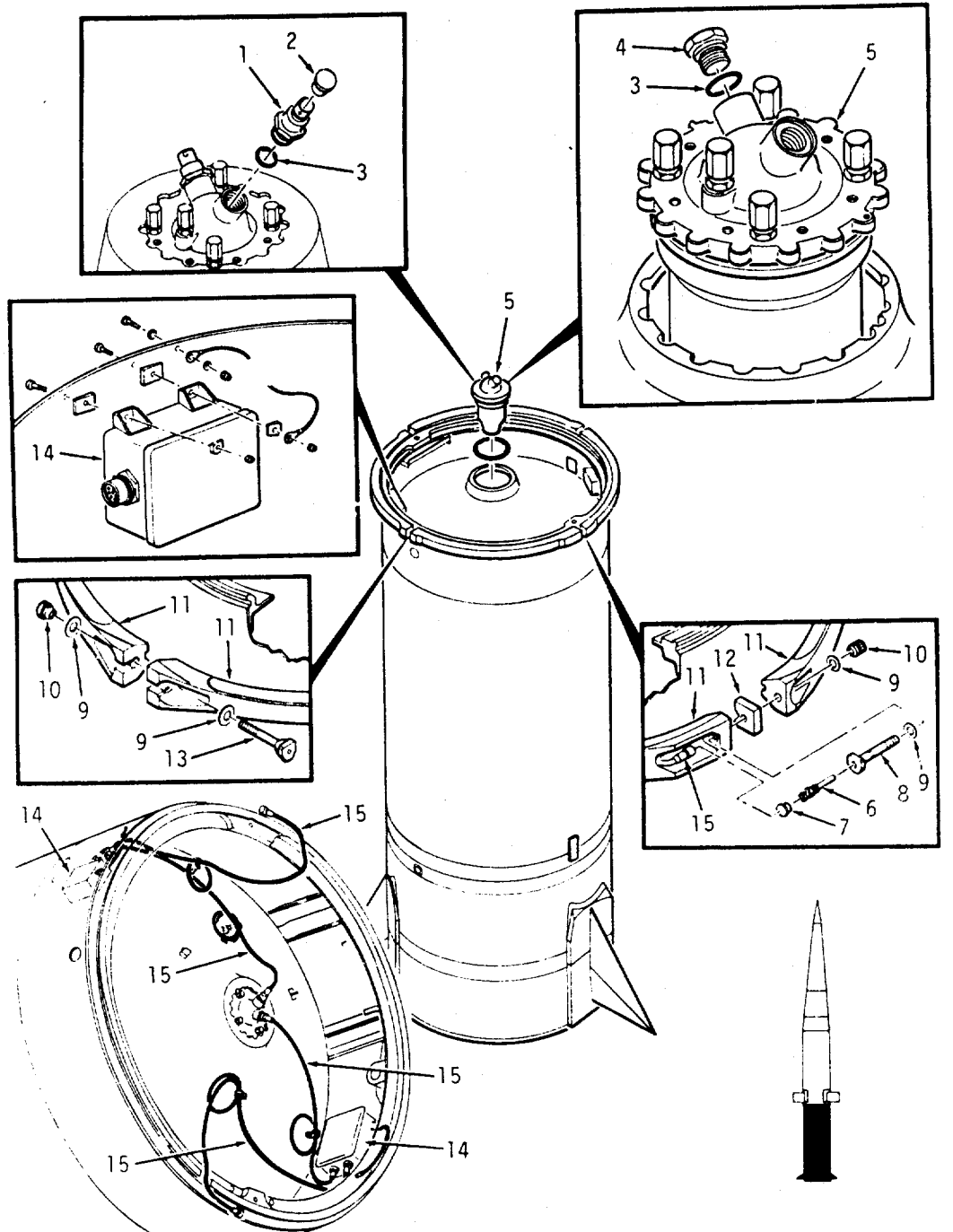
- 1 Phase I Planning and Preparation of Test Procedures (February to September 1970)
- 2 Phase II Inspection, Test, and Assessment (September 1970 to December 1971)
- 3 Phase III Remanufacture (January 1972 to 1973).

The tests, conclusions, and recommendations are discussed herein.

Ten tactical missiles were drawn from Army field units and the Pueblo Army Depot for these tests. The explosive devices were removed from these missiles and subjected to the LEAP assessment and evaluation tests. The results of these tests, conclusions, and recommendations were reported in detail in the Martin Marietta final report OR 11,385(1) to AMICOM. This final report also contains additional detailed information as well as a substantial number of illustrations pertinent to these details.

## **II. MISSILE SYSTEM EXPLOSIVE DEVICES**

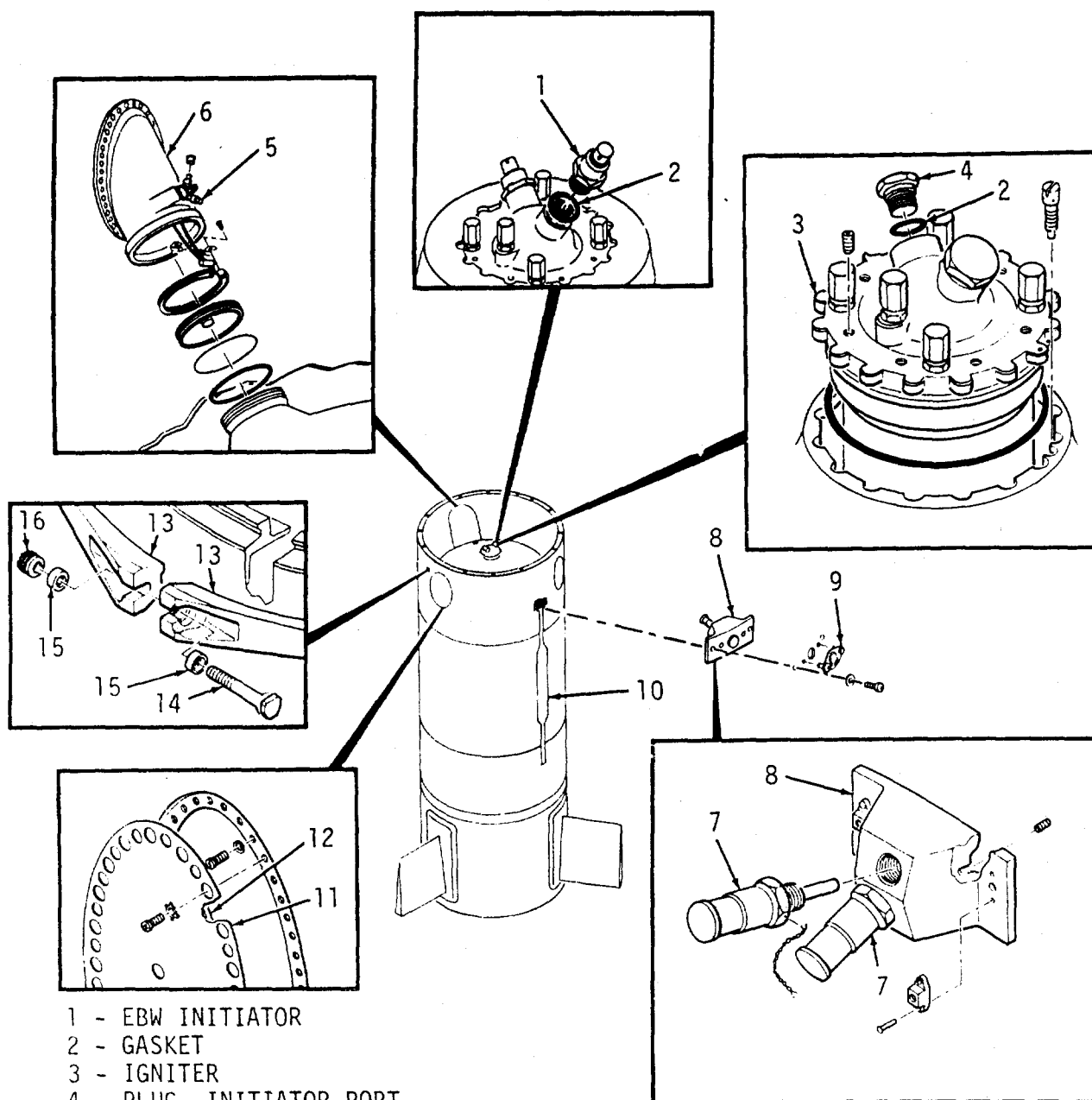
The PERSHING employs several explosive devices in each section of the missile. These configurations are shown in Figures 1 through 5.



LEGEND:

- |                                       |                                     |
|---------------------------------------|-------------------------------------|
| 1 - EBW INITIATOR                     | 9 - WASHER                          |
| 2 - PROTECTIVE CAP                    | 10 - NUT                            |
| 3 - GASKET                            | 11 - RETAINING BAND                 |
| 4 - PLUG                              | 12 - HEAT SHIELD                    |
| 5 - IGNITER                           | 13 - BOLT, NON EXPLOSIVE            |
| 6 - EBW CARTRIDGE, EXPLOSIVE BOLT     | 14 - HIGH ENERGY FIRING UNIT (HEFU) |
| 7 - PROTECTIVE CAP                    | 15 - HIGH VOLTAGE CABLE             |
| 8 - BOLT, STAGE SEPARATION, EXPLOSIVE |                                     |

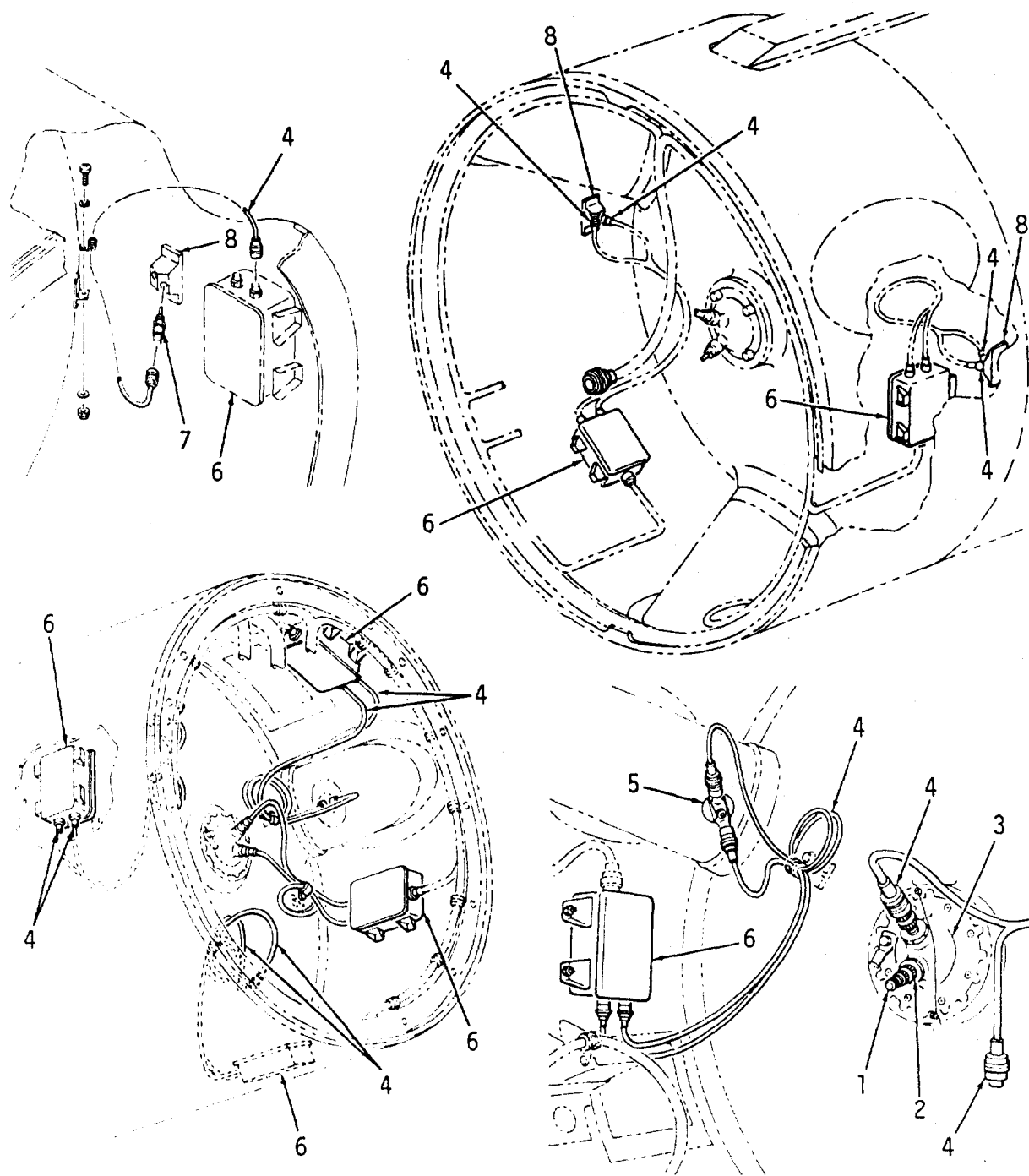
Figure 1. Exploding Bridgewire Explosive Ordnance, High Energy Firing Units and High Voltage Cables Installation in First Stage Assembly



- 1 - EBW INITIATOR
- 2 - GASKET
- 3 - IGNITER
- 4 - PLUG, INITIATOR PORT
- 5 - EBW THRUST REVERSAL DOME RELEASE EXPLOSIVE DEVICE
- 6 - THRUST REVERSAL TUBE
- 7 - EBW DETONATOR
- 8 - MOUNTING BLOCK
- 9 - PROTECTIVE COVER
- 10 - CASE VENT SHAPED CHARGE ASSEMBLY
- 11 - COVER, THRUST REVERSAL PORT
- 12 - SEAL
- 13 - RETAINING BAND
- 14 - BOLT (NON-EXPLOSIVE)
- 15 - WASHER
- 16 - NUT



Figure 2. Exploding Bridgewire Explosive Ordnance and Related Hardware  
Installation in Second Stage Assembly



- 1 - EBW INITIATOR
- 2 - GASKET
- 3 - IGNITER
- 4 - HIGH VOLTAGE CABLE
- 5 - EBW THRUST REVERSAL DOME RELEASE EXPLOSIVE DEVICE
- 6 - HIGH ENERGY FIRING UNIT (HEFU)
- 7 - EBW DETONATOR
- 8 - MOUNTING BLOCK

Figure 3. Exploding Bridgewire Explosive Ordnance, High Energy Firing Units and High Voltage Cables Installation in Second Stage

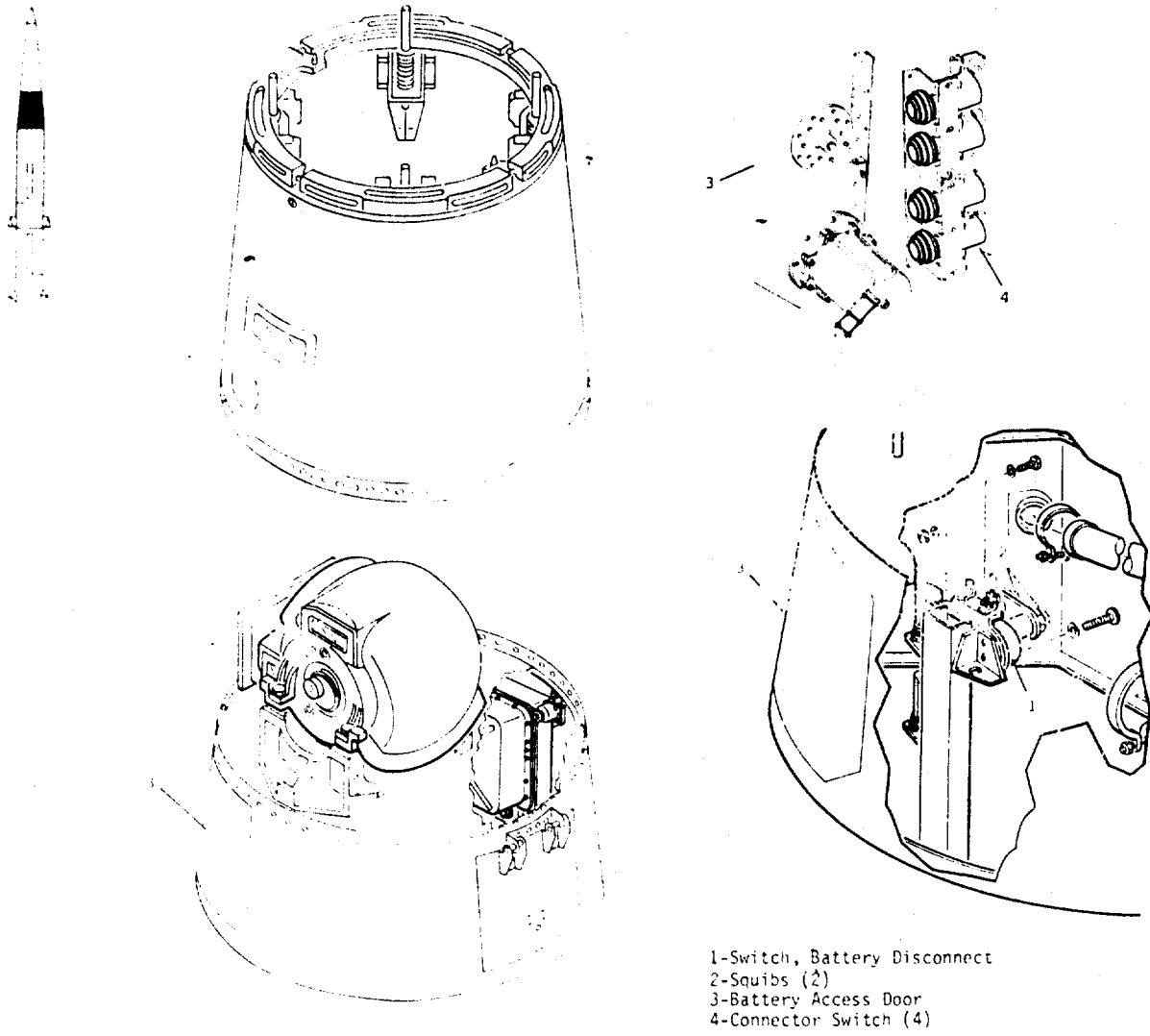
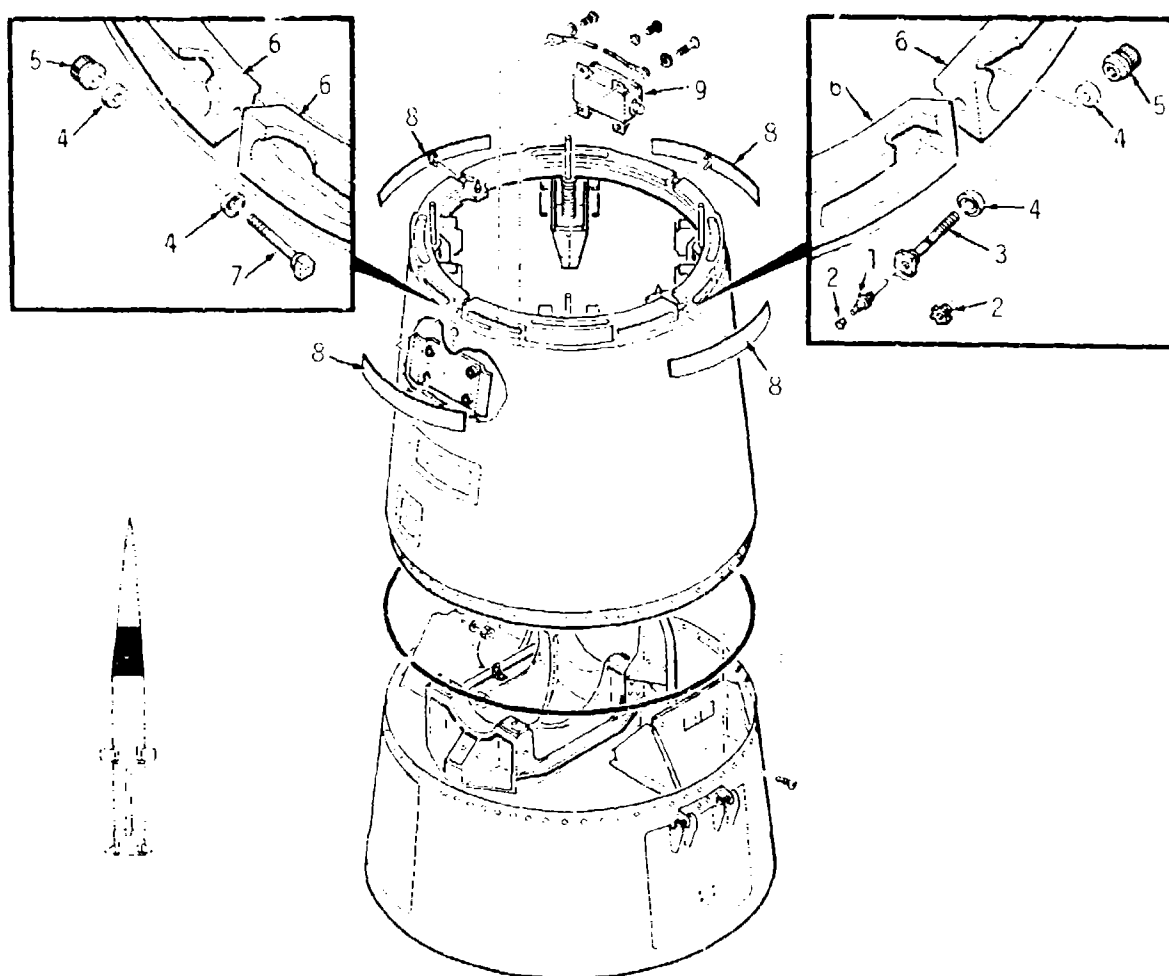


Figure 4. Pershing Guidance and Control Section Showing Connector Switches, Battery Disconnect Switch and Actuating Squibs



- |                                       |                         |
|---------------------------------------|-------------------------|
| 1 - EBW CARTRIDGE, EXPLOSIVE BOLT     | 6 - RETAINING BAND      |
| 2 - PROTECTIVE CAP                    | 7 - BOLT, NON EXPLOSIVE |
| 3 - BOLT, STAGE SEPARATION, EXPLOSIVE | 8 - COVER               |
| 4 - WASHER                            | 9 - HEFU                |
| 5 - NUT                               |                         |

Figure 5. Explosive Bolts and High Energy Firing Unit Installation in Warhead Separation System

### III. TESTS

#### A. INSPECTION AND TEST PLAN

Each type of explosive ordnance device received for LEAP tests was inspected and tested to obtain the maximum amount of information from each specimen tested. A typical test plan is shown in Figure 6.

#### B. INSPECTION

Non-destructive tests were performed on all assemblies to establish their "as received" condition. Bridgewire circuits were checked for continuity and resistance. EBW circuits contain a coaxial spark gap and were tested with a megacycle "grid dip" meter (Figure 7). Information obtained from these tests was compared with the original manufacturer's tests to determine the nature and degree of change, if any. Where the original test data was not available, specification requirements were used as the baseline for comparative evaluation. These explosive devices were subsequently allocated for Bruceton, functional, and explosives analytical tests.

#### C. FUNCTIONAL TESTS

Functional tests were performed on a representative sampling of naturally aged LEAP explosive ordnance devices to obtain performance data. All functional characteristics were monitored and recorded. This included input stimuli, function time, and output characteristics (Figure 8).

#### D. BRUCETON TESTS

Bruceton tests were conducted in accordance with U.S. Army Material Command sensitivity testing requirements document 11199529, Revision A.<sup>(2)</sup> Current Data was recorded for hot wire electroexplosive devices. Voltage and burst current were recorded for exploding bridgewire devices.  $\bar{X}$  and  $3\sigma$  data was determined from this information.

#### E. ANALYTICAL TESTS OF EXPLOSIVES

Analytical tests were conducted on explosive materials obtained from naturally aged tactical explosive devices by the research laboratories of Martin Marietta RIAS.<sup>(3)</sup> These tests were performed to characterize and define any aging of the explosives. The analytical tests consisted of differential thermal analysis, thermogravimetric analysis, sensitivity, spectrometry, calorimetry, and chemical analyses.

##### 1. Differential Thermal/Thermogravimetric Analysis

The Mettler simultaneous DTA/TGA analyzer (Figure 9) provided thermoanalytical and thermogravimetric data. Inasmuch as relatively small quantities of explosives were available



from each explosive assembly, 2 milligram samples were loaded into one cup of the micro-stick (Figure 10). The second cup contained aluminum oxide ( $\text{Al}_2\text{O}_3$ ) reference material. These platinum cups act as one junction of the temperature sensing thermocouples. After the furnace (Figure 11) is placed over the test specimen, the entire measuring head and balance unit is evacuated to approximately  $10^{-4}$  Torr after which purified nitrogen at a steady flow of 5 liters per hour is maintained around the samples. The resulting thermogram (Figure 12) is analyzed for both peak temperature of the exothermic process and sensitivity factor of the exotherm. When comparing the test results of various samples, a shift to higher temperatures for the peak of the exotherm indicates a decrease in thermal sensitivity. The profile of the exotherm, in terms of height to half width ratio, is an indication of the characteristic of the thermal reaction. An increase in the exotherm height to half width ratio is interpreted by RIAS as an increase in thermal sensitivity.

## 2. Physical Sensitivity Tests

Physical sensitivity tests were conducted with a drop test instrument. These tests are normally conducted with 50 milligram samples. However, in order to work with the small quantities of material available, smaller cups were required. After some experimentation, it was found that 5 milligram samples in the small cups (Figure 13) gave satisfactory results. This setup gave drop heights that were roughly one quarter ( $1/4$ ) of the standard drop tests. Ten (10) to twenty (20) samples were tested, depending upon the quantity of material available. The tests were performed using the Bruceton staircase technique where the weight was raised or lowered depending on whether the previous test resulted in a no-fire or fire, respectively. A computer program was developed for calculating the  $\bar{x}$  or nominal drop height and probability data (See Appendix A).

## 3. Spectrometry

Whenever a sample from a particular lot of explosive compound displayed unusual characteristics or test results, additional samples of the material were analyzed on the mass spectrometer. The equipment used was the Bendix Model 14 Time-of-Flight (TOF) mass spectrometer (Figure 14). This TOF mass spectrometer has the advantage of great speed. Ionization, impulse, separation, and detection all occur within 100 microseconds. The instrument is, therefore, well suited to uses requiring high sensitivity and rapid response.

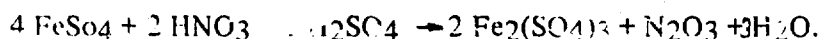
## 4. Calorimetry

Caloric values were determined for boron potassium nitrate ( $\text{B-KNO}_3$ ) obtained from the motor initiators. Tests were conducted with the Parr adiabatic calorimeter Model 1231 (Figure 15).

## 5. Chemical Tests

Chemical tests were conducted on  $\text{B-KNO}_3$  initiator output charges to determine the character and degree of change in its constituents. These tests consisted of titrimetry and Gooch analysis.

The  $\text{KNO}_3$  concentrations were determined by using end point titrimetry to determine nitrate ion concentration by titration with derrous ammonium sulphate solution in a strong sulphuric acid medium:

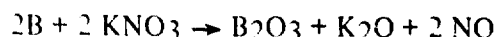


Two platinum wire electrodes were used in a concentrated sulphuric acid containing the nitrate ion to be determined, and a potential of about 200 mV was maintained. When titrated with a 0.04M (moles per liter) ferrous ammonium sulphate solution there is an initial rise in current followed by a gradual fall, with a marked increase at the end point; the latter is easily seen on the 0 to 3 microampere ( $\mu\text{A}$ ) range of a microammeter. The apparatus is shown in Figure 16. The temperature of the solution has some influence on the current reading and so the flask is kept in a constant temperature bath. Before each titration into the acid solution containing a sample of each charge, the ferrous solution was titrated into a sulphuric acid solution of an accurately weighed amount of  $\text{KNO}_3$  to find the amount of ferrous solution required per milligram of nitrate ion.

The boron concentration of each charge was determined using a Gooch crucible (a porcelain crucible with a perforated bottom). An aqueous solution of an accurately weighed amount of the B- $\text{KNO}_3$  mixture is filtered through the crucible leaving the insoluble boron in the crucible. The difference in weight between the crucible alone (measured before the filtering) and the crucible with the boron residue gives the weight of the boron in the mixture.

In all tests, the samples of output charge were always taken as being 94 percent B- $\text{KNO}_3$  and 6 percent laminac binder.

Using the equation



for the decomposition reaction, then if any  $\text{KNO}_3$  has decomposed and boron has oxidized, there should be some boric oxide ( $\text{B}_2\text{O}_3$ ) and potassium oxide ( $\text{K}_2\text{O}$ ) in the output charge. The boric oxide can be detected by analyzing the residue from the Gooch crucible analysis on the TOF mass spectrometer. Potassium oxide is very soluble in water and so gets filtered through in the Gooch analysis along with the  $\text{KNO}_3$ . Boric oxide is soluble in water only after vigorous stirring for a long time in very hot water. Therefore, if it is present in the mixture, it will remain with the boron in the Gooch analysis residue and not get filtered through.

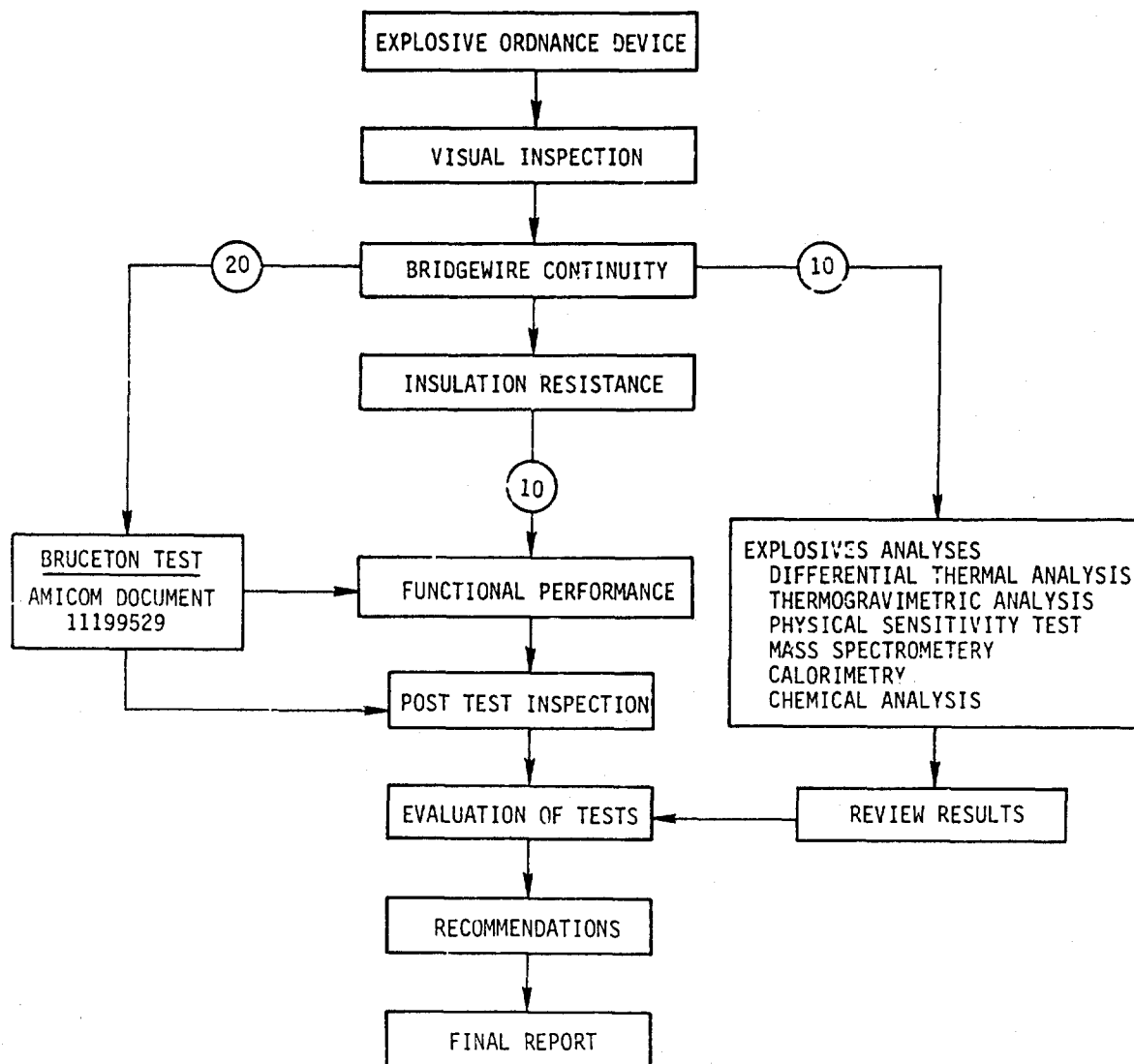


Figure 6. Typical Test Plan

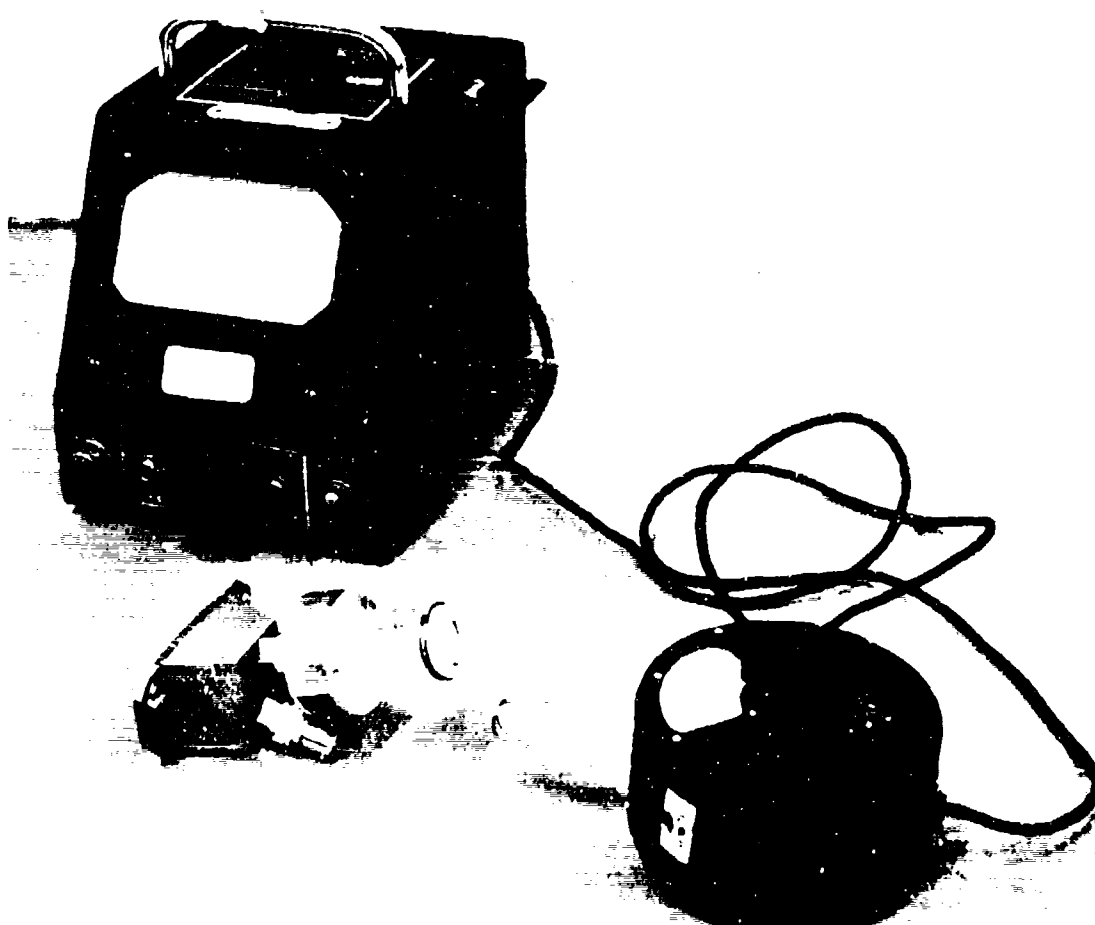


Figure 7. Grid Dip Test of EBW Detonator Showing Coupling Coil on Ordnance Device

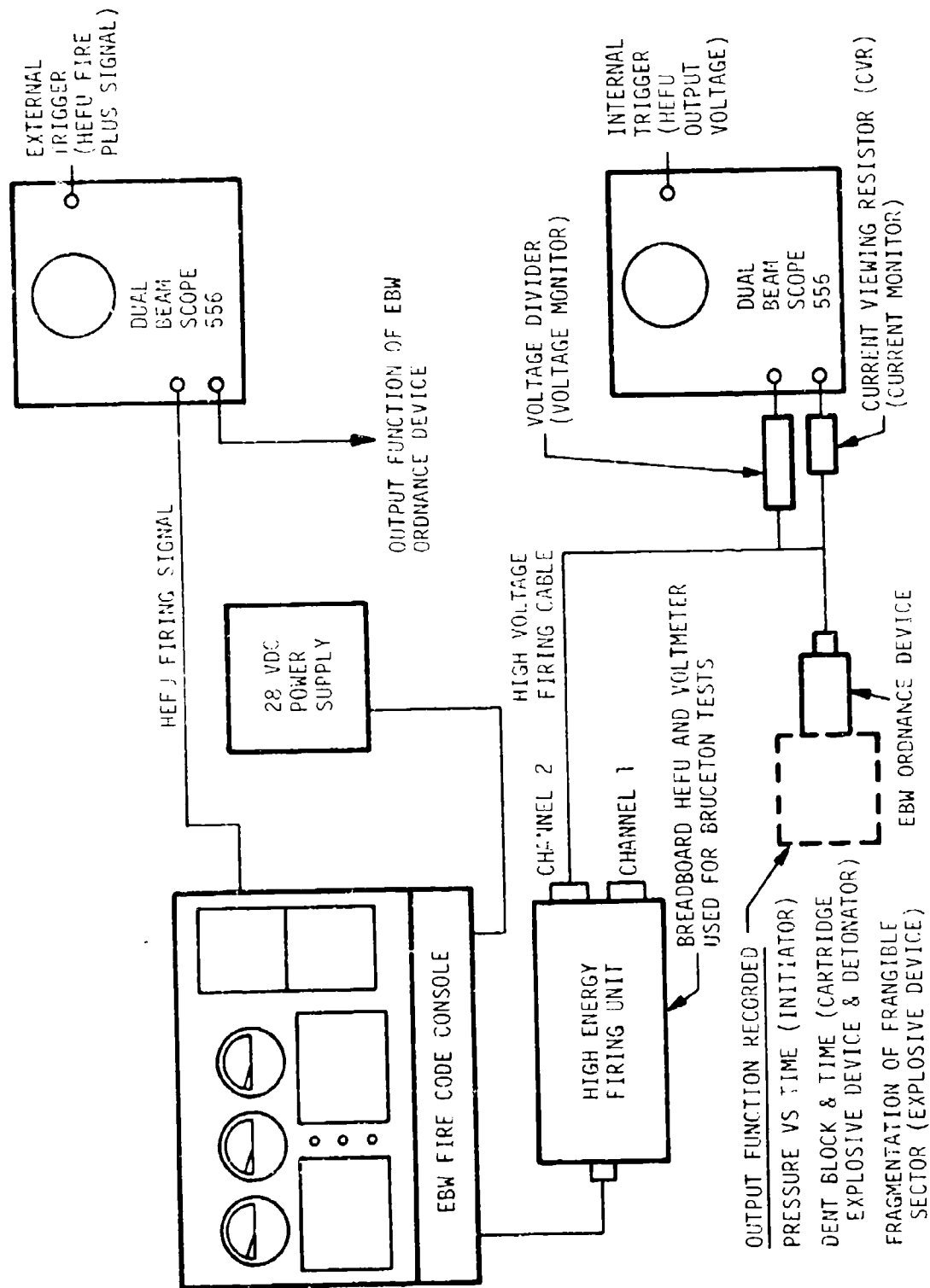


Figure 8. EBW Functional Test Setup

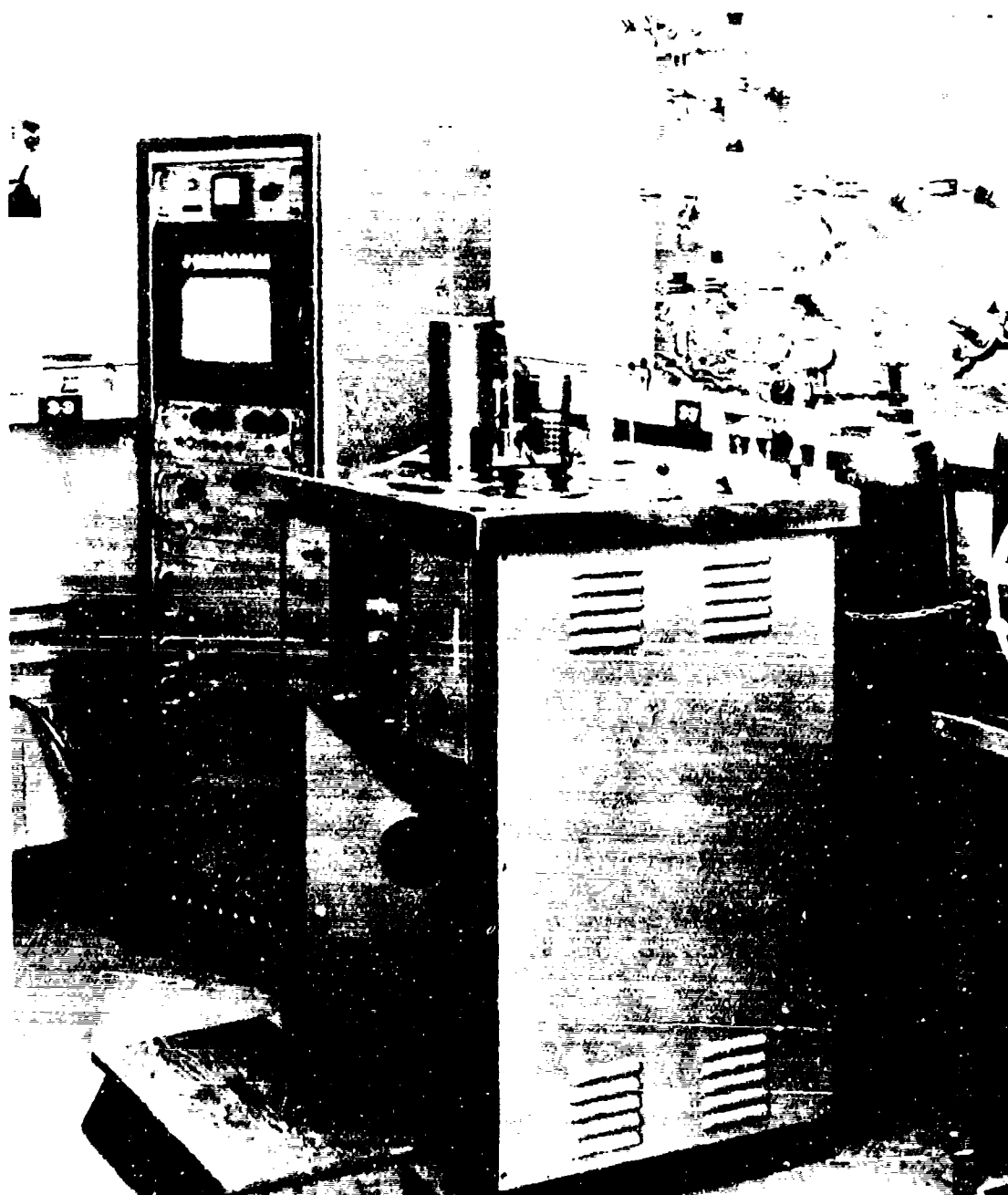


Figure 9. Mettler Simultaneous DTA/TGA Thermoanalyzer (W/Nitrogen Purification Towers in Background)



Figure 10. Platinum Test Cups in Micro-Stick of Mettler Simultaneous DTA-TGA Thermoanalyzer

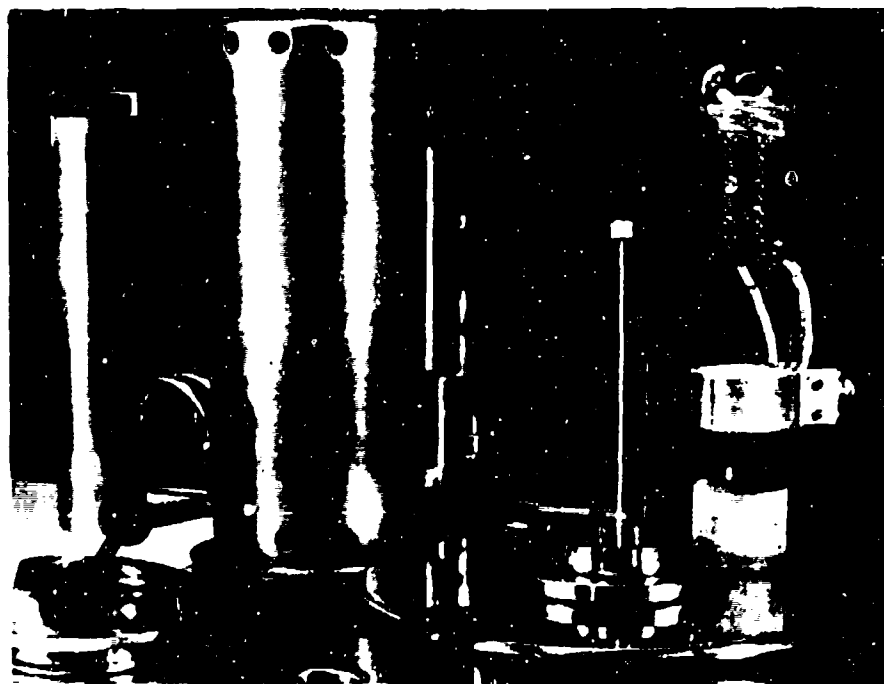
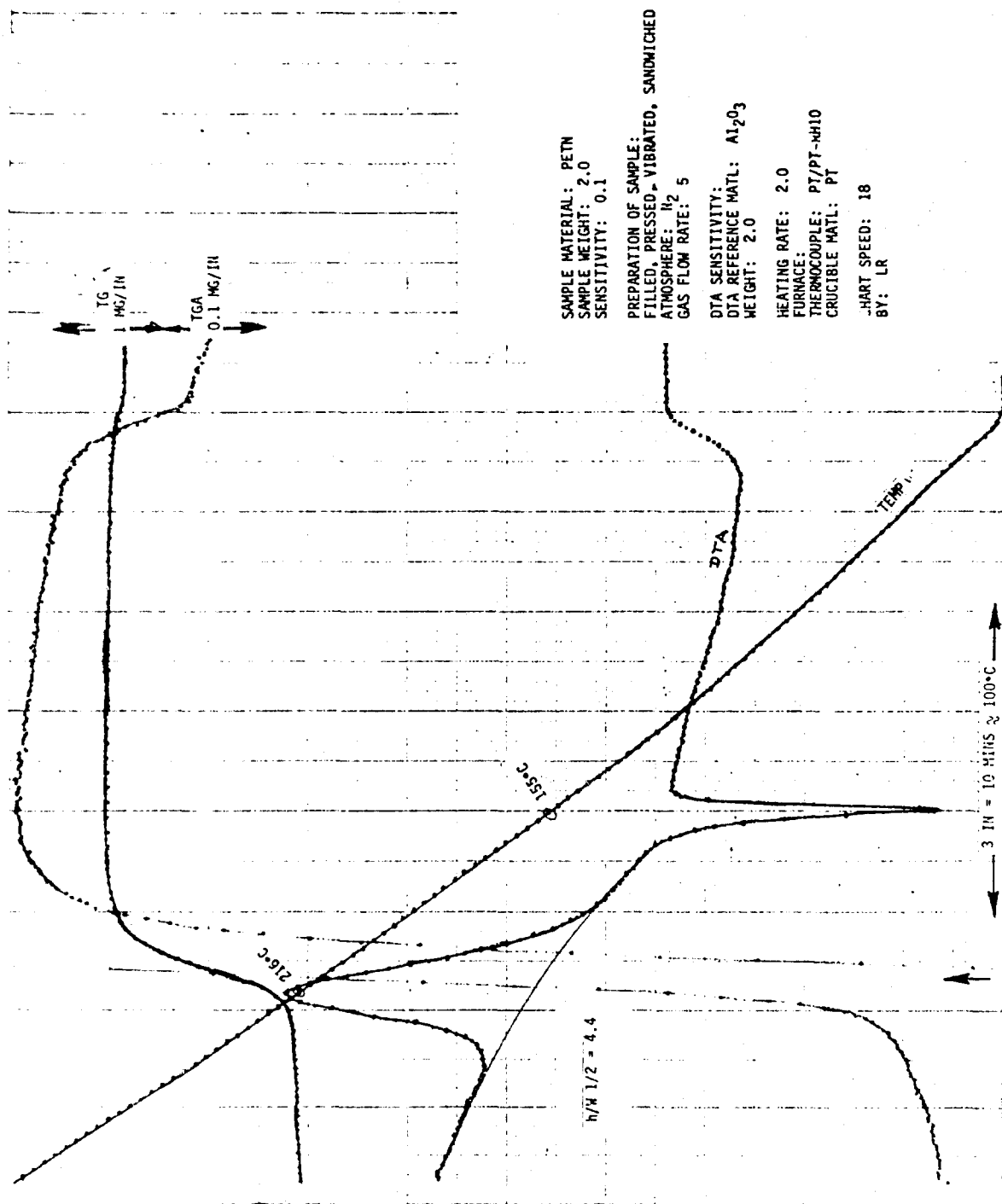


Figure 11. Mettler DTA/TGA Thermoanalyzer Micro-Stick, Furnace and Protective Cover



TEST NO. P/N 8002

IN-HEADER S/N 86

MG MG/IN

VACUUM: TORR

UV/IN

MG

°C/MIN SAMPLE HOLDER:

REF TEMP 25°C

SHAPE: SIZES

IN/HR

BY: LR

HEATING RATE: 2.0

FURNACE: PT/PT-WH10

CRUCIBLE MATL: PT

HEAT SPEED: 18

DTA SENSITIVITY:

DTA REFERENCE MATL:  $Al_2O_3$

WEIGHT: 2.0

PREPARATION OF SAMPLE:

FILLED, PRESSED, VIBRATED, SANDWICHED

ATMOSPHERE:  $N_2$

GAS FLOW RATE: 5

SAMPLE MATERIAL: PETN

SAMPLE WEIGHT: 2.0

SENSITIVITY: 0.1

Figure 12. Typical Simultaneous DTA/TGA Record



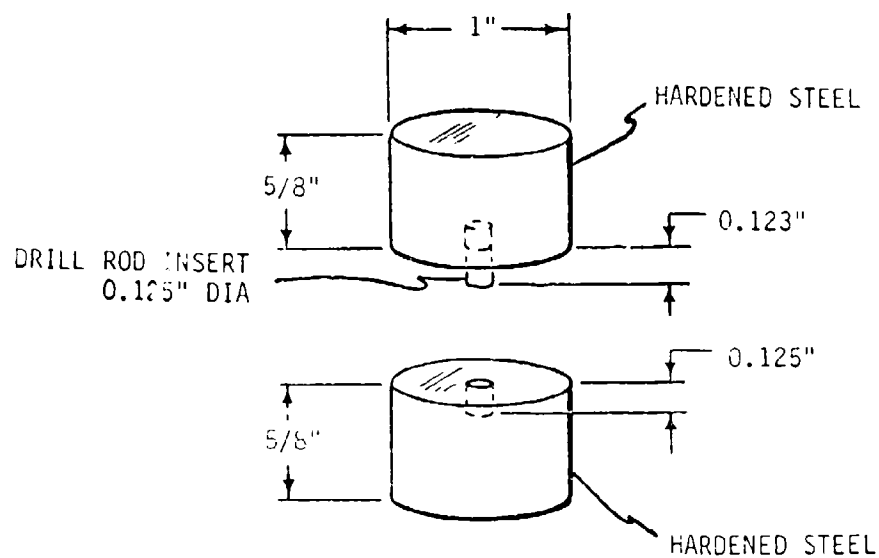


Figure 13. Five Milligram Specimen Cup for Physical Sensitivity (Drop) Test

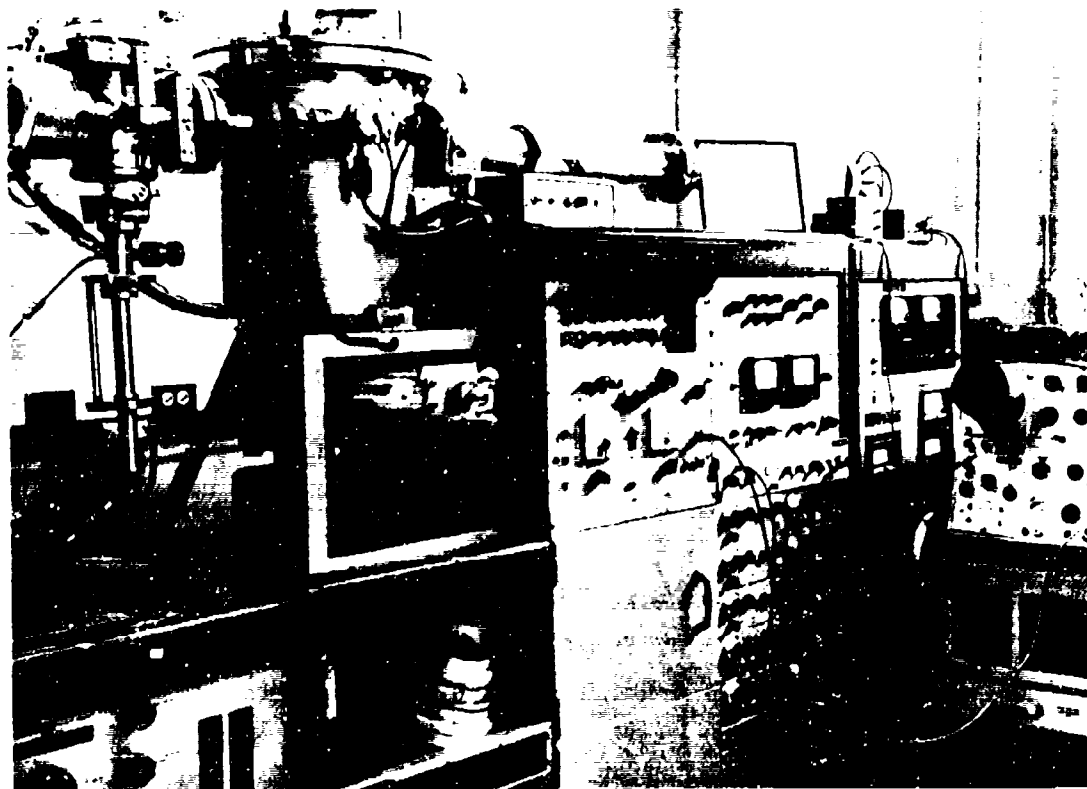


Figure 14. Time of Flight Mass Spectrometer

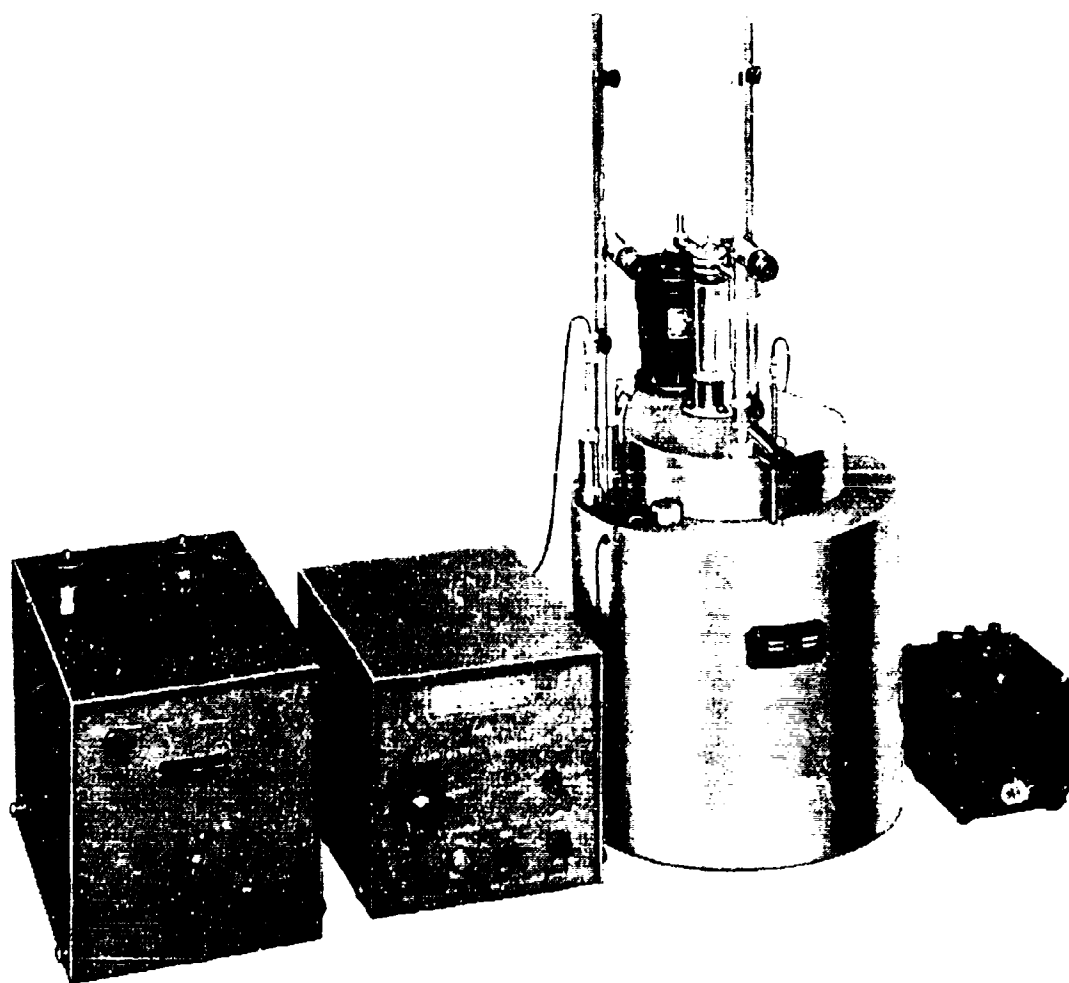


Figure 15. Adiabatic Calorimeter

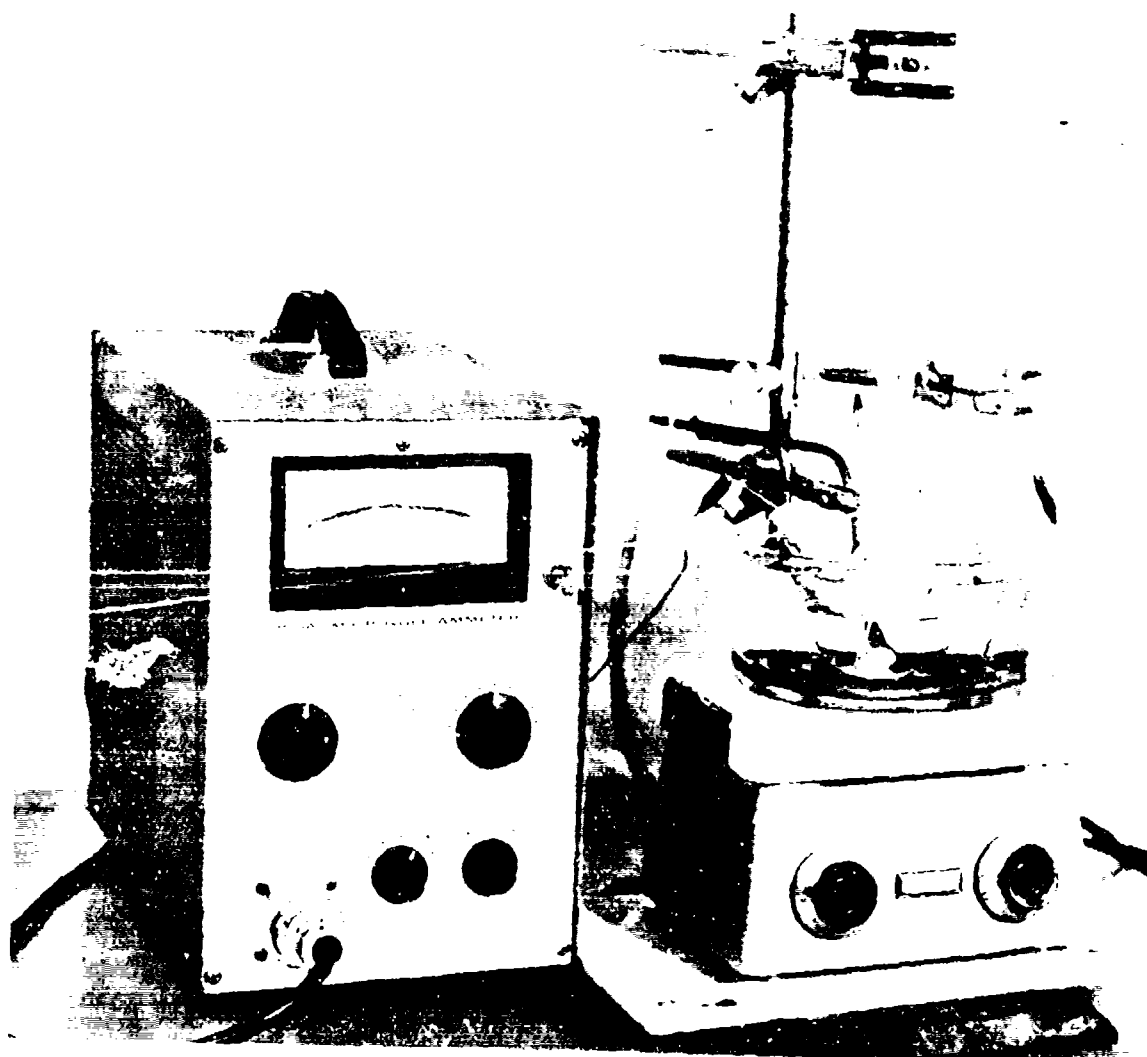


Figure 16. End-Point Titration Set-up to Determine Concentrations of Potassium Nitrate in Initiator B-KNO<sub>3</sub> Output Charge

## IV. TEST RESULTS

### A. EXPLODING BRIDGEWIRE ELECTROEXPLOSIVE DEVICES

PERSHING FBW electroexplosive assemblies employ a common header containing a spark gap in one leg of the bridgewire circuit (Figure 17). Connector keying pin arrangements are different for these assemblies to prevent inadvertent mismatching of firing cables from the high energy firing units (HFFU's).

All FBW devices were fired with the same high energy firing unit and monitoring instrumentation to minimize the variables in the various tests. Figure 18 shows the output circuitry of the HFFU, high voltage cable, and bridgewire circuit common to all PERSHING EBW devices. Output voltage and function time of the HFFU are shown in Figure 19. Voltage and current experienced by the bridgewire are shown in Figure 20. Exothermic data obtained from DTA tests indicate that the PETN bridgewire charge remains very stable through 96 months of age even though the exotherm height-to-half-width ratio ( $h:W_{1/2}$ ) was somewhat variable (Figure 21).

Bruceston tests of the FBW ordnance devices indicated that they were functioning very well. The 50 percent firing voltage ( $\bar{x}$ ) and 3 sigma ( $\sigma$ ) limits were well within the level of output of the HFFU as indicated below in Table I.

TABLE I

Bruceston Tests of EBW Devices

	Initiator (Volts)	Cartridge (Volts)	Explosive Device (Volts)
$\bar{x}$ (50 percent firing voltage)	1213	1283	1293
$\bar{x} + 3\sigma$	1283	1421	1419
$\bar{x} - 3\sigma$	1147	1159	1176

HFFU Output (0.557  $\mu$ fd capacitor) = 2000 - 2700 Volts

#### 1. FBW Rocket Motor Initiator

Fifty FBW initiators (Figure 22) were tested. Some variation in output characteristics of FBW initiators was determined during functional tests (Figures 23, 24, and 25). A substantial range of exotherm temperatures was obtained from DTA tests (Figures 26 and 27). Caloric values were similarly variable (Figure 27). Chemical analyses of the  $B-KNO_3$  revealed that the relative percentages of boron and potassium nitrate were slightly variable but generally within specification limits (Figure 28). No boric oxide was found in TOF mass spectrometer tests.

Examination of cadmium-plated initiator bodies revealed the presence of ferric oxide on the internal surfaces of two units (Figure 29). This was attributed to moisture leakage through the solder seal of the final assembly (Figure 30). Stainless steel bodies with welded closure did not leak.

## 2. EBW Explosive Bolt Cartridge and Case Vent Detonator

Fifty seven EBW cartridges (Figure 31) and eight EBW detonators (Figure 32) were tested. All explosive bolt cartridges and case vent detonators performed very well in functional tests with dent blocks. DTA tests of the transfer, booster, and output charges produced exotherms that were very consistent indicating a lack of aging effects.

## 3. EBW Thrust Reversal Explosive Device

Thirty EBW explosive devices (Figure 33) were tested. Two functional tests were obtained from each explosive device by firing one leg of the MDF into a dent block and firing the other leg into the frangible sector that is installed on the redundant MDF leads (Figure 34). The sector was installed in a thrust reversal dome release test fixture (Figure 35) for simulated dome release tests. Reliable release functions were obtained in all of these tests. Detonation output from the MDF leads was recorded in dent blocks and their equivalent detonation velocities calculated. It was determined from exploratory tests that the detonation stimulus would not propagate across a broken MDF lead (Figure 36).

DTA tests conducted with PETN from the MDF leads indicated that the exotherm data was very consistent over a period of 89 months. There was no discernible aging effects.

# B. HOT WIRE ELECTROEXPLOSIVE DEVICES (EED'S)

Hot wire EED's are employed for less critical applications in the missile system. These units are employed redundantly to provide additional reliability.

## 1. Squib Operated Connector Switch

Forty connector switches (Figure 37) were tested. During the analytical tests of the explosives it was determined that the LMNR bridgewire charge of three switches were wet. This was reflected in the DTA exotherms (Figure 38). Bruceton test data shows that the squib switch continues to meet the specified no-fire and all-fire requirements (Figure 39).

## 2. Squib Pressure Cartridge

Twenty-five squib pressure cartridges (Figure 40) were tested. DTA exotherm data was relatively constant through 98 months of age for the normal lead styphnate bridgewire charge and the Bullseye powder main charge. Functional tests have established that the squib performance is well within the specified requirements of 5000 psi within 25 milliseconds in a 4cc chamber. Bruceton test results show that the squib is well within the specified no-fire and all-fire requirements (Figure 41).

# C. CASE VENT SAFE AND ARM (S&A) DEVICE

Early models of the PERSHING missile contained an S&A initiated case venting system. This S&A (Figure 42) contains two hot wire detonators that are protected by an inductance/capacitance type attenuator. Two rotor leads provide the output explosive stimulus.

Ten S&A's were tested. Output detonation data was determined from dent blocks and found to be very good. Function time from firing signal to explosive output ranged from 20 to 60 milliseconds. Analytical tests of the explosives showed that no aging effects had taken place.

#### D. CASE VENT EXPLOSIVE LEAD ASSEMBLY

On early missiles, with the S&A case venting system, an explosive lead assembly (Figure 43) is employed to transfer the explosive stimulus from the S&A to the shaped charge assembly. Redundancy is provided by dual MDF leads from each S&A output lead to each shaped charge assembly.

Twelve explosive lead assemblies were tested. Functional tests were instrumented to determine function time, rate, and explosive output characteristics (Figure 44). Performance was very good. Analytical tests of the explosives showed that no aging effects were experienced.

#### E. CASE VENT SHAPED CHARGE ASSEMBLY

Case venting of the second stage motor reduces motor pressure to a level that virtually precludes combustion. This eliminates the thrust reversal exhaust plume that envelopes the warhead section and affects stability. The venting function is performed by the shaped charge assembly (Figure 45). Two assemblies are installed on diametrically opposite sides of the motor.

Twenty-one shaped charge assemblies were tested. Units were fired into tapered steel witness plates to determine penetration and cutting performance. It was noted from this data that a substantial variation in performance was being experienced within assemblies as well as from one assembly to another. It was concluded that inadequate stand-off distance accounted for the majority of this effect. However, bending the shaped charge during installation also contributed to the reduced performance.

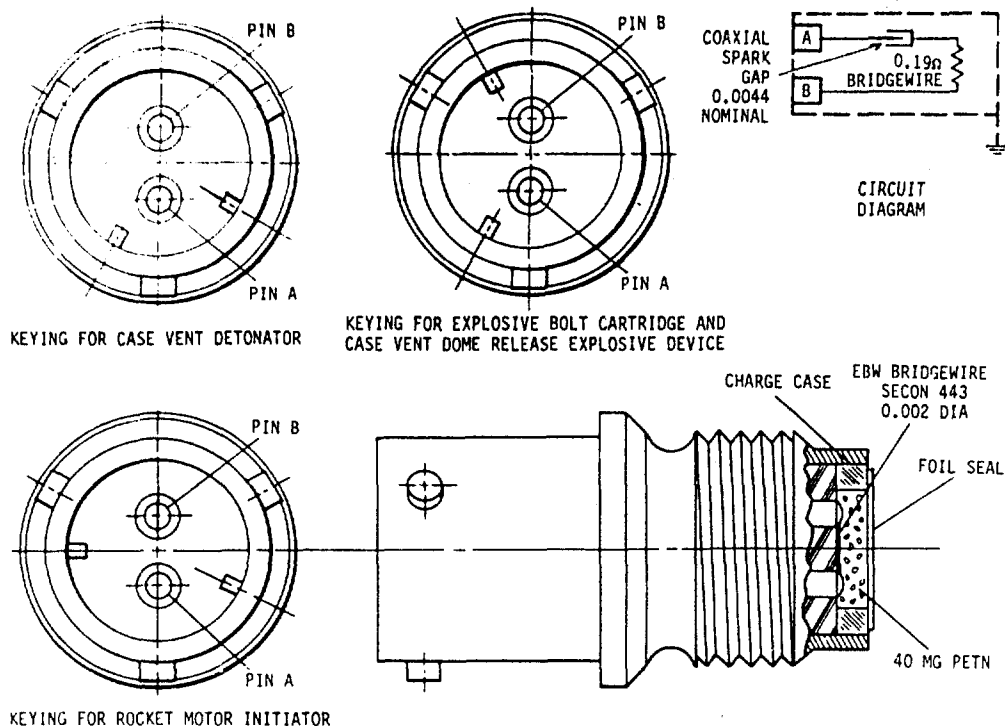
Analytical tests of the explosives indicated that there was no aging effects.

#### F. RECRYSTALLIZED EXPLOSIVES TESTS

Samples of PETN and RDX were recrystallized by the slow evaporation of acetone to provide baseline samples for comparative testing. The results of these tests are shown in Tables II and III. It was determined, primarily from exothermic data of the DTA, that no aging effects were experienced.

#### G. MASS SPECTROMETRY TESTS

Certain samples of explosives were subjected to spectrometry tests on the TOF equipment (Figure 14) in an attempt to determine the cause of some peculiarity noted in other tests. The material tested, reason for investigating, and results of the test are shown in Table IV.



The EBW header assembly is common to all Pershing system exploding bridgewire explosive ordnance devices. These headers become a permanent part of each explosive ordnance device during manufacturing assembly. Headers for each type of EBW ordnance device differ only in their connector keying pin arrangements. These keying pins prevent incorrect mating of the high voltage firing cables from the HEFUs during assembly of the missile sections.

Characteristics of the EBW headers are as follows:

Maximum no fire (no dud) impulse – 650V max (0.33 mfd capacitor)

Maximum possible fire (possible dud) impulse – 650 - 1400V (0.33 mfd capacitor)

Permissible fire zone – 1400 - 2000V (0.33 mfd capacitor)

All fire impulse (50 percent + 3σ) - 2000V (0.33 mfd capacitor)

Normal fire impulse (HEFU) – 2350 ± 350V (0.5 mfd capacitor)

HEFU firing delay – 125 ± 125 microseconds (Act ~ 8-27 μsec)  
(HEFU S/N 508 used in LEAP, Channel 2, 8.8 μsec)

Header response time – Approximately 3 microseconds

Bridge resistance – 0.19 ± 0.02 ohm

Bridgewire – 0.002 inch diameter, Second 443:

Gold 65 - 75 percent

Platinum 5 - 15 percent

Silver 5 - 15 percent

Copper 10 - 15 percent

Explosive loading: 40 mg PETN (MIL-P-387, Class 2)

Figure 17. EBW Header Assembly 10628000 and 10566011





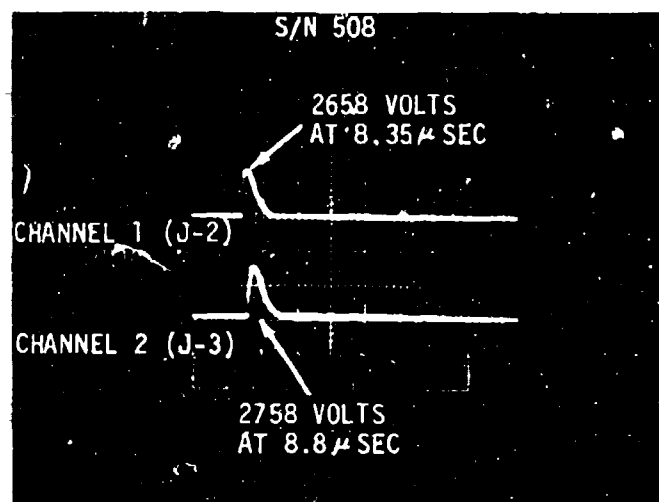


Figure 19. Output Voltage and Function Time Fire Plus Signal, H-FU S/N 508

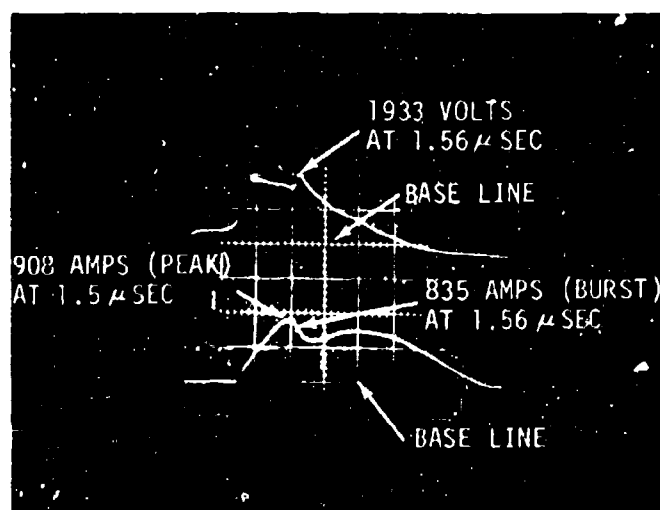


Figure 20. Firing Voltage and Current versus Time, FBW Initiator S/N 123

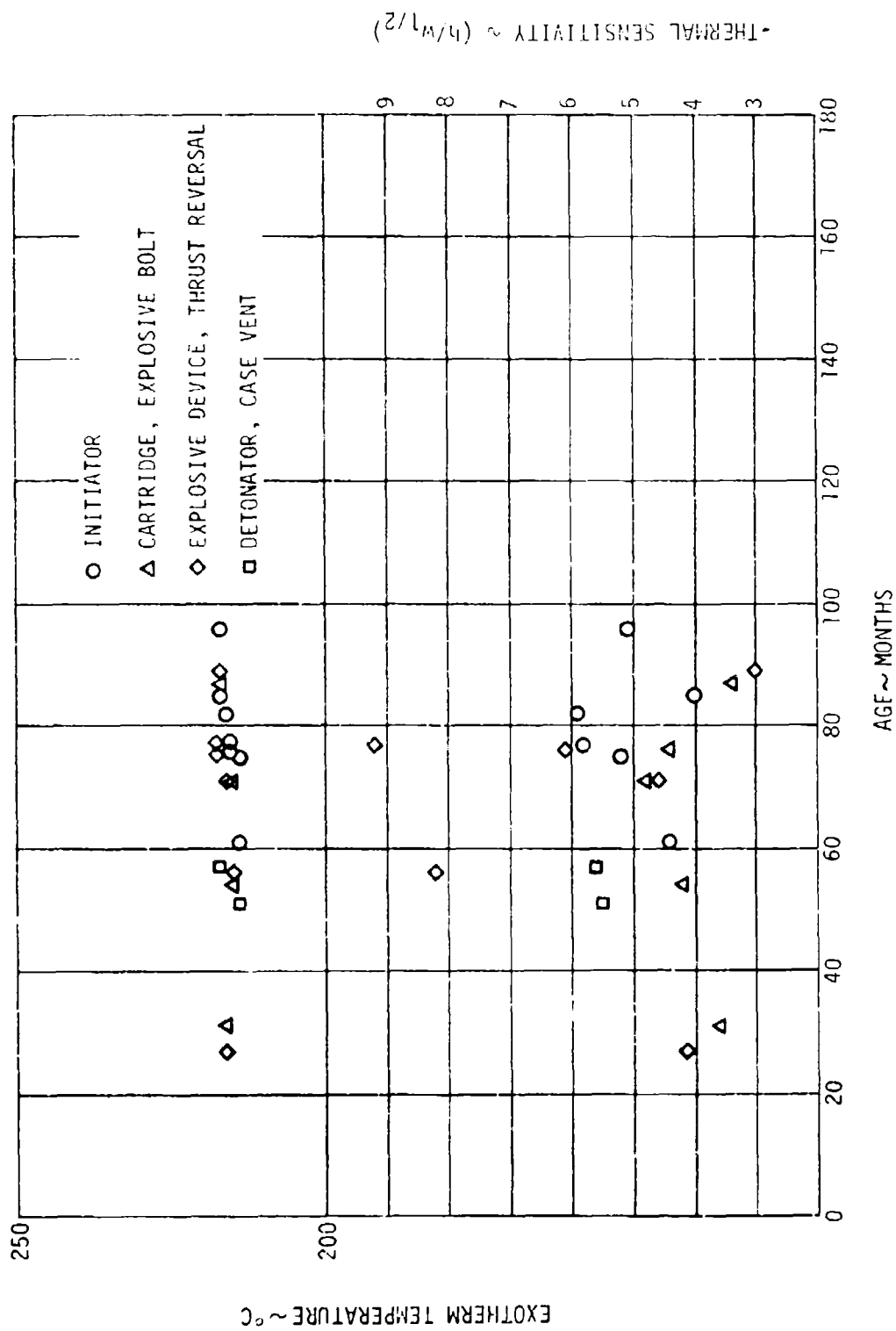
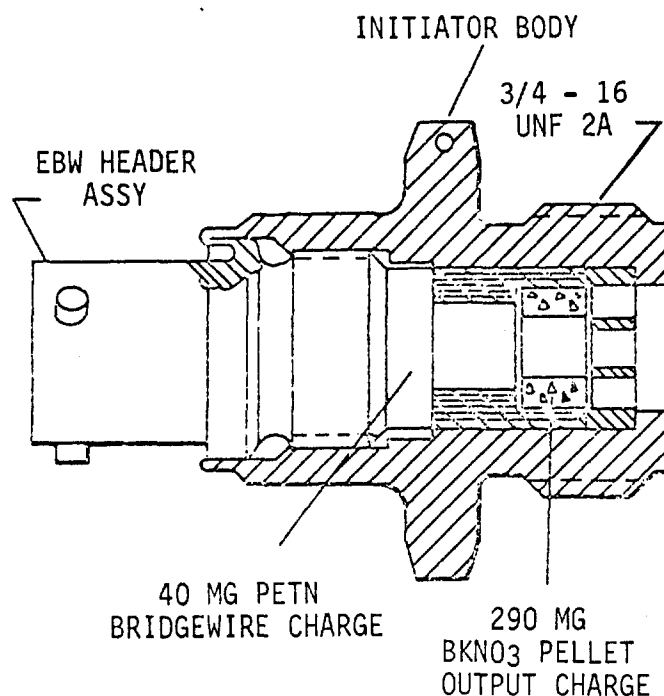
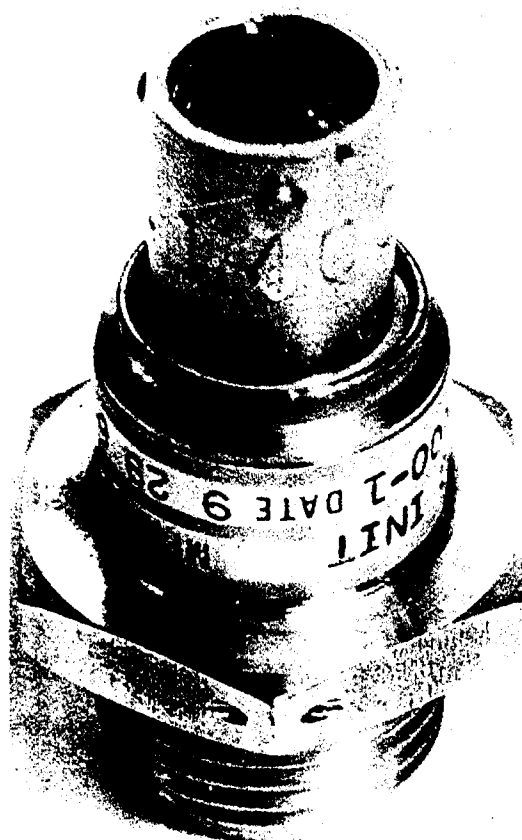


Figure 21. Exotherm Temperature and Thermal Sensitivity of EBW Grade PETN Bridgewire Charge versus Age



The EBW rocket motor initiator is a sealed assembly consisting of an EBW header, with appropriate connector keying pins, permanently assembled to the initiator body, containing an annular pellet of boron potassium nitrate ( $B - KNO_3$  output charge provides a pyrotechnic ignition stimulus to the motor igniter which in turn ignites the rocket motor. Two EBW initiators are installed in each motor to provide operational redundancy. Cadmium plated initiators (10628001-29) and stainless steel initiators (10566012-9) are as follows:

Characteristics of EBW initiators 10628001-29 and 10566012-9 are as follows:

Header characteristics: See Figure 17

Explosive loading:

Header -- 40 mg PETN (MIL-P-387, Class 2)

Output charge --  $290 \pm 10$  mg  $B-KNO_3$

Performance: 120 psig (in 225 cc chamber) within 20 milliseconds required per spec. Actual rise 1.5-2 milliseconds.

Figure 22. EBW Rocket Motor Initiator Assembly, 10628001-29 (MPD 11233) and 10566012-9 (MPD 11521)

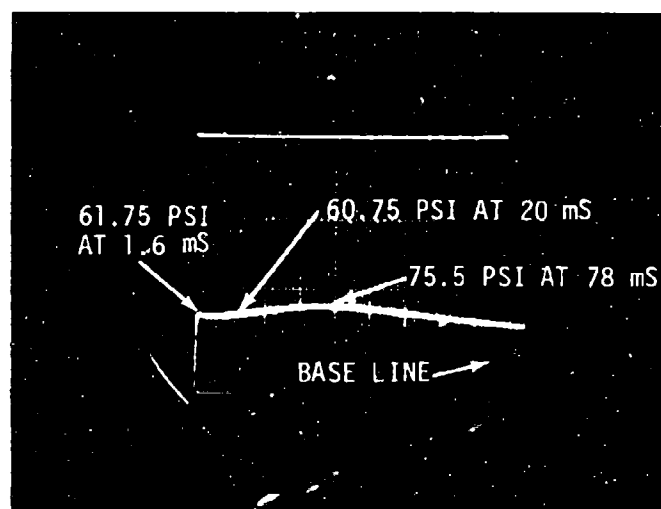


Figure 23. Typical Low Output Pressure versus Time  
Obtained from EBW Initiator (S/N 123)

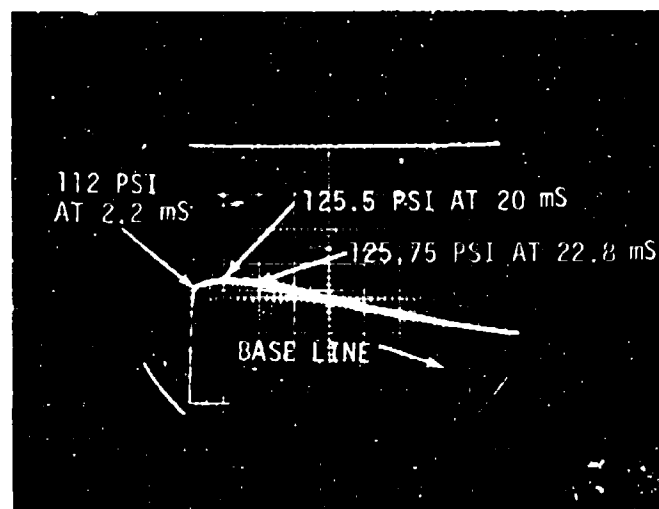


Figure 24. Typical Acceptable Output Pressure versus Time  
Obtained from EBW Initiator (S/N 116)

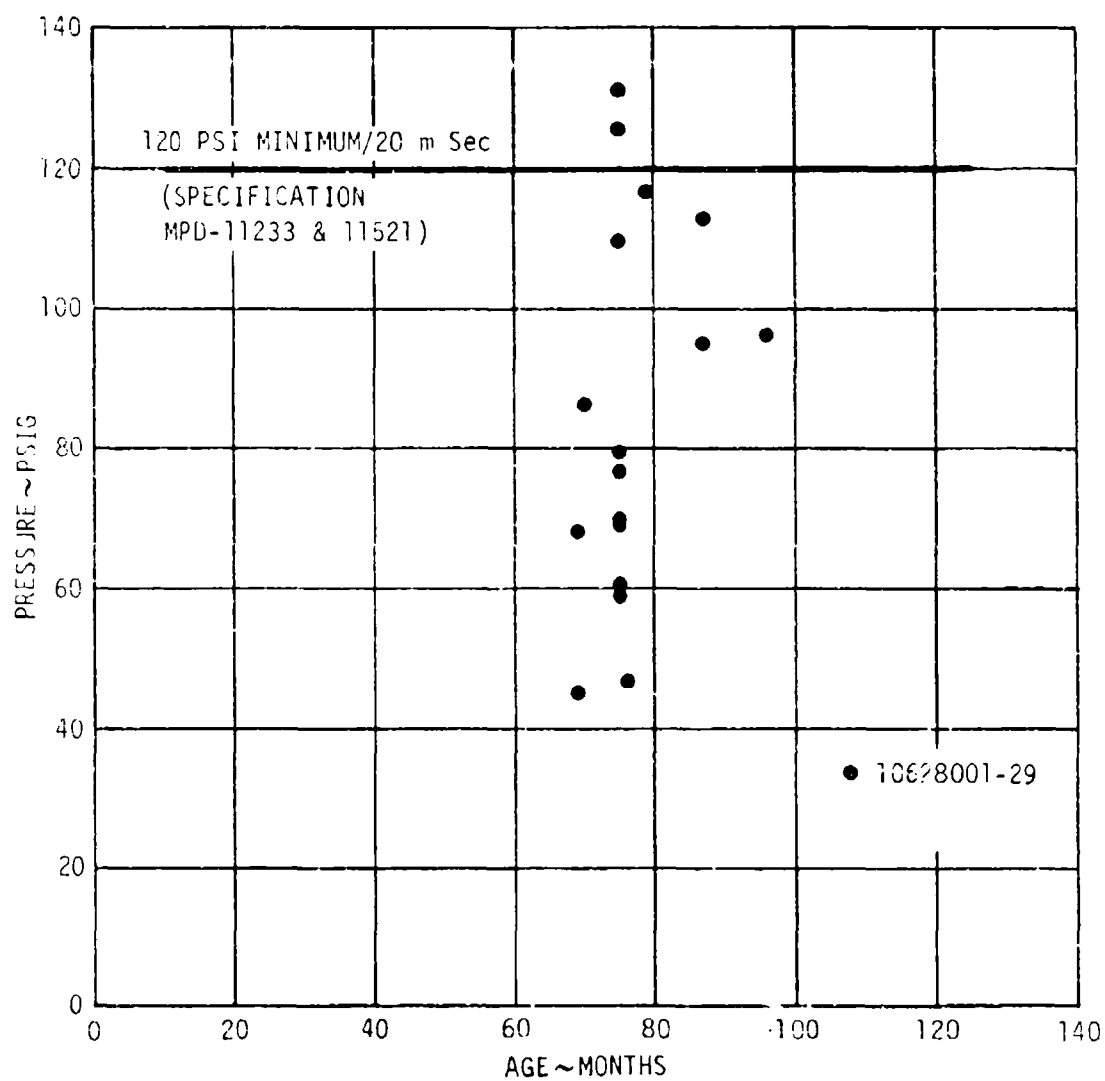


Figure 25. FBW Initiator Output Pressure at 20 Milliseconds versus Age

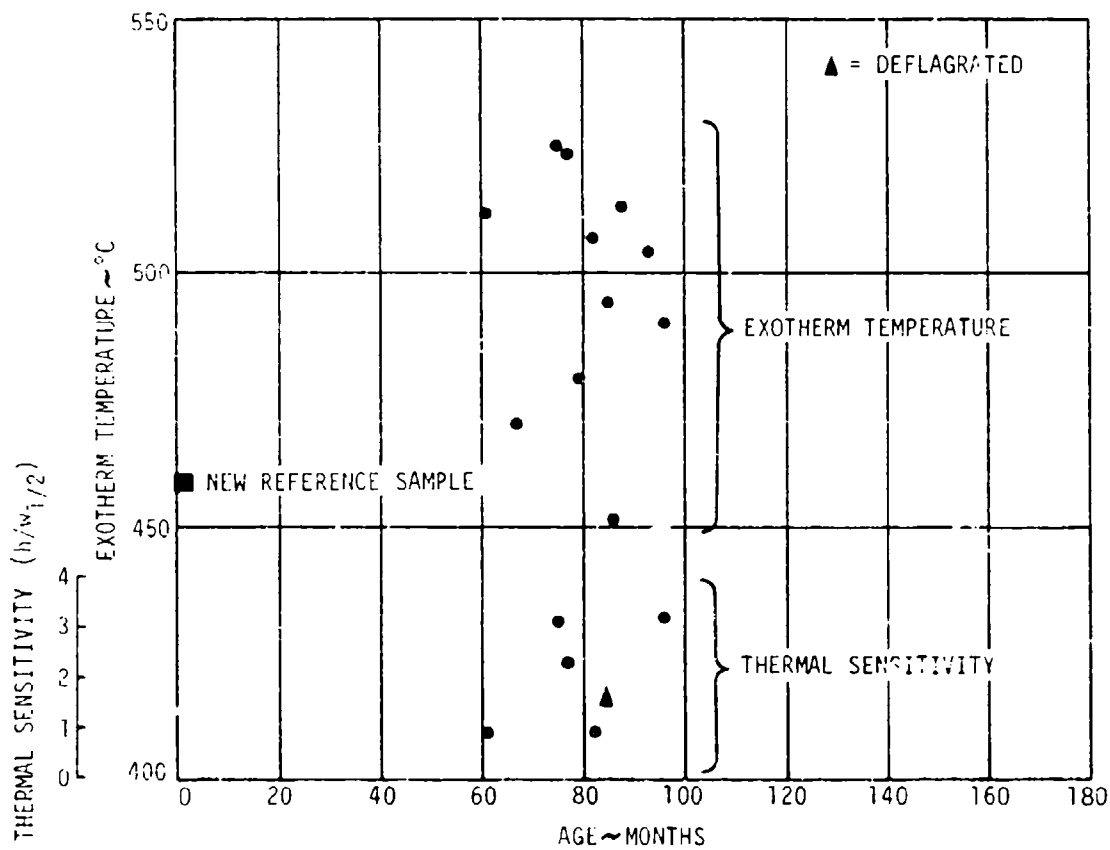


Figure 26. Exotherm Temperature and Thermal Sensitivity of B-KNO<sub>3</sub> EBW Initiator Output Charge versus Age

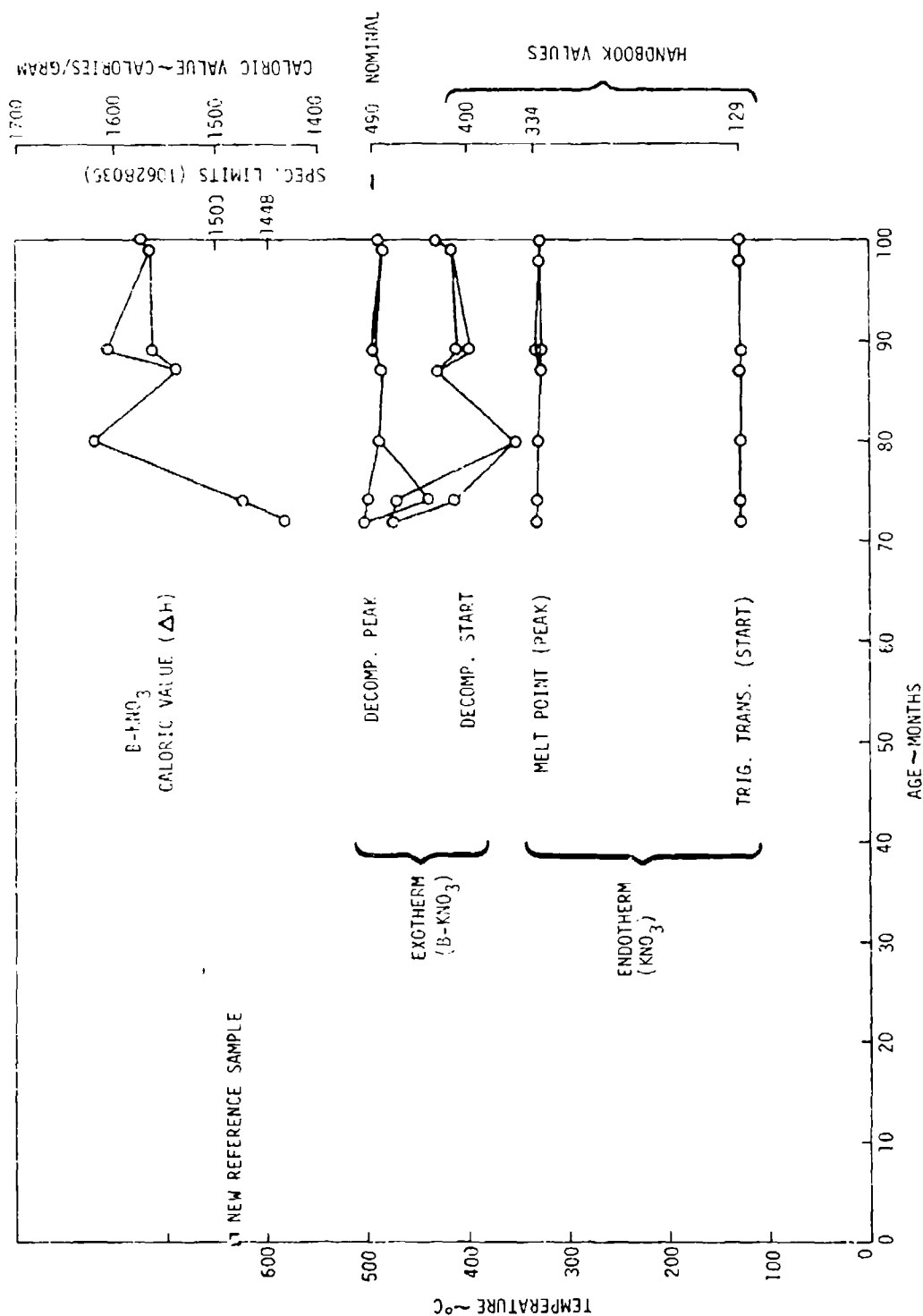


Figure 27. Calorimetry and Thermoanalytical Test Results of B-KNO<sub>3</sub> EBW Initiator Output Charge versus Age

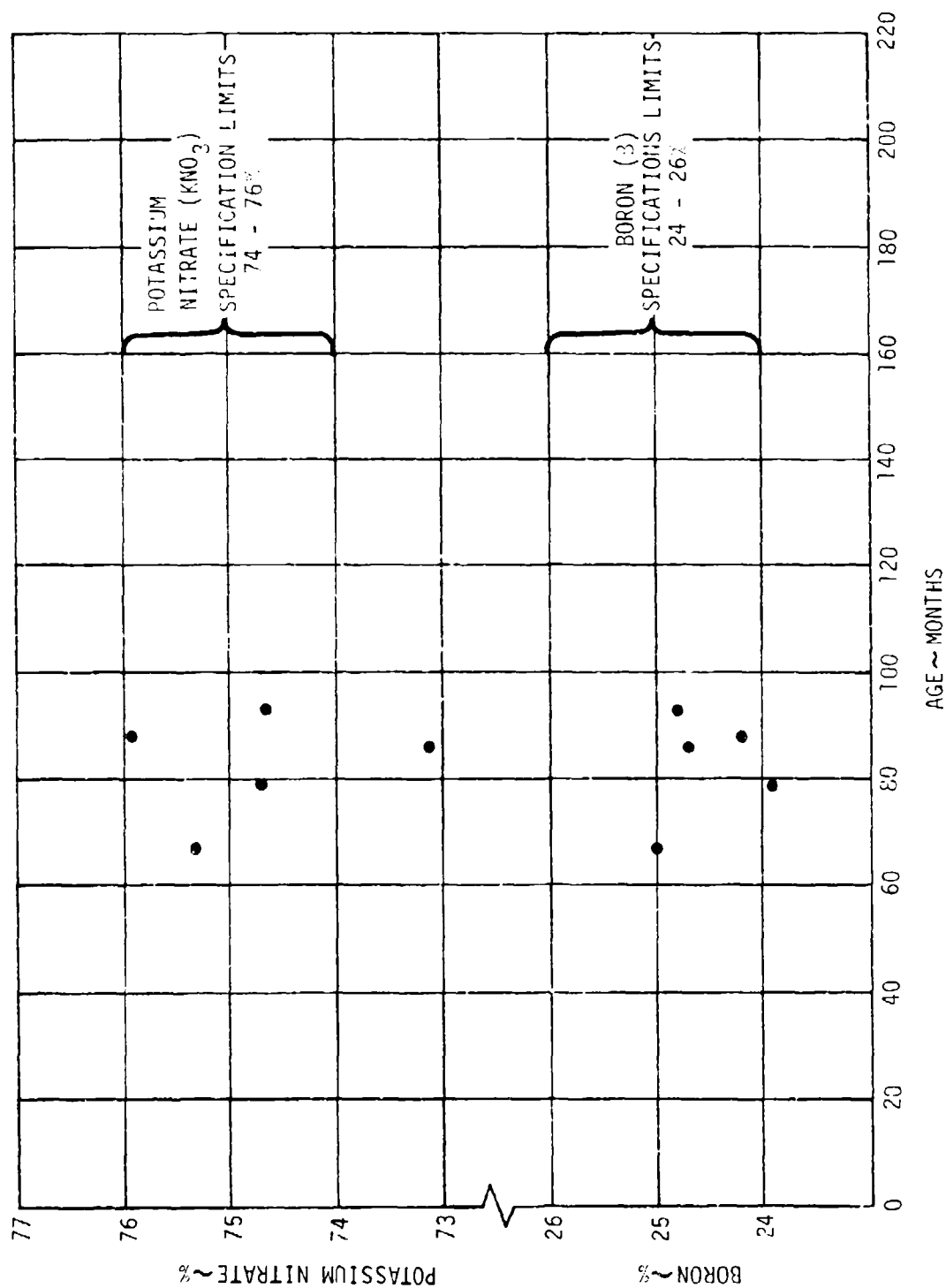


Figure 28. Chemical Analysis of B-KNO<sub>3</sub> EBW Initiator Output Charge versus Age



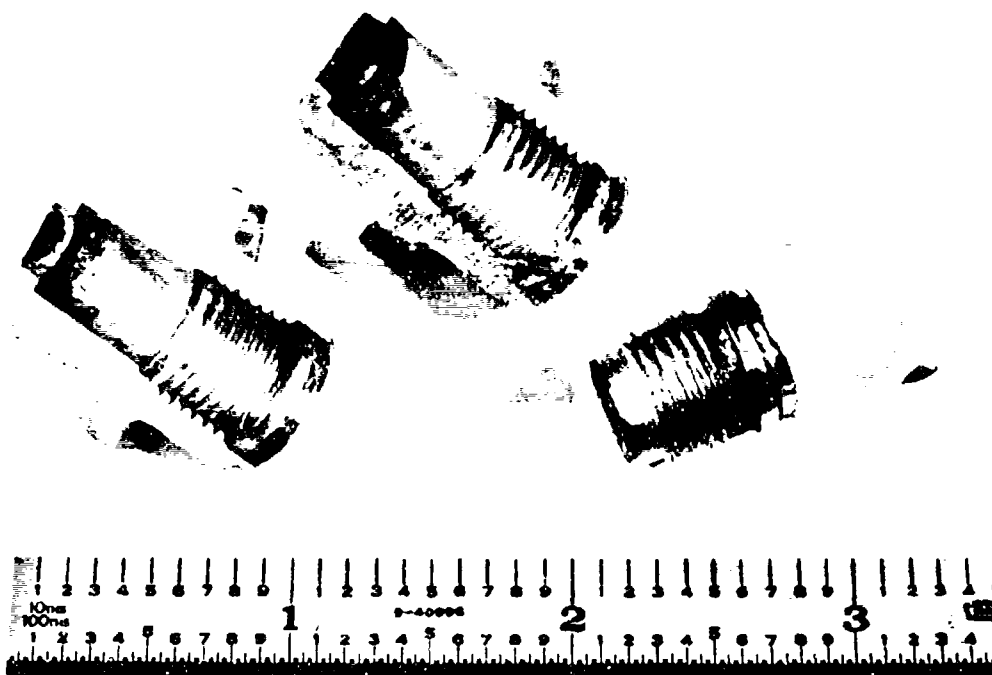


Figure 29. Header and Sectioned Initiator Body Showing Internal Corrosion of Cadmium Plated Steel

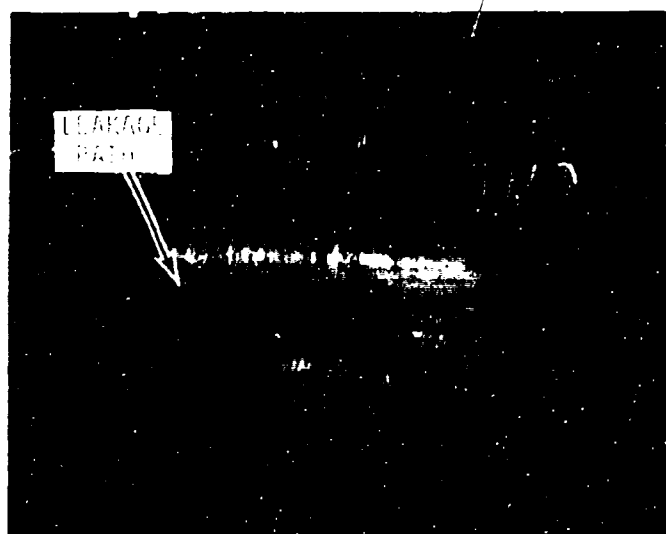
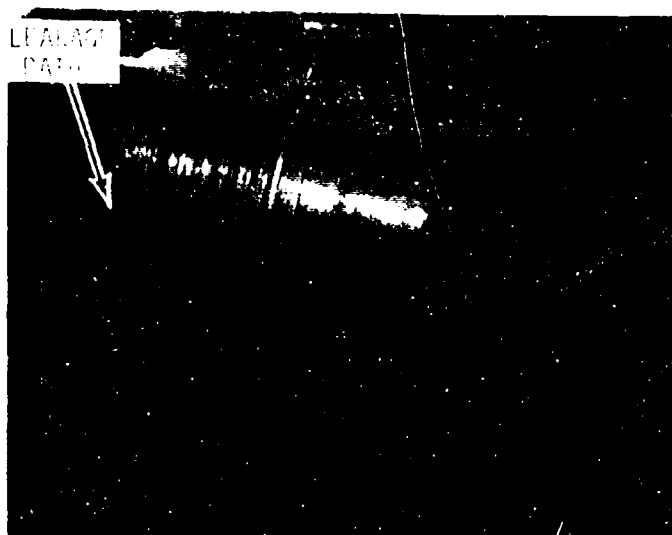
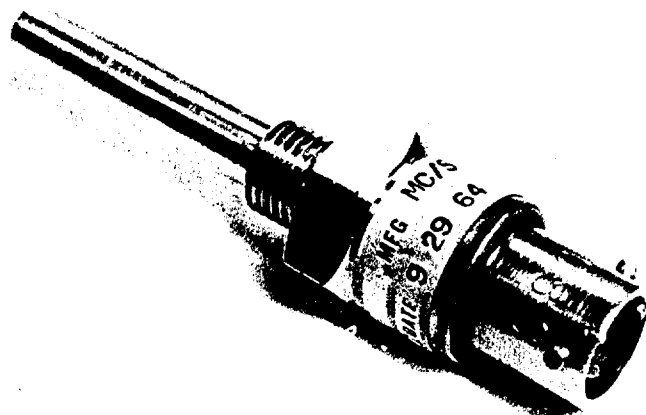
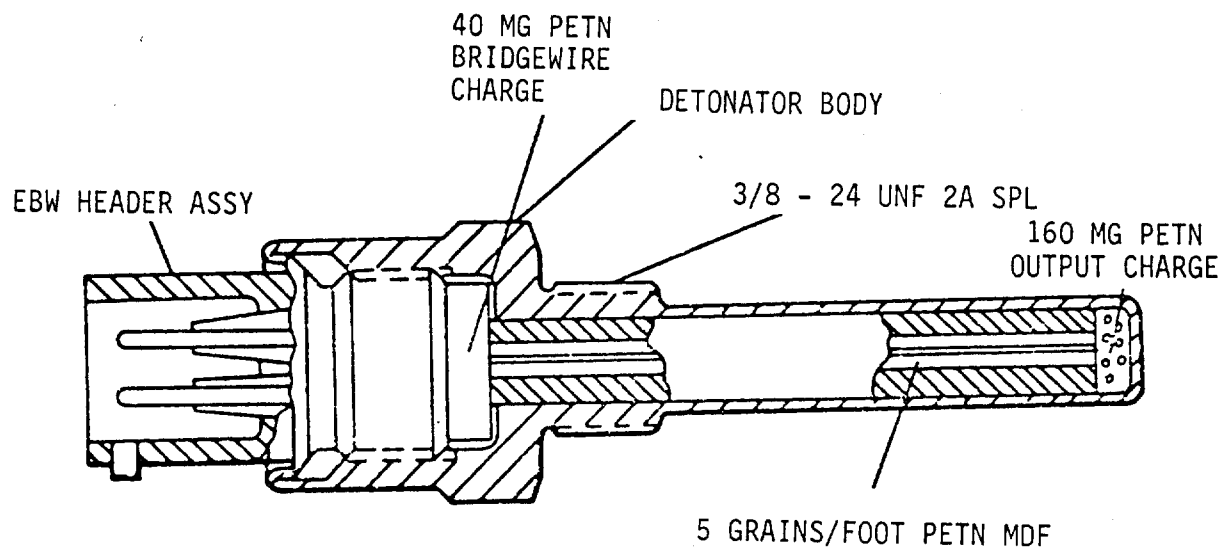


Figure 30. Sectioned Initiator Body Showing  
Leakage Path in Solder Seal



The EBW explosive bolt cartridge is a sealed detonator consisting of an EBW header, with appropriate connector keying pins, permanently assembled to the detonator body containing a PETN transfer lead and output charge. One cartridge is installed in each splice band explosive bolt. Two explosive bolts are installed at diametrically opposite positions in the splice bands to provide redundancy of the splice band release function. Detonator cartridges are installed and high voltage firing cables, are connected after the missile sections are spliced together.

Characteristics of EBW cartridges 10628002-29 and 10566013-9 are as follows:

Header characteristics: See Figure 17

Explosive loading:

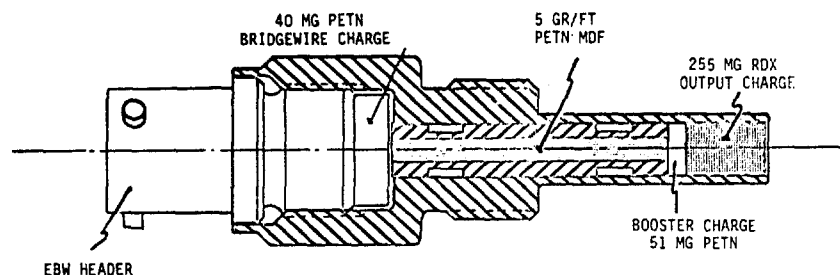
Header — 40 mg PETN (MIL-P-387, Class 2)

5 gr/ft MDF lead — 40 mg PETN (10628032-3)

Output charge — 160 mg PETN (MIL-P-387, Class 2)

Function time: Approximately 7  $\mu$ sec

Figure 31. EBW Explosive Bolt Cartridge (Stage Separation), 10628002-29 (MPD 11234) and 10566013-9 (MPD 11522)



The EBW case vent detonator is similar to, but not physically interchangeable with, the explosive bolt cartridge. The detonator contains an EBW header, PETN transfer lead, PETN booster charge and RDX output charge. Appropriate connector keying pins on the header, provide for correct mating of high voltage cables from the HEFU.

The case vent detonators are installed in mounting blocks on the inside of the second stage forward skirt. These detonators are located directly over and provide a detonation stimulus to the receptor booster in the case vent shaped charge assembly mounted on the outer surface of the second stage motor. Electrical connections of the high voltage firing cables are made when the detonator assemblies are installed.

Characteristics of EBW detonator 10566015-29 are as follows:

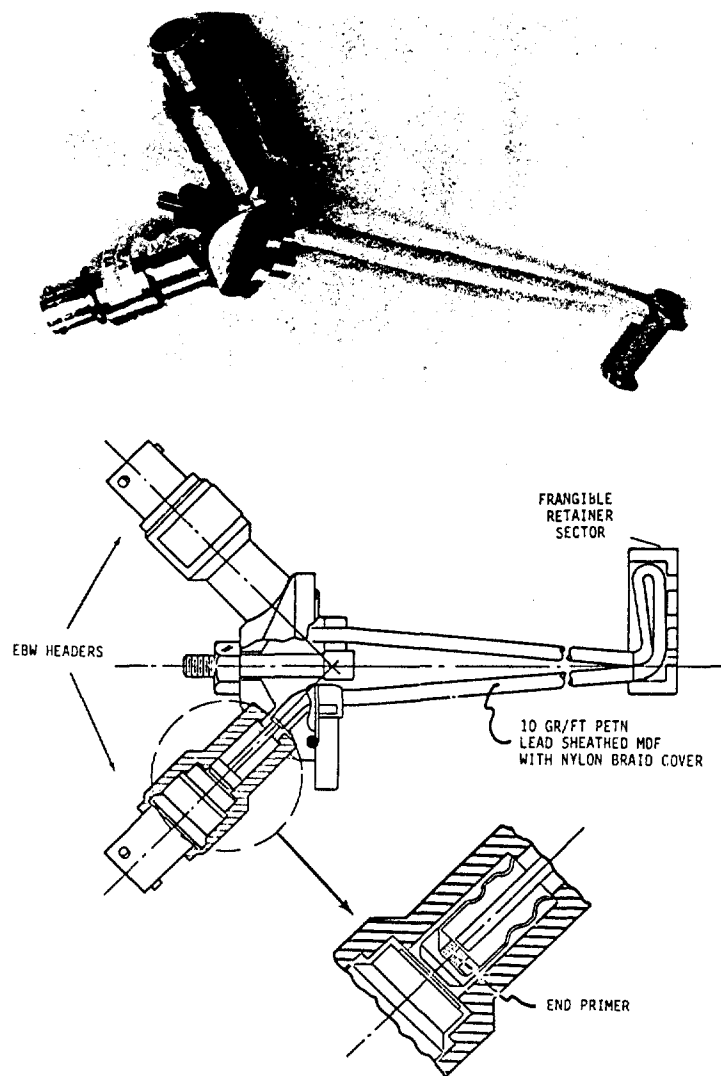
Header characteristics: See Figure 17

Explosive loading:

- Header -- 50 mg PETN (MIL-P-387, Class 2)
- 5 gr/ft MDF lead -- 27 mg PETN (10628032-3)
- Booster charge -- 51 mg PETN (MIL-P-387, Class 2)
- Output charge -- 225 mg RDX (MIL-R-398, Type A Class C)

Function time: Approximately 6  $\mu$ sec

Figure 32. EBW Case Vent Detonator, 10566015-29 (MPD 115,30)



The EBW explosive device is an explosive assembly containing two EBW header assemblies, two end primers, a length of ten grain per foot mild detonating fuse (MDF), and a frangible sector. This design provides redundancy of performance within a single assembly. One explosive device is installed in each thrust reversal tube of the second stage assembly. EBW explosive devices, high voltage firing cables, and HEFUs are installed and connected during second stage assembly. Keying pins in the header, assure correct mating of the high voltage firing cables from the HEFU.

Thrust reversal explosive devices are initiated by high energy electrical pulses from the high energy firing units (HEFUs) upon command from the guidance computer. Thrust reversal (impulse control) of the second stage motor is provided by simultaneously opening three ports on the forward end of the rocket motor. Opening the ports is accomplished by shattering the sector in each port, permitting the retaining rings and closures to be forced out of the ports, and motor gases to escape.

Characteristics of EBW explosive devices 10628003-39 and 10566014-9 are as follows:

Header characteristics: See Figure 17

Explosive loading:

Header -- 40 mg PETN each of two (MIL-P-387, Class 2)

End primers -- 71 mg PETN each of two (10628023-1)

10 gr/ft MDF lead -- 715 mg PETN (10628032-11)

Function time: Approximately 32  $\mu$ sec

Figure 33. EBW Thrust Reversal Dome Release Explosive Device (Sector).  
10628003-39 (MPD 11235) and 10566014-9 (MPD 11523)

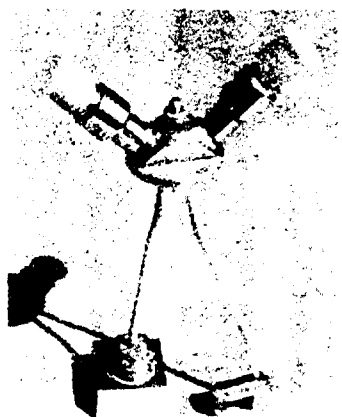


Figure 34. EBW Explosive Device Prepared for Dent Block Test and Thrust Reversal Dome Release Test

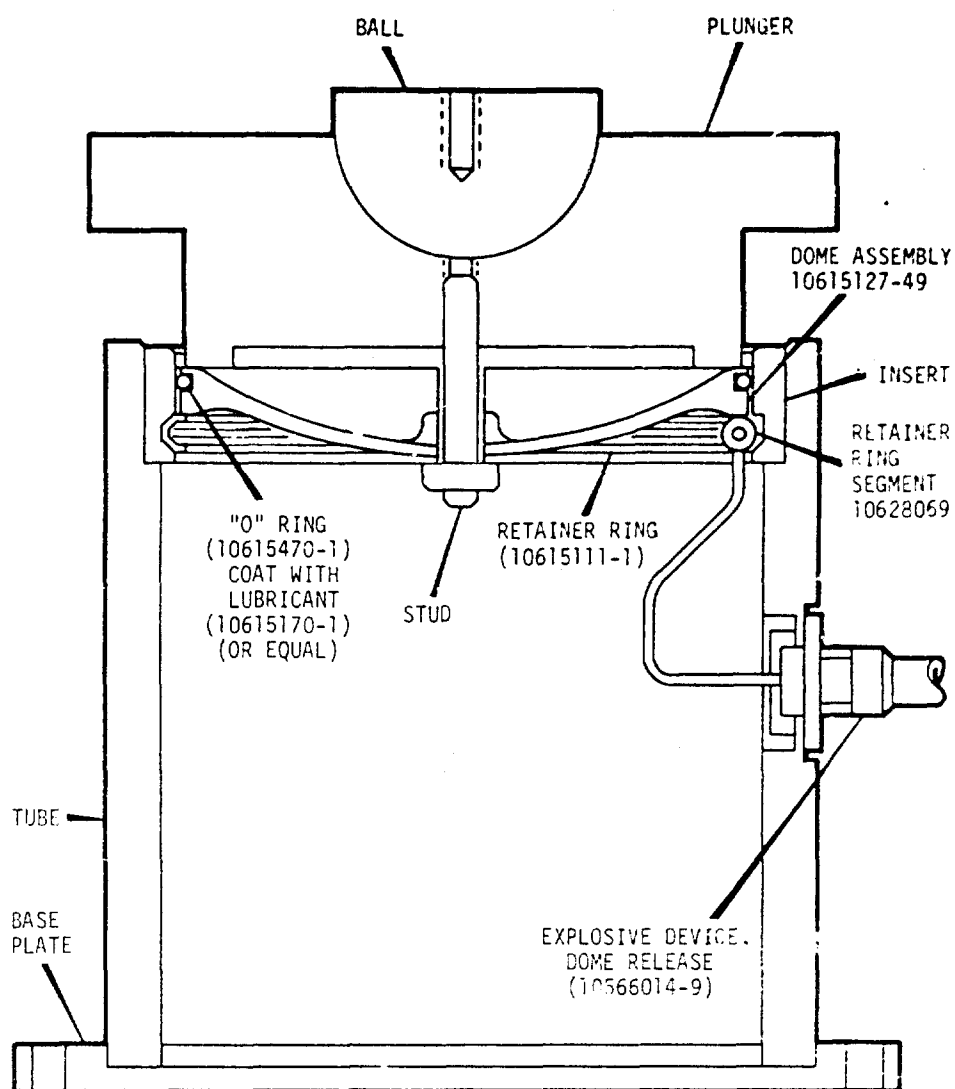


Figure 35. Thrust Reversal Dome Release Test Fixture

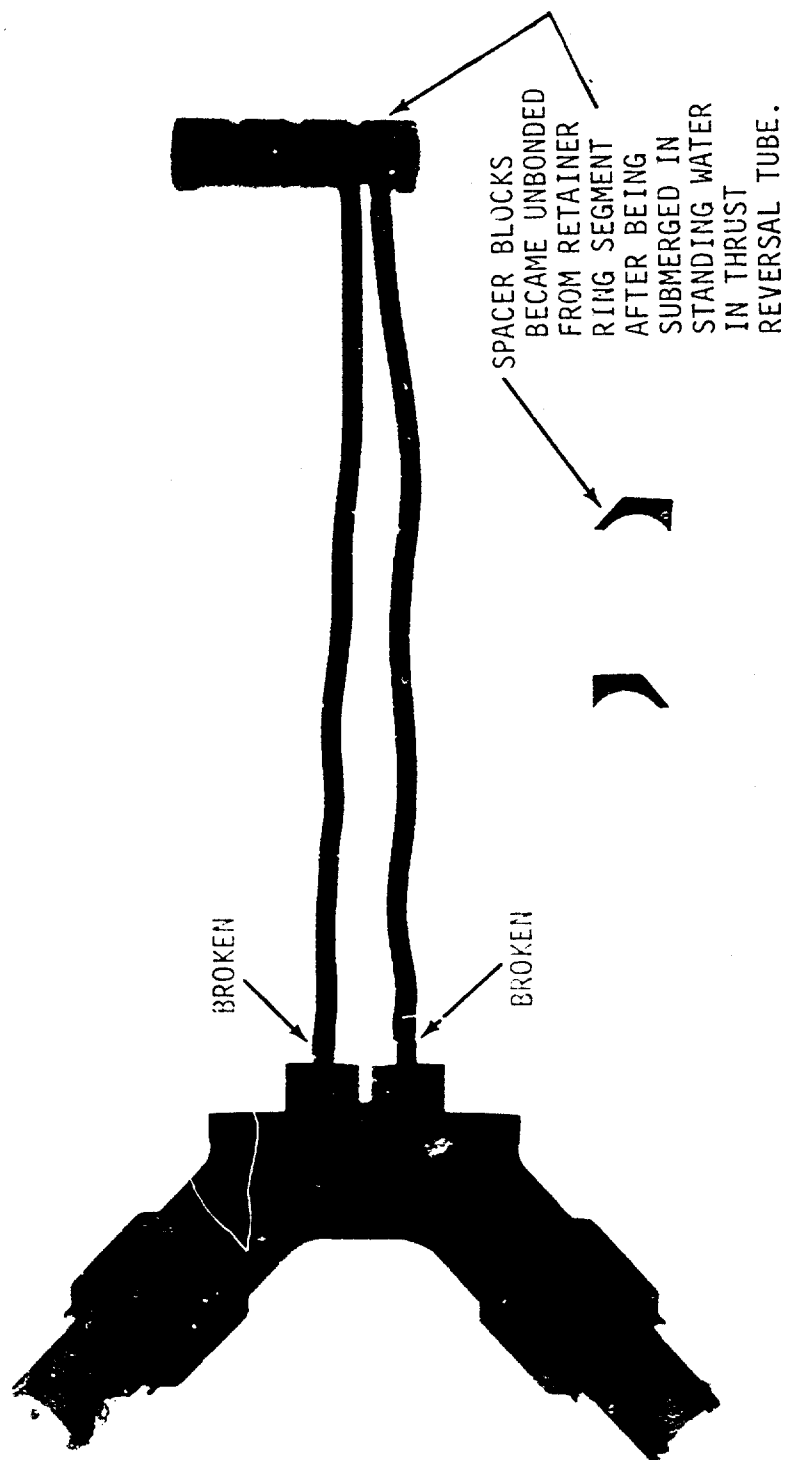


Figure 36. Radiograph of Thrust Reversal Dome Release Explosive Device (S/N 6,  
 Lot 2703-3) Showing Both MDF Explosive Leads Broken (Propulsion Section S/N  
 450, Fall 1971 O.T. Flights)

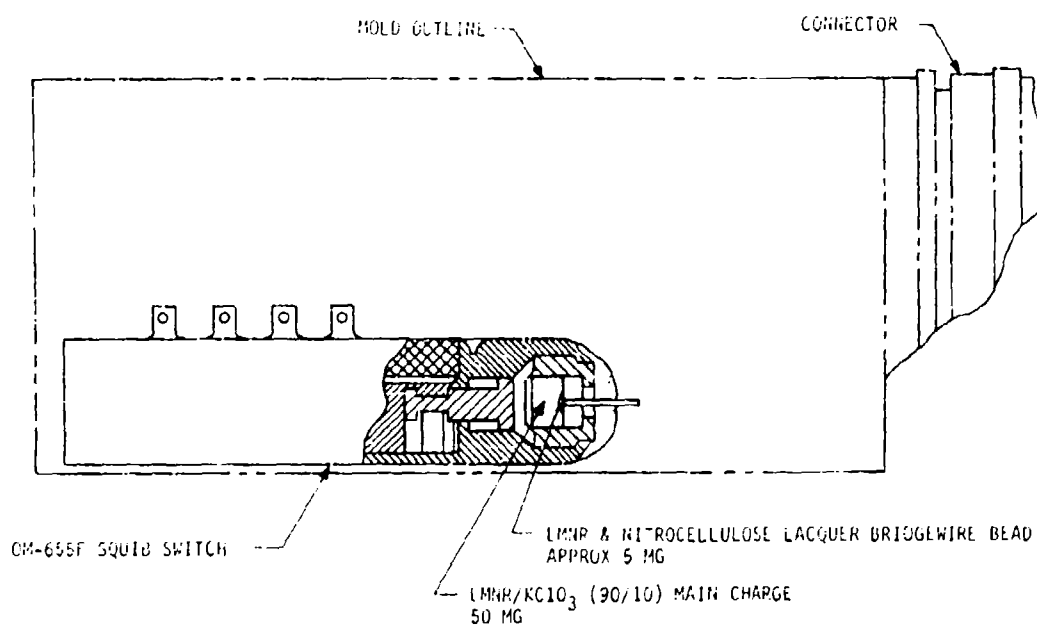
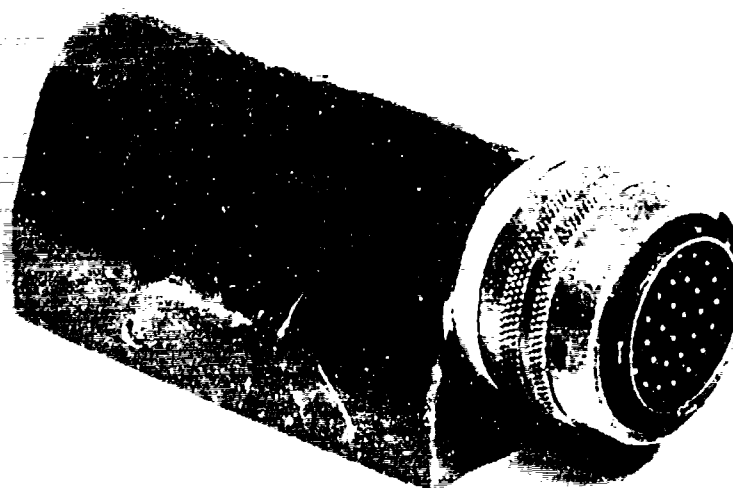


Figure 37. Connector Switch



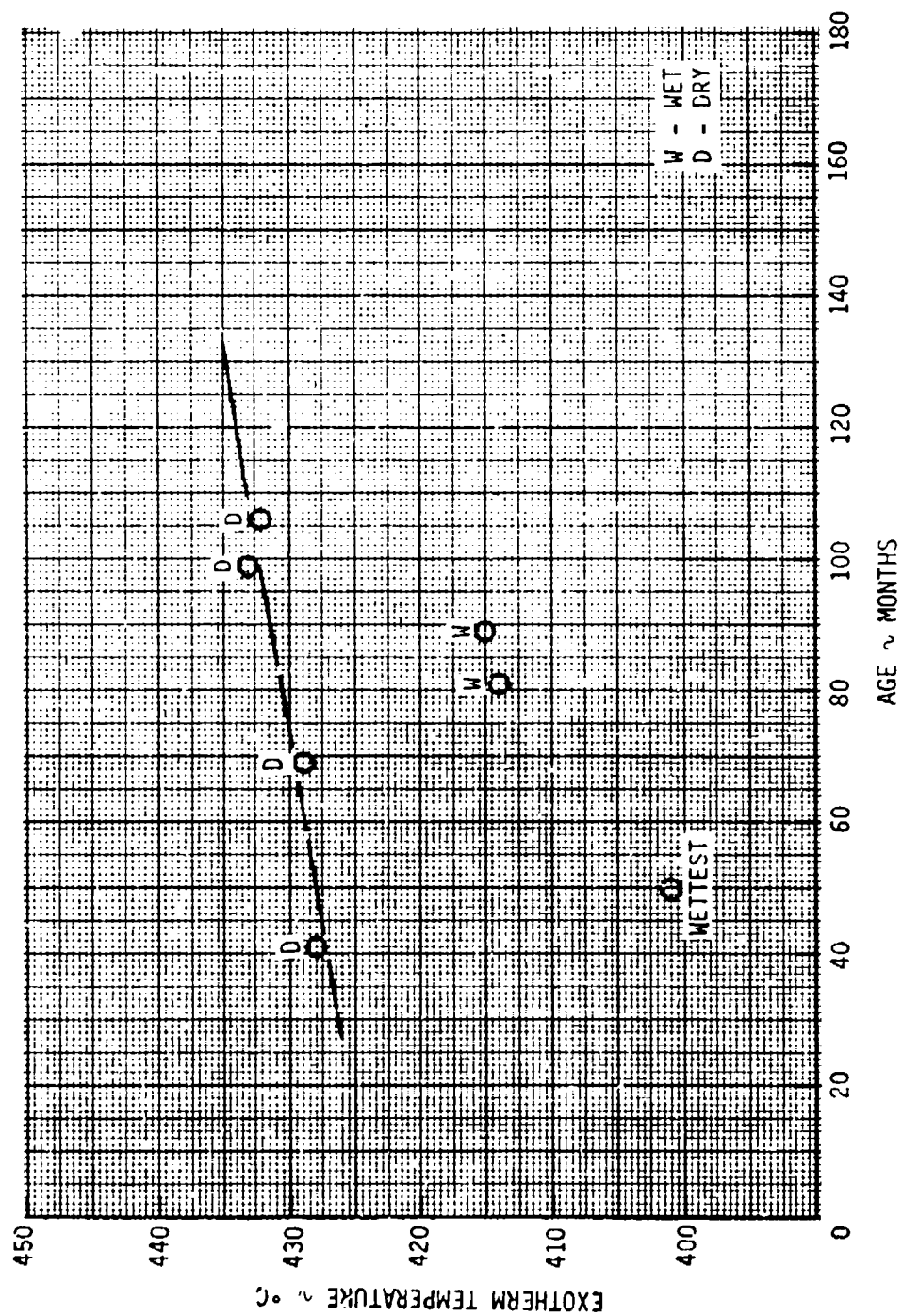


Figure 38. Exotherm Temperature versus Age for LMNR Bridgewire Bead from Connector Switch

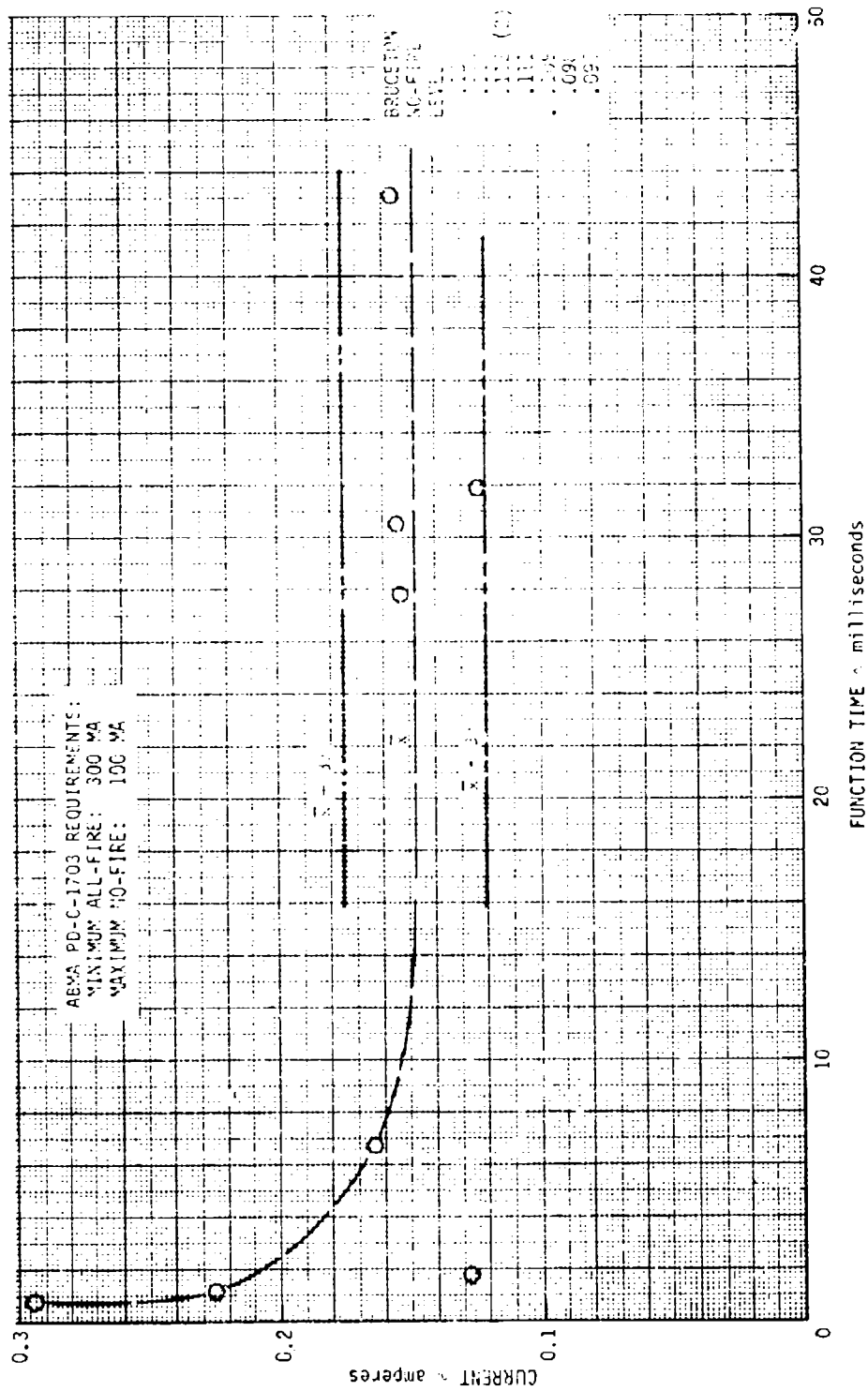


Figure 39. Connector Switch Function Time versus Current from Bruceton Tests Showing Mean Sensitivity Level (x) and Three Sigma (3σ) Deviations

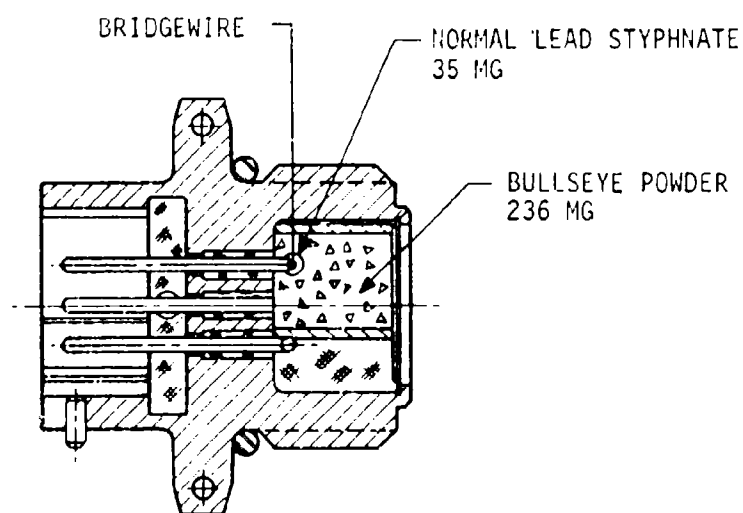
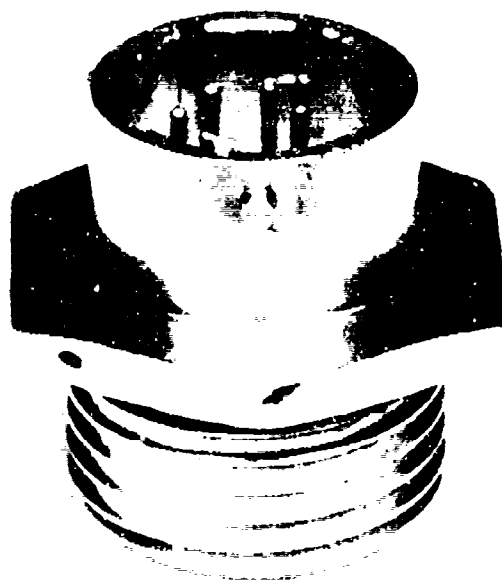


Figure 40. Squib, Battery Disconnect Switch

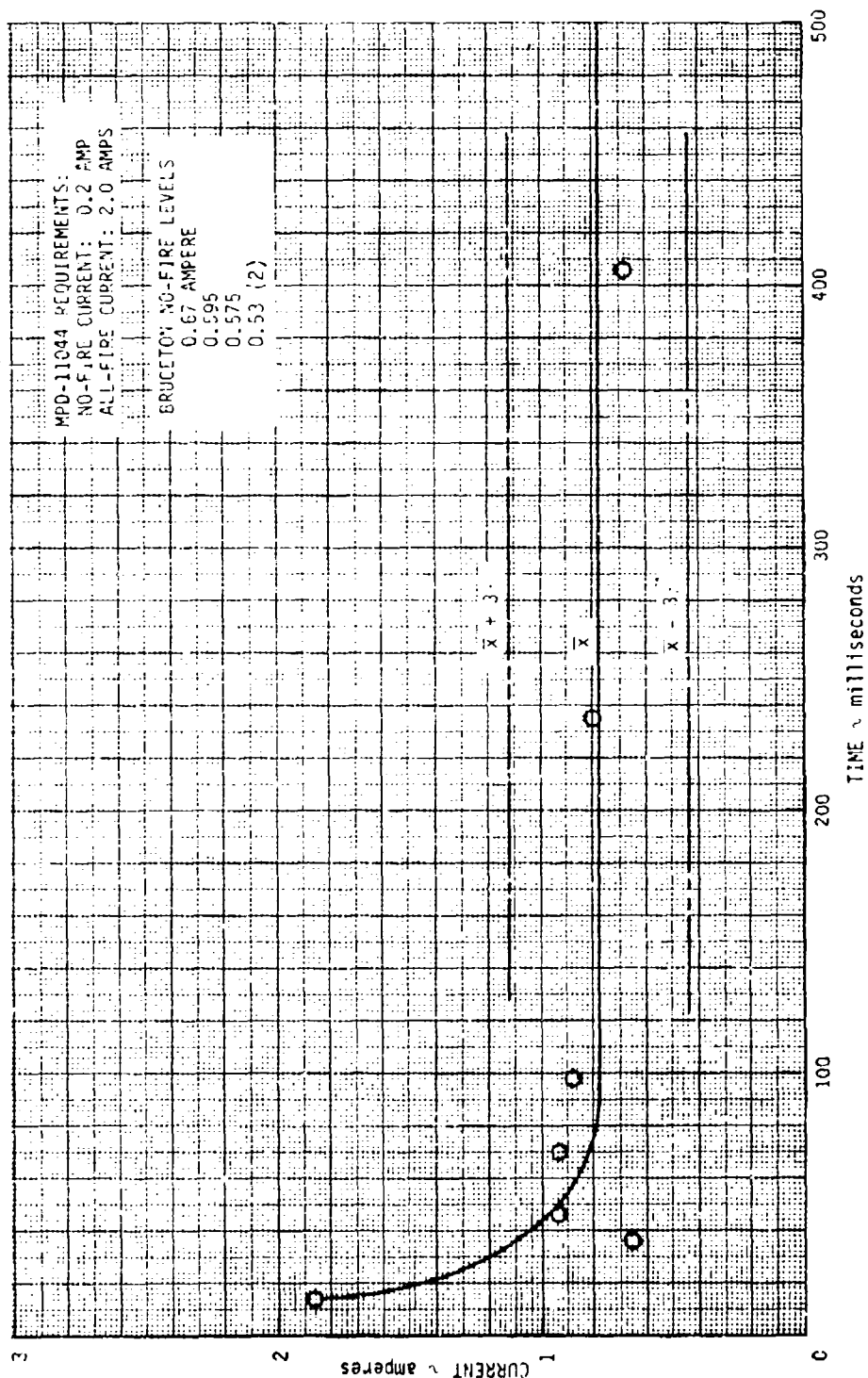


Figure 41. Battery Disconnect Switch Function Time versus Applied Current Showing Mean Sensitivity Level ( $\bar{x}$ ) and Three Sigma ( $3\sigma$ ) Deviations from Bruceton Data

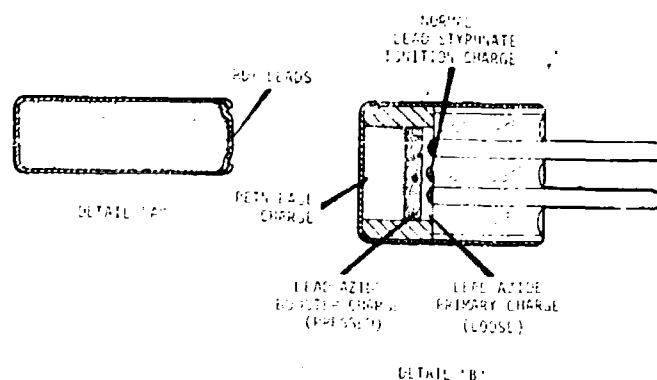
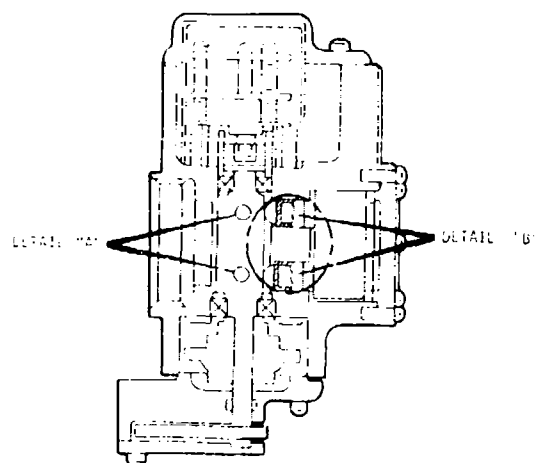
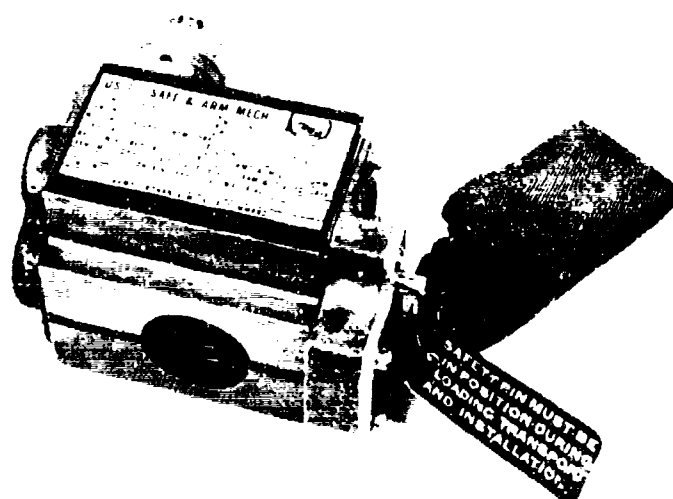


Figure 42. Case Vent S&A Assembly

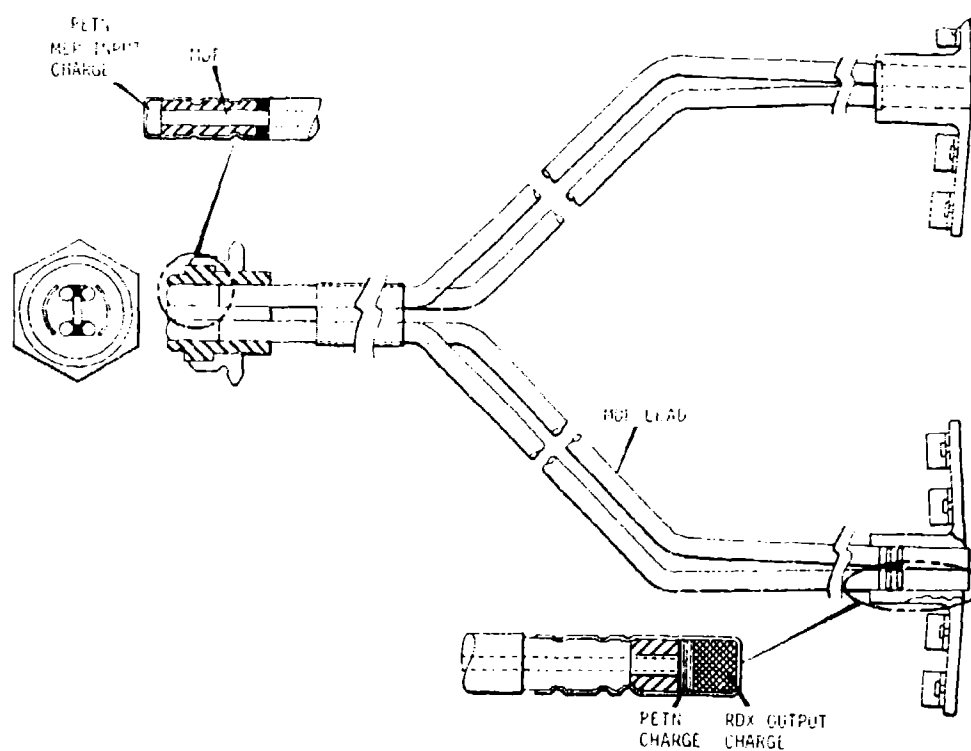
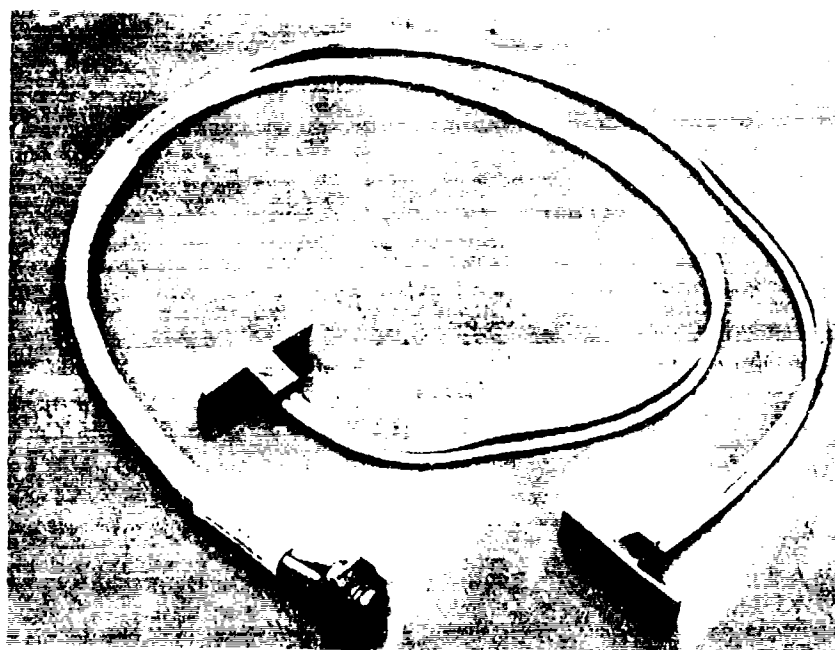


Figure 43. Case Vent Explosive Lead Assembly

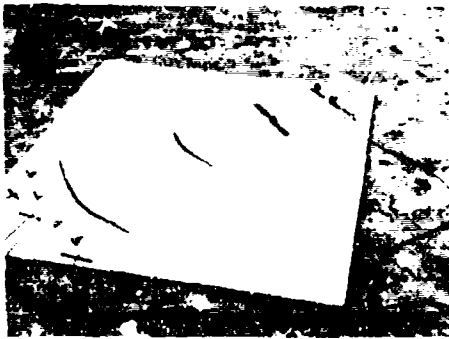


Figure 44. Explosive Lead Assembly Showing Each of the Four Leads Instrumented for Individual Performance

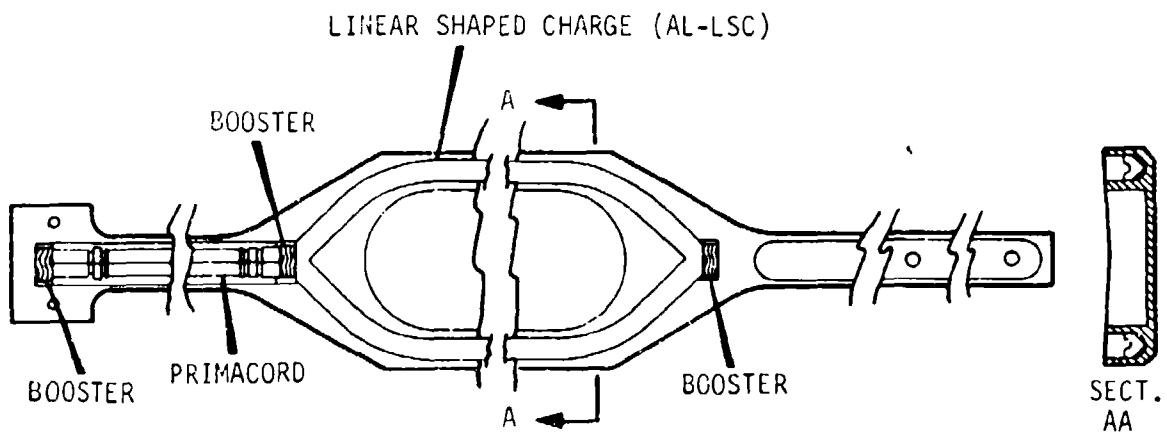
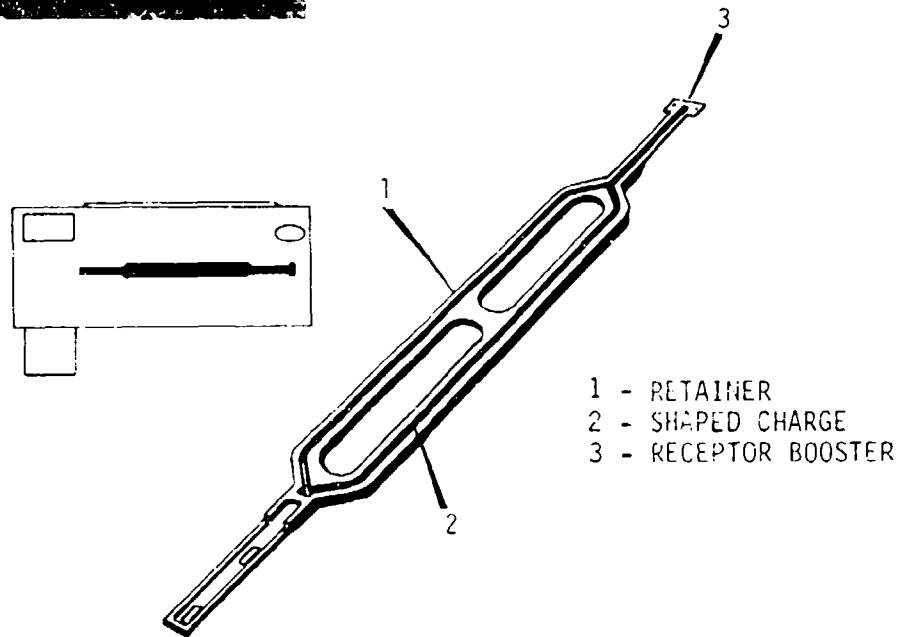


Figure 45. Case Vent Shaped Charge Assembly

TABLE II

## Thermoanalytical and Impact Sensitivity Test Results Recrystallized PETN

Source of Material	Origin Part/Dwg No.	Lot No.	S/N	Age When Tested (Months)	Thermoanalytical Tests			Impact Sensitivity $X_{1/2}$	
					Exotherm (°C)	Rex. (°C)	$W_{1/2}$	Original	Rex.
Bridgewire Charge	10628001-29	2450-5	39	36	213	215	5.2	6.6	-
Bridgewire Charge	10628001-29	M3G-06669		83	216		5.9	9.3	
Bridgewire Charge	10628001-29	2450-2	4	78	215		5.8	5.5	
Bridgewire Charge	10628000-29	2450-5	39	76	213		5.2	6.6	
Bridgewire Charge	10628003-39	M3K-07196		83	216	218	9.1	4.2	-
Bridgewire Charge	10666015-29	1254-3	84	64	217		5.6	5.4	
MDF Charge	10628002-29	2500-2	86	79	215		4.5	-	
MDF Charge	10566013-9	2653-2	60	61	215	218	5.1	-	-
MDF Charge	10628002-39	M3F-03884		83	215		7.1	-	-
MDF Charge	10628003-39	M3C-00594		82	215	217	4.6	3.5	6.1
MDF Charge	10628003-39	M3K-07196		83	215		4.7	4.5	
MDF Charge	10628003-39	2551-1	33	77	215	217	4.4	4.1	9.2 <sup>①</sup>
MDF Charge	10566014-9	2703-1	54	62	215	215	6.0	5.0	
MDF Charge	10566015-29	1254-6	12	58	212	217	4.7	-	-
MDF Charge	10566015-29	1254-3	84	64	215		6.8	-	
Output Charge	10628002-29	M3F-03884		83	215		4.2	7.6	
Output Charge	10628002-29	2500-2	86	79	215	216	6.2	7.6	7.8
Output Charge	10566013-9	2653-2	60	61	210		2.9	11.8	
RIAS PETN	-	-	-		214	215	5.0	-	-
Small amounts of PETN remaining from previous tests were combined as shown to obtain sufficient quantities for these tests.									

① Accrued acetone in recrystallized specimens.



TABLE III

## Thermoanalytical Test Results Recrystallized RDX

Material	Origin Dwg No.	Origin S/N	Exo Temperature		h/W <sub>1/2</sub>		Impact	
			Rex	Orig	Rex (in)	Orig (in)	Rex (in)	Orig (in)
Shaped charge assembly: PRIMACORD RDX	10629280	213	254°C	254°C	8.0	8.0	8.7*	11.9
S&A device: LEADS RDX	10629125	245	252°C	252°C	8.0	8.0		27.2
LEADS RDX	10629125	55	249°C	253°C	5.5	6.3		28.3
EBW detonator: OUTPUT CHARGE RDX	10566015	12	252°C	250°C	7.8	7.9		13.5
OUTPUT CHARGE RDX	10566015	84	252°C	250°C	7.9	8.0		13.8
*Some desensitizing wax removed by recrystallization								

TABLE IV

## Mass Spectrometer Tests

Material	Reason for Investigating	Results
PETN (Recrystallized)	Double peak in thermogram	Exhibited acclused acetone
PETN	Relatively high sensitivity in DTA	Produced the same spectrum
PETN	Relatively low sensitivity in DTA	
RDX	Dark pink, high sensitivity	Produced the same spectrum
RDX	Light pink, relatively high sensitivity	
RDX	Offwhite, relatively low sensitivity	
Lead Styphnate	Hard and brittle	Exhibited a small amount of water loss 2-5 seconds before detonating at 65°C.
Lead Styphnate	Soft and spongy	Exhibited water loss over a wide range of temperatures and for several minutes. Lost over twice as much water as above sample. Did not detonate.

## V. CONCLUSIONS

### A. SUMMARY OF TEST RESULTS

Two types of age-related defects were determined during these tests. Cadmium-plated electroexplosive devices have experienced random corrosion internally as well as externally. Corrosion of the internal surfaces has occurred as a result of the ingress of moisture through leaks in the solder seals. In initiators, this degrades the performance of the B-KNO<sub>3</sub> output charge, however, never to a point of causing a failure to function. Corrosive effects from handling have also been experienced. This is a cosmetic effect without actually degrading the performance of the assemblies.

Moisture was detected in the LMNR bridgewire charge of connector switches. This appeared to affect function time, but no failures were experienced in functional tests of these units.

Handling damage has caused failures of MDF leads when the lead sheath is broken. This results in loss of confinement, the ingress of moisture, and failure to propagate across the break.

The case vent shaped charge assemblies have demonstrated that they are not performing optimally. This is due to the small standoff provided by the retainer assembly. The relatively small bend radius used to form the ends of the linear shaped charge contribute somewhat to this degradation.

### B. RECOMMENDATIONS

The following recommendations were made to the PERSHING Project Manager's Office (PPMO) of AMICOM as a result of the LEAP tests.

- 1 Replace cadmium-plated electroexplosive devices with the stainless steel configurations. This has been implemented by PPMO.
- 2 Limit moisture in the LMNR bridgewire charge of the connector switch to 0.3 percent and insulation resistance to 500 megohms. These changes have been added to the squib switch drawing.
- 3 Add strain relief sleeves to the MDF explosive leads of the thrust reversal explosive device. New hardware has incorporated this improvement. All hardware in the inventory will be modified to incorporate this change.
- 4 Improve the case vent shaped charge assembly to provide optimum performance. This has been approved by PPMO and is being implemented.

## REFERENCES

- 1 Pershing Life Extension and Assessment Program Final Report OR 11,385, December 1971.
- 2 Sensitivity Test. Testing Requirements (Bruceton). U.S. Army Material Command Document 11199529, Revision A, December 1969.
- 3 Martin Marietta Research Institute for Advanced Studies, Baltimore, Maryland.

## APPENDIX A

### Theoretical Treatment of Drop Test Data(A1)

The standard method of analyzing drop test results is the Bruceton staircase method which results in a calculated value for the height,  $h_{0.5}$ , at which the probability is 0.5 that there will be an explosion. This volume is calculated by

$$h_{0.5} = \frac{\sum_i X_i}{\sum_i 1} \pm d/2 \quad \begin{array}{l} \text{use + for failures} \\ \text{use - for successes} \end{array}$$

In this expression  $i$  is the number of successful firings (successes) or nonfirings (failures) at height  $X_i$ ;  $d$  is the increment that the height is varied from test to test, and the summation is carried out over only successes or failures. Some of the problems encountered using the Bruceton method for a very small number of samples are illustrated from the following experimental results. In one experiment we obtained firings at 8, 7, 6, and 5 inches and a failure at 4 inches. Based on the successes  $h_{0.5}$  is calculated to be 6.0. However, this value is heavily biased by the successes at 8 and 7 inches which are likely to be in the range where the probability of a success is near unity. Discounting those two values the calculated value of  $h_{0.5}$  is 5.0 inches. Nonetheless, one is not justified in reporting either of these figures, and clearly a better method of analyzing the data should be sought. This result is not unexpected since the Bruceton method is based on some statistical and mathematical assumptions which are not valid for a small number of samples.

An additional problem with the Bruceton method results from its inherent use of the probability of a failure,  $P_i$ , given approximately by

$$P_i = e^{-KX_i^n}$$

where the exponent,  $n$ , is 2. Levy (A2) has shown that for a number of secondary explosives the proper value of  $n$  is about 4.

For the above reasons a better method of analyzing our drop test data was sought and found. The total probability for a given sequence of successes and failures,  $P$ , is given by

$$\begin{aligned} P(K) &= \prod_i p_i(X_i) \prod_j p_j(X_j) \\ &= \text{Exp}(-K \sum_i X_i^4) \prod_j (1 - \text{Exp}(-KX_j^4)) \end{aligned}$$

where we use the subscript  $i$  for failures and the subscript  $j$  for successes. Since  $h_{0.5}$  is related to  $K$  through the expression  $h_{0.5} = (693/K)^{1/4}$ , all that is required is the optimal value of  $K$  to

determine  $h_{0.5}$ . In Figure A1  $P(K)$  is plotted versus  $h_{0.5}$  for the same data previously discussed. It is seen that it is far more likely that  $h_{0.5}$  is closer to 4.14 than the Bruceton value of 6. Although curves of  $P(K)$  generally show some assymetry about the maximum value, it is not marked near the maximum; so we have used the value of  $h_{0.5}$  determined from the maximum in the  $P(K)$  curves for all drop tests in this report. The value of  $h_{0.5}$  at the maximum is determined by solving the equation

$$\frac{dP(K)}{dK} = 0 = P(K) \left( -\sum_i X_i^4 + \sum_j \left( \frac{X_j^4}{\text{Exp}(-KX_j^4) - 1} \right) \right).$$

A computer program for solving this equation has been written and is included in the report. The program is written in the basic language which is amenable to most time sharing computers. The program also computes the probability that  $K$  is such that  $h_{0.5}$  is within  $\pm 2$ ,  $\pm 1\frac{1}{2}$ ,  $\pm 1$  and  $\pm 0.5$  inches of the previously calculated value of  $h_{0.5}$ . This is accomplished by the numerical integration of

$$\int_{0.693/(h_{0.5} + a)^4}^{0.693/(h_{0.5} - a)^4} P(K) dK / \int_0^{\infty} P(K) dK$$

This probability is of particular importance when trying to determine if the difference between the drop heights for two different samples is significant.

We believe that our method for determining  $h_{0.5}$  is a marked improvement over the Bruceton method for a small number of samples. If the number of samples is greater than about 10, the two methods give similar values of  $h_{0.5}$  as would be expected.

---

A1 Developed by Dr. Maclyn McCarty, Martin RIAS, for the Pershing LEAP program.

A2 P. W. Levy, Nature, 182, 37, (1958).

# COMPUTER PROGRAM FOR CALCULATING DROP HEIGHTS

```

99   DIM H(20)
100  DIM Y(30), Z(30), U(30)
150  READ N1, N2, N5
160  LET S1 = 0
200  FOR I = 1 TO N2
210  READ Y(I)
220  LET Y(I) = (Y(I)/10) + 4
230  LET S1 = S1 + Y(I)
240  NEXT I
300  FOR I = 1 TO N1
310  READ Z(I)
320  LET Z(I) = (Z(I)/10) + 4
330  LET S3 = S3 + Z(I)
340  NEXT I
350  LET N4 = 0.07/Y(1) + 4
400  LET K = K + N4
401  LET F = 0
410  LET J = J + 1
430  FOR I = 1 TO N2
431
440  LET F = F + Z(I)/(EXP(Z(I)*K) - 1)
450  NEXT I
451
470  IF F - S1 > 0 THEN 400
480  LET K = K - N4
490  LET N4 = N4/10
500  LET M = M + 1
510  IF J > 100 THEN 1999
520  IF M < 6.1 THEN 400
539  LET K2 = (0.693/K) + 0.25
540  PRINT "K = "K*1E-4; "X - 1/2 = "10*(0.693/K) + 0.25
600  FOR I = 1 TO 9
610  LET U(I) = 0.693/(K2 + 0.25 - I/20) + 4
620  NEXT I
630  LET U(0) = 0
631  LET U(10) = U(9) + 2
632  LET U(11) = U(10) + 2
700  DATA 3, 2
702  DATA 50
710  DATA 8, 8, 9, 9, 10

```

```

1000 LET B = U(1)/N5
1010 LET K3 = -1
1020 LET K3 = K3 + 1
1025 FOR J1 = 0 TO N5
1030 LET X = U(K3) + J1*B
1040 LET P = 1
1050 FOR I = 1 TO N2
1060 LET P = P*EXP(-X*S1)
1080 NEXT I
1100 LET P = P*EXP(-X*S1)
1110 IF J1 = 0 THEN 1180
1120 IF J1/2 - INT(J1/2) > 0.1 THEN 1170
1130 IF J1/2 - INT(J1/2) > 0.1 THEN 1170
1140 LET S2 = S2 + 2*P
1150 GO TO 1200
1170 LET S2 = S2 + 2*P
1180 LET S2 = S2 + P
1200 NEXT J1
1250 LET H(K3) = S2*B/3
1260 LET S2 = 0
1290 IF K3 = 10 THEN 1350
1300 LET B = (U(K3 + 2) - U(K3 + 1))/N5
1330 GO TO 1020
1350 LET H(K3 + 1) = EXP(-S1*X)/S1 - EXP(-X*(S1 + S3))/(S1 + S3)
1400 FOR I = 0 TO 11
1410 LET S4 = S4 + H(I)
1420 NEXT I
1450 FOR I = 0 TO 11
1460 LET H(I) = H(0) - H(9)
1470 NEXT I
1500 LET SS = 1 - H(0) - H(9)
1501 LET SS = SS - H(10) - H(11)
1510 LET SS = SS - H(1) - H(8)
1520 LET S7 = S6 - H(2) - H(7)
1530 LET SS = S7 - H(3) - H(6)
1600 PRINT "P(1/2) = "SS, "P(1) = "S7, "P(3/2) = "S6, "P(2) = "SS
1999 END

```

To run program insert data as follows:

700 DATA (number of non-firings), (number of firings)

702 DATA (number of segments in integral, 50 is usually adequate)

710 DATA (the height of each non-firing allowed by the height of each firing).

As the program stands, it is for a set of data which gave firing at 8 inches twice and 9 inches once but did not fire at 9 or 10 inches. It is important that the data in line 710 start with the smallest number.

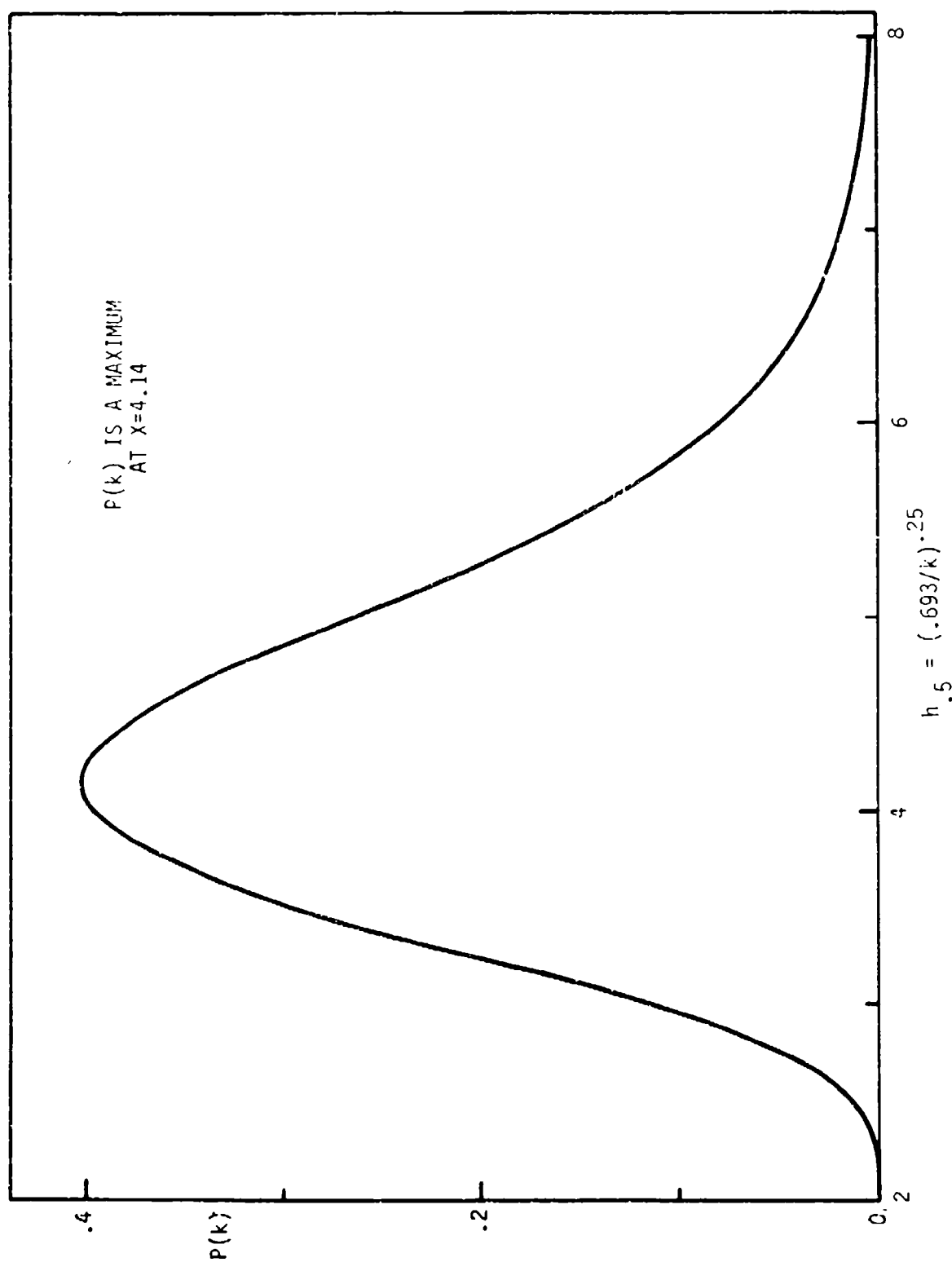


Figure A-1. Plot of  $P(k)$  versus  $h(0.5)$  for Drop Tests



## PROPERTIES AND APPLICATIONS OF BORON/POTASSIUM NITRATE

Paul B. Tweed  
Martin Marietta Corporation  
Orlando, Florida

### ABSTRACT

Boron/potassium nitrate, a replacement for black powder, has been partially characterized by many agencies. This paper contains new data on its aging properties as well as some of its less well known electrical characteristics. The use of boron/potassium nitrate in hot wire and exploding bridgewire devices is also discussed.

### INTRODUCTION

Boron/potassium nitrate compositions are mechanical mixtures of amorphous boron and granular potassium nitrate, with or without binders, that were originally developed as replacements for black powder in rocket igniters. They are superior to black powder with respect to autoignition, hygroscopicity, and heat of reaction. They have also been used as expelling charges and as output charges in electric squibs, and have been in the Department of Defense inventory for approximately 15 years.

Military specification MIL-P-46994 covers pellets of 23.7/70.7/5.6 boron/potassium nitrate/Laminac, which I call Mixture 1. The properties of Mixture 1 are shown in Table I. These values are based on data from Flare-Northern<sup>(1)</sup>, Bermite, Thiokol, the Bureau of Mines, and Allegany Ballistic Laboratory.

Flare-Northern makes a wide variety of boron/potassium nitrate compositions, as shown in Table II. Note that the first seven items are Mixture 1, 2C is 18/82 boron/potassium nitrate and 2K is 15/70/15 boron/potassium nitrate/TNC. The binderless composition is used in applications where the Laminac would be degraded, and the TNC composition is used in ejection devices that require a very fast rise time.

Among the EBW rocket motor initiators which contain Mixture 1 as the output charge are the M6<sup>(2)</sup>, Pershing<sup>(3)</sup>, SPRINT<sup>(4)</sup>, and SAM-D<sup>(5)</sup> devices. The aging characteristics of Mixture 1 when used as an output charge are discussed in this paper. Design requirements which must be considered in applications where boron/potassium nitrate is directly in contact with the bridgewire of an

electroexplosive device are also discussed. Such applications had been previously covered by Menichelli<sup>(6)</sup> of the Naval Ordnance Laboratory in 1965 and Kirkham<sup>(7)</sup> of the United Kingdom Atomic Weapons Research Establishment in 1970.

#### AGING OF MIXTURE 1 OUTPUT CHARGES

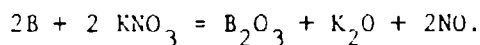
In 1966, Bowman and Knippenberg<sup>(8)</sup> of General Electric reported that Mixture 1 exhibited some deterioration of physical properties when subjected to gas evolution tests for four days at 150°C. Although Mixture 1 did not evolve gas during this period, they recommended 18/82 boron/potassium nitrate as the output charge in sterilizable igniters. Their test data was corroborated by Brownell<sup>(9)</sup> of Thiokol in 1967 when he subjected Mixture 1 pellets to three 53-hour cycles at 135°C. The length increased 10 percent, diameter 8 percent and crush strength dropped from 27,000 to 1000 pounds, but weight did not change. Thiokol concluded that the Laminac binder was responsible for the degradation of the pellets.

Although Mixture 1 deteriorates at sterilization temperatures, it withstands conventional temperatures for long periods of time with only slight loss of performance. References 10 through 13 cover Naval Ordnance Station aging tests of MARK 280 Mod 0, MARK 247 Mod 0, MARK 200 Mod 0, and MARK 270 Mod 0 igniters, respectively. Extrapolation of the results of these tests indicate that Mixture 1 should have a storage life of at least 8 years.

In 1971 Storma<sup>(14)</sup> of Martin Marietta reported on pressure-time tests of 19 Pershing rocket motor initiators after storage from 55 to 96 months. Each Pershing initiator contains an annular output pellet of 290  $\pm$  10 mg of Mixture 1. Figure 1 shows a cross sectional view of this exploding bridgewire device. Eighteen of the 19 initiators had B1113 steel headers and bodies soldered together and cadmium plated; the other initiator had a stainless steel header and body welded together. The latter design is superior to the former with respect to corrosion. The devices were fired in a 225 cc chamber instrumented with a Norwood 111 pressure transducer. Seventeen of the 19 initiators gave pressure rises lower than required (120 psig min within 20 ms). Figure 2(a) shows an output signature that meets the requirements. The pressure rise and slight increase followed by tail-off is characteristic of new initiators. The output signature shown in Figure 2(b) is typical of those units which did not meet the requirements. Here a slow initial pressure rise is followed by a slight decrease and a slight rise before tail-off. Figure 3 shows the relation between age of the initiator and output pressure at 20 ms; no age related rate of change is apparent.

Further investigation of this problem involved thermal, caloric, chemical, and spectroscopic measurements of Mixture 1 samples recovered from aged initiators as well as tests of new Mixture 1. Table III summarizes the results. The highest exotherm is 74°C and 116 percent above the lowest value. The thermal sensitivity (the height to half-width ratio of the exotherm) of the new Mixture 1 is 16.7 times as great as the lowest and 4.7 times as great as the highest aged sample. The highest caloric value is 11.3 percent above the lowest; only the

new sample met the requirement ( $1474 \pm 26$  cal/gm). The relative proportions of boron and potassium nitrate were generally within requirements although 1 to 2 percent below that of the new Mixture 1. No boric oxide was found in the spectrographic tests as was expected; this would have indicated decomposition in accordance with the equation



Since these data indicate that some change took place in the aged Mixture 1, we must look for an explanation of the change which resulted in low pressures. Tulis, Austing, and Hersh<sup>(15)</sup> of Illinois Institute of Technology Research Institute have found that the reactivity of boron with silver difluoride is markedly affected by particle size and magnesium content. Since the original design of the Pershing initiator was known to leak due to an inadequate solder seal, moisture could have reached Mixture 1 and slowly reacted with the magnesium usually present as an impurity in the boron. This could markedly reduce the thermal sensitivity of Mixture 1 without seriously affecting its caloric value; in fact, the caloric value increased probably due to the slower and more complete reaction of the constituents. The same mechanism could also explain the higher exotherm temperatures of the aged Mixture 1. The less reactive mixture should continue to produce gas long after 20 ms has elapsed as the pressure-time curves show.

#### BORON/POTASSIUM NITRATE NEXT TO BRIDGEWIRES

Menichelli reported properties of 25/75 boron/potassium nitrate as well as other metal oxidant mixtures for use next to a bridgewire. His results are summarized in Table IV. Note that the 25/75 composition is somewhat less sensitive to static electricity than Mixture 1. This difference may possibly be due to the use of a different capacitor (1000 pF versus 552 pF) in the tests. Also, Mixture 1 unconfined is more sensitive to static discharge than PETN, whereas the 25/75 composition is less sensitive. Note also that the 25/75 composition is much more sensitive to impact when pelleted than when powdered; this property is the reverse of that for Mixture 1. In both cases, however, the impact sensitivity is less than that of tetryl.

Kirkham reported properties of 50/50 and 30/70 boron/potassium nitrate as well as many other metal oxidant mixtures for use next to a bridgewire. His results are summarized in Table V. Generally, both compositions are more sensitive than RDX to impact, friction, static, hot wire energy, hot wire current, and exploding wire voltage; however, they are less sensitive to heat.

Martin Marietta tested powdered Mixture 1 (obtained by grinding Flare-Northern 2M pellets) in an EBW header. The fixture was a Reynolds SE-1 header with a metal charge cup surrounding a 2.5 x 90 mil gold wire (see Figure 4). The firing circuit is shown in Figure 5. At 2000 volts with a 0.64  $\mu$ F capacitor, the wire burst in 1.0  $\mu$ s and completely ignited Mixture 1. The burst current averaged 1230 amperes at a peak voltage of 1165. Voltage-current traces are

shown in Figure 6. These conditions are not optimum; with 2 x 90 mil gold at 2000 volts, the wire should burst in 0.6  $\mu$ s and yield a burst current of 1200 amperes at 1500 volts.

MIL-I-23659, "Design and Evaluation of Electric Initiators," covers design and testing requirements for hot and exploding bridgewire electroexplosive devices. Typical requirements include statistical sensitivity, safety, and performance after severe environments. Based on the data presented, the binderless compositions should meet these requirements for non-hazardous applications of hot wire devices. Since the mean current sensitivity of 25/75 boron/potassium nitrate is over 3 amperes with a 2 x 60 mil Ney Oro G wire (Table IV), that composition appears to be a good starting point for such a development. Enough information is available from Menichelli and Kirkham so that changes in the wire or boron/potassium nitrate ratio could readily be accomplished if necessary to pass the 1-ampere, 1-watt, and 25000-volt 500-pF no-fire requirements in the design specification.

With regard to using boron/potassium nitrate in an EBW application, the potential user should be thoroughly familiar with MIL-STD-1316A, "Design Safety Criteria for Fuzes." While this military standard does not apply to propellant ignition systems, it does contain some excellent design guides for in-line systems. Some of these are:

- 1 Only tetryl, tetryl pellets, CH6, D1PAM, or HNS are permitted in a position leading to initiation of the main charge without interruption;
- 2 Where electric initiators are employed, a positive means of preventing detonation prior to arming shall be provided;
- 3 When the explosive train does not contain primary explosives and has no provision for interruption, shielding, and other protection, the initiation system is designed to provide at least the same degree of mechanical interruption in the electrical circuit as is obtained with an interrupted train employing primary explosives.
- 4 EBW devices may be used without subsequent explosive train interruption provided:
  - a. The explosive initiated by the EBW is one of those listed in 1 above;
  - b. The arming and triggering signals for initiating the EBW device are switched by two independent features requiring independent sources of energy;
  - c. The sensitivity of the EBW device to electrical initiation is not greater than Group B of MIL-I-23659. The device cannot be initiated by any electrical signal at a peak potential of 500 volts, nor can a 500-volt capacitor discharge, especially from the firing circuit capacitor, initiate the device.

Boron/potassium nitrate compositions must be less sensitive to electrostatic discharge, constant current, capacitor discharge, and shock before they are used for in-line EBW devices. There are techniques such as dichromating the boron or coating it with a plastic that might accomplish the required desensitization, but extensive testing would be required to demonstrate their effectiveness. For existing boron/potassium nitrate compositions, the use of a spark gap in the bridge circuit would allow the device to meet the requirements of MIL-I-23659. However, the device would function by joule heating of the bridgewire and would be less desirable than one with PETN or RDX next to the bridgewire where explosion of the wire is mandatory for functioning.

#### CONCLUSIONS AND RECOMMENDATIONS

In summary, boron/potassium nitrate compositions are widely used as igniters and when properly packaged, are safe and reliable. Tests of electric initiators containing boron/potassium nitrate/binder after 55 to 96 months storage yielded low pressures; this may be attributed to reduction in thermal sensitivity due to ingress of moisture. Squibs containing boron/potassium nitrate next to the bridgewire should be developed for non-hazardous applications and should make excellent high temperature igniters. Finally, boron/potassium nitrate compositions have not yet been desensitized enough to be used in an in-line EBW application.

## REFERENCES

1. Atlantic Research Corporation Flare-Northern Division, "F-ND Bore Potassium Nitrate Ignition Materials," Data Sheet, September 1965.
2. U. S. Army Missile Command Drawing 10120424, "Squib Electric M6", 8 October 1968.
3. U. S. Army Ballistic Missile Agency Drawing 10628001, "Initiator Assy.," 24 May 1965.
4. U. S. Army Materiel Command Drawing, 11177665, "Initiator, Rocket Motor Igniter," 15 September 1970.
5. Martin Marietta Corporation, "EBW Initiator, Rocket Motor, Guided Missile, SAM-D," Specification SPC 10406324-001, 14 February 1972.
6. Menichelli, V. J., "Characterization of Several Igniter Mixtures (U)," U. S. Naval Ordnance Laboratory, June 1965.
7. Kirkham, J., "The Ignitability of Pyrotechnic Compositions from Bridgewires," Proceedings, Second International Pyrotechnics Seminar, July 1970.
8. Bowman, N. J. and Knippenberg, E. G., "Pyrotechnic Devices for Use on Sterilized Spacecraft," Journal Spacecraft, Volume 3, No. 10, 11 July 1966.
9. Martin Marietta Corporation, Private Communication between R. Brownell, Thiokol Chemical Corp., Elkton, Md., and C. Gorzynski, Research Institute of Advanced Studies, 1971.
10. B. D. Biddix, "Igniter Mark 280 Mod 0 for Use in Rocket Mark 32 Mod 0 (HASP): Qualification Test Report," Naval Ordnance Station, Indian Head, Md., 20 August 1968.
11. W. S. Helmrach, "General Surveillance of Navy-Held Mk 247 Mod 0 Igniter," Naval Ordnance Station, Indian Head, Md., December 1968.
12. Weick, K. J., "Surveillance Evaluation Report on Rocket Motor Igniter Mk 200 Mod 0 (Terrier)," Naval Ordnance Station, Indian Head, Md., June 1970.
13. Merchant, D. W., "Surveillance of Terrier Mk 272 Mod 0 Igniter," Naval Ordnance Station, Indian Head, Md., November 1970.
14. Storma, E. M., "Pershing Life Extension and Assessment Program, Phase II Final Report," Martin Marietta Corporation, Orlando, Florida, December 1971.
15. Tulis, A. J., Austing, J. L., and Hersh, C. K., "Water-Ignition of Hypergolically Reactive Pyrotechnic Compositions," Proceedings, Second International Pyrotechnics Seminar, July 1970.

TABLE I  
Properties of Mixture 1

Test	Result
Impact Sensitivity	
Powder	40 kg-cm
Pellets	136-228 kg-cm
Friction Sensitivity	
Powder	0/10 fire at 30 kg-m
Pellets	No fire at 52.6 cm
Static Sensitivity	
Powder	0/10 fire at 0.0069 joule
Pellets	0/10 fire at 5 joules
Density	1.63-1.85 gm/cc
Heat of Reaction	1450-1750 cal/gm
Auto-ignition Temperature	700° to 856°F
Hot Wire Sensitivity (0.0015 PtIr)	1.48 amperes at 10,000 psi
Flame Temperature	4080°F
Burning Rate	1.25-1.75 in/s at 1000 psi
Gas Volume	120 ml/gm
Crush Strength	4000-6500 gm axial
Moisture Content	0.75% maximum

TABLE II

## Flare Northern Boron/Potassium Nitrate Data

PROPERTIES AND CHARACTERISTICS	TYPE OF IGNITION MATERIAL								
	CYLINDRICAL PELLETS			BI-CONVEX PELLETS				GRANULES	
NUMBER	2A	2F	2M	2D	2E	2L	2R	2C	2K
SIZE	0.125 x 0.188	0.250 x 0.250	0.125 x 0.100	0.250 x 0.130	0.250 x 0.250	0.500 x 0.250	0.125 x 0.100	BULK DENSITY (min)	
GRAIN DENSITY (min) gm/cc	1.63	1.70	1.70	1.82	1.70	1.68	1.79		
GRAIN WEIGHT (min) gm	0.060	0.335	0.033	0.140	0.305	1.065	0.031	NOT APPLICABLE	
HEAT OF REACTION (min) cal/gm	1500	1500	1500	1500	1500	1500	1500	1100	1400
AUTO IGNITION TEMPERATURE °F	700°	700°	700°	700°	700°	700°	700°	700°	450°
GRAIN CRUSH STRENGTH (min longitudinally) gm	6.500	6.500	6.500	6.500	6.500	6.500	4.000	NOT APPLICABLE	
OPERATING RANGE °F									
MINIMUM	-80°	-80°	-80°	-80°	-80°	-80°	-80°	-80°	-65°
MAXIMUM	500°	500°	500°	500°	500°	500°	500°	500°	280°



TABLE III  
 Boron/Potassium Nitrate/Laminac Thermoanalytical Data

Unit	Age When Tested (Mo)	Thermal Analysis		Caloric Value* Cal/gm	Chemical Analysis**		TOF Analysis
		Exo Temp (°C)	Sensitivity h/W <sub>1/2</sub>		% Boron	% KNO <sub>3</sub>	
1	96	490	3.2	1571.7			No B <sub>2</sub> O <sub>3</sub>
2	93	504		1565.9	24.8	74.66	
3	88	513		1607.1	24.2	75.94	
4	85	494	D				No B <sub>2</sub> O <sub>3</sub>
5	86	451		1538.8	24.7	73.11	
6	82	507	0.9				
7	77	524	2.3				No B <sub>2</sub> O <sub>3</sub>
8	75	525	3.1				
9	79	479		1619.5	23.9	74.68	
10	67	470		1431.6	25.0	75.33	No B <sub>2</sub> O <sub>3</sub>
11	61	512	0.9				
12	1/2	459	15.1	1482.0	26.2	76.36	

\* Specification requirements: 1474  $\pm$  26 cal/gm

\*\*Specification limits: Boron 24-26%, Potassium Nitrate 74-76%

† Time of flight mass spectrometer test

D-Deflagrated

TABLE IV

## Properties of 25/75 Boron/Potassium Nitrate

Test	Result	
IMPACT SENSITIVITY	Mean Value (cm)	Standard Deviation (log units)
Steel anvil, loose	285	0.17
Steel anvil, pelleted	58	0.13
Sandpaper anvil, loose	204	0.28
Sandpaper anvil, pelleted	73	0.17
VACUUM STABILITY	0.9 cc/gm/h at 260°C	
STATIC SENSITIVITY	Capacitor (LF)	No-fire Voltage (max)
Metal/metal electrodes	1.0	4000
	0.1	6500
	0.01	7500
Metal/rubber electrodes	1.0	1000
	0.1	2000
	0.01	3000
	0.001	7500
DTA (at 2.5°C per minute)	105°C - 8°C exotherm 128°C - Endotherm peaking at 142°C 326°C - Endotherm peaking at 340°C 386°C - Exotherm decomposition begins 446°C - Second exotherm leading to ignition at 488°C	
COOKOFF	Gelatin Capsule	Aluminum Capsule
	400°F - 15+ minutes	500°F - 15+ minutes
	915°F - 20 seconds	900°F - 48 seconds
	1000°F - 13 seconds	1000°F - 42 seconds
SHOCK SENSITIVITY	Mean Value (decibang)	Std. Deviation (decibang)
RDX donor, lucite barrier, 1.39 gm/cc, 4000 psi	4.808	0.654
HOT WIRE SENSITIVITY	Constant Current	Capacitor Discharge
Ney Oro G wire, 2 x 60 mils, phenolic plug	Mean - 3.27 amperes	Not initiated at
	Std. Dev. - 0.016 log units	6.0 µF and 250 V
	Loading - 20,000 psi	
GAP SENSITIVITY	Did not ignite	Did not ignite at 6.0 µF and 250 V

TABLE V

50/50 and 30/70 Boron/Potassium Nitrate

Test	Result	
	Type of Material	
	50/50	30/70
Impact Sensitivity, mean (Figure of insensitivity, Rotter machine)	35	30
Friction Sensitivity (Boxwood against Yorkstone)	0/10 ignitions	5/10 ignitions
Static Sensitivity (Metal/metal electrodes)	>0.045 joule	Not tested
Thermal Stability (Differential scanning calorimeter)	Stable up to 400°C	Stable up to 400°C
Pt Wire Ignition Energy (millijoules, min)		
1 x 40	No ignition	No ignition
2 x 40	13.5 weak	12.5 weak
Pt Wire Ignition Current (amperes, min)		
0.2 x 40	0.2 weak	0.2 weak
0.5 x 40	0.6 weak	0.6 weak
1 x 40	1.3 weak	1.2 weak
2 x 40	3.3 weak	3.1 weak
Au Alloy EBW Voltage		
1.2 x 40 mil wire, 1/4 $\mu$ F capacitor	800 volts weak (0.98 gm/cc)	1300 volts weak (1.07 gm/cc)

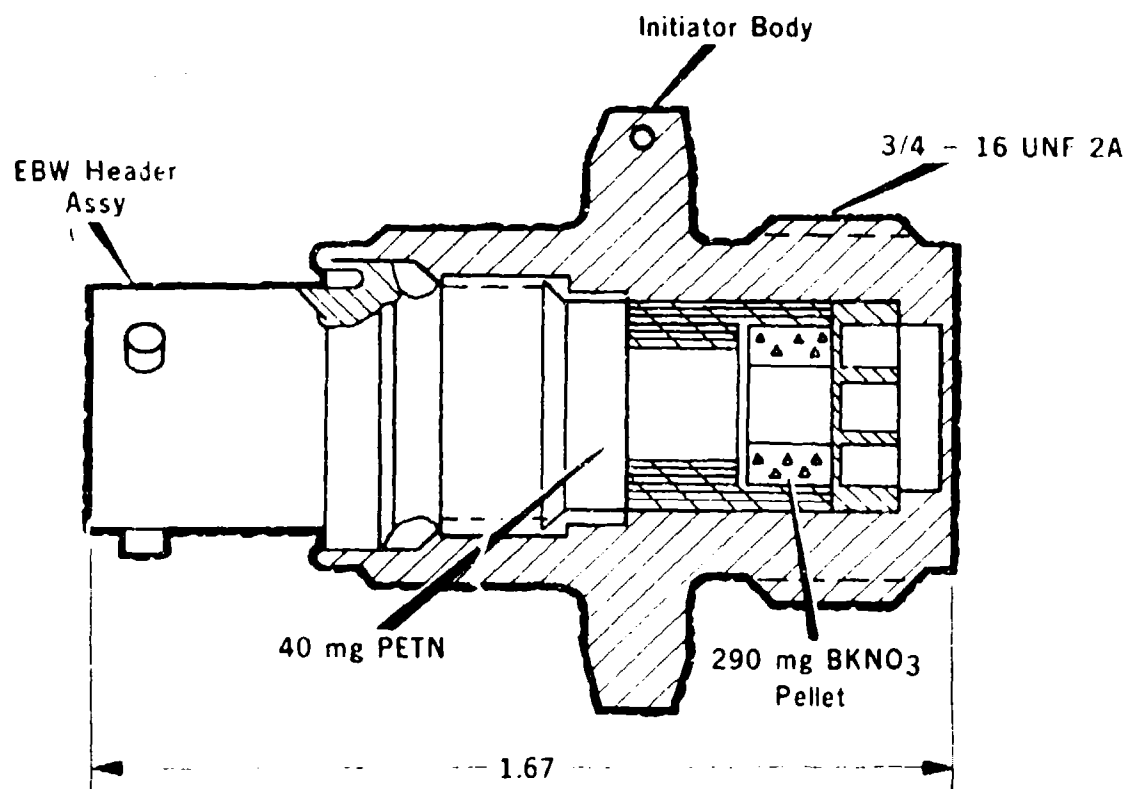
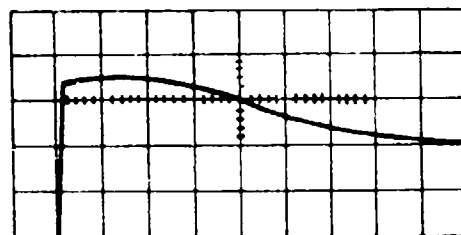


Figure 1. EBW Rocket Motor Initiator

PRESSURE 50PSI PER CM



TIME 20MS PER CM

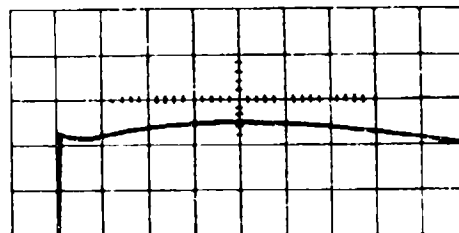
RISE 112PSI IN 2.2MS

PEAK 126PSI IN 22.8MS

PRESSURE AT 20MS 125PSI

(a) Typical Acceptable Output Pressure Versus Time Obtained from EBW Initiator (S/N 116)

PRESSURE 50PSI PER CM



TIME 20MS PER CM

RISE 62PSI IN 1.6MS

PEAK 75PSI IN 78MS

PRESSURE AT 20MS 61PSI

(b) Typical Low Output Pressure Versus Time Obtained from EBW Initiator (S/N 123)

Figure 2. Acceptable and Low Output Pressure Traces

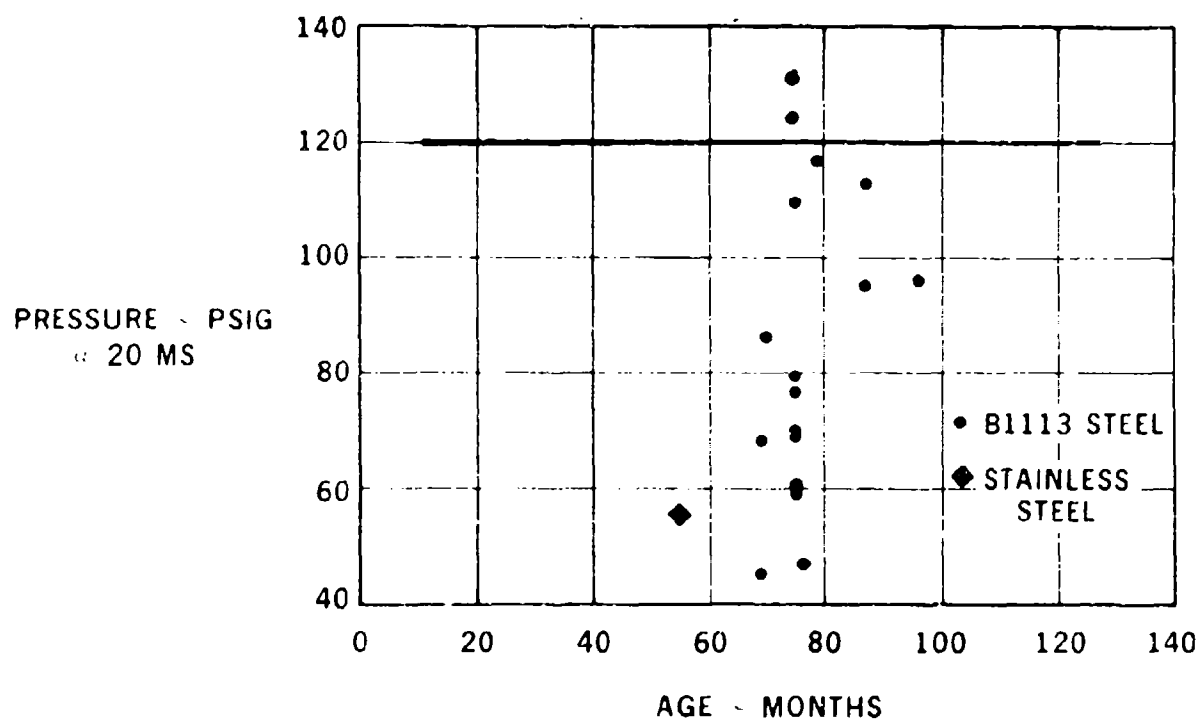


Figure 3. EBW Initiator Output Pressure 11iseconds Versus Age

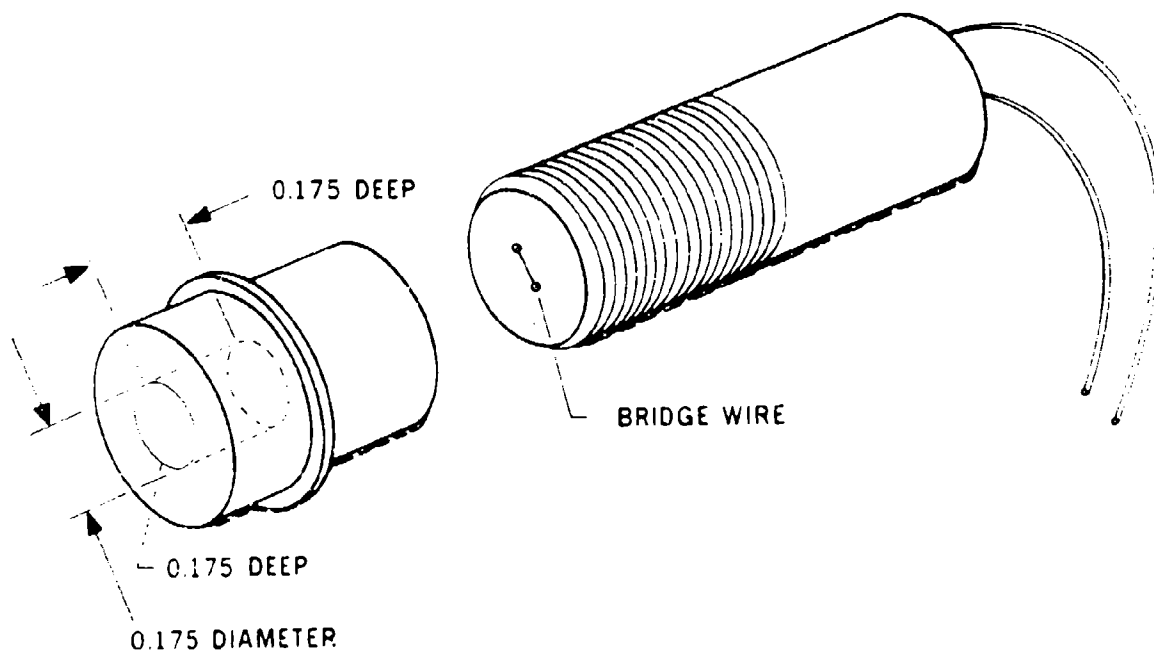


Figure 4. Header/Cup Assembly

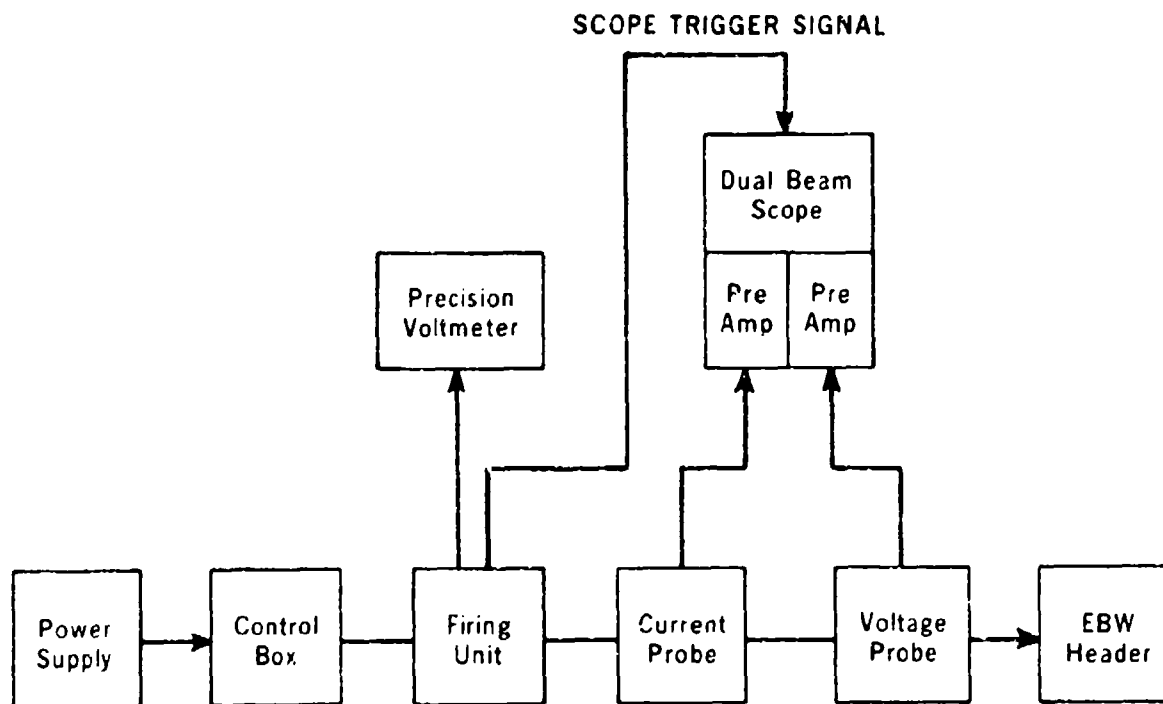
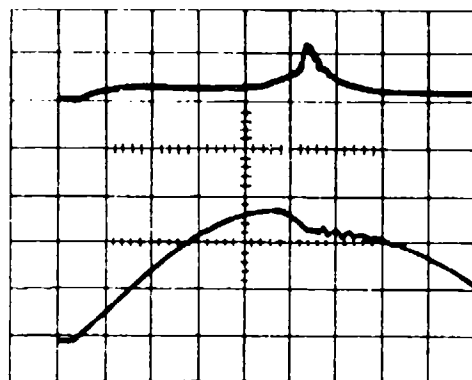


Figure 5. Test Setup for Header Cup/Assembly Voltage/Current Measurements



VOLTAGE  
950 VOLTS PER CM

CURRENT  
500 AMPS PER CM



TIME 0.2  $\mu$  SEC PER CM

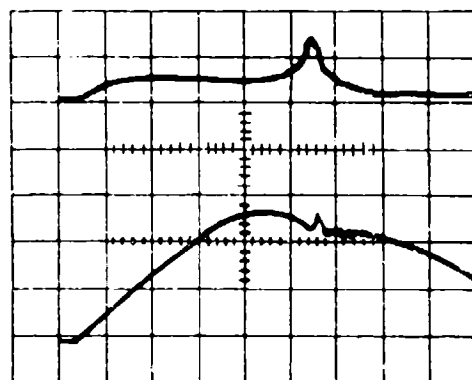
PEAK VOLTAGE 1120 VOLTS

BURST CURRENT 1230 AMPS

BURST TIME 1.03  $\mu$  SEC

VOLTAGE  
950 VOLTS PER CM

CURRENT  
500 AMPS PER CM



TIME 0.2  $\mu$  SEC PER CM

PEAK VOLTAGE 1190 VOLTS

BURST CURRENT 1230 AMPS

BURST TIME 0.97  $\mu$  SEC

Figure 6. Voltage/Current Traces for Mixture 1 in Header/Cup Assembly

THE INFLUENCE OF TRANSITION METAL COMPOUNDS ON  
THE ALUMINUM-SODIUM NITRATE REACTION

P. L. FARNELL, R. P. WESTERDAHL, F. R. TAYLOR  
Pyrotechnics Division, Feltman Research Laboratory  
Picatinny Arsenal, Dover, New Jersey

ABSTRACT

Studies have shown that the presence of small quantities of certain transition metals or transition metal compounds significantly increase the luminous efficiency of aluminum-sodium nitrate flare composition. The magnitudes of the changes in performance are as follows: 4 to 67% decrease in burning rate, 0 to 161% increase in luminous output, and 0 to 466% increase in luminous efficiency. The transition compounds also made the systems initiate easily and burn smoothly. The greatest increase in light output was produced by compounds which caused sodium nitrate to decompose to form oxides of nitrogen rather than its normal decomposition product of nitrogen and oxygen. Other compounds or metals react with aluminum or sodium nitrate at low temperatures, or catalyze the normal decomposition of sodium nitrate. Some additives only reduce the thermal conductivity of the system and hence reduce the burning rate without lowering the luminous output, resulting in an increase in efficiency.

## INTRODUCTION

Although thermodynamic data indicate that aluminum should be a fairly reactive metal, its oxidation reactions proceed poorly due to the impervious oxide shell which immediately forms when the metal is exposed to air ( 1,2 ). For this reason, pressed pyrotechnic compositions of atomized aluminum and sodium nitrate powder ignite poorly, propagate difficultly, and burn very erratically and inefficiently, with the production of large quantities of incandescent particles. However, it has been discovered that adding small quantities of transition metals or transition metal compounds to these compositions makes the systems easy to initiate and smooth burning. Of considerable significance is the fact that these systems burn with a striking decrease in the production of incandescent particles. Furthermore, some of these metals and compounds cause a marked reduction in burning rate, a substantial increase in luminous output, and consequently a significant increase in the overall luminous efficiency of the aluminum-sodium nitrate system. This paper presents the results obtained in a study conducted to determine the mechanism by which these transition metals and compounds alter the performance characteristics of aluminum-sodium nitrate pyrotechnic compositions.

## EXPERIMENTAL

Luminosity studies were conducted by burning pellets of the composition of interest in a large laboratory chamber which was approximately two feet in diameter and five feet long. The pellets were made by pressing 300 mg of the composition at 33,000 pounds per square inch in a metal die. The resulting grains, which were 0.24 inches in diameter and 0.25 inches long, were capped with a non-illuminating igniter composition. The pellets were ignited electrically in the chamber, and the emitted radiation was measured

at a distance of 3.8 feet using a calibrated RCA-926 vacuum phototube. This phototube had a corrective filter which imparts response characteristics essentially equivalent to those of the human eye. The voltage developed by a phototube current flowing through a standard resistor was recorded with a fast response oscillograph. The duration of burning in seconds, the burning rate in inches per minute, the luminous output in kilocandles per square inch of flare surface, and the luminous efficiency in kilocandles-seconds per gram of composition were determined for all of the compositions. The validity of the performance data obtained using these small pellets was established by comparing the data for the small pellets with the data obtained using standard size 1.5 in. diameter by 3.5 in. long flares. Both sizes gave essentially the same performance values.

Thermal conductivity measurements were made using a thermal comparator manufactured by the Thermophysical Properties Research Corporation, Lafayette, Indiana.

All chemicals used were commercially available reagent grade materials. The sodium nitrate was ground to a particle size of 74 microns, and the aluminum had an average particle size of 6 microns.

## RESULTS AND DISCUSSION

Figure 1 presents three photographs of burning aluminum-sodium nitrate pellets. Photograph (a) shows the type of flame produced by simple aluminum-sodium nitrate binaries. This flame produces a profusion of incandescent particles, and always leaves a sphere of unburned metal at the end of burning. Photograph (b) illustrates what happens to the flame when 3%  $\text{MnSO}_4$  is added to the basic composition. It is seen that

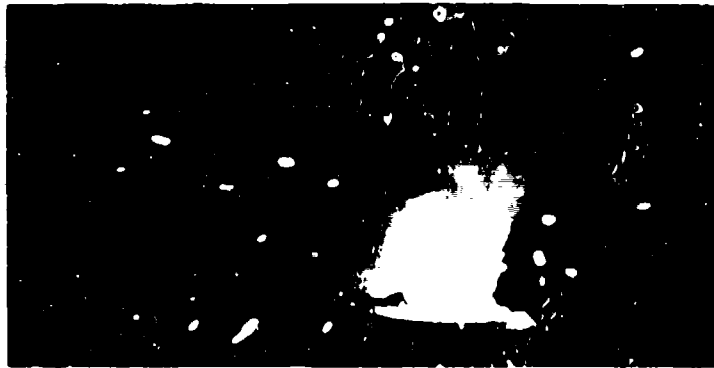
a larger flame is produced, exhibiting a marked reduction in incandescent particles.

Finally, photograph (c) shows that no incandescent particles are ejected from the  $\text{MnSO}_4$  system once equilibrium burning has been established.

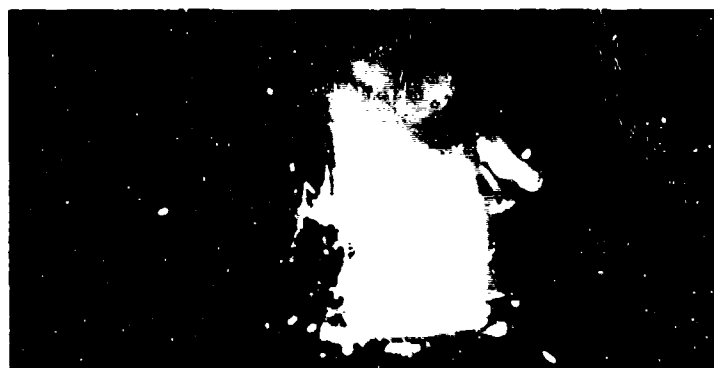
Table 1 presents the performance characteristics obtained for 1-1 Al- $\text{NaNO}_3$  compositions with and without additives. It is seen that the transition metal compounds produce significant changes in either burning rate or luminous output. Since luminous efficiency or total quantity of visible radiation emitted per gram of composition is given by the product of the luminous output and burning time divided by the weight of composition in grams, significant changes in efficiency were observed for most additive systems.

Table 1 is arranged according to classes. There are five classes denoting the reaction occurring when the additive is heated with either aluminum or sodium nitrate. For Class 1 there is no reaction with either component. Class 2 compounds, consisting of manganese oxides, catalyze the normal decomposition of sodium nitrate to evolve oxygen at lower temperatures. Compounds which cause ignition of powdered aluminum at about  $700^\circ\text{C}$  ( a value well below its normal ignition temperature of  $1000^\circ\text{C}$  ) are in Class 3. Class 4 embraces transition metals which all ignite with sodium nitrate at lower temperatures than does aluminum. Finally Class 5 compounds are those which alter the normal decomposition pattern of sodium nitrate, causing the evolution of the oxides of nitrogen at the melting point of the nitrate.

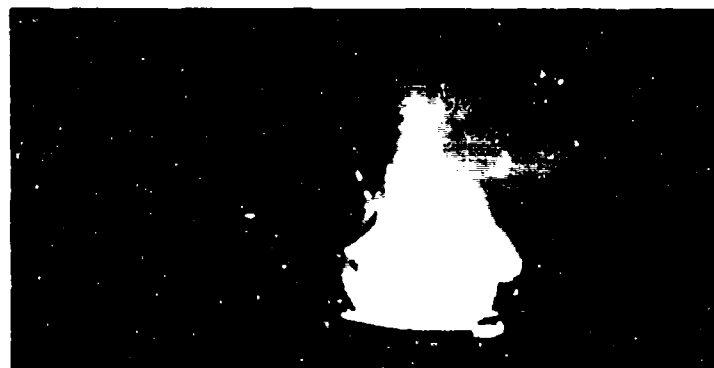
The relative effectiveness of the various additives in changing the performance characteristics of the basic binary can best be surmised by examining Table 2.



(a) 1-1 Al-NaNO<sub>3</sub>



(b) 1-1 Al-NaNO<sub>3</sub> + 3% MnSO<sub>4</sub>



(c) 1-1 Al-NaNO<sub>3</sub> + 4% MnSO<sub>4</sub>

Fig 1 Types of flames produced by burning aluminum sodium nitrate compositions

TABLE 1

Performance Characteristics of 1-1 Aluminum-Sodium  
Nitrate Compositions Containing Transition Metal Compounds

Class	Percent Additive	Additive	Burning Rate (in./min)	Luminous Output *(kc/in. <sup>2</sup> )	Luminous Efficiency *(kc-sec/g)
Binary		None	8.37	21.7	4.36
1	5	TiO <sub>2</sub>	2.80	23.3	14.0
	7	ZrO <sub>2</sub>	6.40	23.9	6.56
	5	Cr	6.48	14.6	3.81
2	5	Mn <sub>3</sub> O <sub>4</sub>	6.32	45.6	12.3
	5	Mn <sub>2</sub> O <sub>3</sub>	4.28	29.4	11.7
	5	MnO <sub>2</sub>	6.78	34.5	8.58
3	5	Na <sub>2</sub> CrO <sub>4</sub>	7.11	22.1	5.24
	5	Na <sub>2</sub> MoO <sub>4</sub> ·2H <sub>2</sub> O	5.85	45.0	13.0
	7	Na <sub>2</sub> WO <sub>4</sub> ·2H <sub>2</sub> O	5.48	36.7	11.3
	5	Fe <sub>2</sub> O <sub>3</sub>	4.17	39.2	15.6
4	5	Fe	6.38	16.0	4.20
	5	Ti	6.23	26.6	7.27
	5	Mo	8.02	52.5	11.0
	7	W	6.26	48.8	13.2

TABLE 1 ( Cont )

<u>Class</u>	<u>Percent Additive</u>	<u>Additive</u>	<u>Burning Rate ( in./min. )</u>	<u>Luminous Output (kc/in.<sup>2</sup>)</u>	<u>Luminous Efficiency (kc-sec/g)</u>
5	3	MnSO <sub>4</sub> · H <sub>2</sub> O	3.78	55.1	24.6
	5	Cr <sub>2</sub> O <sub>3</sub>	4.56	56.5	20.7
	5	Na <sub>2</sub> Cr <sub>2</sub> O <sub>7</sub> · 2H <sub>2</sub> O	4.98	47.0	16.0
	5	CrO <sub>3</sub>	3.09	22.7	12.8
	5	MoO <sub>3</sub>	5.52	29.3	8.94
	7	WO <sub>3</sub>	5.91	30.6	8.69
	7	Zr <sub>2</sub> (O <sub>3</sub> ) <sub>4</sub> · 5H <sub>2</sub> O	3.33	15.9	8.54
	7	H <sub>2</sub> WO <sub>4</sub>	4.53	28.1	10.4

\*kc = kilocandies



TABLE 2

Changes in Performance Characteristics Effected by the Addition of  
Transition Metal Compounds 1-1 Aluminum-Sodium  
Nitrate Compositions

<u>Class</u>	<u>Additive</u>	<u>% Decrease in Burning Rate</u>	<u>% Increase in Luminous Output</u>	<u>% Increase in Luminous Efficiency</u>
1	TiO <sub>2</sub>	67	8	222
	ZrO <sub>2</sub>	23	10	51
	Cr	23	32 <sup>a</sup>	13 <sup>b</sup>
2	Mn <sub>2</sub> O <sub>4</sub>	25	111	182
	Mn <sub>2</sub> O <sub>3</sub>	49	36	169
	MnO <sub>2</sub>	19	59	97
3	Na <sub>2</sub> CrO	15	2	20
	Na <sub>2</sub> MoO <sub>4</sub> · 2H <sub>2</sub> O	30	108	199
	Na <sub>2</sub> WO <sub>4</sub> · 2H <sub>2</sub> O	34	70	160
	Fe <sub>2</sub> O <sub>3</sub>	50	81	258
4	Fe	24	26 <sup>a</sup>	4 <sup>b</sup>
	Ti	25	23	68
	Mo	4	142	153
	W	25	125	203

TABLE 2 ( Cont )

<u>Class</u>	<u>Additive</u>	<u>% Decrease in Burning Rate</u>	<u>% Increase in Luminous Output</u>	<u>% Increase in Luminous Efficiency</u>
5	$\text{MnSO}_4 \cdot \text{H}_2\text{O}$	55	155	466
	$\text{Cr}_2\text{O}_3$	46	161	375
	$\text{Na}_2\text{Cr}_2\text{O}_7 \cdot 2\text{H}_2\text{O}$	40	117	266
	$\text{CrO}_3$	63	5	184
	$\text{MoO}_3$	34	35	105
	$\text{WO}_3$	29	41	99
	$\text{Zr}(\text{NO}_3)_4 \cdot 5\text{H}_2\text{O}$	60	22 <sup>a</sup>	96
	$\text{H}_2\text{WO}_4$	46	30	140

<sup>a</sup> decrease in luminous output

<sup>b</sup> decrease in luminous efficiency

This table shows that while all of the compounds in Class 1 decrease the burning rate, or increase the burning time, these additives ( with the exception of chromium which is discussed below ) do not significantly reduce the luminous output. Consequently these systems exhibit an increase in luminous efficiency. Since these compounds do not react with either aluminum or sodium nitrate, an explanation was sought for their behavior. One of the factors known to effect the burning rates of pyrotechnic compositions is the thermal conductivities of their constituents. Consequently the thermal conductivities of the compositions were determined using a thermal comparator. The results of these measurements are given in Table 3. It is observed that in Class 1 compounds do cause a large decrease in the thermal conductivity of the basic binary. This decrease would reduce the dissipation of heat from the reaction surface, causing more aluminum to vaporize and react, and minimizing the flow of the unreacted molten metal from the surface.

The manganese oxides exert a catalytic effect on the normal decomposition of sodium nitrate (3). The effect of this catalysis would be to flood the reaction surface with oxygen while expending less energy to decompose the nitrate. This would leave more energy available to vaporize the aluminum, resulting in a more efficient consumption of fuel.

The metals and compounds in Classes 3 and 4 have similar effects, for in both cases the ignition temperature is lowered by the reactions occurring with aluminum or sodium nitrate. In Class 3, the compounds act as oxidizers with the aluminum as fuel. This type of reaction is depicted in curve 1 of Figure 2, which is the well known thermite reaction. Curve 2 of Figure 2 shows the case where the metal, e. g. tungsten, becomes the fuel which reacts with sodium nitrate. The reactions which occur

TABLE 3

Comparison of Burning Rate with Thermal Conductivity  
For Aluminum-Sodium Nitrate Compositions  
With and Without Additives

<u>Composition</u>	<u>Burning Rate (in/min)</u>	<u>Thermal Conductivity *(w cm<sup>-1</sup> °C<sup>-1</sup>)</u>
Al-NaNO <sub>3</sub> -TiO <sub>2</sub>	2.80	0.064
Al-NaNO <sub>3</sub> -ZrO <sub>2</sub>	0.0	0.11
Al-NaNO <sub>3</sub> -Cr	6.48	0.18
Al-NaNO <sub>3</sub>	8.37	0.24

\*watts

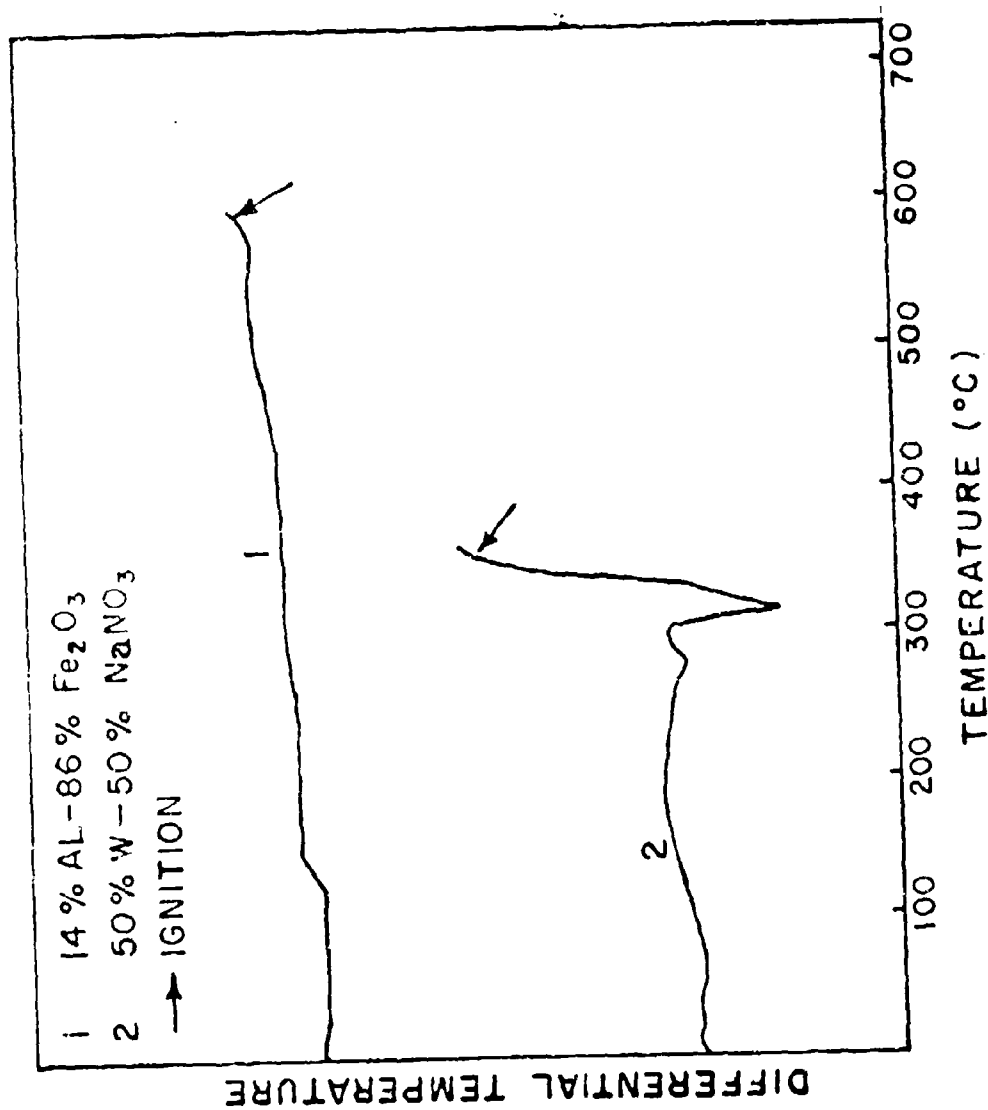
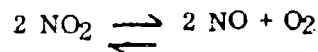


FIGURE 2: LINE 1: 14% AL-86%  $\text{Fe}_2\text{O}_3$  - TRANSITION METAL AND  
 A TRANSITION METAL COMPOUND ACTING AS FUEL AND OXIDIZER

are propagative and provide sufficient heat to ignite the main aluminum-sodium nitrate composition. In addition, less heat is absorbed in the pre-ignition zone due to the lower ignition temperature, providing more heat for the vaporization of the aluminum.

The additives  $\text{Cr}_2\text{O}_3$  and  $\text{MnSO}_4$ , which provide the greatest increase in luminous output and efficiency, are present in Class 5. All of the compounds in this group alter the decomposition of sodium nitrate to form the oxides of nitrogen rather than its normal decomposition products of nitrogen and oxygen. The decomposition reactions occurring in the presence of these additives are listed in Table 4. All of the solid products of these reactions were determined by x-ray diffraction analysis.

That aluminum does react with the NO and  $\text{NO}_2$  gases evolved in the reaction of these additives with sodium nitrate is confirmed by the differential thermograms in Figure 3. In curve 1, aluminum ignited in the solid state when heated to  $375^\circ\text{C}$  in an atmosphere of  $\text{NO}_2$  gas. This gas also contained NO and  $\text{O}_2$  since the  $\text{NO}_2$  undergoes the following equilibrium reaction:



However, the literature (4) shows that only 23-37% of  $\text{NO}_2$  is decomposed in the  $350\text{--}420^\circ\text{C}$  temperature range.

In curve 2 of Figure 3, there is a large exothermal reaction at the melting point of aluminum, caused by the attack of NO gas on the freshly exposed molten metal, followed by ignition at  $825^\circ\text{C}$ . The normal ignition temperature of aluminum in air is  $1000^\circ\text{C}$ ; these data therefore reveal a significant reduction in ignition temperature. In addition the  $\Delta H$  for the reaction of aluminum with  $\text{O}_2$  is 7.4 kcal/gm of Al, with  $\text{NO}_2$

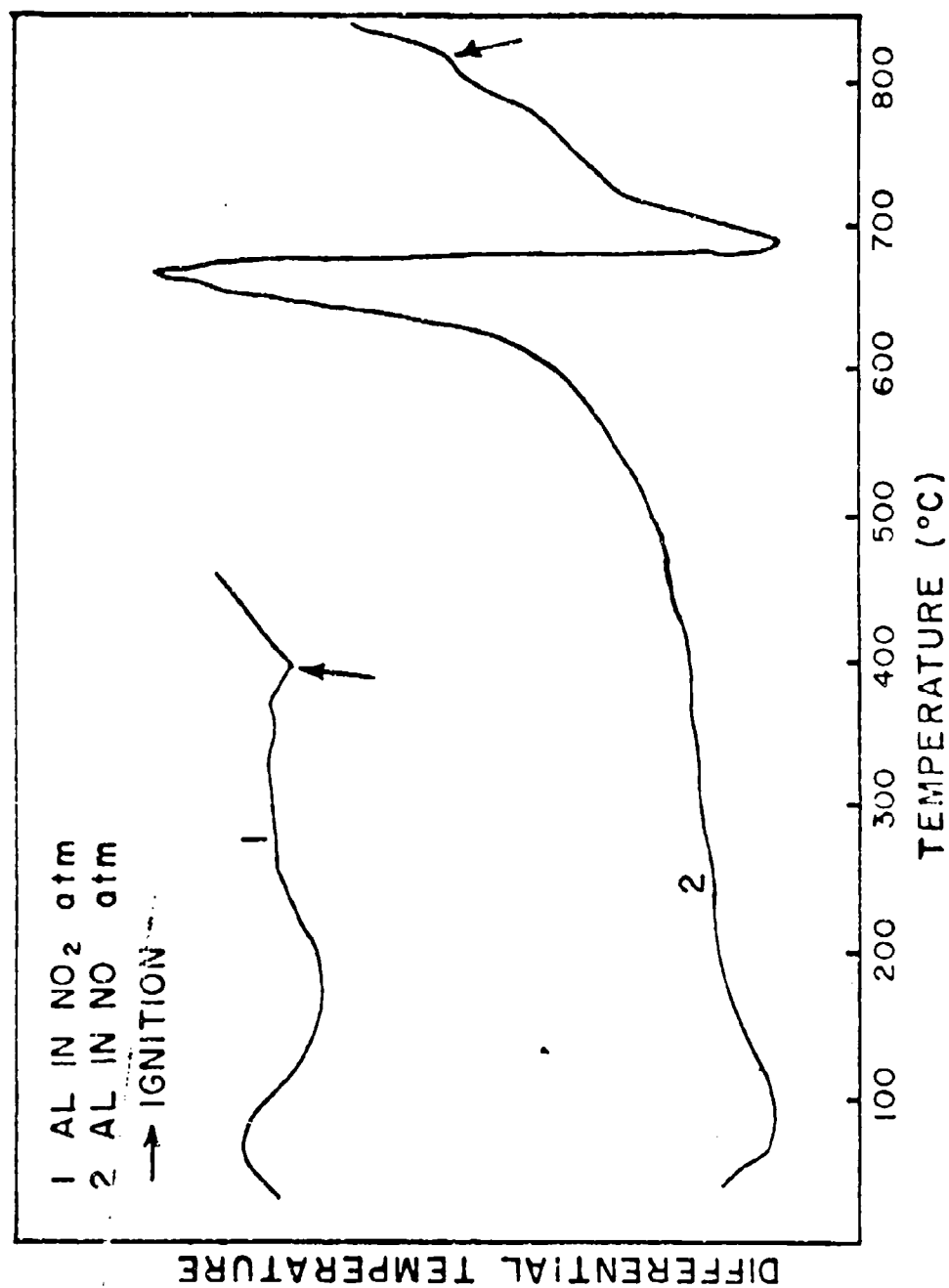
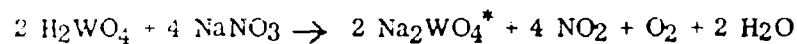
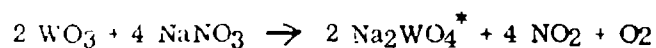
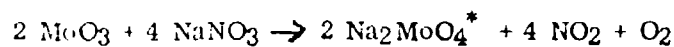
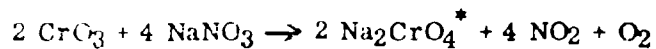
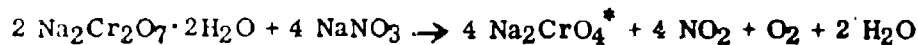
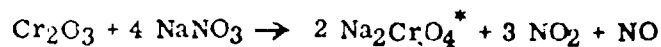
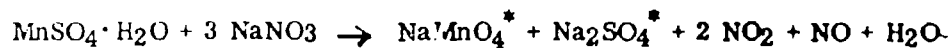


FIGURE 3: DTA CURVES SHOWING THE REACTION OF AL POWDER WITH  
OXIDES OF NITROGEN.

TABLE 4

Reactions of Molten Sodium Nitrate with  
Transition Metal Compounds

\* The presence of these compounds was confirmed by x-ray  
diffraction analysis.



the  $\Delta H$  is 7.6 kcal/gm of Al, and with NO the  $\Delta H$  is 8.6 kcal/gm of Al. Consequently the reaction of the oxides of nitrogen with Al results in the release of greater thermal energy, again resulting in more complete vaporization and subsequent reaction of the metal.

The effect on these compositions of varying the transition metal within a periodic group is shown by comparing the results from Cr, Mo, and W in the metallic state, as the sodium oxy salts ( $\text{Na}_2\text{XO}_4$ ), and as the trioxides ( $\text{XO}_3$ ) ( See Tables 1 and 2 ). The diverse physical and chemical properties play a large role in the differences in performance exhibited within the above groups of additives. Elemental Mo and W act as fuels and ignite propagatively with  $\text{NaNO}_3$  while elemental Cr has no effect. This difference in behavior is produced by the passivation of Cr caused by the strongly oxidizing nitrate, (5) a phenomenon which does not occur for Mo and W.

The sodium oxy salts of these elements react propagatively with aluminum and cause sustained ignition of the three-component system upon heating. However, the luminosity of the composition containing  $\text{Na}_2\text{CrO}_4$  is much lower than for those containing  $\text{Na}_2\text{MoO}_4$  or  $\text{Na}_2\text{WO}_4$ . A comparison of the melting points of these salts reveals that  $\text{Na}_2\text{CrO}_4$  melts around  $400^\circ\text{C}$  while the other salts melt close to  $700^\circ\text{C}$  (6). This low melting point would allow the molten chromate to form a coating on the solid aluminum particles, partially passivating them. The other compounds are solid at the temperature at which aluminum melts, and the molten metal can then react with the melting salt, producing greater heat for the reaction.

The luminous efficiencies obtained using the trioxides of these elements as additives increase in reverse order from the elemental for  $\text{Cr}$ . These data reflect the stability of

the oxides since  $\text{MoO}_3$  and  $\text{WO}_3$  are the common oxides of the respective metals while  $\text{CrO}_3$  is an extremely reactive form. All three of the oxides, however, react with the nitrate to produce oxides of nitrogen, and all three, therefore, give a large boost to the luminous efficiency.

Table 5 compares the performance data obtained for several compositions, pressed at 10,000 and 33,000 PSI. It is evident that, with the exception of the binary, the efficiency is greatly reduced from the values at higher loading pressure; indeed, the luminous efficiencies for  $\text{Mn}_2\text{O}_3$  and  $\text{TiO}_2$  are almost the same as the binary at this loading pressure. It has been reported that the aluminum-sodium nitrate system burns independently from the condensed phase at low loading pressure, but is strongly affected by the condensed phase at 33,000 PSI (6). The above experiments would therefore indicate that the nitrogen oxides formed by the decomposition of nitrate with Class 5 compounds affect the condensed phase, not the vapor phase of the combustion; likewise, the oxygen formed by the catalytic effect of manganese oxides reacts mainly with the condensed phase. Since  $\text{TiO}_2$  reduces the burning rate and allows more time for the metal to vaporize, it too affects the condensed phase, and this effect is almost entirely lost at low loading pressure when the system has become independent of the condensed phase.

Further proof that  $\text{NO}_2$  is involved primarily in the condensed phase reactions was provided by an experiment in which the binary composition was burned in an atmosphere of  $\text{N}_2$  and  $\text{NO}_2$ . It was found that the luminosity of the composition was changed very little from that observed in air (8). Since this atmosphere would have the greatest effect on the vapor phase reactions, the negative results confirm the above conclusion.

TABLE 5

Performance Characteristics of Aluminum-Sodium  
Nitrate Compositions Pressed at 10,000 and 33,000 PSI

Additive	Burning Rate (in./min)		Luminous Output (kc/in <sup>2</sup> )		Luminous Efficiency (kc-sec/g)	
	10K	33K	10K	33K	10K	33K
None	6.49	8.37	27.9	21.7	8.51	4.36
TiO <sub>2</sub>	4.73	2.80	25.8	23.3	10.8	14.0
Mn <sub>2</sub> O <sub>3</sub>	5.04	4.28	22.4	29.4	8.59	11.7
MnSO <sub>4</sub> ·H <sub>2</sub> O	5.55	3.78	32.2	55.1	11.5	24.6
Cr <sub>2</sub> O <sub>3</sub>	4.98	4.56	38.1	56.5	15.1	20.7

## CONCLUSION

The combustion efficiency of the aluminum-sodium nitrate system can be greatly increased by adding small amounts of transition metals and transition metal compounds to the composition. This result arises from minimizing the loss of heat from the reacting surface by reducing the thermal conductivity, as with Class 1 compounds, or by reducing the heat needed to initiate the combustion. The latter effect is caused either by producing the reactive species at a lower temperature, as with the manganese oxides, by reducing the ignition temperature of the composition as with the Class 3 and 4 additives, or by producing a more reactive species and doing so at a lower temperature, as with the production of oxides of nitrogen in Class 5. With more heat available to the reacting surface, more fuel would vaporize, and less would flow from the surface and be lost to the reaction; at the same time there would be a greater tendency to form metal vapor rather than to eject large droplets of molten metal from the flame. Both of these occurrences would result in more complete combustion of the metal, and consequently in a greater amount of light being produced.

## REFERENCES

1. Christensen, H. C., Knipe, R. H., and Gordon, A. S., Pyrodynamics 3, p 99 (1965)
2. Brzustowski, T. A., and Glassman, I., Heterogeneous Combustion, Academic Press, Press, New York, N. Y. (1964) p. 41, 75, 117.
3. Westerdahl, R. P., Farnell, P. L. and Taylor, F. R. "The Reaction of Transition Metal Compounds with Molten Nitrates." ( in preparation )
4. Thorne, P. C. L., Roberts, E. R., and Fritz Ephraim, Inorganic Chemistry, Sixth Edition, Interscience Publishers, Inc., New York, N. Y. (1954), p. 698.
5. Moeller, T., Inorganic Chemistry, John Wiley and Sons, Inc., New York, N.Y. (1952) p. 879.
6. National Research Council Bulletin No. 118, 1949.
7. Farnell, P. L., Beardell, A. J., and Taylor, F. R., Proceedings of the Seventh Symposium on Explosives and Pyrotechnics, Franklin Institute, p. III-3-4 (1971).
8. Westerdahl, R. P., private communication.

## A Flickering Signal Flare

Russell Reed, Jr.  
Richard P. Cornia  
William O. Munson

Thiokol Chemical Corporation/Wasatch Division  
Brigham City, Utah

### ABSTRACT

A unique flickering signal device has been developed in which the flame oscillates at a reproducible 3 cycles per second. The pyrotechnic composition containing a fluorocarbon binder, a halocarbon, magnesium, and ammonium perchlorate is nozzled to burn at a pressure slightly above ambient. By altering the nozzle size, some variation in frequency can be attained. Stable combustion occurs at ambient pressure but when the propellant is burned in a nozzled configuration a regular chuffing has been observed for as long as 10 minutes with no tendency of extinction. The oscillation is thought to be the result of the out of phase coupling of a chemical wave of condensed phase reaction with the thermal wave. As the burning rate decreases, the heat stored in the propellant rapidly increases the temperature of the condensed phase and allows the reaction of the magnesium with

the binder and other halocarbons to occur. These are rapid reactions having high energies of activation and because of the unusual stability of the C-F bond in the fluorocarbon binder, they do not proceed until relatively high temperatures are reached. This reaction,  $(\text{CF}_2)_n + \text{Mg} \rightarrow \text{MgF}_{2(g)} + \text{C}_{(s)}$ , is not sustaining in these compositions, an effect which seems to be caused by the presence of ammonium perchlorate. As ammonium perchlorate is decreased the burning rate increases rapidly, probably because the gaseous decomposition of the ammonium perchlorate is diluting the high flame temperature of the above reaction and increasing the flame front distance from the burning surface.

The fluorocarbon compositions containing aluminum, display oscillatory combustion at higher frequencies (15 to 30 sec depending on the composition) when burned at ambient pressure in an un-nozzled configuration and it is likely that a similar out of phase coupling also occurs in these compositions. The effect is enhanced by using aluminum below 15 micron size. The burning rate of propellants containing halocarbons show a marked dependency on surface area of the metal as would be expected if a condensed phase reaction were occurring.

## FLICKERING FLARE

A flare in which the flame oscillated at a reproducible frequency would be useful as a signal or rescue device. The oscillatory flame should be more easily recognized at a long distance than the conventional steady flame. It would also be useful in identifying friend from foe. Ideally, such a device would oscillate regularly at a frequency of less than 8 cycles per second to allow the oscillation to be detected at a distance. Detection by means of radar and IR detectors might also be advantageous. In order to maximize the difference between minimum and maximum output in a cycle, the flame should essentially extinguish.

Another interesting application of oscillatory flames has been suggested by Breslow (Ref 1) as a means of attaining a more efficient illuminating flare by using a composition in which the flame oscillates at a sufficiently high frequency to appear as a steady light source to the observer.

We have found that a number of compositions containing halocarbons, as binders or additives, and metals exhibit oscillatory combustion. Various fluorocarbon-aluminum compositions, using an oxidizer such as a perchlorate, burn to yield flames oscillating at frequencies of 15 to over 30 cycles per second when burned in the air under ambient conditions.

A typical luminosity time trace for an aluminum/fluorocarbonbinder/ammonium perchlorate composition is shown in Figure 1. As the aluminum particle size is reduced the tendency to produce oscillatory flame is enhanced. However, oscillations



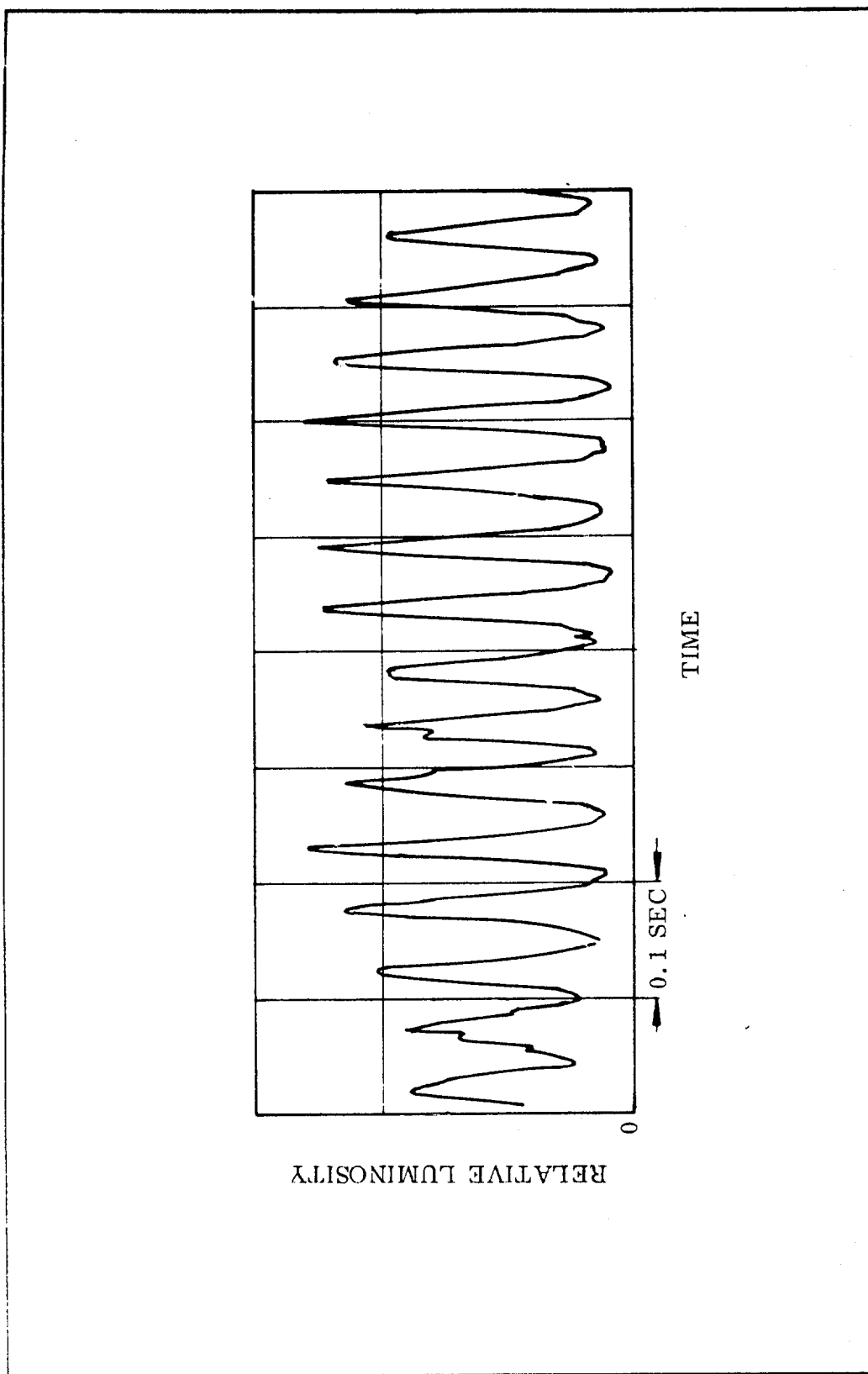


Fig. 1. Luminosity Time Trace of Aluminized Fluorocarbon Composition

at these higher frequencies can be observed only at close range. At distances greater than 100 ft, the flame appears to the eye as a normal steady source of light.

Oscillatory combustion was achieved at lower frequencies using a composition containing a chlorocarbon, magnesium, a perchlorate oxidizer, and a fluorocarbon binder. This composition burns normally at ambient pressure but when nozzled for combustion at pressures only 2 to 5 psi above ambient, it displays a regular oscillation of the flame at 2 to 3 cycles per sec (Figure 2), depending upon the nozzle size.

While this composition has a bright flame due to the presence of Mg (24%, Table I) it also emits in the infrared in view of the formation of carbon and the halide and oxide of magnesium. Carbon is derived from the dehalogenation (by magnesium) of the binder and the aromatic chlorocarbon. The carbon emits largely in the 2 micron region while the MgO emits at longer wavelengths (8 to  $14\mu$ ).

A hand held device (Figure 3) has been demonstrated which employs a pyrotechnic grain (1-3/8 in. dia by 2-1/2 in. long) that burns in a flickering mode (2.5 cycles/sec) for over 2 minutes. A grain (4 in. dia by 25 in. long) has burned for 14 minutes oscillating at 2 cycles/sec. The burning rate is 0.02 in./sec at pressures near ambient. Smaller nozzles increase the pressure and increase the frequency of oscillation; a variation of 1.5 to 3.0 cycles/sec of reproducible oscillation has been attained by varying the nozzle diameters.

The oscillation may be the result of the out of phase coupling of the chemical wave of condensed phase reaction with the thermal wave. As the burning rate decreases, the heat stored in the propellant rapidly increases the temperature of the

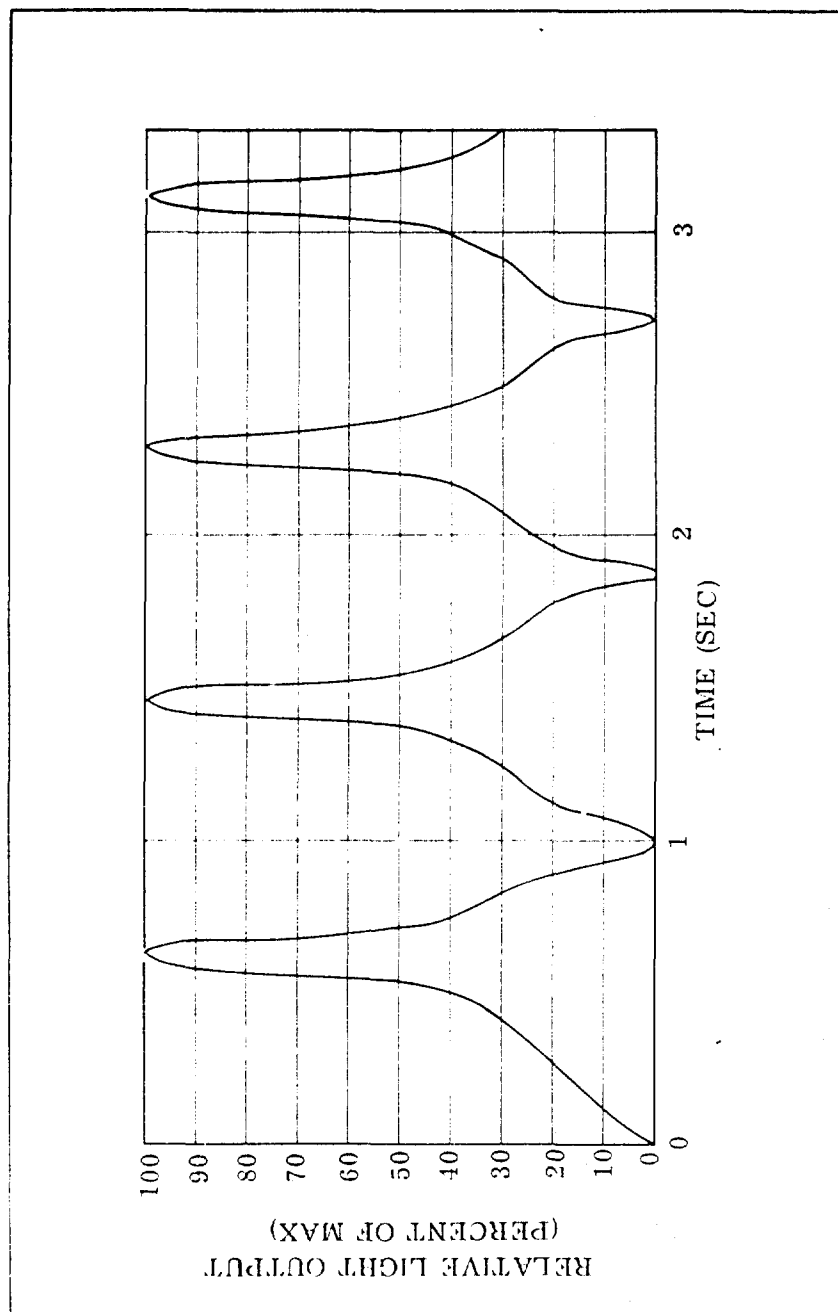


Fig. 2. Low Frequency Oscillatory Combustion of Actual Flare Test

TABLE I

## COMPOSITION AND PROPERTIES OF FLICKERING PYROTECHNIC

Composition (wt %)

Castable fluorocarbon binder	40.0
Oxidizer	16.0
Magnesium	24.0
Chlorocarbon	<u>20.0</u>
	100.0

Mechanical Properties

## Temperature

	<u>+75° F</u>		<u>+150° F</u>
Strain at maximum stress ( $\epsilon_m^t$ , %)	32	46	20
Strain at rupture ( $\epsilon_R^t$ , %)	76	80	30
Stress ( $\sigma_m$ , psi)	60	95	46
Modulus (E, psi)	328	336	232

Cured Density lb/cu in. <sup>3</sup> = 0.0655

( $\pi_p$ ) k  $\cong$  0.64% per °F -60° to +64°F

( $\pi_p$ ) k  $\cong$  0.088% per °F +64° to +150°F

$R_b = 0.02 (P_c / 12.7)^{0.60}$

End of mix viscosity, Kp at 110° F  $\cong$  2

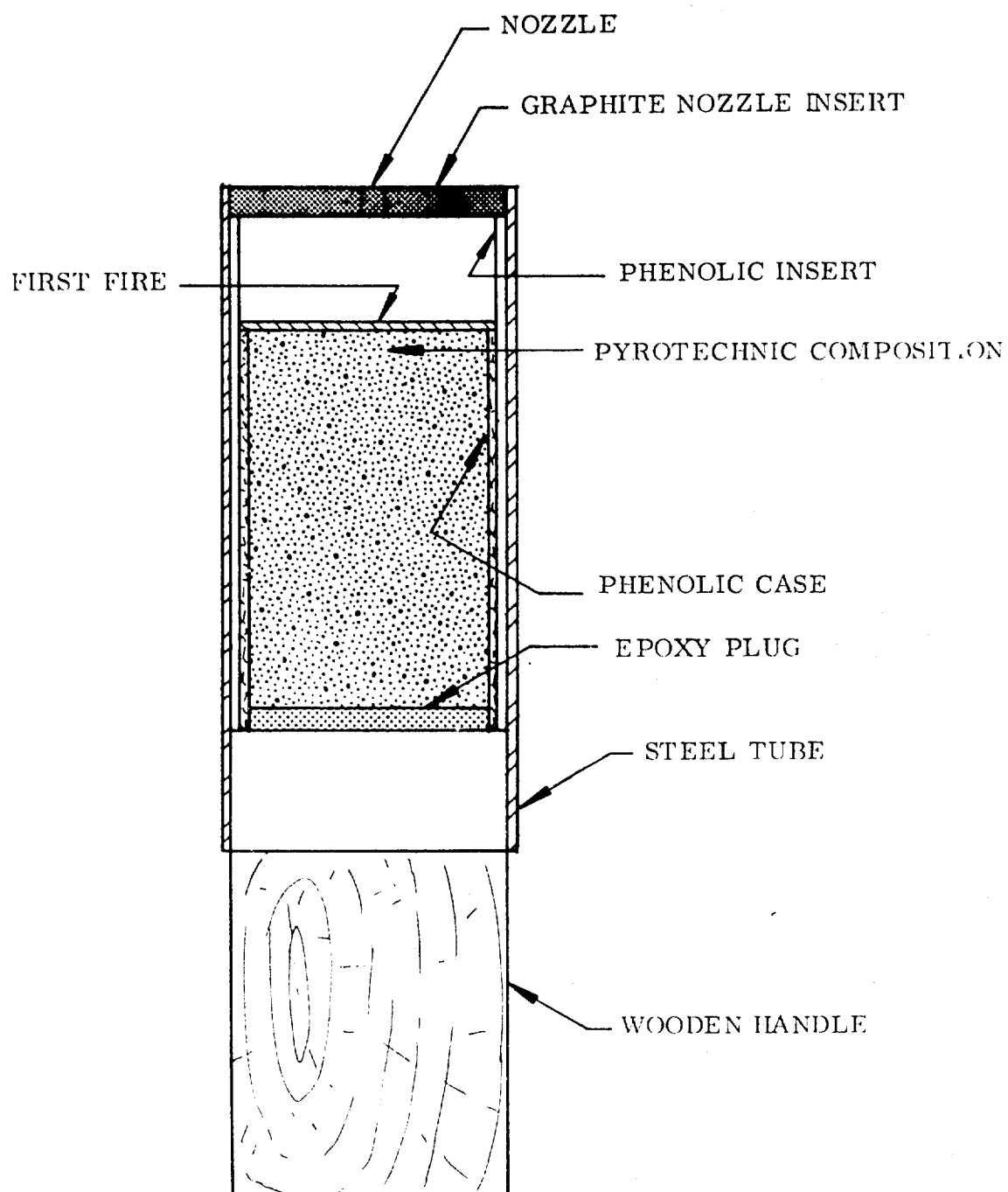


Figure 3. Hand Held Flickering Marker

condensed phase and allows the reaction of the magnesium with the binder and other halocarbons to occur. These are rapid reactions having high energies of activation and because of the unusual stability of the C-F bond in the fluorocarbon binder, they do not proceed until relatively high temperatures are reached. This reaction, in the case of a fluorocarbon,  $(CF_2)_n + Mg \rightarrow MgF_{2(g)} + C_{(S)}$ , is not sustaining in these compositions, an effect which seems to be caused by the presence of ammonium perchlorate. As ammonium perchlorate is decreased, the burning rate increases rapidly, probably because the gaseous decomposition of the ammonium perchlorate is effectively diminishing the high flame temperature of the above reaction; the AP also increases the flame front distance from the burning surface. A DTA thermogram of pulsing flare formulation is displayed in Figure 4 along with the thermogram of a typical AP-hydrocarbon binder (R45 hydroxyl terminated polybutadiene) propellant. Although the thermograms do not give a complete picture, the most obvious difference in the two curves is the longer induction period between the AP endotherm and the first significant exotherm in the case of the flare formulation. Thus, the heat stored in the flare propellant is greater and when ignition does occur the heated portion reacts rapidly.

It is likely that the ammonium perchlorate is decomposing and burning without combustion of the binder or magnesium so that there remains a porous magnesium fluorocarbon mixture which flashes upon reaching the FC-metal reaction temperature of some 500° to 600°C. This porous layer is a poor heat conductor so the energy from the AP flame is stored in the layer rather than being conducted onto the flare grain. The phenomena of AP decomposition without FC binder combustion has been observed in earlier work on AP-FC extinguishable propellants (Ref 2).

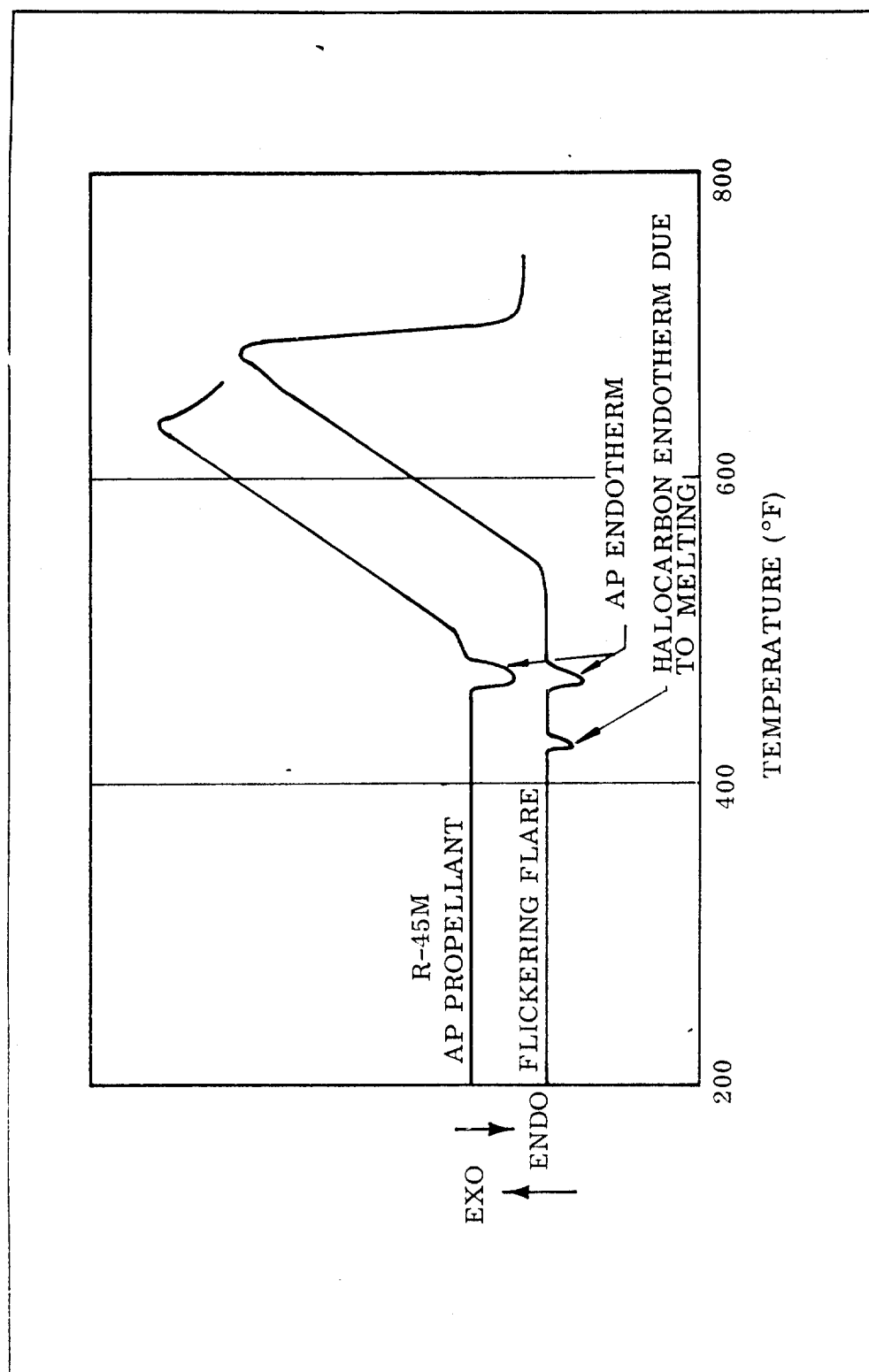


Fig. 4. DTA Thermogram for Flickering Flare Propellant and Typical Hydrocarbon-AP Propellant

The IR spectra shown in Figure 5-7 were attained using a Perkin-Elmer rapid scan 108 spectrophotometer set up to record IR spectra between approximately 2 to 6 microns. The spectrophotometer used an NaCl prism and gold doped germanium detector. Calibration of the spectrophotometer was accomplished by use of a Nernst glower operating at 1800°K and observing the H<sub>2</sub>O and CO<sub>2</sub> adsorption bands along with the carbon-hydrogen bands from a polystyrene film in the light source of the Nernst glower (Figure 5). After calibration of the instrument the spectra of various candles were recorded using an oscilloscope and Polaroid camera. It can be observed from Figure 6 that the emission of Teflon (Vydax)-magnesium is very close to the Nernst glower.

The spectra of the flicker flare (Figure 7) is quite similar to the magnesium-Teflon flare between 2 and 3 microns with somewhat less intensity at 3 microns. However, the slope of the curve between 3 and 4 microns is less so that at comparable intensities at 2.5 microns the flicker flare produces approximately 1.8 times the output at 4.5 micron. The increased output is still less than half that at the shorter wavelengths. Beyond 5.4 microns the traces of both IR flares appear the same.



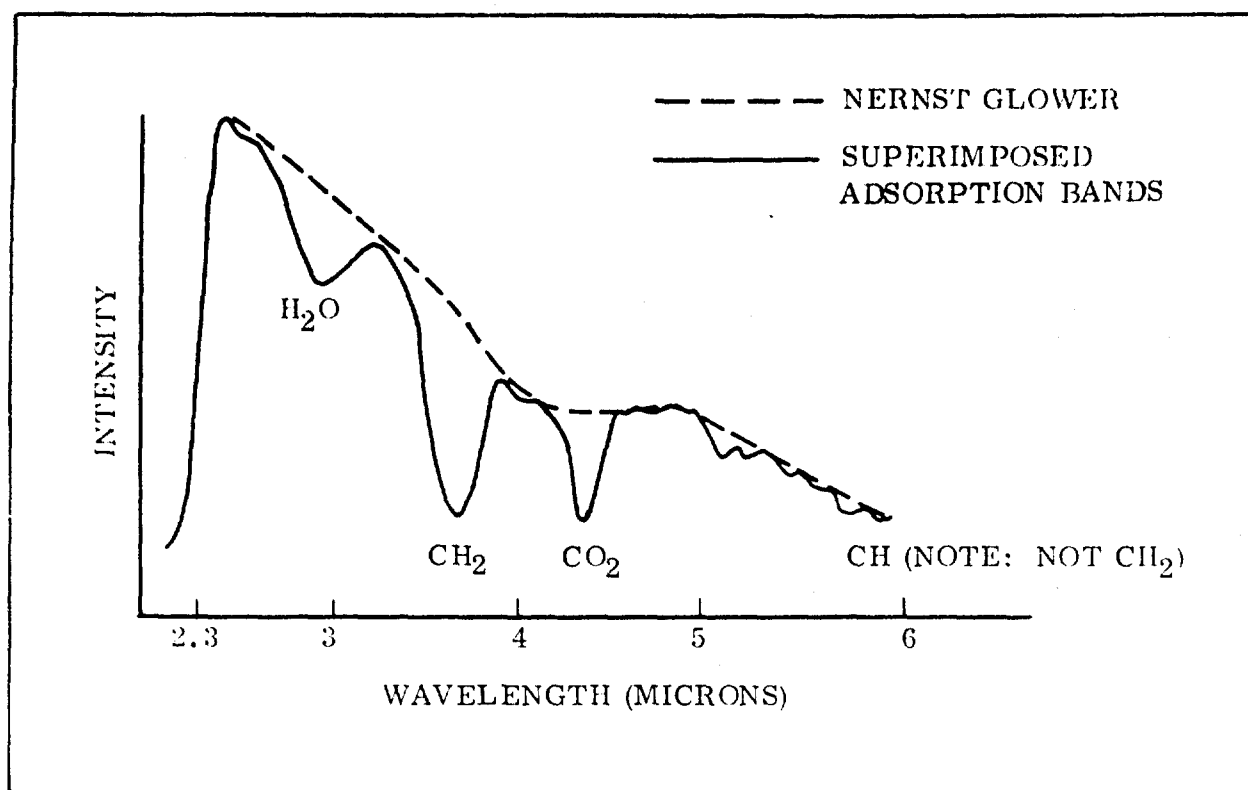


Figure 5. Calibration Curve

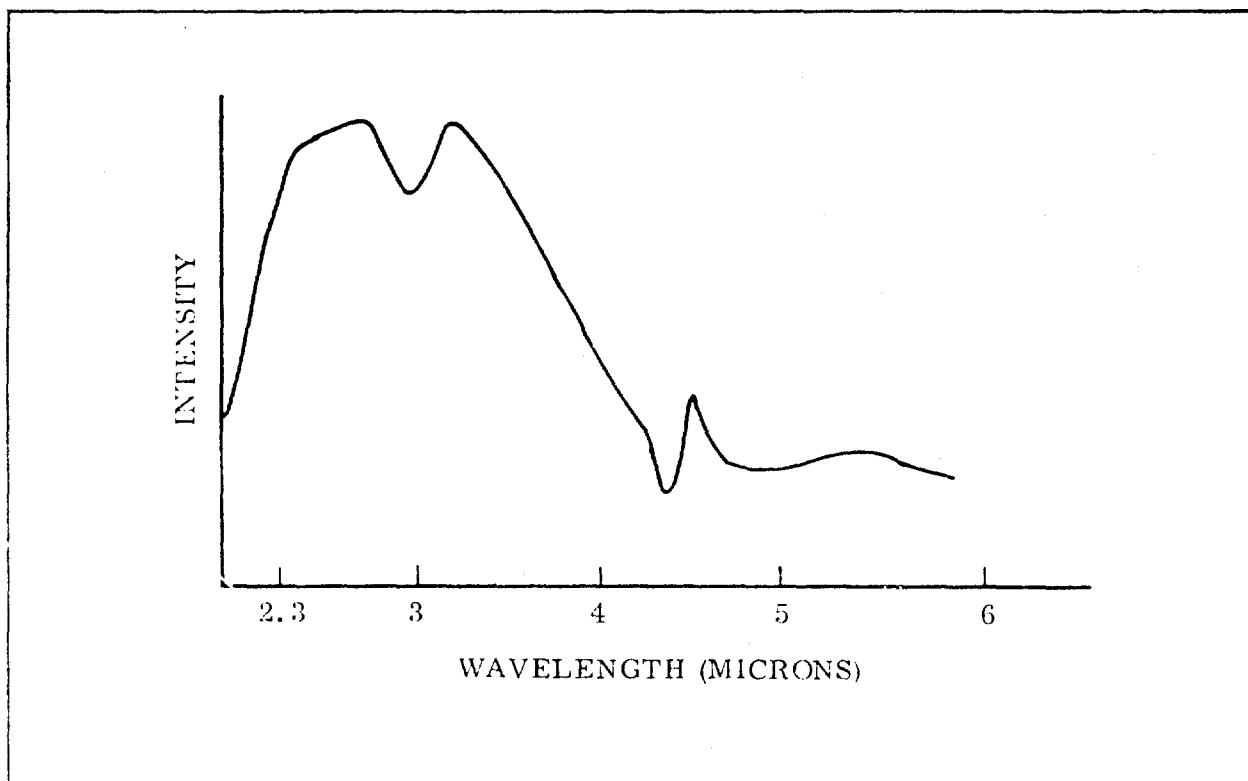


Figure 6. Magnesium-Teflon Flare

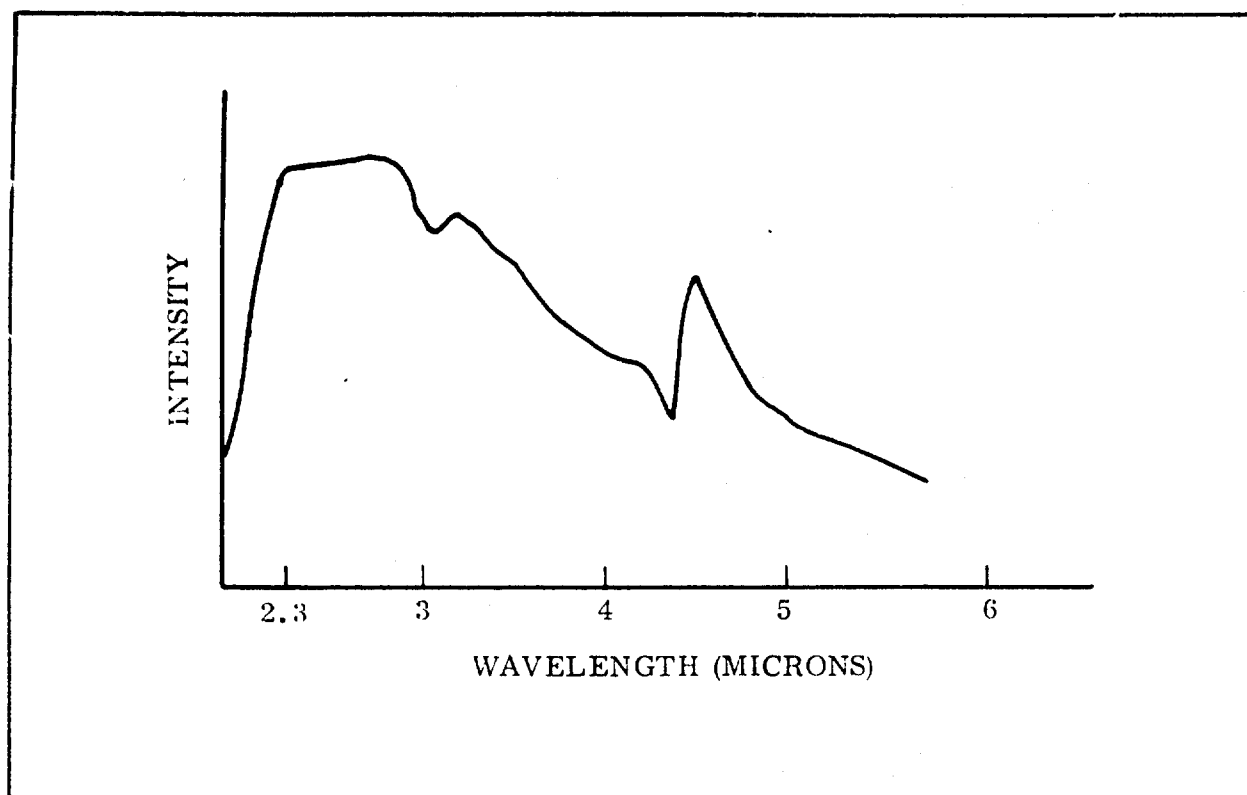


Figure 7. Fluoroacrylate-Mg Flare

## REFERENCES

1. Private Communication from B. A. Breslow, Naval Weapons Center, China Lake, California.
2. Munson, W. O.; Reed, R.; and Cornia, R. P.: "Combustion Bomb Testing of an Extinguishable Fluorocarbon Propellant," presented at 1967 Spring Meeting of Western States, Section 1, The Combustion Institute, 28-29 April 1969.

## Smoke/Flame Pyrotechnics

by

Graham C. Shaw III  
and  
Russell Reed, Jr.

Thiokol Chemical Corporation/Wasatch Division  
Brigham City, Utah

### ABSTRACT

This Air Force sponsored program had as its objective the development of single compositions for use in day-night markers. Formulations producing yellow flame and yellow smoke, orange flame and orange smoke, and red flame and white smoke were achieved. Volatile, colored inorganic halides were formed in the combustion which when condensed yielded highly colored clouds; some are similar to those attained in dye smokes.

Several polymeric binders including fluorocarbon, silicone polyester, chlorinated polyester, and polybutadiene were tested. Oxidizers such as potassium perchlorate were employed to enhance combustion and to oxidize carbon liberated by dehalogenation of the halocarbons. Thermogenic metals such as magnesium were used in some compositions to increase luminosity and the general driving force of combustion. Red and orange colored flames were achieved using strontium compounds; yellow was attained in some cases from sodium salts. It is likely that the metal halides are produced by condensed phase reactions of organic halogen compounds and the finely divided metal.

A yellow smoke/flame composition was demonstrated in the Mk-13 hand held rescue marker and burning times of 3 minutes were realized with a good output of smoke and flame. These compositions were mixed in conventional propellant mixers and processed as castable or tamp compactable formulations that yield grains with adequate to excellent physical properties.

## INTRODUCTION

The major goal of this program was the development of pyrotechnic compositions that simultaneously produced colored smoke of the same color as the flame. Such compositions are desirable because current colored marker pyrotechnics provide either a day or night marker, but not both; and single compositions would simplify target marking operations. Several colors are of interest including: red flame and smoke, red flame and white smoke, and yellow flame and orange smoke. Intensity of the colored flame and the quantity of smoke generated per unit volume of composition consumed should be equivalent to existing marker compositions. Since current colored flame compositions have high flame temperatures and current colored smoke compositions are made with organic dyes which pyrolyze at high temperature, the simultaneous production of colored smoke and colored flame required the use of new concepts.

In addition to the primary objective stated above, compositions that are developed should have the generally desirable properties of pyrotechnic compositions. Safety is a primary concern, and compositions should be safe to manufacture and insensitive to inadvertent initiation, yet easily ignited by standard first-fire compositions. Furthermore, nontoxic combustion products are desirable.

Castable compositions which can be varied in burning rate are desired so that a variety of marking and signalling requirements can be satisfied. The compositions should be castable or tamp castable in order to attain steady combustion at reproducible burning rates. Moreover, they should be strong enough to withstand forces associated with high speed impact, and capable of functioning over a wide temperature range, after being stored for 5 years.

A review of the nature of the composition and combustion of cast smokes and flares is helpful in understanding the problem associated with development of smoke/flame compositions. Conventional pressed colored smokes and the newer castable compositions flamelessly deflagrate, a process that sublimates organic dyes to form vividly colored clouds which then expand due to the evolution of warm gas. Flameless deflagration is facilitated by use of a vigorous condensed-phase oxidizer such as potassium chlorate that is able to oxidize the binders which are typically sugar-like derivatives with pressed smokes and curable liquid polysulfide prepolymers with cast smokes. Both binders are easily oxidized, an essential feature which augments the condensed phase process.<sup>1</sup>

Considerable driving force to reaction is required to sustain such combustion since no flame is present to heat the surface by radiation. Under such conditions, most pyrotechnics (including flares) and propellants rapidly extinguish since these condensed phase reactions are very slow and perhaps even endothermic and, therefore, are incapable of furnishing the heat required to sustain combustion.<sup>2</sup> Potassium chlorate is more reactive in the condensed phase than other common oxidizers such as potassium perchlorate, potassium nitrate, ammonium nitrate, or ammonium perchlorate. The latter two oxidizers function mainly in the gas phase and if added

to smoke compositions, they are remarkably effective in reducing the smoke output (probably by oxidizing the vaporized dye).<sup>3</sup> Polysulfide is an excellent binder since it is preferentially oxidized, thereby protecting the dye from oxidation. Dye pyrolysis is minimized by increasing sulfur content, an effect which lowers the heat of combustion; moreover, sulfur compounds tend to act as scavengers of oxidizing species. Coolants such as oxamide and various other organic nitrogen compounds reduce the deflagration temperature and produce noncombustible gases, effects which tend to prevent flaming.

When flaming occurs, all of the dye is consumed even though the flame temperature is relatively cool ( $1,000^{\circ}\text{C}$ ) compared to conventional colored flares. It is unlikely that organic dyes can be used to achieve a colored smoke in the presence of a flame that results from combustion of conventional ingredients; the flame temperature of current green, yellow, and red flares is in the range of  $2,500^{\circ}\text{C}$ , a temperature which would rapidly and completely pyrolyze even the most thermally stable organic dyes such as the halogenated metallic phthalocyanines.

The rationale of our approach involved the volatilization of metals and metallic derivatives in the flame to yield, via condensation, suitably colored inorganic halides (Table I). It is not necessary that these colored compounds be stable in the flame since they would form upon cooling and condense eventually as submicron particles. Optimum particle size for an orange dye smoke has been determined to be 0.4 micron (diameter). A five-fold variation in the optimum size can occur for variations such as dye type and color, the angle of the viewer to the flame, and the intensity and direction of the incident light.<sup>4</sup> The high specific surface

of the colored compound enhances the vividness of the color and increases the size of the cloud. Moreover, particles of this size do not settle or agglomerate and tend to drift as a cloud. Some of the colored inorganic compounds used are relatively dense and would tend to settle out if the particle size were 10 microns or greater.

TABLE I  
COLOR PRODUCING COMPOUNDS

<u>Color</u>	<u>Iodides</u>	<u>Chlorides and Bromides</u>	<u>Metal Oxides</u>
Red	BiOI + BiI <sub>3</sub> Mol <sub>3</sub> Mesh Metals	FeBr <sub>3</sub> · XH <sub>2</sub> O CoCl <sub>2</sub> · XH <sub>2</sub> O or NH <sub>3</sub> complex	Cu <sub>2</sub> O   Fe <sub>2</sub> O <sub>3</sub> Pb <sub>2</sub> O <sub>3</sub>
Orange	BiOI + BiI <sub>3</sub>		
Yellow	PbI <sub>2</sub>	FeCl <sub>3</sub> · XH <sub>2</sub> O	
Green		CuCl <sub>2</sub> · XH <sub>2</sub> O or NH <sub>3</sub> complex NiCl <sub>2</sub> · XH <sub>2</sub> O - NiBi <sub>2</sub> · XH <sub>2</sub> O or NH <sub>3</sub> complex CrCl <sub>3</sub> · XH <sub>2</sub> O - CrBr <sub>3</sub> · XH <sub>2</sub> O	NiO, Cr <sub>2</sub> O <sub>3</sub> Cr <sub>2</sub> O <sub>3</sub> , Mo <sub>8</sub> O <sub>23</sub> · XH <sub>2</sub> O



These pyrotechnics are in some ways analogous to those forming silver iodide and they may therefore yield nucleating species effective in weather modification.

A large number of widely varying ingredients has been investigated but the most vivid clouds are generally produced by metallic halides. The halide derivatives of bismuth and lead gave dense brightly colored smoke clouds when formed from pyrotechnics. Both bismuth (bp 1,470°C) and lead (bp 1,515°C) are readily vaporized by the flames to yield in the presence of suitable halogen donors, the volatile halides or oxide derivatives. The iodides of lead and bismuth are yellow and orange-red, respectively, depending upon the method of preparation and particle size. The relatively low boiling points of these metals and halides are advantageous since the smokes are formed at a greater distance from the flame thus reducing obscuration. In this approach, either lead, lead oxide or lead halide can be used; however, since bismuth halides (e.g., the triiodide) are easily hydrolyzed, a mixture of bismuth metal and an iodine donor is used. Upon cooling, the iodides condense in particles which are sufficiently small in size so that they show no tendency to settle. Brightly colored clouds of orange, yellow, and red have been obtained and some are comparable to those formed from organic dyes in conventional pyrotechnic smokes.

Lead iodide is probably not pyrolyzed or hydrolyzed to an appreciable extent in the combustion, but bismuth iodide, since it is easily hydrolyzed, may be converted to the oxyiodide, a red tetragonal crystal which decomposes at a red heat to bismuth triiodide and bismuth oxide.

## Yellow Smoke-Flame

Yellow smoke-yellow flame compositions were devised that contained lead or its compounds as the oxide and halides, an alkali perchlorate (as potassium perchlorate) and a liquid curable binder, a highly oxygenated carboxyl terminated polyester, which was generally cured with a multifunctional epoxide. The oxygen content of the binder largely determined the shade of the yellow smokes. The more oxygenated binders produced the brightest light yellow smokes. The direct substitution of polymers higher in carbon and hydrogen such as the carboxyl containing polybutadienes for the polyesters produced yellow smoke clouds which were darker yellow and approached in some cases light browns or sepia colors, an effect which may be caused by the stripping of hydrogen from the polymeric backbone to yield dark carbonaceous species.

When a reactive source of iodine such as iodine pentoxide or iodoform is used in conjunction with the hydrocarbon binders the coloration is intensified much more due to the formation of highly colored organic iodine compounds, possibly radical in nature, which may tend to recombine and become lighter in color as the cloud expands. The use of metallic lead or oxides of lead generally produced yellowish-white clouds of somewhat low color saturation. The metal and oxides in the presence of iodine sources as iodoform, iodine pentoxide, or iodates, produced bright yellow smokes often comparable to those attained with the organic smoke compositions.

The flame is dependent on the binder type and the nature of the oxidizer and fuel. Compositions containing a polyester binder and potassium perchlorate burned

with a bright yellow flame while a similar composition using the carboxyl terminated polybutadiene (CTPB) binder had little flame. When ammonium perchlorate was used as the oxidizer in place of an alkali perchlorate less or no flame was produced; the addition of Mg was required to produce a flame. The presence of Mg in a CTPB binder formulation gave an orange-yellow flame. As anticipated, flame brightness was enhanced by using higher levels of Mg at the expense of smoke density. When sodium nitrate was added in place of potassium perchlorate the flame tended to extinguish followed by a flameless deflagration and increase in smoke output. The addition of both sodium nitrate and magnesium increased the luminosity of the flame while decreasing the smoke evolved. In general there exists a tradeoff between the volume of smoke and flame luminosity.

#### Red Smoke-Flame

Red and violet red smokes were obtained with combinations of Misch metal (a mixture of cerium and other rare-earths), molybdenum or bismuth with iodine donors previously mentioned. The addition of organic binders greatly affect the density and color of smokes produced. For example, a composition yielding bismuth and lead iodides gave good red smoke on combustion but the addition of any appreciable organic materials as a binder resulted in less dense light red or reddish orange smokes. Fluorocarbon binders allowed the formation of red smokes. Thus, a composition containing bismuth, lead iodide, an iodine containing oxidizer and alkali perchlorate is a typical formulation which produced a vividly colored red smoke. The mechanism involved in this effect is not clear, but the formation of a red complex of lead and bismuth iodide is one possibility that must be considered. As the

fluorocarbon binder is increased above minimum levels required for tamp casting, the smoke quality and quantity were adversely affected.

It is likely that the fluorocarbon binder may give a better red smoke because it is a scavenger for water (due to the reaction  $\text{CF}_2 + \text{H}_2\text{O} \rightarrow \text{CO} + 2 \text{HF}$ ); water may decrease the level of the red bismuth iodide via hydrolysis to orange BiOI. The fluorocarbon is not reducing in nature as are the other binders; the loss of the metal halide by reduction would therefore be minimized.

When less expensive polymers such as the highly oxygenated polyesters, the chlorinated polymers or the silicon polymers were substituted for the fluorocarbon binder, even at low levels, orange-red smokes were produced. While the smoke color and density are enhanced as binder level is reduced, a reddish orange or very light red smoke can be obtained in compositions using the oxygenated polyesters with lead iodate. Silicone binders such as Sylgard gave light pink and orange smoke clouds.

While the compositions with fluorocarbon binder gave excellent red smokes, the flames were yellow to yellow-white even in the presence of strontium nitrate, perchlorate, or mixtures of strontium compounds containing halogen sources such as Dechlorane. The presence of fluorine may inhibit the formation of the red emitting  $\text{SrCl}$  fragments as a consequence of the formation of  $\text{SrF}$ , a species emitting in the yellow region. This is not unexpected in view of the generally higher bond energy of the alkaline earth-fluorine linkages.

Compositions in which the fluorocarbon binder was replaced with polyesters or hydrocarbons did not give a bright red smoke although they did burn with a light red flame. Therefore, a pyrotechnic containing a precured red flame composition

was cast into a grain with red smoke formulation. A system containing equal amounts of the red flame and red smoke formulations gave a useful combination of red flame and red smoke; the brightness of the smoke and the color purity of the flame was somewhat degraded in the combined system.

After several tests of conventional type red flare compositions, such as compositions 23-12 and 23-13, Table II, it was found that the perchlorate-glycine adduct<sup>5</sup> used as the major source of red emitter gave better colored flames when burned in combination with the red smoke composition. The addition of a binder to the strontium perchlorate-glycine adduct made it necessary to add more oxidizer and magnesium to achieve an adequate flame temperature. Strontium nitrate and Dechlorane or  $\text{SrCl}_2$  were used as the oxidizer-halogen source to increase the red  $\text{SrCl}$  emitting species in the flame. Compositions containing higher levels of strontium apparently were low in flame temperature and required increased amounts of magnesium for a good red emission (Composition 23-10, Table II). Flares using only strontium nitrate and a halogen source generally burned too slowly and consequently would not attain a sufficient rate of red emission to produce a red flame until after the red smoke composition was consumed.

TABLE II

## RED FLARE COMPOSITIONS FOR COMBINATION RED SMOKE-FLAME

	<u>23-7</u>	<u>23-10</u>	<u>23-11</u>	<u>23-12</u>	<u>23-13</u>
Polyester binder	15.00	15.00	15.00	15.00	15.00
Strontium perchlorate glycine adduct	46.00	38.00	34.00	--	--
Strontium nitrate	30.00	20.00	20.00	47.00	47.00
Dechlorane 510	9.00	7.00	7.00	14.00	14.00
Ammonium perchlorate	--	12.00	12.00	10.00	--
Magnesium (-325)	--	8.00	12.00	14.00	14.00
Potassium perchlorate	--	--	--	--	10.00
Flame color	Orange	Light Red	Good Red	Good Red	Good Red

### Orange Smoke-Yellow Flame

The variations which were made in compositions of the red smoke/flame led to an improved orange smoke-yellow flame composition. With minor modifications, the red smoke composition using an oxygenated polyester binder in place of the fluorocarbon binder produced dense, orange smokes. A high lead content of the composition enhanced the orange smoke density so that it was comparable to that of a dye smoke.

By comparing the smoke from compositions in which lead and an iodine source was replaced with potassium perchlorate (added to enhance the flame) it was concluded that a portion of the lead compounds could be removed, although at some expense to the cloud density.

### White Smoke-Red Flame

Initial investigations using Al, Mg, Zn and Ti metals as a source for white smoke in conjunction with strontium perchlorate showed that when sufficient metal was incorporated in the flare to produce dense oxide smokes the resulting flames were white. The red emission of the strontium chloride species was overwhelmed by the gray body emission of the metal oxides. In view of these results, other means of attaining white smoke were investigated.

It was found that light green to turquoise smokes, believed to be cobalt chloride, accompanied by yellow-orange flames could be achieved by burning compositions (in the hood) containing cobalt, a halogen source (such as hexachloroethane (HCE)), and oxidizer (as potassium perchlorate). The combustion of larger samples outdoors gave a good light green smoke that rapidly faded in color giving dense

white clouds, an effect which may be due to the hydrolysis of the green cobalt chloride by atmospheric moisture. In the absence of a binder, wide variations in the ratio of HCE to cobalt produced clouds of pastel blue and green smokes with good density which also faded to white in larger tests out of doors. The addition of binder such as the oxygenated polyesters greatly decreases the amount of smoke produced. This suggests that hydrogen containing species produced from pyrolysis of the binder are competing with cobalt for the chlorine or are dehalogenating the cobalt chloride.

When chlorinated polyesters, with as much as 30% chlorine, were used in compositions containing cobalt, HCE and an oxidizer, light green smoke clouds of good density were attained; these rapidly faded to white when burned out of doors. A brominated epoxy resin (DER 599) from Dow Chemical gave the same grayish clouds as those obtained from the high oxygen content polyesters. Attempts to use either the brominated epoxy resin or chlorinated polyester as the only source of halogen resulted in dark black or gray smokes, probably due to the stripping of the hydrogen and halogen from the polymer backbone leaving a carbonaceous residue. When Dechlorane, a less volatile source of chlorine was used, gray to black clouds were also produced. Dehalogenation of these organic chloride derivatives yields solid carbon which contributes to the gray color, an effect which can apparently be overcome by using HCE which has a much higher Cl/C ration, 3, as compared to 1.2 for Dechlorane. Moreover, it is likely that the shorter carbon chains of HCE can be oxidized more readily by water (produced in the combustion products) and other oxidizing agents.



The addition of strontium perchlorate to the compositions provides a red flame. The perchlorate appeared to be more efficient than the nitrate. The amount of red light appeared to be equivalent when using 30 to 35%  $\text{Sr}(\text{ClO}_4)_2$  or 40 to 47%  $\text{Sr}(\text{NO}_3)_2$ . The color purity of the flare was considerably less than obtained from the normal red flare compositions because of the emission from the cobalt species. Excellent white smokes (accompanied by light red flames) were attained in compositions using  $\text{Sr}(\text{ClO}_4)_2$ , Co, HCE and chlorinated binders. These smokes were high in density and unlike the HC smoke were white with no grayness.

It is apparent that at the temperatures required for the red emission from the  $\text{SrCl}$  species the gray body emission from other species diminish the color purity of the red flame. As in the previous case the use of separate compositions both cast in the same grain is the technique which is being investigated as a method of improving the quality of the flame.

## REFERENCES

1. "The Phenomena of Flameless Deflagration and High Pressure Deflagration Limits in Propellants," G. Shaw, R. Reed, Jr., 3rd ICRPG/AIAA Solid Propulsion Conference, Atlantic City, New Jersey, June 1968.
2. T. J. Ohlemiller, J. Wenograd, and M. Summerfield, 19th Prog. Report, Contract NONR 1853(32), Princeton University, June 1965.
3. G. Shaw, Unpublished Results, Thiokol Chemical Corporation, Wasatch Division, Brigham City, Utah.
4. D. Sinclair, Handbook of Aerosols, page 96, published by the Atomic Energy Commission, Washington, D. C., 1950.
5. Reported by B. Douda of NAD Crane.

FLOW-CASTABLE COMPOSITIONS FOR  
ILLUMINATION FLARES

by

George A. Lane, E. M. Jankowiak, D. L. Girardin, and K. Roberson,  
The Dow Chemical Company, Midland, Michigan\*

ABSTRACT

A program was undertaken to develop superior flow-cast illuminants based on magnesium, sodium nitrate, and oxygenated binders. A variety of binder resins was studied, including epoxides, vinyl esters, and carbonates. Several amine and anhydride epoxy curing agents were investigated. Plasticizers included nitro, nitrate ester, carbonate, and oxalate compounds. Best results were obtained with a glycerine-based epoxy resin, cured with maleic anhydride-ethylene carbonate eutectic, and plasticized with diethylene glycol dinitrate. This formulation has been optimized with respect to binder level, rheology, magnesium/sodium nitrate ratio, and magnesium particle size distribution. In 3.4 inch candles, efficiencies obtained are at least as good as for the Mark 24 flare candle.

---

\*This work was supported by the Air Force Armament Laboratory (ATTI), Eglin Air Force Base, Florida.

## I. INTRODUCTION

At the Second International Pyrotechnics Seminar in 1970, we reported initial success in developing a pour-castable, high efficiency illuminant. This paper reports a program undertaken since then to improve the binders used, optimize the compositions, study the ingredients and processing, and scale up to larger flares.

Two classes of resins have been studied for binders: epoxy resins and vinyl polyesters. Amines or anhydrides have been used to cure the epoxy resins, and peroxides have been employed with the polyesters. In order to get high luminous efficiency, a nitrate ester plasticizer has been incorporated in the binder.

Composition optimization work has involved improvement of castability by sizing and treatment of the solid ingredients, minimization of the binder level, and optimizing the ratio of  $\text{Mg}/\text{NaNO}_3$  for maximum performance. Since these variables are all inter-related, they must be manipulated simultaneously.

## II. FLARE PREPARATION AND EVALUATION

The sodium nitrate used was ground very fine and thoroughly dried. A Lee attrition mill was used, followed by 16 hours drying at 80°C., regrinding, and screening through a 400 mesh screen. Dried  $\text{NaNO}_3$  passed once through a Mikro-pulverizer was also used in the study. The addition of 0.5% MgO and 0.25% Cab-o-sil aids in preventing agglomeration of the  $\text{NaNO}_3$  particles. Maximum castability can be achieved only by eliminating agglomeration.

Atomized Valley Metallurgical powdered magnesium was used for all this work. Most experiments utilized nominal 40/200 mesh material. The plasticizers used were free of inhibitors.

Three different mixing techniques were employed. In the first a KitchenAid Model K5-A mixer with WW wire loop whip blade was used. The following procedure was followed: add resin, add curing agent, add plasticizer, add Mg, mix 3-5 minutes, add  $\text{NaNO}_3$ , mix 5 minutes. Later it was found that better castability is obtained if the oxidizer is thoroughly dispersed in the binder ingredients. A Hamilton Beach Model 30 mixer was used, with the following procedure: add resin, add curing agent, add plasticizer, mix 1-2 minutes, add  $\text{NaNO}_3$ , mix 5-10 minutes, add Mg, mix 10-15 minutes. These techniques were used on batches up to 650 g. When the mix was scaled up to 10 kg., the KitchenAid mixer was used, with an A-B beater and pastry knife blade, using the following procedure: add curing agent, add plasticizer, add resin, mix 1-2 minutes, add  $\text{NaNO}_3$ , mix 5-10 minutes, add Mg, mix 15-20 minutes. Viscosity of the mixed formulation was determined at 25°C., using a Brookfield RVF viscometer with a T-type spindle. Figure 1 shows the consistency of a typical flow-castable composition.

After mixing, the composition was poured into a plastic funnel and allowed to flow into the flare case or into a mold. The candles were cured overnight at 70°C. After curing, one end of the candle was closed off by casting an epoxy-sand plug to form the flare base.

Many of the flares, especially during the first part of the study, were not cast into cases, but were cast and cured in a mold. These were encased in paper tape after curing by bifilar spiral winding two layers of Crystal Bay masking tape on the candle. Before the tape was applied, a coat of Sprayon No. 321 paint was applied for case bonding.



Figure 1 - Consistency of Cast Flare Composition

The flares were fired in a 18 foot 8-inch deep by 10 foot 5-inch wide by 10 foot 4-inch high concrete block hearth. The bottom of the flare was 4 foot 9 inches above the floor. Ventilation was accomplished by an inlet in the floor, below the flare, and an external 2-speed blower above the flare in the roof. The flare tunnel itself, connected to the hearth by a 4 foot by 9 foot doorway, was 60 foot long by 10 foot 5-inch wide by 14 foot high. The interior of the hearth and tunnel were painted black.

Two Model 856 YYV Weston selenium photovoltaic cells were positioned 51.95 feet and 62.57 feet from the flare, at heights above the floor of 5.1 and 5.5 feet. The outputs of the photocells were amplified by Honeywell Accudata 120 amplifiers. Light output was recorded on a Honeywell Model 906B Visicorder oscillograph. A Dymec Model 2210 voltage-to-frequency converter and a Hewlett Packard Model 523 CR electronic counter were used to integrate the light output and record the integrated luminosity. The photocell was standardized with a General Electric Lamp No. 1M/T20BP, which at a constant amperage yields a specific horizontal candle-power.

The 1 1/4-inch candles were burned vertically, ignited on the upper surface. Air flow was upward. The 3.4-inch candles were tested both in this position and inverted. Time of functioning was determined visually with a stop watch. At least four candles were fired for each data point, unless noted otherwise.

### III. BINDER DEVELOPMENT

In the work on cast flares reported to a previous meeting of this group, a composition was developed based on a binder consisting of the epoxy resin glycerin-diglycidyl ether (XFS-4008L), a nitrate-modified amine terminated polypropylene glycol curing agent (XF-4012), and triethyleneglycol dinitrate (TEGDN) plasticizer. The present work has explored these materials, other oxygen-rich epoxy resins, oxygenated polyesters, alternate oxygen-rich curing agents, and other high-oxygen plasticizers.

#### A. PLASTICIZERS

The role of nitrate-containing binder ingredients was determined by varying the TEGDN level in the binder, as shown in Table I. The effect is dramatic, indicating the unique value of the nitro/nitrate moiety.

TABLE I. EFFECT OF PLASTICIZER CONTENT ON LUMINOUS EFFICIENCY AND BURNING RATE

Composition (Percent)		
49.0 - Magnesium, bimodal 125 $\mu$ and 200 $\mu$		
27.0 - NaNO <sub>3</sub>		
24.0 - Binder - 58.3: 41.7, XFS-4008L:XF-4012		
TEGDN in Binder (Percent)	Luminous Efficiency (Cd-sec/g)	Burning Rate (In/sec)
40.0	53,000	0.037
30.0	36,000 <sup>a</sup>	0.036 <sup>a</sup>
20.0	21,300 <sup>a</sup>	0.039 <sup>a</sup>
10.0	14,000 <sup>a</sup>	0.038 <sup>a</sup>
<sup>a</sup> Single candles.		



Later tests with the high oxygen, non-nitrate plasticizers ethylene carbonate (EC) and diethyl oxalate (DEO) showed them to be inferior to TEGDN or DEGDN (diethyleneglycol dinitrate). To determine the relative effect of nitrate ester groups (as in TEGDN and DEGDN) and nitro groups, the 1:1 solution (BDNPA/F) of bis(2,2-dinitropropyl)acetal (BDNPA) and bis(2,2-dinitropropyl) formal (BDNPF) was studied. The performance of flares with both of these types of plasticizer was about equivalent.

## B. RESINS

The primary emphasis was on two epoxy resins, XFS-4008L and diglycidyl carbonate (DGC). The latter gave somewhat superior performance, but had to be dropped because of poor resin shelf stability.

Polyester, acrylate, and vinyl ester resins were also studied, including HEA (hydroxyethyl acrylate), ADGC (allyl diglycol carbonate), and HEAC (diacrylate of bishydroxyethyl carbonate).

## C. CURING AGENTS

In addition to XF-4012, several amine, anhydride, and carboxylic curing agents were investigated. D.E.H.<sup>®</sup> 24 (triethylene tetramine) gave the most stable compositions. Benzyl dimethyl amine (BDMA) was studied as an epoxy homopolymerization catalyst. Maleic anhydride (MA) and EC-MA (1:1 solution of ethylene carbonate [EC] and MA) yielded improved performance and physical properties.

## D. FORMULATION RESEARCH

### 1. Epoxy Resins

Using neat binders, several epoxy resin systems were studied. The maximum plasticizer compatibility level was ascertained by observing the surface wetness after curing for 16 hours at 70°C. As seen in Table II, nitrate plasticizers proved to be incompatible with XFS-4008L - ethylene glycol - BDMA, DGC - XF-4012, and DGC - D.E.H.<sup>®</sup> 24 binder systems. It is also evident that DGC accepts more plasticizer than XFS-4008L in the presence of an anhydride curing agent. D.E.H.<sup>®</sup> 24-cured XFS-4008L accepts the least plasticizer in this series. Finally, there appears to be no fixed order of plasticization limit for nitro-plasticizers.

---

<sup>1</sup>D.E.H., a trademark of The Dow Chemical Company for epoxy resin curing agents.

TABLE II. PLASTICIZER TOLERANCE OF EPOXY BINDER SYSTEMS

Binder	Binder/Curing Agent Ratio	Plasticizer	Plasticizer Limit (Percent)
XFS-4008L XF-4012	58.3/41.7	TEGDN DEGDN BDNPA/F	40-45.0 50-55.0 65-70.0
XFS-4008L - MA	58.8/41.2	TEGDN DEGDN BDNPA/F	50-55 45-40 40-45
XFS-4008L - EC-MA	41.6/58.4	TEGDN DEGDN BDNPA/F	35-40 40-45 30-35
XFS-4008L - Ethylene glycol - BDMA	78.7/17.1/4.2	TEGDN BDNPA/F	No cure Violent decomposition
XFS-4008L - D.E.H. <sup>Ⓢ</sup> 24	97.0/3.0	TEGDN DEGDN BDNPA/F	30-35 35-40 30-35
DGC - XF-4012	46.8/53.2	All	No cure
DGC - MA	47.3/52.7	TEGDN DEGDN BDNPA/F	55-60 55-60 45-50
DGC - EC-MA	31.0/69.0	TEGDN DEGDN BDNPA/F	50-55 50-55 35-40
DGC - D.E.H. <sup>Ⓢ</sup> 24	78.6/21.4	All	Violent decomposition

Complete flare formulations were prepared from the acceptable binders in Table II. Falling weight impact and spark sensitivity tests showed all these compositions to be quite safe. Flare candles were fabricated and functioned, with the results shown in Table III.

The most promising plasticized binder systems, on the basis of lowest viscosities and highest efficiencies, were the XFS-4008L - EC-MA, XFS-4008L - MA, XFS-4008L - D.E.H.<sup>Ⓢ</sup> 24, and XFS-4008L - XF-4012 compositions.

TABLE III. GENERAL PROPERTIES OF COMPLETE FLARE COMPOSITIONS

Sample	Aluminum (%)	Mg (%)	Carbon (%)	Black (%)	Binder (%)	DEGN (%) in Binder	Viscosity (cps) 25°C.	Impact <sup>c</sup> Pst. (Kg. cm)	Density (g/cc)	Luminous Efficiency (Cd-sec/g)	Burning Rate (In/sec)
6.1		6.0					775,000	300+	1.44	29,400	0.064
6.2		7.5					674,000	300		24,000 <sup>d</sup>	0.053
6.3		6.0					115,000		1.70	31,000 <sup>d</sup>	0.052
7.0		5.0				50.0	100,000	300	1.50	31,700 <sup>e</sup>	0.052
6.4		6.0					300,000	300+		28,000 <sup>d</sup>	0.054
6.5		5.9				40.0	125,000	105	1.74	33,800 <sup>d</sup>	0.057
7.2		7.2				40.0	75,000		1.60	29,500 <sup>d</sup>	
6.0		6.0				50.0	250,000	275	1.51	36,400	0.060
7.6		5.4					55,000	225	1.62	34,200 <sup>d</sup>	0.069
7.1			2.5			20.0	250,000	200	1.53	37,300	0.062
6.5			9.1				100,000	190	1.58	40,500	0.060
6.0			8.4			40.0	142,000	177	1.58	44,500	0.069
16.3	6.2	7.0				30.0	190,000	300+	1.59	30,900	0.051
15.1	5.1		0.5			35.0	137,500	300+	1.57	31,400	0.069
	5.1	5.7					165,000	230	1.57	36,000 <sup>d</sup>	0.067
	5.1	5.7				55.0	Too high	300	1.39	26,500	0.090
	5.1	5.7					42,000	100	1.67	32,700 <sup>d</sup>	0.073
	5.1						Too high	300+	1.36	29,000	0.101
	3.7		10.8			50.0	Dry	200	1.46	25,600	0.125
	3.7		6.3				Dry	220	1.51	29,300	0.032

<sup>a</sup> 50/200 mesh Mg, half each 50/100 and 100/200 mesh.

<sup>b</sup> 50/200 mesh Mg, half each 50/100 and 100/200 mesh.

<sup>c</sup> 100/200 mesh Mg, half each 50/100 and 100/200 mesh.

<sup>d</sup> 100/200 mesh Mg, half each 50/100 and 100/200 mesh.

<sup>e</sup> 100/200 mesh Mg, half each 50/100 and 100/200 mesh.

<sup>f</sup> 100/200 mesh Mg, half each 50/100 and 100/200 mesh.

All compositions were also tested for spark sensitivity using the

open cup. None ignited at the highest setting, 18.75 joules.

One third each 50/50, 50/100, and 100/200 mesh.

Surprisingly, the DGC - EC-MA binder system, one of highest in oxygen content, registered low efficiency and rapid burning rate. However, poor grain integrity, due to very high viscosity and poor wettability, probably is responsible. The DGC - MA - TEGDN composition also displays an unexpectedly high viscosity, increased burning rate and low efficiency. These poor results are undoubtedly due to shelf instability of the DGC.

The composition containing the XFS-4008L - XF-4012 - TEGDN binder system was studied extensively for storage surveillance stability at 70°C. (Table IV).

TABLE IV RESULTS OF HIGH TEMPERATURE STORAGE<sup>a</sup>

TEGDN in Binder (Percent)	Initial	12 Weeks (Ambient)	4 Weeks (70°C)	8 Weeks (70°C)	12 Weeks (70°C)
	<u>Luminous Efficiency (Cd-sec/g)<sup>b</sup></u>				
40	31,000	28,400	25,900	26,600	26,300
30	27,000	22,900	21,500	20,100	20,000
20	16,500	16,500	16,700	15,100	15,130
	<u>Burning Rate (In/sec)<sup>b</sup></u>				
40	0.051	0.050	0.062	0.049	0.047
30	0.049	0.050	0.050	0.050	0.049
20	0.049	0.050	0.053	0.051	0.050
	<u>Weight Loss (Percent)</u>				
40		(0.02) <sup>c</sup>	0.17	0.43	0.36
30		(0.02) <sup>c</sup>	0.10	0.34	0.34
20		(0.11) <sup>c</sup>	0.08	0.16	0.18

<sup>a</sup>49% Trimodal Mg, 27% NaNO<sub>3</sub> (-400 mesh), 24% XFS-4008L - XF-4012 - TEGDN binder (XFS-4008L/XF-4012 = 1.4).

<sup>b</sup>1 1/4 Inch diameters tape-wrapped candles.

<sup>c</sup>Weight gain.

The data indicate an adequate degree of thermal stability for three levels of plasticizer after 12 weeks exposure at either ambient conditions or 70°C.

A comparison of various binder systems after four weeks surveillance at 70°C. is shown in Table V. The XFS-4008L - XF-4012 - TEGDN binder composition is included for comparative purposes.

Because of relatively high weight loss and poor physical appearance no further work was done on BDNPA/F. Similarly, rapid burning and questionable shelf-life contributed to suspension of further work with DGC. Of the remaining systems, XFS-4008L - XF-4012, XFS-4008L - MA, and XFS-4008L - EC-MA, plasticized with TEGDN or DEGDN, were chosen for optimization studies.

## 2. Polyester Resins

### a. Hydroxyethyl Acrylate (HEA)

An experimental vinyl ester resin, based on HEA and MA at a 54.2/45.8 ratio, diluted with 40 percent HEA, required 24 hours to cure at 100°C. in the absence of catalyst. Free radical catalysis with cumene hydroperoxide or lauroyl peroxide accelerated the cure rate significantly and produced a more densely cross-linked gumstock. This relatively high oxygen (40 percent) binder, formulated as a complete flare mix, gave a luminous efficiency at 24 percent binder of only 9,000 cd-sec/g. Attempts to increase light output by adding TEGDN resulted in extreme gassing and poor curability.

### b. Allyl Diglycol Carbonate

It was found possible to increase the oxygen content of the low viscosity monomer ADGC by free radical copolymerization with MA. A 100.0-gram flare mix was prepared with 19 percent binder containing a ratio of 3 moles of ADGC to 2 moles of MA, catalyzed with 1.0 percent lauroyl peroxide. Castability was threshold, the cured grain was firm but low in cohesive strength, and grain expansion was totally absent. Flare compositions based on this binder seemed compatible, and relatively high oxygen content (42 to 44 percent) was attainable. Time did not permit complete evaluation of this system.

### c. Diacrylate of Bishydroxyethyl Carbonate (HEAC)

HEAC, used as a primary binder component, displayed excellent wetting qualities, good pot life, a high level of compatibility, and rapid cure rate at elevated temperatures. Free radical initiators MEK peroxide, cumene hydroperoxide, and lauroyl

TABLE 1. COMPOSITE LUMINOUS EFFICIENCY RESULTS

Test No.	Plasticizer (%)	Lum. Gain (%)	Lum. Gain (%)	EDHFA/F (%)	Weight Loss 4 wks. 70°C (%)	Luminous Efficiency <sup>d</sup> (cd sec / ft)		Burning Rate <sup>d</sup> (in / sec)	
						Initial	4 Weeks	Initial	4 Weeks
XFS-4006L	NI-4006L								
	6.0	12.0(40 <sup>a</sup> )	--	--	0.17	21,000 <sup>b</sup>	25,900	0.052	0.062
	5.0	--	12.0(50 <sup>a</sup> )	--	0.34	31,700	39,500	0.052	0.062
	6.0	--	--	9.6(40 <sup>a</sup> )	2.20	29,400	19,900	0.064	0.064
XFS-4006L	MA								
	6.0	12.0(50 <sup>a</sup> )	--	--	1.42	36,400	42,300	0.061	0.061
	5.4	--	10.8(45 <sup>a</sup> )	--	0.98	34,200 <sup>b</sup>	34,500	0.069	0.070
	5.9	--	--	9.6(40 <sup>a</sup> )	1.51	33,800 <sup>b</sup>	35,500	0.057	0.076
XFS-4006L	D.E.H. 24								
	0.5	7.2(30 <sup>a</sup> )	--	--	(0.27 <sup>c</sup> )	30,900	35,700	0.051	0.051
	0.5	--	8.4(35 <sup>a</sup> )	--	0.02	31,400	34,700	0.069	0.059
	EC-MA								
XFS-4006L	9.1	8.4(35 <sup>a</sup> )	--	--	0.84	40,500	38,200	0.060	0.059
	8.4	--	9.6(40 <sup>a</sup> )	--	0.76	44,500	36,500	0.069	0.068
	9.8	--	--	7.2(30 <sup>a</sup> )	1.77	37,300	35,300	0.062	0.059
	EC-MA								
DGC	8.3	12.0(50 <sup>a</sup> )	--	--	0.52	25,500	37,000	0.125	0.072
	8.3	--	12.0(50 <sup>a</sup> )	--	0.38	29,300	40,300	0.092	0.065
	10.8	--	--	8.4(35 <sup>a</sup> )	1.32	29,000	34,400	0.101	0.093
	MA								
DGC	5.7	13.2(55 <sup>a</sup> )	--	--	0.62	26,500	42,900	0.090	0.070
	5.7	--	13.2(55 <sup>a</sup> )	--	0.24	32,700 <sup>b</sup>	34,600	0.073	0.063
	7.0	--	--	10.8(45 <sup>a</sup> )	0.21	36,000 <sup>b</sup>	33,500	0.067	0.066

<sup>a</sup>Plasticizer in binder.

<sup>b</sup>Trimodal Mg blend. Others listed contained 40/200 Mg.

<sup>c</sup>Weight gain.

<sup>d</sup>1 1/4 Inch diameter tape-wrapped candles.

peroxide were found to catalyze homopolymerization of HEAC efficiently. A 0.3 percent concentration of lauroyl peroxide is recommended for curing at 70°C.

Initial studies of unplasticized 10 g. mixes indicated that a 1:1 ratio of HEAC to MA, with EC added in a quantity equal to the MA (for higher oxygen content), resulted in a promising composition containing 24 percent binder. The viscosity was very low, (<100,000 cps, at 25°C.), and the polymerization rate and exotherm were easily controllable. Grain integrity appeared excellent with no evidence of expansion or doming during cure. At 17.4 percent binder, with no nitrate ester plasticizer, approximately 34,000 cd-sec/g efficiency was obtained at a burn rate of 0.070 in/sec.

Since it appeared that an acceptable efficiency level could not be reached without a nitrate ester plasticizer, work was begun on TEGDN plasticization of a homopolymerized HEAC binder. These compositions produced excellent viscosities, ranging from 37,500 to 55,000 cps at 25°C with TEGDN levels of 0 to 40 percent of the binder. Interestingly all the candles containing TEGDN, even 40 percent TEGDN, displayed very dry surfaces, indicative of the high plasticizer tolerance capacity of HEAC. Performance studies, shown in Table VI revealed that 47,000 cd-sec/g, luminous efficiency and favorable burning rates can be achieved with 40 to 50 percent TEGDN or DEGDN levels. Initial data indicate that the 52/28 ratio is an approximate optimum for the Mg/NaNO<sub>3</sub> ratio.

These compositions show a slight surface softness at the 50 percent plasticizer level, possibly indicating overplasticization. A duplicate 500 g batch prepared for surveillance studies (Table VII) gave no indication of migration or incompatibility at a slightly higher (0.30 percent) catalyst content. Thus it appears that more than 50 percent DEGDN or TEGDN could be tolerated. These surveillance data show that a composition based on HEAC - DEGDN binder shows promising surveillance stability. Weight loss is acceptably low. Combustion data points (representing only one candle) show varying luminous efficiency values. It is believed that this reflects observed varying chimney effects and side burning, rather than composition degradation.

Safety tests showed an impact sensitivity ( $E_{50}$ ) of 280 kg cm for the composition with 20 percent TEGDN in the binder. At 30 and 40 percent TEGDN, values of 251.0 and 218.0 Kg cm were obtained, respectively. It can be predicted that ( $E_{50}$ ) for the 50 percent TEGDN composition will fall in the range of 150 to 200 Kg cm.

TABLE VI COMPOSITIONS CONTAINING HEAC

Ingredient	Percent Composition				
Mg , 40/200 mesh	49.0	52.0	49.0	52.0	52.0
NaNO <sub>3</sub>	27.0	28.0	31.0	28.0	28.0
HEAC	14.4	12.0	12.0	10.0	10.0
TECAX	9.6	8.0	8.0	10.0	--
DEGUN	--	--	--	--	10.0
Lauroyl Perox.	0.2	0.2	0.2	0.2	0.2
Binder	24.0	20.0	20.0	20.0	20.0
Plasticizer in Binder	40.0	40.0	40.0	50.0	50.0
	Performance <sup>a</sup>				
Viscosity, cps 25°C	52,500	500,000	220,000	245,000	265,000
Burn Rate, in/sec	--	0.067	0.064	0.071	0.082
Luminous Eff., cd-sec/g	38,300	45,000	38,200	45,200	46,800
<sup>a</sup> 1 1/4 Inch diameter tape-wrapped candles.					



TABLE VII SURVEILLANCE OF HEAC - DEGDN  
BASED COMPOSITION<sup>a</sup>

Parameter	Days at 70°C			
	0	10	24	31
Weight Loss, %	--	0.18	0.17	0.14
Color and Integrity	--	No Change		
Plasticizer Exudation	--	None Detected		
Ignition		Immediate		
Lamp. Eff., cd-sec/g <sup>b</sup>	40,600	36,200	26,700	31,650
Burn. Rate, in/sec <sup>b</sup>	0.082	0.077	0.084	0.082

<sup>a</sup>Highosilac (40/200 mesh), 51.0%; NANO, 28.4%; HEAC, 10.0%; DEGDN, 10.0%.

<sup>b</sup>Single candles, 1 1/4 in. diameter tape-wrapped candles.

#### IV. OPTIMIZATION STUDIES

Three systems, based on the binders XFS-4008L - EC-MA - DEGDN, XFS-4008L - MA - TEGDN, and XFS-4008L - XF-4012 - DEGDN, were studied for optimum composition. The goal was maximum luminous efficiency maintaining flow castability.

##### A. FORMULATION OPTIMIZATION

##### 1. XFS-4008L - EC-MA - DEGDN

Figure 2 shows the effects of magnesium to sodium nitrate ratio and binder content on viscosity for XFS-4008L - EC-MA - DEGDN compositions. The 49/27 Mg/NaNO<sub>3</sub> ratio appears well optimized for maximum castability, displaying minimal viscosity over the ranges of 21.4 to 24 percent binder. Optimization results for XFS-4008L - EC-MA - DEGDN compositions are given in Table VIII. The unfavorable effect of increased binder content on luminous efficiency and burning rate is apparent.

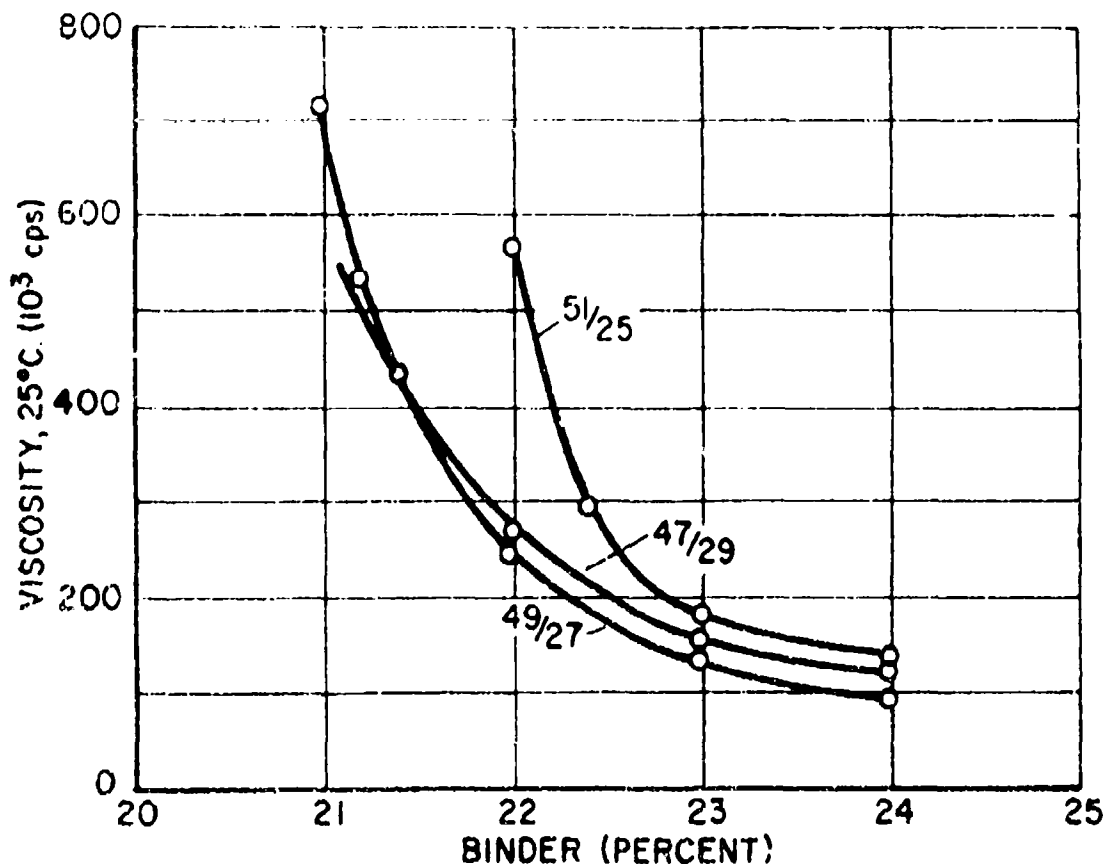


Figure 2. Effects of Binder Content and Magnesium/Sodium Nitrate Ratio on Viscosity (XFS-4008L - EC-MA - DEGDN)

TABLE VIII. OPTIMIZATION STUDIES OF COMPOSITIONS  
CONTAINING XFS-4008L - EC-MA - DEGDN BINDER<sup>a</sup>

Binder (%)	Mg <sup>b</sup> /NaNO <sub>3</sub> Ratio	Viscosity (cps)	Luminous Efficiency <sup>c</sup> (cd-sec/g)	Burning Rate <sup>c</sup> (in/sec)	Density (g/cc)
24.0	47/29	127,500	56,400	0.0480	1.64
24.0	49/27	87,000	50,000	0.0550	
24.0	51/25	130,000	55,400	0.047	1.59
23.0	47/29	155,000	60,000	0.048	1.62
23.0	49/27	132,500	50,500	0.0567	1.61
23.0	51/25	175,000	54,900	0.047	
22.0	45/31	315,000	52,200	0.0514	1.60
22.0	47/29	265,000	57,700	0.0517	1.66
22.0	49/27	245,000	61,000	0.0600	1.61
22.0	51/25	563,000	70,000	0.0563	1.59
22.0	53/23	712,500	61,800	0.0505	1.57
22.4	51/25	290,000	58,800	0.049	1.58
21.4	47/29	437,500	62,000	0.051	1.65
21.2	49/27	525,000	60,600	0.0564	1.62
21.0	49/27	712,500	66,900	0.0646	1.60
<sup>a</sup> XFS-4008L:EC-MA:DEGDN = 6.0:8.4:9.6 <sup>b</sup> 40/200 mesh Mg <sup>c</sup> 1 1/4 Inch diameter tape-wrapped candles.					

The completed optimization study at 22 percent binder shows that maximum burning rate and minimum viscosity occur at the 49/27 Mg/NaNO<sub>3</sub> ratio (Figure 3). However, the highest efficiency (70,000 cd-sec/g) was obtained at a Mg/NaNO<sub>3</sub> ratio of 51/25 and binder content of 22 percent.

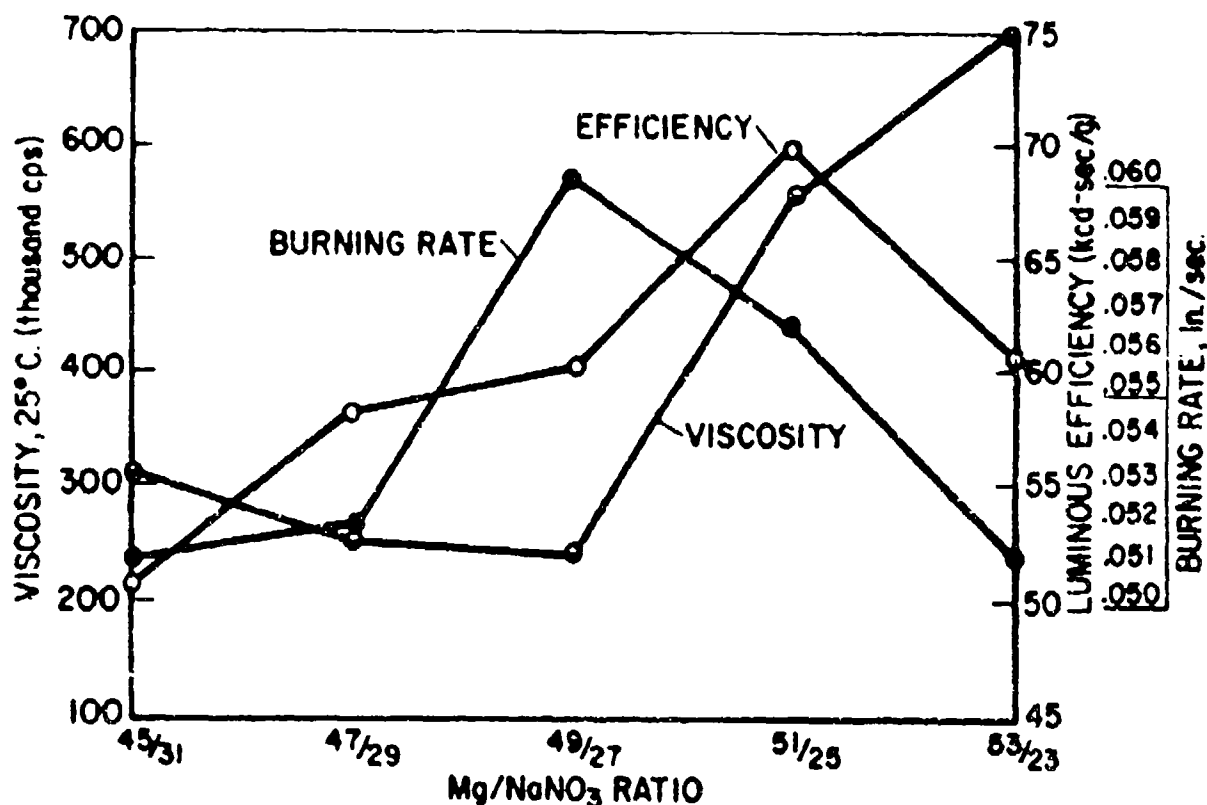


Figure 3. Effect of Magnesium/Sodium Nitrate Ratio on Viscosity and Combustion Behavior (22% XFS-4008L - EC-MA - DEGDN Binder)

## 2. XFS-4008L - MA - TEGDN and XFS-4008L - XF-4012 - DEGDN

Optimization results for compositions containing the XFS-4008L - MA - TEGDN and XFS-4008L - XF-4012 - DEGDN binders are presented in Table IX.

As seen in Figure 4 compositions containing either MA or XF-4012 curing agents display the expected viscosity increase with reduced binder levels. The XF-4012 cured compositions show superior castability. While the MA system required 21.8 percent binder to attain 500,000 cps viscosity, only about 20.5 percent of the XF-4012 system should produce equivalent castability. The burning rate of XF-4012 cured

TABLE IX. OPTIMIZATION STUDIES ON COMPOSITIONS<sup>a</sup>  
CONTAINING XFS-4008L - MA - TEGDN  
AND XFS-4008L - XF-4012 - DEGDN

Ingredient	%	Plasticizer <sup>b</sup>	Viscosity (cps, 25°C)	Density (g/cc)	Luminous <sup>c</sup> Efficiency (Cd-sec/g)	Burning Rate (In/sec)
XFS-4008L - MA	24.0	TEGDN	135,000	1.63	54,000	0.052
XFS-4008L - MA	23.0	TEGDN	185,000	1.62	63,700	0.058
XFS-4008L - MA	22.0	TEGDN	410,000	1.62	52,600	0.056
XFS-4008L - MA	22.0	DEGDN	415,000	1.63	59,100	0.057
XFS-4008L - XF-4012	24.0	DEGDN	72,500	1.64	47,700	0.048
XFS-4008L - XF-4012	23.0	DEGDN	105,000	1.63	53,300	0.048
XFS-4008L - XF-4012	22.0	DEGDN	195,000	1.59	55,000	0.049
XFS-4008L - XF-4012	21.0	DEGDN	360,000	1.59	50,200	0.051
XFS-4008L - XF-4012 (800 gram-batch)	20.0	DEGDN	345,000	1.72	--	--

<sup>a</sup> Mg/NaNO<sub>3</sub> = 1.815, 40/200 mesh.

<sup>b</sup> 50.0 percent of Binder

<sup>c</sup> 1/4 Inch diameter tape-wrapped candles.

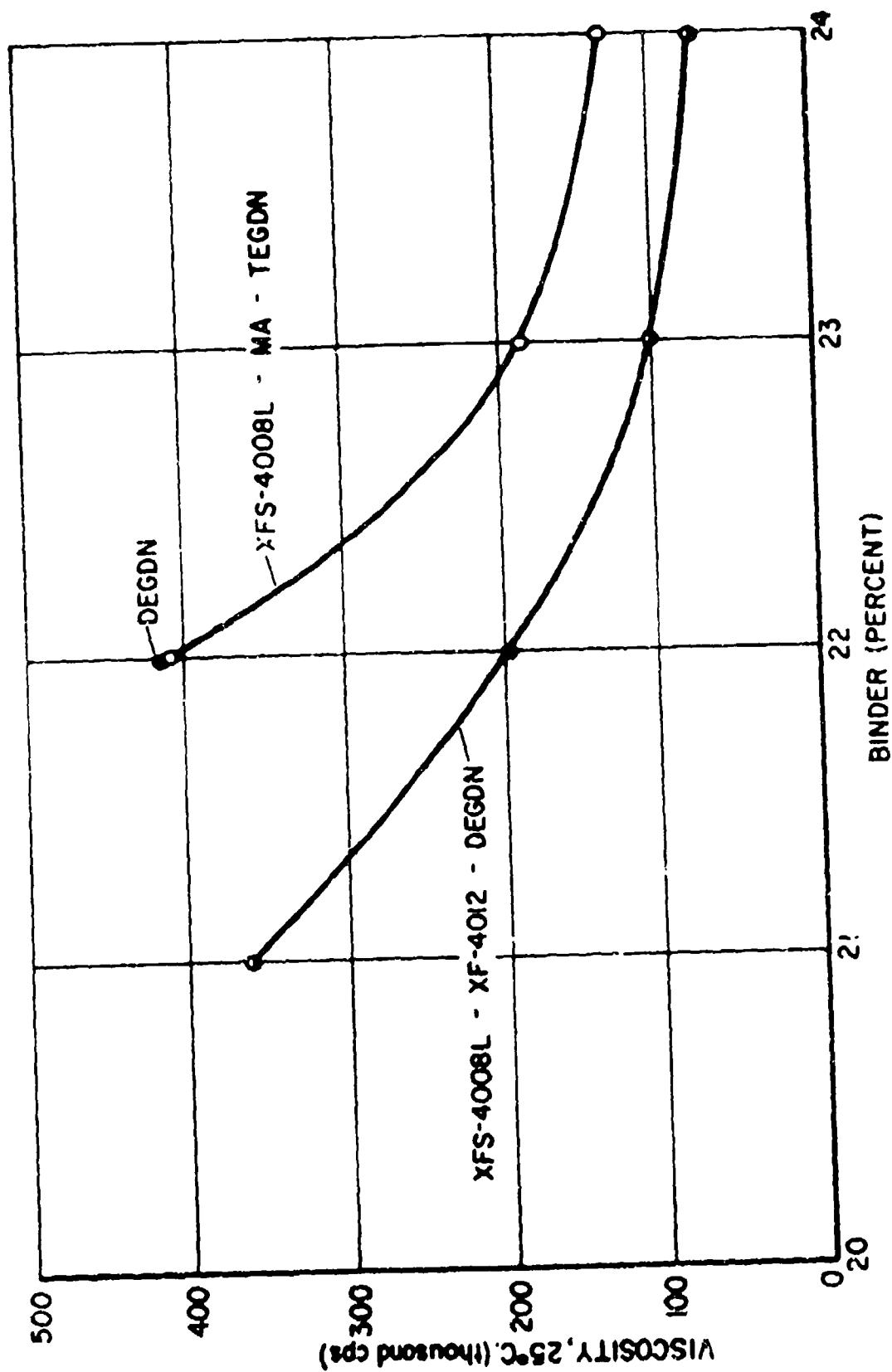


Figure 4 . Effect of Binder Content on Viscosity

compositions was found to decrease smoothly as binder level increases. For MA cured formulations the burning rates at 22 and 23 percent binder are slightly anomalous. At equivalent binder levels, the MA-based flares burn 10 to 20 percent faster than those containing XF-4012.

As the binder level decreases, the luminous efficiency generally improves, as expected. However, for both MA and XF-4012 cured systems an anomalous low result was obtained at the lowest binder level studied. Because the  $Mg/NaNO_3$  ratio was not varied, these compositions are not fully optimized for these binder systems. The data do indicate, however, significantly lower efficiencies for FP-4012 containing compositions at all binder levels.

### 3. Choice of Binder

Figure 5 shows the effect of binder level on viscosity for the binders studied. Although the compositions containing XF-4012 - DECDN binder are more castable than the others, those based on EC-MA - DECDN generally give higher efficiencies and faster burning rates. A light output trace of one of these candles is shown in Figure 6. The XF-4008L - EC-MA - DECDN system was chosen for scale up to larger diameter flares. The first step in this scale up was to study flare case materials that are more practical than taped cases for operational flares.

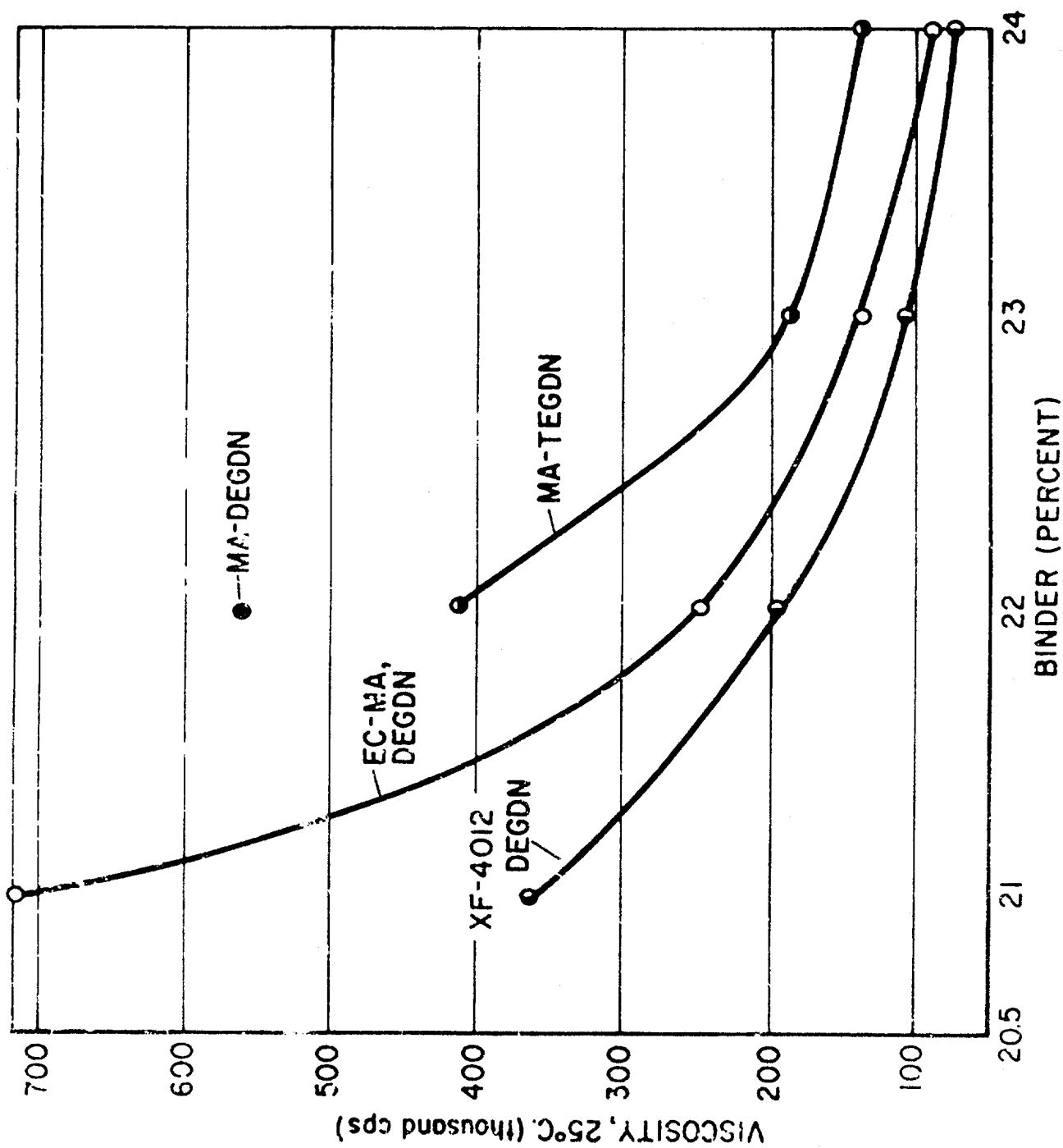


Figure 5. Comparative Effects of Binders on Mix Viscosity (1.815 Mg/ $\text{NaNO}_3$  Ratio, XFS-4008L Resin)



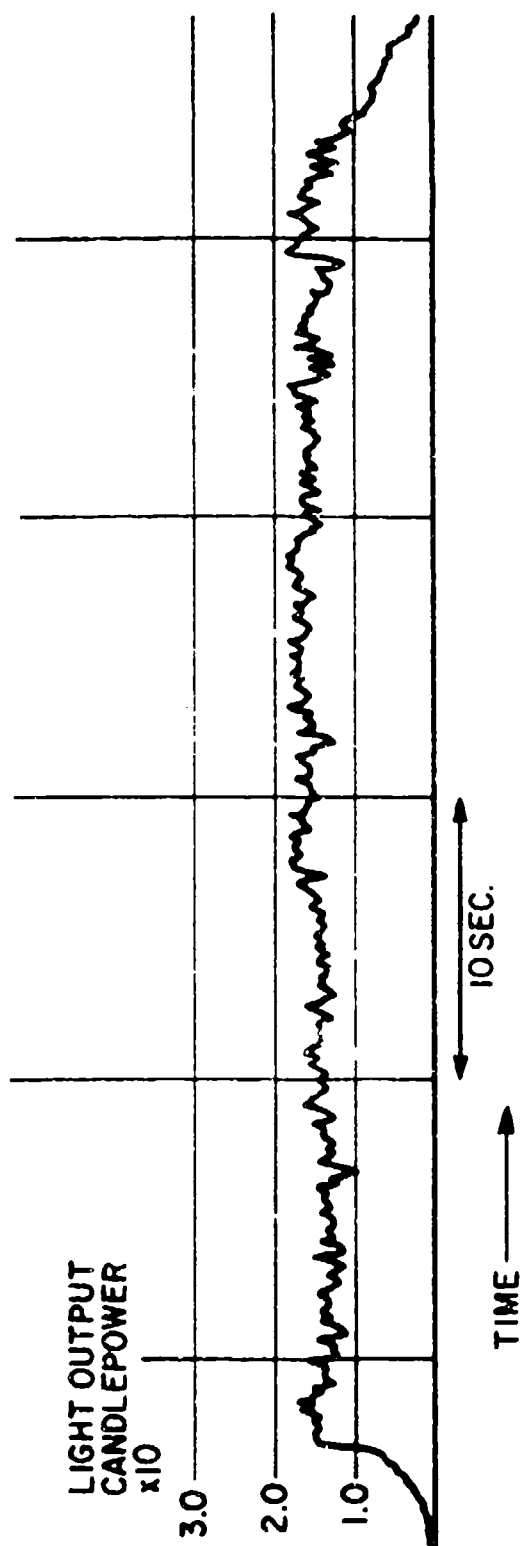


Figure 6. Light Output Trace From Cast Flare Composition  
(2.04 Mg/NaNO<sub>3</sub> Ratio, 22 percent XFS-4008L - EC-NA - DEGDN Binder)

## V. CASE MATERIALS

The cases studied were paper phenolic, cotton phenolic, and fish paper.

### A. PAPER-PHENOLIC CASES - 1.25 INCH DIAMETER

Initial studies were conducted in 1.25 inch diameter paper-phenolic cases to determine the compatibility and case bonding properties of this composition with the case material. As shown in Table X initial tests showed a failure in case-bonding, as indicated by marked increase in combustion rate and reduction in luminous efficiency. Lining paper-phenolic cases with Viton fluoroelastomer lacquer (3,000 to 3,500 cps, solution of acetone and Viton fluoroelastomer) gave enough improvement to warrant an immediate investigation of paper-phenolic cases of 3.4 inch diameter lined with Viton fluoroelastomer.

TABLE X COMBUSTION BEHAVIOR OF CANDLES IN  
PAPER-PHENOLIC TUBES

	Cast Composition <sup>a</sup>		
	1.25 inch Paper-Phenolic		Paper-Tape
	Unlined	Lined With Viton	
Burn Rate in/sec	0.086	0.046	0.055
Efficiency cd-sec/g	24,000	39,200	49,800
Flame	Split	Smooth Straight	Smooth Flared
Chimney	Large	Small	None
<sup>a</sup> 50.29 percent magnesium, 27.71 percent NaNO <sub>3</sub> , 5.96 percent XFS-4008L, 8.04 percent EC-MA, 7.70 percent DEGDN.			

### B. PAPER-PHENOLIC CASES - 3.4 INCH DIAMETER

Initial investigation yielded consistently low luminous efficiencies for 3.4 inch candles in paper-phenolic cases, lined with Viton when fired in either the upright or inverted

position. This was attributed primarily to chimney effects. However, smoke obscuration also was evident in the inverted firings. The data in Table XI indicate good case-bonding with the 0.110 inch wall cases. Attempts were made to overcome the chimney effect and improve luminous efficiency by (1) reducing wall thickness from 0.110 inch to 0.055 inch and (2) using cases with 1/2 inch alternating bands of 0.110 inch and 0.056 inch thickness or 0.077 inch and 0.056 inch thickness. As may be seen in Table XI good case bonding and higher luminous efficiencies were achieved in some tests. However, because the 0.055 inch wall proved unacceptable, and the 0.077 inch wall was unpredictable, further work was done on flare preparation procedures. This showed that modifications in casting and case bonding procedures resulted in acceptable combustion behavior for the 0.110 inch wall 3.4 inch I.D. paper-phenolic cases. These data are shown in Table XII.

Good combustion results were obtained by using a thinner ling of Viton (2,500 to 2,700 cps lacquer viscosity), and by bonding the epoxy-sand plug to the flare base. Efficiencies comparable to the ribbed case and approaching the results with 2 ply paper tape were obtained. This type of case and method of flare preparation were adopted for optimization purposes.

#### C. FISH PAPER AND COTTON-PHENOLIC CASES

Data are presented in Table XIII for 1.75 inch diameter fish-paper cases. The thicker 1/16 inch wall cases give the best results in the inverted position. Flare composition XFS-4008L - EC-MA - DEGDN cast in these Viton lined cases displays a luminous efficiency and burning rate equivalent to the 2 ply paper-tape wrapped case. Interestingly, lining of the fish-paper cases with Viton is detrimental in the thinner 1/32 inch wall cases. This strongly suggests that Viton contributes to case bond failure during functioning in this case. The 1/16 inch wall thickness appears practical for either lined or unlined cases.

Cotton-phenolic cases were tested (0.075 inch wall), and displayed good case-bonding, as indicated by the burning rate, 0.055 in/sec. However, luminous efficiency, 20,000 cd-sec/g, was surprisingly low, considering there was no residual chimney.

Thus, the preferred 1.75 inch diameter case appears to be 1/16 inch wall fish-paper, followed closely by the paper phenolic lined with Viton. Fish-paper cases need to be investigated for 3.4 inch diameter candles. 3.4 Inch (I.D.) paper phenolic cases were selected for studying the large diameter flares.

TABLE XI STUDY OF 3.4 INCH DIAMETER FLARES<sup>a</sup>

Number of Firings	Case	Case Wall inch	Flare Attitude	Burr Rate in/sec	Luminous Efficiency cd-sec/g
2	Viton lined paper phenolic	0.110	Upright	0.057	30,600
2 <sup>b</sup>	Viton lined paper phenolic	0.110	Inverted	0.056	27,800
1	Viton lined paper phenolic	0.077	Inverted	0.063	46,700
1	Viton lined paper phenolic	0.077	Inverted	0.132	27,800
1	Viton lined paper phenolic	0.077	Inverted	0.105	21,800
1	Viton lined paper phenolic	0.077	Inverted	0.106	23,200
2	Viton lined paper phenolic	0.055	Upright	0.122	27,400
2	Viton lined paper phenolic	0.055	Inverted	0.138	24,800
1	Viton lined paper phenolic	0.077-0.056 <sup>c</sup>	Inverted	0.074	45,200
1	Viton lined paper phenolic	0.110-0.056 <sup>c</sup>	Inverted	0.057	43,400
2	2 Ply paper tape	---	Upright	0.052	51,400

<sup>a</sup> Composition 52/26/22 - Mg (40/200 mesh)/NaNO<sub>3</sub>/XFS-4008L - EC-MA- DEGDN.

<sup>b</sup> Flare and case fell during functioning of one flare. Data based on single flare.

<sup>c</sup> Banded case, alternating 1/2 inch segments of different thickness.

TABLE XII EFFECT OF PREPARATION METHOD OF 3.4 INCH DIAMETER FLARES

Composition <sup>a</sup>		Case	Case Wall inch	Viton Lining	Burn Rate in./sec	Luminous Efficiency cd-sec/g
Mg <sup>b</sup>	NaNO <sub>3</sub> Binder <sup>b</sup>					
52	26	22	Unbonded sand plug <sup>c,d</sup>	Heavy <sup>e</sup>	0.056 <sup>a</sup>	27,800 <sup>a</sup>
52	26	22	Bonded sand plug <sup>c</sup>	Thin <sup>f</sup>	0.055 <sup>a</sup>	43,400 <sup>a</sup>
52	28	20	Bonded sand plug <sup>c</sup>	Thin	0.061 <sup>a</sup>	42,600 <sup>a</sup>
50	30	20	Bonded sand plug <sup>c</sup>	Thin	0.059 <sup>a</sup>	45,000 <sup>a</sup>
52	26	22	2 Ply paper tape	--	0.052	51,400

<sup>a</sup>Inverted firings.

<sup>b</sup>XFS-4008L - EC-MA - DEGN.

<sup>c</sup>Paper phenolic case.

<sup>d</sup>Dow Corning release agent between sand plug and flare base.

<sup>e</sup>Significantly thicker than 0.0035 inch.

<sup>f</sup>Measured to be 0.0035 inch thick.

<sup>g</sup>40/200 mesh.

TABLE XIII STUDY OF 1.75 INCH FLARES IN FISH-PAPER CASES<sup>a</sup>

Number of Firings	Case	Wall Thickness inch	Flare Position	Length inch	Density g/cc	Weight g	Burn Rate in/sec	Luminous Efficiency cd-sec/g
4	Fish-Paper Lined w/Viton	1/16	Inverted	3.59	1.63	229.8	0.053	44,000
4	Fish-Paper Lined w/Viton	1/32	Inverted	3.52	1.64	237.4	0.121	25,000
2	Unlined fish-paper	1/16	Inverted	3.78	1.55	231.5	0.064	41,000
1	Unlined fish-paper	1/32	Inverted	2.60	1.57	164.5	0.060	40,700
4	2 ply <sup>b</sup> paper-tape	--	Upright	4.07	1.62	125.9	0.057	41,700

<sup>a</sup> Composition - 52/26/22 - Mg (40/200 mesh)/NaNO<sub>3</sub>/XFS-4008L - EC-MA - DEGDN.

<sup>b</sup> 1.25 Inch diameter.

## VI. LARGE DIAMETER FLARES

The compositions shown in Table XIV result from a composition optimization, conducted in 3.4 inch I.D. paper-phenolic cases lined with Viton and fired in the inverted position.

At the 20 percent binder level about 50 to 52 percent Mg and 28 to 30 percent  $\text{NaNO}_3$  appear to be optimum.

TABLE XIV OPTIMIZATION, CAST CANDLES

Comp. Number	Composition <sup>a</sup>	Viscosity cps 25°C	Burn Rate in/sec	Luminous Efficiency cd-sec/g
1942-112	52/28/20	275,000	0.061	42,600 <sup>b, c</sup>
1942-113	50/30/20	306,000	0.059	45,000 <sup>b, c</sup>
1942-117	48/32/20	537,500	0.057	38,400 <sup>b, c</sup>
1942-109	52/28/20	275,000	0.066	53,000 <sup>d</sup>
1942-110	50/30/20	306,000	0.060	50,800 <sup>d</sup>
1942-117	48/32/20	537,500	0.057	37,800 <sup>d</sup>
Mark 45 Comp.	"		0.055	55,700 <sup>d</sup>
Mark 45 Comp.			0.055	53,200 <sup>d</sup>

<sup>a</sup> Mg/ $\text{NaNO}_3$ /Binder: Magnesium Lot 2097, 40/200 mesh;  $\text{NaNO}_3$  by Mikro-pulverizer, 0.50" MgO and 0.25" Cab-o-sil, un-screened; Binder - 27.1% XPS-4008L, 37.9% EC-MA, 35% DEGDN.

<sup>b</sup> Inverted firing.

<sup>c</sup> 3.4 Inch diameter paper phenolic case.

<sup>d</sup> 1.25 Inch diameter paper tape case.

A 5,000.0 g batch of the 50/30/20 composition of Table XII was prepared to study castability and combustion behavior. It contained the 58.5/22.5/9.0/10.0 blend of magnesium<sup>1</sup>, and the NaNO<sub>3</sub> was freshly screened just prior to use.

A very favorable viscosity was obtained for this mix, 185,000 cps at 25°C. A lower binder level might be achieved, with better performance.

---

<sup>1</sup>See Section VIID, Magnesium Particle Size.



## VII. FLARE PROCESSING

### A. SCALING-UP

Successful scaling-up from 100 g to 400-600 g and then to 5000-8000 g, batches was accomplished. The viscosities obtained in smaller batch sizes were maintained or improved. No mass effect on cure rate or exotherm was noted in the larger scaled-up batches, indicating adequate pot life at ambient temperatures, irrespective of batch size. Thus, production scale operation should present no difficulties.

### B. CURE TEMPERATURE AND VIBRATION EFFECTS ON DENSITY

Because curing at a constant 70°C yielded some variations in flare densities, a study was undertaken to optimize curing conditions. Table XV indicates that density decreases with higher temperature curing. However, maximum density was obtained with an initial low temperature cure, followed by a post cure at 70°C. Presumably this contributes to degassing of the mix. In an effort to eliminate the two-temperature cure cycle, it was found that 1/2 hour exposure of cast flares to mechanical vibration produced similar or increased densities.

TABLE XV EFFECT OF CURING TEMPERATURE ON DENSITY<sup>a</sup>

Composition Number	Curing Temperature °C.	Density g/cc	Burning Rate <sup>b</sup> in/sec	Luminous Efficiency <sup>b</sup> cd-sec/g
1942-92-1	46	1.60	0.061	44,500
1942-92-3	60	1.53	0.064	43,100
1942-92-5	70	1.47	0.072	45,200
1942-95-7	45-70	1.69	0.056	44,800
Mark 45 Composition	70	1.70	0.060	51,200

<sup>a</sup>Composition - 52/26/22 - Magnesium (40/200 mesh)/NaNO<sub>3</sub>/ Binder (XFS-4008L - EC-MA - DEGDN).

<sup>b</sup>1.25 Inch diameter tape-wrapped candles.

### C. SODIUM NITRATE PARTICLE SIZE

To conduct meaningful composition optimization and also achieve minimum binder levels, effective control of castability is necessary. The particle size of  $\text{NaNO}_3$  has the greatest single effect on castability. It was found that screening dried Lee-Attrition milled  $\text{NaNO}_3$  through 400 mesh immediately prior to use consistently produced a low viscosity. It is believed that  $\text{NaNO}_3$  exhibits a great tendency to agglomerate or coalesce on storage, a phenomenon that is aggravated by atmospheric humidity.

It also was discovered that the anti-caking agents  $\text{MgO}$  and Cab-o-sil minimize the rate and extent of coalescence during storage. Therefore, all  $\text{NaNO}_3$  used in this program contained 0.5 percent  $\text{MgO}$  and 0.25 percent Cab-o-sil.

#### 1. Mikro-Pulverizer "Grinder"

Screening through 400 mesh is tedious and inefficient, and probably is unacceptable for large scale processing. Attempts proved successful to substitute a production type grinder, the "Mikro-Pulverizer," for the preparation of acceptably fine  $\text{NaNO}_3$ . Table XVI shows that while compositions employing unscreened  $\text{NaNO}_3$  (Mikro pulverizer) may be slightly less efficient, burning rate and castability are favorably affected. Screening through 400 mesh appears unnecessary. Anti-caking agents may be added prior to or after grinding. Figure 7 is a photomicrograph of the  $\text{NaNO}_3$  powder. Particles of  $\text{NaNO}_3$  range from approximate 1 micron to 80 microns, where greater than 50 percent by weight are larger than 25 microns, only about 1.0 percent are less than 5 microns, and only about 1.0 percent are larger than 50 microns.

#### 2. Wetting Agents

Because reagglomeration of the finely divided  $\text{NaNO}_3$  occurs upon addition to hydrophobic binder systems, prewetting with surfactants was investigated for possible further reduction in binder levels. Prewetting  $\text{NaNO}_3$  with non-ionic Tergitol E-35 proved most efficient, followed closely by non-ionic Dow surfactant 9N4. However, at surfactant/ $\text{NaNO}_3$  concentrations of 10-15 percent, the quantity necessary for thoroughly wetting  $\text{NaNO}_3$ , there was evidence of incompatibility. Subsequent studies revealed that only 0.5 percent added to the binder reduced viscosity and improved castability consistently and effectively (Table XVII).

TABLE XVI PROCESSING  $\text{NaNO}_3$ 

Composition A - 50.29/27.71/22.0 - $\text{Mg}^a/\text{NaNO}_3/\text{XFS-4008L}$ - EC-MA - DEGDN						
Batch Number	$\text{NaNO}_3$ Type	Batch Size g	Brookfield Viscosity cps	Luminous Efficiency cd-sec/g	Burning Rate in/sec	
1942-86	Lee-Attrition (<400 mesh)	500	460,000	39,200	0.056	
1942-89	Lee-Attrition (unscreened)	500	430,000	37,700	0.056	
1942-87	"Mikro-Pulverizer" 0.032" round hole screen (unscreened)	800	420,000	36,500	0.065	
1942-91	"Mikro-Pulverizer" 0.020" HB x 3/64B (unscreened)	800	180,000	36,600	0.062	
Composition B - 52/26/22 - $\text{Mg}/\text{NaNO}_3/\text{XFS-4008L}$ - EC-MA - DEGDN						
1942-92	"Mikro-Pulverizer" 0.020" HB x 3/64B	800	290,000	38,200	0.066	
1942-95	"Mikro-Pulverizer" 0.020" HB x 3/64B	8000	200,000	38,600	0.056	
<sup>a</sup> 40/200 mesh.						
<sup>b</sup> 1 1/4 inch diameter tape-wrapped candles.						

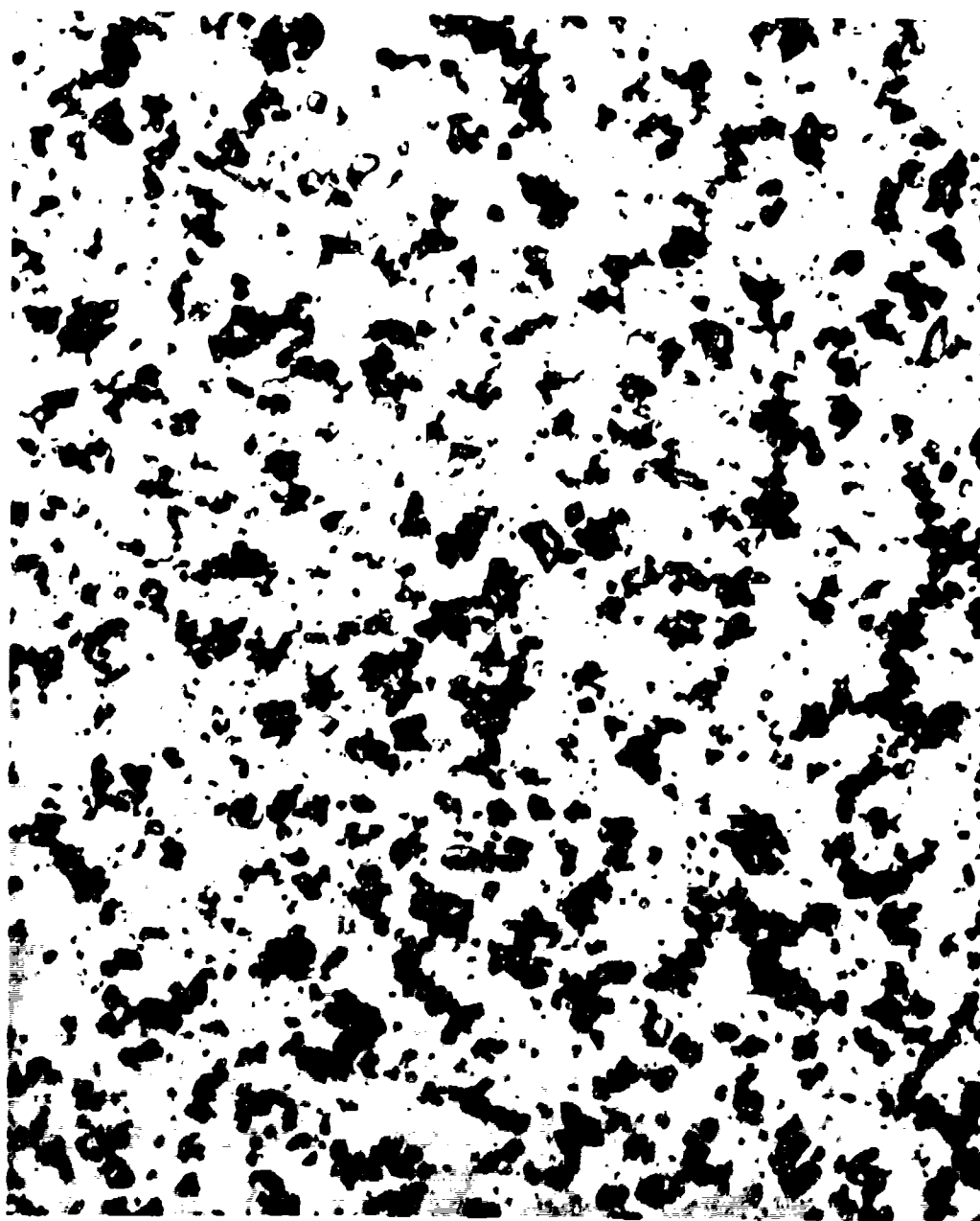


Figure 7 Photomicrograph of Sodium Nitrate - 350X

TABLE XVII SURFACTANT CONCENTRATION EFFECTS<sup>a</sup>

Viscosity, cps	Tergitol E-35, %
240,000	0.0
173,000	0.25
145,000	0.50
130,000	0.75
115,000	1.00
<sup>a</sup> 50% Mg (40/200 mesh), 30% NaNO <sub>3</sub> , 20% XFS-4008L - EC-MA - DEGDN binder.	

#### D. MAGNESIUM PARTICLE SIZE

Particle size variations in commercially available atomized magnesium are common. Earlier studies indicated that an excess of material finer than 100 mesh is undesirable and leads to high viscosity and poor castability at the desired low binder levels. It is believed that if the 40/200 grade magnesium contains about 10-15 percent -100 mesh material, maximum efficiency and minimum viscosity are possible. Table XVIII shows a screen analysis and resulting comparative viscosities of the five lots of 40/200 magnesium used in this research.

Lots V05-70 and V12-70 were used before the work began on 3.4 inch candles, and the other lots were used after this point. Figure 8 is a photomicrograph of the Lot V05-70 material. Both the coarser 34273 and finer 033992 lots lead to high mix viscosities. Because 2097 was in short supply, a study was undertaken to determine the most efficient magnesium particle size distribution for maximum castability by blending the above three lots. Furthermore, because 033992 contained a broad distribution, it was separated into +100 and -100 mesh fractions to study particle size effects more easily.

TABLE XVIII MAGNESIUM PARTICLE SIZE DISTRIBUTION

Mesh No. on	Lot No. V05-70	Lot No. V12-70	Lot No. 2097	Lot No. 033992	Lot No. 034273
60	17.8	23.1	31.1	15.1	50.2
80	49.4	67.2	24.6	31.1	38.3
100	28.8	8.9	32.2	11.6	6.5
140	3.6	0.7	4.3	23.0	4.4
200	--	--	4.0	16.8	0.3
230	--	--	3.0	1.5	0.1
Pan	0.4	0.1	2.0	--	0.1
Viscosity cps	--	--	306,300	>1,000,000	750,000
50/30/20 Mg/NaNO <sub>3</sub> /binder (XFS-4008L - EC-MA - DEGDN).					

The most efficient combination was a 50/50 blend of 2097 and +100 mesh 033992. However, the quantity of 2097 available was insufficient to complete the project. It was found that a 65/25/10 ratio of +100 mesh 033992/2097/034273 produces a viscosity of 175,000 cps at 25°C, in a 50/30/20 - Mg/NaNO<sub>3</sub>/binder composition.

An attempt was made to increase the burning rate by adding 10 percent magnesium fines (-100 mesh 033992). Data presented in Table XIX show the significant effect of this particle size distribution.

Figure 9 shows the comparative particle size distribution of Lot 2097, the blend which gave minimum viscosity, and the blend shown in Table XIX.

On basis of these studies it was decided to use the 58.5/22.5/9.0/10.0/magnesium blend and freshly screened Mikro-pulverized NaNO<sub>3</sub> for the preparation of 3.4 inch candles for comparison with Mark 24 flare candles.

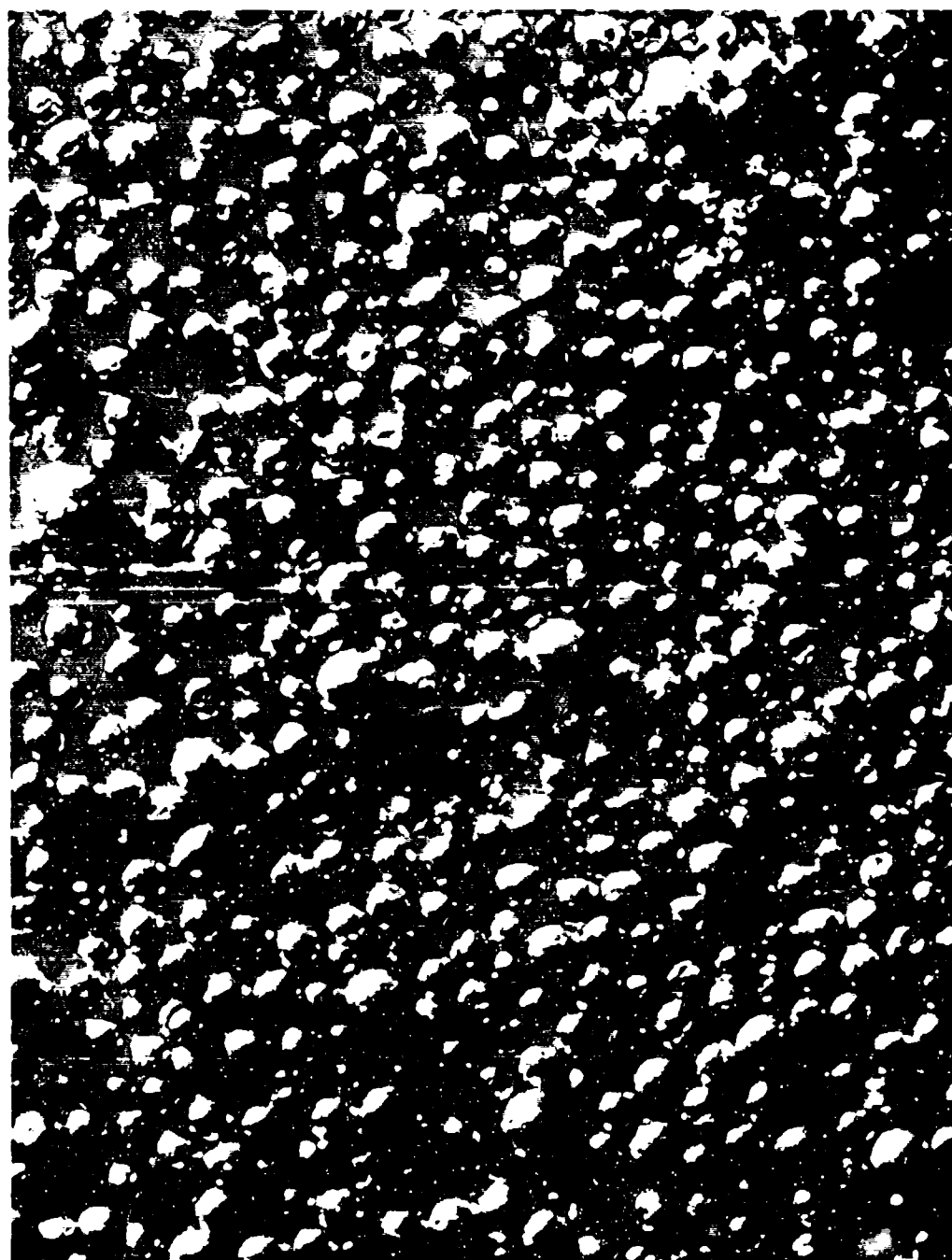


Figure 8 Photomicrograph of 40/200 Magnesium - 45.6X

TABLE XIX EFFECTS OF MAGNESIUM PARTICLE SIZE DISTRIBUTION

	Lot 2097	Blend
50% Magnesium	100%	58.5%, 033992, +100 mesh 22.5%, 2097 9.0%, 034273 10.0%, 033992, -100 mesh
30% NaNO <sub>3</sub>	"Mikro-Pulverizer"	"Mikro-pulverizer" freshly screened
20% Binder (XFS-4008L, EC-MA, DEGDN)	Same	Same
Viscosity, 25°C cps	306,000	185,000



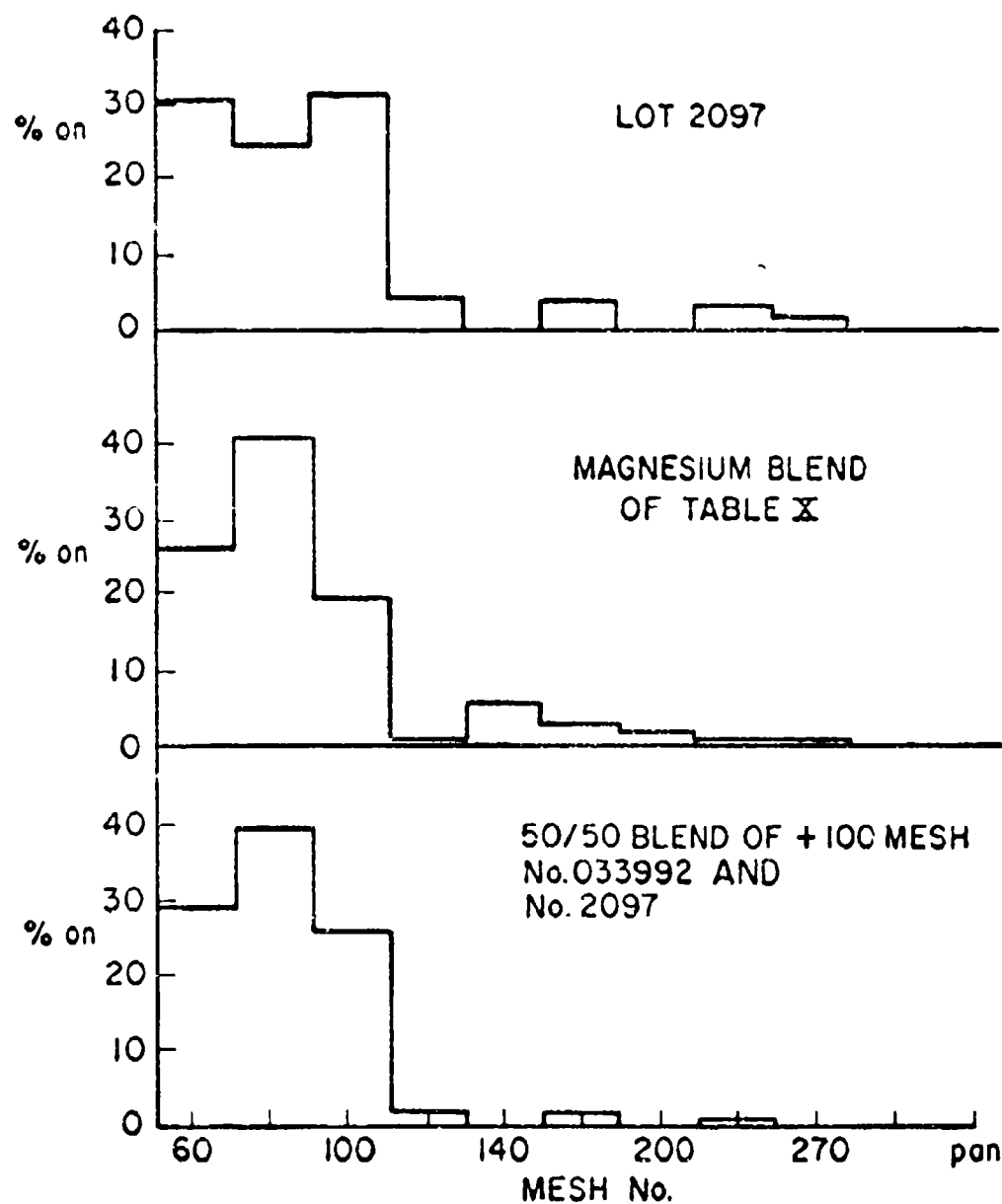


Figure 9 Particle Size Distribution of Magnesium Powders

## VIII. STANDARD FLARES

Throughout these studies flares containing standard pressed compositions were fired in order to have a basis for comparison. For the 1 1/4 inch diameter cast flares, 1 1/4 inch pressed flares containing the composition used in Mark 45 candles were used. For the 3.4 inch flares, Mark 24 candles, obtained from Eglin Air Force Base, were employed.

### A. MARK 45 COMPOSITION FIRINGS

About 100 standardized pressed 1.25-inch diameter candles containing Mark 45 composition were fired at frequent intervals in conjunction with firings of developmental flares. These candles, wrapped with a 4-ply tape case, consistently gave about 60,000 cd-sec/g average efficiency. A group of these flares with 2-ply taped cases gave an average efficiency of 75,000 cd-sec/g.

### B. MARK 24 CANDLES

Mark 24 candles received from Eglin Air Force Base were functioned for purposes of comparison with the best cast flares. Most of these candles were fired in the inverted position. Several of the Mark 24's burned significantly faster than the nominal burning time of  $180 \pm 10$  sec. Most of them broke up and fell to the floor near the end of functioning, the faster-burning ones sooner. Table XX shows the results on these Mark 24 candles, along with comparative data on the 3.4 inch cast candles.

The average efficiency of all the Mark 24 candles fired was 27,900 cd-sec/g. If only those with burning times of 170 sec or greater are selected, the average is 29,100 cd-sec/g. The average of the latter group is 30,000 cd-sec/g for inverted firings and 27,400 cd-sec/g for upright attitude, not a meaningful difference. In some firings smoke obscuration was evident. Because of the higher burning rate and greater diameter of the Mark 24 candles, it would be expected that smoke problems would be more severe than for the 3.4 inch cast flares.

The average efficiency for the cast candles was 40,650 cd-sec/g, 43,400 cd-sec/g for the inverted firings. The average burning rate is 0.057 in/sec.

TABLE XX MARK 24<sup>a</sup> AND CAST<sup>b</sup> CANDLES: COMPARATIVE FIRINGS

Candle	Burning		Efficiency cd-sec/g	Attitude
	Time, sec	Rate, ips		
Mark 24	177	0.090	32,000	Inverted
Mark 24	187	0.085	28,800	Inverted
Mark 24	180	0.089	27,700	Inverted
Mark 24	176	0.091	27,000	Inverted
Mark 24	152	0.105	25,000	Inverted
Cast, 80-1	82	0.057	42,800	Inverted
Mark 24	157	0.102	27,000	Inverted
Cast, 80-2	80	0.059	43,800	Inverted
Mark 24	197	0.082	34,000	Inverted
Cast, 80-3	84	0.056	43,600	Inverted
Mark 24	147	0.109	23,900	Inverted
Mark 24	187	0.086	29,900	Upright
Cast, 80-4	90	0.056	32,400	Upright
Mark 24	174	0.092	24,500	Upright
Mark 24	182	0.080	27,900	Upright
Mark 24	192	0.080	30,300	Inverted
Mark 24	158	0.101	24,100	Inverted
<sup>a</sup> 4.25 Inch diameter, cardboard case. <sup>b</sup> 3.4 Inch diameter, paper phenolic case.				

## IX. CONCLUSIONS

The cast candles in 3.4 inch paper phenolic cases give very promising performance. They are at least equal in efficiency to the Mark 24 candles tested, although it is felt the latter suffered from poor reproducibility, case bond failure, and tunnel smoke problems. In 1.25 inch taped cases, the cast composition is nearly equivalent to the Mark 45 composition.

Two polyester binders studied during this program merit further effort. A minimum of work was done on ADGC and ADGC with M/ or EC-MA. This research should be carried forward. Compositions based on Tex-R-1939 appear very desirable. This type of composition should be scaled to 3.4 inch candles and the composition optimized.

Because of the promise of these formulations, and the advantages of forming flare candles by casting, flow cast compositions should be considered for new flare items and as an alternate in current illumination devices.

USE OF PROPELLANT GAS GENERATORS FOR THE  
EMPTYING OF CAPACITIES AT GREAT DIVING DEPTHS

J. DELGENDRE and D. KURTZEMANN

DIRECTION TECHNIQUE DES CONSTRUCTIONS NAVALES

Groupe d'Etudes et Recherches de Pyrotechnie

Summary : While studying the most efficient method of emptying the ballast tanks of submarines, the engineers of G.E.R.Py have been able to show the interest of using gas generators running on solid propellant which will be seven times less heavy than all the equivalent compressed-air installations.

The object of this paper is to describe the experimental methods employed in this development :

- Use of the Mach similarity where speed and pressure are maintained
- Trials at sea at scale I confirming the results obtained on a model and proving the efficiency of the system at great depths.

Besides displacing water from ballast tanks, these generators would find their use in refloating operations and in operating autonomous underwater devices.

Studies on these lines are being pursued.

-----  
INTRODUCTION-

The recent loss of two of our submarines has shown all the interest of operating a rapid lightening of the submarine by the flushing out of ballast at her diving depth. The current compressed-air installation however does the water expelling not under one minute at a depth of 40 meters only, while at greater depths the equipment is ineffective. In order to reduce this delay, several solutions have been proposed :

- To increase the compressed-air output by increasing the module of the pipes and cocks,
- to use gas generators running on propellant.

The latter solution will be studied in the present article. It will

.../...

be shown that besides the advantage of rapid water expelling, weight and dimensions of the installation are considerably reduced. On the other hand, current developments in oceanography and undersea operations have increased the demand for a simple lightweight autonomous device able to assist in gathering objects at great depths.

We cannot affirm, of course, that the study presented is of an absolute novelty in all its aspects, but

no information whatever concerning any precedence has been received by the authors.

## 2. Advantage of Gas Generators running on Solid Propellant-

### 2.1 - Comparison of the potential energy of propellant and compressed air-

When comparing the potential energy of propellant with the potential energy of compressed air at various pressures, we get the following results :

1 gram of compressed air at 250 bars (expansion up to 1 bar)	700 joules
1 gram of compressed air at 500 bars	890 joules
1 gram of current propellant	3240 joules

Even when accounting for the attenuation of thermal energy due to Carnot's law, the potential energy of propellant available for use exceeds by far the potential energy of compressed air, and that at a ratio varying from 2 to 5.

### 2.2.- Comparison of volumes and weights-

The higher density of current propellant presents another advantage :

- 1 gram of propellant is occupying a space of  $0,58 \text{ cm}^3$
- 1 gram of compressed air at 250 bars is occupying a space of  $3,7 \text{ cm}^3$

It is not easy of course to assess the exact data for vessels and accessories, but an overall evaluation of several cases has shown that an installation running on propellant

.../...

- weighs seven times less than an equivalent compressed-air installation
- is occupying a space reduced to a tenth of the space occupied by the compressed-air installation.

### 2.3.- Use of compressed-air installations is limited by depth-

In the most favourable case, i.e. when the compressed-air bottles are submitted to Archimedes' Law,

the whole system of water expelling by compressed air has to be considered as totally ineffective when the apparent weight in water of the expelling device exceeds the buoyancy of the expelled water volume. This absolute limit to the use of compressed air appears at a certain depth, i.e. at 2000 m, considering the current technology of compressed-air bottles.

This statement has however only theoretical value as it is practically impossible to use bottles loaded at more than 250 bars (the bottles are loaded at shallow depths).

On the other hand, there are some types of propellant with an r.m.s. pressure of 500 to 600 bars; they would be effectively used with a back-pressure of 250 to 300 bars. We may be justified in supposing that from a depth of 1000 meter downward propellant will have to replace compressed air.

### 2.4.- Comparison of the output-

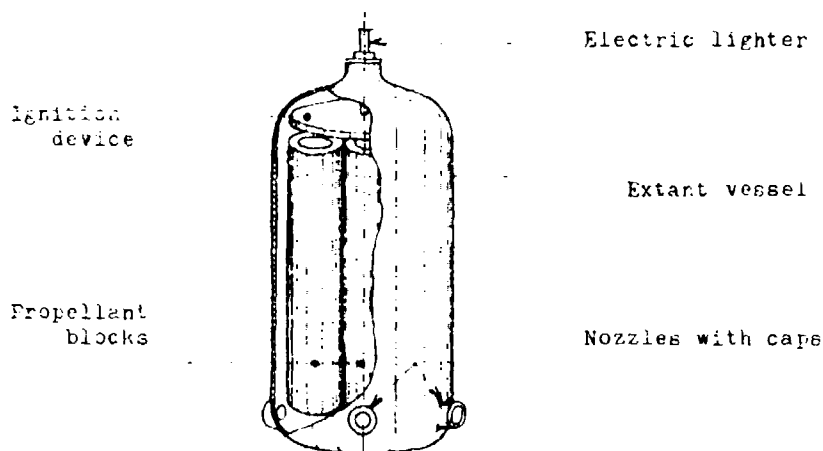
The speed of water displacement by propellant generators may be ten times the speed attained by standard compressed-air installations. It would indeed be possible to accelerate the output of compressed air by increasing the module of the pipes and cocks, but not without increasing also their weight. The ratio of 7 (paragr. 2.2) comparing the weights of the installations would be largely exceeded.

.../...

### 3.- Principle and Basic Formulae-

#### 3.1- Functioning of the generator-

The generator consists essentially of a combustion chamber fitted with one or more blocks of solid propellant and an electric ignition device. The gas is evacuated through nozzles with caps, two of them placed opposite the other two in order to eliminate thrust. A patent has been taken out for this device under Nr. 175 279 on November 26, 1968.



The combustion laws being already established for jet propulsion, we are recalling the essential elements as follows :

The combustion speed  $v$  of propellant is an increasing function of the pressure  $p$  in the combustion chamber; the formulae are varying with the propellant type, and are written :

$$v = ap^n \quad (1)$$

$$0,015 < a < 0,40$$

$$0,40 < n < 0,85$$

The mass output of the gases is a product of  $v$  by the combustion surface  $S$  and the density of the propellant.

When the pressure  $p$  exceeds the critical pressure caused by the sonic flow of the gases through the nozzle necks with the section  $s$ , the maintaining of the output yields the

.../...



following equation for the internal pressure of the combustion  
chambre :

$$p = K \left( \frac{S}{s} \right)^{\frac{1}{1-n}} \quad (2)$$

K being a function of the nature of the gas, in this case of the  
propellant.

The internal chambre pressure will only be stabilized when  $n < 1$ .

It will be found that by varying the ratio  $S/s$ ,

, it is possible to adjust the chambre pressure,  
the combustion speed and, accordingly, the displaced water output.  
Within the limits of de Barré de St. Venant's hypothesis which  
supposes the gas flow to be isentropic, and in the case of the  
chambre pressure exceeding the critical pressure which is nearly  
twice as high as the downward pressure, the downward pressure has  
no effect on the chambre pressure.

Features of a gas generator :

- Mass gas output which will remain constant when the combustion  
surface remains constant. (This case will be discussed in the  
present article).
- The quantity of propellant fitted into the vessel,
- and the running time of the generator depending on this quantity.
- The manner how the gases are bubbling in the water must also be  
taken into account, this being a decisive factor for the final  
gas temperature in the ballast.

### 3.2.- Near relations between the generator data and the ballast data-

The ballast structure will tolerate a limited overpressure which  
determines the maximum output flowing through the filling apertures  
and also the output of one or more gas generators. There will have  
to be established a formula presenting the mass output of gas  
produced as a function of the hydrostatic pressure at diving depth

.../...

and specifying the maximum overpressure to be tolerated in the ballast as well as height and filling section of the ballast. The weight of propellant and the running time of one or more generators are a function of the ballast volume.

Mass output of gases :

- E      Filling section where water is evacuated
- P      Hydrostatic pressure at E level
- $\Delta P$     Overpressure in ballast as compared with P
- $z_0$     Height of ballast
- z      Displaced water level at instant t
- q      mass output of propellant
- $\alpha$       Striction coefficient of the aperture E
- $\gamma$       Adiabatic gas constant
- V      Specific volume of released gases
- K      Dimensioned constant entering into the relation of adiabatic gases.

This constant will be defined experimentally using the simplifying hypothesis that the thermal exchanges gas-water at the instant of displacement are independent of  $(P + \Delta P)$ .

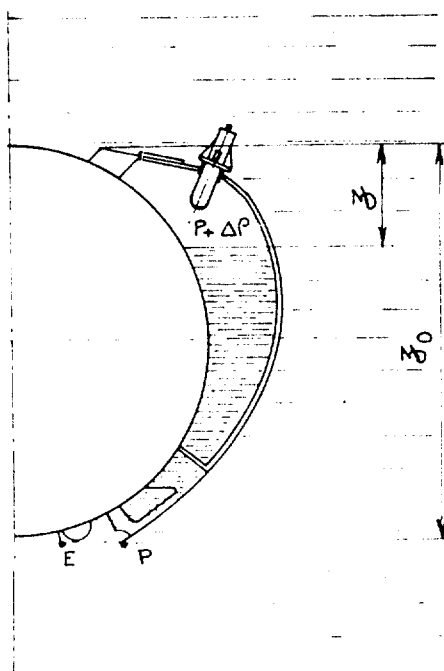


Figure 2

.../...

When writing the formula for the maintaining of flow, we extract :

$$q = \left( \frac{P + \Delta P}{k} \right)^{\frac{1}{2}} \propto E \left[ \frac{2}{p} \Delta P + pg(z_0 - z) \right]^{\frac{1}{2}} \quad (3)$$

Supposing the output to be constant, we find a maximum  $\Delta P$  when  $z = z_0$ , i.e., at the end of the flushing out; the admissible maximum output for the ballast will be :

$$q_{\max} = \left[ \frac{P + \Delta P_{\lim}}{K} \right]^{\frac{1}{2}} \propto E \left[ \frac{2}{p} \Delta P_{\lim} \right]^{\frac{1}{2}} \quad (4)$$

where  $\Delta P_{\lim}$  is the overpressure limit in the ballast.

Fig. 3 shows  $q$  as a function of  $P$  et  $\Delta P_{\lim}$ ,  $K$  having been determined experimentally during two trials at depths of 36 m and 200 m.

Figure 3

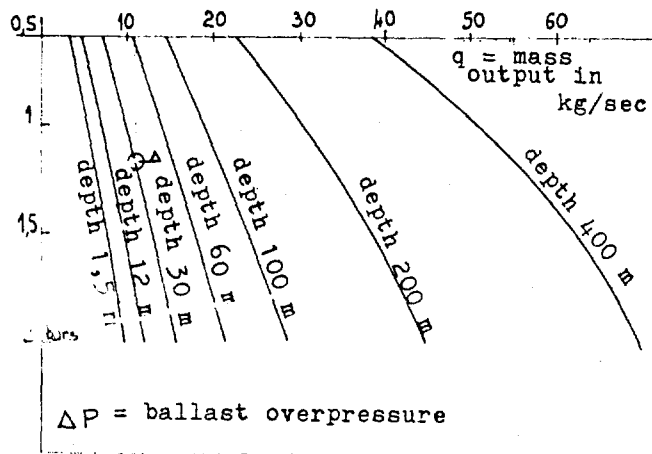
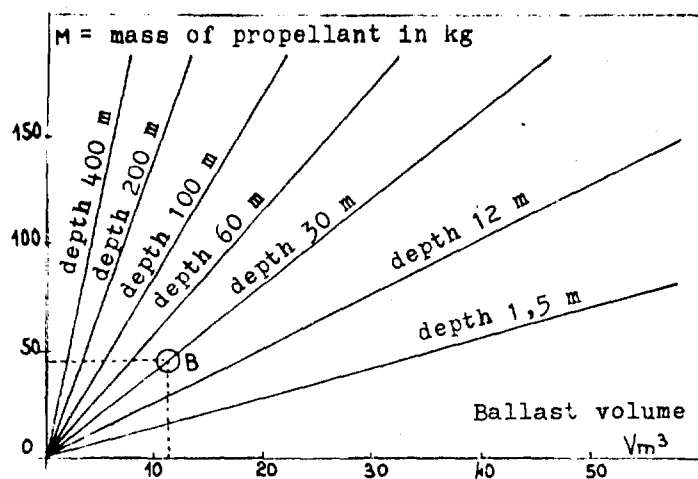


Fig. 4 shows the quantity of propellant  $Q$  as a function of the ballast volume to be expelled and as a function of depth, using the formula  $(P + \Delta P) = K$ .

It will not do however to consider only the stress by overpressure the ballast has to undergo, the stress by depression has also to be taken into account. When the water has been displaced at great speed, there will succeed to a phase of overpressure in the ballast a phase of depression, the gas capacity going into a

.../...

pulsation movement similar to an undersea explosion.



Let us view the simple case of a spheric gas bubble with the radius  $r$  expanding in water, the internal pressure of this bubble being  $\pi$  and the hydrostatic pressure  $P$ .

By writing that the variation of kinetic energy of water per time unit is equal to the pressure stress during the same period, we have the relation

$$\pi - P = \frac{1}{2a^2} \frac{d}{dt} (a^3 \dot{a}^2) \quad (5)$$

During an underwater explosion the internal pressure of the sphere may decrease to some hundredth only of  $P$ .

The expansion of gases due to the expelling of water from the ballast will be of course be more gentle than the expansion due to an underwater explosion. But by neglecting viscosity and by establishing that the live forces working in a particle of expelled water are equal to the stress of pressure forces, we find that to the maximum particle speed of 10 m/s corresponds to a depression of the order of 0.5 bar at the end of the gas expansion. A cylindrical ballast designed for overpressure might well be buckling under these conditions.

.../...

Finally we may note another dynamic effect water is having on the ballast and by which we may benefit : that is to say a dynamic lightening of the ballast during the flushing-out; a fact which is illustrated by the design of fig. 5 :

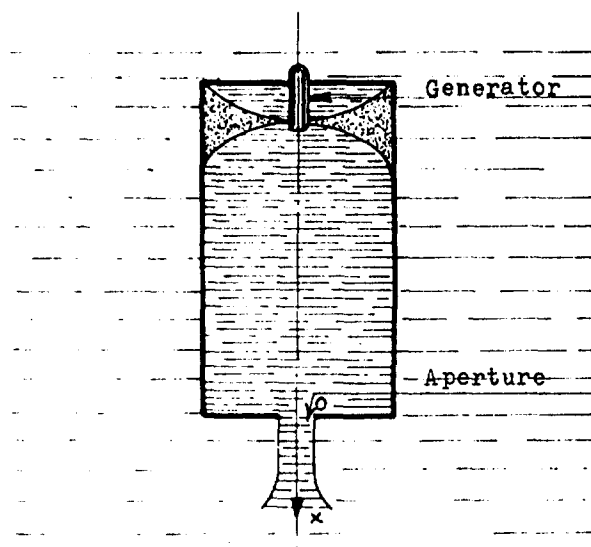


Figure 5

The water will be flowing at the average speed  $V$  through the aperture  $O$  with an output  $M$ . The force operating on the ballast is equal to the quantity of the fluid movement  $MV$  flowing through  $O$ , in whatever direction the generator nozzles may point. In paragraph 5,2 it will be shown that during a special trial this dynamic thrust has amounted to 2,2 tons during 2,3 seconds while the static thrust amounted to 4,7 tons at the end of this flushing-out period. These two thrusts combined would result in a take-off effect very useful in refloating operations.

The same would be true for a water displacement by compressed air if it could be done at the same speed.

#### 4.-Opportuneness of the Use of Similarity in Experimentation-

Trials at sea being expensive and dependent on weather conditions, it has been tried to reproduce a similarity of the functioning of the generator, of the hydrodynamic conditions and of the bearing up under stress of the ballast.

It has been well established that the Mach similarity, maintaining the pressure and accordingly stress and speed (the time scale remains in accordance with the scale of dimensions), may be applied to the elastic deformation of statically charged structures.

In the case of dynamic charges, we can write the dimensional matrix of the system and determine the number of dimensionless terms .

If the determinant variables are :

L	characteristic length of the structure
M	mass of a particle having made contact with the structure
V	particle speed
E	modulus of elasticity
$\gamma$	Poisson coefficient
$\rho$	specific mass of the structure
n	maximum stress brought to bear upon all points of the structure,

the resolution of the linear and homogeneous equations of the system yields the following dimensionless terms :

$$\frac{nL^3}{MV^2}, \frac{EL^3}{MV^2} / \frac{MV}{\rho L^3}$$

If the metal of the mock-up is identical with that of the model, the similarity coefficients  $K_E$ ,  $K_V$ ,  $K_p$  are equal to unity; what is called similarity coefficient or scale  $K_E$  is the relation existing between E as defined by its relation to the mock-up, and E as defined by its relation to the model. The same applies to

.../...

$K_V, K_P, K_M, K_L, K_n$ . When writing the conservation of the dimensionless numbers, we have :

$$K_M = K_L^3$$

$$K_V = 1$$

$$K_n = 1$$

that is to say that model and mock-up will have to undergo the same stress when similar particles are striking the structure at the same speed. If the damage is due to stress, mock-up and model will be subjected to the same deformation.

Plastic deformations however are not due to stress. Indeed, for the same resulting plastic deformation, the stress may depend on the path that has been followed; the similarity may be only approximate<sup>1)</sup>; but the aim is always not to warp the structure when flushing out the ballast. It is therefore sufficient to keep in mind that if the mock-up has been damaged in the plastic domain, the model will have been damaged in the same domain, i.e. the processus of flushing-out has been too rough.

4.2.- Let us now try to apply the Mach similarity to the aqueous element and there to the speed necessary for a rapid flushing out of the ballast.

The classic similarity of the flow of incompressible fluids preserves the Reynold number; which number, however, is not an invariable in the Mach similarity.

We shall now consider the movement of some water particle with the mass  $m$ , which is defined by the fundamental principle of dynamics

$$F - m\gamma = 0$$

where  $m\gamma$  is the inertial force of the particle.

$F$  represents the entirety of the exterior forces brought to bear

-----  
 1) It is interesting to notice that with the help of simplifying calculations it has been possible to establish a mach similarity of deformation in the plastic domain, a theory which has been confirmed by numerous experiments (resistance to underwater explosions, buckling of structures struck by targets). .../...

upon the particle : an overall pressure force composed of static pressure, dynamic pressure and viscosity forces.

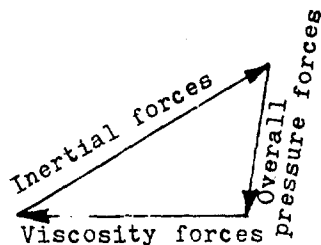


Fig. 6

In order that the particles of the two flows may execute a similar movement maintaining their speed while hitting a solid obstacle, the triangles formed by the three acting forces must be identical.

The overall pressure of the two flows is maintained in Mach similarity. For two similar sections which are in the ratio of the square of the dimensions, the overall pressure forces will be in the ratio of the square of the dimensions. Per unit of volume these forces will be in the inverse ratio of the dimensions.

The inertial forces of the particles in the two flows in Mach similarity are in the ratio of the square of the dimensions ( $m$  is in the ratio of the cube of the dimensions, the ratio of the accelerations is the inverse of the ratio of the dimension). Per unit of volume, the inertial forces (with a component

$$\rho \frac{du}{dt} = \rho u \frac{\partial u}{\partial t} + \rho w \frac{\partial v}{\partial t}$$

$u$  being the speed according to  $Ox$ ), are proportional to  $\rho V^2/D$ , they are therefore in the inverse ratio of the dimensions.

The forces of viscosity per unit of volume (with a component  $\mu \partial^2 u / \partial x^2 + \dots$ ,  $\mu$  being the dynamic viscosity), are proportional to  $V/D^2$ ; contrary to the aforementioned forces they are varying with the inverse square of the dimensions.

.../...



It will be shown that in the case of a rapid flushing-out of the ballast the viscosity forces are negligible with respect to the inertial forces.

The ratio of the inertial forces to the viscosity forces is as follows :

$$\frac{\frac{\rho V^2}{D}}{\mu \frac{V}{D^2}} = \frac{\rho V D}{\mu}$$

This ratio is none other than Reynold's number. If the particular speed is near 10 m/s, the principal dimension being evaluated as 1 m, we have :

$$\rho = 10^3 \text{ kg/m}^3$$

$$V = 10 \text{ m/s}$$

$$D = 1 \text{ m}$$

$$\mu = 102,6 \text{ kg/s/m}^2$$

$$\frac{\rho V D}{\mu} = 10^2$$

The inertial forces are therefore one hundred times more powerful than the viscosity forces which latter may be neglected, the more so when the structure is of a large size.

The force applied to a particle has therefore only two components

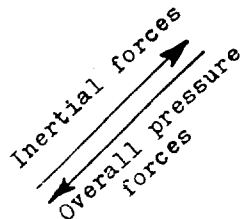


Fig. 7

These forces are in accordance with the Mach similarity (where pressure and speed are maintained). If the flushing-out is done on a mock-up, the particles will have the same dynamic pressure and the same speed as those in a model, on condition that the time scale remain in accordance with the scale of dimensions. As a rule, depth must be maintained at Mach similarity.

.../...

When the mock-up is on a scale  $N$  times reduced, the expelling generator will have to function with a speed  $N$  times increased, the output being diminished by  $N^3/N = N^2$  concerning the mock-up. The flow speed of the water flowing through a similar aperture is however maintained.

#### 4.3- Similarity of gas generators-

The receiving and transmitting elements of energy being in accordance with the Mach similarity, the generators will have to be designed for the same conditions.

Without going into details or applying the theory of mock-ups to gas generators, it will be immediately seen that running on the same propellant, the functioning (1) and (2) is in accordance with the Mach similarity.

The generators being geometrically similar and running on the same propellant, the internal chamber pressure and the combustion speed will be approximately the same. The gases having sufficiently cooled down by bubbling in the water they will occupy a volume proportional to the cube of the dimension when the depth is maintained. The density of the propellant being in the ratio of the dimensions, the combustion time is in the same ratio. With gas generators which are geometrically similar, the time scale is in near accordance with the scale of dimensions, - we may therefore apply the Mach similarity with a good approximation.

#### 5. EXPERIMENTATION-

The development of water expelling generators, their fitting into the ballast, and the choice of filling apertures have been a matter of trial.

##### 5.1.- Trials in similarity-

5.1.1.- In order to develop a generator running on 25 gr of propellant, to study the water flow as a function of the generator

.../...

position in the capacity to be flushed out, the direction in which to place the nozzles, the form of the filling aperture, the measurement of overpressure and water temperature, - we have proceeded in the following manner :

A glass bell holding 20 litres has been immersed in a water tank with side windows; the flushing-out has been filmed externally with a fast motion camera. The expelling time has been of the order of 350 ms, the maximum volume of displaced water being 19 litres at a depth of 1,7 m. The internal overpressure of the bell remained under 1 bar. Figure 8 represents three frames of a film sequence :



Frame N°78  
t = 26 ms  
2 jets hit the  
wall of the bell



Frame N°376  
t = 225 ms  
a liquid dihedron  
is persisting in  
the centre of the  
bell



Frame N°981  
t = 330 ms  
end of the  
flushing-out  
process

Fig. 8 - Filming at 3000 frames per second

5.12.- The ultimate aim of the trials being the flushing-out of a submarine ballast tank, a mock-up on the scale of 1:10 has been designed (fig.9). The flushing-out has been filmed in the same manner as described above, and the internal overpressure of the ballast has been recorded in order to assess the efficiency of the system and to evaluate the shortest possible time in which to accomplish the flushing-out without damaging the ballast structure.

.../...

With 20 gr of propellant 11,6 litres have been expelled in 350 ms at a depth of 1,7 m. Maximum overpressure : 1,8 bar.

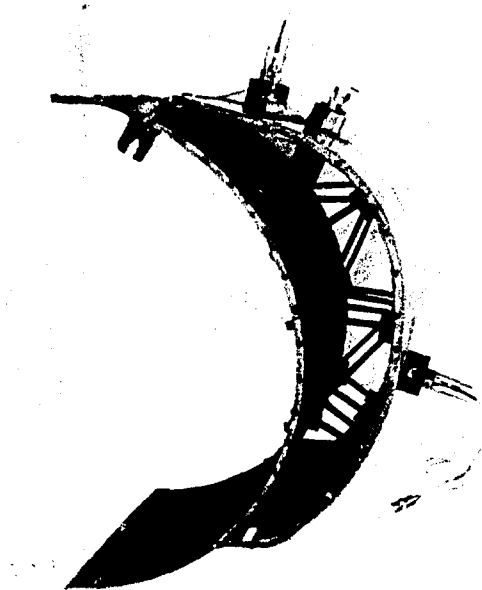


Fig. 9 - Mock-up of a ballast fitted with sensors the faces being of plexiglass.

#### 5.2.- Trials with ballast tanks of 3 m<sup>3</sup> and 6 m<sup>3</sup>-

In a first trial we have compared a flushing-out with compressed air and with propellant: a cylindrical ballast has been fixed on a concrete block of 35 t on the bottom at a depth of 35 m (fig.10). The results obtained are :

- 4820 litres have been expelled in 48 sec. with a standard compressed-air installation
  - 2000 litres have been expelled in 1 s with 9 kg of propellant
  - 4000 litres have been expelled in 1 s with 18 kg of propellant, the ballast gates, having slightly buckled towards the interior.
- The temperature was stabilized at 27°C.

The following trials have allowed to evaluate the efficiency

.../...



Figure 10 - Ballast at a depth of 35 ■

of generators running on 25 and 35 kg of propellant at ever increasing depths.

A cylindrical ballast fitted with a generator and weighted with an anchor of 5 to 7 tons has been immersed in the coastal waters off Toulon. The device was suspended from the gaffs of a pram which was set adrift, or, in bad weather, anchored by the stern. The functioning of the generator was checked by immersed probes containing Seignette salt and also by cathodic or magnetic recording. (Fig.11).

#### Results :

- Experiment of October 30, 1968 :

At a depth of 50 m, 3800 litres have been expelled in 2,3 s using 25 kg of propellant; a certain loss has been observed due to too large a filling aperture.

- Experiment of February 24, 1969 :

At a depth of 60 m, 4700 litres have been expelled in 2,3 s with 25 kg of propellant. Then the entire system surfaced which was believed to be due to the hydrodynamic thrust mentioned in paragraph 3.2; the emptying speed through the aperture had been 11 m/s, the output 2000 kg/s, the corresponding average thrust was 22 000 Newtons.

- Experiment of July 11, 1969 :

At a depth of 200 m, 2000 litres have been expelled in 2,5 s using 35 kg of propellant.

- Experiment of September 18, 1969 :

Same results as obtained by the preceding trial. The ballast temperature was stabilized at 50°C.

#### 5.4.- Trials with a submarine ballast tank-

In two successive trials the ballast tank of a submarine of the DAPHNE class has been flushed out, the filling

.../...

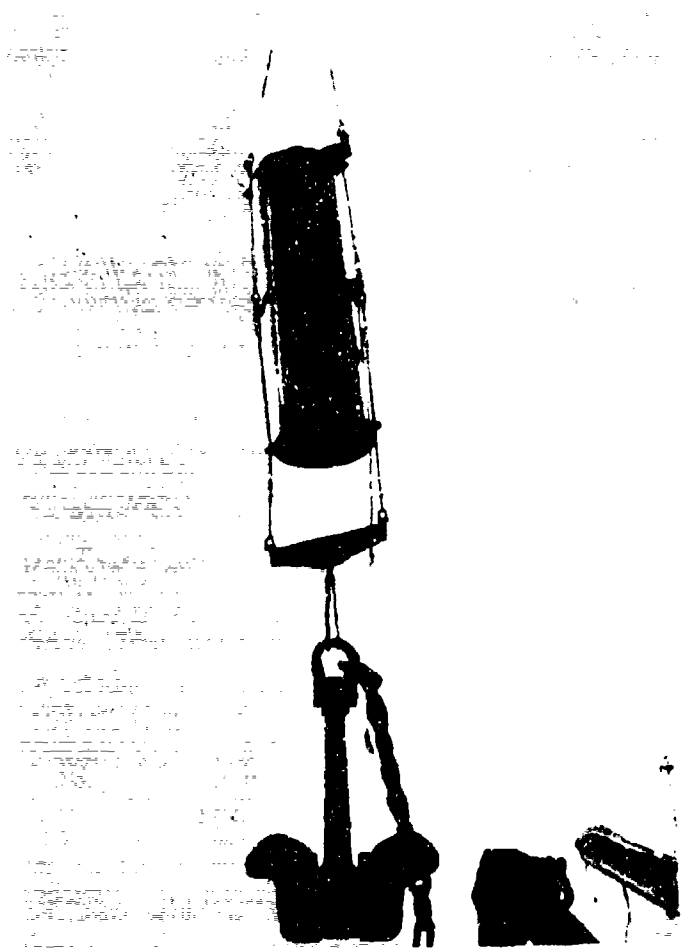


Figure 11 - Ballast of 6 m<sup>3</sup> weighted with a  
7 ton anchor

apertures being placed at a depth of 31 m.

A caisson representing part of a submarine has been used in these trials. It has been lowered into the water by means of the set-up represented in figure 12, which had been designed and realized by the "Centre d'Etudes des Techniques Sous-marines" of the "Direction des Constructions et Armes Navales" of Toulon. (Photograph of the caisson see fig.14).

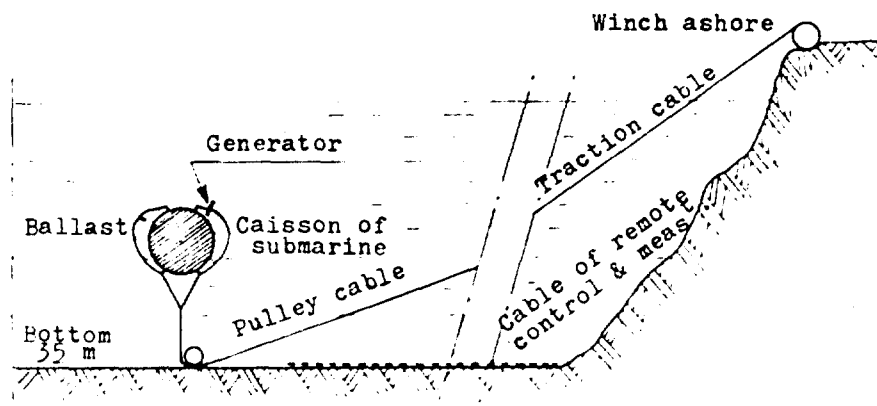


Figure 12

In the first trial, a generator containing 25 % of the propellant deemed necessary for emptying the ballast of 11 500 litres, has been used; 2400 litres have been expelled in 5 s using 11,75 kg of propellant; overpressure in the ballast remained below 0,15 bar.

In the second trial, a generator containing 50 % of the propellant necessary for the emptying of the ballast has been used; 4800 litres have been expelled in 5 s using 23,5 kg of propellant in a generator as represented in figure 11. Overpressure in the ballast remained below 0,5 bar.

#### 6.- PURSUIT OF THE STUDY

o .- When flushing out submarine ballasts, the gases used will have to be entirely free of reducing agents such as hydrogen and carbon monoxide.

.../...





Fig. 13 - Generator used in submarine ballasts

There is indeed a risk of ignition of the gases during a further flushing-out with compressed air.

The propellants currently in use are still producing 10 to 25 % of  $\text{CO} + \text{H}_2$ ; we are therefore considering to set up a study with the participation of the "Société Nationale des Poudres et Explosifs" in order to develop a propellant with combustion gases entirely free of these reducing agents.

6.2.- These problems are absent when it is a question of raising.

Generators containing 1,5 kg of propellant have been tried in these operations at depths of 160, 200, 300 and 400 m with encouraging results.

Yet smaller generators may come in useful in the activities of autonomous divers; the lifting of a relative mass of 111 kg under water has been realized by flushing out a barrel of 200 litres with a generator containing 300 gr of propellant.

In salvage and refloating operations the gas generator presents the following advantages :

- There is no need for flexible pipes to be inflated by compressed air from the surface,
- operations can be carried out at great depths where compressed-air devices are ineffective,
- the propellant device weighs seven times less than the compressed-air device,
- the gas is released at great speed.

The experimental results described above will help to bring to a successful issue a development of generators suitable for particular salvage operations, e.g. bringing to the surface, either automatically or by remote control, scientific or industrial equipment functioning at great depths, recovery of lost missiles, refloating of wrecks, a.s.o.

.../...

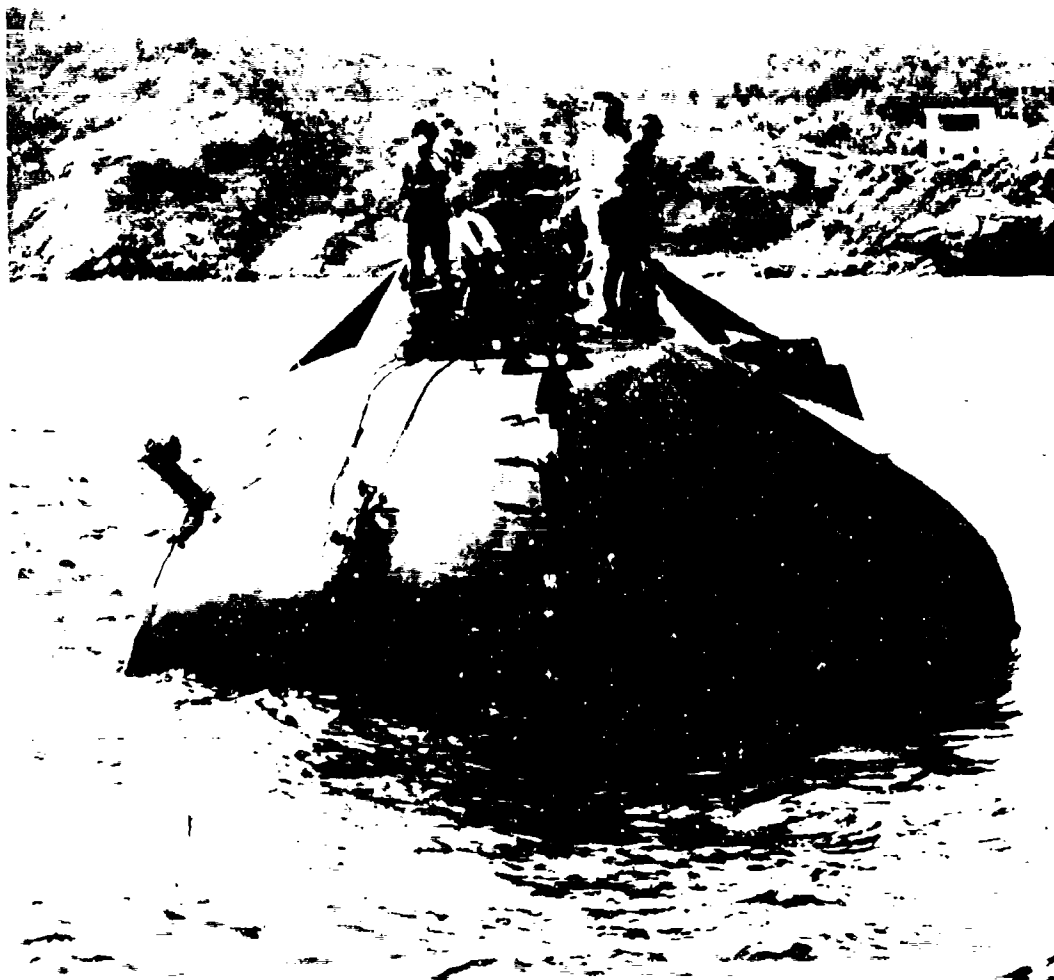


Figure 14 - Conning tower of a submarine of the DAPHNE class  
fitted with generator

A first notion of using liquid propellant in this development has been abandoned in favour of solid propellant, the former equipment being complex and cumbersome besides weighing the double of a generator running on solid propellant. No interesting results could therefore have been expected.

On the other hand, the use of elements which, while decaying in water release an ample supply of gas seems to be very promising. We have already realized generators of this type which have the advantage of an adjustable output. But as the released gas consists generally of hydrogen, they may not be used where there is a risk of ignition.

However, these equipments which we have used for inflating antenna carrying balloons, may yet come in handy for the operation of autonomous underwater devices.

----

BIBLIOGRAPHY :

- (1) LANGHAAR, H.L. : "Analyse dimensionnelle et théorie des maquettes" (DUNOD)
- (2) COMOLET, R : "Mécanique expérimentale des fluides" (MASSON & Cie.)
- (3) SUTTON, G.P. : "Rocket Propulsion Elements" (John WILEY & Sons)
- (4) WILLIAMS, F.A. "Fundamental Aspects of Solid Propellant Rockets" (Library of Congress Catalog N° 68.3/381)

# PYROTECHNIC SPECIAL EFFECTS IN MOTION PICTURES

Frank P. Clark

The Research Center of the Association  
of Motion Picture and Television Producers, Inc.

## ABSTRACT

Pyrotechnic chemistry and special effects applications in the motion picture industry are limited by several unique parameters. Camera shutter speed, size and scale of the sets, film sensitivity and ambient illumination are among those items which dictate the pyrotechnic compounds, quantities and their uses.

The paramount factor governing pyrotechnics in motion pictures, however, is safety. This means not only protection against injury to actors, powder men and other personnel, but also against the premature destruction of sets that may cost many thousands of dollars and weeks of delay to replace.

Since virtually all motion picture pyrotechnic special effects are electrically initiated, the main portion of this paper describes a unique Electro-Explosives Safety Program developed by the Research Center of the Association of Motion Picture and Television Producers, Inc. to drastically reduce the hazards involved in employing pyrotechnic special effects.

## PYROTECHNIC SPECIAL EFFECTS

### IN MOTION PICTURES

Pyrotechnic special effects have been a vital part of motion picture production since the days of the silent movies. Their primary purpose is to produce visible and audible effects for the camera and the sound recorder rather than to perform "work", as is the case with most normal pyrotechnic devices.

The application of pyrotechnics in motion pictures is governed by a number of parameters unique to the motion picture industry. Among these are the speed of the film running through the motion picture camera (24 frames per second); sensitivity and color response of the film being used; day or night photography; size or scale of the scene being photographed; proximity of actors to the effect; animal action, etc.

If a pyrotechnic special effect reaches its full development in  $1/25$ th of a second or less, it will appear to "pop on" the screen. Ideally an effect should "bloom" to full size in a period of several frames of film, or between  $1/4$  to  $1/2$  a second. In essence, we must use "slow motion" pyrotechnic effects.

If a pyrotechnic illuminant is too bright, the color will appear washed out due to an over-exposure of the film. White flame is not particularly photogenic, saturated colors are much more effective. Therefore we need not-too-bright pyrotechnics - particularly for night-time filming. Some films are balanced to give correct color rendition at a color temperature of  $6000^{\circ}\text{K}$ , and others at  $3200^{\circ}\text{K}$ . For this reason a flame may appear differently to different types of film stock. Often a scene will be shot in miniature. It therefore becomes necessary to scale a pyrotechnic effect down in size to match the size of a small set.

Of all the limitations imposed on pyrotechnic special effects, however, safety is the most important. Actors are often required to work in close proximity to vigorous effects - sometimes even to be bowled-over by them. We must neither injure them nor poison them with our pyrotechnic devices. Great care is exercised by our experienced powder men to insure that an effect will go off at exactly the right time and that the force will be directed in precisely the proper direction with a pre-determined magnitude.

With all of the expertise employed in the manufacture of photogenic pyrotechnic items, and with the careful application of these devices to special effects by skilled pyrotechnic operators, there still remains one area of hazard that is common to all electrically initiated pyrotechnic items - that of premature or accidental ignition.

The Research Center of the Association of Motion Picture and Television Producers, Inc. (AMPTP) recognized this potentially dangerous situation and originated a project to analyze and identify the various hazards which might be encountered in using electrically initiated pyrotechnic devices in the motion picture environment. These hazards were found to include:

1. Static Electricity: This can be due either to atmospheric conditions or to charges built up on the individual powder man as a result of synthetic fabric garments, touching an ungrounded vehicle, using an ungrounded CO<sub>2</sub> fire extinguisher, and many other causes.
2. Induced Currents: These might result in premature ignition when lead wires are inadvertently laid next to AC lighting cables. (No significant induction was achieved, however, when squib lead wires were intentionally air-coupled with a 225 ampere DC arc light cable and the arc repeatedly struck and extinguished.)
3. Leakage Currents: Many motion picture sequences are filmed in wet, rainy and muddy locations. Lighting and other power cables can provide quite substantial leakage currents which may be picked up by squib or detonator lead wires.
4. Accidental Shorts: The many lighting cables, junction boxes and power cords strewn about during the filming of motion picture sequences, in conjunction with moving equipment, camera dollies and with dozens of people milling around, create numerous opportunities for accidental shorts between lead wires and 120/240 volt AC and DC power sources.
5. Radio Frequency Induction: Although this hazard is recognized, tests conducted with tuned antennas under the Mount Wilson television antenna array, as well as at the base of a 50,000 watt commercial AM radio station, failed to produce currents sufficient to ignite a test flashbulb or a squib. Even direct coupling to a 40 watt radio transmitter antenna did not fire these devices. Motion picture pyrotechnics are almost

always fired singly, with twin lead wires, or in small multiples hooked up in parallel circuits. Thus, they are relatively insensitive to RF induction. The single-wire, series hook-ups used in some commercial blasting operations, such as in mining and quarrying, constitute a giant loop which is much more highly susceptible to radio frequency induction.

6. Lightning: Conditions which lead to a lightning strike are preceded by the development of very considerable voltage gradients. These gradients can represent a definite hazard. A lightning strike itself, of course, constitutes the ultimate hazard.
7. Accidental Firing: The human factor must always be considered when analyzing hazards. Lead wires connected to improper sources of power (lighting circuits, field telephones, etc.), premature connection to the firing battery, faulty firing switches or careless or accidental cycling of firing switches constitute some of the human hazards.
8. Ultra-Sensitive Devices: Certain circumstances, including borderline manufacturing tolerances, damage to the bridgewire and ageing of ignition compounds can cause electric squibs or detonators to become quite a bit more sensitive than the average. It is the belief of the Research Center that some of these ultra-sensitive devices, in rare combinations with a mild form of any of the above-mentioned hazards, may produce premature ignitions.

#### THE AMPTP ELECTRO-EXPLOSIVES SAFETY PROGRAM

In order to provide protection against these various hazards the AMPTP has proposed the following Electro-Explosives Safety Program. The full program consists of three phases:

1. Pre-test all squibs or detonators which will be employed to initiate larger explosions.
2. Develop an electro-explosives safety system which will safely attenuate all of the hazards listed above - except a lightning strike.
3. Adopt a lightning warning meter to provide an indication of excessive voltage gradients.



## PRETESTING OF SQUIBS

In any process involving the manufacture of large numbers of any given item, there will be a statistical distribution of each of its properties. In the case of squibs and detonators, depending upon manufacturing quality controls, these variables may combine to produce a few units per thousand which will be more sensitive than the average. In addition, an initiating compound may become less stable or more sensitive with age.

Under the safety program, any squib or detonator which is to be used in any device capable of injuring an individual or causing property damage should be tested by applying a brief electric impulse at a substantial fraction of its nominal firing circuit (but not sufficiently long to cause thermal damage to a normal unit) to destructively weed out those rare units which may be super-sensitive. This procedure need not apply to such small pyrotechnic devices as electric spark effects, small "bullet hits", fire igniters, etc.

(The principle supplier of pyrotechnic special effects to the motion picture and television industry has readily agreed to such a test procedure.)

## AMPTP ELECTRO-EXPLOSIVES SAFETY SYSTEM

The System consists of three parts:

1. The Attenuator Unit.
2. The Power Unit.
3. The Circuit Test Unit.

### THE ATTENUATOR UNIT

This device reduces to a safe level all of the above mentioned hazards. It consists of an electronic network, epoxy potted in a rugged plastic case in order that it might withstand considerable abuse and still be a reusable item. It is intended to be placed as near the explosion site as possible. The manner in which it attenuates each of the hazards is described as follows: (See Fig.1)

Static discharges capable of being generated on a human body (tested at 12,500 volts through a 500 picofarad condenser), and atmospheric gradient: or other continuously generated static charges are harmlessly shunted to ground through the

bleed resistors  $R_1$  and  $R_2$  and an attached grounding wire. It is possible that static discharges in excess of 50,000 volts could jump across  $L$  and  $C_1$  and enter transformer  $T$ . At this point it is possible for the current to jump to the transformer core where the charge is then harmlessly shunted to ground. The secondary winding of the transformer is further shielded and insulated, and thus the preferred electrical path is to ground by means of the shield through a suitable ground wire.

In order to be effective, the ground terminal, located between the lead-line terminals, should be connected to earth if the explosive is lying or buried in the earth. If the pyrotechnic effect is to be used in a metal mortar or located in a metal housing, vehicle, etc., then the ground terminal of the attenuator should be bonded to the metal object.

Direct Current will provide a single pulse to the transformer  $T$  as it charges capacitor  $C_1$ . The pulse leaving the attenuator - even when 250 VDC is applied to the lines - provides less energy to the squib than does a standard blasting galvanometer.

Alternating Current 50-400 Hz AC is blocked by the high impedance of  $C_1$ . It is further attenuated by the saturation of the iron transformer core. This occurs when the secondary voltage is in the order of 1/100 volt.

Leakage and Induced Currents, either AC or DC, are similarly attenuated. Care must be exercised, however, to insulate squib or detonator leg wires and the output terminals of the attenuator unit when special effects are to be set off in wet locations. Induction hazards are minimized due to the short lines between the attenuator and the squib, however leakage currents may pose a hazard if these lines are not properly insulated. Special marine grease has proved to be an effective insulator in overnight immersion tests in sea water.

Radio Frequency Induction, although not considered to be a substantial hazard in motion picture locations, is effectively attenuated by the inductor  $L$  and the capacitor  $C_2$ .

Areas directly in front of high powered radar may pose a hazard due to direct thermal heating. Normally no filming is done in such locations, since these energy levels are dangerously harmful to people.

Lightning itself cannot be protected against by any simple device. A direct strike will fire any explosive effect. Prior to a strike, however, substantial atmospheric voltage gradients will appear, and these may cause considerable differences in potential between the two ends of any lead-lines in the area.

Resistors  $R_1$  and  $R_2$ , if properly connected to a ground wire, will effectively bleed such charges to earth.

One of the most unique safety features of the Attenuator Unit is the impedance of the secondary winding of transformer T. It is equivalent to 12 inches of No. 20 wire. (.010 ohms) This means, in effect, that when attached to the Attenuator Unit, squib or detonator leg wires are shunted - and that the device is actually fired while in a shunted condition.

The Attenuator Unit's electronic network functions not only to attenuate the various hazards described, but is designed to be a tuned circuit. The particular resonant frequency, 8,500 Hz, was chosen so as to be above the voice range of motion picture sound recording, and well above the power line frequencies of 60 and 400 Hz. At the sametime it is well below the radio frequency bands.

### THE POWER UNIT

The purpose of the Power Unit is to supply adequate firing power, at the correct frequency and voltage, as required by the Attenuator Unit. It also incorporates several safety and convenience features. From an operational standpoint the Power Unit simply replaces the standard firing current source - in motion picture applications this is normally a 49 1/2 volt "B" battery. (See Fig.2)

The Power Unit consists of a high voltage (130 V.), high-frequency (8,500 Hz) inverter that operates from a 12 volt DC power source. A small 12 volt, high current output, lead-acid motorcycle battery is located in a compartment of the Power Unit case. Also provided is an accessory cable with a cigarette lighter plug at one end for quickly recharging the battery from any vehicle with a negative ground. For added convenience in transportation, a 12 volt dry cell battery or any 12 volt sealed or gel-cell type battery may be substituted.

In order to maintain constant power, a storage capacitor is built into the Power Unit. Besides delivering large amounts of power, this capacitor permits reliable firing even when the battery is nearly exhausted. When the battery plug is disconnected, the capacitor is shorted so that there is no residual charge remaining anywhere in the circuit.

A voltmeter is incorporated in the capacitor circuit to indicate the voltage stored in the capacitor. By noting the rate of charge, the condition of the battery may also be evaluated.

A power switch is attached to the Power Unit by means of a plug-in extension cord which permits the pyrotechnic operator

to move about so that he always has the location of his special effects in view (or he can employ another pyrotechnic operator to give signals when direct vision is obstructed). The switch itself is in a clear plastic housing so that the contacts are always visible as a double check on the safety condition of the switch.

The power switch is not primarily intended to serve as a firing switch. Its function is to turn on the Power Unit which supplies power to the main firing switch. This two-handed operation is designed to reduce the possibility of accidentally triggering a single firing switch. The pyrotechnic operator must really intend to fire the shot when two hands are required.

The output terminals of the Power Unit are normally shunted and the inverter is disconnected from the capacitor power source until the power switch is plugged in. When the power switch plug is inserted, power is available and the output terminals are ready to be deshunted only when the hand-held power switch is closed. At this time a neon lamp will light, indicating that 130 volts are present at the output terminals.

The inverter is an efficient transistor/inductor circuit which converts 12 volts DC into 130 volts at 8,500 cycles AC. It is frequency stabilized for optimum Attenuator Unit performance. Protection for the Power Unit circuitry is provided, in the event that the output terminals might be short circuited while power is applied.

A dummy load is provided, with an indicator lamp to test individual Attenuator Units. When an Attenuator Unit is connected to the output terminals of the Power Unit, and the "squib terminals" are held against the test-load binding posts, the indicator lamp will light when the power switch is closed and the Attenuator Unit is functioning normally. A "press to test" feature permits checking the condition of the indicator lamp.

The Power Unit is supplied with two carrying case options. One is a sturdy wooden instrument case, the other is a clear plastic case. Both provide a separate compartment which houses the 12 volt motorcycle battery, the various operating cables and two or three Attenuator Units. The clear case provides a visual check on the condition of the electronic circuitry for possible damage, and also a ready inventory of cables and Attenuator Units.

#### OPERATION

In operation, as many as four standard one amp, one ohm bridgewire-type devices may be connected in parallel to a single Attenuator Unit. As many as three Attenuator Units may be

hooked up in parallel on any one single circuit - or a total of twelve initiators at a single firing. This has been demonstrated through 2,000 feet of No. 18 stranded zip-cord wire. As many such charges as may be necessary may be connected to a stepping relay and fired in sequence with machine-gun rapidity - or as rapidly as the pyrotechnic operator can cycle his firing switch. (See Fig.3)

### CIRCUIT TESTER

Since the Attenuator Unit blocks DC current, it is not possible, with conventional equipment, to check continuity through any squibs or detonators attached to the unit. All that can be read on a standard blasting galvanometer is the value of the two bleed resistors,  $R_1$  and  $R_2$ , plus an insignificant line resistance. Therefore a unique circuit tester has been designed to indicate:

1. That continuity exists to the attenuator and back.
2. That the firing lines are not shorted.
3. That an open-circuit squib or a shorted squib is not connected to the attenuator.
4. The number of normal squibs connected to the attenuator.

The Circuit Tester may also be used to test normal blasting circuits. There are provisions for measuring the resistance of the lead lines, as well as provisions to test the internal battery.

The Circuit Tester employs a very small transistor oscillator to generate a low energy tone at 8,500 Hz. This sampling current is on the order of 1/2 to one milliampere - or about 1/20th the output of a standard blasting galvanometer. Fail-safe limiters are incorporated in the circuit design and, if overloaded, the circuit simply quits oscillating and no power is delivered to the line. Measurements are made by sampling the actual power consumed (in microwatts) by the firing circuit and the various components attached to the attenuator.

### LIGHTNING WARNING METER

The third phase of the Electro-Explosives Safety Program is the recommended use of any one of several commercially available Lightning Warning Meters to monitor exterior locations when atmospheric conditions are likely to generate potentially hazardous gradients.

Prior to a lightning strike, the static potentials that develop between clouds and earth, or between various spots on the earth surface are quite considerable. It has been noted that the least gradient known, prior to a lightning strike, is 10,000 volts/meter. When this voltage gradient is reached, a strike may occur. Even if the lightning does not directly strike the lead lines to a pyrotechnic special effect, the enormous energy released into the earth can induce very high voltage in the lines. An even greater hazard of course is the direct danger to personnel by the lightning itself. When the meter on the Lightning Warning instrument indicates 5,000 volts/meter, the potential is half way to the value at which a strike can occur, and it is time for those personnel remaining to rapidly clear the area and seek shelter.

At potential gradients of less than 10,000 volts/meter any current induced in the lead lines is harmlessly shunted to earth through the bleed resistors and ground wire at the Attenuator Unit. No attempt should be made to place, wire or remove electrically initiated pyrotechnic devices when there is any significant reading on the Lightning Warning Meter (i.e., any reading above 1,000 volts/meter).

To date the safety record of the motion picture industry powder men is an enviable one. This does not preclude, however, the application of state-of-the-art electronics to the development of novel safety systems to further reduce the possibility of premature or accidental ignition of pyrotechnic special effects.

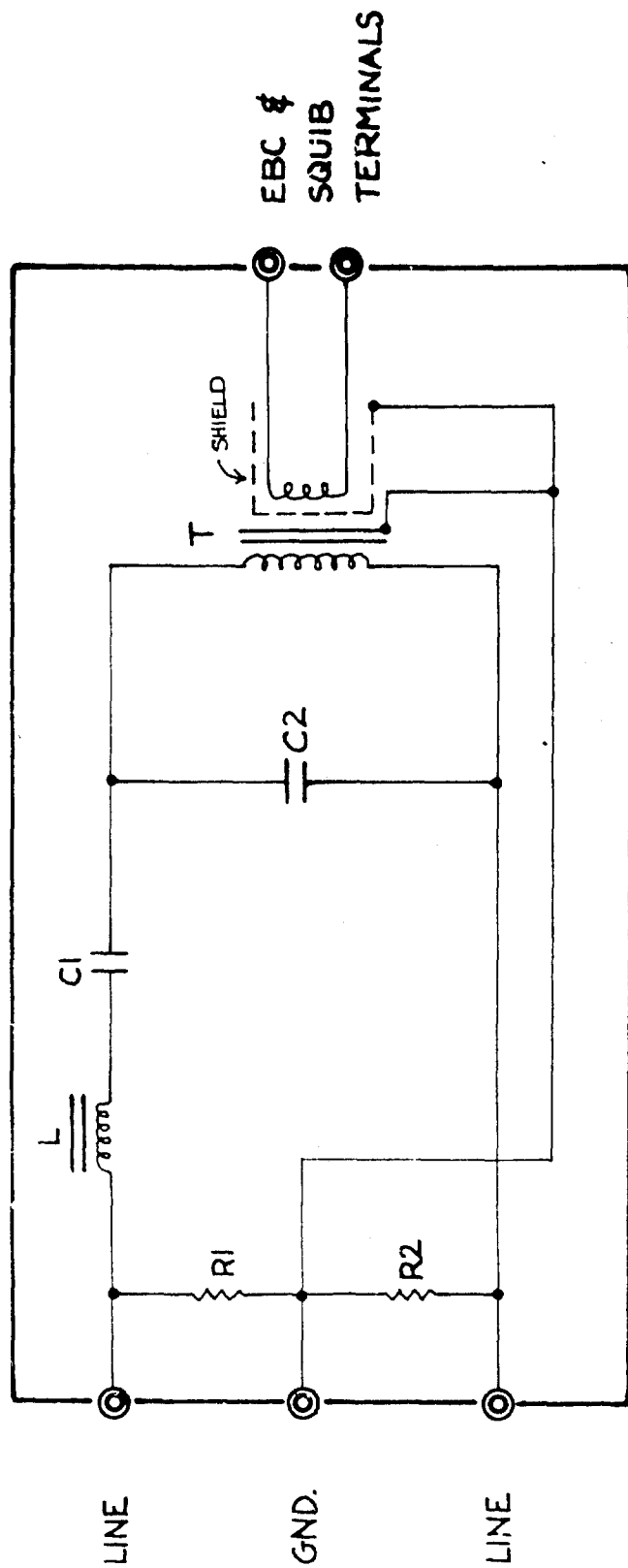
### CONCLUSIONS

The AMPTP Electro-Explosives Safety Program was developed to significantly lower the hazards involved in the motion picture pyrotechnic special effects. The program consists of three phases:

1. Pretesting of all squibs and detonators to be used in dangerous effects in order to weed out any ultra-sensitive units.
2. The use of the newly developed AMPTP Electro-Explosives Safety System which consists of the following items:
  - A) Attenuator Unit
  - B) Power Unit
  - C) Circuit Tester

3. The use, where indicated, of a Lightning Warning Meter to detect dangerous voltage gradients which might pose a hazard to personnel.

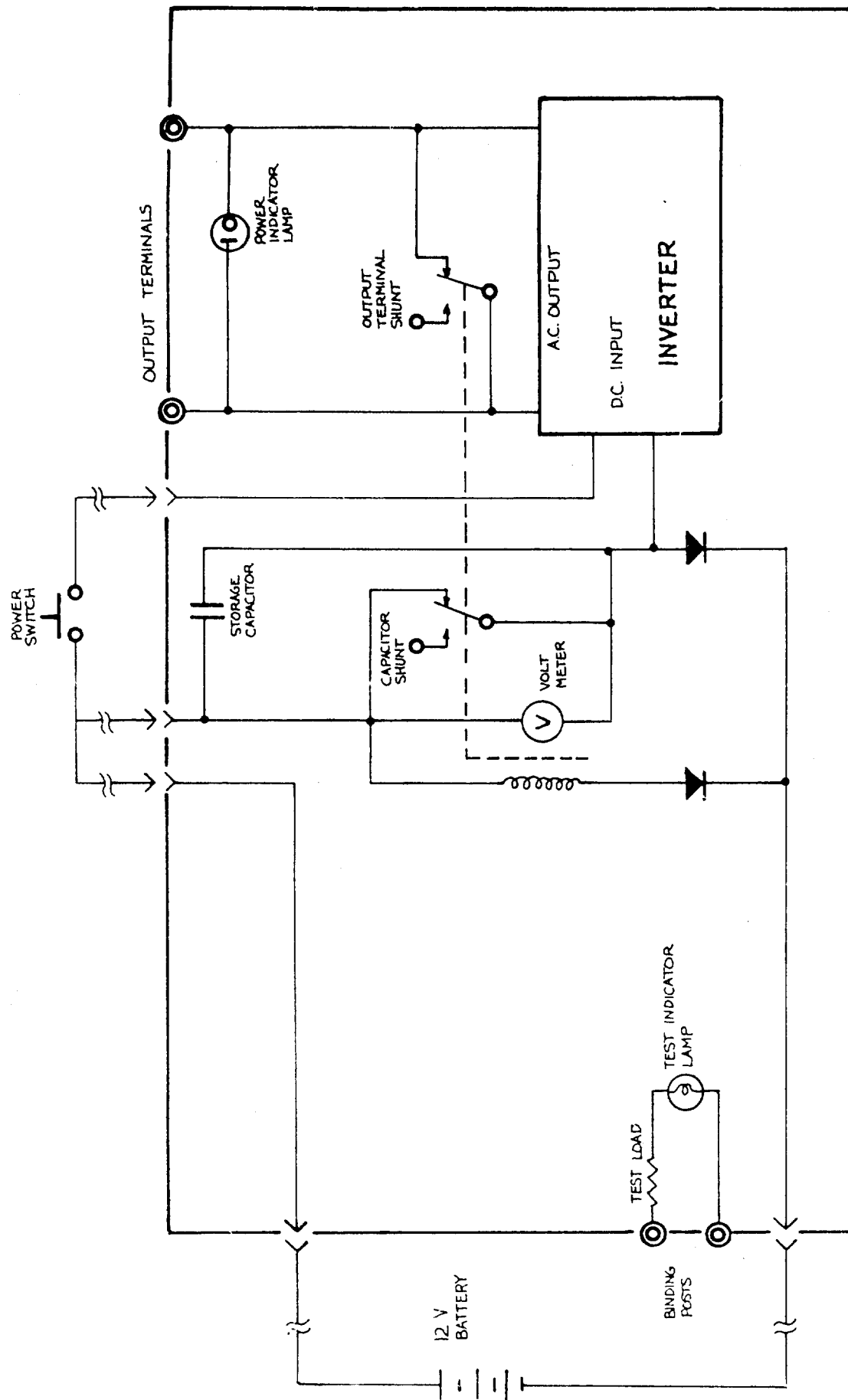
For photographic reasons, the motion picture industry employs low intensity, low velocity pyrotechnic materials to simulate explosive events. Safety, however, is of paramount concern. The AMPTP Electro-Explosives Safety System provides a significant margin of safety over conventional pyrotechnic and explosives firing practices. In many other occupational areas, certain military and commercial blasting operations for instance, unwanted electrical energy may also enter the blasting circuit from numerous sources. A system similar to that described in this paper will provide valuable protection against the same extraneous electrical sources as described above.



AMPTP ELECTRO-EXPLOSIVES SAFETY SYSTEM  
ATTENUATOR UNIT

FIGURE 1



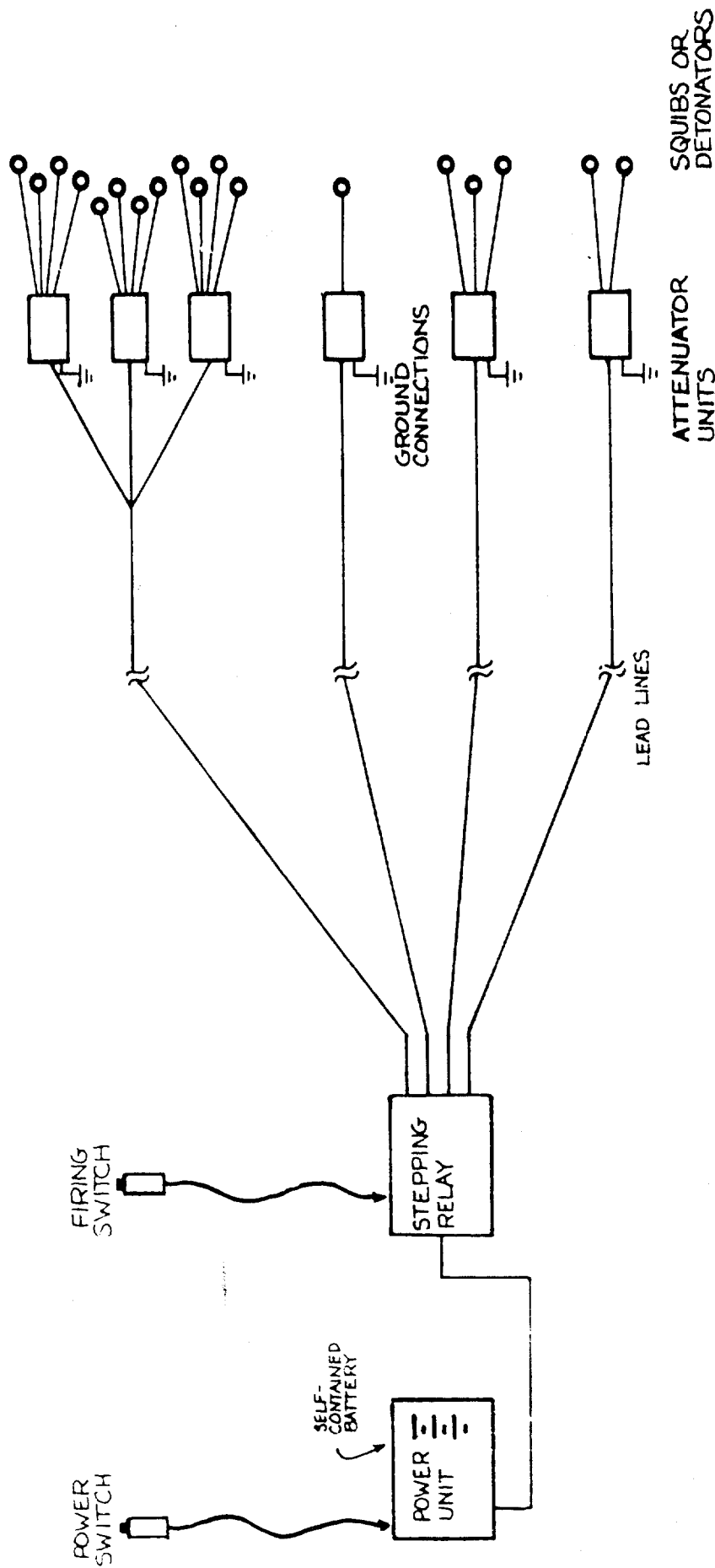


A PTP ELECTRO-EXPLOSIVES SAFETY SYSTEM

POWER UNIT

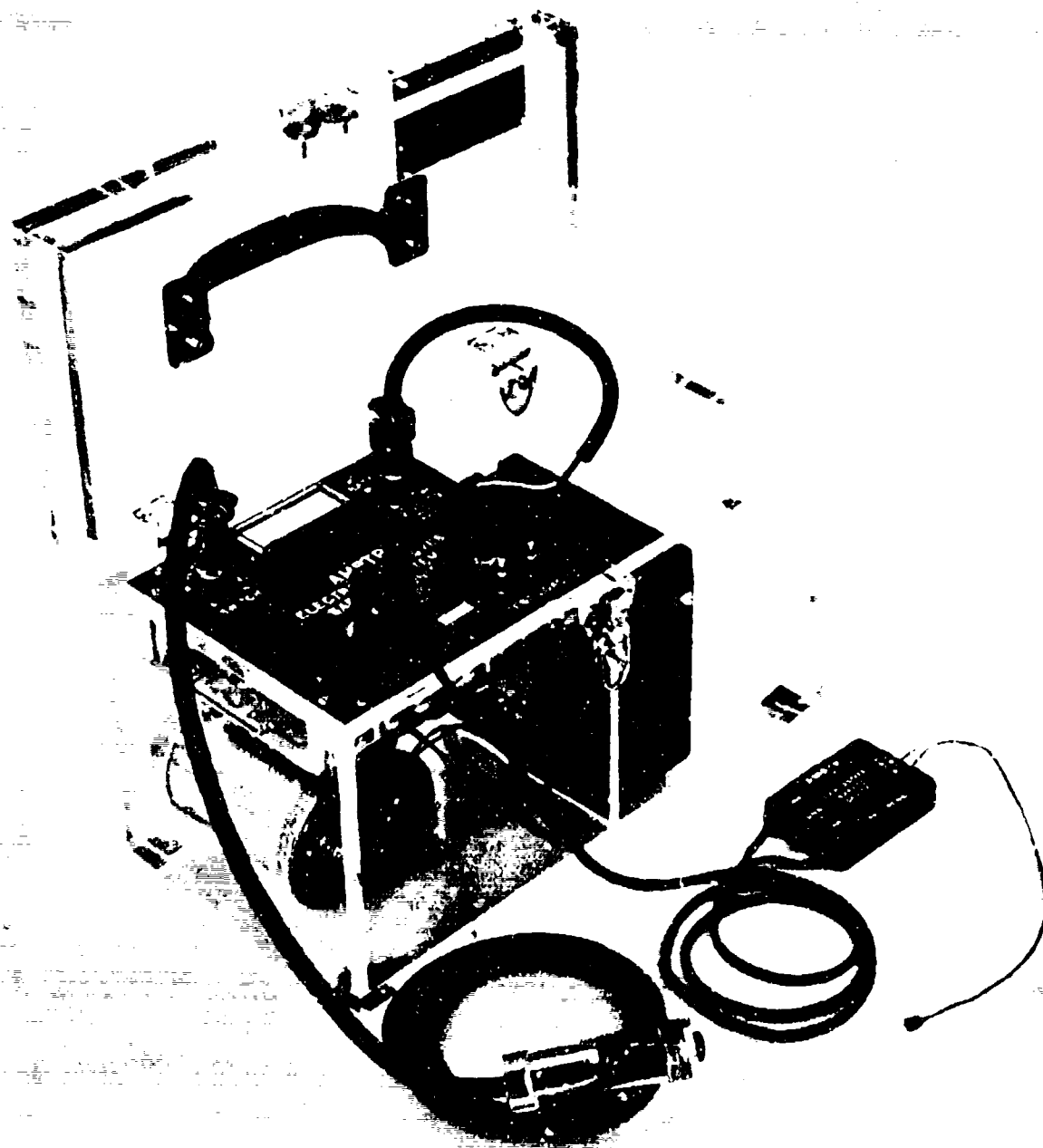
(Simplified Schematic)

FIGURE 2



AMPTP ELECTRO-EXPLOSIVES SAFETY SYSTEM  
TYPICAL FIRING HOOK-UPS

FIGURE 3



AMPTP ELECTRO-EXPLOSIVES SAFETY SYSTEM

IMPROVED BINDER SYSTEMS  
FOR  
FLARE COMPOSITIONS

by

H. E. Filter and D. L. Stevens

The Dow Chemical Company, Midland, Michigan

ABSTRACT

A program was undertaken to develop improved binder systems for pressed and tamp-cast flares. Work was concentrated on the processing and stability properties of the binders and their effect on burning rate, efficiency and light output of flare compositions. Variation of resin and curing agent compositions produced significant changes in the burning rate of both pressed grain and tamp-cast flares without changing the efficiency of the flares. Binder systems were developed for the MK 24, MK 45 and LUU-2B flares. Data are presented for use in selecting binders for new flares. A new family of binders based on carboxyl terminated polyols was developed and several of these materials have shown promise in tamp-cast flare compositions. Flare compositions based on these binders have the advantage of long pot life, good processability, and desirable performance properties.

PRECEDING PAGE-BLANK-NOT FILMED

## I. INTRODUCTION

The binder is the predominant factor in determining the mechanical properties and processing characteristics of any type of flare composition, and can have considerable influence on the combustion properties. Proprietary work has shown that even at the low (3-5%) binder level used for pressed grain flares large variations in burning rates and efficiency can be obtained by varying the binder composition.

In 1965 an in-house program on pressed, tamped, and pour-cast flares was initiated. Initial work was with epoxy resins, but a variety of other binder materials has been tested. Efforts were concentrated on the curing properties and pot life of the binders and their effect on the burning rate, efficiency and light output of flare compositions.

Many variables are known to affect flare performance, among them particle size of the magnesium and sodium nitrate powders, magnesium/sodium nitrate ratio, density, flare configuration and additives. Changing the magnesium/sodium nitrate ratio and magnesium particle size are methods which are frequently used to alter the burning rate of flares. Work at Dow has shown that the binder has a greater effect on burning rate than the above variables. Variation of resin and curing agent compositions has produced two to threefold changes in the burning rate and intensity of the tamp-cast flare compositions, without significantly changing the efficiency of the flares.

Binder systems are available which can be used to produce flares with low burning rates (0.04-0.05 in./sec.) through ultra-high burning rates (0.14-0.19 in./sec.). The combination of ultra-high burning rate (0.19 in./sec.) and high efficiency (50,000 cd. sec./g.) has resulted in extremely high intensity flares.

## II. FLARE PREPARATION AND EVALUATION

The sodium nitrate used was Grade B Class II, MIL-S-322-B (15-45 micron particle size) material. It was vacuum dried at 110°C., screened and stored in tightly sealed glass jars. The dried  $\text{NaNO}_3$  was passed through a 200-mesh screen for the pressed-grain flare formulations. Initial work on tamp-cast flares was with a bimodal particle size distribution  $\text{NaNO}_3$  of one-third 400-mesh and two-thirds 60-micron. Dried  $\text{NaNO}_3$  which passed through an 80-mesh screen had approximately the same particle size distribution and produced flares with equivalent burning rates and efficiencies as the bimodal  $\text{NaNO}_3$ . Most of the data

presented in this paper was obtained with -80 mesh material. When a new lot of  $\text{NaNO}_3$  was obtained, the performance of flares prepared from the old and new lot were compared to assure consistent results.

Atomized powdered magnesium was used for all the pressed grain flare work. A standard 30/50 mesh material was used. Ground powdered magnesium was used for all the tamp-cast flare work. Screen analysis and performance data were compared before switching lots to assure consistent data were obtained.

A five-or twelve-quart Hobart mixer was used for mixing the flare compositions. The following procedure was used: add resin and curing agent, mix 1-2 minutes, add magnesium, mix 5 minutes, add  $\text{NaNO}_3$ , mix 10 minutes, press into a mold, and cure overnight (16 hours) at  $70^\circ\text{C}$ . The pressed grain flares contained 4% binder and were pressed in a Dake press at 8,450 psi. The tamp-cast flares contained 9% binder and were pressed at a pressure (3,200 psi) which would produce optimum density with every binder system evaluated, assuring equivalent performance data.

Many of the flares were cast into Mylar plastic-lined cases and cured. The flares were then removed from tubes lined with Mylar plastic film and encased in paper tape by bifilar spiral winding two layers of masking tape on the candle. One end of the candle was closed off by casting an epoxy sand-plug to form the base.

The flares were fired in a 18.66 feet deep by 10.42 feet high concrete block hearth. The bottom of the flare was 4.75 feet above the floor. The hearth was ventilated by an inlet in the floor, below the flare, and an external 2-speed blower above the flare in the roof. The flare tunnel connected to the hearth by a 4 feet by 9 feet doorway, is 60 feet long by 10.42 feet wide by 14 feet high. The interior of the hearth and tunnel is painted black.

Two Model 856 YV Weston selenium photovoltaic cells were positioned 51.95 feet and 62.57 feet from the flare, and 5.1 and 5.5 feet above the floor. The outputs of the photocells, after passing through Honeywell Accudata 120 amplifiers, were recorded on a Honeywell Model 906B Visicorder oscillograph. A Dymec Model 2210 voltage-to-frequency converter and a Hewlett Packard Model 523 CR electronic counter were used to integrate the light output and record the integrated luminosity. The photocells were standardized with a General Electric Lamp No. 1M/T20BP, which at a constant amperage yields a specific horizontal candle-power.

The 1.25-inch and 2.9-inch candles were burned vertically, ignited on the upper surface. Air flow was upward. The 3.4-inch candles were tested in an inverted position. Time of functioning was determined with a stop watch. At least four candles were fired for each datum point, unless noted otherwise.

### III. PRESSED-GRAIN FLARE BINDER STUDIES

The normal method of manufacture for pressed flares is to mix 3-5% of a polyester binder with a mixture of magnesium powder fuel and sodium nitrate oxidizer. This mixture is pressed into the desired flare configuration at pressures of 7,500-10,000 psi. The small amount of binder used in this technique serves to cement the solid particles together, resulting in flares of acceptable strength and dimensional stability.

Since pressed flares use a minimum amount of liquid binder ingredients, the binder must be carefully selected to achieve maximum wetting of the solid fuel and oxidizer and to impart maximum strength and stability to the cured candle. This is important if the flare is to have the thermal stability and moisture resistance needed to pass the standard JAN cycle tests for temperature and humidity cycling (MIL-STD-331) and resistance to vibration and handling (MIL-STD-810).

Research involved various binder resins, including polyesters, vinyl esters, conventional epoxy resins (glycidyl ethers), epoxy novalacs and carboxyl-containing polymers. Several amine and anhydride curing agents as well as free radical polymerization catalysts were studied.

Several epoxy resins produced the best results and were selected for further development. The goal was the development of a binder which would impart improved properties to the flares and could be substituted directly for the existing binder (polyester) without changing any production procedures.

#### A. BINDER EVALUATION

Efforts were directed at developing a binder system for the MK 24 and MK 45 pressed-grain flares. Initial work showed that a binder system composed of a 70/30 mixture of D.E.R.<sup>®</sup> 321 resin (a low viscosity glycidyl ether epoxy resin produced by The Dow Chemical Company) and D.E.R.<sup>®</sup> 732 resin (a polyglycol diepoxide produced by The Dow Chemical Company) cured with XD-3482.01 (an amine hardener), produced flares with burning rates and efficiencies equivalent to flares in production.

## 1. Effect of Binder Composition on Flare Performance

Work with small (1.25-inch diameter flares showed that, even at 4% binder level, the ratio of D.E.R.<sup>®</sup> 321 and D.E.R.<sup>®</sup> 732 had a significant effect on the burning rate and efficiency of the flares. The effect was clearly demonstrated in a joint program between Dow and the Naval Ammunition Depot, Crane, Indiana (NAD - Crane). Epoxy based flare compositions selected by Dow and NAD - Crane personnel were evaluated in full size MK 45 flares at NAD - Crane. The data from one of the tests are summarized in Table I.

The data in Table I show that the burning time of MK 45 flares can be increased by increasing the concentration of the D.E.R.<sup>®</sup> 732 in the binder. Increasing the concentration of D.E.R.<sup>®</sup> 732 from 30%-100% caused a corresponding decrease of 32.2 seconds (15.6%) in the burning time of the flares. It is very significant that the higher concentrations of D.E.R.<sup>®</sup> 732 also produced higher luminous efficiencies. Since light intensity (candle-power) is a direct function of efficiency (candle power-seconds/gram) and burning time (seconds), a higher efficiency must be obtained for flares of equal weight and slower burning time to maintain equivalent intensity. The large increase in efficiency (7,900 cd.-sec./g. or 20.6%) shown in Table I resulted in a slight increase in the intensity of the flares containing larger concentrations of the D.E.R.<sup>®</sup> 732 resin.

Table I

Effect of Binder Composition on MK 45  
Flare<sup>a, b</sup> Performance

Binder System <sup>c</sup>	Flare Performance		
	Burning Time sec.	Luminous Efficiency cd.-sec./g.	Light Intensity cd. x 10 <sup>6</sup>
70/30 D.E.R. <sup>®</sup> 321/D.E.R. <sup>®</sup> 732:XD-3482.01	207.8	38,300	1.347
30/70 D.E.R. <sup>®</sup> 321/D.E.R. <sup>®</sup> 732:XD-3482.01	233.4	45,600	1.465
D.E.R. <sup>®</sup> 732:XD-3482.01	240.4	46,200	1.434

<sup>a</sup>58.7/38.2/4.0 Mg/NaNO<sub>3</sub>/Binder

<sup>b</sup>Average of 4 candles.

<sup>c</sup>All binder compositions were at a 1:1 amine to epoxy equivalent ratio.



Past practice has been to adjust the burning time of flares by varying the magnesium/sodium nitrate ratio. The ability to keep the solids ratio constant and adjust the burning time by varying the ratio of epoxy resins gives the Dow epoxy binder system an added advantage over competitive systems, such as the polyester binder.

## 2. Effect of D.E.R.<sup>®</sup> 732 Resin Content on Physical Properties and Water Sensitivity of Flares

The use of the binder system composed of 70/30 D.E.R.<sup>®</sup> 321/D.E.R.<sup>®</sup> 732 instead of the polyester system was based on improved temperature and humidity stability and equivalent physical integrity of the candle (cured flare composition). To assure that increasing the content of D.E.R.<sup>®</sup> 732 in the binder would not adversely effect flares, the effect of increased D.E.R.<sup>®</sup> 732 on flare properties was investigated.

Tensile specimens were prepared from a series of epoxy resin gumstocks (epoxy resin and curing agent) at a 1.0/1.0 epoxy equivalent/amine hydrogen equivalent ratio. The epoxy resin and curing agent were thoroughly mixed and poured into silicone rubber molds (Die "C" as specified in ASTM Standard D-412-51T). A minimum of ten specimens was prepared for each gumstock, cured 16 hours at ambient temperature and conditioned 40 hours minimum at ambient temperature and humidity as specified in ASTM Standard D-618 (Standard Methods of Conditioning Plastics and Electrical Insulating Materials for Testing). All specimens were tested on an Instron tensile tester at a strain rate of 2.0 in./min. All elongation measurements were extension until fracture and were obtained from the Instron chart.

Compression specimens of flare compositions were prepared from a series of epoxy resins using the pressed grain flare formulation shown in Table I. One hundred-gram batches of the flare composition were prepared in a KitchenAid mixer and 5.4-gram specimens were pressed into 0.5 in. diameter x 1 in. long cylindrical molds at 8,450 psi on the Dake press. The specimens were cured 16 hours at 80°C., conditioned 40 hours at ambient temperature and tested in compression at 0.5 in./min. crosshead speed.

The tensile strengths and extensions to failure of the gumstocks and the compressive strengths of the cured flare compositions, based on the corresponding epoxy systems, are summarized in Table II. The data for the systems based on D.E.R.<sup>®</sup> 321 and D.E.R.<sup>®</sup> 331 resin are in close agreement with published values for these resins when cured with D.E.H.<sup>®</sup> 24 epoxy curing agent (a curing agent very similar to XD-3482.01). Replacing either D.E.R.<sup>®</sup> 321 or D.E.R.<sup>®</sup> 331 with D.E.R.<sup>®</sup> 732 reduces the tensile strength of the two systems.

Table II

Effect of D.E.R.<sup>®</sup> 732 Resin Content on Mark 45  
Flare Binder Physical Properties

<u>Binder Composition<sup>c</sup></u>	<u>Tensile Strength psi</u>	<u>Extension to Failure, %</u>	<u>Flare Compressive Strength<sup>a</sup>, psi</u>
D.E.R. 331 <sup>b</sup>	10,239	5.2	--
D.E.R. 321 <sup>b</sup>	9,985	5.0	--
70/30 D.E.R. 321/ D.E.R. 732 <sup>b</sup>	3,732	21.0	8,287
30/70 D.E.R. 321/ D.E.R. 732 <sup>b</sup>	137	27.9	2,759
D.E.R. 732 <sup>b</sup>	60	21.0	2,114
Polyester Control	8,463	6.0	4,752

<sup>a</sup> Binder content.

<sup>b</sup> XD-3482.01 used as curing agent.

<sup>c</sup> All binder compositions were at a 1:1 amine to epoxy equivalent ratio.

The compressive strengths of the cured flares appeared more significant than the gumstock tensile properties. Even the gumstocks which had poor tensile properties (30/70 D.E.R. 321/D.E.R. 732 and D.E.R. 732) produced flare compositions with compressive strengths in excess of 2,000 psi.

The polyester control was brittle when compared with the epoxy formulations. The polyester gumstock tensile specimens shattered when they broke under test, while none of the epoxy specimens shattered. In addition, the epoxy based flare composition broke evenly in compression while the polyester based composition shattered as it broke.

No specifications have been written for the physical properties of pressed grain flare binders or flare compositions. The only requirement is that the flares withstand a 40-foot drop test without detonating or catching fire. The data in Table II indicate that even flares based on the 100% D.E.R. 732 have enough strength to meet present specifications. The ability of the epoxy binders to resist shattering indicates that they would also absorb a shock more readily than the polyester system and would be less likely to explode or burn on impact.

The water sensitivity of the epoxy resin gumstocks was determined by casting 1" x 3" x 1/8" thick specimens into silicone rubber molds and curing the specimens for 16 hours at ambient temperature. The specimens were conditioned 40 hours at ambient temperature and six specimens of each binder composition were suspended in distilled water as described in ASTM Standard D-543-60-T (Resistance of Plastics to Chemical Reagents). The effect of the water on the appearance (color, shape, degradation) of the samples was observed and they were removed from the water after 7, 15, and 30 days, blotted dry, and weighed to determine water pickup.

In addition to the gumstock immersion tests, pressed cylinders (1/2" x 1") of flare composition prepared as previously described for the compressive tests were also immersed in water. The specimens were observed daily for the first 30 days and less frequently for the next 30 days and any indication of reaction or change in appearance was noted. The water pick-up and appearance of the immersed gumstocks are summarized in Table III and the appearance of the cured flare compositions after water immersion is shown in Table IV.

The data in Table IV show that increasing the content of D.E.R. 732 in the binder system does not seriously effect the water sensitivity of the flare composition. All of the epoxy based flare compositions maintained their configuration and physical integrity after 60 days immersion in water, while the polyester based flare composition reacted immediately with the water (severe bubbling) and disintegrated within two days after immersion. This is consistent with the data in Table III which show that the polyester gumstocks turned white and chalked within two hours immersion in water, while the epoxy resins maintained their original appearance. While the water pickup of the epoxy resin gumstocks increased with increasing content of D.E.R. 732, the water sensitivity of the cured flares was not seriously affected.

The data in Table IV show the main advantage of epoxy resin binders for illumination flares. While the sodium nitrate is water soluble and the magnesium powder is highly reactive with water, only 4% of an epoxy resin binder greatly inhibits reaction of a mixture of these compounds with water. These data have been verified by personnel at NAD-Crane who have immersed Mark 45 flares in water for two weeks with no significant change in appearance or grain integrity.

While no attempt was made to fire any flares after immersion in water, the test does give an indication of the excellent hydrolytic stability of the amine-cured epoxy resin binder system.

Table III

Effect of D.E.R. 732 on Water Sensitivity  
of Epoxy Resin Gumstocks

Binder Composition	Water Sensitivity		Gumstock Appearance
	Immersion Time, days	Water Pickup, %	
D.E.R. 331-D.E.H. 24	7 30	0.34 0.71	Straw colored-translucent-hard. <sup>b</sup> No visible change after 30 days. <sup>c</sup>
D.E.R. 321-D.E.H. 24 <sup>a</sup>	7 30	0.34 0.72	Light amber-translucent-hard. <sup>b</sup> No visible change after 30 days. <sup>c</sup>
D.E.R. 334-D.E.H. 24	7 30	0.40 0.97	Nearly clear-very hard. <sup>b</sup> Very slight surface chalking after 7 days. <sup>c</sup>
D.E.R. 331-CX-3482.1	7 30	0.33 0.77	Amber-translucent-hard. <sup>b</sup> Very slight surface chalking after 7 days. <sup>c</sup>
D.E.R. 321-CX-3482.1	7 30	0.52 0.97	Amber-translucent-hard. <sup>b</sup> No visible change after 30 days. <sup>c</sup>
D.E.R. 334-CX-3482.1	7 30	0.39 1.07	Amber-translucent-hard. <sup>b</sup> No visible change after 30 days. <sup>c</sup>
70/30 D.E.R. 321/ D.E.R. 732a	7 30	1.55 2.88	Amber-translucent-hard. <sup>b</sup> No visible change after 30 days. <sup>c</sup>
70/30 D.E.R. 334/ D.E.R. 732a	7 30	1.52 2.93	Amber-translucent-hard. <sup>b</sup> No visible change after 30 days. <sup>c</sup>
30/70 D.E.R. 321/ D.E.R. 732a	7 30	8.88 13.70	Light amber-translucent-rubbery. <sup>b</sup> Slight warp after 7 days.
30/70 D.E.R. 321/ D.E.R. 732a	7 30	9.35 14.60	Light amber-translucent-rubbery. <sup>b</sup> Slight warp after 30 days. <sup>c</sup>
D.E.R. 732a	7 30	27.40 38.70	Light amber-translucent-cheeseey. <sup>b</sup> Warped after 7 days.
Polyester Control	7 30	1.56 2.28	Crystal clear-very hard. <sup>b</sup> Snow white, chalky surface after 2 hrs. <sup>c</sup>

<sup>a</sup> XD-3482.1 used as curing agent at 1:1 amine to epoxy equivalent ratio.

<sup>b</sup> Before water immersion.

<sup>c</sup> After immersion for time indicated.

Table IV  
Effect of Water Immersion on Pressed  
Grain Flare Compositions<sup>a</sup>

<u>Binder Composition</u>	<u>Flare Appearance After Water Immersion</u>
D.E.R. <sup>®</sup> 334 <sup>b</sup> Resin	Slight bubbling-no visible change after 15 days. Darkening and slight white, crystal growth after 30-60 days.
70/30 D.E.R. <sup>®</sup> 321/ D.E.R. <sup>®</sup> 732 <sup>b</sup>	Slight bubbling-slight darkening after 15 days. Darkening and some white, crystal growth after 30-60 days.
70/30 D.E.R. <sup>®</sup> 334/ D.E.R. <sup>®</sup> 732 <sup>b</sup>	Slight bubbling-slight darkening after 15 days. Darkening and some white, crystal growth after 30-60 days.
30/70 D.E.R. <sup>®</sup> 321/ D.E.R. <sup>®</sup> 732 <sup>b</sup>	Slight bubbling-slight white, crystal growth after 2 days. Darkening and white crystal growth after 30-60 days.
30/70 D.E.R. <sup>®</sup> 334/ D.E.R. <sup>®</sup> 732 <sup>b</sup>	Slight bubbling-slight white, crystal growth after 2 days. Darkening and white, crystal growth after 30-60 days.
D.E.R. <sup>®</sup> 732 <sup>b</sup>	Slight bubbling-slight white, crystal growth after 2 days. Darkening and white, crystal growth after 30-60 days.
Polyester Control	Severe bubbling-disintegrated within 2 days.

<sup>a</sup>4 binder content.

<sup>b</sup>XD-3482.01 used as curing agent at 1:1 amine to epoxy equivalent ratio.

#### B. EVALUATION OF OTHER PRESSED GRAIN BINDER SYSTEMS

In effort to develop a more improved binder system, the combustion properties of a series of flares based on other Dow epoxy binder systems were compared with the properties of flares prepared from the binder of XD-3482.01 cured 70/30 D.E.R.<sup>®</sup> 321/D.E.R.<sup>®</sup> 732. The performance properties of the flares prepared from the various binder systems are compared in Table V. All the binder systems shown in Table V produced flares with higher light efficiencies than the standard system; however, the burning rates and light intensities of the flares varied considerably.

Table V

Comparative Performance of Pressed Grain Flares<sup>a,b</sup>

Binder System <sup>c</sup>		Flare Performance			
Resin	Curing Agent	Oxygen in Binder, %	Burning Rate in./sec.	Efficiency cd.-sec./g.	Average Intensity cd.
Epoxy Blend of Standard 70/30 D.E.R. <sup>®</sup> 32/D.E.R. <sup>®</sup> 732	XD-3482.01 Poly-amine	20	0.058	51,600	103,000
XF-4013L, Sulfur-Containing Epoxy	D.E.H. <sup>®</sup> 14 Poly-amide	19	0.081	54,900	153,000
XF-4013L	XF-4010, aminated polyglycol	19	0.084	59,200	171,200
XF-4008L, High Oxygen Epoxy	XF-4010	31	0.071	54,100	132,200
5611-78A Epoxy Novolac	Maleic anhydride	31	0.096	58,000	191,600
5611-73C Experimental Epoxy	XF-4010	21	0.090	57,000	176,600
FORMREZ 17-80 Carboxyl Terminated Polyester	ERLA 0510 Trifunctional epoxy	39	0.081	54,400	151,700

<sup>a</sup>58/38/4 Mg/NaNO<sub>3</sub>/Binder.<sup>b</sup>All flares 1.25" diameter and pressed at 8,450 psi.<sup>c</sup>All binder compositions were at 1:1 epoxy to curing agent equivalent ratio.

While none of the binder systems in Table V could be used as a direct replacement for the standard binder, the data can be used to select binders to meet new flare requirements. For instance, if a fast burning high intensity flare is needed, flares which burn about 65% faster and have approximately 40% higher light output than the MK 24 or MK 45 flares can be prepared from the 5611-73C/maleic anhydride system.

#### IV. TAMP-CAST FLARE BINDER STUDIES

Work funded by Eglin Air Force Base has lead to the development of tamp-cast flare systems with higher binder content (9%) which can be consolidated at greatly reduced pressures (50-100 psi). A result of this work has been the LUU-2B flare, which utilizes a tamp-cast candle containing a binder based on Formrez 17-80 carboxyl terminated polyester (Witco Chemical Company) cured with ERLA 0510, a trifunctional epoxy resin (Union Carbide Corporation).

Dow has been developing tamp-cast binder based flare compositions with combustion properties equivalent to the system presently used in the LUU-2B flare.

##### A. INITIAL BINDER EVALUATION

The combustion properties of tamp-cast flares prepared with a series of potential Dow binder systems and the binder system of Formrez 17-80/ERLA 0510 are summarized in Table VI. The data show that both the binder resin and the curing agent have an effect on the burning rate and efficiency of the tamp-cast flares. The use of maleic anhydride as a curing agent for either the XF-4013L or the epoxy novolac doubled the burning rates of flares over those based on the same binders with an aminated polyglycol curing agent. The combination of fast burning rate and high efficiency produced flares of extremely high intensity. The XF-4013L/maleic anhydride based flare had twice the burning rate (0.132 vs. 0.066 in./sec.) and intensity (236,900 cd. vs. 108,900 cd.) as the standard flares based on Formrez 17-80/ERLA 0510. The epoxy novolac/maleic anhydride based flares were almost three times as fast and bright as the standard flares. The 0.194 in./sec. burning rate and 301,500 candlepower intensity of the 1.25 in. diameter epoxy novolac/maleic anhydride based flares made them the fastest burning and brightest candles ever tested at Dow. This binder system is a prime candidate for any high intensity flare applications.

Table VI

Comparative Performance of Tamp-Cast Flares<sup>a,b</sup>

Binder System		Flare Performance			
Resin	Curing Agent <sup>c</sup>	Oxygen in Binder, %	Burning Rate in./sec.	Efficiency cd.-sec./g.	Average Intensity cd.
Standard FORMREZ 17-80 Resin	ERLA 0510	39	0.066	53,500	108,900
XF-4008L High Oxygen Epoxy	XF-4010 Aminated polyglycol	31	0.061	54,200	102,000
XF-4013L, Sulfur Containing Epoxy	XF-4012 Aminated polyglycol	21	0.082	47,800	120,900
XF-4013L	Maleic anhydride	25	0.132	58,200	236,900
50/50 XF-4008L/XF-4013L	Maleic anhydride	33	0.111	61,100	209,100
Epoxy Novolac	XF-4010	20	0.111	50,000	171,100
Epoxy Novolac	Maleic anhydride	31	0.194	50,400	301,500

<sup>a</sup> 61/30/9 Mg/NaNO<sub>3</sub>/Binder.<sup>b</sup> All flares 1.25 diameter and pressed at 3,200 psi.<sup>c</sup> All binder compositions were at 1:1 epoxy to curing agent equivalent ratio.



The XF-4008L/XF-4010 binder system was chosen for further development in tamp-cast flares. Data from flare producers verified the performance data, but indicated that the binder had borderline pot life and could present processing problems.

#### B. IMPROVED BINDER DEVELOPMENT EFFORTS

Efforts were concentrated on the development of a binder system which would retain the performance properties of the XF-4008L/XF-4010 binder, but would significantly increase pot life. Recent work has resulted in a family of carboxyl terminated polyol polymers which have excellent pot life, possibly 8-12 hours in large batches of flare composition, with performance properties equivalent to the present LUU-23 binder system. The performance and aging properties of flares based on several of these binders with varying polymeric structures are summarized in Table VII.

The data in Table VII show that the binder composition still has an effect on the burning rate. The particular polyol structures for the polymers in Table VII were selected because they produced flares with burning rates in the same range as the Formrez 17-80/ERLA 0510 (0.070 in./sec.). The flares based on the Dow binders were prepared at a Mg/NaNO<sub>3</sub> ratio of 58/33, while the flares using Formrez 17-80/ERLA 0510 were prepared at the 61/30 Mg/NaNO<sub>3</sub> ratio specified for the LUU-2B flare. Even at the reduced Mg content, the performance of the Dow flares was comparable to the standard flares and one-month aging at 70°C. resulted in no significant changes in performance.

The carboxyl terminated polyglycol structure 5615-44A was selected for further evaluation and was designated XF-4062L. To determine the effect of a case material on the XF-4062L/4008L binder system, flares were pressed into 3.4-inch diameter, cotton-phenolic tubes lined with Viton A fluoroelastomer. All the flares were pressed at 1,500 psi in a Dake press to assure equivalent density. The flares were burned in an inverted position with the air flow upward to simulate conditions normally encountered.

Table VIII compares the performance data of the 3.4-inch flares based on the XF-4062L/XF-4008L with flares based on the binder of Formrez 17-80/ERLA 0510. The data show that the XF-4062L/XF-4008L flares gave slightly higher efficiency and intensity at a slower burning rate (longer burning time). These data are being repeated by another laboratory to verify our results.

Efforts are being directed toward further evaluation of the carboxyl terminated polyol binders and optimization of flare performance based on several of the most promising of these binders. The combination of long pot life, good processability, and good flare performance make these binders outstanding candidates for all types of illuminating flares.

Table VII

Comparison of Performance and Aging Properties of Tape-Cast Flares<sup>a</sup>

Binder System <sup>c</sup>		Flare Performance <sup>b</sup>			
		Burning Rate in./sec.	Original Efficiency cd.-sec./g.	Burning Rate in./sec.	Efficiency cd.-sec./g.
Resin	Curing Agent				
FORMREZ 17-80	ERLA 0510	0.070	51,600	0.072	50,600
6041-44F	XF-4008L	0.071	51,100	0.069	50,300
5615-44A (XF-4062L)	XF-4008L	0.063	53,300	0.066	50,000
5615-56A	XF-4008L	0.068	56,100	0.075	51,400
5615-56B	XF-4008L	0.073	50,300	0.077	49,100

<sup>a</sup>58/33/% M<sub>3</sub>/N<sub>2</sub>O<sub>5</sub>/Binder (FORMREZ 61/30/9).<sup>b</sup>All flares 1.25" diameter and pressed at 3,200 psi.<sup>c</sup>All binder compositions were at 1:1 resin to curing agent equivalent ratio.

Table VIII

Comparative Performance of Flares in 3.4"  
Diameter Cotton-Phenolic Cases

<u>Binder System<sup>e</sup></u>		<u>Flare Performance<sup>a, b</sup></u>		
		<u>Burning Rate</u>	<u>Efficiency</u>	<u>Average</u>
<u>Resin</u>	<u>Curing Agent</u>	<u>in./sec.</u>	<u>cd.-sec./g.</u>	<u>Intensity</u>
				<u>cd.</u>
FORMREZ 17-80 <sup>c</sup>	ERLA 0510	0.068	31,500	495,000
XF-4000L <sup>d</sup>	XF-4062	0.063	35,200	512,000

<sup>a</sup>Cases lined with Viton A.

<sup>b</sup>Flares at 9% binder and pressed at 3,200 psi - 3.4" diameter.

<sup>c</sup>61/30/9 Mg/NaNO<sub>3</sub>/Binder.

<sup>d</sup>58/33/9 Mg/NaNO<sub>3</sub>/Binder.

<sup>e</sup>All binder compositions were at 1:1 resin to curing agent equivalent ratio.

V. CONCLUSIONS

The binder composition of both pressed-grain and tamp-cast flares has a significant effect on the burning rate and luminous efficiency of the flares. Binder systems are available which will vary the burning rates of pressed grain flares from approximately 0.055-0.095 in./sec. while maintaining the efficiency of the flares at about 50,000 cd.-sec./g. Tamp-cast flares have been prepared with burning rates from about 0.055-0.196 in./sec. and efficiencies in the 50,000-55,000 cd.-sec./g. range. Binder systems are available to design flare compositions to meet a wide range of burning time and light intensity requirements.

Variations in the binder ingredients can be used to control the burning rate of flares, while maintaining a constant Mg/NaNO<sub>3</sub> ratio. An amine-cured epoxy resin binder system has been designed and is being used in the MK 24 and MK 45 flares to improve the temperature and humidity stability of the flares. Changes in the ratio of the D.E.R.<sup>®</sup> 321 and D.E.R.<sup>®</sup> 732 epoxy resins have been shown to vary burning times of the flares by at least 15% even at a 4% binder level.

A new family of carboxyl terminated polyol binders has been developed and shows promise in tamp-cast flare formulations. The long pot life and performance properties of flares prepared from these binders make them candidates for further evaluation in both tamp-cast and pressed-grain flares.

# POUR-CASTABLE COMPOSITIONS

FOR

## COLORED SMOKE SIGNALS

by

Harold E. Filter, Erwin M. Jankowiak, George A. Lane, and  
Don L. Stevens

The Dow Chemical Company, Midland, Michigan

### ABSTRACT

Work funded by Picatinny Arsenal resulted in the development of a pour-castable pyrotechnic composition for the dissemination of colored dyes. The polymeric binder composed of SA-1455, tris[2-(1-aziridinyl)ethyl]trimellitate, and XF-4018L, triethylenetetramine, used with  $\text{KClO}_3$  oxidizer and a smoke dye produced a castable formulation which generated a smoke of good quality and density.

This paper reports a proprietary program undertaken to improve the binders developed in the contract efforts, optimize the composition, and develop applications for the resulting smoke compositions. By varying the concentration of the dye, oxidizer and binder-fuel in the formulation the burning rate of the composition could be controlled.

Application development work involved the use of red and white smokes in 105 mm. smoke canisters, the use of red smokes to identify and mark the flight path of aircraft, and the use of red, yellow, green, and violet smokes in M-18 hardware.

New pour-castable binder systems are presented which are generally applicable to all smoke colors and have good surveillance properties.

## I. INTRODUCTION

At the First Pyrotechnic Seminar, August 1968, at Estes Park, Colorado, Dr. Goerge A. Lane presented a paper on, "Colored Signal Smokes: Castable Compositions". The work, funded by Edgewood Arsenal [Contract Nr. DA-18-035-AMC-118(8)], resulted in the development of a promising castable pyrotechnic composition for the dissemination of red smoke. Further efforts under contract to Picatinny Arsenal [Contract Nr. DA-28-017-AMC-3412(A)] were concentrated on the development of castable, polymer-bonded green smoke formulations. A new polymeric binder system based on tris[2-(1-aziridinyl)ethyl]trimellitate was used for the more heat sensitive green smoke dye. The binder system also appeared to be generally applicable to white, yellow, and red smoke formulations.

A proprietary program was undertaken to continue the development of castable colored smoke formulations and to develop applications for the smoke compositions. This paper reports the results of the program. Data are presented on the optimization of castable smoke compositions; application of the compositions in 105 mm. M1 smoke units, aircraft markers, and M-18 smoke grenades; and a promising new binder system for pour-castable smokes.

## II. OPTIMIZATION STUDIES

The development of promising castable, polymer-bonded colored smokes based on a binder system composed of SA-1455, tris[2-(1-aziridinyl)ethyl]trimellitate, cured with XF-4018L, triethylencetetramine was funded by Picatinny Arsenal.<sup>1</sup> Smoke quality and yield were good and were approximately constant over a week storage at 72°C. An examination of the most promising red, green, yellow, and white smoke formulations listed in Table I show that the burning rates of the green and yellow formulations in particular were too fast for practical application. An in-house program was undertaken to decrease the burning rates of these smokes and optimize each of the colored smoke formulations.

### A. EFFECT OF THE BINDER RESIN/CURING AGENT RATIO

Initial burning rate studies involved an evaluation of various curing agents for the SA-1455 binder resin. The work involved

---

<sup>1</sup>"Exploratory Development of Colored Smoke Formulations," G. A. Lane, E. M. Jankowiak, J. P. Flynn, Final Report Contract Nr. DA-28-017-AMC-3412(A).

Table I

Colored Smoke Formulations

<u>Composition and Properties</u>	<u>Smoke Formulations</u>		
	<u>Red</u>	<u>Green</u>	<u>Yellow</u> <u>White</u>
Granular Dye, %	50.0	45.0	40.0
KClO <sub>3</sub> , %	24.9	27.5	32.0
SA-1455-tris[2-(1-aziridinyl) ethyl]trimellitate, %	21.9	22.0	24.2
XF-4018L, Triethylene- tetramine, %	3.2	5.5	3.8
Burning Rate, in./sec.	0.024	0.070	0.061
Color	Good	Good	Good
Stability	Good	Not tested	Good

curing agents which had shown promise with epoxy resin systems in earlier smoke development programs. Several sulfur-containing curing agents gave indications of producing good binder systems, especially from the standpoint of low formulation viscosity (castability) and good smoke quality (color and yield).

However, further investigation showed that these curing agents used with SA-1455 also produced smokes with very rapid burning rates and the work was terminated.

The most successful method of controlling burning rate was the use of higher ratios of curing agent in the SA-1455 binder. The data in Table II show the effect of increasing the amount of the XF-4018L curing agent from 20.0% to 38.2% of the total binder compositions. The burning time of the smoke grains was increased from 10 seconds (0.085 in./sec.) to 22 seconds (0.039 in./sec.) by increasing the XF-4018L content. However, only the fast burning formulation (20% XF-4018L) was stable after 12 weeks of aging at 72°C.

The effect of increasing the amount of DSEH-97 in the SA-1455 binder on green smoke performance is summarized in Table III. The DSEH-97 has an effect directly opposite that of XF-4018L in the SA-1455 binder. Increasing the DSEH-97 content decreases the burning time of the green smoke from 12-15 seconds (0.071 in./sec.) to 3-4 seconds (0.283 in./sec.). The green smokes prepared from the lower DSEH-97 concentration show the least change in burning time and color quality after 12 weeks of aging at 72°C.

The data in Tables II and III indicate there is a very definite limit in the concentration of XF-4018L or DSEH-97 which can be used with the SA-1455 binder. The use of the XF-4018L curing agent is limited to approximately 20-25% of the total binder, while the limit of DSEH-97 is 25-29% of the total binder. While the data shown is only for green smoke formulations, similar data was obtained on red, yellow, and violet smokes.

The effects of varying the ingredients of green smoke compositions on the burning rate and color are summarized in Table IV. All the smoke grains were in insulated M-18 cans and were off-center internal-burning configurations. The configuration produced a web thickness of 1.42 inches. The XF-4018L concentration was held at approximately 23.5% of the total binder to assure good thermal aging stability of the smoke compositions. Similar data were obtained on red, yellow, and violet smokes.

The dye concentration and the binder-fuel/oxidizer ratio of the smoke compositions have a significant effect on burning rate and color quality. It appears there is an optimum binder-fuel/oxidizer/dye ratio which will give the best color at any specified burning rate. Formulation 5612-75 was burned in an end-burning and internal-burning configuration and gave identical burning rates.

### III. POUR-CASTABLE 105 mm. M1 TYPE SMOKE UNITS

The superior physical properties of the polymer-bonded smoke

Table II

Effect of XF-4018L Content On Green Smoke Performance

<u>Composition and Properties</u>	<u>Smoke Formulations<sup>a</sup></u>		
	<u>416</u>	<u>260</u>	<u>420</u>
Granular Dye, %	45.0	45.0	46.0
KClO <sub>3</sub> , %	27.5	27.5	26.5
SA-1455, %	22.0	20.0	17.0
XF-4018L, %	5.5	7.5	10.5
% XF-4018L in Binder	20.0	27.3	38.2
Burning Time, sec.			
Initial	10	15	22.0
After 12 weeks at 72°C.	8	Deflagrated in oven	No ignition
Burning Rate, in./sec.			
Initial	0.085	0.056	0.039
After 12 weeks at 72°C.	0.108	Deflagrated in oven	No ignition
Color			
Initial	Good	Good	Good
After 12 weeks at 72°C.	Good	Deflagrated in oven	No ignition

<sup>a</sup>All smoke grains were cast in 35 mm. film cans - 25 grams weight and 0.85 inch high.



Table III

## Effect of DSEH-97 Content on Green Smoke Performance

Composition and Properties	Smoke Formulations <sup>a</sup>		
	544	545	543
Granular Dye, %	47.0	47.0	47.0
KClO <sub>3</sub> , %	25.5	25.5	25.5
SA-1455, %	19.35	16.7	14.6
DSEH-97, %	8.15	10.8	12.9
% DSEH-97 In Binder	29.6	39.2	52.0
Burning Time, sec.			
Initial	12-15	10-11	3-4
After 12 weeks at 72°C.	18-19	35.0	20.0
Burning Rate, in./sec.			
Initial	0.071-0.037	0.085-0.077	0.283-0.213
After 12 weeks at 72°C.	0.047-0.045	0.025	0.043
Color			
Initial	Excellent	Good	Good
After 12 weeks at 72°C.	Good	Fair	Poor

<sup>a</sup>All smoke grains were cast in 35 mm. film cans - 25 grams weight and 0.85 inch high

Table IV

Effect of Smoke Composition on Green Smoke Performance

Composition and Properties	Smoke Formulations <sup>a</sup>		
	5612-75	5613-2A	5613-4A
Granulated Dye, %	45.0	50.0	53.0
KClO <sub>3</sub> , %	27.5	22.5	22.5
SA-1455, %	21.0	21.0	18.7
XF-4018L, %	6.5	6.5	5.8
Burning Time, sec.	105.0	86.5	67.0
Burning Rate, in./sec.	0.33	0.016	0.021
Color	Good-Fair	Good	Excellent-Good
			Excellent

<sup>a</sup>All smoke grains were cast into insulated M-13 cans - 250 grams weight and 1.42 inches thick.

compositions make them prime candidates for gun-fired projectiles. Therefore, efforts were directed toward adopting our pour-castable red and white smoke compositions to the 105 mm. M1 type smoke canisters used in the M84A1 smoke cartridge.

The 105 mm. metal canister is approximately 2.9 inches diameter by 3.5 inches high with a 0.6 inch diameter tube down the center. An epoxy coated insulator was adhered to the sides and bottom of the container to insulate the metal can from the burning smoke composition and assure case bonding and uniform combustion. A castable igniter compound was applied to the outside diameter of the metal center tube and cured at room temperature. Enough material was used to fill and bridge the ignition holes in the tube and to bond to the metal between the holes.

The smoke compositions used and the burning times achieved are shown in Table V. All the compositions were prepared on a Hobart mixer. Approximately 390 grams of the white composition or 375 grams of the red composition were cast into the metal canisters and cured 48 hours at 40°C. The canisters were cooled, an epoxy inhibitor was applied to the cured surface, the metal top was placed on the epoxy surface, and the completed unit was cured 2-3 hours at 70°C. Forty-five units of each color were sent to Edgewood Arsenal for evaluation.

Table V

Pour-Castable 105 mm. Smoke Compositions

<u>Composition and Burning Time</u>	<u>White</u>	<u>Red</u>
Dye, %	43.0	45.0
Oxidizer (KClO <sub>3</sub> ), %	27.0	27.5
SA-1455, %	24.2	21.0
FPS-4018L, %	5.8	6.5
Burning Time, Sec.	45	36

Several of the white units were loaded into M84A1 smoke cartridges and statically fired. Duplicate firings were made and the smokes ignited and burned for the specified time (45 seconds). The color and density of the resulting smoke clouds were compared with standard HC units and rated equivalent by test personnel.

Both the red and white units were ballistically tested in gun firings at Jefferson Proving Ground. All of the pour-castable smoke units ignited prematurely. The gunnery officer reported that all of the units ignited upon firing and appeared to eject

from the cartridges upon leaving the gun barrel. The cause was premature ignition of the first fire. The units appeared to function normally on the ground 400-700 yards down range from the gun. The smoke color and density was impressive to the test personnel.

#### IV. POUR-CASTABLE RED SMOKES FOR AIRCRAFT MARKING

A program to demonstrate the feasibility of using colored smokes to identify and mark the flight path of target drones was undertaken as a joint effort between Dow and the Pace Corporation, Memphis, Tennessee. Dow provided the smoke units and Pace the hardware required in the program.

The goal was the development of a smoke unit to emit a large enough volume of red smoke, when functioned on a flying drone, to be visible from the ground and from aircraft in flight. A fast burning smoke composition was chosen.

The pour-castable smoke composition was adapted to containers prepared from 5-inch diameter cardboard tubes. An epoxy resin based smoke formulation, designated Formulation No. 285 and previously developed on an Edgewood Arsenal contract by G. A. Lane and E. M. Jankowiak was used. The composition had been shown to produce red smokes with good color and density. The epoxy resin based red smokes showed no change in color or burning times after 12 weeks at 70°C. The smoke formulation used is shown in Table VI.

Table VI

#### Composition of Red Smoke Formulation No. 285

<u>Ingredients</u>	<u>Wt. % Solids</u>
MAAQ <sup>a</sup> (red dye)	40.0
KClO <sub>3</sub>	30.0
XF-4013L (Sulfur based epoxy resin)	12.9
XF-4008L (Glycerin based epoxy resin)	3.5
XF-4008L (Polysulfide resin)	3.5
BDMA (Benzyl dimethylamine)	10.1

<sup>a</sup>85% Methylaminoanthraquinone, 15% dextrin.

A small particle size red dye, was used in the smoke formulation. A tamp-cast, rather than a flow-castable smoke composition was obtained. Due to the time and cost limitations of the feasibility study, the tamp-cast formulation was considered acceptable for our work.

The work was concentrated on a 5-inch diameter by 5-inch long smoke unit with a burning time of 35-45 seconds. To obtain the proper burning time a configuration composed of six cylindrical holes, 0.5 inch in diameter, were equally spaced in a hexagonal pattern, 0.63 inch from the edge of the unit. An additional cylindrical hole was placed in the center of the unit. The final unit contained approximately 4.85 pounds of smoke composition, had a burning time of 35-40 seconds and produced a dense red smoke cloud.

Eleven of the large red smoke units were sent to the Pace Corporation and placed in their hardware. The completed units were sent to Holloman Air Force Base for feasibility testing. Feasibility tests consisted of placing four of the smoke units on the wings of a subsonic drone. The smoke units were functioned individually while the drone was flying at 18,000 feet and in excess of 400 mph.

The tests were a success. The smoke trail from a single 5-inch by 5-inch unit was seen by the naked eye at ground level at a distance of at least 28 nautical miles. Observers in aircraft following the drone at distances of 200-12,000 feet, reported the red smoke was more visible against the hazy horizon and the yellow desert than a white oil smoke used as a standard in the test.

#### V. POUR-CASTABLE M-18 TYPE COLORED SMOKE GRENADES

A program was undertaken to develop pour-castable red, green, yellow, and violet smokes in M-18 hardware. The major portion of the program concerned the development of smokes which would produce a uniform color for the required burning time. At the time the program was begun, green and yellow formulations in particular, had burning times in excess of 50 to 90 seconds.

An epoxy coated insulator was adhered to the sides and bottom of the metal M-18 cans. An end-burning configuration was found unsatisfactory, due to the need for extremely slow burning smoke compositions and the filtering of the smoke through the ash. Filtering through the ash changed the color quality of the smoke from a deep color to a pale color during the functioning of the munition.

An off-center, internal-burning (OCIB) configuration was adapted. The OCIB configuration consisted simply of a 0.75-inch diameter

cylindrical hole down one side of the grain. This resulted in burning of the grain at the periphery of the cylindrical hole. Placing the hole at the edge of the grain produced a web thickness of 1.42 inches and no significant filtering occurred from the resulting ash.

The required burning rates were obtained by proper adjustment of the dye concentration, oxidizer level, and binder-fuel content of the formulations as previously discussed in the Optimization Studies (Part II) section of this paper. The starting point formulations used are shown in Table VII and the final formulations used to prepare the M-18 grenades are summarized in Table VIII.

Combustion data on smokes of both end-burning and OCIB configurations have been included in Table VII. The combustion data show the configuration makes no significant difference in the burning rate of the smoke composition if proper insulation is used to prevent side burning.

The formulations shown in Table VIII were used to prepare M-18 type grenades which were submitted to Edgewood Arsenal for evaluation. Colloidal silica had to be added to the low viscosity yellow and violet compositions to prevent the dye from settling during cure. All the metal M-18 cans were insulated with an epoxy coated cardboard insulator. The formulations were mixed on a Hobart mixer, cast into the insulated cans, cured in a circulating air oven for at least 20 hours at 40-45°C., and post cured at 70°C. for 4 hours.

A total of 120 of the M-18 type grenades, 30 of each color (red, green, yellow, and violet), were submitted to Edgewood Arsenal for evaluation. Data obtained from Edgewood Arsenal indicated that all four colors of grenades functioned satisfactorily on initial firing and after 12-week storage at ambient conditions. Under these conditions the smoke grenades functioned within the specified time limits of 50 to 90 seconds and produced good color and volume of smoke. However, after 12 weeks of storage at 155°F., only the red and violet grenades performed comparable to standard M-18 grenades used as controls. The burning time of green pour-castable smokes increased to approximately 130-150 seconds and the yellow smokes would not ignite.

## VI. BINDER IMPROVEMENTS

New binder systems composed of a family of carboxyl terminated polyols cured with epoxy resins have recently shown promise as castable smoke binders. Since most of the problems with stability appeared to occur with yellow smokes, work was concentrated on this color. Several binder systems have shown promise in initial evaluations.

Table VII

## Initial Formulations Used For Orientation

Of

## Burning Rates and Mixing Properties

Composition and Burning Properties	Red	Pour-Castable Smoke		
		Green	Yellow	Violet
Granulated Dye %	45.0	45.0	47.5	50.0
KClO <sub>3</sub> (-200 Mesh, includes 3% MgCO <sub>3</sub> ), %	27.5	27.5	30.0	27.5
SA-1455 (tris[2-1-aziridinyl)ethyl] trimellitate), %	21.0	21.0	17.5	18.0
XF-4018L (Triethylenetetramine), %	6.5	6.5	5.0	4.5
Burn Time, End Burners <sup>a</sup> , sec.	200.0	105.0	53.0	54.0
Burning Rate, End Burners <sup>a</sup> , in./sec.	0.018	0.033	0.065	0.064
Burn Time, OCIB, sec.	78.0	43.0	21.0	Not tested
Burning Rate, OCIB, in./sec.	0.018	0.033	0.068	Not tested

<sup>a</sup>The smoke filters noticeably with all end burners.

Table VIII

Final Formulations Used In The M-18 Grenades

Composition and Burning Properties	OCIB Pour-Castable Smoke			
	Red	Green	Yellow	Violet
Granulated Dye, %	45.0	52.0	51.0	51.0
KClO <sub>3</sub> (-200 Mesh, includes 3% MgCO <sub>3</sub> ), %	27.5	22.5	21.6	21.3
SA-1455 (tris[2-(1-aziridinyl)ethyl], % trimellitate)	21.0	19.47	21.08	21.08
XF-4018L (Triethylenetetramine), %	6.5	6.03	6.02	6.02
CAB-O-SIL, %	--	--	0.30	0.60
Burn Time, sec.	71.0	70.0	57.0	62.0
Burning Rate, in./sec.	0.020	0.020	0.025	0.023



Work with the carboxyl terminated polyol binders has been done in insulated 35 mm. film cans. No side burning has occurred and excellent results have been obtained. The binder systems have a long pot life (in excess of 4 hours) and can be cured at 70-80°C. in 16-24 hours.

Data on three of the most promising systems are shown in Table IX. All data was obtained on 25 gram samples cast in insulated 35 mm. film cans and cured for 24 hours at 80°C. Aging data on the 5613-49A resin has shown no significant changes in burning time or rate after 12-weeks aging at 70°C. The use of a 50/50 mixture of XF-4013L/D.E.R.<sup>2</sup> 334 produced relatively slow burning rates with both yellow and violet smokes. No significant change in combustion properties was found with either the yellow or violet smoke after 12-weeks aging at 70°C. The green smoke based on the XF-4062L/XF-4013L binder shows good initial properties, but aging data are not completed. The color of all the smoke compositions in Table IX appears excellent (good quality and density).

In addition to the 12-week aging data on the yellow and violet smokes, additional smoke munitions containing these compositions have been aged 16 weeks at 70°C. The munitions were then cold soaked at -65°F. and fired at -65°F. Neither the yellow or the violet compositions showed any change in grain geometry or any evidence of cracking. The yellow composition showed an increase in burning time from 34 to 73 seconds when fired at -65°F., while the violet composition only increased from 37 to 52 seconds. The change in burning time appears to be due to the low functioning temperature (-65°F.) rather than the long-term thermal aging.

Work is continuing with the promising castable, polymer-bonded colored smoke compositions based on the carboxyl terminated polyol resins.

## VII. CONCLUSIONS

The dye concentration and the binder-fuel/oxidizer ratio of castable smoke formulations have a significant effect on the burning rate and color quality of the smokes. There is an optimum binder-fuel/oxidizer/dye ratio which will give the best color at any specified burning rate.

Successful static firings were obtained with M84A1 smoke cartridges containing pour-castable white smokes in 105 mm. M1 type smoke canisters. Ballistic firings of red and white smoke units resulted in premature ignition of the first fire which caused the units to function on the ground 400-700 yards down range from the gun. Work is being conducted to eliminate the premature ignition of the first fire.

Table IX

Combustion Properties of Colored Smokes

Based On

Carboxy Terminated Polyol Binder Systems

Composition and Burning Properties	Smoke Formulations		
	CD-561-3-49A	CD-561-3-50	CD-561-3-83A
Granulated, Yellow Dye, <sup>a</sup>	51.0	---	---
Granulated, Violet Dye, <sup>a</sup>	---	51.0	---
Granulated, Green Dye, <sup>a</sup>	---	---	50.0
KClO <sub>3</sub> , <sup>a</sup>	21.6	21.6	25.0
5613-49A, <sup>a</sup>	7.40	7.40	---
XF-4062L, <sup>a</sup>	---	---	10.4
50/50 XF-4013L/D.E.R. <sup>5</sup> 334, <sup>a</sup>	20.1	20.1	---
XF-4013L	---	---	14.6
Burning Time, sec.			
Initial	34	37	35
After 12 weeks at 70°C.	38	34	Not tested
Burning Rate, in./sec.			
Initial	0.025	0.023	0.024
After 12 weeks at 70°C.	0.022	0.025	Not tested

<sup>a</sup>Carboxyl terminated polyol resins

Castable red smokes were used to identify and mark the flight path of aircraft. Red smoke units placed on the wings of drones flying at 420 mph and 18,000 feet, produced a smoke trail which was visible on the ground at a distance of 28 nautical miles.

Internal-burning grenades in M-18 hardware were prepared from pour-castable red, yellow, green, and violet smoke compositions. All four colors initially met the specifications for standard pressed M-18 grenades, but only the red and violet grenades met specifications after surveillance.

Promising castable colored smokes have been prepared from binders based on a new family of carboxyl containing polyols. The long pot life and stability of smoke compositions prepared from these binders make them candidates for further evaluation as general purpose binders for smoke dissemination.

# Observations of the Surface Details of Burning $\text{Mg}/\text{NaNO}_3$ /Binder Flares

John L. Eisel

Aerothermochemistry Division

Naval Weapons Center, China Lake, Calif.

## ABSTRACT

Because the physical - chemical details of flare combustion are largely unknown, a study was undertaken to elucidate certain aspects of these processes. The surface processes of the combustion were observed using high speed (up to 4000 frames per second) and high magnification (up to 4x on the film) color cinematography.

It was observed that at the surface the  $\text{NaNO}_3$  melts, flows together into large masses and decomposes. Non-molten Mg particles are captured at these decomposition sites and are ejected - still non-molten - into the flame zone away from the surface. Although sodium D line radiation accompanies this ejection process most of the illuminating radiation appears to take place in the metal combustion region away from the surface. The degree of activity and surface structure are observed to vary as a function of particle size and composition.

## OBSERVATIONS OF SURFACE DETAILS OF BURNING $\text{Mg}/\text{NaNO}_3$ /BINDER FLARES

### INTRODUCTION

Only in recent years have the physical and chemical details of pyrotechnic flare combustion come under close scrutiny. These efforts have emphasized such aspects as the spectral distribution and how it can be affected (<sup>1,2,3</sup>), the chemistry of component reactivity and decomposition (<sup>4,5</sup>), and the effects of such variables as binder type and constituent particle size on flare efficiency (<sup>6,7</sup>).

The present preliminary study is aimed at elucidating some of the details of decomposition and combustion occurring at the burning surface of  $\text{Mg}/\text{NaNO}_3$ /binder flares. The means for making the observations to be reported herein have been high speed, high magnification color motion pictures. The understanding of the details seen comes, to a great extent, from careful repeated observations of a number of films. For this reason only a summary of the observations and some discussion based on these observations will be presented here. The films on which these judgements are based will be made available here. The films on which these judgements are based will be made available to qualified agencies upon request.\*

Reference to Table 1 will indicate that a rather limited selection of flare ingredients and compositions was investigated. For this reason generalization based on observations reported here must be avoided without further investigation.

---

\*Requests may be made to Commander (Code 6082), Naval Weapons Center, China Lake, Calif. 93555, Attn: Dr. John L. Eisel.

### THE EXPERIMENTAL SETUP

The motion pictures from which observations were made and conclusions drawn in this study were of 0.25 inch diameter pressed strands of the flare materials listed in Table 1. The strands were ignited on their upper end by an electrically heated bridgewire, usually tungsten. The flares were burned at one atmosphere pressure with a sheath of nitrogen to carry the products of combustion away from the field of view and to prevent secondary burning with inducted atmospheric air. The combustion platform is shown in Fig. 1. Illumination of the burning surface was provided by a focused 2500 watt xenon lamp which could be periodically interrupted by a chopper wheel to permit observation of self-luminosity. The camera used was a Redlakes Laboratories Hycam framing rates of up to 4000 frames per second and provided with lens extensions necessary to achieve magnification of up to 4X on the film.

Illumination was generally at 60 degrees with respect to the line of camera sight when surface illumination was desired. In some cases to be discussed later, it was desirable to silhouette the condensed phase particles leaving the burning surface. In this case the xenon lamp radiation was directed down the camera line of sight, across the burning surface, and through a blue filter which minimized the yellow flare radiation as seen by the camera.

Certain restrictions of the experiment must be kept in mind while assessing the results. First, the small diameter of the flare led to a less efficient energy feedback due to heat losses at the edges. Second, the flare was burned in a "flame up" configuration with a nitrogen gas purge in the direction of product gas flow. This discouraged secondary combustion with inducted air. And finally, as noted before, only a limited number of composition variations were observed which precluded generalizations.

## OBSERVED DETAILS OF COMBUSTION AND DISCUSSION OF RESULTS

Certain observations were general and will be described without respect to composition or ingredient particle size. Others were the result of variations in composition and particle size and will be discussed later.

When observing the surface details of  $\text{Mg}/\text{NaNO}_3$ /binder flares the first thing that impresses itself on the viewer's consciousness is the fact that sodium nitrate melts and decomposes on the surface. The molten oxidizer draws up into bubbling "balls" or "globules" at isolated sites on the burning surface whose size and activity are dependent upon variables to be discussed later on. These globules tend to grow by gathering up newly melted material or by coalescing with other fully formed globules. These, from the time of their formation, undergo a boiling decomposition which appears to be the major mechanism by which the oxidizing species reach the gas phase and subsequently the flame. There appears to be greater cohesive or surface tension forces than adhesive forces between the molten globules and the solid surface with the result that little wetting of the surface by the molten oxidizer is apparent. As new particles of  $\text{NaNO}_3$  become exposed at the surface they are seen to first melt and then to begin to decompose, usually joining nearby larger globules.

The magnesium, on the other hand, appears never to be molten at the flare surface. Magnesium particles leave the surface by two routes with apparently random distribution between the two. The exposed particle becomes free due to regression and melting of the surrounding material and can either be carried from the surface into the gas-phase region by evolving gas flow, or by a second, more spectacular route. By this second mechanism magnesium particles free on the surface, but not in a strong gas stream, are deposited on the surface of a decomposing oxidizer globule where it either remains temporarily or where it is totally engulfed. Upon contact between the magnesium particle and the oxidizer globule, no increase in the decomposition activity of the globule can be visually detected indicating a similarity of temperatures. After an induction period, which is not constant, the magnesium particle is ejected from the globule at high velocity accompanied by a flash of what appears to be sodium D radiation and often some oxidizer fragments. Never were such expelled magnesium particles seen to deform or divide as they left. Although very spherical, carefully sized magnesium was used in most of this study two mixes were made using non-spherical, rather flattened

magnesium particles with considerable irregularity. When observed during combustion these particles were seen to leave the surface in their original, irregular shape rather than in a spherical configuration. The implication of these observations and of the lack of deformation during expulsion from the surface have been taken as evidence that the magnesium leaves the flare surface in its solid state.

Finally, experiments as previously described, in which the burning sample is back-lighted and filtered and in which the magnification is reduced to increase the field of view, demonstrate that the magnesium particles produce their characteristic dense cloud of MgO smoke after they are well away from the regressing flare surface.

It is well known that  $\text{NaNO}_3$  melts at about  $308^\circ\text{C}$  and magnesium at  $649^\circ\text{C}$ . It has further been reported<sup>4</sup> that  $\text{NaNO}_3$  begins its thermal decomposition as a result of slow heating at about  $450^\circ\text{C}$ . It must therefore be concluded that the temperature of the burning flare surface must be in this region between  $450^\circ\text{C}$  and  $649^\circ\text{C}$ . As the further effects of specific variables on the physical configuration of the flare surface will show, very likely no constant value of the surface temperature exists even with the limited class of flares being considered here.

These, then, were the general observations. As composition and particle sizes were varied other details were seen.

A change in  $\text{Mg}/\text{NaNO}_3/\text{Viton A}$  from 55/41/4 to 70/26/4 with gran 17 magnesium leads to a smaller size and shorter lifetime of the decomposing oxidizer globules. On the other hand, if the magnesium particle size is reduced from gran 17 (nominally 200  $\mu\text{m}$ ) to gran 15 (nominally 100  $\mu\text{m}$ ) for a 55/41/4 mix the globule size is reduced even more, the burning rate greatly increased and the radiating region brought closer to the surface. In addition, or more likely as a consequence, the activity of the surface becomes very frenetic. All of these observations lead to the conclusion that the energy feed back is higher than before and the surface temperature has increased.

When the 4 percent binder is changed to Vitel the behavior becomes again somewhat different. With Vitel as a binder the oxidizer globules appear to have even less affinity for the flare surface and tend to wander about collecting more oxidizer as well as magnesium particles. Now when a magnesium particle has been encapsulated by the oxidizer globule there is a tendency for the whole or part of the magnesium-oxidizer mass to leave the surface together rather than simply to expel the metal particle. In addition, the burning rate of the vitel



containing flares is significantly increased at high magnesium loading as compared to those containing Viton A, while remaining nearly the same at low magnesium levels (See Fig. 2).

### CONCLUSIONS

What has been observed, in summary, is that the surface processes during combustion of these flare variations are extremely heterogeneous; are sensitive of fuel to oxidizer ratio; to fuel particle size and to a lesser extent to binder type; that the reactions directly yielding the major portion of the heat release and visible radiation take place well away from the surface, but influence it through varied energy feedback; and that the temperature of the surface, while dependent upon all of these variables, must be bracketed by the temperature of initial decomposition of  $\text{NaNO}_3$  and the melting temperature of magnesium.

The goal of the work - to make known some of the physical-chemical details of the surface conditions of a limited selection of  $\text{Mg}/\text{NaNO}_3$ /binder flare - has been realized. Further work, both in terms of the variety of materials observed and in terms of quantitative measurements, must be done before adequate understanding of these complex processes is attained.

## REFERENCES

1. Douda, B.E., *Spectral Observations in Illuminating Flames* in *Proceedings of First Pyrotechnic Seminar*, AD679911 (Defence Documentation Center), Cameron Station, Alexandria, Virginia, 1968.
2. Hamerick, J.T., J.D. Stanitz, and P.L. Blackshear, Jr., *Exploratory Development of Illuminating Flares*, AD848086 (Defence Documentation Center), Cameron Station, Alexandria, Virginia, 1968.
3. Blunt, R.M., *Study of Illuminating Flames From Solid Reactants*, Naval Ammunition Depot, Crane, Indiana, RDTR No. 77, 1 June 1970.
4. Bond, B.D. and P.W.M. Jacobs, *The Thermal Decomposition of Sodium Nitrate*, J. Chem. Soc. London (A), 1966, p. 1265 ff.
5. Gordon, S. and C. Campbell, *DTA in Inorganic Compounds*, Analytic Chem., 27, p. 1102, 1956.
6. Howlett, S., *The Effect of Particle Size of  $\text{NaNO}_3$  on the Performance of Flare Compounds*, Naval Ammunition Depot, Crane, Indiana, RDTR No. 139, 1 April 1969.
7. Hamrick, Joseph T., *Exploratory Development of Illuminating Flares*, in *Proceedings of Second International Pyrotechnics Seminar*, Denver Research Institute, Denver, Colo., 20 July 1970.

TABLE I

Designation	Magnesium		NaNO <sub>3</sub>	Binder	
CT #	wt. %	granulation	wt. %	wt. %	type
257	70	17	26	4	Viton A
258	55	17	41	4	Viton A
259	40	17	56	4	Viton A
261	55	15	41	4	Viton A
262	70	17	26	4	Vitel
263	55	17	41	4	Vitel
264	40	17	56	4	Vitel
266	55	15	41	4	Vitel
344	55	15	41	4	Viton A
289	55	17	41	4	Viton A
290	55	17	41	4	Viton A

TABLE I. Designations, compositions, and particle sizes of the flares observed.

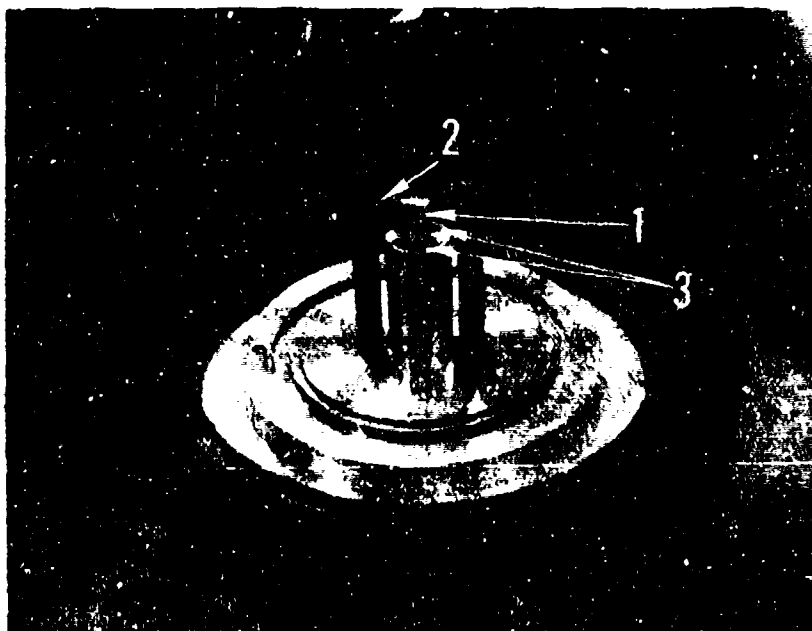


FIGURE 1. View of the combustion platform showing: 1) flare sample, 2) tungsten bridge wire, and 3) nitrogen-purge vents.

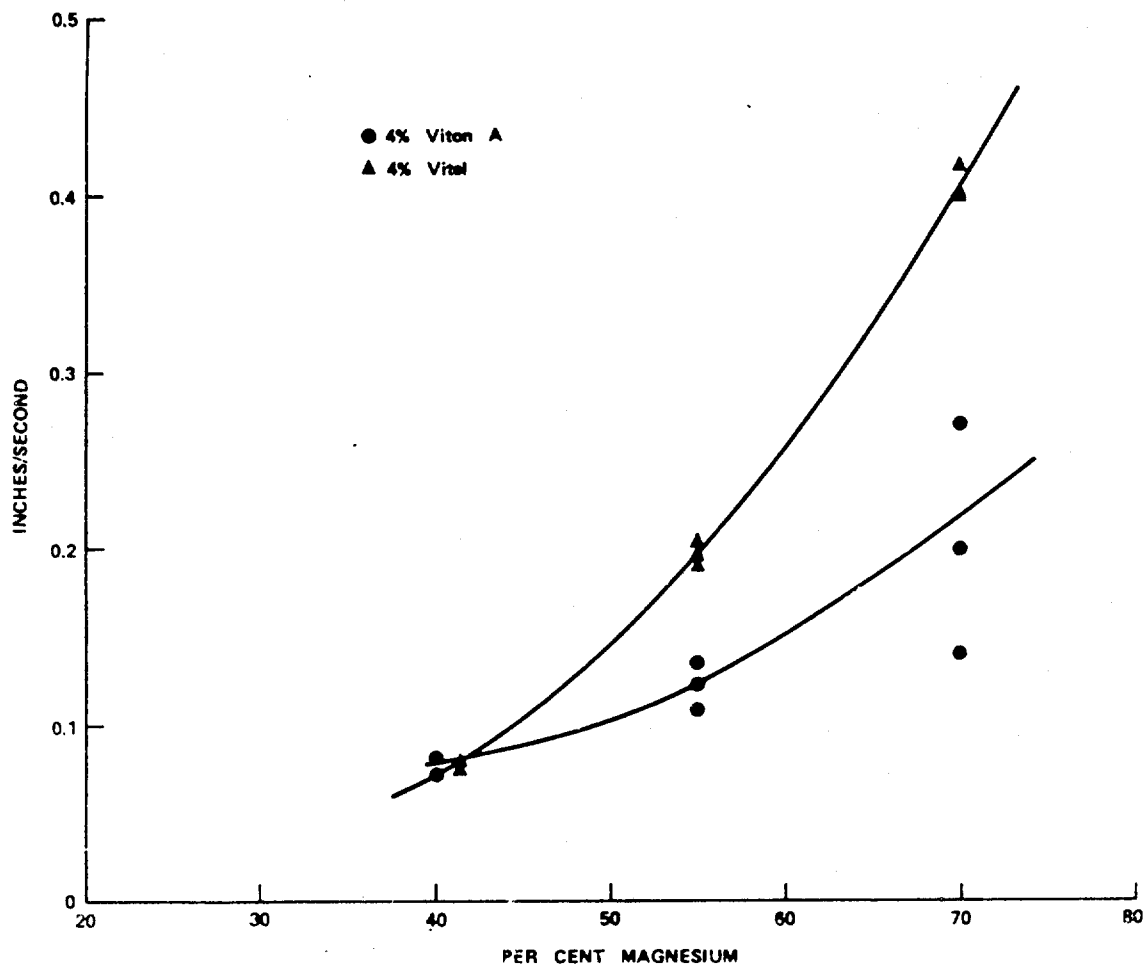


FIGURE 2. Burning rates as a function of per cent magnesium loading at a constant 4 per cent binder for both Viton A and Vitel binders. Data taken from burn times of 7/8 inch diameter pressed flares burning in ambient air.

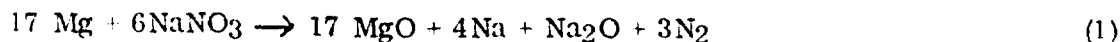
# FACTORS AFFECTING THE STOICHIOMETRY OF THE MAGNESIUM-SODIUM NITRATE COMBUSTION REACTION

by

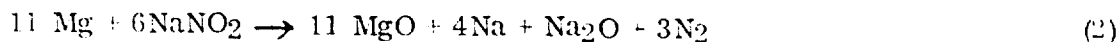
A. J. Beardell and D. A. Anderson  
Pyrotechnics Division, Picatinny Arsenal, Dover, New Jersey

## ABSTRACT

A mass balance investigation of the magnesium-sodium nitrate combustion reaction was made to determine its stoichiometry and the factors which influence the stoichiometry and completeness of reaction. Pressed pellets of the mixture were burned in a sealed bomb under a controlled gaseous atmosphere and the gaseous and solid products were analyzed. Factors investigated were gaseous atmosphere, magnesium particle size, and composition. Using fine particle size Mg (22  $\mu$ ) and a Mg/NaNO<sub>3</sub> mole ratio of 3 it was found that the reaction follows the stoichiometry



When the particle size of the Mg was 350  $\mu$ , the reaction was only about 80% complete. The Na/Na<sub>2</sub>O mole ratio was reduced to 1.4 and sodium nitrite was observed as a major product. The completeness of reaction of coarse Mg was increased by about 5% using 20% O<sub>2</sub> in He atmosphere. Fine particle size Mg reacts completely with NaNO<sub>2</sub> under combustion conditions according to the reaction

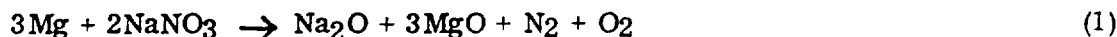


Data is presented which show the relative rates of the combustion reactions and the reactions leading to the final combustion products are discussed.

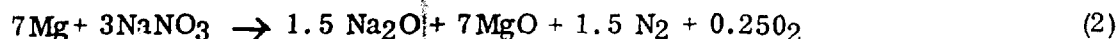
## INTRODUCTION

The importance of the magnesium-sodium nitrate reaction in producing high intensity illumination in the visible region of the spectrum has led to numerous investigations of the reaction mechanism (1, 2, 3). Some investigations have been made over the temperature region of 560 to 700°C, which constitutes the ignition and pre-ignition regime. Other investigations have been concerned with flame studies which are exemplified by the work of Louda (4) in which the emission spectra was emphasized. There is no known study in which the detailed investigation of the stoichiometry of the combustion reaction has been clarified nor is there specific information on the combustion efficiency of the system.

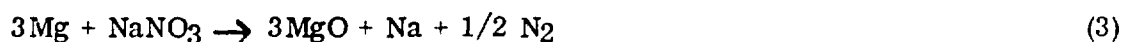
Shidlovsky (5) expresses the reaction stoichiometry as



or



In both cases, sodium oxide is assumed to be the reaction product. Douda (4) expresses the reaction as



in which sodium metal is produced. Thermodynamically, equation (3) appears to be the preferred reaction (6). Previous studies in this laboratory on the effect of gaseous environment on the luminous energy of Al-NaNO<sub>3</sub> flare compositions (7) indicated that metallic sodium is a major product of the reaction. To clarify this situation, a study is being made to identify and analyze the products formed from the combustion of the magnesium-sodium nitrate mixture under a variety of conditions and to determine the combustion efficiency. This report describes the initial phases of this work.

#### EXPERIMENTAL APPARATUS AND ANALYTICAL PROCEDURES

Apparatus. The vessel used to contain the combustion products of the magnesium sodium reaction consists of a standard Parr bomb, 350 ml in volume to which is attached a pressure transducer (0 - 200 psi), and ports which contain a water reservoir and ignition wires. The bomb is also connected to a Bourdon type pressure gauge (0 - 800 Torr) and to a flow loop (6 cc in volume) which leads to a gas chromatograph.

In a typical run, a two or three gram pellet, pressed at 10 K psi, is sealed into the bomb and the system is evacuated to about 0.1 Torr. Helium or other gases are introduced to a pressure of 1 atmosphere. The bomb is then closed off, the remainder of the system is evacuated and the pellet is ignited with an ignition wire. Successful ignition is indicated by a rise in pressure as sensed from an oscillograph connected to the pressure transducer. The pressure-time trace also serves to provide a qualitative measure of the time-to-ignition, combustion efficiency and mass burning rate.

#### Analytical Procedures

Gases. The total nitrogen gas produced was measured by two methods. The combustion bomb was opened to the rest of the system and the gas pressure

was measured directly on the pressure gauge. The gas trapped in the flow loop was then fed into a molecular sieve chromatographic column, which had been calibrated for nitrogen. The procedure also allows the measurement of  $O_2$ , and, with an alternate column ( Poropak ), for nitrogen oxides and ammonia. In almost all instances, the quantity of  $N_2$  measured by both techniques agreed to within 1%. A sample of the gases was also expanded into an IR cell for analysis. However, in no instance were IR absorptions observed.

Sodium. The bomb was evacuated and about 75 cc of degassed water was added to the mixture through the attached closed cylinder. The bomb was swirled to assure water contact at all surfaces in the system. The hydrogen produced in the reaction was then analyzed using the molecular sieve chromatographic column.

Nitrate and Nitrite. A spectrophotometric procedure reported by Wetters and Uglum (8) was used to analyze for unreacted nitrate and nitrite. The method depends on the observation that nitrite has a characteristic band at 355 and a shallow band at 302  $\mu$  in which the absorbance ratio is 2.5 while nitrate has a characteristic band at 302  $\mu$ .

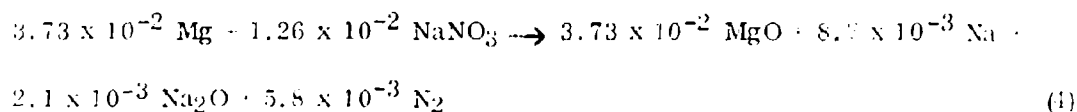
The water solution of soluble products was separated from the solid residue by centrifugation and filtration and the nitrite content was measured using UV spectrophotometry. The solution is basic, having a pH of approximately 11.5, which is due to the sodium hydroxide produced from the reaction of metallic sodium with water and from the solubility of sodium oxide in water. The sodium hydroxide has been shown to be non-interfering in the analysis of nitrate or nitrite (8). However, it was observed that the absorption peak for nitrite shifted from 355 to 362 - 365  $\mu$  for the experimental solution in which the magnesium-sodium nitrate reaction did not go to completion. It is possible that the shift occurs because of interfering effects due to the presence of soluble metallic salts or oxides which may have formed during the combustion process, their source being the ignition wire, the porcelain cup which contained the pellet or the wall of the combustion vessel. For this report, however, the peak observed at 363 - 365  $\mu$  is assumed to be due to nitrite. The impurity effect is considered to be negligible since the  $A_{355}/A_{302}$  is close to 2.5 in every case.

Sodium Oxide. The basic solution was titrated with standard 0.1 N HCl to obtain total sodium ion. The difference between this value and the hydroxide produced in the reaction of sodium was used to calculate the sodium oxide content. Sodium peroxide was assumed to be present if oxygen was produced when water was introduced into the bomb.

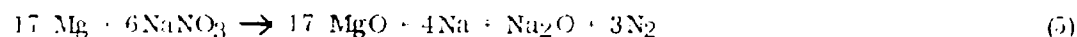
Magnesium and Magnesium Oxide. The insoluble solid residue is dried to a constant weight. It contains magnesium oxide and unreacted magnesium. The magnesium content is determined by the amount of evolved hydrogen produced from the reaction of Mg with dilute sulfuric acid; the magnesium oxide is then determined by difference.

Reaction Stoichiometry. It is convenient to specify a stoichiometry for the magnesium-sodium nitrate combustion reaction to provide a basis for the analysis of the data. It was therefore desirable to oxidize the magnesium completely with the sodium nitrate. The initial study was therefore made using fine Mg powder ( 22  $\mu$  ) in which the particle size is comparable to the sodium nitrate ( 23  $\mu$  ).

A two gram pellet having a Mg/NaNO<sub>3</sub> mole ratio of 3 to 1 was burned in 1 atmosphere of helium. The experimentally determined stoichiometric equation is



or



The reaction appears to have gone to completion. All of the nitrate was decomposed and only  $7 \times 10^{-5}$  moles or about 0.2% unreacted magnesium was recovered. Bomb calorimetry studies on the mixture gave a value of 2000 cal/g which is 97% of the value ( 2060 cal/g ) calculated from heats of formation data according to equation (5). The most significant aspect of the results is that the major portion of the sodium is reduced to metallic sodium and the remainder appears as sodium oxide, the Na/Na<sub>2</sub>O ratio being 4. The sodium oxide may be produced either from the decomposition of the nitrate or, more likely, from the oxidation of sodium. In the latter case the sodium vapor in the flame zone must compete with vaporizing magnesium for the oxygen produced in the decomposition of the nitrate.



The reaction of sodium with oxygen to produce sodium oxide rather than sodium peroxide requires an oxygen deficient atmosphere, which is the condition that exists in the bomb environment. Sodium oxide can also be produced from the decomposition of the nitrate (9). If this is the case, it must escape from the

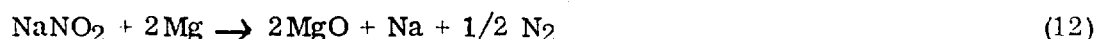
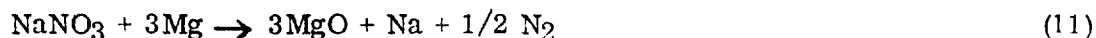


flame zone where it is unstable and likely to react with Mg according to





However, this analysis cannot discern the source of oxide nor of metallic sodium. The mass balance was therefore performed assuming the following reactions



It was further assumed that the quantity of Na shown in equation (4) was correct and the difference between the stoichiometric amount, according to equation (11), and the analyzed amount represented the sodium content. The results are shown in Table 1. The most serious discrepancy is the low nitrogen values ( 8% ), which cannot be readily explained. It is speculated that the low nitrogen might be due to the formation of magnesium nitride. The nitride is easily hydrolyzed to ammonia and, indeed, in one case, the combustion vessel was opened immediately after burning a magnesium-sodium nitrate mixture, and water was introduced into the bomb. The solution had a distinct ammoniacal odor. However, ammonia was never detected on the gas chromatograph after water addition to the closed vessel or by IR analysis. If magnesium nitride is formed, the low sodium and high oxygen content can also be explained. Possibly, the reaction products are contaminated by the formation of refractory materials from the porcelain cup used to containing the pellet. The overall mass balance is approximately 2.5% high which tends to confirm this conclusion.

Combustion of Coarse Magnesium. The magnesium normally used in operational flares has an average particle size of about 350  $\mu$  ( 30/50 mesh ). It was therefore desirable to study the combustion products of the reaction between coarse magnesium and sodium nitrate. A three gram pellet containing coarse particle size magnesium and sodium nitrate ( 23  $\mu$  ) in a 3 to 1 mole ratio was burned in a helium atmosphere in one trail. These experiments were performed to determine (1) the effect of particle size on the stoichiometry and mode of decomposition of the nitrate and (2) the combustion efficiency. Similar trials were conducted on the same mixture in a 80% helium 20%  $\text{O}_2$  atmosphere. Oxygen was added to the system to determine the effect of air-augmentation and to provide sufficient oxygen to burn all of the Mg where it was in excess.

The pellets burned in the inert atmosphere were found to burn incompletely, the remainder decomposing only as far as the nitrite. The experimentally determined heat of reaction gave a reproducible value of 1656 cal/g which is 80.7% of the calculated value ( based on equation 5 ) as compared to 78.4% based on the amount of unreacted magnesium.

TABLE 1

Mass Balance Results of Reaction Between Fine Particle  
Size Mg and  $\text{NaNO}_3$  ( Mole Ratio 3/1 )

<u>Reactants</u>	<u>Quantity ( Moles )</u>		<u>Deviation ( % )</u>
	<u>Calc. ( <math>\times 10^3</math> )</u>	<u>Obs. ( <math>\times 10^3</math> )</u>	
Magnesium	35.7	37.3	-5.4(*)
Sodium Nitrate	12.6	12.6	0(**)
<u>Combustion Products</u>			
Mg	-	0.07	-
MgO	37.3	37.3	0
Na	8.2	8.2	0(**)
$\text{Na}_2\text{O}$	2.2	2.1	-4.5
$\text{N}_2$	6.3	5.6	- 8
Total Na	12.6	12.4	- 1
Total Mg	37.3	37.4	0.27
Total N	12.6	11.6	- 8
Total O	37.8	39.4	+ 4
Overall mass balance (g)	1.9385	1.9861	+2.4

(\*) Excess Mg

(\*\*) Basis for calculations

For the mass balance evaluation, the assumed reaction sequence was based on equation 9, 10 and 11 and equation 13 which is required to account for some of the oxygen produced in the decomposition of the nitrate to nitrite.



The results are shown in Table 2.

While the overall mass balance agrees within 2.5% there are some discrepancies in the data which must be recognized. The Mg content is accounted for to within two percent but the MgO content is high by 11%. This value is determined gravimetrically by difference, a method which would not account for the previously mentioned contaminants. The most serious discrepancy is the low value obtained for N<sub>2</sub> (14%) which was observed in the previous trial. The total experimentally analyzed sodium content is within 2% of the calculated value but the sodium oxide molar content is high by 5.2%. The mass balance evaluation assumed that the sodium metal and sodium nitrite concentrations were correct and therefore this discrepancy is not surprising. In general, it is believed that an adequate mass balance was achieved.

A second series of experiments were performed on the 3:1 mole ratio coarse Mg-NaNO<sub>3</sub>. In these trials the mixtures were burned in a 80% He - 20% O<sub>2</sub> atmosphere. There was sufficient atmospheric oxygen (  $2.7 \times 10^{-3}$  moles ) and oxygen produced in the decomposition of the nitrate to the nitrite (  $2.8 \times 10^{-3}$  moles ) to oxidize the unreacted magnesium (  $\sim 9 \times 10^{-3}$  moles ) observed from the combustion of the mixture in the inert atmosphere.

In this series of experiments with air augmentation sodium peroxide was detected as a reaction product and only a small amount of metallic sodium was detected. Approximately 85% of the Mg was consumed while 74% of the nitrate was completely decomposed.

For the mass balance evaluation of the reaction was assumed to occur via equations 9, 10, 11, 13 and 14. The data are shown in Table 3.



There is in general, a decrease in the accuracy of the data from the previous run, the most serious discrepancies occurring with the sodium content ( 10% high ) and the MgO content (  $\sim 12\%$  high ) while the overall mass balance is about 5.7% high. It is believed that during and immediately after the

TABLE 2

Mass Balance Results on Reaction of Coarse Mg ( 30/50 Mesh )  
With  $\text{NaNO}_3$  in an Inert Atmosphere

<u>Reactants</u>	<u>Quantities ( Moles x 10<sup>3</sup> )</u>		
Mg	57.3		
NaNO <sub>3</sub>	19.1		
<u>Products</u>	<u>Quantities ( Moles x 10<sup>3</sup> )</u>		<u>Deviation</u>
	<u>Calc.</u>	<u>Obs.</u>	<u>( % )</u>
Mg	15.6	12.7	-19.1
NaNO <sub>2</sub>	-	5.8	-
MgO	41.9	45.8	+11
Na	5.7	5.7	0
Na <sub>2</sub> O	3.8	4.0	+5.2
N <sub>2</sub>	6.6	5.7	-14
Total Na	19.1	19.5	+2
Total Mg	57.3	58.4	+2
Total N	19.1	17.2	-10
Total O	57.3	61.4	+7
Overall mass balance (g)	3.0158	3.0932	+2.6

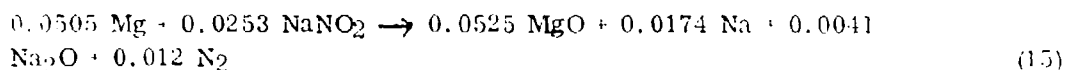
TABLE 3

Mass Balance Results of Combustion Reaction Between  
Mg ( 30/50 Mesh )  $\text{NaNO}_3$  in 80% He - 20%  $\text{O}_2$  Atmosphere

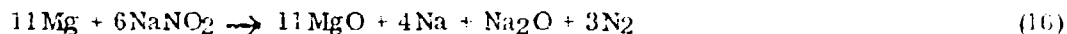
<u>Reactants</u>	<u>Quantities ( Moles x 10<sup>3</sup> )</u>		
Mg	56.9		
NaNO <sub>3</sub>	18.9		
Oxygen	2.7		
<u>Combustion Products</u>	<u>Quantity ( Moles x 10<sup>3</sup> )</u>		<u>Deviation</u>
	<u>Calc.</u>	<u>Obs.</u>	<u>( % )</u>
Mg	13.1	8.8	-33
NaNO <sub>2</sub>	5.7	5.7	-
MgO	42.8	49.0	+11.9
Na	0.4	0.4	-
Na <sub>2</sub> O	6.0	7.0	+16.6
Na <sub>2</sub> O <sub>2</sub>	0.4	0.4	-
N <sub>2</sub>	6.6	6.4	-3
O <sub>2</sub>		0.03	-
Total Na	18.9	20.9	+10
Total Mg	56.9	57.8	+1.6
Total N	18.9	18.5	-2.2
Total O	62.1	68.23	+9.9
Overall mass balance (g)	3.0758	3.2358	+5.2

combustion reaction, secondary reactions of oxygen with the internal environment of the combustion vessel may occur which can influence the mass balance. A comparison of the calculated amount of Mg oxidized and the analyzed amount is 33%. The calculated amount is based on the oxygen made available from both the decomposed nitrate and atmospheric oxygen and therefore is dependent upon the accuracy of the  $\text{NO}_2^-$  content of the mixture. This analysis is in some question because of the shift observed in the characteristic band due to  $\text{NO}_2^-$  from 357  $\mu$  to 365  $\mu$ . This matter requires further investigation. One possibility is the presence of  $\text{NO}_2$ , which has a characteristic peak at 400  $\mu$  and has a high extinction coefficient. If  $\text{NO}_2$  is present and not accounted for, the  $\text{NO}_2^-$  would tend to be high and the  $\text{N}_2$  content would be low.

Magnesium-Sodium Nitrite Combustion. A three gram pellet of  $\text{Mg-NaNO}_2$  in a 2:1 mole ratio was burned in a helium atmosphere in the closed combustion vessel. The observed reaction is



By chemical analyses the MgO content was found to be about 4% high, while the sodium content of the products agreed closely with that of the reactants. The oxygen content was about 10% high, mostly because of the high MgO content. The nitrogen analysis was low by about 4%. The reaction went to completion as indicated by the fact that the nitrite concentration were negligible and the unreacted Mg content was  $10^{-4}$  moles. The mole ratio of  $\text{Na}/\text{Na}_2\text{O}$  was 4 as was observed using  $\text{NaNO}_3$ . A reasonable stoichiometry that can be written is



The reaction requires confirmation because of the unaccounted for discrepancies in the MgO and  $\text{N}_2$  content of the products.

Pressure-Time Relationships. Shown in Figure 1 are the pressure-time traces obtained from the combustion of the four compositions. The difference in the ignitibility and burning rate of the 22  $\mu$  Mg flare ( Curve 1 ) and the 350  $\mu$  Mg flare ( Curve 2 ) are clearly shown. The pertinent data are shown in Table 4.

TABLE 4

Results of Pressure-Time Investigation on Magnesium  
Containing Flare Compositions

Composition* ( Mole Ratio )	Particle Size of Mg	Atmosphere	Time-To Ignition (sec)	Time-To Peak Pressure (sec)	Peak Pressure (PSI)
Mg/NaNO <sub>3</sub> (3:1)	22	He	0.7	1.0	184
Mg/NaNO <sub>3</sub> (3:1)	350	He	1.25	2.7	56
Mg/NaNO <sub>3</sub> (3:1)	350	80% He - 20% O <sub>2</sub>	1.25	2.3	80
Mg/NaNO <sub>2</sub> (2:1)	22	He	0.6	0.85	164

As expected, the 22  $\mu$  Mg composition burned at a faster rate and the time-to-ignition was lower than the 350  $\mu$  Mg composition. The addition of oxygen to the atmosphere ( for the 350  $\mu$  Mg composition ) did not alter the ignitibility but the rate of pressure rise and the peak pressure was increased.

A comparison of the pressure-time traces of the 22  $\mu$  Mg with NaNO<sub>3</sub> or NaNO<sub>2</sub> show that the time-to-ignition of the NaNO<sub>2</sub> composition is slightly lower and the time-to-peak pressure is lower. This observation is in line with findings in this laboratory that Mg flares containing mixtures of NaNO<sub>3</sub> and NaNO<sub>2</sub> burn at a faster rate than compositions containing only NaNO<sub>3</sub>. This result is expected since the decomposition of the nitrate to the nitrite is endothermic by about 12 kcal/mol.

#### DISCUSSION

It has been shown that fine particle size Mg ( 22  $\mu$  ) can be oxidized completely by sodium nitrate and that metallic sodium is a major product. If the particle size of the Mg is  $\sim$ 350  $\mu$  the amount oxidized is 80 to 85% depending on the oxygen content of the atmosphere. In an oxygen deficient atmosphere, sodium oxide is present while in an oxygen rich atmosphere sodium oxide and sodium peroxide are present. Brewer (10) indicates that sodium oxide on subliming at 920°C undergoes simple decomposition to the gaseous elements while sodium peroxide dissociates at about 450°C. Thus, it is likely that these products are formed outside of the combustion zone and during the cooling process. However, particles ejected on the periphery of the burning surface may not pass through

the flame zone and  $\text{Na}_2\text{O}$  may escape intact. Blackshear, et. al. (11) indicate that the temperature of the flame plume of a 2.25 in. flare has a temperature of about  $1250^\circ\text{C}$  about 4 inches above the flare surface. If the oxide is in the proximity of a Mg particle the reaction



may therefore occur. Sodium oxide is known to form from the decomposition of the nitrate (9) and it may exist sufficiently long in the flame zone to react with Mg.

A few interesting observations were made in the mass balance analysis of the  $\text{Mg}/\text{NaNO}_3$  combustion reaction. Thus, the nitrogen gas content of the products was consistently low indicating that nitrogen is present in another form. Two possible explanations are (1) the nitrogen is present as  $\text{Mg}_3\text{N}_2$  and (2) it is present as  $\text{NO}_2$  occluded by cooled solid products. Nitrogen oxides were never observed but a shift in the UV spectrum of unreacted nitrite indicates the presence of another species, possibly  $\text{NO}_2$ .

Sodium nitrite was observed as a reaction product only in the cases where the Mg reacted incompletely. Particle ejection from the surface may account for some of the nitrite, that is, molten sodium nitrate which undergoes ejection decomposes endothermically and is not in contact with a heat source to cause further decomposition. Another possibility is that large Mg particles absorb the energy which otherwise might be utilized to decompose the nitrite.

It is also likely that the ejection mechanism can account for the inefficient combustion of coarse Mg. Another reason is that large particles do not have sufficient time to evaporate and burn as they pass through the combustion zone. According to Friedman and Macek, single particle burning time is directly proportional to the diameter squared (12). Calculations by Tischer (13) and Blackshear, et. al. (11) showed that unreacted Mg may be observed when the flare is burned in a limited atmosphere of  $\text{O}_2$ . It is surprising, however, that coarse particle Mg flares produce a greater luminous energy than fine particle Mg flares, which has been observed by Blackshear, et. al. (11). This observation coupled with our observation that fine particle size Mg burns with a high efficiency with  $\text{NaNO}_3$  might indicate that atmospheric air oxidation of Mg is a necessary condition for high luminosity.



## REFERENCES

1. Freeman, E. S. and Gordon, S. "Application of Absolute Rate Theory to the Ignition of Propagatively Reacting Systems. Thermal Ignition of Lithium Nitrate + Magnesium, Sodium Nitrate + Magnesium", J. Phys. Chem 60, p 67 (1956).
2. Bond, B. D. and Jacobs, P. W. M., "Chemical Reaction and Ignition in Mixtures of Magnesium and Sodium Nitrate", Combustion and Flame 10, 349 (1966).
3. Hogan, V. D. and Gordor, S., "Pre-ignition and Ignition Reactions of the Propagatively Reacting System Magnesium-Sodium Nitrate-Laminac, " Combustion and Flame, 3, 3 (1959).
4. Douda, B. E. and Bair, E. J., "Visible Radiation from Illuminating Flares. II. Formation of the Sodium Resonance Continuum", J. Opt. Soc. of America 60, 1257 (1970).
5. Shidlovsky, A. A., "Foundations of Pyrotechnics" Moscow USSR, 1954.
6. AMC Pamphlet, "Military Pyrotechnic Series. Part I. Theory and Application", AMCP 706-185, April 1967.
7. Farnell, P. L., Beardell, A. J. and Taylor, F. R., "The Performance of Aluminum-Sodium Nitrate Flares in Various Oxygen-Nitrogen Atmospheres", Proceedings of the Seventh Symposium on Explosives and Pyrotechnics, Franklin Institute, September 1971.
8. Walters, J. H. and Uglum, K. L., "Direct Spectrophotometric Simultaneous Determination of Nitrite and Nitrate in the Ultraviolet", Anal. Chem. 42, 335 (1970).
9. Bond, B. D. and Jacobs, P. W. M., "The Thermal Decomposition of Sodium Nitrate", J. Chem. Sec. A, 1265 (1966).
10. Brewer, L., "Thermodynamic Properties of the Oxides," Chem. Rev. 52, 1 (1953).
11. Blackshear, P. L., Marty, K. A. Barnes, K., and Dorman, F. D., "Exploratory Development of Illuminating Flares," Section IV, AFATL-TR-68-91, August 1968.
12. Friedman R., and Macek, "Studies of Single and Combustion of Aluminum Particles," Ninth Symposium ( International ) on Combustion", Academic Press, N. Y., 1963, pp 703-712.

Best Available Copy

13. Tischer, R. L., "Effect of Entrained Air in Determining Optimum Flare Compositions", Proceedings Second International Pyrotechnic Seminar, July 1970, p 425.

ADDENDUM: After completion of this paper, the reason for the shift in the characteristic band due to nitrite ion from 355 to 365  $\mu$  was uncovered. The shift was found to be due to chromate which is formed by the oxidation of the chromel wire used to ignite the composition. Chromate has a characteristic band with a maximum at 375  $\mu$  and has an extremely high extinction coefficient. Preliminary determination of nitrite in the presence of chromate in a basic solution indicates that the nitrite ion concentration reported in this paper is high by a factor of 2.5 to 3. This correction would, in effect, account for the discrepancies in the calculated sodium oxide and MgO values given in Tables 2 and 3.

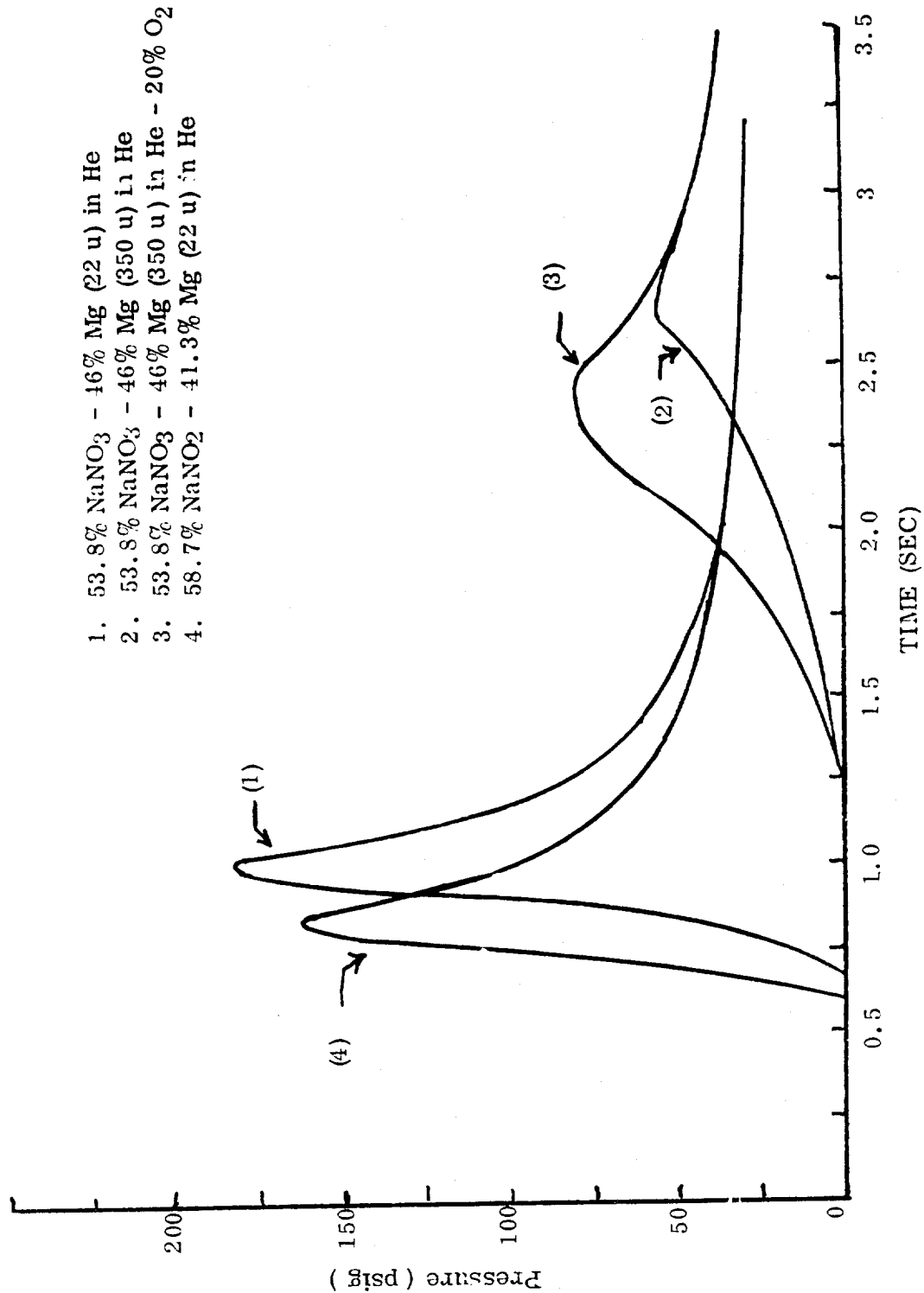


FIG 1. P-T TRACES RESULTING FROM THE COMBUSTION 3 G PELLETS OF  $\text{Mg-NaNO}_3$  AND  $\text{Mg-NaNO}_2$ .

Best Available Copy